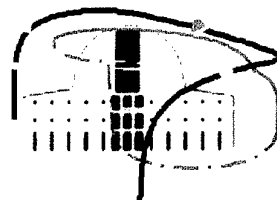




Universidad Pública de Navarra
Public University of Navarre

5th International Symposium
On Quantitative Feedback Theory
and Robust Frequency Domain
Methods



Pamplona, Spain.
23 - 24 August, 2001.

20010927 068

Edited by
Mario García-Sanz

DOCUMENTA
SERIES
IN
CONTROL THEORY AND APPLICATIONS
VOLUME 100

REPORT DOCUMENTATION PAGE

Form Approved OMB No. 0704-0188

Public reporting burden for this collection of information is estimated to average 1 hour per response, including the time for reviewing instructions, searching existing data sources, gathering and maintaining the data needed, and completing and reviewing the collection of information. Send comments regarding this burden estimate or any other aspect of this collection of information, including suggestions for reducing this burden to Washington Headquarters Services, Directorate for Information Operations and Reports, 1215 Jefferson Davis Highway, Suite 1204, Arlington, VA 22202-4302, and to the Office of Management and Budget, Paperwork Reduction Project (0704-0188), Washington, DC 20503.

1. AGENCY USE ONLY (Leave blank)		2. REPORT DATE 2001	3. REPORT TYPE AND DATES COVERED Conference Proceedings	
4. TITLE AND SUBTITLE 5 th International Symposium on Quantitative Feedback Theory and Robust Frequency Domain Methods			5. FUNDING NUMBERS F61775-01-WF049	
6. AUTHOR(S) Conference Committee				
7. PERFORMING ORGANIZATION NAME(S) AND ADDRESS(ES) Universidad Publica de Navarra Dept. de Automatica y Computacion Pamplona 31006 Spain			8. PERFORMING ORGANIZATION REPORT NUMBER N/A	
9. SPONSORING/MONITORING AGENCY NAME(S) AND ADDRESS(ES) EOARD PSC 802 BOX 14 FPO 09499-0200			10. SPONSORING/MONITORING AGENCY REPORT NUMBER CSP 01-5049	
11. SUPPLEMENTARY NOTES				
12a. DISTRIBUTION/AVAILABILITY STATEMENT Approved for public release; distribution is unlimited.			12b. DISTRIBUTION CODE A	
13. ABSTRACT (Maximum 200 words) The Final Proceedings for International Symposium on Quantitative Feedback Theory and Robust Frequency Domain Methods, 23 August 2001 - 24 August 2001 This is an interdisciplinary conference. Topics include; <ul style="list-style-type: none"> - Quantitative Feedback Theory - Robust Control - Frequency-based Methods - Robust Stability and Performance - Uncertain Dynamic Systems - Identification for Robust Control - Fault Detection in Uncertain Systems - Applications 				
14. SUBJECT TERMS EOARD, Control, Quantitative Feedback Theory (QFT), Frequency Domain Methods			15. NUMBER OF PAGES 303	
			16. PRICE CODE N/A	
17. SECURITY CLASSIFICATION OF REPORT UNCLASSIFIED	18. SECURITY CLASSIFICATION OF THIS PAGE UNCLASSIFIED	19. SECURITY CLASSIFICATION OF ABSTRACT UNCLASSIFIED	20. LIMITATION OF ABSTRACT UL	

NSN 7540-01-280-5500

Standard Form 298 (Rev. 2-89)
Prescribed by ANSI Std. Z39-18
298-102

**5th INTERNATIONAL SYMPOSIUM ON
QUANTITATIVE FEEDBACK THEORY
AND ROBUST FREQUENCY DOMAIN METHODS**

PROCEEDINGS

Edited by: Mario García-Sanz

**Public University of Navarre
Pamplona (Spain), 23-24 August 2001**

Supported by
The European Office of Aerospace Research and Development
The organisers wish to thank the United States Air Force European Office of Aerospace
Research and Development for its contribution to the success of the conference.

AQ F01-12-2608

Title: Proceedings of the 5th INTERNATIONAL SYMPOSIUM ON
QUANTITATIVE FEEDBACK THEORY AND ROBUST FREQUENCY
DOMAIN METHODS

Editor: Mario García-Sanz
Editorial Committee: Javier Castillejo, Igor Egaña
Published by: Universidad Pública de Navarra
© The Authors
© Universidad Pública de Navarra

ISBN: 84-95075-56-3

D. L.: NA-1926-2001

Printed by: Lankopi S. A.

Copies may be
ordered from: Prof. Mario García-Sanz
Dpto. Automática y Computación
Universidad Pública de Navarra
Campus Arrosadía
31006 Pamplona - Navarra (España)

Responsibility for the contents rests entirely with the authors. The editors
accept no liability for errors or omissions.

No part of this publication may be reproduced, stored in a retrieval system or
transmitted in any form or by any means without prior permission of the
editors. Permission is not required to copy abstracts of papers, provided that a
full reference to the source is given.

International Program Committee

Chairman: Mario García-Sanz (Spain)

Edward Boje (South Africa)

Constantine H. Houpis (USA)

Eduard Eitelberg (South Africa)

Isaac Horowitz (USA)

Per-Olof Gutman (Israel)

Yossi Chait (USA)

Alfonso Baños (Spain)

Roberto Tempo (Italy)

Pedro Albertos (Spain)

Mathew A. Franchek (USA)

Oded Yaniv (Israel)

Dave Thompson (USA)

Bor-Chyun Wang (Taiwan)

Donald Ballance (United Kingdom)

John O'Reilly (United Kingdom)

Suhada Jayasuriya (USA)

National Organization Committee

Mario García-Sanz

Igor Egaña

Javier Castillejo

Pablo Vital

Javier Villanueva

Marta Barreras

Juan Carlos Guillén

Montserrat Gil



Universidad Pública de Navarra
Public University of Navarra



European Office of Aerospace
Research and Development

CAJA NAVARRA



CEA

comité
español de
automática

INDEX

EDITORIAL	ix
PLENARY SPEAKERS	xiii

PLENARY TALKS

SOME PECULIARITIES OF LOAD SHARING CONTROL	
<i>E. Eitelberg</i>	1
CONTROL OF THE AERO-ELECTRIC POWER STATION. AN EXCITING QFT APPLICATION FOR THE 21 ST CENTURY	
<i>P. O. Gutman, E. Horesh, R. Gueta, M. Borshchevsky</i>	9

1ST PAPER SESSION

LOOP SHAPING AND ACHIEVABLE PERFORMANCE WITH PID CONTROLLERS	
<i>L.H. Keel, S.P. Bhattacharyya</i>	31
ON THE EXISTENCE CONDITIONS FOR ROBUST STABILITY AND PERFORMANCE OF PID CONTROLLERS	
<i>U. I. Ukpai, S. Jayasuriya</i>	39
POINTING CONTROL FOR PRECISION FLIGHT TELESCOPES USING QUANTITATIVE FEEDBACK THEORY	
<i>A. Bentley</i>	47
SOME IDEAS FOR QFT RESEARCH	
<i>I. Horowitz</i>	57
PRE-FILTER DESIGN FOR TRACKING ERROR SPECIFICATIONS IN QFT	
<i>E. Boje</i>	63
QUANTITATIVE MULTIVARIABLE FEEDBACK DESIGN FOR A SCARA ROBOT ARM	
<i>I. Egaña, J. Villanueva, M. García- Sanz</i>	67

2ND PAPER SESSION

IDENTIFICATION FOR ROBUST CONTROL OF A FAST FERRY	
<i>J. Aranda, J. M. de la Cruz, J.M. Díaz, P. Ruipérez</i>	73
ROBUST QFT CONTROLLER FOR MARINE COURSE-CHANGING CONTROL	
<i>T.M. Rueda Rodríguez, F.J. Velasco González, E. Moyano Pérez, E. López García</i>	79
MULTIVARIABLE CONTROL FOR COOLING MACHINES BASED ON VAPOR COMPRESSION	
<i>J.M. Galvez, L. Machado, A. Gomes da Silva</i>	85

QFT CONTROL DESIGN FOR AN APPROXIMATELY LINEARIZED PNEUMATIC POSITIONING SYSTEM

F. Xiang, J. Wikander 95

A NOTE ON THE USE OF THE STRUCTURED SINGULAR VALUE IN DECENTRALISED CONTROL

P. S. Rao, E. Boje 107

COMPENSATOR SELECTION USING QFT FOR H_{∞} LOOPSHAPING WITH COPRIME UNCERTAINTIES

F. del Valle, F. Tadeo, O. Pérez 113

QFT DESIGN WITH PHASE SPECIFICATIONS

J. C. Moreno, A. Baños, M. Berenguel 123

A GEOMETRIC APPROACH TO ROBUST PERFORMANCE OF PARAMETRIC UNCERTAIN SYSTEMS

J. Bondia, J. Picó 133

3RD PAPER SESSION

DIGITAL IMPLEMENTATION OF CONTROLLERS

E. Eitelberg 141

OPTIMAL IMPLEMENTATION OF A MULTIVARIABLE CONTROLLER IN A FIXED POINT DSP

L. González, L. A. Salas 151

ROBUST FEEDBACK SYNTHESIS FOR NARMAX MODELS USING GENERALIZED DESCRIBING FUNCTIONS

P.S.V. Nataraj, K. Kotecha 161

HOROWITZ: BRIDGING THE GAP

C. H. Houpis 171

INTERVAL QFT: A MATHEMATICAL AND COMPUTATIONAL ENHANCEMENT OF QFT

P.S.V. Nataraj, S. Sheela, A.K. Prakash 177

SIMULTANEOUS MEETING OF CONTROL SPECIFICATIONS IN QFT

M. Gil-Martinez, M. García-Sanz 193

COMPARING ROBUST CONTROL DESIGN STRATEGIES FOR PRACTICAL IMPLEMENTATION IN AUTONOMOUS VEHICLES

L. Ganselmeier, J. Helbig, E. Schnieder 203

4TH PAPER SESSION

ONE-DIMENSIONAL ACTIVE NOISE CONTROL USING THE INTERNAL MODEL PRINCIPLE

M. O'Brien, P. Pratt, C.J. Downing 207

APPLICATION OF A ROBUST FAULT-TOLERANT CONTROL SCHEME TO A NONLINEAR SYSTEM

A. Cardoso, A. Dourato 215

INTERACTIVE EDUCATIONAL ENVIRONMENT FOR DESIGN BY QFT METHODOLOGY

S. Dormido, J. Aranda, J.M. Díaz, S. Dormido Canto 223

HIGH-ORDER CONTROLLERS MODEL REDUCTION USING QFT TOOLS

J. Castillejo, M. Barreras, P. Vital, M. García-Sanz 231

GENERATION OF FREQUENCY RESPONSE TEMPLATES FOR LINEAR SYSTEMS WITH AN UNCERTAIN TIME DELAY AND MULTILINEARLY CORRELATED PARAMETER PERTURBATIONS

C. Hwang, S. F. Yang 239

COMPUTATION OF SISO GENERAL PLANTS TEMPLATES

J. Cervera, A. Baños, I. M. Horowitz 247

FREQUENCY DOMAIN FEEDFORWARD COMPENSATION

F.J. Pérez Castelo, R. Ferreiro Garcia 255

CPP, LQG OR GPC?

T. OMahony, C.J. Downing 261

PAPERS OUT OF SESSION

ON HOROWITZ'S CONTRIBUTIONS TO RESET CONTROL

Y. Chait, C.V. Hollot 269

QFT CONTROLLER SYNTHESIS USING EVOLUTIVE STRATEGIES

C. Raimúndez, A. Baños, A. Barreiro 291

A METHOD FOR NONLINEAR QUANTITATIVE STABILITY

A. Baños, I. Horowitz 297

LIST OF AUTHORS 303

**International Symposium on Quantitative Feedback Theory
and Robust Frequency Domain Methods**

Wright Patterson Airforce Base, Dayton, Ohio, USA, August 1992

Purdue University, West Lafayette, Indiana, USA, August 1995

University of Strathclyde, Glasgow, Scotland, UK, August 1997

University of Natal, Durban, South Africa, August 1999

Public University of Navarre, Pamplona, Spain, August 2001

EDITORIAL

QFT & RFDM International Symposia. Past, present and future.

Much of the current interest in frequency domain robust stability and robust performance dates from the original work of H.W. Bode (1945), and I. Horowitz (1963). Since then, and during the entire second half of the twentieth century, there has been a tremendous advance in the state-of-the-art of robust frequency domain methods. One of the main techniques, introduced by Prof. Isaac Horowitz in 1959, which characterises closed loop performance specifications against parametric plant uncertainty, mapped into open loop design constraints, became known as Quantitative Feedback Theory (QFT).

Since the seventies until now, the association of the Air Force Research Laboratory (AFRL-USA) with the Department of Electrical and Computer Engineering of the Air Force Institute of Technology (AFIT-USA) has resulted in a large amount of research in QFT. In fact, the first research grant that Prof. Horowitz, the founder of QFT, received was in 1973 from the Air Force Office of Scientific Research (AFOSR). Further support came from their European Office Aerospace Research and Development (EOARD). Indeed, much of the early Air Force support for Prof. Horowitz came through EOARD.

Great strides were made by the U. S. Air Force researchers in the application of QFT to the design of robust multivariable flight control systems. Prof. Constantine H. Houppis of AFIT, along with his graduate students, and in conjunction with Prof. Horowitz, extended the state-of-the-art in the development and application of QFT. As a result Prof. Houppis, as General Chairman, with the sponsorship of AFRL, organised the first international scientific meeting on QFT, with the name: *Quantitative Feedback Theory Symposium*. It was held at Wright Patterson Airforce Base, Dayton, Ohio (USA), in August 1992. As Prof. Houppis stated in those days, "*Quantitative feedback theory (QFT) has achieved the status as a very powerful design technique for the achievement of assigned performance tolerances over specified ranges of plant uncertainties without and with control effector failures*".

The awareness of the power of QFT to solve real world problems has evoked the interest and involvement of a greater number of control engineers and researchers. The methodology has been used to solve SISO, MISO, and MIMO plants, single and multiple loops, linear and nonlinear processes, lumped and distributed plants, etc. Since 1989 until 2000 there have been published 322 international papers on QFT: 210 at international scientific conferences and 112 at international scientific journals of the Science Citation Index (data according to INSPEC and the QFT Symposia). Figure 1 shows the evolution.

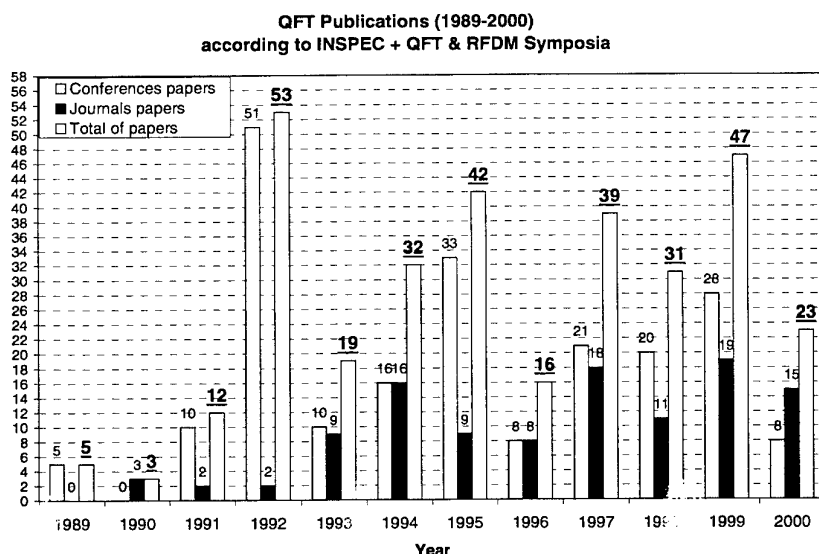


Figure 1

Prof. Horowitz said in the first QFT symposium: "*there is room in QFT for highly diverse talents: the nonmathematical practical engineer with physical insight and inventive talent, the skilled mathematician interested in existence theorems and abstract generalisations, up to the stubborn, even plodding researcher who by hard dedicated work acquires deep understanding of this subject*". However, he also said "*QFT is as yet in its infancy, pointing to vast, available problems areas*".

Since then, there has been an increasing interest in the frequency domain methods. The second international symposium was held at the Purdue University, West Lafayette, Indiana (USA), in August 1995, with the name: *Quantitative and Parametric Feedback Theory Symposium*. The third one was at the University of Strathclyde, Glasgow, Scotland (UK), in August 1997, with the name: *Symposium on Quantitative Feedback Theory and other Frequency Domain Methods and Applications*. The fourth symposium was held at the University of Natal, Durban, South Africa, in August 1999, with the name: *International Symposium on Quantitative Feedback Theory and Robust Frequency Domain Methods*.

Now, I would like to introduce the fifth international scientific meeting being held this year at the Public University of Navarra, Pamplona, Spain, for which I am keeping the same name as the last symposium: *International Symposium on Quantitative Feedback Theory and Robust Frequency Domain Methods* (QFT & RFDM). Its purpose is to bring together practitioners and researchers in the field of frequency domain methods and to promote the development of these methods and their practical application. The Symposium covers new developments in Quantitative Feedback Theory and Robust Frequency Domain methods, algorithms, software and applications.

The number of papers that have been published in the five international symposia is 138 ($= 37 + 18 + 27 + 21 + 35$). Their distribution per symposium is shown in Figure 2. In terms of subject, at the beginning almost 95% of the papers were about QFT, and only 5% about other Robust Frequency Domain Methods. However, from the third symposium until now the rate has been stabilised in 62% about QFT against 38% about other RFDM (Figure 3).

The total number of authors that have attended any symposium is 253 ($= 61 + 41 + 43 + 42 + 66$), and the number of different authors that have attended the symposia is 190. Their distribution per continent and symposium is shown in Figures 4 and 5.

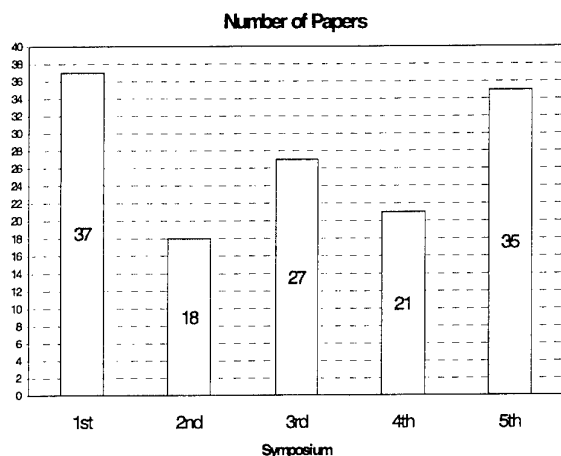


Figure 2

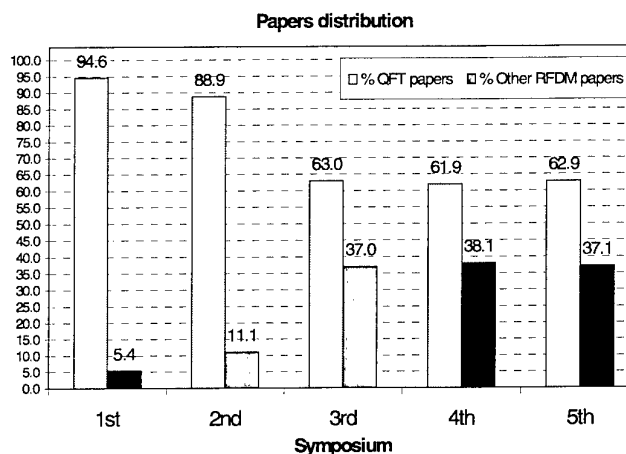


Figure 3

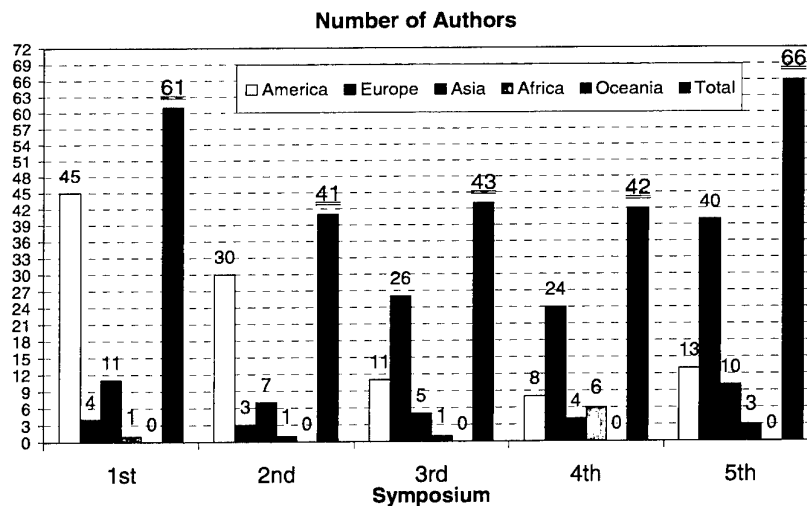


Figure 4

Authors distribution per continents

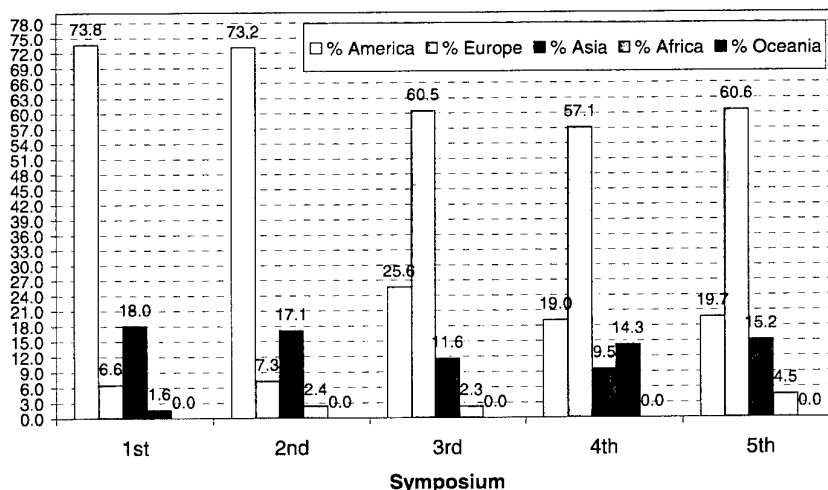


Figure 5

Among the set of 190 different authors that have attended the symposia, 15 of them have been present in more than 60% of the events. They are: I. Horowitz, C.H. Houpis, F.N. Bailey, Y. Chait, M.A. Franchek, S. Jayasuriya and O.D.I. Nwokah from USA; E. Eitelberg and E. Boje from South Africa; M. García-Sanz and A. Baños from Spain; P.O. Gutman and O. Yaniv from Israel; P.S.V. Nataraj from India; and B.C. Wang from Taiwan. In this context only one author has taken part in all of the symposia: Prof. Constantine H. Houpis.

The number of countries participating in the biennial symposium has increased through the years, as it is shown in Figure 6. The number of different countries that has attended the symposia is 16. Table I shows the countries where the authors came from per symposium.

Number of Countries

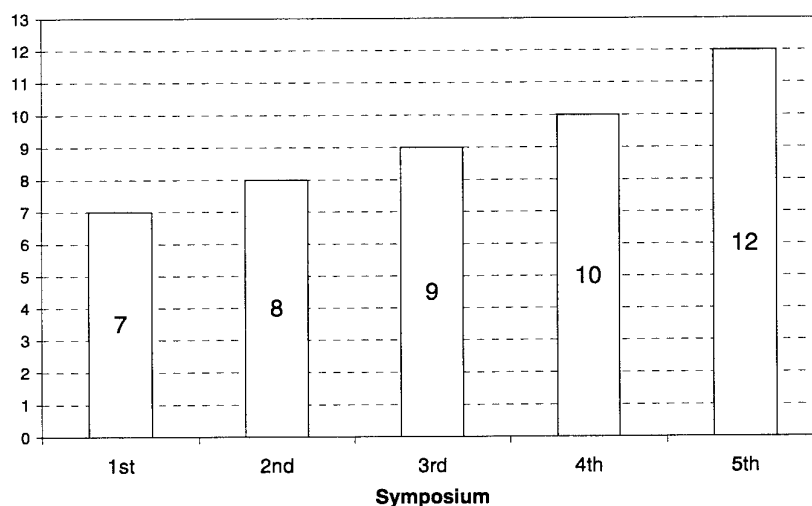


Figure 6

Table I. Authors distribution per countries

Symp	America			Europe									Asia			Africa	SUM
	USA	Mexico	Brazil	UK	Spain	France	Germany	Poland	Sweden	Switzer land	Portugal	Ireland	Israel	Taiwan	India	South Africa	
1st	44	1	0	4	0	0	0	0	0	0	0	0	5	3	3	1	61
2nd	29	1	0	2	1	0	0	0	0	0	0	0	2	3	2	1	41
3rd	11	0	0	10	6	6	3	1	0	0	1	0	4	0	0	1	43
4th	5	3	0	7	9	1	2	0	2	3	0	0	0	4	0	6	42
5th	9	2	2	0	29	0	3	0	2	0	2	4	4	2	4	3	66
%	38.7	2.8	0.8	9.1	17.8	2.8	3.2	0.4	1.6	1.2	1.2	1.6	5.9	4.7	3.6	4.7	

The countries with the most representation, in terms of number of authors, are the four that have been organisers: USA (38.7%), United Kingdom (9.1%), South Africa (4.7%) and Spain (17.8%); plus Israel (5.9%).

Two countries have attended the five symposia: USA and South Africa. Five countries have attended four: Mexico, United Kingdom, Spain, Israel and Taiwan. Three countries have attended three: France, Germany and India. Two countries have attended two: Sweden and Portugal. Four countries have attended one symposium: Brazil, Poland, Switzerland and Ireland.

More than 60 successful engineering control applications of robust frequency domain methods, mainly QFT controllers, have been reported through the five symposia. The following list highlight the next real implementations:

- Flight control: F-16 flight control system, Lambda remotely-piloted airplane, C-135 military transport aircraft, UH-60 Black Hawk helicopter flight control, SAAB AB flight control system, Advance combat aircraft, Autopilot flight control design, Missile control systems, X-29, etc.
- Process control: Distillation columns, Continuous stirred tank reactors CSTRs, Heavy oil fractionator, pH neutralisation process, Heating systems, Multiple-effect evaporator, Gasifier control, Superheater temperature control, Cooling machines, Arc welding penetration control, Pinch weld quality control, Hydraulic positioning systems, Storage vessel processes, Flow control, Pneumatic positioning system, etc.
- Robotics: Distributed mechanical structures, Flexible beam with variable coupling, 3 DOF Robot manipulators, Autonomous path tracking robot, SCARA Robot manipulator, etc.
- Combustion motors control: Aircraft engines, V-6 fuel-injected combustion engine, Allison Pd-514 aircraft turbine engine, GE16 variable cycle engine, Ford 4.6L-2 valve V-8 fuel injected engine, Turbofan engine, etc.
- Special vehicles control: Intelligent vehicles, Autonomous vehicles, Fast Ferry control, Citroen BX active suspension, etc.
- Electronics systems control: 741 BJT Operational amplifier, Audio power amplifier, Fixed point DSP, DC motor position servo prototype, etc.
- Power systems control: Fast control coil system of a Tokamak, Aero-electric power station, etc.
- Biological systems control: Active sludge wastewater treatment plant, etc.
- Advanced systems: Flight telescope control, Earthquake simulator machine, etc.

After the large covered itinerary, we can state that the international QFT & RFDM symposia have reached the maturity of a periodic and referenced scientific meeting on Robust Frequency Domain Methods. Progress has been made in having IFAC take over the management. The outlook in IFAC assuming the sponsoring of the symposia is favourable. We expect a final decision later this year. Until then, I would like to thank all the people and institutions that have worked and supported the symposia, since the first ideas of Prof. Isaac Horowitz and the first symposium organised by Prof. Constantine Houpis, and from many different countries and through the years.

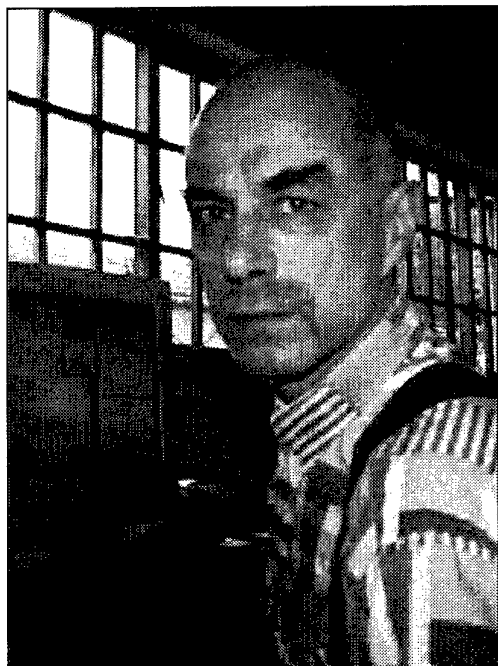
References

- Bode, H.W. *Network Analysis and Feedback Amplifier Design*. Van Nostrand Company, 1945.
- Horowitz, I. *Synthesis of Feedback Systems*. Academic Press, 1963.
- Horowitz, I. *Fundamental Theory of Linear Feedback Control Systems*. Trans. IRE on Automatic Control, AC-4, 5-19, December 1959.
- 1st International Symposium. *Quantitative Feedback Theory*. Edited by C.H. Houpis & P.R. Chandler. Wright Patterson Airforce Base, Dayton, Ohio (USA), August 1992. WL-TR-92-3063.
- 2nd International Symposium. *Quantitative and Parametric Feedback Theory*. Edited by O.D.I. Nwokah & P.R. Chandler. Purdue University, West Lafayette, Indiana (USA), August 1995.
- 3rd International Symposium. *Quantitative Feedback Theory and other Frequency Domain Methods and Applications*. Edited by L. Petropoulakis & W.E. Leithead. University of Strathclyde, Glasgow, Scotland (UK), August 1997.
- 4th International Symposium. *Quantitative Feedback Theory and Robust Frequency Domain Methods*. Edited by E. Boje & E. Eitelberg. University of Natal, Durban, South Africa, August 1999. ISBN: 1-86840-330-0.

Mario García-Sanz
Editor

5th QFT & RFDM International Symposium
Public University of Navarra
Pamplona, Spain (2001)

PLENARY SPEAKERS



Eduard Eitelberg, Dr.-Ing. habil., Pr. Eng., LL.M.
Professor of Electrical & Control Engineering

Born in 1949, Estonia. Married with very attractive Esther and four children. Dr.-Ing. habil. (control engineering) from the University of Karlsruhe, Germany. Full professor since 1983, first at the University of Natal, since 1987 at the University of Durban-Westville, both in South Africa. LL.M. (*cum laude*) in 2000. 24 years of under-graduate and post-graduate teaching in various electrical, mechanical, computer and control engineering subjects; and commercial law. 79 publications, including 8 books (or chapters), 45 research papers, 2 patents.

Research interests include: mathematical modelling, computer simulation and estimation; control engineering — current favourite is load sharing in engineering, management and economic spheres; topics in physics and bio-medical applications; international commercial law.

Business activities (as NOY Business™) include: boiler dynamics; control system design; process industry and instrumentation projects; signal processing in acoustic and sonar applications; naval systems' engineering, integration and project

management; manufacturing and ISO 9000.



Per-Olof Gutman, Ph.D., Civ.-Ing
Associate Professor of Control Engineering

Born in Hoganas, Sweden on 21 May 1949. He received the Civ.-Ing. degree in Engineering Physics (1973), the Ph.D. in Automatic Control (1982) and the title of Docent in Automatic Control (1988), all from the Lund Institute of Technology, Lund, Sweden. He received the MSE degree from the University of California, Los Angeles in 1977 as a Fulbright grant recipient.

From 1973 to 1975 he taught mathematics in Tanzania. 1983-84 he held a post-doctoral position at the Faculty of Electrical Engineering, Technion - Israel Institute of Technology, Haifa, Israel. 1984-

1990 he was a scientist with the Control Systems Section, El-Op Electro-Optics Industries Ltd, Rehovot, Israel. From 1989 he is with the Faculty of Agricultural Engineering, Technion, currently holding the position of Associate Professor.

Gutman was a visiting professor with Laboratoire d'Automatique, ENSIEG, Grenoble, France in 1995-96, and spent most summers since 1990 as a visiting professor at the Division of Optimization and Systems Theory, Department of Mathematics, Royal Institute of Technology, Stockholm, Sweden.

His research interests include robust and adaptive control, control of complex non-linear systems, computer aided design, off-road vehicle control and other control applications in agriculture, such as greenhouse control, and water supply systems control.

PLENARY TALK

SOME PECULIARITIES OF LOAD SHARING CONTROL

Eduard Eitelberg

NOY Business, 58 Baines Road, Durban 4001, South Africa
e-mail: controle@pixie.udw.ac.za

Abstract: In the recently published book, "Load Sharing Control" (Eitelberg, 1999), a frequency domain, loop-by-loop load sharing control system design methodology was developed and demonstrated with engineering examples. A number of new concepts were introduced in order to characterise some peculiarities that are not relevant in single-loop control systems, or have been overlooked in the general multivariable control system theory. Some of these concepts and peculiarities will be elaborated during this presentation.

Keywords: load sharing, cross sensitivity, stability, floating supply.

1. INTRODUCCION-THE CONCEP OF LOAD SHARING

In many engineering and in most economic systems, the burden of producing material, energy, goods (or signals in general) to satisfy some demand is shared between two or more distinct sources with limited supply capabilities (plants, suppliers, controllers, ...) — these sources share the load. In fact, all systems, where at least one output depends on at least two inputs, are load sharing.

Figure 1 defines the basic additive load sharing structure with N supply plants P_i , the associated supply and manipulated variables y_{si} and u_i , a common plant A , a common output y and a common disturbance d — the load. Disturbance may be added after the 'accumulator' A , without affecting the general validity of the presented results.

Some prominent load sharing examples are:

- process steam supply by multiple boilers to a common header with y signifying the header pressure;

- boiler feed-water pumps in parallel and in series with y signifying the total feed-rate;
- electric power supply grid with multiple power stations with y signifying the grid frequency;
- competitive markets with multiple suppliers for substitutable goods or services with y signifying the price.

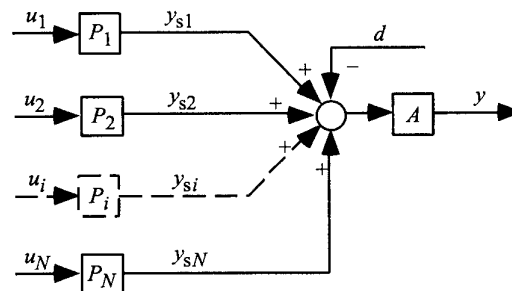


Figure 1: The basic load sharing system model.

In my book "Load Sharing Control", fundamental properties of load sharing control systems are investigated and procedures for designing independent and co-ordinated control systems are derived

constructively and demonstrated. It is shown there that systems with multiple feedback loops often (unintentionally) contain load sharing structures of significance to the designer. The load sharing properties and abilities of some new and some well-known industrial multi-loop and multivariable feedback control structures are analysed in this book.

2. CONTROL OF LOAD SHARING SYSTEM

The **primary control problem** is to control the common output y via the supply plants P_i . The same load d can be balanced by an infinite number of combinations of the individual supplies y_{si} . In real systems, there are generally very strong technical, economic and political reasons to prefer certain combinations over others. Therefore, maintaining some predetermined distribution of the load between individual supply plants is the **secondary control problem**. In special cases, however, control of one of the individual supplies y_{si} may be the most important task.

One could attempt to counteract the influence of load variation on y by feed-forward only. Despite the undeniable usefulness of load feed-forward, the practical difficulties of measuring the total system disturbance/load accurately and the uncertainties in the supply plants P_s make it seldom sufficient on its own. Hence, with or without feed-forward, a feedback control system from y to at least some of the individual u_i has to be designed.

There are N feedback signal transfers to define — from y to each u_i . In addition, the system can have N independent reference signals r_i for each independent supply plant. Figure 2 shows one possible implementation of these $2N$ design degrees of freedom.

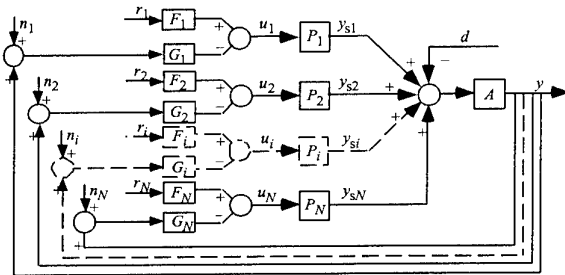


Figure 2: Independent load sharing control system: with common load d and output y ; and N individual supplies y_{si} , supply plant inputs u_i , supply references r_i , and feedback measurement or transmission noises/errors n_i .

An independent implementation of load sharing control is an attractive option, especially when individual supply plants P_i are in geographically distant locations. Power plant control for grid frequency stabilisation is implemented in many plants individually, see Knowles (1990). Sometimes individual supply plants are supplied with built-in load control instrumentation, such as the small electrode boilers that are used in the textile industry, industrial refrigerant compressors and others. These 'packaged deal' supply plants are designed to work well when carrying a specified load range alone. They are sometimes implicitly expected to work just as well or better when sharing a load — they might, but not without additional control system design effort.

It is convenient to introduce the individual supply loop transfer function as

$$L_i(s) = A(s)P_i(s)G_i(s) \quad (1)$$

L_i represents the feedback loop around the supply plant P_i when all other supply plants P_j are 'on manual' — all $G_j = 0$ for $j \neq i$. This is not necessarily the same as having all the other plants physically disconnected from the load, because that could significantly modify the accumulator A — for example, the steam volume or the rotating inertia. Now, the load regulation loop transfer function around the accumulator is simply

$$L(s) = \sum_{i=1}^N L_i(s) = A(s) \sum_{i=1}^N P_i(s)G_i(s) \quad (2)$$

The common output in Figure 2, is given by

$$Y = -\frac{A}{1+L}D + \frac{\sum_{i=1}^N AP_iF_iR_i}{1+L} - \frac{\sum_{i=1}^N L_iN_i}{1+L} \quad (3)$$

A detailed expression for individual supply outputs, in Figure 2, is given by

$$Y_{si} = \frac{L_i}{1+L}D + \frac{A^{-1}}{1+L} \left[L_i \frac{F_i}{G_i} R_i + \sum_{j=1}^N L_j L_i \left(\frac{F_j}{G_j} R_j - \frac{F_i}{G_j} R_j \right) \right] - \frac{A^{-1}}{1+L} \left[L_i N_i + \sum_{j=1}^N L_j L_i (N_i - N_j) \right] \quad (4)$$

The pre-eminence of the load regulation loop L is evident in the first right-hand term of eq. (3). In order to eliminate the effect of the load D on the system

output Y a high-gain loop L is needed. As a minimum, in order to justify the introduction of feedback, the design must achieve $|L(j\omega)| \gg 1$ in some (usually low) frequency range. This technical expression of the previously mentioned *primary control problem* will remain in the focus for the rest of this presentation.

A high gain L can only be achieved by implementing some of the individual supply loops L_i with high gain in the required frequency range — see eq. (2). As a first rough idea, all load sharing supply loops must have a gain in the order of $|L|$. This is evidenced by the first right-hand term of eq. (4). The supplies with $|L_i(j\omega)| \ll |L(j\omega)|$ do not participate in the load sharing at the corresponding frequency ω — as if they were 'on manual'.

This discussion brings us to the first peculiarity of Load Sharing Control.

Cross sensitivity:

Pair-wise discrepancies between feedback signal errors $(N_i - N_j)$ and mismatches between the filtered references $((F_i/G_i)R_i - (F_j/G_j)R_j)$ — see eq. (4) — are amplified by the 'supply distribution cross sensitivities' $(L_i L_j)/(A(1 + L))$ in the individual supplies Y_{si} . If both loops number i and j are high-gain supply regulating loops then the cross sensitivity between them has a quadratic numerator $|L_i L_j|$ that dominates the denominator.

Independent load sharing control systems are generally unsuitable for high gain control due to potentially infinite supply distribution cross sensitivities. The supply outputs in loops with high gain in the independent controllers G_i or plants P_i are hugely sensitive to differences in independent measurement errors and output references — the supplies will saturate easily and thus not be party to controlled load sharing.

The electrical power supply grid frequency is essentially controlled independently by a number of power plants by feeding the difference between an independent frequency reference and the independently measured grid frequency through a generally low-gain proportional controller to the turbine governor valve, see Knowles (1990). It should be noted, that the grid frequency control loop for an entire area, or country, does have high gain in the single central controller (Glover and Sarma, 1989).

Cascaded control systems contain two or more loops around some common plant. Hence one needs to be concerned about the cross sensitivity and some other

load sharing peculiarities. Cascaded control system design is handled quite thoroughly in my book.

Further, it is shown in my book that MIMO control systems can become inoperable due to large cross sensitivity — this is the case when the controlled plant is strongly interacting in the sense of Bristol's relative gain (Bristol, 1966). In 1998/1999, I was involved in an automotive component production scheduling and productivity improvement project. Fundamental market changes had been followed by a drop in the achievable production rates to somewhere between 50 and 70%. This is a very interesting story but must be left for another occasion. Besides a number of significant middle and top managerial deficiencies (in my very carefully considered opinion) there was an interesting technical problem with one of the manufacturing bottlenecks' — an aluminium brazing furnace. The original multivariable control system contained temperature control loops that had high cross sensitivity from temperature sensors to individual heaters. My analysis indicated that small temperature measurement errors led to such dramatically uneven heater power distribution that local thermal safety switches tripped the furnace. Management was very sensitive to the resulting loss of production and had suspected sabotage! The problem and its solution are described in my book and have been published separately (Eitelberg, 1999a). In essence, I simplified the control system structure and eliminated the high cross sensitivity. The general idea is as follows.

An alternative implementation of the $2N$ design degrees of freedom is shown in Figure 3. For convenience of designing and operating the whole system and in view of the presence of a co-ordinating controller, a common master reference is added — it does not add another degree of freedom for control.

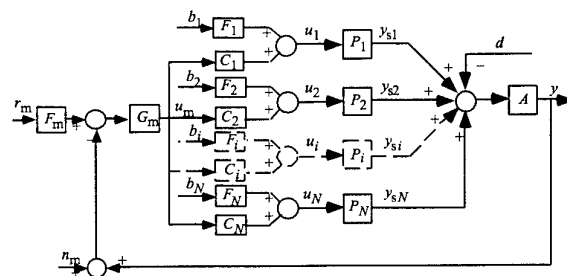


Figure 3: Co-ordinated load sharing control system: with common load d , output y , master sensor/transmission noise n_m and master reference r_m ; as well as N individual supplies y_{si} , supply plant inputs u_i , and supply references/biases b_i .

The feedback control co-ordination is achieved by using a common master controller G_m . The possibly dynamic feedback blocks C_i distribute the feedback control effort between the individual supply plants P_i . It is assumed that the gains of all (except possibly one) $C_i P_i$ are sufficiently low. The accumulator A may have high gain, but this does not help in load disturbance rejection. Any necessary high gain for load regulation is implemented in the master controller G_m . Because of the availability of the master reference R_m , the gains of all (except possibly one) F_i (feeding into closed loops) can and should be kept low.

Although the independent and co-ordinated control systems are formally equivalent for the purpose of the combined supply control in the linear regime with respect to the common output y , the co-ordinated control structure has no such cross sensitivity problem with high gain feedback as was the case in the independent control structure, because the high gain is provided by the common equipment in the load control loop. If necessary, the plant gains can be kept low with local supply regulating feedback loops around the individual plants.

Now I would like to turn the attention to peculiarities that help to understand the design of load sharing systems. In this context, there is no difference between independent and co-ordinated load sharing control structures. Fifteen years ago I heard Professor Horowitz stressing the difference between design and implementation and I agree. For example, a good design can be badly implemented — like in an independent structure with high cross sensitivity — but good implementation of a bad design makes no useful sense.

3. CONTRIBUTION OF A SUPPLY PLANT TO GLOBAL PERFORMANCE

Important design insights are gained by defining the feedback loop transfer function around an individual supply plant P_i under the condition that all other loops are closed:

$$L_{si} = \frac{L_i}{1 + L_{-i}} \quad \text{with} \quad L_{-i} = L - L_i = \sum_{\substack{j=1 \\ j \neq i}}^N L_j \quad (5)$$

L_{si} is important for determining the conditional stability and limit cycling conditions for the plant P_i , but it has other uses as well. L_{si} is called the **conditional supply loop transfer function**, as opposed

to the individual supply loop transfer function L_i that assumed all other loops to be open. L_{-i} is the load control loop transfer function when P_i is 'on manual'.

By elementary substitution, one can show that

$$(1 + L) = (1 + L_{-i})(1 + L_{si}) \quad (6)$$

All zeros of $(1 + L)$, that are not zeros of $(1 + L_{-i})$, must be zeros of $(1 + L_{si})$. A zero of $(1 + L) = (1 + L_{-i}) + L_i$ can be a zero of $(1 + L_{-i})$ if and only if, at this zero, $L_i = 0$ as well. This permits us to judge the stability of the entire load control system from the design of the individual supply control loop.

Stability:

Stability of the closed conditional supply loop transfer function L_{si} around any individual supply plant P_i guarantees stability of the overall load control closed loop L , if none of the right half-plane poles of $1/(1 + L_{-i})$ is cancelled by L_i in eq. (5).

The closed loop load regulation is characterised by the first right-hand term in eq. (3). It can be split into the contribution of L_{si} and all the other supply loops as

$$\frac{A}{1 + L} = \frac{A}{1 + L_{-i}} \frac{1}{1 + L_{si}} \quad (7)$$

Equation (4) expresses each supply plant's share in load regulation as $L_i/(1 + L)$, which can be expressed as

$$\frac{L_i}{1 + L} = \frac{L_{si}}{1 + L_{si}} \quad (8)$$

I should point out that eq. (8) does not indicate the share of supply number i in the total load, merely its share in the dynamic load regulation. The former depends on the freely prescribed load reference or bias too. Now the contribution of supply number i to the control system performance can be clearly stated.

Contribution to performance:

The individual supply plant P_i improves the load regulation by the factor $1/(1 + L_{si})$ as indicated by eq. (7) and carries $L_{si}/(1 + L_{si})$ of the total load variation as indicated by eq. (8).

4 SUPPLY AUGMENTATION WITH FAST PLANT

The following design scenario is quite common in load sharing systems. A set of $N-1$ plants are operating, but an additional plant is needed. If this need has arisen due to increased load, then the management should seriously consider buying more of the same — because of the familiarity with the plant and because of the relative ease of slotting an identical plant into the existing load sharing control system.

However, if this need has arisen due to inadequate speed of load regulation with the existing complement of the supply plants, then a faster (and probably more expensive) plant P_N must be considered. The existing control system speed is obviously limited by the non-minimum phase-lag characteristics of the existing plant. Note that a new and more expensive plant may actually have lower running costs and perhaps even lower total cost of ownership, or it may increase the overall profit of the business despite higher running and total costs! Some economic and safety related aspects are discussed in my book.

One can proceed conservatively (cautiously) and use the existing load control loop as is, with allowance for the possible but usually quite simple modification of the accumulator A . This way, taking the additional plant P_N out of the loop returns the total system to a previously designed known stable operational mode. The existing load control loop transfer function is L_{-N} and the new conditional supply loop $L_{sN} = L_N/(1 + L_{-N})$ will be designed so that the augmented system is stable. Equation (7) indicates the improvement in the load regulation and eq. (8) indicates the load share that the additional plant has to be able to balance with its own supply.

The algebraic simplicity of this design problem suggests a similar simplicity of the quantitative feedback design. I think I have moved significantly in this direction but much still remains to be done. Horowitz (1993) uses the very powerful concept of 'design perspective' to judge various properties and consequences of a successful design before the actual feedback system design. His main concern is satisfaction of low frequency specifications and judging the necessary gain cross-over frequency ω_{gc} , as well as other consequences. I prefer the 'reverse' perspective — from known gain cross-over frequencies to judging the best possible performance. This frequency domain perspective is solidly based on the understanding of the analytic function phase and magnitude integral relationships. Bode and then Horowitz must be credited with recognising the

tremendous importance of these abstract mathematical relationships for the design of feedback systems.

One of the most important of these relationships, in an approximate form, states that the average magnitude slope of a stable minimum phase-lag transfer function is $40 \text{ dB/decade}/(\pi \text{ radians}) = 0.222 \text{ dB/decade/degree}$ of phase angle. An extremely important consequence of this relationship is the elementary fundamental relationship between the achievable gain cross-over frequency ω_{gc} and the non-minimum phase-lag characteristics of the equipment in the loop. For example, in a practical design, $\omega_{gc} < 1/T_d$ where T_d is the dead-time (transport delay). In my book, other relationships are derived as well.

The corresponding design perspective is shown with the help of straight line approximations on the Bode magnitude plot in Figure 4.

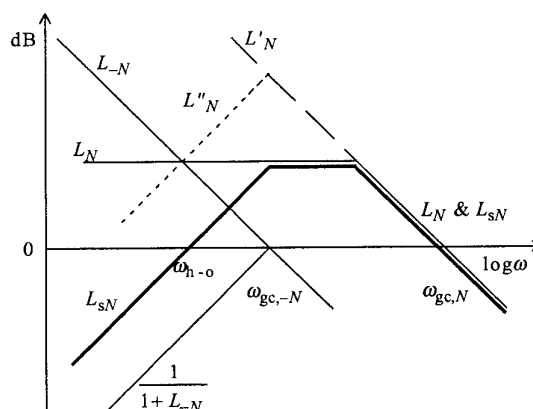


Figure 4: Design perspective when L_N is faster than L_{-N} .

Thus, if a phase margin of $\pi/4$ is required then the loop transfer function will 'roll-off' at about 30 dB/dec around the gain cross-over frequency ω_{gc} . If not only unconditional stability, but also 'unconditional stability margin' is required, then this roll-off cannot be exceeded for any frequency below ω_{gc} . In reality, the non-minimum phase-lag component will reduce the phase margin for the assumed roll-off, but the amount of reduction depends on the required gain margin (among other things).

If the accumulator A is an integrator (or integrating), then the above unconditional stability margin of $\pi/4$ may be an unaffordable luxury and a roll-off of closer to 40 dB/dec may be needed below the gain cross-over frequency ω_{gc} — to make L dominate A in $A/(1 + L)$ at low frequencies.

With these explanations, one can start by assuming that the slope of L_{-N} in Figure 4 is often in the vicinity

of -30 dB/dec with a phase angle of about $-3\pi/4 = -135^\circ$. The gain cross-over frequency of L_{-N} $\omega_{gc,-N}$ is determined by the non-minimum phase-lag of the existing plant. The new plant P_N has for example smaller dead-time and the corresponding loop L_N has a correspondingly higher maximum gain cross-over frequency $\omega_{gc,N}$, but the same slope of, say, -30 dB/dec.

If L_N has the same slope of -30 dB/dec for all $\omega < \omega_{gc,N}$, as indicated by L'_N , then all load regulation will be done in a stable manner by the totally dominating new plant. In this case, all the other supply plants are kept at a constant individual supply level either by their bias set-points or in the manual mode and the feedback design is trivial. However, the new plant must be sufficiently powerful to cover all load excursions.

If the new plant is not sufficiently powerful, one can still design a totally dominating loop transfer function around it. However, the fast regulation dynamics is enabled only when the new plant is not saturated. Either $L = L_{-N}$ or $L = L_N$. The individual supply biases affect the load level(s) at which the switch-over happens. Figure 5 illustrates this design. The usefulness of this option is doubtful.

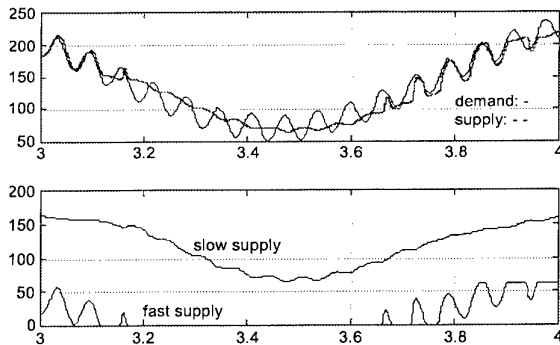


Figure 5: Illustration of load distribution between slow and dominating fast loop. The fast supply limits are 0 and 60. The slow supply limits are 0 and 200, it is biased to 150.

The power and (especially the operating) cost of the new plant can be limited by requiring L_N to regulate only in the frequency range where L_{-N} cannot — around and above $\omega_{gc,-N}$. This is achieved by reducing the roll-off of L_N as indicated in Figure 4. Note that L_N does not have to be horizontal, it just has to cross L_{-N} at some '*hand-over*' frequency $\omega_{h-o} (< \omega_{gc,-N})$ to be determined by the designer) — Horowitz (1963, Chapter 8) uses the term 'transition frequency' in a similar design situation. The corresponding magnitude of the conditional supply loop $L_{sN} = L_N/(1 + L_{-N})$ is

indicated by the thick line in Figure 4. According to eq. (7), the load regulation is improved in the approximate frequency range of ω_{h-o} to $\omega_{gc,N}$.

The hand-over frequency ω_{h-o} must be significantly less than $\omega_{gc,-N}$ in order to avoid regulation gaps in the frequency range below $\omega_{gc,N}$, and in order that significant gain can be put into the new loop L_N . According to eq. (8), the new plant carries the entire dynamic load in the frequency range from ω_{h-o} to $\omega_{gc,N}$ and the old plant set follows load changes below ω_{h-o} — *slower than it would do without the new plant*. Therefore, the choice of the hand-over frequency ω_{h-o} is a matter of compromise.

If, around the hand-over frequency $\omega_{h-o} (< \omega_{gc,-N})$, the slopes of L_{-N} and L_N are -30 and 0 dB/dec respectively, then the slope of L_{sN} is $+30$ dB/dec. This yields a sufficiently small L_{sN} phase angle of 135° at ω_{h-o} (a low frequency phase margin of 45°). Sometimes, L_N is made zero at steady-state. This is so in the inner loop design of the plant modifying cascaded system by Horowitz (1993) and it happens automatically when the 'valve position control scheme' of Shinskey (1988) is inserted into a control loop. This requires positive slope of L_N at some low frequency. If this positive slope is designed around the hand-over frequency, such as indicated by L''_N in Figure 4, the overall system may become unstable. If, for example, the slope of L_N is 20 dB/dec, around $\omega_{h-o} (< \omega_{gc,-N})$, then the slope of the conditional L_{sN} is $+50$ dB/dec. This yields an L_{sN} phase angle of 225° at ω_{h-o} — and an **unstable system!**

The above conservative design process results in a Bode magnitude plot of the load control loop transfer function L that looks like a terraced mountain side. In a single loop system this would generally indicate under-design. Furthermore, perhaps more importantly, the 'corner' at ω_{h-o} introduces a slow mode at about this frequency in addition to the intended dominant closed loop fast mode at about $\omega_{gc,N}$. The general problem of slow modes in control systems with 'wiggling' loop transfer functions is analysed in my latest book (Eitelberg, 2000).

Although the slow supply redistribution mode at ω_{h-o} cannot be avoided in the supply plant outputs, its residual in the accumulator output can be reduced to zero by 'straightening out the terrace' in L . That means that the hand-over will have to take place along the line L'_N in Figure 4 and some low frequency portion of L_{-N} must become (significantly) steeper than the previously mentioned -30 dB/dec. If the hand-over frequency ω_{h-o} is sufficiently low the modified L_N

will be conditionally stable, otherwise it will be unstable without the new loop closed and *operating within its supply limits*. The main condition for overall stability is that L_N dominates L_{-N} by magnitude where the non-minimum phase-lag is significant in L_{-N} — then one should be able to design a stable L with the gain cross-over frequency $\omega_{gc,N}$ of L_N .

The advantage of increasing the hand-over frequency ω_{h-o} is in more small signal load regulation burden falling on the existing plants and correspondingly less on the new plant. Therefore, according to linear system theory, a less powerful and cheaper new plant needs to be purchased than in the case of the cautious design.

Achieving better small signal economy or performance with unstable (or conditionally stable) L_{-N} could (and very probably would) be a *Pyrrhic victory*! Even temporary saturation of the plant P_N by sufficiently large load deviations can lead to overall system limit cycling ('instability' of the linear system theory). In my opinion, this is the most amazing peculiarity of load sharing systems.

Avoid Pyrrhic victories:

Base your design of the conditional supply loop L_{sN} on an unstable (or conditionally stable) closed loop L_{-N} , only if you really know what you are doing (or if you have adequate insurance).

Be very circumspect when designing master controllers for combined plants with fixed load sharing structures — important information is in the individual loops.

Be very circumspect when tuning slow loops while fast loops are operating — impressive (small signal) linear performance can be achieved at the cost of potentially disastrous (large signal) operating problems.

I did not suspect the above stability problem during my development of the design procedures, it surprised me when I could not make one of my apparently good designs work, took some considerable effort to explain, and much more effort to overcome the obstacle without compromising the performance. Figure 7 gives an idea of what can be achieved with some non-trivial design effort.

I should point out that well-designed cascaded feedback loops inherently suffer from the 'Pyrrhic victory syndrome'. A solution seems to be in acquiring an inner loop sensor with sufficiently wide range. This is a question of implementation which goes beyond what I can explain here, but see Eitelberg (1999).

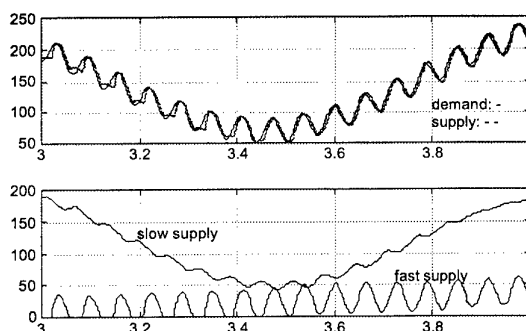


Figure 7: Illustration of load distribution between slow and floating fast supply. The fast supply limits are 0 and 60, it is biased to 20. The slow supply limits are 0 and 200. Same plant and load as in Figure 6, different control system structure.

5 CONCLUSION

Two of the arguably most interesting peculiarities of load sharing control are the *cross sensitivity* and the *Pyrrhic victory syndrome* (the conflict between small signal performance and plant operability). Both concerns are just as relevant in general multivariable control systems.

REFERENCES

- Bristol, E. H. (1966). On a new measure of interaction for multivariable process control. *IEEE Trans. Autom. Control*, AC-11, pp. 133–134.
- Glover, J. D. and Sarma, M. (1989). *Power System Analysis and Design*. Boston: PWS-KENT.
- Eitelberg, Ed. (1999). *Load Sharing Control*. Durban: NOYB Press, ISBN 0-620-23537-3.
- Eitelberg, Ed. (1999a). Load sharing in a multivariable temperature control system. *Control Engineering Practice*, Vol. 7, No. 11, pp. 1369–1377.
- Eitelberg, Ed. (2000). *Control Engineering Course Notes*. Durban: NOYB Press, ISBN 0-620-26359.
- Horowitz, I. (1963). *Synthesis of Feedback Systems*. Academic Press.
- Horowitz, I. (1993). *Quantitative Feedback Design Theory (QFT)*. Boulder: QFT Publications.
- Knowles, J. B. (1990). *Simulation and Control of Electrical Power Stations*. New York: John Wiley.
- Shinskey, F. G. (1988). *Process Control Systems*. Third Edition, New York: McGraw-Hill.

PLENARY TALK

Control of the Aero-Electric Power Station – an exciting QFT application for the 21st century

Per-Olof Gutman¹, Eran Horesh, Rami Gueta, and Michael Borshevsky

Faculty of Agricultural Engineering
Technion – Israel Institute of Technology
Haifa 32000, Israel

¹Corresponding author. E-mail: peo@tx.technion.ac.il

Abstract: The Aero-Electric Power Station is the ultimate solar power station, utilizing the dry, hot air of Earth's desert zones. By spraying water at the top of e.g. a 1200 m tall chimney with a diameter of 400 m, the air is cooled by evaporation and flows downwards through turbines at the bottom, generating 380 MW of net electric power. The Aero-Electric Power Station is still on the planning stage, and this paper belongs to a long series of feasibility studies.

The current “truth” model of the Aero-Electric Power Station is a one-dimensional computational partial differential equation model, having the air density, the air velocity, the temperature, the humidity of the air, and the mass of the evaporating droplets as state variables, combined with a turbine model whose state variables are the air velocity through the turbine and the rotor angular velocity.

The external weather conditions, defined as the air pressures, temperatures, and humidity at the top and bottom of the tower, determines the optimal operating point, i.e. the optimal water spray flow and turbine velocity that give the largest net power. The gross power produced by the turbine is partly delivered to the grid that is assumed to accept all it gets, and partly to pump sea water to the lower water reservoir at the bottom of the tower, and from the lower reservoir to the upper reservoir at the top. The reservoirs make it possible to use the pumping power as a control input in addition to the spray flow rate.

For each operating condition it is possible to approximately model the Aero-Electric Power Station plant as an uncertain unstable irrational transfer function, with the deviations from the nominals of the delivered turbine power and spray flow as control inputs, and the deviation from the nominal of the rotor velocity as the output. Changes of external humidity and temperatures are typically very slow with diurnal and slower variations, and hence these changes can be taken into account by slowly changing the operating condition. The same holds with respect to the slowly varying mean external air pressures. Wind changes, however, will cause significant disturbances in the external air pressures at the top and bottom of the tower in the frequency range 0.002 – 0.2 Hz. Therefore deviations from the nominals of the external top and bottom air pressures are included as disturbances in the model for regulation, whereby the regulator is to be designed to keep the rotor velocity constant at its nominal value. Thus the plant model has two disturbances (external air pressures at top and bottom), two control variables (turbine power, and spray flow), and one output (rotor velocity), without a cascaded structure. Hence this problem is a paramount case for robust *load sharing* control.

It turns out the set of possible operating conditions impose such a large uncertainty in the transfer function model that it is impossible to solve the regulation problem with one linear feedback regulator. The set of operating conditions is thus divided into overlapping subsets. For each subset a robust linear feedback regulator is designed by QFT, in such a way that the load of regulation is shared between the two control inputs. Gain scheduling should then be implemented to follow the slowly changing operating condition from subset to subset.

In this paper the load sharing QFT design is demonstrated for one subset of operating conditions, with closed loop simulations using the “truth” model. Problems that remain to be solved include, *inter alia*, the design of the gain scheduling algorithm, the use of feed-forward from disturbances, and the development of a multi-turbine three dimensional “truth” model and the solution of the subsequent MIMO design problem.

1. Introduction

The Aero-Electric Power Station is the ultimate solar power station, utilizing the dry, hot air of Earth's desert zones. By spraying water at the top of e.g. a 1200 m tall chimney with a diameter of 400 m, the air is cooled by evaporation and flows downwards through turbines at the bottom, generating 380 MW of net electric power. An artist's view of an Aero-Electric Power Station is found in Figure 1. The Aero-Electric Power Station is still on the planning stage, and this paper belongs to a long series of feasibility studies. An overview of the principles and main design issues is found in e.g. Gueta (19993), Zaslavsky (1997) and Zaslavski *et al.* (1999).

One of the major operational problems of the Aero-Electric Power Station is to avoid so

called salt spray. The water sprayed at the top of the tower will of course be salt ocean water, in order not to waste costly and scarce fresh water. If the droplets evaporate completely, powdered salt will pass through the turbines and potentially harm the surroundings. Studies have shown that at optimal operation, the amount and size of the droplets should be such that the evaporation increases the salt concentration in the drops from 4% to about 20%. Then the remaining salty drops will be collected outside the turbines, and led back into the ocean. As an additional benefit, the humid outlet air will in part dew irrigate the surrounding areas. It is clear that to avoid salt spray, efficient feedback control might be of importance. The present study does not deal with the salt spray avoidance control problem directly, but with maintaining the operation near optimum.

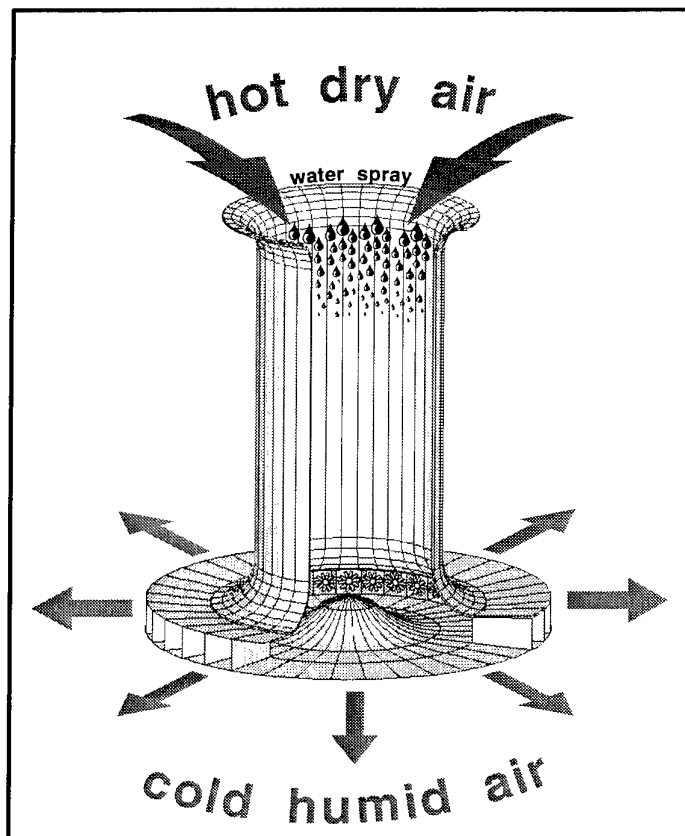


Figure 1. An artist's view of the Aero-Electric Power Station. Note that this view is inexact since the drops will not evaporate completely, but exit through the turbines to be collected outside.

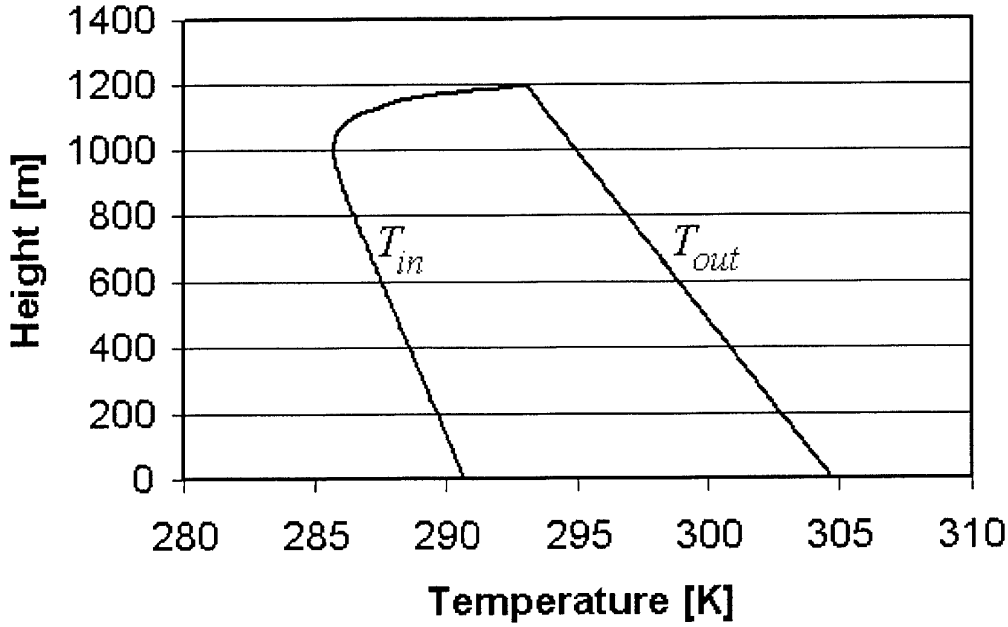


Figure 2. The air temperature inside, T_{in} , and outside, T_{out} , the tower vs. altitude, when water droplets of diameter $150 \mu\text{m}$ are sprayed at the top of the tower, in a quantity sufficient to saturate the air with vapor.

The thermodynamic principle of the Aero-Electric Power Station is the different adiabatic heating of the humid and cool air inside the tower and the dry and hot air outside the tower, as displayed in Figure 2. The cool and humid air inside the tower is heavier than the outside air and flows downwards. The created pressure difference between the inside and outside air at the bottom of the tower drives the turbines. The potential gross energy due to the cooling, E_c [J/m³] is given by

$$E_c = \int_0^{H_c} (\rho_a(x) - \rho_{at}(x)) g dx \approx \rho_a g H_c \frac{\overline{T_{out}} - \overline{T_{in}}}{\overline{T_{in}}} \quad (1)$$

where ρ_a [kg/m³] is the density of the air inside the tower, ρ_{at} [kg/m³] is the density of the air in the atmosphere, g is the constant of gravity, H_c [m] is the total height of the tower, and T_{in} [K] and T_{out} [K] are the temperatures inside and outside the tower, respectively. Note that E_c is approximately proportional to the mean difference between T_{in} and T_{out} ,

$\overline{T_{out}} - \overline{T_{in}}$. $\overline{T_{in}}$ denotes the mean inside temperature. It is hence important to spray a sufficient quantity so that the air inside the tower is saturated with vapor and the temperature profile follows the wet adiabatic at all heights, as T_{in} in Figure 2. With an insufficient spray discharge, complete evaporation will take place at some height, and from that height and below the T_{in} profile will be parallel to the dry adiabatic of T_{out} in Figure 2, and hence $\overline{T_{out}} - \overline{T_{in}}$ will be less than maximal.

A slow initial cooling at the top of the tower will decrease the value of E_c in (1). It has been shown (Zaslavski *et al*, 1999) that for net power optimal operation, surplus spray discharge is necessary, in order to ensure fast evaporation and a fast drop in temperature at the top of the tower, see Figure 2. Consequently, water drops will exit the turbines together with the humid air. Ideally, infinitesimal droplets should be used. Available spraying equipment is capable to produce droplets with a diameter of $150 \mu\text{m}$. The optimal surplus discharge is such that the

size of the droplets will decrease to a diameter of about $87 \mu\text{m}$ at exit, thus also avoiding salt spray. As stated above the salt concentration in the droplets will increase from 4% to 20%, the latter figure also being the limit for efficient water vapor evaporation from the droplets at the bottom of the tower. Larger surplus spray

discharge will increase gross power production, since a large part of the kinetic energy of the remaining droplets can be retrieved in the turbines, but net power production will decrease due to the pumping losses.

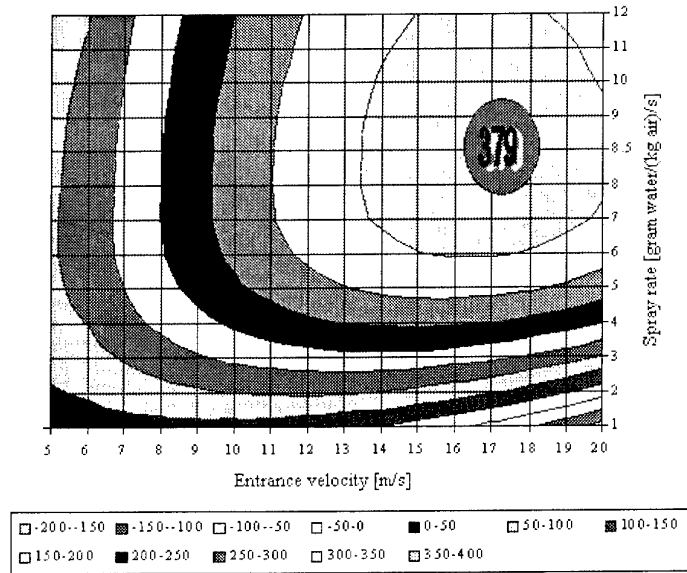


Figure 3. Potential net power [MW] as function of constant entrance air velocity, and constant spray rate, for a 1200 m high tower with diameter of 400 m, sprayed with droplets of $150 \mu\text{m}$ diameter. An ideal tower model with an ideal turbine is used for the computation. The weather conditions are $T_{out}(top,t)=293 \text{ [K]}$, $T_{out}(bottom,t)=304 \text{ [K]}$, atmospheric vapor density (humidity) = 20 [kg water/kg air], $P_{out}(top,t) = 93000 \text{ [Pa]}$, $P_{out}(bottom,t) = 106700 \text{ [Pa]}$, where t denotes time [s].

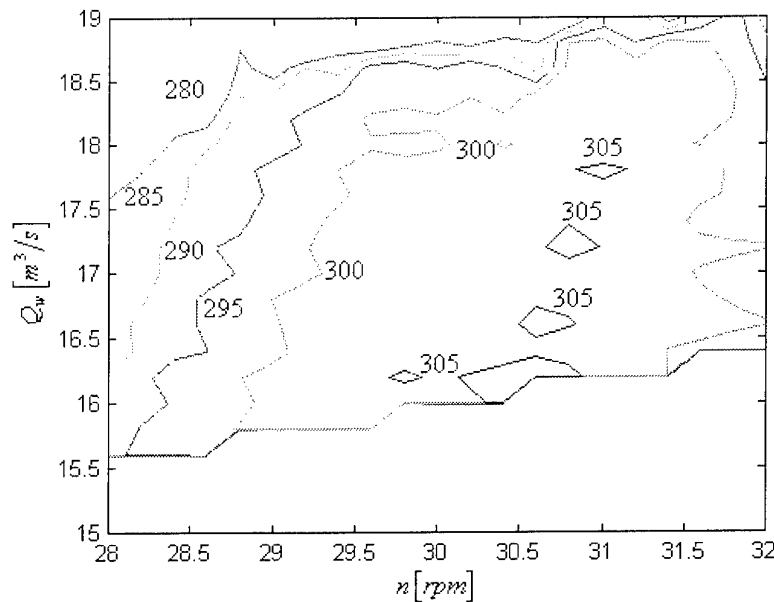


Figure 4. Net power [MW] as a function of constant rotor angular velocity and constant spray discharge, for the tower and conditions described in Figure 3. The computation is done with a static model that approximates the "truth" model in steady state with at most 15% error (Horesh, 2001), and the turbine described in section X.

The power production is proportional to the product of air mass flow, and the air pressure difference between inside and outside air at the bottom of the tower, (or, alternatively, head at the turbine). Both of these variables are functions of the entrance velocity of the air into the tower, v_{top} [m/s]. In Horesh (2001), on which this paper is based, it is shown that in steady state, v_{top} is a monotonous function of the turbine rotor angular velocity, n [rpm], for the studied weather conditions. It can be shown, (Zaslavsky *et al*, 1999) that there exists an optimal constant entrance velocity for which the net power production is maximized. Figure 3 shows the potential net power as a function of constant spray rate and constant v_{top} . The dependence of the net power on constant spray rate and constant rotor velocity is similar, see Figure 4.

The “truth” model of the Aero-Electric Power Station is a one-dimensional computational partial differential equation model, having the air density, the air velocity, the temperature, the humidity of the air, and the mass of the evaporating droplets as state variables, developed in Borshchevski (1998). The “truth” model took its current form in Horesh (2001) where Borshchevski’s model was combined with a variable rotor speed turbine model, Ekelund (1994), whose state variables are the air velocity through the turbine and the rotor

angular velocity. The model is described in Section 2.

The external weather conditions, defined as the air pressures, temperatures, and humidity at the top and bottom of the tower, determines the optimal operating point, i.e. the optimal water spray flow and turbine velocity that give the largest net power. The gross power produced by the turbine is partly delivered to the electric grid that is assumed to accept all it gets, and partly to pump sea water to the lower water reservoir at the bottom of the tower, and from the lower reservoir to the upper reservoir at the top. The reservoirs make it possible to use the pumping power as a control input in addition to the spray flow.

Figure 4 is generated by a static model from Horesh (2001) that approximates with at most 15% error the steady state of the current “truth” model (Section X) for the weather condition defined in the figure caption. The net power was computed for combinations of the spray rate Q_w [m³/s] and rotor velocity n [rpm] in a grid in Figure 4. The net power N_{net} [Watt] and the pumping power, N_p [Watt], follows from the computation. In this way *optimal operating points* are found also for other given weather conditions, yielding set points for all input and output variables.

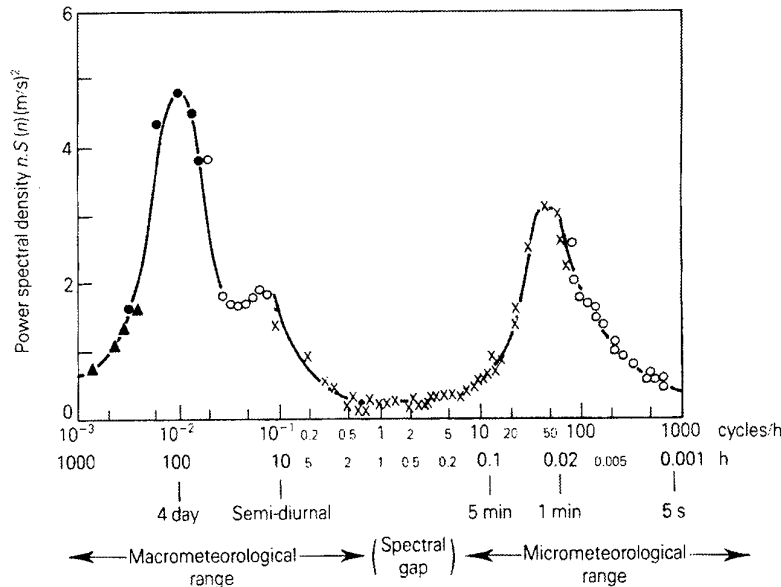


Figure 5. Wind spectrum, from Freris (1990)

For each operating condition it is possible to “locally” model the Aero-Electric Power Station plant as an uncertain unstable irrational transfer function, with the deviations from the nominals of the delivered turbine power (or equivalently rotor load torque) and spray flow as control inputs, and the deviation from the nominal of the rotor velocity as the output. Changes of external humidity and temperatures are typically very slow with diurnal and slower variations, and hence these changes can be taken into account by slowly changing the operating condition. The same holds with respect to the slowly varying mean external air pressures. Wind changes, however, will cause significant disturbances in the external air pressures at the top and bottom of the tower in the frequency range 0.002 – 0.2 Hz, see Figure 5. Therefore deviations from the nominals of the external top and bottom air pressures are included as disturbances in the model for regulation, whereby the regulator is to be designed to keep the rotor velocity constant at its nominal value. Thus the plant model has two disturbances (external air pressures at top and bottom), two control variables (turbine power, and spray flow), and one output (rotor velocity), without a cascaded structure. The local transfer function model is described in Section 3.

It turns out the set of possible operating conditions impose such a large uncertainty in the transfer function model that it is impossible to solve the regulation problem with one linear feedback regulator. The set of operating conditions is thus divided into overlapping subsets. For each subset a robust linear feedback regulator is designed by QFT, in such a way that the load of regulation is shared between the two control inputs, using the load

sharing ideas of Eitelberg (1999). Gain scheduling should then be implemented to follow the slowly changing operating condition from subset to subset.

In Section 4 the load sharing QFT design is demonstrated for one subset of operating conditions. The design was done with *Qsyn* – the *Toolbox for Robust Control Systems Design*, Gutman (1995). Some Closed loop simulations using the “truth” model are presented in Section 5. The results and their implications are discussed in Section 6. One of the conclusions is that QFT is eminently suited to solve this challenging control problem.

Problems that remain to be solved include, *inter alia*, the design of the gain scheduling algorithm, the use of feed-forward from disturbances, and the development of a multi-turbine three dimensional “truth” model and the solution of the subsequent MIMO design problem.

2. The one-dimensional “truth” model

In this section a short overview is given of the computational one-dimensional partial differential model of Borshchevski (1998) which is partially based on Gueta (1993). In this model, the tower is sliced into $h=20$ m tall slices (cells), and the time is discretized by $\theta=0.05$ seconds, such that a pressure wave that travels with the speed of about 340 m/s will hit each slice at least once in discrete time. Let j denote the time step, and i the cell number. The balance equations defining the operation inside the tower follow. The *air mass balance equation* (continuity equation) is

$$\rho_a(i,j) = \rho_a(i,j-1) + \frac{\theta}{h} (U(i,j-1) \rho_a(i-1,j-1) - U(i+1,j-1) \rho_a(i,j-1)) + \frac{\theta}{h} S_v(i,j) \quad (2)$$

where ρ_a [kg/m³] is the humid air density, U [m/s] is the air velocity, and S_v [kg/m²/s] is the vapor source. The *momentum balance equation* is

$$\begin{aligned} U(i,j) = & U(i,j-1) - \frac{\theta}{h} U(i,j-1) (U(i+1,j-1) - U(i,j-1)) - \\ & \frac{\theta}{h \rho_a(i,j-1)} (R(i-1,j) (\rho_a(i,j-1) T(i,j-1) - \rho_a(i-1,j) T(i-1,j))) + \\ & + \theta \left(g - f \frac{U(i,j-1)^2}{2H_c} \right) + \frac{\theta}{h} \frac{S_F(i,j)}{\rho_a(i,j-1)} \end{aligned} \quad (3)$$

where R [J/kg/K] is the gas constant for air, T [K] is the temperature of the air, g [m/s/s] is the constant of gravity, f is the friction coefficient, H_c [m] is the height of the tower, and S_F [N/m²] is the momentum source due to drag. The *energy balance equation* is

$$\begin{aligned} T(i, j) = & T(i, j-1) - \frac{\theta}{h} U(i+1, j-1) (T(i, j-1) - T(i-1, j)) - \\ & - \frac{\theta}{h} \frac{R(i, j-1)}{C_v(i, j-1)} T(i, j-1) (U(i+1, j-1) - U(i, j-1)) - \\ & - \frac{\theta}{h} \frac{S_Q(i, j)}{\rho_a(i, j-1) C_v(i, j-1)} + \frac{U(i, j-1)^3}{C_v(i, j-1)} \frac{f}{2H_c} \end{aligned} \quad (4)$$

where C_v [J/kg/K] is the specific heat of air at constant volume, and S_Q [J/m²/s] is the energy source caused by the interaction with the water drops. The *vapor balance equation* is

$$\omega_b(i, j) = \omega_b(i, j-1) + \frac{\theta}{h} (U(i, j-1) \omega_b(i-1, j) - U(i+1, j-1) \omega_b(i, j-1)) + \frac{\theta}{h} S_v(i, j) \quad (5)$$

where ω_b [kg water/m³ air] is the vapor density. The equations for the *evaporation of a drop*, E_d [kg/s], the *mass of a drop*, m_d [kg], the *drop diameter*, d_d [m], and the *velocity of a drop*, U_d [m/s], are

$$\left\{ \begin{aligned} E_d(i, j) &= -\rho_a(i, j) \sigma \pi D_a d_d(i, j) (\omega_a(i, j) - \omega_b(i, j)) \\ \frac{dm_d}{dt} &= E_d(i, j) \\ d_d &= \sqrt[3]{\frac{6m_d}{\pi \rho_d}} \\ U_d(i, j) &= U(i, j) + \frac{g \rho_d d_d(i, j)}{18 \mu_a (1 + 0.15 R_e^{0.687})} \end{aligned} \right. \quad (6)$$

where σ is the Sherwood number, D_a is the diffusion coefficient, d_d [m] is the water drop diameter, ω_a [kg water/kg air] is the saturation humidity of the air, ρ_d [kg/m³] is the density of the drop, μ_a [kg/m/s] is the elasticity of the air, R_e is the Reynolds number, and ω_a [kg water/kg air] is the humidity of the air, computed from (5). The *vapor source* in (1) and (5) is given by

$$S_v(i, j) = -\frac{n_d(i, j)}{A_c} E_d(i, j) \quad (7)$$

where n_d is the number of drops in cell i at time j , and A_c [m²] is the cross section area of the tower.

The *momentum source due to drag* in (3) is given by

$$S_F = \frac{n_d}{A_c} g m_d \quad (8)$$

The indices i, j are dropped for convenience. The equation for the *energy source* caused by the interaction with the water drops is

$$\begin{cases} S_Q = \frac{n_d}{A_c} (\nu \cdot k_a \pi d_d (T_d - T) + LE_d) \\ \frac{dT_d}{dt} = \frac{1}{m_d C_{pd}} (\nu \cdot k_a \pi d_d (T_a - T_d) + LE_d) \end{cases} \quad (9)$$

where ν is the Nusselt number, k_a [J/(Ksm)] is the thermal conductivity of air, T_d [K] is the temperature of the drops, and L [J/kg] is the evaporation energy for water. C_{pd} [J/K/kg] = drop specific heat at constant pressure. The indices i, j are omitted.

The boundary conditions for the tower are governed by the following equations. The *humid air density at the top of the tower*, $\rho_a(0, t/0.05)$ [kg/m³] is given by

$$\rho_a(0, t/0.05) = \frac{P_{out}(top, t)}{RT_{out}(top, t)} \quad (10)$$

where $P_{out}(top, t)$ [Pa] is the outside atmospheric air pressure at the top of the tower, $T_{out}(top, t)$ [K] is the outside atmospheric temperature at the top of the tower, and, as mentioned above, R [J/kg/K] is the gas constant for air. The *air velocity at the bottom of the tower*, $v_{bot}(t) = U(61, t/0.05)$ [m/s] is given by

$$v_{bot}(t) = \frac{m\pi D^2 v_{tur}(t)}{4A_c} \quad (11)$$

$$\begin{cases} v_{pot} = \frac{25600(3200 \cdot n(t) \cdot p + 2\sqrt{-82944q^2n(t)^2 + 81q^2H_{pot} + 2500p^2H_{pot}q^2})}{81q^2 + 2500p^2} \cdot \frac{4}{\pi D^2} \\ H_{pot} = \frac{P_{in}(61, j) - P_{out}(61, j)}{g\rho_a(61, j)} \\ P_{in}(61, j) = \frac{\rho_a(61, j)}{RT(61, j)} \end{cases}$$

(13)

where m is the number of turbines, D [m] is the diameter of the turbine, and $v_{tur}(t)$ [m/s] is the velocity of the air through the turbines, given below by (12). $T_{out}(top, t)$ constitutes the boundary condition for (4), while the atmospheric vapor density equals $\omega_b(0, j)$ in (5). The initial water drop velocity at the top of the tower, $v_d(0, j)$, is neglected since it tends very quickly to the drop velocity in (6). The initial drop diameter, $d_{d0} = d_d(0, j)$ [m], is assumed to be constant in this study = 150 μ m, but could be used as a control variable. The initial mass of a drop follows from (6). The spray flow rate, $Q_w(t)$ [m³/s], is a control variable, from which the number of initial water drops, $n_d(0, j)$, follows from $d_d(0, j)$ and (6).

The turbine model is adapted from Ekelund (1994), and contains two differential equations. The differential equation for the *air velocity through the turbine*, $v_{tur}(t)$ [m/s], is

$$\dot{v}_{tur}(t) = \frac{C_p}{2L_T} (v_{pot}^2(t) - v_{tur}^2(t)) \quad (12)$$

where C_p is the efficiency of the turbine and diffuser system, given by a table (Krivchenko, 1994) L_T [m] is the length of the turbine, and $v_{pot}(t)$ [m/s] is the “potential” air velocity, given by

where $n(t)$ [rpm] is the rotor angular velocity, p and q are constant turbine parameters, H_{pot} [m] is the “potential” head, computed according to static head in Pnueli and Gutfinger (1992), $P_{in}(61,j) = P_{in}(\text{bottom}, t/0.05)$ [Pa] is the internal pressure at the bottom, $P_{out}(61,j) = P_{out}(\text{bottom}, t/0.05)$ [Pa] is the atmospheric pressure at the bottom, see the atmospheric model in Wallace and Hobbs (1977). $P_{in}(0,j) = P_{out}(\text{top}, t/0.05)$ is a boundary condition. $T(i,j)$ is given by (6), $T(0,j) = T_{out}(\text{top}, t/0.05)$ is the boundary condition for (6), and R [J/kg/K] is the gas constant for air. Note that it is via (13), (11) that the water spray enters as a control variable that influences the air velocity through the turbine in (12).

The differential equation for the *rotor angular velocity*, $n(t)$ [rpm], is

$$\dot{n}(t) = \frac{1}{J_T} \left(\frac{\pi \rho_a D^2 v_{bot}^3(t)}{8n(t)} C_p - \left(\frac{2\pi}{60} \right)^2 \frac{N_{th}(t)}{m \cdot n(t)} \right) \quad (14)$$

where J_T [kgm²] is the turbine moment of inertia, m is the number of turbines, and $N_{th}(t)$ [W] is the power delivered from the turbines. Note that

$$N_{th}(t) = N_{net}(t) + N_p(t), \quad (15)$$

where $N_{net}(t)$ [W] is the net power delivered to the grid, and $N_p(t)$ [W] is the pumping power. The pumping power needed to lift the water from the bottom of the tower to the sprayers is

$$N_p(t) = \frac{\rho_w g Q_w(t) (H_c + H_{loss})}{\eta_p} \quad (16)$$

where H_{loss} [m] is the loss of head in the water intake and in the sprayer, and η_p is the efficiency of the pumps. When optimizing the steady state operation, (16) is used. (16) prescribes that $N_p(t)$ cannot be a control variable independent of $Q_w(t)$. If there is water storage capacity at the bottom and top of the tower, $N_p(t)$ may however be used as an independent but limited control variable. In this paper it is assumed that for dynamic regulation, $Q_w(t)$ and $N_p(t)$ are independent,

and that the capacities of the storage tanks are sufficient.

3. The linear model around an optimal operating point.

With the tower-and-turbine model in Section 2, and a given constant weather it is possible to find the constant spray flow rate Q_w and rotor angular velocity n that maximizes the net production of electrical power, N_{net} .

To compute N_{net} for given Q_w and n , one may, e.g. solve the equations in Section 2 in steady state, i.e. letting all derivatives and differences with respect to time in each cell be zero. Another route is to simulate the model in Section 2 until steady state is reached which is however very time consuming. In Gueta (1993) a simple “ideal” model of the tower without turbines was assumed and the optimum was found with relative ease. Figure 3 is generated with the method of Gueta (1993). Horesh (2001) formulated a simplified algebraic steady state model based on the equations in Section 2, that was shown in few cases to give an optimum at most 15% off the the optimum found by simulating the equations in Section 2 to steady state. Figure 4 is generated with the use of the simplified model in Horesh (2001), combining equidistantly gridded values of Q_w and n . The local optima in Figure 4 are due to different values turbine efficiency as a function of Q_w and n .

One may notice Figure 4 that the optimum is not very sensitive to $Q_w \in [16, 18]$ m³/s for $n \approx 30.7$ rpm.

The results both in Figure 3 and Figure 4 indicate that insufficient spray flow (in Figure 4, $Q_w < 16$ m³/s) causes the net power to decrease sharply. In Figure 4 the decrease of turbine efficiency contributes to the sharp decrease in net power for insufficient spray flow. Surplus spray flow also decreases net power but in a less drastic way, since the potential energy of the water drops may be partly recovered. This fact is beneficial for avoiding salt spray.

In view of Figure 4, one possible way to control the aero-electric power station is to make use of an *extremum-seeking controller* (Sternby, 1979) whereby set points for Q_w and n are “probed” in the vicinity of the current set point, in order to track an optimum that is changing slowly due to the slowly changing weather conditions. Such a configuration will

require feedback control to keep Q_w and n at their respective set points. An extremum-seeking controller has to be designed wisely in order not to lose too much produced power during probing due to local optima and the sharp drop in net power due to insufficient spray flow.

In this paper another approach is taken. It is assumed that a pre-computed *operating table* prescribes the *operating points* for the spray flow rate, and turbine rotor angular velocity, Q_{w0} [m³/s] and n_0 [rpm] respectively, as a function of current weather, yielding the corresponding net optimal power, N_{net0} [W] and pumping power $N_{p,0}$. The task of the feedback controller is to keep Δn zero, where $\Delta n = n - n_0$, using $\Delta Q_w = Q_w - Q_{w0}$, and $\Delta N_{lh} = N_p - N_{p0}$, thereby, in view of (15), keeping the net power $N_{net} = N_{net0}$, in response to micro-meteorological wind induced pressure disturbances, whose spectrum is given in Figure 5. Such a scheme is feasible if the water storage tanks are sufficiently voluminous to accept temporary deviations from nominal levels until the operating points are adjusted

anew with the use of the operating table. In fact, the storage tank water levels may be used as indicators that new operating points are needed.

In this section the simplified linearized model around an operating point is presented. For the detailed development, see Horesh (2001). Section 5 contains the design of the feedback controller.

By linearizing the turbine equations (12)-(14) around the state operating point $[n_0 \ v_{tur0}]^T$, one gets a second order state space description with constant coefficients:

$$\begin{cases} \dot{x}(t) = Ax(t) + [B_1 \ B_2] w(t) \\ y(t) = Cx(t) \end{cases} \quad (17)$$

where $x(t) = [\Delta n(t) \ \Delta v_{tur}(t)]^T = [(n(t) - n_0) \ (v_{tur}(t) - v_{tur0})]^T$, $w(t) = [\Delta N_{lh}(t) \ \Delta H_{pot}(t)]^T = [(N_{lh}(t) - N_{lh0}) \ (H_{pot}(t) - H_{pot0})]^T = [(N_p(t) - N_{p0}) \ (H_{pot}(t) - H_{pot0})]^T$, since $N_{net} = N_{net0}$, $y(t) = \Delta n(t) = (n(t) - n_0)$,

$$A = \begin{bmatrix} -\left(\frac{60}{2\pi}\right)^2 \frac{\pi \rho_a D^2 C_p v_{tur0}^3}{8 J_T n_0^2} & \left(\frac{60}{2\pi}\right)^2 \frac{3\pi \rho_a D^2 C_p v_{tur0}^2}{8 J_T n_0} \\ \frac{v_{tur0} C_p}{L_T} \frac{\partial v_{pot}}{\partial n} \Big|_0 & -\frac{v_{tur0} C_p}{L_T} \end{bmatrix},$$

$$B = [B_1 \ B_2] = \begin{bmatrix} \left(\frac{60}{2\pi}\right) \frac{1}{J_T m n_0} & 0 \\ 0 & \frac{v_{tur0} C_p}{L_T} \frac{\partial v_{pot}}{\partial H_{pot}} \Big|_0 \end{bmatrix}, \text{ and } C = [0 \ 1].$$

From (17) the transfer function from w to y is easily computed,

$$\left\{ \begin{aligned} Y(s) &= [P_1 | P_2'] W(s) \\ P_1(s) &= \frac{s \left(\left(\frac{60}{2\pi} \right) \frac{1}{mJ_T n_0} \right) + \left(\frac{C_p v_{tur0}}{L_T} \left(\frac{60}{2\pi} \right) \frac{1}{mJ_T n_0} \right)}{s^2 + s \left(\left(\frac{60}{2\pi} \right)^2 \frac{\pi \rho_a D^2 C_p v_{tur0}^3}{8J_T n_0^2} + \frac{C_p v_{tur0}}{L_T} \right) + \left(\left(\frac{60}{2\pi} \right)^2 \frac{\pi \rho D^2 C_p^2 v_{tur0}^3}{8J_T L_T n_0} \left(\frac{v_{tur0}}{n_0} - 3 \frac{\partial v_{pot}}{\partial n} \Big|_0 \right) \right)} e^{-\tau_a s} \\ P_2'(s) &= \frac{\left(\frac{60}{2\pi} \right)^2 \frac{3\pi \rho_a D^2 C_p^2 v_{tur0}^3}{8J_T L_T n_0} \frac{\partial v_{pot}}{\partial H_{pot}} \Big|_0}{s^2 + s \left(\left(\frac{60}{2\pi} \right)^2 \frac{\pi \rho D^2 C_p v_{tur0}^3}{8J_T n_0^2} + \frac{C_p v_{tur0}}{L_T} \right) + \left(\left(\frac{60}{2\pi} \right)^2 \frac{\pi \rho_a D^2 C_p^2 v_{tur0}^3}{8J_T L_T n_0} \left(\frac{v_{tur0}}{n_0} - 3 \frac{\partial v_{pot}}{\partial n} \Big|_0 \right) \right)} \end{aligned} \right. \quad (18)$$

where the delay $e^{-\tau_a s}$ was inserted to reflect the dynamics of the turbine to load power changes. While $P_1(s)$ connects y with a physically manipulable control input, ΔN_h , the input into $P_2'(s)$ is the intermediate variable ΔH_{pot} . It is thus necessary to find the transfer function or frequency function from ΔQ_w to ΔH_{pot} , as well as the transfer functions from the assumed pressure disturbances at the top and the bottom, $\Delta P_{top}(t) = P_{out}(top, t) - P_{out0}(top, t)$, and $\Delta P_{bot}(t) = P_{out}(bottom, t) - P_{out0}(bottom, t)$, respectively, to ΔH_{pot} . In fact, ΔH_{pot} was chosen as a control input in (17) rather than e.g. Δv_{tur} or Δv_{bot} because this enables the decoupling between the tower and the turbine. Approximate expressions for these frequency functions were developed in Horesh (2001), and summarized here.

Assuming that the tower is filled with an ideal gas than undergoes in isentropic process, then the pressure changes $\Delta P(x, t)$ [Pa] around a

stationary point can be modeled with the wave equation,

$$\frac{\partial^2 \Delta P(x, t)}{\partial t^2} = c^2 \frac{\partial^2 \Delta P(x, t)}{\partial x^2} \quad (19)$$

where c [m/s] is the velocity of sound. Assume further that the boundary condition at the top (i.e. equal to the pressure disturbance at the top) is sinusoidal, with frequency ω [rad/s],

$$\Delta P_{top}(t) = \Delta P(0, t) = A_{mp} \sin(\omega t). \quad (20)$$

The turbine imposes the boundary condition

$$\frac{\partial \Delta P(H_c, t)}{\partial x} = 0. \quad (21)$$

Then (19)-(21) yield that

$$\Delta P(x, t) = A_{mp} \sin(\omega t) \left(\cos\left(\frac{\omega}{c} x\right) + tg \left(\frac{\omega}{c} H_c \right) \sin\left(\frac{\omega}{c} x\right) \right) \quad (22)$$

From (22) it is easy to find that the resonance frequency is $\omega_{res} = (\pi c)/(2H_c) \approx 0.445$ rad/s for $H_c=1200$ m. According to Figure 5,

the subset of the micrometeorological range in which the pressure disturbance has a significant contribution is about to 0.02

$\text{Hz}=0.126$ rad/s, and hence one may assume that $\omega < \omega_{\text{res}}$. Then, one has from (22) that

$$\Delta P(H_c, t) = \frac{A_{\text{top}} \sin(\omega t)}{\cos(\omega H_c/c)} = \frac{1}{\cos(\omega H_c/c)} \Delta P(0, t) \quad (23)$$

By the use of Bernoulli's equation (Pnueli and Gutfinger, 1992) on which also equation (13b) is based, one gets

$$\Delta H_{\text{pot}}(t) = \frac{1}{g \rho_a(H_c, t) \cos(\omega H_c/c)} \Delta P(0, t). \quad (24)$$

Equation (24) can be interpreted that a sinusoidal pressure disturbance of sufficiently low frequency is amplified with a frequency dependent gain. If the time dependent variable $\rho_a(H_c, t)$ is replaced by an uncertain constant $\hat{\rho}_a$ that covers the range of $\rho_a(H_c, t)$, then one gets the frequency function

$$\Delta H_{\text{pot}}(j\omega) = \frac{1}{g \hat{\rho}_a \cos(\omega L_D/c)} \Delta P_{\text{top}}(j\omega). \quad (25)$$

Note that for $\omega = \omega_{\text{res}}$ and its harmonics (25) has infinite gain. In the "truth" model, the gain is but very large. In a similar way, one finds

$$\Delta H_{\text{pot}}(j\omega) = \frac{1}{g \hat{\rho}_a \cos(\omega L_D/c)} \Delta P_{\text{bot}}(j\omega) \quad (26)$$

where L_D [m] is the length of the diffuser.

For the details of the development of the approximate transfer function from ΔQ_w to ΔH_{pot} , see Horeish (2001). It is based *inter alia* on an averaging procedure of the equations in Section 2. With reference to (4), (6), (9), the use of the approximation $\delta\omega_a \approx -C_{pa} \delta T / L$ where $\delta\omega_a$ [kg water/kg air] is the change in humidity of the air due to the temperature change δT [K], and C_{pa} [J/kg/K] is the

specific heat of air at constant pressure, one may obtain the following approximation for the *static* dependence of the temperature change ΔT [K] at the bottom of the tower as a result of a change of the spray flow ΔQ_w [m^3/s],

$$\Delta T = -\frac{d_{d0}^3 A_c \bar{U}^2}{6 Q_{w0}^2 \sigma D_a \bar{d}_d} \left(1 - \frac{1}{\gamma}\right) \frac{g}{C_{pa}} \Delta Q_w \quad (27)$$

where \bar{U} [m/s] is the average air velocity, \bar{d}_d [m] is the average drip diameter, and γ is the difference between the temperature gradient for humid and dry air, as in Figure 2. However evaporation is a dynamic process, see (6a) that may be approximated by a linear first order model and the droplets have a finite velocity, see (6d), which causes a delayed response. One may therefore turn (27) into a dynamic equation in the Laplace domain,

$$\Delta T(x, s) = \frac{-\frac{\bar{U}}{Q_{w0}} \left(1 - \frac{1}{\gamma}\right) \frac{g}{C_{pa}} e^{-\frac{x}{\bar{U}_d} s}}{s + \frac{1}{\tau_2}} \cdot \Delta Q_w(s) \quad (28)$$

$\Delta T(x, s)$ is the Laplace transform of the temperature change x m down the tower, $\tau_2 = (d_{d0}^3 A_c \bar{U}) / (6 Q_{w0} \sigma D_a \bar{d}_d)$ [s] is the time constant of the evaporation of the drops, cf. (6b), and x/\bar{U}_d [s] is the time delay of the droplets. With the help of Bernoulli's equation, (1) may be turned into an alternative formula for ΔH_{pot} ,

$$\Delta H_{\text{pot}} = \int_0^{H_c} \frac{-\Delta T(x)}{\bar{T}} dx \quad (29)$$

where $\bar{T} = \bar{T}_{\text{in}}$ [K] is the average temperature inside the tower, we get from (28), (29) after integration

$$\Delta H_{pot}(s) = \frac{1}{T} \cdot \frac{\frac{\bar{U}}{Q_{w0}} \left(1 - \frac{1}{\gamma}\right) \frac{g}{C_{pa}} \bar{U}_d}{\left(\frac{1}{\tau_2} + s\right)s} \left(1 - e^{-\frac{H_c s}{\bar{U}_d}}\right) e^{-\tau_b s} \Delta Q_w(s), \quad (30)$$

where also $\Delta Q_w(s)$ was replaced by $e^{-\tau_b s} \Delta Q_w(s)$ in order to represent in a simple way the dynamics of the spraying equipment, whereby $\Delta Q_w(t)$ should from now on be interpreted as the command to the spraying equipment. The model (18), (25), (26), (30) is now complete..

It can be shown that the plant parameter values for the studied aero-electric power station are such that one of the poles of $P_1(s)$ and $P_2(s)$ is unstable. Let the unstable pole be $-p_1$, and the stable pole $-p_2$. Let $-z_1$ be the zero of $P_1(s)$, k_1

the high frequency gain of $P_1(s)$, k_2 the high frequency gain of $P_2'(s)$, $k_p = k_2 / (g \hat{p}_a)$, and

$$k_Q = \frac{1}{T} \cdot \frac{\bar{U}}{Q_{w0}} \left(1 - \frac{1}{\gamma}\right) \frac{g}{C_{pa}} \bar{U}_d. \quad (31)$$

With this simplified notation, the block diagram of the plant model (18), (25), (26), (30), (31) is drawn in Figure 6, and its frequency function becomes, with $s = j\omega$,

$$\Delta n(s) = \begin{bmatrix} P_1(s) & P_2(s) \end{bmatrix} \begin{bmatrix} \Delta N_{th}(s) \\ \Delta Q_w(s) \end{bmatrix} + \begin{bmatrix} P_3(s) & P_4(s) \end{bmatrix} \begin{bmatrix} \Delta P_{top}(s) \\ \Delta P_{bot}(s) \end{bmatrix} \quad (32)$$

where

$$\begin{cases} P_1(s) = \frac{k_1(s+z_1)}{(s+p_1)(s+p_2)} e^{-\tau_b s} \\ P_2(s) = \frac{k_2}{(s+p_1)(s+p_2)} \cdot \frac{k_Q}{(s+1/\tau_2)s} \left(1 - e^{-\frac{H_c s}{\bar{U}_d}}\right) e^{-\tau_b s} \\ P_3(s) = \frac{k_p}{(s+p_1)(s+p_2) \cos((sH_c)/(jc))} \\ P_4(s) = \frac{k_p}{(s+p_1)(s+p_2) \cos((sL_D)/(jc))} \end{cases}$$

It should be pointed out that the model errors introduced by the approximations is partly "compensated" by letting the parameters have an extended uncertainty range with respect to the ensuing robust control systems design.

The set of all operating conditions is characterized by the following set of uncertain parameter ranges (nominal values are

underlined): $p_1 \in [-0.054, -0.015]$, $p_2 \in [0.33, 0.71]$, $z_1 \in [0.27, 0.53]$, $k_1 \in [2.4, 5.1] \cdot 10^{-11}$, $k_2 \in [0.006, 0.071]$, $k_Q \in [1.28, 21] \cdot 10^{-4}$, $\tau_a \in [0.09, 0.11]$, $\tau_2 \in [3.3, 50]$, $\tau_b \in [1.8, 2.2]$, $H_c = 1200$, $\bar{U}_d \in [9.5, 19]$, $k_p = k_2/12$, $L_D = 160$, and $c = 340$.

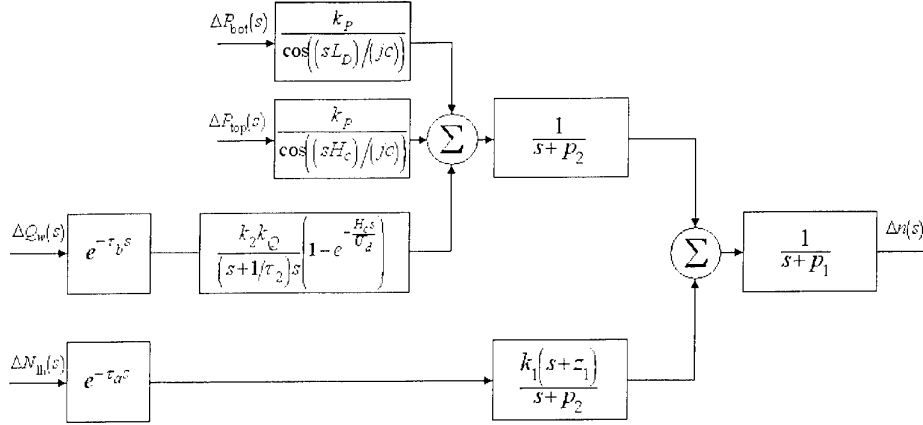


Figure 6. Block diagram of the plant model (18), (25), (26), (30), with the parameters defined in (31) and above.

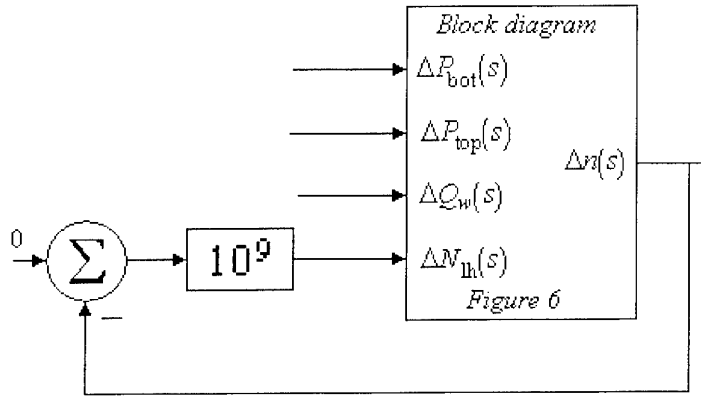


Figure 7. Block diagram of the initially closed loop system, stabilized by the proportional regulator $k = 10^9$ in the $\Delta N_{th}(t)$ loop. The plant block represents the block diagram in Figure 6.

4. Load sharing QFT design for regulation

The control systems should be designed such that for all operating points the following *specifications* be satisfied: *i*) the closed loop system must be asymptotically stable; *ii*) include an integrator such that $\Delta n(t) \rightarrow 0$ for step disturbances; *iii*) the gain of the output sensitivity function must be less than 2 for all frequencies; *iv*) $|\Delta n(j\omega)/\Delta P_{top}(j\omega)| < 0.001$ and $|\Delta n(j\omega)/\Delta P_{bot}(j\omega)| < 0.001$ for $\omega < 1$ rad/s, excluding a small frequency range around the resonance 0.445 rad/s; *v*) minimum use should be made of the control variable $\Delta N_{th}(t)$. Specification *iv*) implies that all disturbances in the micrometeorological range are damped, as well as disturbances near the first resonance frequency. Specification *v*) is meant to ensure that $\Delta N_{th}(t)$ will be operated within the capacity of minimal storage tanks.

It turns out the set of possible operating conditions impose such a large uncertainty in the transfer function model of Section 4 that it is impossible to solve the regulation problem with one linear feedback regulator. It is also even impossible to stabilize the closed loop system with ΔQ_w only, because of the combination of an unstable pole, significant delay, and uncertainty. On the other hand it is easy to understand with root locus arguments that it is possible to stabilize $k P_1(s)/(1 + k P_1(s))$ with a sufficiently large k provided τ_a is sufficiently small, i.e. *globally stabilize the closed loop system with a P-regulator* in the $\Delta N_{th}(t)$ loop. In our system $k = 10^9$ was sufficient. The initially closed loop is displayed in Figure 7. The compensated open loop, $k P_1(s)$, is displayed in a Nichols chart in Figure 8, together with the uncertainty templates for the

global set of operating conditions. It follows from Figure 8 that the sensitivity specification *iii* is satisfied. The still insufficient disturbance rejection is demonstrated in the Bode diagram in Figure 9 of $|\Delta n(j\omega)/\Delta P_{\text{top}}(j\omega)| = |P_3(j\omega)/(1+kP_1(j\omega))|$ for the closed loop configuration of Figure 7.

It should be noted that no attempt was made to make the $\Delta N_{\text{th}}(t)$ loop satisfy specifications

beyond stability and sensitivity, since, firstly, as mentioned above, this was found impossible for the full uncertainty set emanating from all operating points, and secondly, specification *v* prescribes that as much as possible of the feedback burden should fall on the ΔQ_w loop. It is however important that the system may be globally stabilized by a simple controller in the $\Delta N_{\text{th}}(t)$ loop, even if other control loops fail.

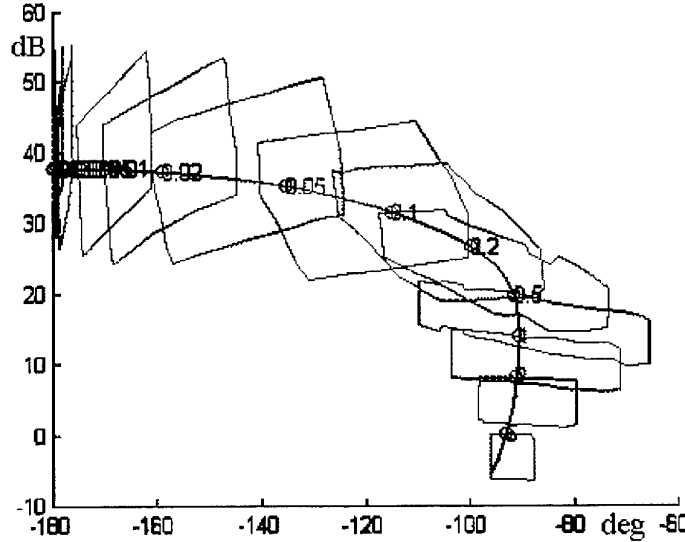


Figure 8. Templates of the open loop $kP_1(s)$ for the parameter combinations characterizing the complete set of operating conditions (full uncertainty set), in a Nichols chart. The nominal plant is marked with the template frequencies [rad/s].

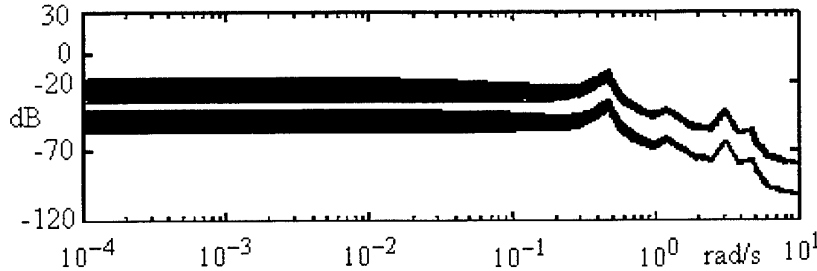


Figure 9. The disturbance transfer function $|\Delta n(j\omega)/\Delta P_{\text{top}}(j\omega)| = |P_3(j\omega)/(1+kP_1(j\omega))|$ for the closed loop configuration of Figure 7 in a Bode diagram. Due to finite numerical resolution, the resonance peak at 0.445 rad/s does not reach infinity. The plant cases cover the full uncertainty set.

Due to the failure to find one linear feedback regulator to solve the problem of regulation, the set of operating conditions is thus divided into overlapping subsets. For each subset a robust linear feedback regulator is designed by QFT, in such a way that the load of regulation is shared between the two control inputs, using the load sharing ideas of Eitelberg (1999). Gain scheduling should then be implemented

to follow the slowly changing operating condition from subset to subset, but this topic is not treated in this paper.

Here, we will demonstrate the design for one particular subset of operating conditions. It is defined by the following *shrunk* parameter intervals (nominal values are underlined): $p_1 \in [-0.042, -0.029]$, $p_2 \in [0.55, 0.60]$,

$z_1 \in [0.44, 0.46]$, $k_1 \in [2.77, 3.05] \cdot 10^{-9}$,
 $k_2 \in [0.020, 0.024]$, $k_Q \in [3.31, 4.85] \cdot 10^{-4}$,
 $\tau_a \in [0.09, 0.11]$, $\tau_2 \in [5.3, 11.9]$, $\tau_b \in [1.8, 2.2]$,
 $H_c = 1200$, $\bar{U}_d \in [9.5, 19]$, $k_p = k_2/12$,
 $L_D = 160$, and $c = 340$.

According to Eitelberg (1999) the “slowest” loop should be closed first, which in the present case is the loop whose control input is the water discharge ΔQ_w . Closing this loop first will also satisfy specification *v*. The open conditional water discharge supply plant is given by the transfer function from ΔQ_w to Δn in Figure 7,

$$G_d(s) = \frac{3 \cdot 10^{-2} \left(1 + \frac{s}{0.0003}\right) \left(1 + \frac{s}{0.002}\right) \left(1 + \frac{2 \cdot 0.6s}{0.02} + \frac{s^2}{0.02^2}\right) \left(1 + \frac{2 \cdot 0.7s}{0.009} + \frac{s^2}{0.009^2}\right)}{s \left(1 + \frac{s}{0.0007}\right) \left(1 + \frac{s}{1000}\right) \left(1 + \frac{s}{0.03}\right)^2 \left(1 + \frac{s}{0.0011}\right)^2 \left(1 + \frac{s}{0.01}\right)} \quad (34)$$

thus satisfying specification *ii*. See Figure 12 for a block diagram of the system. Figure 13 displays the Bode diagram of $|\Delta n(j\omega)/\Delta P_{\text{top}}(j\omega)| = |P_3(j\omega)/(1 + kP_1(j\omega) + G_d(j\omega)P_2(j\omega))|$ for the configuration in Figure 12. Clearly specification *iv* is not satisfied. Hence an

$$L_{s2}(s) = \frac{P_2(s)}{1 + kP_1(s)} \quad (33)$$

whose templates for the shrunk uncertainty are given in Figure 10. Due to the significant phase lag and time delay in $L_{s2}(s)$, it was found possible to satisfy only closed loop stability together with an 8 dB output sensitivity specification, rather than specification *iii*, see Figure 11. It was not possible to raise the bandwidth further. However, an integrator was included in the controller $G_d(s)$,

additional ΔN_{th} loop stronger than the previously designed P-regulator has to be designed, also to meet specification *iii*. The ΔN_{th} loop could also be made such that specification *iv* be satisfied in a “robust” way, and to increase the bandwidth in order to get a rapid disturbance response.

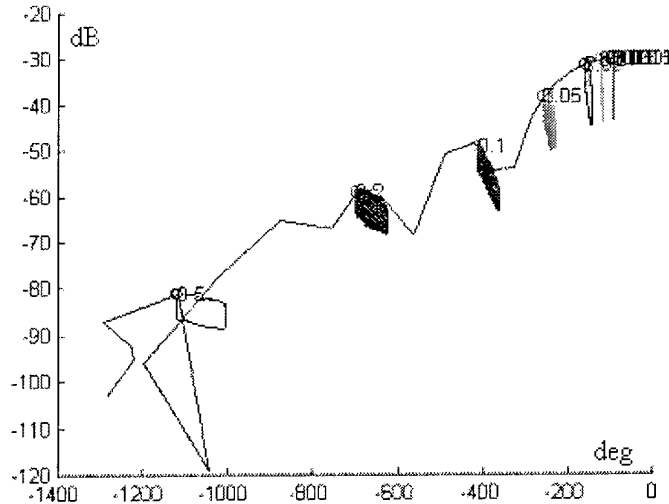


Figure 10. Templates for (33) for the shrunk uncertainty set, in a Nichols diagram. The nominal is parameterized by frequency, [rad/s].

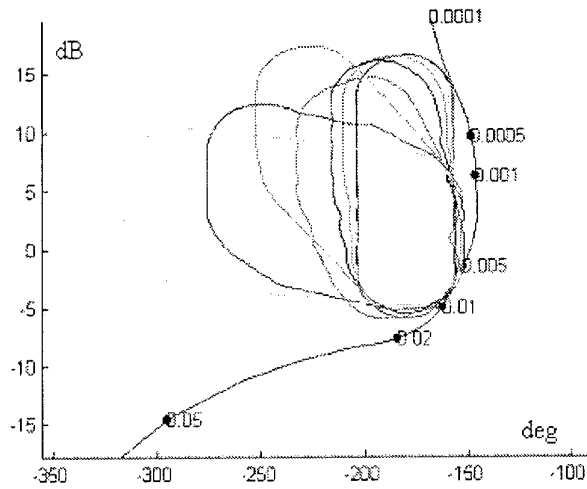


Figure 11. The nominal compensated open conditional water discharge supply loop $G_d(s)L_{s2}(s)$ from (33), (34), in a Nichols diagram, together with Horowitz bounds emanating from the closed loop output sensitivity specification, $|S| < 8\text{dB}$.

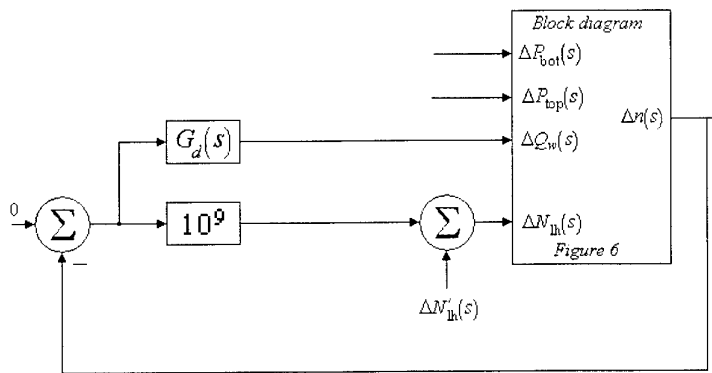


Figure 12. Block diagram of the system after the closure of the conditional water discharge supply loop with the controller $G_d(s)$ in (34). ΔN_h is the control input for the subsequent final control loop.

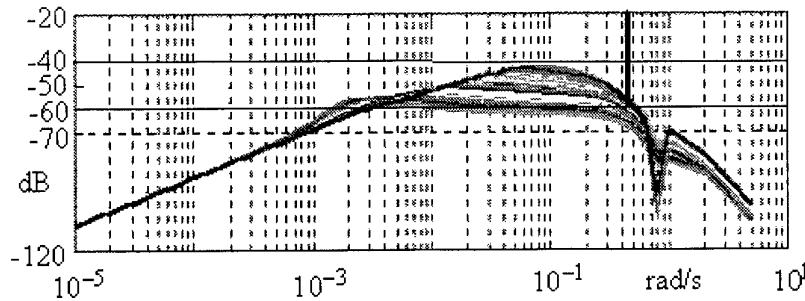


Figure 13. Bode diagram of $|\Delta n(j\omega)/\Delta P_{top}(j\omega)| = |P_3(j\omega)/(1 + kP_1(j\omega) + G_d(j\omega)P_2(j\omega))|$ which is the disturbance transfer function for the closed loop configuration of Figure 12. Due to finite numerical resolution, the resonance peak at 0.445 rad/s does not reach infinity. The plant cases cover the shrunk uncertainty set.

The open conditional supply loop for the design of the final ΔN_{ih} controller is given as the transfer function between $\Delta N'_{ih}$ and Δn in Figure 12,

$$L_{s3}(s) = \frac{P_1(s)}{1 + kP_1(s) + G_d(s)P_2(s)} \quad (35)$$

The templates of $L_{s3}(s)$ for the shrunken uncertainty set are displayed in Figure 14. In order to attenuate $|\Delta n(j\omega)/\Delta P_{top}(j\omega)|$ further in the frequency range $[0.0002, 0.03]$ rad/s, cf. Figure 13, the following disturbance rejection was introduced:

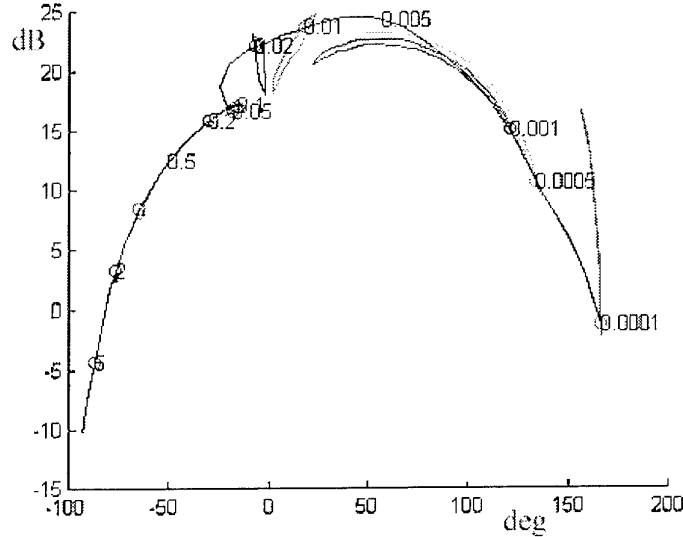


Figure 14. Templates for $10^9 L_{s3}(s)$, with $L_{s3}(s)$ defined in (35) for the shrunken uncertainty set, in a Nichols diagram. The nominal is parameterized by frequency, [rad/s]. Notice the size of the templates in comparison with Figure 8.

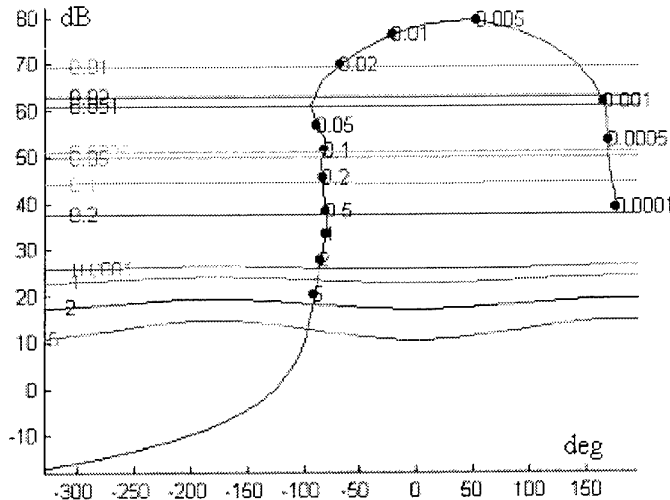


Figure 15. The nominal compensated open conditional pumping power supply loop $G_f(s)L_{s3}(s)$ from (35), (37), in a Nichols diagram, together with Horowitz bounds emanating from (36).

$$\left| \frac{\Delta n(s)}{\Delta P_{\text{top}}(s)} \right|_{\text{spec}} \leq \left| \frac{(s+2 \cdot 10^{-3})(s+5 \cdot 10^{-3})}{(s+2 \cdot 10^{-5})(s+5)} \right| \quad (36)$$

The nominal compensated open conditional pumping power supply loop $G_f(s)L_{s3}(s)$, together with the Horowitz bounds emanating from (36), with

$$G_f(s) = \frac{10^{13}(1.67s^2 + 0.5s + 0.0002)}{s^3 + 1000s^2 + 9s + 0.025}$$

(37)

is displayed in Figure 15. Comparing Figure 14 and Figure 15, it is clear that specification *iii* is satisfied. The block diagram of the final system is found in Figure 16. Figure 17 displays the Bode diagram of $|\Delta n(j\omega)/\Delta P_{\text{top}}(j\omega)| =$

$$\left| P_3(j\omega) / \left(1 + (k + G_f(j\omega))P_1(j\omega) + G_d(j\omega)P_2(j\omega) \right) \right|$$

for the configuration in Figure 12.

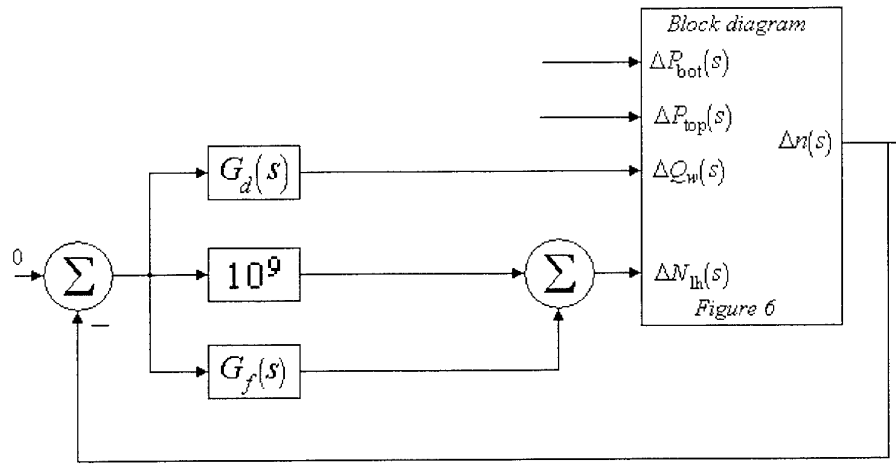


Figure 16. Block diagram of the final control system. $G_f(s)$ is given in (37), and $G_d(s)$ in (34).

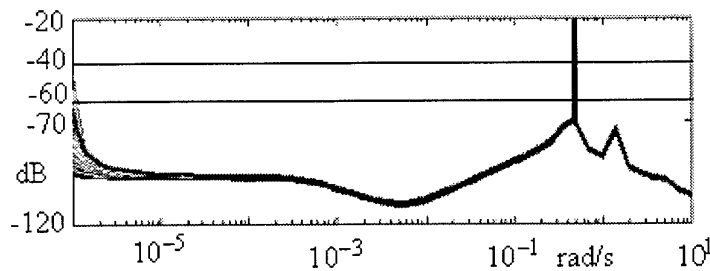


Figure 17. Bode diagram of the disturbance transfer function for the closed loop configuration of Figure 16, $|\Delta n(j\omega)/\Delta P_{\text{top}}(j\omega)| = \left| P_3(j\omega) / \left(1 + (k + G_f(j\omega))P_1(j\omega) + G_d(j\omega)P_2(j\omega) \right) \right|$. Due to finite numerical resolution, the resonance peak at 0.445 rad/s does not reach infinity. The plant cases cover the shrunk uncertainty set.

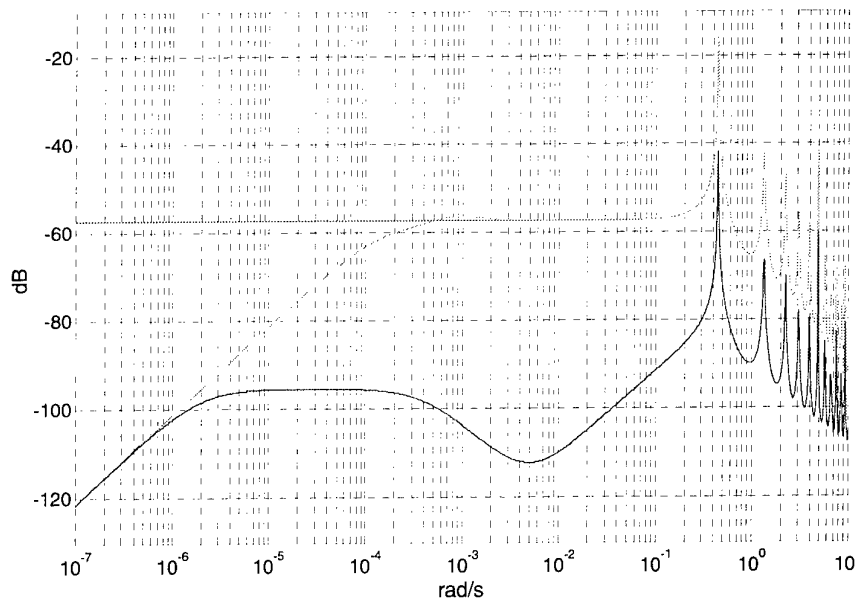


Figure 18. Bode diagram of the disturbance transfer functions $|\Delta n(j\omega)/\Delta P_{\text{top}}(j\omega)|$ from Figures 9, 13, and 17, for the nominal case of the shrunk uncertainty set.

5. Simulations.

The “truth” model of the Aero-Electric Power Station in Section 2 will not exhibit the infinite resonances seen in Figures 9, 13, 17, and 18, since internal damping and friction is not neglected. To check the control system, the pressure disturbance at the top was however defined at a frequency near the first resonance,

$$\Delta P_{\text{top}}(t) = 10 \cdot \sin(0.45t) \quad (38)$$

in a simulation where the final controller defined in Figure 16, and the plant was defined by the “truth” model in Section 2. The results in Figures 17 and 18 make us expect an attenuation of about -40 dB. Figures 19, 20, 21 display the time domain response of $n(t)$, and the control signals $\Delta N_h(t)$, and $Q_w(t)$, respectively. It is clearly seen in Figure 19 that $\Delta n(t)$ is attenuated to an amplitude of about 0.075 (around the nominal $n_0=34$ rpm) that is by -42 dB in comparison with (38).

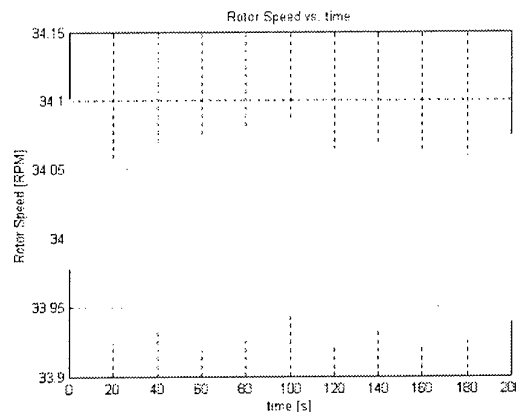


Figure 19. The simulated response of $n(t)$, as a result of a disturbance according to (38) in a simulation where the controllers of Figure 16 were integrated into the truth model of Section 2.

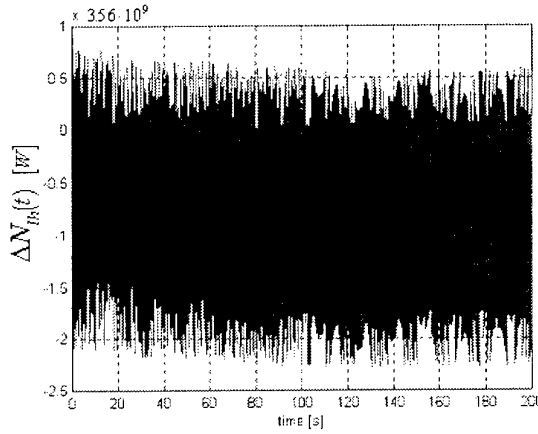


Figure 20. $\Delta N_{lh}(t)$ The simulated response of $\Delta N_{lh}(t)$, as a result of a disturbance according to (38) in a simulation where the controllers of Figure 16 were integrated into the truth model of Section 2. Note that $N_{lh} = (2\pi n/60)M$, where M [Nm] is the control torque exerted on the axis. With $n_0=34$ rpm, it holds that $3.56M=n$. Note in the figure the controller needs about 3 MW peak-peak for control purposes which is negligible in comparison to the produced net power.

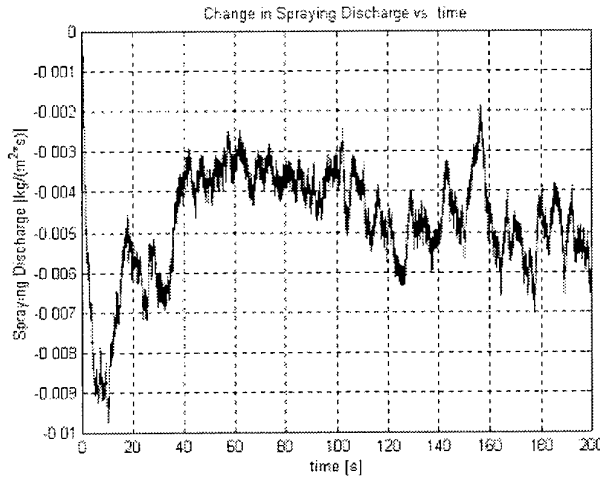


Figure 21. The simulated response of $\Delta Q_w(t)$, as a result of a disturbance according to (38) in a simulation where the controllers of Figure 16 were integrated into the truth model of Section 2.

6. Conclusions

The general conclusion is that it is possible to design a regulator for the Aero-Electric Power Station that satisfies stringent specifications, using QFT and load sharing, for an uncertainty set around a given operating point. Indeed one might perceive a certain over-design in this paper.

However, the design results implicitly demonstrate the trade-off between the size of uncertainty and achievable specifications. If the disturbance attenuation specifications are relaxed then the design problem would have

been solvable for a larger uncertainty set around the chosen nominal. With larger local uncertainty sets it will become easier to design the global regulator by gain scheduling among the local regulators. One way to gain schedule is to switch regulators when the operating point belongs to the intersection of two adjacent uncertainty sets, for which local controllers were designed. Such robust gain scheduling is impossible if robustness and uncertainty sets are not taken into account in the local regulator design stage.

Another interesting issue is the presence of the resonances at harmonic frequencies, see Figure Damping these is a problem similar to echo

cancellation in telecommunication systems or active vibration damping. In this paper no special measures were taken except strong attenuation, but one could contemplate e.g. comb filters or other measures.

It is expected that Aero-Electric Power Stations will contribute significantly to the needs of electrical power during the 21st century, particularly in desert areas where part of the power will be used to desalinate sea water. It is expected that their controllers will be designed using QFT.

7. References

- Borshchevski, Michael (1998), "One-dimensional model for the description of air flow and droplets in the Energy Tower", Internal report, Technion – Israel Institute of Technology, Haifa, Israel (in Hebrew).
- Ekelund, Tommy (1994), "Control of variable speed wind turbines in a broad range of wind speeds. Chalmers University of Technology, Göteborg, Sweden.
- Eitelberg, Eduard (1999), *Load Sharing Control*, NOYB press, Durban.
- Freris, Leon L. (1990), *Wind Energy Conversion Systems*, Prentice Hall, New York.
- Gueta, Rami (1993), *Energy from dry air – a mathematical model to describe the air flow and droplet evaporation in the Energy Tower*, Ph.D.-thesis, Technion – Israel Institute of Technology, Haifa, Israel (in Hebrew).
- Gutman, Per-Olof (1995), *Qsyn – the Toolbox for Robust Control Systems Design, User's Guide*. El-Op Electro-Optics Ind., Rehovot, Israel.
- Horesh, Eran (2001), *Design of Control for the Energy Tower*, M.Sc.-thesis, Technion – Israel Institute of Technology, Haifa, Israel (in Hebrew).
- Krivchenko, Grigory. (1994), *Hydraulic machines: Turbines and Pumps*, Lewis, London.
- Pnueli, David, and Gutfinger, Chaim (1992), *Fluid Mechanics*, Cambridge University Press, U.K.
- Sternby, Jan (1979), "A review of Extremum Control", Internal report, Department of Automatic Control, Lund Institute of Technology, Lund, Sweden.
- Wallace, J. M. and Hobbs, P. V. (1977), *Atmospheric Science - An Introductory Survey*, Academic Press, New York.
- Zaslavsky, Dan (1997), "Solar energy without a collector for electricity and water in the 21st century", Internal report, Technion – Israel Institute of Technology, Haifa, Israel.
- Zaslavsky, Dan (1999), *Aero-Electric Power Stations – a summary of R&D 1982-1998*, Technion – Israel Institute of Technology, Haifa, Israel (in Hebrew).

LOOP SHAPING AND ACHIEVABLE PERFORMANCE WITH PID CONTROLLERS

L.H. Keel * and S.P. Bhattacharyya **

** Center of Excellence in Information Systems, Tennessee State University
330 Tenth Avenue North, Campus Box 139,
Nashville, TN 37203-3401, USA*

*** Department of Electrical Engineering, Texas A\&M University
College Station, TX 77843, USA*

Abstract: A recent result characterizing the set of all stabilizing Proportional-Integral-Derivative (PID) controllers for a given linear time invariant (LTI) plant is used here to address the issue of achievable performance with PID control. Specifically, we show how to determine constructively a) the attainable set of closed loop characteristic roots b) the set of achievable frequency responses and c) a prescribed set of loop shaping specifications. Items a) and b) utilize standard results from parametric robust control theory on polytopic sets of polynomials and transfer functions. The problem of loop shaping for the given LTI plant using PID controllers is formulated as a set of gain and phase specifications to be attained pointwise at a prescribed set of frequencies. By describing these in the Nyquist plane with prescribed tolerances specified using rectangular windows we are able to formulate the loop shaping problem as a linear programming problem parameterized by a proportional gain. This combined with the linear constraints describing the stabilizing set allows us to constructively intersect the stabilizing and specification sets and obtain a yes or no answer to the question of whether a given loop shaping specification can be achieved using some controller from the set of stabilizing PID controllers. The usefulness of such a formulation in control system design cannot be overstated and is illustrated here

1. INTRODUCTION¹

Despite revolutionary advances in control theory, the PID controller retains its status as one of the most widely used control techniques. This is largely due to its built-in characteristics. It provides feedback; it has the ability to eliminate steady state offsets through integral action; it can also anticipate the future through derivative action. In fact, the PID control has gone through and adapted to many technological changes ranging from pneumatics to microprocessors

via electronic tubes, transistors, and integrated circuits (Astrom et al., 1995). However, the research in PID control mainly focused in implementation issues such as auto-tuning, gain scheduling, continuous adaptation, etc...

In recent years, attention has turned to more fundamental issues which provide theoretical insights into PID control in the modern control context. One notable development is the determination of the set of all stabilizing controllers for a given single-input, single-output plant and the resulting efficient computational schemes for depicting this set. This development revealed interesting aspects of the set

¹ This research was supported in part by NASA Grant NCC-5228 and NSF Grant HRD-9706268.

and the topology of the stabilizing set can be exceedingly complicated (Datta et al., 2000). It was found in (Datta et al., 2000) that, for a fixed proportional gain K_p , the stabilizing set is characterized by a set of linear inequalities in the integral gain K_I and the derivative gain K_D . As a result, the two dimensional stabilizing set in K_I - K_D space, for fixed K_p becomes a union of bounded or unbounded convex polygons.

The present paper builds on the above development and investigates the following questions. First, for a given single-input, single-output linear-time invariant system, how can we characterize the entire root space in the complex plane that is achievable for closed loop poles by all possible choices of stabilizing PID controllers? Second, what is the achievable frequency response in the Bode plot sense? In this paper, these two questions are elegantly answered by using the result of in conjunction with standard results in parametric control theory (Bhattacharyya et al., 1995; Keel, 1994) on polytopic sets of polynomials and rational functions.

Answers to above questions are directly related to the achievable performance of PID controllers. For example the achievable frequency responses give us the maximum achievable gain and phase margins. Despite extensive use of PID controllers, these questions regarding the achievable performance of ID controllers have never been analytically investigated before.

We next consider the problem of loop shaping for a given LTI plant with a PID controller. The loop shaping problem can be stated as follows: the designer desires that the frequency response of the open loop controlled system should have prescribed gain and phase, within tolerances, at a chosen set of frequencies. This is a standard approach to design: for example, see (Zhao et al., 1996) and references therein. Our approach to this problem consists of requiring that the frequency response of the controlled system loop gain function should pass through prescribed rectangular windows in the Nyquist plane.

This formulation in conjunction with the characterization of all stabilizing PID controllers (Datta et al., 2000) leads to a linear programming problem whose solution determines the set of PID controllers attaining the specifications within the stabilizing set. The advantage of this formulation, from the designer's point of view, is that it gives a yes or no answer to the question of whether a given loop shaping specification can be achieved with a PID controller from the stabilizing set. In case the answer is yes the entire set attaining specifications is also obtained, and in case the answer is no, the

specifications have to be relaxed or changed. An example is given for illustration.

2. CHARACTERIZATION OF ALL STABILIZING PID CONTROLLERS

The central result underlying the characterization of all stabilizing PID controllers for a given SISO LTI plant is the Generalized Hermite-Biehler Theorem (Ho et al., 1999), which is essentially a root counting formula. An alternative root counting formula was given in (Keel et al., 2000). This is the version we use here. To state this, let

$$\begin{aligned}\delta(s) &= \delta_n s^n + \dots + \delta_1 s + \delta_0 \\ &= \delta_e(s^2) + s\delta_o(s^2)\end{aligned}\quad (1)$$

where $\delta_e(s^2)$ and $\delta_o(s^2)$ are components of $\delta(s)$ made up of even and odd powers of s , respectively. Then for every frequency $\omega \in \mathbb{R}$, we write

$$\delta(j\omega) = p(\omega) + jq(\omega) \quad (2)$$

where $p(\omega) = \delta_e(-\omega^2)$ and $q(\omega) = \omega\delta_o(-\omega^2)$.

Let $r(l)$ denote the open right half plane (RHP) (open left half plane (LHP)) roots of the given polynomial. Introduce the notation:

$$\text{Sgn}[x] = \begin{cases} +1 & \text{if } x > 0 \\ -1 & \text{if } x < 0 \\ 0 & \text{if } x = 0 \end{cases} \quad (3)$$

and let

$$f^{(k)}(x_i) := \left. \frac{d^k f(x)}{dx^k} \right|_{x=x_i} \quad (4)$$

Theorem 1 (Keel et al., 2000): Let the nonnegative real zeros of $q(\omega)$ be

$$0 = \omega_0 < \omega_1 < \omega_2 < \dots < \omega_t$$

with respective multiplicities k_i , $i = 0, 1, \dots, t$, and let $\omega_{t+1} = \infty$.

Then **A. degree** $[\delta(s)]$ is even,

$$\begin{aligned}l - r &= \text{Sgn}[q^{(k_0)}(\omega_0)](\text{Sgn}[p^{(k_0-1)}(\omega_0)] - \text{Sgn}[p(\omega_1)]) \\ &\quad + \sum_{i=1}^t \text{Sgn}[q^{(k_i)}(\omega_i)](\text{Sgn}[p(\omega_i)] - \text{Sgn}[p(\omega_{i+1})])\end{aligned}$$

B. degree $[\delta(s)]$ is odd,

$$\begin{aligned}l - r &= \text{Sgn}[q^{(k_0)}(\omega_0)](\text{Sgn}[p^{(k_0-1)}(\omega_0)] - \text{Sgn}[p(\omega_1)]) \\ &\quad + \sum_{i=1}^{t-1} \text{Sgn}[q^{(k_i)}(\omega_i)](\text{Sgn}[p(\omega_i)] - \text{Sgn}[p(\omega_{i+1})]) \\ &\quad + \text{Sgn}[q^{(k_t)}(\omega_t)] \cdot \text{Sgn}[p(\omega_t)]\end{aligned}$$

We apply the above results to the PID problem. Let $P(s)$ be a given plant and $C(s)$ be a PID controller where

$$P(s) = \frac{N(s)}{D(s)} = \frac{N_e(s^2) + sN_o(s^2)}{D_e(s^2) + sD_o(s^2)} \quad (5)$$

and

$$C(s) = \frac{K_I + K_P s + K_D s^2}{s}. \quad (6)$$

Then the closed loop characteristic polynomial becomes

$$\delta(s, K_I, K_P, K_D) = s D(s) + (K_I + K_D s^2) N(s) + K_P s N(s) \quad (7)$$

Let us introduce

$$N(-s) = N_e(s^2) - s N_o(s^2). \quad (8)$$

Then it is easy to verify that we have

$$\delta(s, K_I, K_P, K_D) N(-s) \Big|_{s=j\omega} = p(\omega, K_I, K_D) + jq(\omega, K_P) \quad (9)$$

where

$$p(\omega, K_I, K_D) = p_1(\omega) + (K_I - K_D \omega^2) p_2(\omega) \\ q(\omega, K_P) = q_1(\omega) + K_P q_2(\omega)$$

with

$$p_1(\omega) = -\omega^2 [N_e(-\omega^2) D_o(-\omega^2) - D_e(-\omega^2) N_o(-\omega^2)] \\ p_2(\omega) = N_e^2(-\omega^2) + \omega^2 N_o^2(-\omega^2) \\ q_1(\omega) = \omega [D_e(-\omega^2) N_e(-\omega^2) + \omega^2 D_o(-\omega^2) N_o(-\omega^2)] \\ q_2(\omega) = \omega [N_e^2(-\omega^2) - \omega^2 N_o^2(-\omega^2)]$$

Let $r(\cdot)$ and $l(\cdot)$ denote the number of open RHP and open LHP roots of the given polynomial (\cdot) , respectively. Then we see that

$$l(\delta(s, K_I, K_P, K_D) N(-s)) - r(\delta(s, K_I, K_P, K_D) N(-s)) \\ [l(\delta(s, K_I, K_P, K_D)) - r(\delta(s, K_I, K_P, K_D))] \\ + [l(N(-s)) - r(N(-s))].$$

From the definition

$$\sigma_i[\cdot] = r(\cdot) - l(\cdot), \quad (10)$$

we therefore conclude that $\delta(s, K_I, K_P, K_D)$ of n^{th} order is Hurwitz if and only if

$$\sigma_i[\delta(s, K_I, K_P, K_D) N(-s)] = n + [(N - s) - r(N(-s))] \quad (11)$$

Now let us observe eq. (9). It is easily seen that the coefficients of the polynomial $p(\omega, K_I, K_D)$ are linear functions of K_I and K_D , and K_P also appears linearly in the coefficients of the polynomial $q(\omega, K_P)$. Thus, once we determine the real positive roots, $0 = \omega_0 < \omega_1 < \omega_2 < \dots < \omega_{l-1}$ of $q(\omega, K_P)$ for a fixed value of K_P , we can determine the set of sign sequences $\text{Sign } p(\omega_i, K_I, K_D)$, $i = 0, 1, \dots, l$ that satisfy the condition given in eq.(11) from the Theorem 1. Each of these sequences is a set of linear inequalities, in K_I and K_D to be solved to determine the stability region in (K_I, K_D) space. By repeating this over the K_P axis, the entire stability region in (K_I, K_D, K_P) is obtained. In the following sections, we use the above characterization of the stabilizing set to constructively formulate and solve the problems related to achievable performance with PID control.

3. ACHIEVABLE CLOSED LOOP POLES

In this section, we consider the problem of determining the root space attainable in the complex plane where the closed loop poles can be obtained by all choices of stabilizing PID controllers. We call this set the *achievable root space*. In other words, it is not possible to find stabilizing PID controllers, for the given system, such that the closed loop poles can be located outside the achievable root space. Let

$$P(s) = \frac{N(s)}{D(s)} = \frac{n_{n-1}s^{n-1} + \dots + n_1s + n_0}{s^n + d_{n-1}s^{n-1} + \dots + d_1s + d_0}. \quad (12)$$

Then the characteristic polynomial is

$$\delta(s) = s D(s) + (K_I + K_P s + K_D s^2) N(s) \\ = (1 + K_D n_{n-1}) s^{n+1} + (d_{n-1} + K_D n_{n-2} + K_P n_{n-1}) s^n \\ + (d_{n-2} + K_D n_{n-3} + K_P n_{n-2} + K_I n_{n-1}) s^{n-1} + \dots \\ + (d_0 + K_P n_0 + K_I n_1) s + K_I n_0. \quad (13)$$

The coefficients of the characteristic polynomial $\delta(s)$ are linear functions of the controller parameters K_I , K_P and K_D . Furthermore, it was established in the previous section that the stability region in (K_I, K_D) space, for every fixed K_P , is a single polytope or a union of polytopes. For each such polytope, with fixed K_P the set of characteristic polynomials in eq.(13) is a polytope. Therefore, by the Edge Theorem (Bhattacharyya et al., 1995; Bartlett et al., 1988) the boundary of the root space of the set of $\delta(s)$ can be determined by computing the root loci along the exposed edges of this polytope. By repeating this computation over the stabilizing range

of K_P , we can determine the set of characteristic roots achievable. The example given in Section 6 illustrates the use of this root space computation in design.

4. ACHIEVABLE FREQUENCY RESPONSES

The open loop transfer function of the system with the PID controller is

$$L(s) = C(s)P(s) \quad (14)$$

As $C(s)$ ranges over the stabilizing set, $L(s)$ ranges over the corresponding stabilizing set which we denote as $Stab(L)$. The frequency response of each $L(s)$ in $Stab(L)$ is the set of achievable frequency responses. As we have seen before, the stabilizing set is described for a fixed K_P by linear inequalities in (K_I, K_D) . Thus, the set of achievable $L(s)$ transfer functions for a fixed K_P by a polytopic set of transfer functions. This fact allows us to determine the corresponding achievable Bode plots by $Stab(L)$ using results on frequency response of polytopic sets of transfer function developed in (Bhattacharyya et al., 1995; Keel, 1994). Basically, the Bode magnitude and phase envelopes that are achievable can be obtained by scanning the exposed edges of the polytope. Once again, the example in Section 6 illustrates the use of this in design.

5. LOOP SHAPING VIA PID CONTROLLERS

In this section, we consider the problem of loop shaping, i.e., for the given plant $P(s)$, find $C(s)$ such that magnitude and phase plots of the loop transfer function $L(s) = P(s)C(s)$ are as close as those of a prespecified loop transfer function $L_0(s)$. Typically, the complete description of $L_0(s)$ is not known. Instead, data points (magnitude and phase) over several frequencies are available. It is important to note, at the outset, that, from the properties shown in Sections 3 and 4, it is necessary that the frequency plots of $L_0(s)$ (or data points over chosen frequencies) must lie inside the admissible envelopes. Otherwise, it is impossible to determine a stable set (K_I, K_D, K_P) that approximates $L_0(s)$. However, it is in general difficult to find a stabilizing controller that has the magnitude and phase plots of its loop transfer function to exactly coincide with those of a chosen $L_0(s)$. Therefore, it is reasonable to attempt to achieve these within tolerances. To formulate this problem, write

$$\begin{aligned} L(j\omega) &= P(j\omega)C(j\omega) \\ &= P(j\omega) \underbrace{\left[\frac{(K_I - \omega^2 K_D) + j\omega K_P}{j\omega} \right]}_{C(j\omega)} \\ &= \underbrace{[P_r(j\omega) + P_i(j\omega)]}_{P(j\omega)} \underbrace{[(K_I - \omega^2 K_D) + j\omega K_P]}_{j\omega C(j\omega)} \\ &= \underbrace{[(K_I - \omega^2 K_D)P_r(\omega) - \omega K_P P_i(\omega)]}_{R(\omega, K_I, K_P, K_D)} \\ &\quad + j \underbrace{[(K_I - \omega^2 K_D)P_i(\omega) - \omega K_P P_r(\omega)]}_{I(\omega, K_I, K_P, K_D)}. \end{aligned} \quad (15)$$

Let $\omega_1, \dots, \omega_k$ denote the prescribed set of frequencies where we wish to enforce frequency response specifications. As state before, these specifications must be stated with some tolerance so that the chances of finding a controller are improved. This leads to the following set of linear inequalities on the real and imaginary parts of $L(j\omega_i)$.

$$\alpha_i^- \leq R(\omega_i, K_I, K_P, K_D) \leq \alpha_i^+, \quad i=1, \dots, k \quad (16)$$

$$\beta_i^- \leq I(\omega_i, K_I, K_P, K_D) \leq \beta_i^+, \quad i=1, \dots, k \quad (17)$$

for all selected i . The set of loop gain transfer functions attaining the specifications above may be denoted as $Spec(L)$. This set is depicted in Figure 1. Note that this set of inequalities describing $Spec(L)$ is linear in (K_I, K_D) . To determine if the specification can be met, they need to be solved in conjunction with the stability conditions. In other words we need to intersect the stability set $Stab(L)$ with the specification set $Spec(L)$. Since the latter are linear in (K_I, K_D) for a fixed K_P , our strategy for design is clear. First, fix K_P to solve the linear programming problem in (K_I, K_D) obtained by adding the stability conditions to the loop shaping conditions in eqs.(16) and (17).

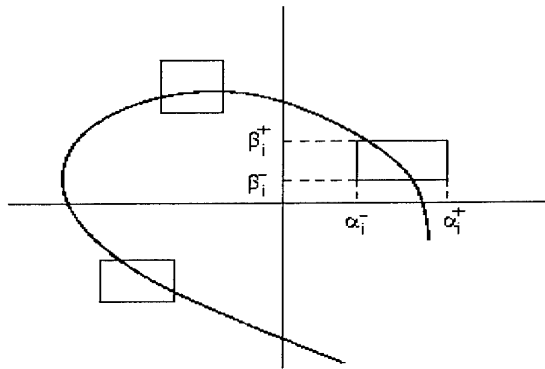


Fig. 1. Loop shape satisfying specifications

Repeat this procedure for different values of K_P within the stabilizing range. If no solution exists to

such linear programming problems, the specifications cannot be achieved. Conversely, the set of all (K_I, K_D) which satisfy the augmented linear programming conditions for a given K_P represent the set of solutions that achieve the specifications. This type of computation is illustrated in the example.

6. EXAMPLE

Consider the control system with the plant

$$P(s) = \frac{N(s)}{D(s)} = \frac{s^3 - 4s^2 + s + 2}{s^5 + 8s^4 + 32s^3 + 46s^2 + 46s + 17}.$$

and the PID controller be

$$C(s) = K_P + \frac{K_I}{s} + K_D s.$$

The characteristic polynomial is

$$\begin{aligned} \delta(s, K_I, K_P, K_D)N(-s) = & [s^2(-12s^6 - 180s^4 - 183s^2 \\ & + 75) + (K_I + K_D s^2)(-s^6 + 14s^4 - 17s^2 + 4)] \\ & + s[(-s^8 - 65s^6 + 246s^4 - 22s^2 + 34) \\ & + K_P(-s^6 + 14s^4 - 17s^2 + 4)]. \end{aligned}$$

We have

$$\begin{aligned} p_1(\omega) &= -12\omega^8 + 180\omega^6 - 183\omega^4 - 75\omega^2 \\ p_2(\omega) &= \omega^6 + 14\omega^4 + 17\omega^2 + 4 \\ q_1(\omega) &= -\omega^9 + 65\omega^7 - 246\omega^5 + 22\omega^3 + 34\omega \\ q_2(\omega) &= \omega^7 + 14\omega^5 + 17\omega^3 + 4\omega \end{aligned}$$

and

$$\begin{aligned} \delta(s, K_I, K_P, K_D)N(-s) \Big|_{s=j\omega} \\ = p(\omega, K_I, K_D) + jq(\omega, K_P) \end{aligned}$$

where

$$\begin{aligned} p(\omega, K_I, K_D) &= p_1(\omega) + (K_I - K_D \omega^2) p_2(\omega) \\ q(\omega, K_P) &= q_1(\omega) + K_P q_2(\omega) \end{aligned}$$

For a fixed K_P , we compute the distinct finite zeros of $q(\omega, K_P)$ with odd multiplicity's, say, $\omega_0 = 0$, $\omega_1, \dots, \omega_k$. We have

$$\begin{aligned} \text{degree}[\delta(s, K_I, K_P, K_D)] &= n = 6 \\ \text{degree}[N(s)] &= m = 3 \\ l(N(-s)) &= 2 \\ r(N(-s)) &= 1. \end{aligned}$$

Suppose, for example that $K_P = -4$, then we have $\omega_0 = 0$, $\omega_1 = 0.4265$, $\omega_2 = 2.3639$, $\omega_3 = 7.4531$. From eq. (11),

$$\begin{aligned} l(\delta(s, K_I, K_P, K_D)) - r(\delta(s, K_I, K_P, K_D)) \\ \underbrace{\hspace{10em}}_{\text{required to be 6}} \\ - \underbrace{[l(N(-s)) - r(N(-s))]}_{2-1=1} = 7 \text{ (required for stability)} \end{aligned}$$

By applying the formula in Theorem 1 (for the odd case) we have

$$\begin{aligned} 7 = & \text{Sgn}[\dot{q}(\omega_0, -4)](\text{Sgn}[p(\omega_0, K_I, K_D)] \\ & - \text{Sgn}[p(\omega_1, K_I, K_D)]) \\ & + \text{Sgn}[\dot{q}(\omega_1, -4)](\text{Sgn}[p(\omega_1, K_I, K_D)] \\ & - \text{Sgn}[p(\omega_2, K_I, K_D)]) \\ & + \text{Sgn}[\dot{q}(\omega_2, -4)](\text{Sgn}[p(\omega_2, K_I, K_D)] \\ & - \text{Sgn}[p(\omega_3, K_I, K_D)]) \\ & + \text{Sgn}[\dot{q}(\omega_3, -4)]\text{Sgn}[p(\omega_3, K_I, K_D)] \quad (18) \end{aligned}$$

Since

$$\text{Sgn}[\dot{q}(\omega_0, -4)] = 1, \text{Sgn}[\dot{q}(\omega_1, -4)] = -1,$$

$$\text{Sgn}[\dot{q}(\omega_2, -4)] = 1, \text{Sgn}[\dot{q}(\omega_3, -4)] = -1,$$

the only feasible sign sequence that satisfies eq. (18) is

$$\begin{aligned} \{\text{Sgn}[p(\omega_0, \cdot)], \text{Sgn}[p(\omega_1, \cdot)], \text{Sgn}[p(\omega_2, \cdot)], \text{Sgn}[p(\omega_3, \cdot)]\} \\ = \{1, -1, 1, -1\}. \end{aligned}$$

This leads the following set of linear inequalities in (K_I, K_D) space that characterises the stabilising parameters.

$$\begin{aligned} p_1(\omega_0) + (K_I - K_D \omega_0^2) p_2(\omega_0) &> 0 \\ p_1(\omega_1) + (K_I - K_D \omega_1^2) p_2(\omega_1) &< 0 \\ p_1(\omega_2) + (K_I - K_D \omega_2^2) p_2(\omega_2) &> 0 \\ p_1(\omega_3) + (K_I - K_D \omega_3^2) p_2(\omega_3) &< 0 \end{aligned} \quad (19)$$

Typically, the loop shaping constraints are selected using Bode plots. A designer selects a number of frequencies of interest, and the upper and lower bounds of magnitude and phase at each selected frequency. These selected windows can be reinterpreted in terms of the Nyquist plot windows in our formulation, as shown in Figure 2. Thus the wedge shaped regions are approximated by appropriate rectangular windows shown in the figure. For this example, we select four frequency points of interest, ω_i^* for $i=1,2,3,4$, in this example and

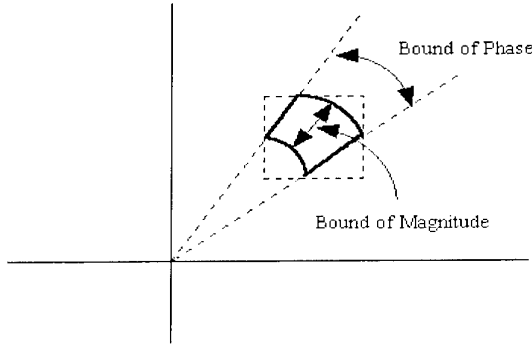


Fig. 2. Bounds of magnitude and phase

approximate the corresponding wedge shape windows by rectangles, and have

$$\alpha_i^- \leq R(\omega_i^*, K_I, K_P, K_D) \leq \alpha_i^+, \quad i=1, \dots, k$$

$$\beta_i^- \leq I(\omega_i^*, K_I, K_D) \leq \beta_i^+, \quad i=1, \dots, k$$

where (α_i^-, α_i^+) represent the lower and upper limits of the real and image parts of the rectangle shown in Figure 1. Thus, the additional linear inequalities are

$$\begin{aligned} R(\omega_i^*, K_I, K_P, K_D) &\leq \alpha_i^+, & i=1, 2, 3, 4 \\ -R(\omega_i^*, K_I, K_P, K_D) &\leq -\alpha_i^-, & i=1, 2, 3, 4 \\ I(\omega_i^*, K_I, K_D) &\leq \beta_i^+, & i=1, 2, 3, 4 \\ -I(\omega_i^*, K_I, K_D) &\leq -\beta_i^-, & i=1, 2, 3, 4 \end{aligned} \quad (20)$$

As discussed, the region satisfying the set of inequalities in eq. (19) gives the stabilizing parameter set. On the other hand, the set of inequalities in eq. (20) gives the set of controller parameters satisfying loop shaping conditions or specifications. Therefore, by solving eqs. (19) and (20) simultaneously, we have the controller parameter set satisfying both stabilization and loop shaping conditions. Figure 3 shows these two sets.

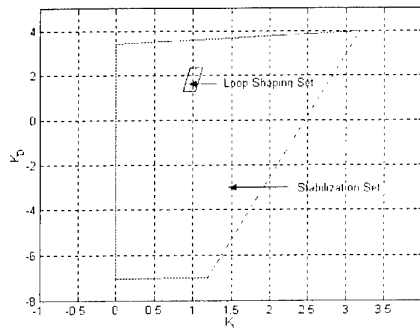


Fig. 3. Stabilization and loop shaping for $K_P = -4$

Figure 4 shows admissible Bode plots (bounded by dotted lines) that correspond to the stabilisation region. This means that any Bode plots passing outside this region cannot be realized by any

stabilizing PID controllers when $K_P = -4$. ω_i^* for $i=1,2,3,4$ indicate the set of design frequencies and the envelopes depicted by solid lines are the design envelopes. The design objective is to find a set of controller parameters that results the Bode plots of the controller loop transfer function $L(j\omega)$ located inside the design envelopes.

Finally, we select a set of controller parameters inside the loop shaping region shown in Figure 3, that is $K_P = -4$, $K_I = 1$, $K_D = 2$

or

$$C(s) = \frac{1 - 4s + 2s^2}{s}$$

The controller is verified in Figure 5. With this PID controller, feedback stabilization as well as loop shaping are achieved.

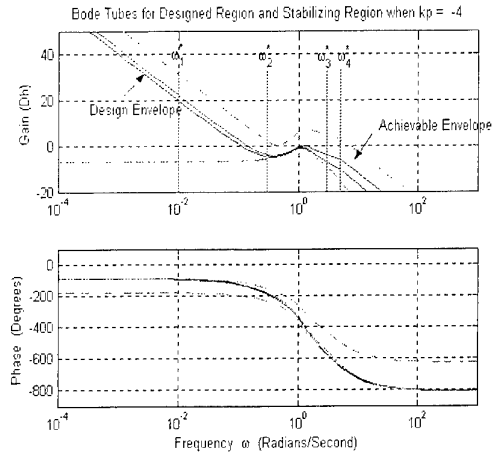


Fig. 4. Admissible Bode envelopes and design envelopes for $K_P = -4$

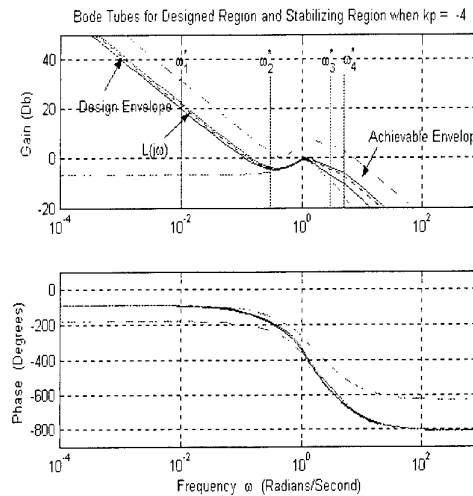


Fig. 5. Admissible Bode envelopes and design envelopes for $K_P = -4$, and Bode plots of $L(j\omega)$

Figure 6 shows the achievable closed loop poles discussed in Section 3. As expected, the achievable closed loop poles from the design set are inside those from the stabilization set.

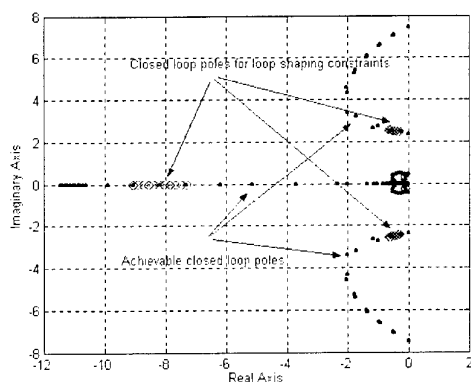


Fig. 6. Achievable closed loop poles and design closed loop poles for $K_P = -4$

7. CONCLUDING REMARKS

In this paper we have given procedures to determine the performance achievable by a control system consisting of a given LTI plant in closed loop with PID controllers. By exploiting recent results giving a "linear" characterization of the stabilizing set of controllers we are able to determine the root space attainable and the frequency response attainable. Moreover we have developed a loop shaping procedure based on linear programming that can systematically search through the stabilizing set and determine a PID controller if it exists. We expect these results to significantly impact design methodologies for PID control and to further research on PID controller performance.

REFERENCES

- Astrom, K. and T. Hagglund, (1995). *PID Controllers: Theory, Design, and Tuning* (2nd Edition)}. Instrument Society of America, Research Triangle Park, NC..
- Bartlett, A.C., C.V. Hollot, and H.Lin (1988). Root location of an entire polytope of polynomials: it suffices to check the edges. *Mathematics of Controls, Signals and Systems*, **1**, 61 - 71.
- Bhattacharyya, S.P., H. Chapellat, and L.H. Keel (1995). *Robust Control: The Parametric Approach*. Prentice Hall PTR, Upper Saddle Rive, NJ.
- Datta, A., M.T. Ho, and S.P. Bhattacharyya (2000). *Structure and Synthesis of PID Controllers*. Advances in Industrial Control Series, Springer-Verlag, London.
- Ho, M.T., A. Datta, and S.P. Bhattacharyya (1999). Generalization of the Hermite-Biehler Theorem. *Linear Algebra and its Application*, **302**, pp. 135 -153.
- Keel, L.H. and S.P. Bhattacharyya (1994). Robust parametric classical control design. *IEEE Transactions on Automatic Control*, **39**, 7, 1524 -1530.
- Keel, L.H. and S.P. Bhattacharyya (2000). A generalization of Mikhailov's criterion with applications. *Proceedings of the 2000 American Control Conference*, Chicago, IL.
- Zhao, Y. and S. Jayasuriya (1996). Robust stability of closed loop systems resulting from nonsequential MIMO-QFT design. *Journal of Dynamic Systems, Measurement and Control*, **118**, 4, 753 - 756.

ON THE EXISTENCE CONDITIONS FOR ROBUST STABILITY AND PERFORMANCE OF PID CONTROLLERS

Ukpai I. Ukpai and Suhada Jayasuriya

*Department of Mechanical Engineering,
 Texas A&M University, College Station, TX 77843, U. S. A*

Abstract: PID controllers are widely used due to the ease in their design and implementation. Existence conditions of Quantitative Feedback Theory (QFT) controllers have been established by previous studies. In this paper, some of these results are extended to the PID controller implemented with a filter in the derivative term. It is shown that the PID controller gains cannot span the entire real space for a proper plant family. In addition, the Nevalinna-Pick interpolation problem is used to establish a lower limit on the peak magnitude of the nominal complimentary sensitivity function. Also, certain plant structures are excluded from PID control if stability is to be achieved.

Keywords: Loop transfer, PID, QFT, Robust performance, Sensitivity function, SISO, Stability criteria, Time delay.

1. INTRODUCTION

In traditional QFT, the controller is obtained by shaping the nominal loop transfer function, L_o , on the Nichols chart that has the stability and performance bounds superimposed on it (Horowitz, 1991). This stage relies heavily on the experience of the designer. Several existence conditions for QFT controllers have been developed in order to establish, a priori, if the tedious process of loop shaping can produce a controller for the general robust performance problem (Jayasuriya and Zhao, 1994). In this paper some of these existence conditions are extended to the case where the controller structure is constrained to be a PID controller according to:

$$K_{PID}(s) = k_p \left[1 + \frac{1}{k_i s} + \frac{s k_d}{Ts + 1} \right] = \frac{k_1 s^2 + k_2 s + k_3}{s(Ts + 1)} \quad (1)$$

where k_p is the controller gain, k_i is the reset time, k_d is the derivative coefficient and T is the time constant of the filter in the derivative term. k_1 , k_2 and k_3 are defined as $k_d + k_p T$, $k_p + T/k_i$, $1/k_i$ respectively.

2. STABILITY OF A TWO DEGREE-OF-FREEDOM QFT PROBLEM

The QFT problem for a single-input-single-output (SISO) system is stated (Nordgren et al., 1994): synthesize a controller such that the uncertain feedback system is internally stable and:

- 1) $\frac{L}{1+L}$ is exponentially stable $\forall \alpha \in \Omega \subset \mathbb{R}^q$ (Robust Stability) where α is the vector of q bounded and continuous uncertain

parameters belonging to the differentiable manifold Ω .

$$2) \quad A(\omega) \leq |T_{yr}(j\omega)| \leq B(\omega) \quad \forall \omega \text{ (Robust}$$

$$\text{tracking performance), } T = F \frac{L}{1+L}$$

$$3) \quad |S(j\omega)| = \left| \frac{1}{1+L(j\omega)} \right| \leq M_D(\omega) \quad \forall \omega,$$

$\forall \alpha \in \Omega$ (robust disturbance accommodation)

The above is a statement of the general QFT robust performance problem. It was shown in Nordgren et al (1994) that robust performance of a system is guaranteed if

$$|M^{-1}(\omega)S(\alpha, j\omega)| + |H(\alpha, j\omega)m(\omega)| \leq 1, \quad \forall \omega, \quad \forall \alpha \in \Omega$$

subject to the satisfaction of the robust stability

$$\text{condition of } H = \frac{L}{1+L} \quad \forall \alpha \in \Omega \text{ where the general}$$

uncertain plant family is given by

$$P(s) = P(\alpha, s)[1 + \Delta_n(s)]$$

and

$$|\Delta_n(j\omega)| < m(\omega) \subset \Re H^\infty,$$

$$P(\alpha, s) = \begin{cases} \frac{k \prod_i (s + z_i) \prod_j (s^2 + 2\zeta_j \omega_j s + \omega_j^2) e^{-s\tau}}{s^2 \prod_k (s + p_k) \prod_l (s^2 + 2\zeta_l \omega_l s + \omega_l^2)}, & \forall \omega < \omega_h \\ \frac{ke^{-s\tau}}{s^c}, & \forall \omega \geq \omega_h \end{cases}$$

where

$$L(\alpha, s) = K_{PID}(s)P(\alpha, s),$$

$$L(s) = K_{PID}(s)P(s), \quad L_o(s) = L(\alpha_o, s) = K_{PID}(s)P_o(s)$$

$P_o(s) = P(\alpha_o, s)$, ω_h is the Horowitz's universal high frequency (defined as the frequency after which the phase variation of the parametric plant set is essentially zero) and $M(\omega)$ is the infimum of all sensitivity specifications. $k, z_i, \zeta_j, \zeta_l, \omega_j, \omega_l, \tau, p_k$ belong to α . It is noted that the tracking specification can be transformed to a sensitivity specification. It is also noted that the relative degree of the plant remains constant over the plant set.

A condition on the feasibility of the QFT problem is that the feedback system involving only the parametric plant set $P(\alpha, s)$ is robustly, internally stable $\forall \alpha \in \Omega$.

Define

$$L'(\Omega, s) = K \frac{N(\Omega, s)}{D(\Omega, s)}.$$

Defining $A(\Omega, s) \equiv A(\alpha, s)$, $\forall \alpha \in \Omega$, as an uncertain polynomial function, let D_N be the semicircular contour varying along the imaginary axis from $-jR$ to jR avoiding the poles of $L'(\Omega, s)$ on the imaginary axis by arbitrarily small semicircles centered at these poles and then into the right-half plane from $(0, +R)$ to $(0, -R)$ along a circle of radius R , centered at the origin and chosen such that all right-half plane zeros are included in it. Stability is established by the following theorem for the general plant with time delay:

THEOREM 1: (NORDGREN ET AL., THEOREM 2)

Given the loop transmission function, $L'(\Omega, s)e^{-s\tau} = K \frac{N(\Omega, s)e^{-s\tau}}{D(\Omega, s)}$, assume that

$$= K \frac{N(\Omega, s)}{D(\Omega, s)} = L'(\Omega, s) \text{ is strictly proper and that there}$$

is no closed right half plane, ζ_+ , pole-zero cancellation in $L'(\Omega, s)$. Then the time delay feedback system with the characteristic function given by:

$$Z(\Omega, s) = D(\Omega, s) + Ke^{-s\tau}N(\Omega, s) =$$

$$a_n(\Omega)s^n + \dots + a_0(\Omega) + Ke^{-s\tau}[b_m(\Omega)s^m + \dots + b_0(\Omega)]$$

has no zeros in the closed set $D_N \in \zeta_+$ if and only if:

i) for some $\alpha = \alpha_o \in \Omega, Z(\alpha_o, s) \neq 0 \quad \forall s \in D_N$ and

ii) $0 \notin Z(\Omega, s), \quad \forall s \in \partial D_N$ where ∂D_N is the contour of D_N

Proof:

See (Nordgren et al., 1994)

For the special case of plants without time delay, the above theorem reduces to the lemma in Jayasuriya and Zhao (1994) given here as Lemma 1.

Let the proper compensator transfer function be

$$G(s) = \frac{Q_1(s)}{Q_o(s)} \text{ and the plant be } P(\alpha, s) = \frac{N_p(\alpha, s)}{D_p(\alpha, s)}$$

and strictly proper:

Lemma 1:[Lemma 2.1 (Jayasuriya and Zhao, (1994))]

$G(s)$ stabilizes the whole plant family if and only if:

- i) there exists an $\alpha_0 \in \Omega$ such that $G(s)$ stabilizes $P(s, \alpha_0)$
- ii) $0 \notin \delta_1(j\omega, \Omega)$, $\forall \omega \in [0, \infty]$ where $\delta_1(j\omega, \Omega) \triangleq 1 + K_{PID}(j\omega)P(j\omega, \alpha)$

$$= 1 + \frac{Q_1(j\omega)N_p(j\omega, \alpha)}{Q_0(j\omega)D_p(j\omega, \alpha)}$$
- iii) there are no imaginary axis pole-zero cancellations in $\frac{Q_1(j\omega)N_p(j\omega, \alpha)}{Q_0(j\omega)D_p(j\omega, \alpha)}$.

Proof:

See (Jayasuriya and Zhao, 1994)

Robust stability thus requires the zero-exclusion principle given as condition (ii) in Lemma 1 and discussed in Jayasuriya (1993). To satisfy the robust stability condition, there should be no closed right-half plane pole-zero cancellations in the product $P(s)K(s)_{PID}$, where $K(s)_{PID} \equiv G(s)$ is the controller of equation 1 in this situation.

Also there exists an $\alpha = \alpha_0$ such that $P_0(j\omega) = P(j\omega, \alpha_0) \neq 0$ or $P(j\omega, \alpha_0)$ does not contain any imaginary-axis poles or zeros. In other words, according to condition (ii) of Lemma it can be shown that:

$$L_0(j\omega) \neq \frac{-P(j\omega, \alpha_0)}{P(j\omega, \alpha)} \quad \forall \omega, \forall \alpha \in \Omega \quad (2)$$

If there is no α_0 such that $P(j\omega, \alpha_0) \neq 0$ then there must exist several fixed frequencies $\omega_1, \dots, \omega_r$ such that $P(j\omega_i, \alpha_0) = 0$ (or ∞) $\forall \alpha \in \Omega$ and no more imaginary-axis poles or zeros.

3. EXISTENCE CONDITIONS OF QFT CONTROLLERS WITH A PID STRUCTURE

In this section, results would be developed that deal specifically with PID controllers. Let the parametric plant be:

$$P(s, \alpha) = \frac{N_p(s, \alpha)}{D_p(s, \alpha)} e^{-s\tau}, \quad \alpha \in \Omega \in \mathbb{R}^q$$

where α is the uncertain parameter vector of length q .

Let the PID controller be $K_{PID}(s) = \frac{N_k(s)}{D_k(s)}$ as given

by equation 1. The loop transfer function is

$$L(s, \alpha) = \frac{N_p N_k}{D_p D_k} e^{-s\tau} = \frac{N(\Omega, s)}{D(\Omega, s)} e^{-s\tau}.$$

It is assumed that $P(s, \alpha)$ is strictly proper. $K_{PID}(s)$, as implemented here, is proper. The characteristic polynomial is:

$$\delta(s, \alpha) = D(\Omega, s) + KN(\Omega, s)e^{-s\tau} \quad (3)$$

where $N_p(s, \alpha) = p_{im}(\alpha)s^m + \dots + p_{10}(\alpha)$,

$D_p(s, \alpha) = p_{on}(\alpha)s^n + \dots + p_{00}(\alpha)$, $m < n$.

$N_k(s) = k_1 s^2 + k_2 s + k_3$ and $D_k(s) = Ts^2 + s$.

The coefficient of the highest order term in $\delta(s, \alpha)$ is $T p_{on}$ with order $= (n+2)$.

Allowing no change in plant order, i.e. $T p_{on} \neq 0 \quad \forall P \in \mathcal{P}$. In other words, $0 \notin p_{on}(\Omega)$.

The controller has only two poles, one at the origin and one at $-T$. To avoid loss of degree in the loop transfer function, and also to insure it is proper, there can be no pole-zero cancellation of the controller poles. As is seen from the stability theorem given earlier, the pole at the origin cannot be cancelled. This reasoning lead to the following Lemma.

Lemma 2:

Plants of the form $sP'(\alpha, s)$ where $P'(\alpha, s)$ is of the

form $\frac{N_p(s, \alpha)}{D_p(s, \alpha)} e^{-s\tau}$ with $N_p(s, \alpha)$ and $D_p(s, \alpha)$ as

rational polynomials with no zeros at the origin cannot be stabilized by PID control.

Proof:

Since no pole-zero cancellation is allowed on any of the controller poles (at $-T$ and 0) in order to insure it is proper, it follows that the plant cannot have a zero at the origin since this would cancel the pole of the controller at the origin

From the third condition of Lemma 1 follows corollary 1:

Corollary 1:

Since there are no right half plane poles of $K_{PID}(s)$, it is not possible to have closed right half plane pole-zero cancellation in the loop transfer function

$L(s, \alpha) = \frac{N_p N_k}{D_p D_k} e^{-st}$ provided such do not occur in the plant transfer function.

This makes the condition, that there be no right half plane pole-zero cancellation, of Lemma 1 and Theorem 1 unnecessary.

The next corollary is only applicable to strictly proper plants.

Let the nominal plant be $P(s, \alpha_0) = P_0(s)$.

Corollary 2: [Corollary 2.2 (Jayasuriya and Zhao, 1994)]

The plant family $P(s, \alpha) = \frac{N_p(s, \alpha)}{D_p(s, \alpha)}$ cannot be stabilized if $0 \in \{P_0(s)/P(s, \alpha)\}_{s=j\omega}$.

Proof:

The loop transfer function is $L(s, \alpha) = P(s, \alpha)K_{PID}(s)$.
But

$$K_{PID}(s) = \frac{L(s, \alpha_0)}{P(s, \alpha_0)} = \frac{L_0(s)}{P_0(s)} \Rightarrow L(s, \alpha) = \frac{P(s, \alpha)}{P_0(s)} L_0(s)$$

From Lemma 1 the robust stability is achieved if $L_0(s)$ is stable and

$$\delta(j\omega, \alpha) = 1 + L_0(j\omega) \frac{P(j\omega, \alpha)}{P_0(j\omega)} \neq 0 \quad \forall \alpha \in \Omega, \omega \in [0, \infty] \quad (4)$$

$$\delta(j\omega, \alpha) = 0 \text{ if and only if } L_0(j\omega) \frac{P(j\omega, \alpha)}{P_0(j\omega)} = -1,$$

which is true if and only if the polar plot of $L_0(j\omega)$ intersects the value set $\left\{ -\frac{P_0(s)}{P(s, \alpha)} \right\}_{s=j\omega}$. Since the plant

is strictly proper and $K_{PID}(s)$ is proper, $L_0(j\omega)$ is strictly proper so that $\lim_{\omega \rightarrow \infty} L_0(j\omega) = 0$. So if

$0 \in \{P_0(s)/P(s, \alpha)\}_{s=j\omega} \Rightarrow \delta(s, \alpha)|_{s=j\omega} = 0$ and the plant family cannot be stabilized.

For a plant family that is proper the following corollary is useful.

Corollary 3:

For a proper plant family, let $\left\{ \frac{P_0(s)}{P(s, \alpha)} \right\}_{s=j\omega} = \{\Psi\}$, a

value set, then the PID controller parameters must be such that $\{\Psi\} \notin L_0(j\omega)|_{\omega=\infty}$.

Proof:

$$\delta(j\omega, \alpha) = 1 + L_0(j\omega) \frac{P(j\omega, \alpha)}{P_0(j\omega)} \neq 0 \text{ for stability.}$$

So if $L_0(j\omega) \frac{P(j\omega, \alpha)}{P_0(j\omega)} = -1$, then the plant family is

unstable $\forall \alpha \in \Omega$ or $\forall \omega \in [0, \infty]$ which is true if and only if the polar plot of $L_0(j\omega)$ intersects the value

$$\text{set } \left\{ -\frac{P_0(s)}{P(s, \alpha)} \right\}_{s=j\omega}.$$

Let $\forall \alpha \in \Omega, \left\{ -\frac{P_0(j\omega)}{P(j\omega, \alpha)} \right\}_{\omega=\infty} \in \{\Psi\}$, a value set,

then for stability $L_0(j\omega)|_{\omega=\infty} \notin \{\Psi\}$.

Since $L_0(j\omega) = P_0(j\omega)K_{PID}(j\omega)$ and $P_0(j\omega)$ is fixed, then certain values of $K_{PID}(s)$ must be excluded.

Sometimes the PID controller is implemented without the filter in the derivative term. In such a case, corollary 3 reverts to the general case of the zero exclusion principle.

Corollary 3 leads to theorem 2 below.

THEOREM 2:

If $\left\{ -\frac{P_0(s)}{P(s, \alpha)} \right\}_{s=j\omega}$ is finite (plant is proper) then the

PID controller (implemented as a proper transfer function) parameter gains cannot span the entire real space.

Proof:

Follows from corollary 3.

Another result that will be developed uses the theory that parameterizes all stabilizing controllers and solves the Nevanlinna-Pick interpolation problem. Certain theorems and definitions useful in developing the results are first reviewed.

Let RH^∞ be the family of all stable, proper, real and rational functions.

THEOREM 3:

Assume $P \in RH^\infty$. The set of all stabilizing controllers, G for which the feedback system is internally stable is: $G = \left\{ \frac{Q}{1-PQ} : Q \in RH^\infty \right\}$.

If P is no longer assumed to be stable let $P = \frac{N}{M}$ be the coprime factorization of P over \mathcal{H}^∞ and let X, Y be two functions in RH^∞ satisfying the equation $NX + MY = 1$.

THEOREM 4:

The set of all G 's for which the feedback system is internally stable is given by: $\left\{ \frac{X+MQ}{Y-NQ} : Q \in RH^\infty \right\}$.

Theorem 4 reduces to Theorem 3 when $P \in RH^\infty$.

THEOREM 5:

Let $C = N_c / M_c$ be a coprime factorization over RH^∞ . Then the feedback system is internally stable if and only if $(NN_c + MM_c)^{-1} \in RH^\infty$.

Theorems 3 to 5 are well known theorems and the proofs are omitted. For the proofs see, for example, (Doyle et al, 1992).

Let $\{a_1, \dots, a_n\}, \{b_1, \dots, b_n\}$ be sets of points in the complex plane such that for $a_i, \operatorname{Re} s > 0, a_1, \dots, a_n$ are distinct and $|b_i| \leq 1, i=1, \dots, n$. Then if $\|G\|_\infty \leq 1$, the Nevanlinna-pick (NP) problem is to find G such that $G(a_i) = b_i, i=1, \dots, n$, that is, the graph of G is to pass through the point (a_i, b_i) where $G \in RH^\infty$ and $\|G\|_\infty \leq 1$.

Definition 1:

The NP problem is said to be solvable if G exists.

Definition 2:

Associated with the NP problem data $a_i, b_i, i=1, \dots, n$ is the $n \times n$ matrix Λ whose ij^{th} element is $\frac{1 - b_i \bar{b}_j}{a_i + \bar{a}_j}$, called the pick matrix.

Definition 3:

The NP problem is solvable if and only if $Q \geq 0$.

Lemma 3:

If the NP problem is solvable, then $Q \geq 0$.

Proof:

Doyle et al, 1992

Definition 4:

Let A be the matrix with ij^{th} element $\frac{1}{a_i + \bar{a}_j}$ and B with elements $\frac{b_i \bar{b}_j}{a_i + \bar{a}_j}$.

Then the pick matrix, $\Lambda = A - B$.

Lemma 4:

If at least one of the $b_i \neq 0$, then $\gamma_{\max} = \frac{1}{\sqrt{\lambda_{\max}}}$

where λ_{\max} is the largest eigenvalue of $A^{-1}B$. For the NP problem $G(a_i) = \gamma b_i, i=1, \dots, n, \gamma \geq 0$ the maximum γ is γ_{\max} such that $\gamma \leq \gamma_{\max}$.

Proof:

(Doyle et al., 1992)

For the standard 2-dof system, the transfer function from the reference input to the output is:

$$T = \frac{PG}{1+PG} \quad (5)$$

Since $P = \frac{N}{M}, G = \frac{X+MQ}{Y-NQ}$, then

$$T = N(X+MQ) \quad (6)$$

The frequencies at which $1 + P(s, \alpha)G(s) = 1 + L(s, \alpha)$ is zero are characterized by $L(s, \alpha)|_{s=j\omega} = -1$ or

$$L_o(j\omega) = -\frac{P_o(j\omega)}{P(j\omega, \alpha)} \text{ and the system is unstable.}$$

$$1 + L_o(j\omega) = \frac{P(j\omega, \alpha) - P_o(j\omega)}{P(j\omega, \alpha)}$$

$$\frac{L_o(j\omega)}{1 + L_o(j\omega)} = \frac{L_o(j\omega)P(j\omega, \alpha)}{P(j\omega, \alpha) - P_o(j\omega)}$$

$$= \frac{P_o(j\omega)K(j\omega)P(j\omega, \alpha)}{P(j\omega, \alpha) - P_o(j\omega)}$$

so the plant family is stable if and only if:

$$\left| \frac{L_o(j\omega)}{1 + L_o(j\omega)} \right| \neq \left| \frac{P_o(j\omega)K(j\omega)P(j\omega, \alpha)}{P(j\omega, \alpha) - P_o(j\omega)} \right| \quad \forall \omega \in [0, \infty] \quad (7)$$

Let

$$\gamma_{\min} = \inf_{K \text{ stabilizing}} \left\| \frac{L_o(j\omega)}{1 + L_o(j\omega)} \right\|_{\infty} \quad (8)$$

Define $T_o(s) = \frac{1}{\gamma} (NX + NMQ)$

The following NP interpolation problem is then posed: Find T_o such that the following interpolation conditions are satisfied:

$$T_o(z_i^1) = \frac{1}{\gamma} NX(z_i^1), \quad i = 1, \dots, n$$

where $z_i^1, i = 1, \dots, n$ are the zeros of NM including those at infinity. It is assumed that plant is strictly proper. Satisfaction of the interpolation condition implies:

$$NMQ(z_i^1) = 0 \quad (9)$$

This further imply no right hand plane zero cancellation in NM and Q and it follows that Q must be stable.

The pick matrix is

$$\Lambda = A - \gamma^2 B$$

$$\text{where } A_{ij} = \frac{1}{a_i + \bar{a}_j}, \quad B_{ij} = \frac{b_i \bar{b}_j}{a_i + \bar{a}_j}, \quad a_i = z_i^1,$$

and $b_i = NX(z_i^1)$. z_i^1 are the right half plane zeros of NM .

Therefore, γ_{\max} for which the problem is solvable is

$$\frac{1}{\sqrt{\lambda_{\max}}} \quad \text{where } \lambda_{\max} \text{ is the largest eigenvalue of } A^{-1}B.$$

Then a stabilizing controller exists such that:

$$\inf_{\omega \in [0, \infty]} \min_{\alpha \in \Omega} \left| K \frac{P_o}{1 - P_o/P} \right| > \gamma_{\min} \quad (10)$$

Since

$$\left| K \frac{P_o}{1 - P_o/P} \right| \in [\mu, \infty] \quad \forall \omega \in [0, \infty], \alpha \in \Omega$$

where $\mu \in \Omega$.

Let $\mu_{\min} = \inf_{\omega \in [0, \infty]} \mu$ then the following corollary is obtained.

Corollary 4:

If $\left\| \frac{L_o}{1 + L_o} \right\|_{\infty} < \mu_{\min}$, then the family of plants is

robustly stable (i.e. $\left| \frac{L_o}{1 + L_o} \right| \neq \left| K \frac{PP_o}{P - P_o} \right|$).

The above corollary can be used to check if a compensator, K_{PID} (that stabilizes the nominal plant) is robustly stable. In other words, if we can find a member of the plant family for which the maximum

peak (i.e. $\left\| \frac{L_o}{1 + L_o} \right\|_{\infty}$ since any member of the family

can be chosen as the nominal) value specified is violated, then that K is unacceptable.

Theorem 6:

If $\inf_{\omega \in [0, \infty]} \min_{\alpha \in \Omega} \left| K(j\omega) \frac{P_o(j\omega)}{1 - P_o(j\omega)/P(j\omega, \alpha)} \right| > \gamma_{\min}$, where

$$\gamma_{\min} = \min_{K \text{ stabilizing}} \left\| \frac{L_o(j\omega)}{1 + L_o(j\omega)} \right\|_{\infty}, \quad \text{then } K \text{ stabilizes the}$$

entire family $P(s, \alpha)$.

Proof:

Follows from corollary 4.

Theorem 6 is a variation of Theorem 3.1 in (Jayasuriya and Zhao, 1994):

If $\inf_{\omega \in [0, \infty]} \inf_{\alpha \in \Omega} \left| \frac{P(j\omega, \alpha)}{P(j\omega, \alpha) - P_o(j\omega)} \right| > \gamma_{s \min}$, then there exists a stabilizing controller for the entire family

$$P(s, \alpha) \quad \text{where } \gamma_{s \min} = \inf_{K \text{ stabilizing}} \left\| \frac{1}{1 + L_o(j\omega)} \right\|_{\infty}.$$

Corollary 5:

$$\text{Let } \inf_{\omega \in [0, \infty]} \left| \frac{L_o}{1 + L_o} \right| = \mu_T.$$

If $\gamma_{\min} < \mu_T$ and the plant family satisfies the conditions of Lemma 1, then the QFT controller satisfies the performance specification characterized in terms of the maximum allowable peak μ_T , on the complimentary sensitivity function.

Proof:

Obvious.

This corollary is useful in verifying whether a given controller can achieve a specified allowable peak value.

4. CONCLUSION

The result that the PID terms cannot span the whole real space have been shown by using the zero exclusion principle and the requirement that there can be no right half plane or imaginary axis pole-zero cancellations in forming the open loop transfer function. This restriction on the pole-zero cancellations was used to exclude plants with a zero at the origin from possible PID control as implemented in this paper. The Nevalinna-Pick interpolation was used to establish a lower limit on the peak magnitude of the complimentary sensitivity function. This would be useful in controller performance analysis to check if a specified peak value of the complimentary sensitivity function can be realized.

REFERENCES

- Doyle, J. C., B. A. Francis and A. R. Tannebaum (1992). *Feedback Control Theory*, Macmillan, pp. 66-75, New York.
- Horowitz, I. M.. (1991). 'Survey of Quantitative Feedback Theory (QFT)', *International Journal of Control*, **53**, pp. 255-291.
- Jayasuriya, S. (1993). 'Frequency Domain Design for Robust Performance Under Parametric, Unstructured or mixed uncertainties', *Journal of Dynamic Systems, measurements and control*, vol. **115**, pp. 439.
- Jayasuriya, S. and Y. Zhao (1994). 'Stability of quantitative feedback designs and the existence of robust QFT controllers', *International Journal of Robust and Nonlinear Control*, pp. 21-46 **4**(1).
- Nordgren, R. E., O. D. I. Nwokah and M. A. Franchek (1994). 'New Formulations for Quantitative Feedback Theory', *International Journal of Robust and Nonlinear Control*, **4**, pp. 47-64.

POINTING CONTROL FOR PRECISION FLIGHT TELESCOPES USING QUANTITATIVE FEEDBACK THEORY

Anthony E. Bentley

*Control Subsystems Department, Sandia National Laboratories, Mail Stop 0501, PO Box
5800, Albuquerque, New Mexico 87185-0501*

A pointing control system is developed and tested for a flying gimbaled telescope. The two-axis pointing system is capable of sub-microradian pointing stability and high accuracy in the presence of large host vehicle jitter. To achieve the design specifications, high-accuracy, high-resolution, two-speed resolvers were used, resulting in gimbal-angle measurements stable to 1.5 microradians. In addition, on-axis inertial angle displacement sensors were mounted on the telescope to provide host-vehicle jitter cancellation. The feedback compensation was designed using Quantitative Feedback Theory.

1. INTRODUCTION

The two-axis gimbaled telescope is shown below in Figure 1. This project was funded to retrofit the telescope (which was built over ten years ago) to incorporate the latest advances in servo technology and thereby achieve an "order-of-magnitude" improvement in pointing accuracy and line-of-sight stability. The telescope was retrofitted with precision resolvers and new (higher torque) motors. On-gimbal Inertial Angle Sensors were also added to enhance inertial pointing stability. A servo system was developed that blends feedback from the resolvers together with the inertial angle sensors to achieve less than one microradian line-of-sight pointing stability or jitter, ± 1.5 microradian pointing resolution and ± 30 -microradian accuracy.

This paper will describe, the new servo system including each sub-system, namely: the gimbal, Inertial Angle Sensors (IAS), resolvers, Inertial Measurement Unit (IMU), feedback compensators, motor power amplifiers, and IAS notch filters. The pointing performance of the refurbished telescope is also presented.

Two separate models were used depending on the operating mode of the telescope. For large re-targeting maneuvers, the telescope is a *Multiple-Input Multiple-Output* (MIMO) servo system with significant non-linear interactions between the two gimbal

axes. However, for small maneuvers, gimbal interactions can be ignored—which reduces the model to two de-coupled *Single-Input Single-Output* (SISO) systems with disturbances. The command input is labeled "R" while the main output is the inertial pointing angle. Although, the gimbal angle is also an output, it will not be controlled independently of the inertial pointing angle. Axis de-coupling is possible because both axes of the telescope are balanced—the center of mass is very close to the center of rotation.

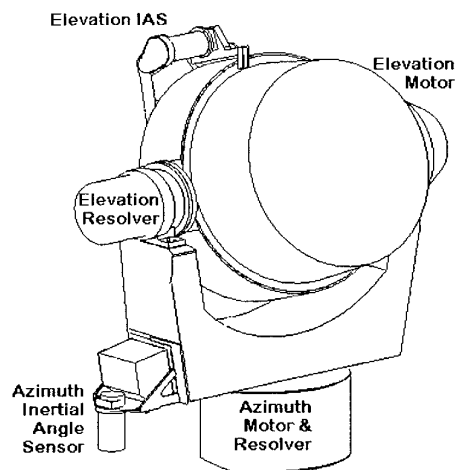


Figure 1. Telescope gimbal.

A simplified flow graph of the servo system is shown below in Figure 2. While only one axis is shown, with a few parameter substitutions the flow diagrams for both are identical. In Figure 2, and throughout this study, the telescope angle definitions are as follows. The gimbal angle of either axis with respect to its base is referred to as " θ ," the inertial gimbal angle is " Y ," and the angular position of the gimbal base is a disturbance and is therefore labeled " D ." The relationship between these angles is: $\theta = Y - D$.

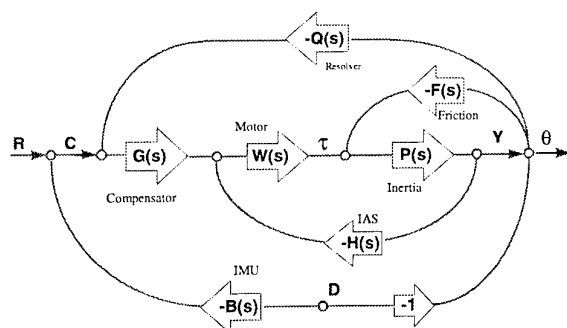


Figure 2. Single-axis (de-coupled) servo model

The pointing *resolution* and *accuracy* requirements are imposed on the gimbal angle θ measurement and are achieved by using high accuracy resolvers and resolver-to-digital converters. The resolvers provide absolute knowledge of the gimbal angle relative to the telescope base to ± 30 -microradian *accuracy*. This is a physical limitation of the resolvers due mainly to alignment limitations. The resolvers provide an output, which is an analog modulated AC signal. In order to use the resolvers as feedback sensors, the output must be demodulated and digitized. The resolver-to-digital converter circuits provide digitized resolver measurements that are stable to 22 bits. Thus the *resolution* of the resolvers is $2\pi / (2^{22}) = 1.5$ microradians.

The reference command " R " is the *absolute line-of-sight* pointing requirement on the inertial output " Y ." Because there is no low-frequency inertial sensor on the telescope, we have no absolute DC measurement of the inertial pointing angle " Y ." Thus, " Y " must be estimated based on the attitude of the vehicle " D " (which acts as a disturbance) as measured by the Inertial Measurement Unit (IMU) and the gimbal angle θ . An on-board navigation processor computes the inertial command needed to track a point on the ground, and subtracts from that command the attitude of the vehicle, to issue the gimbal command " C " which is the absolute pointing requirement on the gimbal angle θ . These navigation computations are not part of the servo system as described in this paper. The command input to the servo system herein described is the gimbal command " C ."

The commanded input " C " is the desired gimbal angle θ , which if followed perfectly at low frequency would cause the telescope to track the desired point on the ground. It contains both the inertial attitude data of the vehicle " D " and the line-of-sight informa-

tion from the navigation solution. However, the high-frequency information contained in the command " C " is less than ideal for frequencies above about 2 Hz due to bandwidth limitations of the IMU as well as a variable latency in the vehicle attitude data stream. Thus the on-gimbal Inertial Angle Sensors (IAS) are used as local feedback sensors to cancel high frequency telescope *jitter*.

In summary, the *accuracy* and *resolution* of the telescope are performance measurements on the gimbal angle θ , while the *absolute line-of-sight* and *line-of-sight jitter* specifications are requirements on the inertial angle " Y ." All four requirements must be met in order for the telescope to track a point on the ground with a stable (jitter-free) image. However, since all pointing requirements are related by the equation $\theta = Y - D$, the two outputs θ and Y need not be controlled independently of each other. The system *accuracy* and *absolute line-of-site* performance limit how closely the telescope can acquire and center a given target in the field-of-view. Once a target has been acquired, the system *resolution* limits how well the target can be tracked. The *line-of-sight jitter* determines how much *shaking* and *blurring* are seen in the final image. Assuming that the servo system has large DC gain, the *accuracy* and *resolution* specifications are both met by the resolver and resolver-to-digital converter designs, while *absolute line-of-sight* requirements are the responsibility of the aforementioned navigation processor (not described in this paper). Finally, the *line-of-sight jitter* requirements are met by the careful design of the servo system whose description follows herein.

The *plant* in Figure 2, labeled $P(s)$, models the effect of gimbal inertia " J ," that is: $P(s) = 1/(Js^2)$. In reality there are also structural resonances in the plant $P(s)$ that are not represented in the model. The telescope was being refurbished while the servo controls were being designed, so it was not available for study and identification of structural resonances. Because of a tight delivery schedule, neither was there enough time nor opportunity to fully study the plant once the refurbished telescope was completed. Thus, the structural resonances were never incorporated into the plant model. However, the effects of said resonances were successfully dealt with in an empirical manner using notch filters installed shortly before delivery of the telescope. This is described in a subsequent section of this paper.

The input to $P(s)$ is torque " τ ," while the output is the inertial angle " Y ." The torque input to $P(s)$ comes from two sources: 1) $W(s)$ which collectively represents the motor windings, the power amplifiers (which deliver current to the motor), and a feedback compensator, and 2) $F(s)$ which represents gimbal friction. Of course, friction opposes the relative motion and thus carries a negative sign.

The gimbal angle θ is measured by two high-accuracy resolvers (a 1x and a 64x resolver). In Figure 2, the resolvers together with the *Resolver-to-*

Digital (R/D) converters are lumped together and labeled Q(s)—and for simplicity, will hereafter be referred to as the resolver. The inertial angle “Y” is measured with a Systron Donner *Inertial Angle Sensor*¹ (IAS) and is labeled H(s) in Figure 2.

Because H(s) rolls-off at low frequencies, another sensor was needed to cancel the low-frequency components of the disturbance “D.” A connection to the Inertial Measurement Unit (IMU) on the host vehicle was added to the telescope pointing system to provide low-frequency *feed-forward* cancellation of the base disturbance. Of course, since the IMU is located off-gimbal, a transformation is necessary to convert host attitude data into gimbal coordinates. The frequency response of the IMU together with the coordinate transformation are lumped together in Figure 2, and labeled B(s). The transformed host attitude data are subtracted from the desired pointing angle “R” to produce the commanded angle “C.” This calculation, together with the coordinate transformation are computed on a navigation processor outside the servo controller system as described in this report, however, these components are shown in Figure 2 for completeness.

Finally, there is the compensator G(s). The function of G(s) is to blend the low-frequency data coming from B(s) and Q(s) with the “high-frequency” feedback data coming from the inertial sensor H(s)—producing a “smooth” transition between the two sensors.

2. IDENTIFICATION OF FIXED COMPONENTS

In this section we identify the *transfer functions* of those components in the servo that are *fixed* in the sense that they are not available for modification by the design process. We also quantify the uncertainties in their parameters. For example, elevation gimbal inertia is estimated at 0.6 kg-m². This estimate was made prior to the telescope being completed so for design purposes elevation inertia was allowed to vary between 0.5 and 0.7 kg-m². Azimuth gimbal inertia depends on elevation angle θ as per Equation 1 below. For an elevation angle of 90 degrees, azimuth inertia is approximated at 1 kg-m², for 180° it is estimated at 0.75 kg-m².

$$J_{az} \approx 0.35 + 0.4 \cos^2(\theta) + 0.65 \sin^2(\theta) \text{ kg-m}^2 \quad (1)$$

The Inertial Angle Sensor H(s) is a *band-pass* device whose bandwidth is between 2 Hz and 10 kHz. The theory of operation, application and evaluation of the IAS is further explained in Reference 1.

The nominal transfer function of the IAS is, given by Equation 2 below, has been found to vary slightly with temperature. The manufacturer provided four different transfer functions to represent H(s) at various temperatures (Equations 3 through 5). This

set of four was used to represent the variation in H(s) as a function of temperature.

$$H_n(s) \equiv \frac{s^3[s+187][s+7.6]}{[s+201][s+4][s+1][s^2+17s+15^2]} \quad (2)$$

$$H_2(s) \equiv \frac{s^3[s+151][s+6.9]}{[s+163][s+4][s+2][s^2+21s+15^2]} \quad (3)$$

$$H_3(s) \equiv \frac{s^3[s+151][s+8.5]}{[s+163][s+4][s+1][s^2+20s+15^2]} \quad (4)$$

$$H_4(s) \equiv \frac{s^3}{[s+0.47][s^2+17s+13^2]} \quad (5)$$

A Bode plot of the IMU, B(s) was provided from the host vehicle contractor. From this plot, a nominal transfer function B_n(s) was empirically determined that matched the Bode plot. The transfer function, given by Equation 6 (excluding the time delay), is shown below. For design purposes, the dominant pole at 300 rad/sec was varied $\pm 20\%$, while its damping ratio of 0.6 was varied $\pm 10\%$. A sample space of sixteen variations on B(s), plus the nominal, was used to represent the uncertainty in the IMU.

$$B(s) \equiv \frac{300^4(1000)[0.205s+1]}{[0.201s+1][s^2+360s+300^2][s+1000]} \quad (6)$$

The nonlinear behavior of bearing friction was simulated with the Dahl friction model²—whose differential equation is shown below in Equation 7. The telescope manufacturer estimated the Dahl friction model parameters as shown below in Table 1.

$$\frac{dF}{dt} \equiv \text{abs} \left\{ 1 - \text{sign} \left(\frac{d\theta}{dt} \right) \frac{F}{F_{\max}} \right\} (\text{slope}) \frac{d\theta}{dt} \quad (7)$$

Axis	Running Torque F _{max} (Nm x 10 ⁻³)			Slope (Nm/rad.)		
	Min.	Nom.	Max.	Min.	Nom.	Max.
El.	5	10	21	3.5	7	14
Az.	21	42	85	26	52	104

Table 1. Dahl friction model parameters

In order to include the nonlinear effect of bearing friction into the design process it was convenient to convert the nonlinear Dahl effect into an equivalent frequency response. This was done using the *describing function technique*. That is, the response of the nonlinear model to various sinusoidal inputs was measured, and the input/output transfer function was derived from these data. Sinusoidal inputs to equa-

¹ Harold Morris, “The Inertial Angular Displacement Sensor, Theory and Application,” (Systron Donner Inertial Division), February 18, 1987.

² P. R. Dahl, “A Solid Friction Model,” *The Aerospace Corporation, Space and Missile Systems Organization Air Force Systems Command*, Report No. TOR-0158 (3107-18)-1, May 1968.

tion 7 produce outputs with the same fundamental frequency, plus higher harmonics due to the nonlinear nature of Equation 7. The describing function technique tests the nonlinear system at one frequency at a time. The transfer function is determined at each frequency by ignoring the harmonics and computing the input/output ratio for the fundamental.

Accordingly, the Dahl equation was simulated at various frequencies, under various conditions. The input to the Dahl model simulations was the first derivative of angle with respect to time (θ dot), and the output was bearing friction torque. When the data for these simulations were reduced, it was found that the Dahl frequency response varies as a function of both frequency, and input magnitude. The Dahl friction behaves much like a single-order low-pass filter—whose roll-off frequency is a function of not only the Dahl parameters of F_{max} and $Slope$, but also a function of input magnitude. From these data, it was empirically determined that the describing function equivalent of Equation 7 could be written as shown in Equation 8. (Note that because the input to the Dahl equation is $d\theta/dt$ instead of θ , Equation 8 must be multiplied by “ s ” in order to yield the transfer function $F(s)$ with bearing friction as the output and θ as the input.)

$$\left| \frac{F(s)}{s} \right| = \left| \frac{slope}{s + a} \right| \quad (8)$$

$$\text{Where: } a = \frac{\pi \cdot slope \cdot \text{input magnitude}}{4F_{max}}$$

3. DESIGN PROCEDURE

Applying standard flow graph techniques to Figure 2 yields the transfer function shown below in Equation 9 for the inertial angle “ Y .” The first term in Equation 9 is the response due to the control reference signal “ R ,” while the second term represents the system response due to the disturbance “ D .”

$$Y(s) = \frac{RGWP}{1 + P[F + W(GQ + H)]} + \frac{DP[F + GW(Q - B)]}{1 + P[F + W(GQ + H)]} \quad (9)$$

The design goals for this project were: 1) 1.5 μ radian pointing resolution—that is, steady-state pointing to within one bit of the 22 bit commanded gimbal angle, 2) 1 microradian RMS line-of-site pointing jitter in the presence of host vehicle attitude disturbance “ D ” and 3) high agility—that is, *fast* re-targeting capability. Note that the transfer function for goal 1 is represented in the first term of Equation 9, while the stability performance (goal 2) is represented in the second term of Equation 9. The most challenging design goal is the stability criterion.

3.1 Resolver to Digital (R/D) Converter Design

By observing the second term in Equation 9, it is clear that the system response to disturbance “ D ” can be significantly reduced by designing $Q(s) \approx B(s)$. That is, we want the frequency response of the resolvers to match as closely as possible that of the IMU shown in Equation 6.

An Analog Devices chip (AD2S80A) was used for the R/D converter. It is a “type II feedback system” that requires external compensation to achieve the desired closed-loop response.³ The converter can be summarized as shown in Figure 3. In order for the transfer function of $Q(s)$ to closely match that of the IMU $B(s)$, another pole was added to the compensator, as shown in Figure 4. This produced the desired closed-loop response shown in Equation 6.

Figure 3. Block diagram of R/D converter

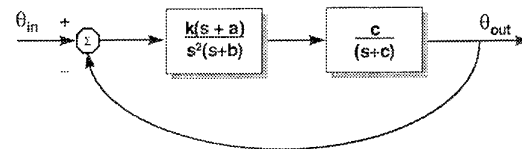


Figure 4. Modified block diagram of resolver-to-digital converter

3.2 Design of Feedback Sensor Blending Compensator $G(s)$

The most challenging aspect of this design was that of the compensator $G(s)$. The function of $G(s)$ is to blend the low-frequency data coming from $B(s)$ and $Q(s)$ with the *high-frequency* feedback data coming from the inertial sensor $H(s)$. The effective feedback sensor is the composite $G(s)Q(s) + H(s)$. Since $H(s)$ rolls-off for frequencies below 2 Hz, we want to use the resolver feedback data from $Q(s)$ for all frequencies below 2 Hz, and use the inertial angle sensor $H(s)$ for all frequencies above 2 Hz. Therefore, ideally $G(s)$ should cut-off $Q(s)$ *sharply* at 1 Hz, however, this presents a significant problem. Factoring the equation $G(s)Q(s) + H(s)$, reveals zeros in the right-half of the s -plane—resulting in unstable poles in the closed-loop system, (since according to root-locus analysis, closed-loop poles “seek” the open-loop zeros at high gain).

Using the root-locus technique, it is possible to modify $G(s)$ to cause $G(s)Q(s) + H(s)$ to have all zeros (and poles) in the left-half plane. However, this proved to be quite difficult when taking into account the divergence in $H(s)$ and $Q(s)$ due to temp-

³ Mark L. Schirmer, “Using Laplace and Fourier Transform Techniques to Model the Performance of Resolver to Digital Converters,” (Analog Devices Inc.: Memory Devices Division, 3 Technology Way, Norwood Massachusetts)

erature and component variations. That is, finding a compensator that meets this specification (no right-half-plane poles and zeros) is relatively simple for each combination of $H(s)$ and $Q(s)$ individually. But finding *one* compensator that satisfied this criterion for *all* combinations of H and Q in the set proved to be quite impractical using the root-locus technique. It was therefore necessary to find another method.

Quantitative Feedback Theory (QFT) is ideally suited for such a design challenge. Typical QFT designs specify *upper* and *lower* performance bounds on the closed-loop frequency response. In this case the design specifications on $G(s)Q(s) + H(s)$ were quite simple: 1) First we needed a *smooth transition* between the $Q(s)$ and $H(s)$ feedback sensors (that is, there should be no significant *peaking* over the desired operating range). 2) Secondly the composite sensor $GQ + H$ must be minimum phase (no right-half-plane zeros). To be more precise on the first specification, *smooth transition* was defined as $-2.3 \text{ dB} \leq |GQ + H| \leq 2.3 \text{ dB}$ for frequencies less than 100 Hz. Here $\pm 2.3 \text{ dB}$ was used for the upper and lower bounds which correspond to damping ratio of about 0.42—that is, the composite feedback sensor $GQ + H$ should have no poles or zeros with damping ratios less than 0.42. Designing to both of these specifications simultaneously, while taking into account plant uncertainty, turned out to be relatively simple using QFT.

Designing to requirement 1) is straightforward using QFT, however, meeting criterion 2) requires some problem manipulation. The sensor equation simply needs to be *rearranged* to fit the classical QFT approach: $GQ + H = H(1 + GQ/H) = H(1 + L)$, where $L = GQ/H$.

If $1 + L$ is minimum phase and stable, then the composite sensor $GQ + H$ will be also. As long as G and Q are stable, and H is minimum phase $1+L$ will be stable. To guarantee that $1+L$ is minimum phase the Nyquist criterion needs to be satisfied. Since $L(s)$ has neither right-half plane poles nor zeros, we can simply design $L(s)$ to have no encirclements of the critical point. On the Nichols chart, the critical point is found at 0 dB and -180 degrees. Thus if $L(s)$ crosses 0 dB to the right of this critical point, then we will have no encirclements, and our system will be stable and minimum phase. Ideally, of course, we would want to have some phase margin when $L(s)$ crosses 0 dB, so we will stay a considerable distance away from the critical point—specifically, we will stay outside the 2.3 dB Nichols chart contour.

Figure 5 shows the Nichols plot of the compensated nominal plant $GL_n(s) = GQ_n/H_n$. The performance bounds were defined as $-2.3 \text{ dB} \leq |GQ + H| \leq 2.3 \text{ dB}$ with respect to the nominal plant Q_n/H_n . At each frequency where bounds were calculated, there are two bounds shown in Figure 5. The dashed lines represent the upper bound of $|GQ + H| \leq 2.3 \text{ dB}$, while the solid lines represent the lower bound $-2.3 \leq |GQ + H|$. As long as the compensated nominal plant $GL_n(s)$ lies below the dashed lines, and above the solid lines at each frequency, the design criteria will be satisfied for all combinations of Q and H in the set. A lead-lag compensator $G(s)$ was designed to meet the design specifications at all frequencies— $G(s)$ is given in Equation 10.

$$G(s) = \frac{27[s+4]}{[s+9][s+12]} \quad (10)$$

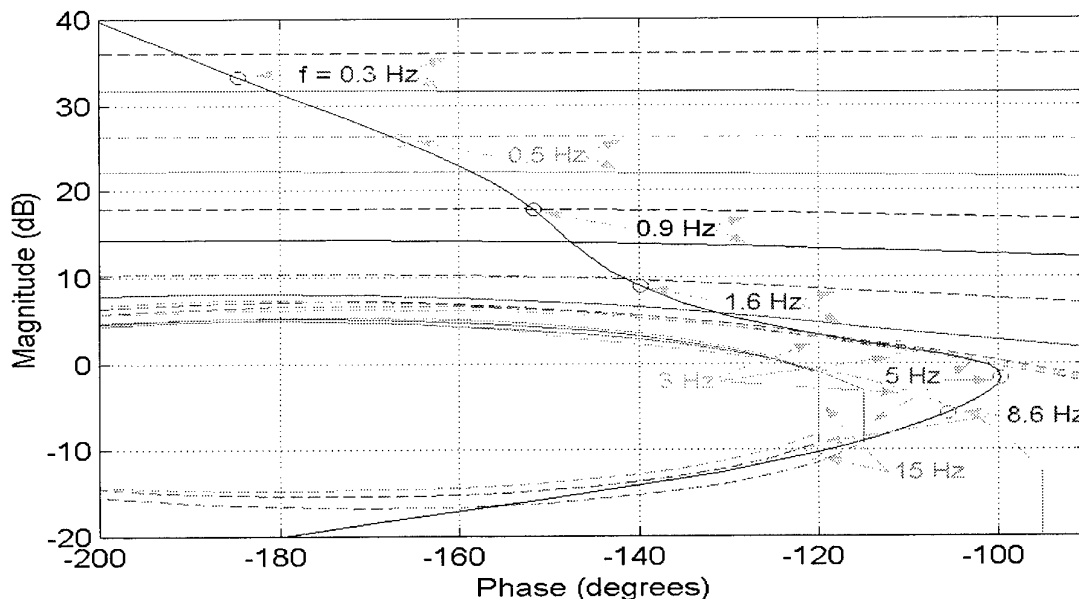


Figure 5. Nichols plots of GQ_n/H_n with bounds on $GQ + H$.

Figure 6 shows a Bode plot of $GQ(s)$ along with $H(s)$, and a simulated disturbance $D(s)$ as measured by $B(s)$. This sample disturbance is taken as the absolute worst case that could be expected on the host vehicle. Note the large spike at 4.5 Hz. Figure 7 shows the Bode plot of the composite sensor $G(s)Q(s) + H(s)$.

3.3 Redesign of Feedback Sensor Blending Compensator $G(s)$

The simulated host vehicle pointing error $d(t)$ contains a ± 6 microradian jitter at 4.5 Hz. The host vehicle attitude data from $B(s)$ is sampled at 40 Hz, and contains a variable latency. Every other sample has a maximum latency of 15 milliseconds, with the remaining samples having a latency of 25 milliseconds. Since this delay is not inside the feedback loop, it will not affect stability, but it severely restricts the disturbance rejection performance. Detailed simulations revealed that because of this variable latency, attenuation of the 4.5 Hz jitter was quite difficult. The impasse is due to the fact that the 4.5 Hz disturbance is measured by both the inertial angle sensors $H(s)$ as well as IMU $B(s)$, but is corrupted in $B(s)$ by the variable latency. The delay becomes more significant at higher frequency, causing the two sensors $B(s)$ and $H(s)$ produce conflicting information on $D(s)$ at 4.5 Hz, which seriously limits disturbance attenuation.

Ideally, we would have rolled-off $B(s)$ at a lower frequency so it would not see the 4.5 Hz. However, as it turns out, a certain amount of over-lap between the two sensors is needed in order to satisfy the minimum phase requirement.* Thus, another approach was needed to further attenuate $D(s)$. To accomplish this, $G(s)$ was modified (as shown in Equation 11) to purposely violate the upper bound $|GQ + H| \leq 2.3$ dB for frequencies local to 4.5 Hz. The idea was to allow the 4.5 Hz jitter to come through the feedback sensor with a higher gain so that it could be acted upon more aggressively than its neighboring frequencies. In an effort to emphasize the uncorrupted information coming from $H(s)$ with respect to

$$G(s) = \frac{42[s + 4]}{[s + 14][s + 12]} \quad (11)$$

$B(s)$, a gain of 3 was added to $H(s)$.

* This conclusion is not immediately obvious and is not proved in this paper. It was reached while attempting to shape the nominal loop GQ_n/H_n . Suffice it to say that while shaping the loop it became clear that the QFT bounds could not be satisfied without some frequency overlap between Q and H . The high-frequency roll-off of Q is provided by G and if G is rolled off at too quickly the nominal loop approaches the critical point and ultimately violates the Nyquist criterion.

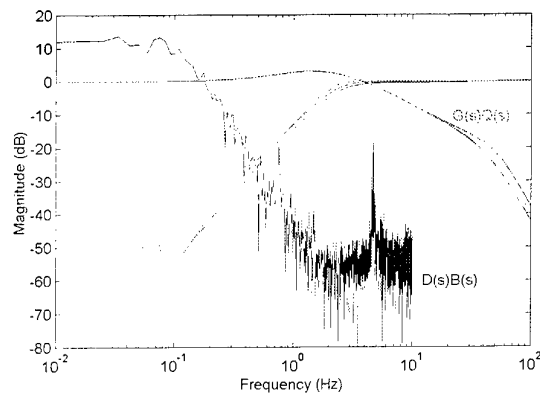


Figure 6. Bode plot of $G(s)Q(s)$ and $H(s)$ along with $D(s)B(s)$.

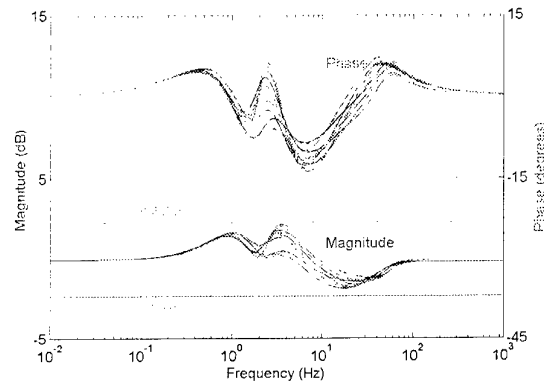


Figure 7. Bode plot of $G(s)Q(s) + H(s)$

This significantly improved the disturbance attenuation at 4.5 Hz, however, when the servo was implemented on the actual telescope, large structural resonances in the inertial angle sensor mounts that attach the *Inertial Angle Sensors* to the telescope were discovered. The lowest of these resonances were too close to the system bandwidth to effectively notch-out, so it became necessary to sacrifice performance in order to avoid exciting the structural resonances. (These resonances will be discussed later in this report.) The gain on $H(s)$ was thus lowered from 3 to 1.5. The Bode plot of the composite sensor $GQ + H$ in Figure 8 includes the gain of 1.5 on the inertial angle sensor $H(s)$.

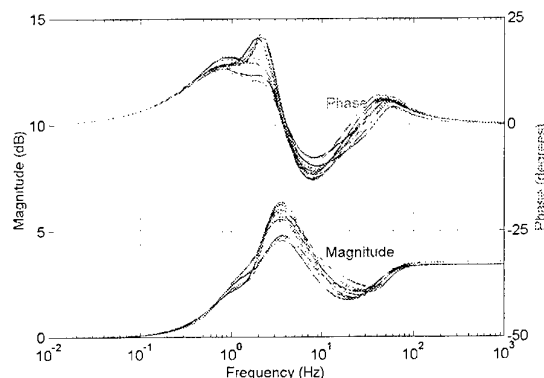


Figure 8. Bode plot of composite sensor $G(s)Q(s) + 1.5 H(s)$

3.4 Design of Feedback Compensator $W(s)$

As mentioned in the system overview, $W(s)$ collectively represents the motor windings, the power amplifiers (which deliver current to the motor), and a feedback compensator. The power amplifiers were designed as current drivers with current feedback from the motor windings. This effectively removed the motor winding dynamics from the design process, and the bandwidth of these amplifiers was large enough to be ignored with respect to the design of $W(s)$. The driving factor in the design of $W(s)$ was that of disturbance attenuation. The desired pointing stability is ± 1 microradian.

The worst-case host-vehicle attitude data contains disturbances of about ± 250 microradians at low frequency and ± 5 microradians at 4.5 Hz. For design purposes, it was assumed that the disturbance $D(s)$ would be no greater than the bound shown in Figure 9—derived by taking the Fourier transform[†] of the azimuth data shown in Figure 22. To achieve a factor-of-two design margin, the system was designed to attenuate this disturbance down to ± 0.5 μ radian.

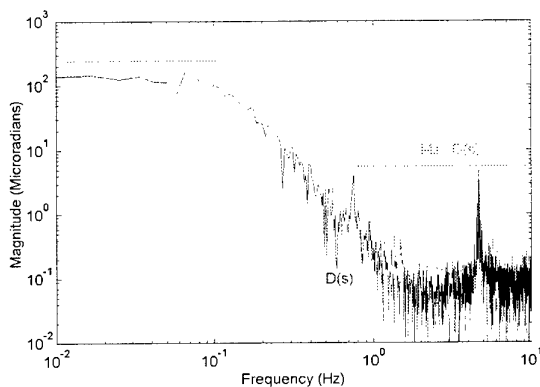


Figure 9. Fourier transform of $D(s)$ with maximum disturbance limits.

To accomplish this, an attenuation of 55 dB is needed at low frequencies and 22 dB is needed at the higher frequencies. The only other quantitative specification imposed on the design of $W(s)$ was the stability criterion—that the closed-loop system must have less than 2.3 dB of peaking.

Nichols chart stability and disturbance attenuation bounds were calculated from Equation 9 with respect to $L_n(s)$. To stabilize the servo loop, a compensator $W(s)$ was designed as given by Equation 12. Figure 10 shows the intersection of the stability and dis-

turbance attenuation bounds. Also in Figure 10 is shown the Nichols plot of the compensated nominal loop $W(s)L_n(s) = W(s)P_n(s)[G(s)Q_n(s) + H_n(s)]$. Note that the servo system is stable, and meets the bounds at all frequencies. A Bode plot of the open-loop compensated system is shown in Figure 11.

$$W(s) = \frac{k \times 10^6 b[s + a]}{a[s + b]} \text{ where, } \begin{bmatrix} a \\ b \\ k \end{bmatrix} = \begin{bmatrix} \text{Az.} & \text{El.} \\ 500 & 170 \\ 4400 & 2800 \\ 9 & 2 \end{bmatrix} \quad (12)$$

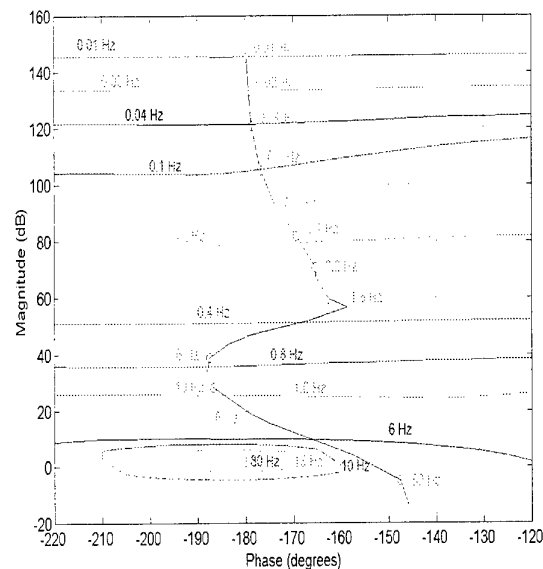


Figure 10. Nichols plot of compensated nominal loop $W(s)L_n(s)$ with bounds.

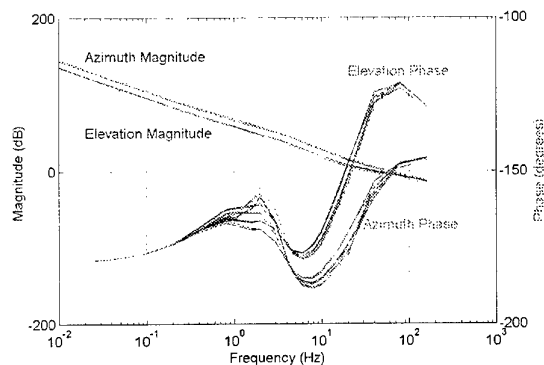


Figure 11. Bode plot of open-loop system $W(s)L(s)$.

A Bode plot of the closed-loop disturbance attenuation is shown in Figure 12 along with the disturbance attenuation design criteria—which are met at all frequencies. The disturbance attenuation criteria were derived from the disturbance bound shown in Figure 9, which was derived from the FFT of the simulated disturbance data $d(t)$.

[†] The FFT data presented in Figure 9 has been scaled such that there is a one-to-one correspondence in magnitude between the time $d(t)$ and frequency $D(s)$ domains. That is, the ± 5 μ radian time-domain disturbance at 4.5 Hz shows up in the FFT data as a spike of magnitude 5 microradians at 4.5 Hz. Likewise with other frequency components of the disturbance $d(t)$.

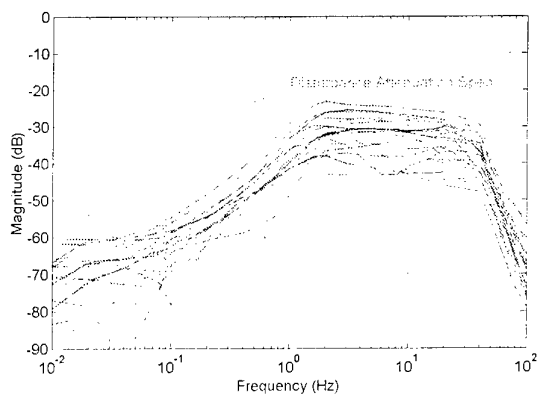


Figure 12. Disturbance rejection Bode plot.

3.5 Design of the Inertial Angle Sensor Notch Filters

The system was first tested on a single-axis gimbal with the same resolver, *Inertial Angle Sensor* (IAS) and roughly the same inertia, torque and bearing friction as the actual telescope. This provided an ideal test-bed for debugging servo hardware and software. However, once implemented on the actual telescope, structural resonances on the IAS mounts caused the telescope to oscillate. The single-axis test gimbal did not exhibit this phenomenon since the IAS was mounted rigidly at the center of the gimbal, while the makeshift telescope mounts, being retrofits, were significantly more compliant (see Figure 1). The open loop* frequency response of the servo system was measured using a network analyzer, and is shown in Figure 13. This revealed several destabilizing resonances starting at about 200 Hz.

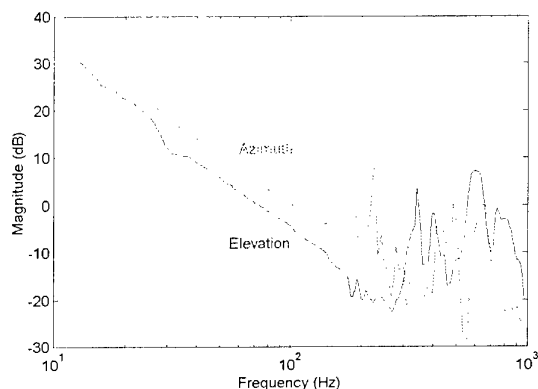


Figure 13. Open-loop frequency response showing resonances in the IAS mounts

The tight delivery schedule did not allow time to fully analyze and re-design the controller to account for these structural resonances. Instead, in-line notch filters were added to modify the IAS feedback sensor transfer function to ignore the jitter data at certain frequencies. The notch-filter board provided a maximum of six, second-order active-notch filters, together with a third-order low-pass filter for each axis.

* The input for these measurements was motor current while the output was angular displacement as measured by the Inertial Angle Sensors (IAS).

The transfer function of the notch filter is shown in Equation 17, while that of the low-pass filters is shown in Equation 18. Note that for elevation, ω_3 is infinite. The specific notch frequency for each filter is given in table 2 in Hz.

$$N(s) = \frac{s^2 + \omega^2}{s^2 + 2(0.18)\omega s + \omega^2} \quad (17)$$

Az.	264	335	406	504	2500	5000
El.		335	555	635	720	875

Table 2. Notch filter locations in Hz

$$LP(s) = \frac{\omega_1^2 \omega_2 [s + \omega_3]}{\omega_3 [s^2 + \omega_1 s + \omega_1^2] [s + \omega_2]} \quad (18)$$

where:

$\begin{bmatrix} \omega_1 \\ \omega_2 \\ \omega_3 \end{bmatrix}$	$=$	$\begin{bmatrix} 5000 & 1500 \\ 10000 & 10000 \\ 1500 & \infty \end{bmatrix}$
--	-----	---

The frequency responses of Figure 13 provided a general idea of what notch filters would be needed. However, the process used to select the number of filters used as well as their frequencies (described below) was not based on this preliminary data—since it was gathered before the telescope was entirely assembled, and would most likely be different than the final configuration. Also, since each notch filter adds unwanted phase lag below the notch frequency it was important to not use more notches than absolutely necessary to avoid eroding the phase margin.

The notch filters were selected as follows. The loop was closed around the telescope and allowed to resonate while the dominant oscillation frequency for each axis was measured. A notch filter was then built to eliminate that frequency and inserted in front of the IAS signal. The loop was again closed, while the next most dominant mode was identified. This continued until all oscillations were eliminated. The low-pass filter was then added to roll-off all high frequency resonances. The azimuth low-pass filter includes a zero at 239 Hz needed to restore phase margin that was lost due to the several notch filters.

IMPLEMENTATION RESULTS

Figure 14 shows the telescope step response. The top graph in Figure 14 shows the gimbal angles in degrees, while the bottom graph shows the output of the *Inertial Angle Sensor* (IAS) in microradians. Figure 15 shows actual in-flight pointing performance with typical host vehicle base motion disturbances. The azimuth pointing jitter as measured by the IAS's over this time interval is 295 nanoradians (rms) while the elevation pointing jitter is 385 nanoradians (rms). Note that both axes exceed the design goal of 1 microradian pointing stability.

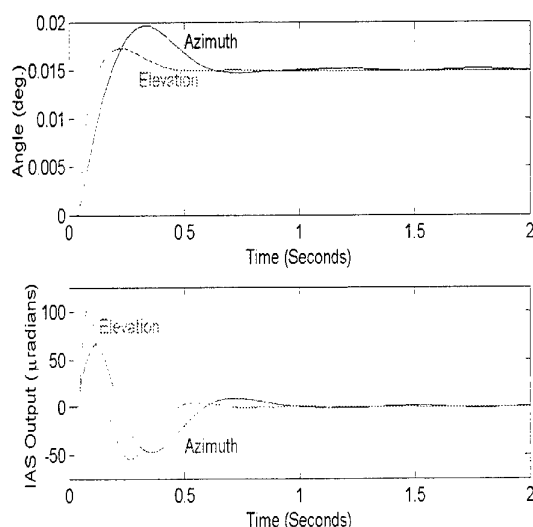


Figure 14. Telescope step response

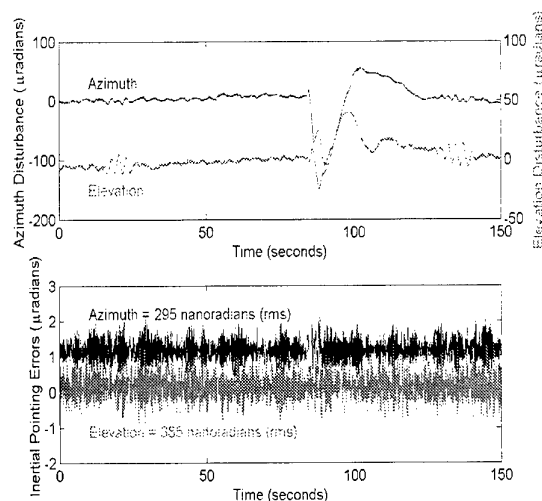


Figure 15. In-flight tracking performance

CONCLUSIONS

Quantitative Feedback Theory (QFT) provided a simple, yet powerful design tool which resulted a solution that exceed the performance goal of 1 microradian pointing stability in spite of large host vehicle pointing errors. One of the most challenging aspects of this project was the blending of feedback and feed-forward sensors to achieve *optimum** performance. These feedback sensors included the gimbal resolvers and Inertial Angle Sensors (IAS), whose signals were blended with the variably-delayed host vehicle attitude data coming from the Inertial Measurement Unit (IMU). The blending of these sensors was greatly simplified using QFT. Using this technique, design trade-off options could be easily weighed against each other in terms of cost versus performance benefit.

Another significant challenge was overcoming the structural resonances in the telescope. The performance goal of 1 microradian pointing stability resulted in a relatively high gain/bandwidth controller. Because of the large bandwidth, several structural reso-

nances were excited, causing pointing performance degradation. Several notch filters were added to the controller to eliminate the possibility of exciting these structural resonances. The extra phase lag introduced by these notch filters decreased the phase margin of the closed-loop system, which in turn further degraded pointing performance. Ultimately the *optimum** trade-off between gain-bandwidth and stability margin was obtained to produce a controller that exceeds the design goals without exciting structural resonances.

All components of the feedback compensator and notch filters were implemented in analog hardware. Thus, the controller modifications, which were necessary to avoid exciting the structural resonances, were more difficult to create. Because of the short design cycle, it was not possible to fabricate new printed circuit boards in time to meet the delivery schedule. Therefore, all modifications had to be carefully reworked on the original flight hardware. This provided another significant challenge.

Yet despite these obstacles, the pointing control system was delivered on time, with measured in-flight performance that meets the design goal with significant margin.

ACKNOWLEDGMENTS

Many people have contributed to this work. The author wishes to thank Dr. Isaac Horowitz, Professor Emeritus of the University of California at Davis, the University of Colorado and the Weizmann Institute of Science in Rehovot Israel, who developed "Quantitative Feedback Theory" (QFT)—which made this design both practical and understandable.

Sandia is a multiprogram laboratory operated by Sandia Corporation, a Lockheed Martin Company, for the United States Department of Energy under Contract DE-AC04-94AL8500.

* The trade-offs mentioned are only "optimum" in the sense that the design goals were satisfied with enough phase margin to allow for the full range of parameter variations anticipated in the system. Higher disturbance rejection capability could have been achieved at the expense of phase margin, however the designer selected the "optimum trade-off" between conflicting design goals based on measured performance data rather than any mathematical proof.

SOME IDEAS FOR QFT RESEARCH

Isaac Horowitz

QFT Publications, Boulder, Colorado. O132012@aol.com

Abstract: Feedback theory is much less popular now than 5 years ago. However, there is little question that the problem of achieving desired system tolerances from Uncertain Plants, at minimum Cost of Feedback, will remain an important, enduring one for many future generations. Although much progress has been made, it is minuscule in comparison with the extent of the problem. The purpose here is to suggest some significant QFT research problems, some tantalizingly on the boundary of the unknown. There have been in the past many suggestions for improvements in Feedback Synthesis. Most have been illusory, e.g. the Smith Regulator [9], because they were formulated in a qualitative context, without the disciplines of quantitative uncertainty and performance specifications, degrees of freedom, sensor noise, plant modification etc. Without such disciplines, it is impossible to properly evaluate competing techniques. The reader is referred to the 1991 Survey paper for some background, I. Horowitz, 1991, Survey of QFT, Int. J. Control, 53, 2, 255-91.

1. SINGULAR G COMPENSATION

Consider a SISO plant whose range of uncertainty includes right half-plane (rhp) poles and zeros, some even so close as to appear like dipoles. Ordinary design (even only for stability for one plant case at a time) results in impractical, negligibly small stability margins. In this approach [1], the Stability Problem is separated from the Sensitivity problem, by transforming the SISO system into a MIMO system for stability purposes, by use of MIMO compensation (G a matrix). It was shown that stability can then be achieved over the entire plant set. However, the system stability is highly sensitive to the G compensator. Since G can be a simple digital controller or active network, it can usually be designed much more 'robust' than a typical plant P (which may be highly complex and massive in extent), so much has been achieved. This is a fantastic result, violating normal Feedback tradition. Somehow, the very high system sensitivity to the plant, has been shifted to the G compensator. Note that Performance Sensitivity has been sacrificed. The loop transmission

has been dedicated to Stability. What is the mechanism involved here? Can similar results be obtained for highly uncertain unstable, 'nmp' nonlinear plants? There has been hardly any follow-up to this pioneering work.

2. NONLINEAR NETWORK SYNTHESIS

The following is a classical much-researched LTI synthesis problem: Given a desired transfer function, find a passive (or active) network for this purpose. An equivalent nonlinear problem is: Given a set $F_i(s)$ of transfer functions and a set of deterministic signal inputs $R_i(s)$, find a network such that for a given desired output set $Y_i(s)$, each Y_i has the transform $Y_i(s) = F_i(s)R_i(s)$. This is a very difficult problem. See [2] for a stab at it using Linear Time-Varying (LTV) elements, but with unsolved problems of sensitivity and stability. Obviously, such nonlinear feedback synthesis would be tremendously useful in feedback design, and in other applications.

3. THE SISO MULTIPLE-LOOP FEEDBACK PROBLEM (WITH AND WITHOUT PLANT MODIFICATION)

(a). There is available a finite (n) number of internal sensors, in addition to the usual output sensor, giving a $(n+2)$ degree of freedom system (one due to the prefilter). The research objective is to find a systematic means of designing the available $n+1$ feedback loops, to satisfy the quantitative specifications at minimum cost of feedback, i.e. with consideration of the $n+1$ sensor noise sources. (b). The solution of this permits solution of the much more complex analogous MIMO problem, i.e. given a n by n MIMO plant, with m available internal feedback sensors, and the usual n output sensors, develop a synthesis procedure for exploiting the available freedom to satisfy the quantitative specifications, with minimum cost of feedback. The 'equivalent disturbance' technique described in [3], enables the solution of this problem, by means of the above SISO technique of (3a). Furthermore, for both 3a, b, the techniques are applicable to Nonlinear, Time-Varying Plants, because for NO Plant Modification systems, the desired outputs determine the Plant internal signals. Needless to say, this is a much more complex problem if 'plant modification' is allowed [4, 11]. It is surely time for QFT researchers to provide some competition to Prof. B. C. Wang in the very important area of Feedback Systems with allowed plant modification. So far, he and his students have had the field to themselves.

4. NON-DIAGONAL COMPENSATION IN MIMO FEEDBACK SYSTEMS.

There has been disappointingly little work in this area. Most design problems have apparently been solvable by diagonal compensation. One might tackle this, by formulating a design problem which is not thus solvable. The ill conditioned high purity distillation column Challenge Problem (1992 CDC Conference) is herewith suggested for this purpose (see P. 419 of Ref. 5). Besides being on the verge of uncontrollability, the Plant has up to one minute pure time delay. To best of author's knowledge, the only solution to this Challenge Problem has been due to QFT. The H-infinity solutions offered at the Conference (Brighton, Gt. Britain), were quite inadequate. The QFT solution [5] was forced to use a nondiagonal prefilter, and barely satisfied the specs., but diagonal G was satisfactory. It is suggested that the specifications be made more difficult, in order to force use of nondiagonal G . This should be a good problem for thorough study of nondiagonal compensation in MIMO systems.

5. LOAD SHARING (PARALLEL PLANT) CONTROL

H. W. Bode, the great pioneer of feedback theory once noted that after he had deduced the 'cost of feedback' in single loop systems (see [5, Sec. 10.8]), he devoted much time to decrease of the cost, which was achieved by others [7,p.400]. It involves use of a family of plants, with feedback available from the outputs of the individual plants to the inputs of other family members. The relation between cost and benefits of feedback can then be dramatically different that in the normal feedback system. For example, in the single loop system, 40 db of feedback over (0,10) rps has a cost of about 400rps [5, 291]. But in a properly designed 2-plant parallel system, for the same cost, 80 db of feedback is available [7]; 120 db in a 3 plant system. Eitelberg [6] has pioneered in the control and stability aspects of these systems, but much work remains to be done to integrate this, to achieve the available superior Sensitivity properties of such systems.

6. COST OF FEEDBACK REDUCTION BY MEANS OF SPECIALIZED NONLINEAR DEVICES

FORE is a simple first order device which responds linearly to input $r(t)$ not equal to zero, but its output is zero when the input is zero. It has been shown [8] that for a large class of systems, this nonlinear device can be used to significantly reduce the cost of feedback, especially for plants with large high frequency gain uncertainty. It should be emphasized that many nonlinear devices have been suggested in the literature, which have describing function models which promise such properties (have phase lags smaller than in LTI elements, for the same magnitude slopes). The difficult challenge is how to integrate such nonlinear elements into a systematic quantitative design technique. To best of author's knowledge, this has been done only by FORE. There must surely be many more such nonlinear elements, awaiting the ingenious inventor.

7. TIME DOMAIN QFT, TIME-VARYING FEEDBACK, ON-LINE IDENTIFICATION

The great progress made by QFT has been thanks to its Frequency Domain formulation, because thereby the real time-domain system (differential equations, convolution), is transformed mathematically into an algebraic system, (transforms, multiplication), in the complex domain. One can hardly visualize achieving analogous results by working in the time domain. In a brilliant tour de force [10], Barnard has presented a Time Domain QFT synthesis theory for the two-degree-of-freedom SISO system.

Obvious criticisms are: its lack of the 'cost of feedback' concept, the effect of sensor noise, the difficulty of extensions to multiple-loop structures, the high mathematical expertise needed for practical design, compared to the very much simpler mathematics needed in Frequency Domain QFT, and the latter's easy, flexibility of extension to highly complex structure systems. Nevertheless, a detailed consideration and comparison of Barnard's work, would be highly desirable. No doubt much insight will be thereby obtained in time-transform relations in QFT, and the basic feedback mechanism. Also, one might then think in terms of time-varying feedback, for example if there is significant change in the extent of plant uncertainty as a function of time.

The latter idea is related to of On-Line Identification, almost totally ignored in existing QFT. There can be no question that even gross identification could tremendously reduce the cost of feedback. For example, suppose the zero frequency uncertainty, which is say 1000 to 1, could be even sloppily measured by a 2 to 1 error factor, then the LTI uncertainty is only 6 db rather than 60db; similarly for high\ frequency uncertainty the Oscillating Adaptive system is intended to do precisely that, and disciplined (quantitative) study of its many forms has led to a scientific theory for such systems, revealing feedback problems for which it is superior to ordinary LTI systems.[1 2].

Consider the following simple scheme for on-line identification, applied to the following: a 3 pole, 1 zero Plant, with Transfer Function: $[s(3)+As(2) + Bs(1) + C] / [Ds(1) + E]$, where $s(i)$ is s to i th power. In the time-domain, by repeated integrations (from 3 to 7), and letting $I(m)y$ represent the m th integral of $y(t)$ over some fixed interval, one obtains a set of 5 simultaneous equation in the unknowns A, B, C, D, E. For example, the first is: $y + (I_1y)A + (I_2y)B + (I_3y)C = (I_2u)D + (I_3u)E$, where u, y are the plant input and output. The fifth equation is $(I_4y) + (I_5y)A + (I_6y)B + (I_7y)C = (I_6u)D + (I_7u)E$. This is an ill-conditioned set of simultaneous equations, but can be readily solved, and gives good results. One must decide of course on interval of integration etc. Identification is then good, but only in absence of measurement noise; quite poor otherwise. The following technique was found useful to obtain fairly good results for even fairly significant y (output unbiased measurement) noise. A variety of methods can be used to do finite-time interval smoothing of the noise contaminated $y(t)$, giving say $y_x(t)$. Then use $y_x(t)$, instead of $y(t)$, to obtain the needed 5 equations to solve for A, B,..E. One can experiment to find better preliminary modification of the $y(t)$ measurement. This can, of course, be done to $u(t)$ it is also noisy. The fair success achieved by the above primitive technique, suggests that online identification is highly worth pursuing. The eventual objective is a

Unified theory for the optimum combination of ordinary QFT, and On - Line Identification. Sensor noise must be included, if the theory is to be meaningful.

8. DISTRIBUTED SYSTEMS

The Ordinary, Lumped (differential or difference) equation is a very small subclass of Distributed Systems (partial differential or difference equations). For many years, it was mainly treated by approximation, as a cascaded multiple loop system. By means of the double transform, QFT was extended to $y(x,t)$ type pde systems, involving only 2 variables [13]. An extension of the Nyquist Criterion was essential, because it is in the same mathematical language that is used in QFT quantitative design. Without it, QFT would be seriously impaired. Prof. Yakar Kannai was prevailed upon to supply us this essential tool [14]. However, the above [13] approach is pretty well limited to 2 variables x, t . By a brilliant tour de force, Dr M. Kelemen broke through this seemingly impenetrable barrier, basically extending QFT rigorously to Distributed (PDE) systems. This is done by Laplace Transform for the time variable, and Fourier Series for the others, or in many cases, Green functions, as in several of the references below. As with lumped multiple-loop systems with Plant Modification, in which advanced research has been the exclusive domain of one group, so QFT Distributed System theory has been almost the sole domain of one individual with various coworkers. (The author acknowledges the assistance of Dr. Kelemen in the following, briefly summarizing significant features of the progress made in Distributed QFT system theory). The System quantitative performance specifications can be functions of space or other non-directional variables, as well as of time (directional variable), to be achieved despite the Uncertainties in the analogous distributed plant variables. The same applies to the Boundary Conditions, which are absorbed as Disturbances [15]. As to be expected, Existence conditions are more complex than in Lumped systems. Other QFT features are carried over, such as applicability to Multiple-Loop, and to Nonlinear/Time-Varying Systems. However, the issues are very complex, as can be seen in Fritz-John [16]. Even for a linear PDE, the transfer function will be non-rational in the Laplace variable, with the other variables entering as highly nonlinear coefficients. The kind of great care one must take with lumped nonminimum- phase unstable systems is essential for the simplest PDE problem.

Even the simplest problem, like the heat equation with zero boundary conditions, involves a considerable amount of computations; the transfer functions are non-rational, and the time domain simulations are far from trivial.

A laboratory tested DETAILED QFT DESIGN procedure, with non rational plant, parametric uncertainty and boundary conditions, is described in [17,18]. A systematic theoretical study has been made concerning the enhancement by linear distributed feedback, of stability of LTI PDE plants. The space variable was assumed unbounded. So rational functions in two variables, Laplace and Fourier were involved. The main technical innovation was extension of the Gaarding hyperbolicity condition to infinite time. The PDE problem was thereby transformed into an ODE one in time, with coefficients the Fourier transforms on the space variables of the plant equation [19]. The conclusion of both these references is: Arbitrary regularity in space of the data (initial conditions) leads to arbitrary polynomial enhancement in time of stability, and uniformly in space applicable to both exponential and undamped plants -poles in left plane, but not bounded away from imaginary axis- the degree of stability depends not only on the system, but on the DATA (initial conditions and the input functions, both distributed in space) as well. This phenomenon is typical of distributed systems, but is lost in any finite dimensional approximation. Are such results the best obtainable, or is exponential enhancement of stability possible in general? See Sun [20] for some results. The practical designer need not be skilled in the mathematics of the above, only be aware of the practical limitations, so that he does not try to do the impossible. The extension to nonlinear PDE plants can be done with the second Nonlinear QFT Equivalent Disturbance technique. This is to be attempted [22].

The above cryptic summary reveals that THE DOOR HAS BEEN OPENED TO THE CREATION OF A TRULY QUANTITATIVE FEEDBACK THEORY FOR UNCERTAIN DISTRIBUTED SYSTEMS. THERE IS TREMENDOUS AMOUNT OF RESEARCH TO BE DONE, BOTH OF A PURE MATHEMATICAL NATURE, AND ESPECIALLY OF APPLIED COMPUTATIONAL NATURE.

9. THE SECOND QFT NONLINEAR TECHNIQUE

This method was originally meant for disturbance attention for Nonlinear Plants [22], in which the highest derivative of the plant output y appears linearly, and the input u appears linearly. The nonlinear terms become disturbances in an overall LTI equivalent system, and the design problem is one of disturbance attenuation of a LTI plant with only high-frequency gain uncertainty, which is a relatively easy design problem. Unlike the first QFT nonlinear technique, there is no need to solve backwards from a family of acceptable y , to the resulting family of u ; no need for plant templates and possibly difficult loop

shaping -- a considerable saving in design labor. See [5, Sec. 14.11], of a 4 by 4 highly interacting, uncertain, nonlinear time-varying mimo problem, solvable by this technique, within half a day without use of a computer. It is possible also to apply the technique to the Command input problem, by use of a nominal output, so that the allowed deviation from the nominal becomes a disturbance. It is also very convenient to use this technique to guarantee Quantitative stability, i.e. quantitative performance in response to deviations in original command or disturbance sets, or plant set, or of compensators, even for designs originally made by first QFT nonlinear technique, in which the nonlinear/time-varying plant set is replaced by an equivalent LTI plant set (see forthcoming book by Baños, Horowitz, Notes for European Nonlinear Course, Universidad de Murcia, Spain, September 2000). However, the applicability constraints noted in first sentence above is a very severe shortcoming, and the eliminations of the restrictions worthy of significant research. One suggested bulllike method to generalize the technique is as follows: (a) the nonlinear plant output y terms are treated as before, available from the specifications on the outputs due to the disturbances (they must include the bounds on the derivatives of the output, up to highest order). One solves backwards (as in the first QFT nonlinear technique) to find the nonlinear plant input u terms, and combines them with (a) to obtain their resulting extremes. Then, all the nonlinear terms due to both input and output, (and mixed ones), appear as equivalent disturbances, on a LTI plant with only high-frequency gain uncertainty. The design problem then becomes again, to shape the LTI loop to satisfy the performance bounds on y . The extra work needed, of the simple problem is solving backwards for the u inputs. But there is still no need for plant templates, and the loop shaping is much easier than in the first QFT nonlinear technique. For the case of nonlinear y terms with leading nonlinear derivatives, the plant prefilter technique of [23] can be used. It is worth investing much research effort to generalize and streamline this equivalent disturbance technique, because of its relative simplicity and versatility.

Conclusion: One can obviously conclude from all the above, that it is fallacious to say that most QFT problems have been solved. Rather, as of this date only a tiny part of the battle for "Achieving Desired Quantitative Performance Despite Uncertainty" has been won.

REFERENCES

1. Horowitz I., Yaniv O., 1987, Quantitative design for SISO non-minimum phase unstable plants by the Singular G method. Int. J. Control, 46, 1, 281-94.

2. Horowitz I., 1980, A nonlinear synthesis problem. Int. J Systems Science, 10, 1025-40.
3. Ibid, 1982, Uncertain MIMO systems with internal variable feedback, Int J Control, 36, 989-1009.
4. Horowitz I., Wang B.C., 1979, Quantitative Synthesis of Uncertain Cascade Feedback Systems with Plant Modification. Ibid, 30, 837-62.
5. Horowitz I. 1993. Quantitative Feedback Design Theory (QFT). Book. OFT Pubs., 4470 Grinnell Ave., Boulder, Colorado 80305. O132012@aol.com; Yaniv O. 1999. Quantitative Feedback Design, Linear and Nonlinear Control Systems. Book. Kluwer Academic Pub. Boston.
6. Eitelberg, E., 1999. Load Sharing Control NOYI3 Press, 58 Baines Road, Durban 4001, S. Africa. Controle@pixie.udw.ac.za
7. Horowitz, I., 1963. Synthesis of Feedback Systems Book. Academic Press, Secs. 8.8,9.
8. Horowitz I., Rosenbaum P., 1975, Nonlinear design for cost of feedback reduction in systems with large plant uncertainty, Int. J Control, 21, 977-1001.
9. Horowitz I., 1983. Some properties of delayed controls (Smith Regulator), Ibid, 38, 977-90.
10. Barnard R., 1993, Time domain OFT based on fixed points and homotopic invariance in Linfinity. Ibid, 58, 5, 1169-82.
11. Wang, B. C., Horowitz I., 1988. Quantitative synthesis of a 5-loop plant modification control system Ibid, 47, 1649-64.
12. Yaniv O., Horowitz I., Oldak S., 1968. Disturbance attenuation in singleloop dithered adaptive systems. Ibid, 48, 179-92.
13. Horowitz I., Azor R., Uncertain partially noncausal distributed feedback systems. Ibid, 40, 5, 989-1002,
14. Kannai, Y., 1982, Causality and stability of linear systems described by partial differential operators, Siam J on Control and Optim. 20, 669-74.
15. Kannai, Y., Kelemen, M., Horowitz, 1993. Spatial discretization and approximation of distributed loops and inputs. Int. J Control, 58, 933-45.
16. Fritz-John 1978. Partial Differential Equations. Springer, Berlin.
17. Kelemen, M., Bagchi, A., 1993. Modeling and feedback control of a flexible arm of a robot for prescribed frequency domain tolerances. Automatic 29, 899-909.
18. Kelemen, M., 1996. Time decay rates for undamped constant coefficients linear pde. J Diff. Equations, 125, 1, 215-38.
- 19 Ibid, 2001. Input\output stability degrees for undamped constant coefficient linear pde, IJC, 74, 387-97.
20. Sun, S. H., 1981. On spectrum distribution of completely controllable linear systems. Siam J Control, 19, 730-43.
21. Kelemen M., Akhrif O., Linear QFT control of a highly nonlinear multimachine power system, to appear in Int. J Robust & Nonlinear Control, to appear in Special Horowitz issue.
22. Horowitz I., 1982, Feedback systems with nonlinear uncertain plants, Int J Control, 36, 155-171.
23. Ibid, 1981, Improvement in nonlinear feedback technique by cancellation, ibid 34, 547-60.

PRE-FILTER DESIGN FOR TRACKING ERROR SPECIFICATIONS IN QFT

Edward Boje

School of Electrical and Electronic Engineering
University of Natal, Durban, 4041, South Africa
email: boje@nu.ac.za

Abstract: This paper shows how the pre-filter may be designed in quantitative feedback design of single-input, single-output systems with tracking error specifications (Eitelberg, 2000). The method uses gain and phase information for the pre-filter design. The design is conveniently performed on the log polar complex plane using standard CAD tools.

Keywords: Quantitative feedback design; QFT.

1. INTRODUCTION

Eitelberg (2000) investigated quantitative feedback theory (QFT) design for single-input, single-output systems with tracking error specifications. This note shows how the pre-filter is designed for this approach.

A two-degree-of-freedom control system is shown in Fig. 1. As usual in quantitative control system design, it is assumed that the linear(ised) plant transfer function is an element of a set, $P(s) \in \{P\}$, and this may include structured and unstructured uncertainty. (The dependence on the Laplace variable, s , or projection onto the imaginary axis ($j\omega$) will not be shown where it is obvious from the context.) In order to undertake engineering design, there must also be some closed loop specifications available. In most QFT work (see Horowitz (1991 or 1993) for a general reference), the tracking (and other) specifications are assumed to be only on the magnitude of the closed loop transfer functions. As Eitelberg (2000) has argued, bounding the closed loop transfer function within a disk around a nominal (model) performance often makes engineering sense. Such performance specifications result in sensitivity designs for tracking performance. They are compatible with norm-based methods, but the exact (structured and/or unstructured) plant uncertainty description is retained. QFT design with norm bounded specifications has previously been discussed for example by Horowitz (1979, 1991), and Nwokah, Jayasuriya & Chait (1991).

Given the system in Fig. 1 and client-specified model, $M(s)$, with model output, $Y_m(s) = M(s)R(s)$, the design task is to specify feedback controller, $G(s)$ and pre-filter, $F(s)$ to meet relative tracking error specifications. The relative tracking error transfer function, E_k^r , of the k^{th} plant is defined as follows:

$$E_k^r R = Y_m - Y_k \quad (1)$$

Eitelberg (2000) does not use a model reference (i.e. $M(s)=1$) which means that the relative tracking error

must become large at frequencies where the closed loop transfer function (reference to output) has low gain. A model reference extends the frequency range over which the relative tracking error specification is useful as it captures knowledge of the expected closed loop roll-off. Eitelberg (2000) accounts for unstructured uncertainty in the measurement system and pre-filter. This important consideration will not be pursued here. Let $H=1$ (no significant measurement dynamics) and $D=0$ (no disturbance as tracking behaviour is the subject of the paper). Define the complimentary sensitivity, $T_k = (I + L_k)^{-1} L_k$, with $L_k = P_k G$. Simple specifications on the relative tracking error would be to contain the relative error (element-wise) within a disk of client-specified, frequency-dependant radius, $A(\omega)$,

$$\begin{aligned} |E_k^r(j\omega)| &= |M(j\omega) - T_k(j\omega)F(j\omega)| \leq A(\omega) \\ \forall P_k &\in \{P\} \end{aligned} \quad (2)$$

A two-degree-of-freedom design is required to properly solve the design problem with minimum feedback bandwidth and to take care of unstructured and structured uncertainty in the plant. The design is performed at a set of discrete design frequencies, ω_i , $i = 1, 2, \dots$

2. PRE-FILTER DESIGN

Suppose that a controller, G , has been designed to meet or exceed the feedback design constraints. The pre-filter, F , can then be designed to satisfy the tracking error specification, eq(2). A simple approach to the design of F is to make use of the assumption that the nominal relative tracking error is zero,

$$F = F_0 = M / T_0 \quad (3)$$

By correct (realistic) specification of the model, M , the designer can ensure that F is rational, (strictly) proper and stable (even if L_0 is transcendental). The model would be required to exactly anticipate and replicate

right hand plane transmission zeros and other singularities in the nominal loop transfer function. If, as would be usual, the model is approximate, direct application of eq(3) may yield nuisance right hand plane singularities with small residuals that should obviously be discarded. Direct use of eq(3) may also result in a pre-filter of unnecessarily high order for practical problems.

To avoid high order feedback controllers, practical QFT designs usually have higher bandwidth than strictly necessary, meaning that there is some over-design. As opposed to "standard" QFT designs where the choice of nominal plant is arbitrary, there may also be over-design as a result of a poor or constrained choice of the nominal plant. At each design frequency, ω , any over-design of the feedback controller can be exploited to reduce the complexity of the pre-filter by finding the exact region (around F_0) within which F may lie. For any particular L , M , and A , eq(2) is a linear fractional mapping of F and therefore results in simple quadratic inequalities on a plant by plant basis.

For example, (unknown) $F = re^{j\phi}$, and (known)

$$T = L/(1+L) = x e^{j\alpha}, \quad M = y e^{j\beta} \text{ gives,}$$

$$\begin{aligned} & (y \cos(\alpha) - x r \cos(\phi + \beta))^2 + \\ & + (y \sin(\alpha) - x r \sin(\phi + \beta))^2 \leq A^2 \end{aligned} \quad (4)$$

Eq(4) can be solved for r , given any $\phi \in [-360^\circ, 0^\circ]$, for example using the Matlab QFT toolbox (Borgesani, Chait & Yaniv, 1998). The solution of eq(4) for a particular plant case and design frequency will divide the complex plane of F into acceptable and unacceptable regions. If the feedback controller design was successful, by construction, there is a non-empty intersection (over the plant set) of the acceptable regions for F at each frequency (or at worst the point, $F = M/T_0$). ($F(s)$ must satisfy Bode gain-phase relationships and, as discussed above, correctly specifying the model will ensure that a proper, rational and stable $F(s)$ exists.) Usually, in QFT the pre-filter is designed by magnitude only but the design outlined here is conveniently undertaken on the log-complex plane ($\arg\{F\}$ vs. $dB\{F\}$). The intersection of the regions given by eq(4) at frequency ω provides an exact bound for the design of $F(\omega)$.

3. EXAMPLE

The example is based on Example 2 in the Matlab[®] QFT toolbox (Borgesani, *et al*, 1998).

Original specifications:

$$\text{Plant: } P(s) = \frac{k}{s(s/a+1)}, \quad a, k \in [1, 10].$$

Tracking specifications:

$$\left| \frac{0.6584(s+30)}{s^2+4s+19.75} \right|_{s=j\omega} \leq |T_{Y/R}(j\omega)| \leq \left| \frac{120}{s^3+17s^2+82s+120} \right|$$

Design Nominal (specifically chosen):

$$P_0(s) = \frac{3}{s(s/3+1)}.$$

Approximately equivalent tracking error specifications, (illustrated at $s=j3$ in Fig. 2):

Model response (for specific P_0)

$$M(s) = \frac{1}{(s/4)^2 + 1.4s/4 + 1}$$

Tracking error tolerance:

$$A(\omega) = \left| \frac{0.12s}{((s/4)^2 + 1.2s/4 + 1)(s/11 + 1)} \right|_{s=j\omega}$$

The original feedback controller design,

$$G(s) = \frac{(s/1.1 + 1)(s/114 + 1)}{(s/43 + 1)((s/1000)^2 + 1.5s/1000 + 1)}$$

obviously satisfies the above tracking error bounds. The constraints on the pre-filter design are illustrated in Fig. 3 along with the (original) pre-filter,

$$F(s) = \frac{1}{(s/4)^2 + 1.4s/4 + 1}, \quad \text{that satisfies the}$$

constraints with low order and low bandwidth.

4. CONCLUSIONS

This paper has shown how to design the pre-filter in quantitative feedback design with tracking error specifications

5. REFERENCES

- Borgesani C, Chait Y & Yaniv O (1998), *MatlabTM Quantitative Feedback Theory Toolbox*, Mathworks Inc.
- Eitelberg E (2000), "Quantitative feedback design for tracking error tolerance", *Automatica*, vol. 36, no. 2, pp319-326.
- Horowitz I (1979), "Quantitative synthesis of uncertain multiple input-output systems", *International Journal of Control*, vol. 30, pp81-106.
- Horowitz I, (1991) "Survey of Quantitative Feedback Theory (QFT)", *International Journal of Control*, Vol. 53, No. 2, pp. 255-291.
- Horowitz, I (1993), *Quantitative Feedback Design Theory (QFT)*, Vol. 1, QFT publications, 4470 Grinnell Ave., Boulder, Colorado, 80303.
- Nwokah ODI, Jayasuriya S & Chait Y (1991), "Parametric robust control by Quantitative Feedback Theory," *American Control Conference*, pp. 1975-1980.

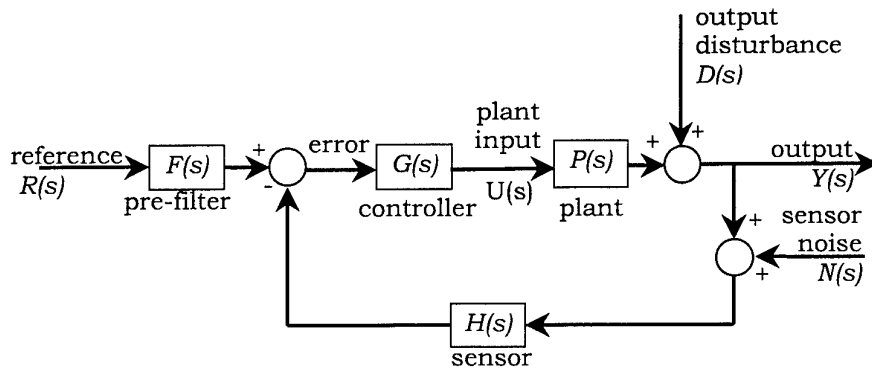


Figure 1 – Two-degree-of-freedom feedback system

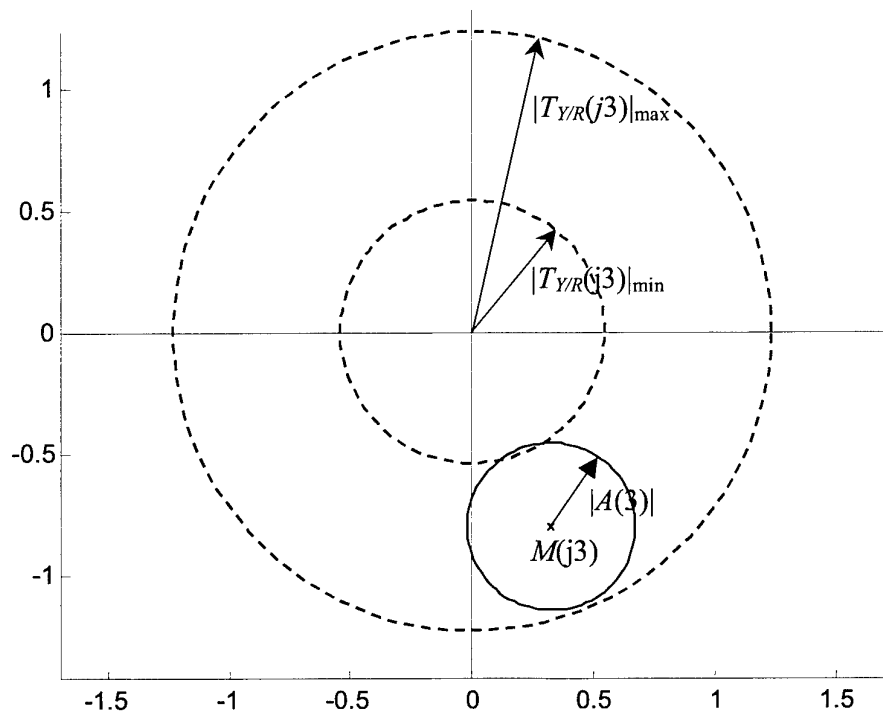


Figure 2 – Illustration of magnitude and nominal tracking error specifications

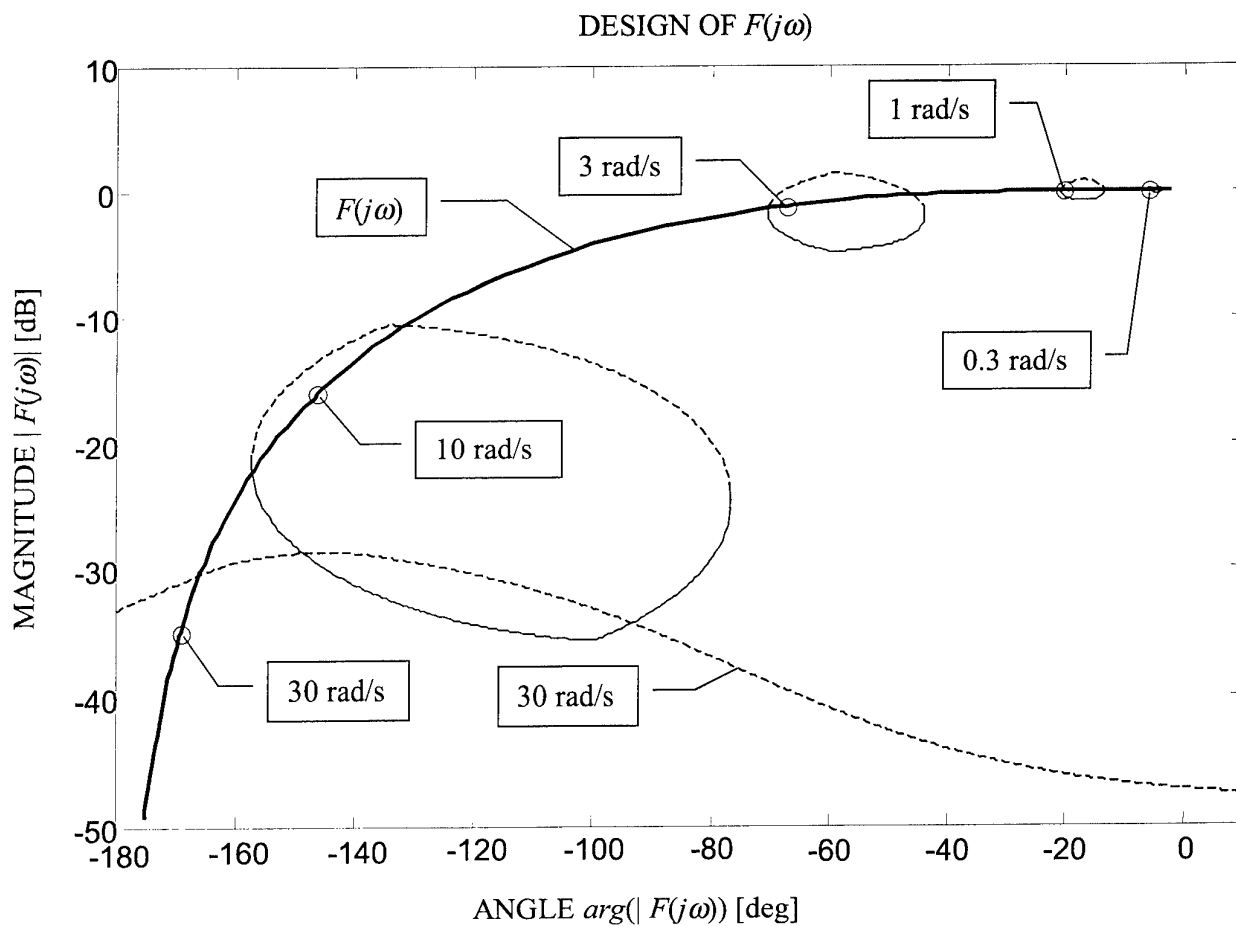


Figure 3 – Pre-filter design for tracking error specifications (dashed lines = “below” bounds, solid lines = “above” bounds)

QUANTITATIVE MULTIVARIABLE FEEDBACK DESIGN FOR A SCARA ROBOT ARM

I. Egaña, J. Villanueva, M. García-Sanz

Automatic Control and Computer Science Department, Public University of Navarre
 31006 Pamplona (SPAIN) Tel: +34 948 169387. Fax: +34 948 168924. Email: mgsanz@unavarra.es

Abstract: *Multivariable systems are currently considered one of the most challenging problems within Control Engineering. Loop interaction reduction and stability under the presence of plant uncertainties as well as system integrity are some of the problems attached to those processes. In this context, some previous papers have dealt with the loop coupling reduction in the QFT frame, taking into account the definition of a coupling matrix. Those techniques are applied in order to design the controller of a SCARA robot manipulator.*

Keywords: QFT, Robust Control, Multivariable Systems, Non-diagonal Matrix Controller, SCARA robot arm.

1. INTRODUCTION

Consider a $n \times n$ linear multivariable system, -see Figure 1-, composed of a plant P , a non-diagonal controller G , and a prefilter F , where $P \in \mathbf{P}$ and \mathbf{P} is a set of possible plants due to uncertainty.

The quantitative feedback design problem (Horowitz, 1979) of specifying a controller G , and a prefilter F to achieve certain tracking specifications will be considered. This work will focus on those systems with a high interaction level due to loop coupling.

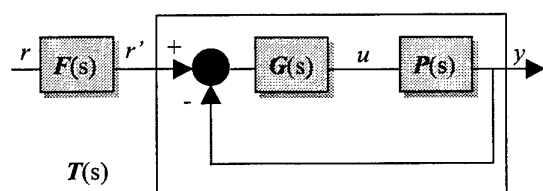


Fig. 1. Structure of a 2 Degree Of Freedom system composed of a linear uncertain plant $P(s)$, an two designed elements: a feedback controller $G(s)$ and a prefilter $F(s)$

In the last decades, many papers dealing with the design of controllers for uncertain multivariable systems have appeared: Rosenbrock (1970) used the Inverse Nyquist Array; Kidd (1984) extended the Direct Nyquist Array to uncertain systems; Horowitz (1979), and Horowitz and Sidi (1980), first used the Schauder's fixed point theory to justify a *quantitative* multivariable technique, improving it later (Horowitz, 1982); the Perron-Frobenius root method was used by Boje and Nwokah (1997 and 1999) in the QFT frame, as well as Yaniv (1995) and Franchek *et al.* (1997) included non-diagonal elements in the feedback controller; O'Reilly and Leithead (1991) proposed the Individual Channel Analysis and Design -ICAD-, etc.

Analogously to the gamma function of ICAD, the loop interaction with non-diagonal elements was studied in order to reduce the loop coupling in (Egaña and García-Sanz, 1999; Egaña and García-Sanz, 2000) and (García-Sanz, and Egaña, 2002). This yielded the development of a new design methodology for fully populated matrix controllers.

In this paper a controller design of a multivariable controller for a two-input/two-output SCARA robot arm is presented. Thus, the present work is a detailed

application of some considerations -explained in Egaña and García-Sanz (1999; 2000) and García-Sanz and Egaña (2002)- about multivariable design techniques for uncertain systems with a strong coupling behaviour.

The arrangement of the paper is the following. In Section 2 the performance specifications for the design problem are stated. In Section 3, a detailed description of the controller design is explained, and Section 4 concludes the paper emphasising the most relevant ideas.

2. UNCERTAIN MODEL AND PERFORMANCE SPECIFICATIONS

The process to control is a SCARA robot arm, manufactured by Adept Technologies. Figure 2 shows the Adept One robot manipulator, and Figure 3 the two joints -angles q_1 and q_2 - that are considered in this paper.

In order to present the control of two joints of a SCARA robot arm, in this Section the plant model and the desired performance specifications are presented, as well as a brief description of the theoretical principles that will be applied.

2.1 Plant Model

The Lagrange equations' method is used to find Equation (1) and Equation (2), which describe the dynamic behaviour of the two-link system. The real inputs are torques τ_1 and τ_2 -applied through power amplifier as u_1 and u_2 - commanded by electrical motors on joints 1 and 2, and the outputs are angles q_1 and q_2 .

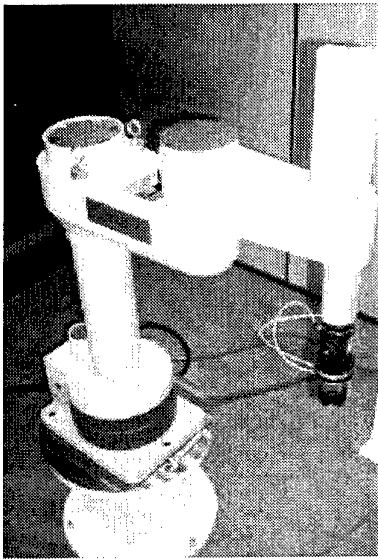


Figure 2. Adept One SCARA robot

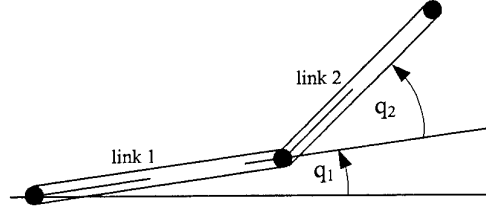


Figure 3. Considered joints of SCARA robot arm

$$(p_1 + 2 \cdot p_3 \cdot \cos(q_2)) \cdot \ddot{q}_1 + (p_2 + p_3 \cdot \cos(q_2)) \cdot \ddot{q}_2 + r_1 \cdot \dot{q}_1 + \tau_{c1} \cdot \text{sgn}(\dot{q}_1) = \tau_1 = \frac{u_1}{k} \quad (1)$$

$$(p_2 + p_3 \cdot \cos(q_2)) \cdot \ddot{q}_1 + p_2 \cdot \ddot{q}_2 + r_2 \cdot \dot{q}_2 + \tau_{c2} \cdot \text{sgn}(\dot{q}_2) = \tau_2 = \frac{u_2}{k} \quad (2)$$

where k is the power amplifiers' gain, r_i are coefficients of viscous friction, τ_{ci} Coulomb friction parameters associated with link i , and

$$\left. \begin{aligned} p_1 &= I_1 + I_2 + m_1 \cdot x_1^2 + m_2 \cdot (l_1^2 + x_2^2) \\ p_2 &= I_2 + m_2 \cdot x_2^2 \\ p_3 &= m_2 \cdot l_1 \cdot x_2 \end{aligned} \right\}$$

denoting I_i , moment of inertia of the i -th link; m_i , mass of the i -th link; l_1 , length of link 1.

Input signals u_1 and u_2 will be computed in counts [ct] and will be commanded to the robot motors by the amplifiers. Hence the robot parameters included in Table 1 are multiplied by a gain of 75 [ct/N·m] due to the power amplifier equipment.

Table 1: Coefficients of uncertain plant

	Minimum	Maximum	Nominal
$p_1 \cdot k$ [ct·s ² /rd]	719	813	766
$p_2 \cdot k$ [ct·s ² /rd]	186	200	193
$p_3 \cdot k$ [ct·s ² /rd]	134	230	182
$r_1 \cdot k$ [ct·s/rd]	67	381	224
$r_2 \cdot k$ [ct·s/rd]	11.6	91.9	51.75
$\tau_{c1} \cdot k$ [ct]	344	358	351
$\tau_{c2} \cdot k$ [ct]	262	323	292.5

Now it is possible to consider the Coulomb frictions as disturbances and the cosine value of q_2 as an uncertain parameter h between -1 and +1. Taking into account Equation (1) and Equation (2), it is easy to find the following transfer functions, which are the elements of the plant P defined as,

$$\begin{bmatrix} Q_1 \\ Q_2 \end{bmatrix} = \mathbf{M} \cdot \begin{bmatrix} u_1 \\ u_2 \end{bmatrix} = \begin{bmatrix} M_{11} & M_{12} \\ M_{21} & M_{22} \end{bmatrix} \cdot \begin{bmatrix} u_1 \\ u_2 \end{bmatrix} \quad (3)$$

$$M_{11}(s) = \frac{p_2 \cdot s + r_2}{s \cdot \Delta(s)} \cdot \frac{1}{k} \quad (4)$$

$$M_{12}(s) = \frac{-(p_2 + p_3 \cdot h)}{\Delta(s)} \cdot \frac{1}{k} \quad (5)$$

$$M_{21}(s) = \frac{-(p_2 + p_3 \cdot h)}{\Delta(s)} \cdot \frac{1}{k} \quad (6)$$

$$M_{22}(s) = \frac{(p_1 + 2 \cdot p_3 \cdot h)s + r_1}{s \cdot \Delta(s)} \cdot \frac{1}{k} \quad (7)$$

where,

$$\Delta = z_2 \cdot s^2 + z_1 \cdot s + z_0 \quad (8)$$

with the following coefficients,

$$\left. \begin{aligned} z_2 &= p_2 \cdot (p_1 + 2 \cdot p_3 \cdot h) - (p_2 + p_3 \cdot h)^2 \\ z_1 &= p_2 \cdot r_1 + r_2 \cdot (p_1 + 2 \cdot p_3 \cdot h) \\ z_0 &= r_1 \cdot r_2 \end{aligned} \right\}$$

2.2 Specifications

Consider the quantitative feedback design problem (Horowitz, 1979) of specifying a controller G , and a prefilter F , to achieve certain tracking specifications $A(\omega) = \{a_{ij}(\omega)\}$ and $B(\omega) = \{b_{ij}(\omega)\}$ for the function $T_{Y/R} = \{t_{ij}^{Y/R}\}$,

$$b_{ij}(\omega) \leq |t_{ij}^{Y/R}(j\omega)| \leq a_{ij}(\omega) \text{ for } i, j = 1, \dots, n \quad (9)$$

when,

$$y = [I + P \cdot G]^{-1} \cdot P \cdot G \cdot F \cdot r = T \cdot F \cdot r = T_{Y/R} \cdot r \quad (10)$$

and where all the matrices are 2×2 .

The desired performance specifications are the following,

- robust stability: at least 50° lower phase margin and at least 1.8333 (5.26 dB) lower gain margin (not simultaneously),
- control signals lower than 32767 [ct] for disturbance rejection of and tracking commands,
- reduction of coupling effect as much as possible,
- tracking specifications on $|T_{Y/R}(j\omega)|$ are to achieve tracking tolerances defined by,

$$a(\omega) \leq |t_{ii}^{Y/R}(j\omega)| \leq b(\omega) \text{ for } i = 1, 2 \quad (11)$$

where,

$$a(\omega) = \frac{3.5^2 \cdot (s/30 + 1)}{s^2 + 2 \cdot 0.75 \cdot 3.5 \cdot s + 3.5^2} \quad (12)$$

$$b(\omega) = \frac{2^2}{(s^2 + 2 \cdot 1.5 \cdot 2 \cdot s + 2^2) \cdot (s/10 + 1)} \quad (13)$$

The design presented below is part of a normal engineering design process, and is the first approach to design a competitive controller for the Adept One robot arm. The above specifications are limited by the achieved sampling time for the practical implementation, that is actually 10 ms. Further designs for force control are subjected to the improvement of this critical parameter.

2.3 Brief description of theoretical principles

García-Sanz and Egaña (2002) include a detailed description of the transfer function matrix of the system T expressed as in Equation (14).

$$\begin{aligned} T \cdot r' &= \left(I + (\hat{P}_d)^T \cdot G_d \right)^{-1} \cdot (\hat{P}_d)^T \cdot G_d \cdot r' + \\ &+ \left(I + (\hat{P}_d)^T \cdot G_d \right)^{-1} \cdot (\hat{P}_d)^T \cdot (G_b - (\hat{P}_b + G_b) \cdot T) \cdot r' = \\ &= \left(I + (\hat{P}_d)^T \cdot G_d \right)^{-1} \cdot (\hat{P}_d)^T \cdot G_d \cdot r' + \\ &+ \left(I + (\hat{P}_d)^T \cdot G_d \right)^{-1} \cdot (\hat{P}_d)^T \cdot C \cdot r' \quad (14) \end{aligned}$$

denoting \hat{P} as the plant inverse, and \hat{P}_d , \hat{P}_b , G_d and G_b the diagonal part -subscript d- and non-diagonal part -subscript b- of \hat{P} and G respectively.

The term of Equation (14) that includes the non-diagonal parts G_b and \hat{P}_b of the feedback controller and the plant inverse is called the *coupling matrix C*.

One hypothesis is needed to simplify the expression of each element of the coupling matrix C .

Hypothesis H1: suppose that,

$$|t_{jj} \cdot (\hat{p}_{jj} + g_{jj})| \gg |t_{kj} \cdot (\hat{p}_{ik} + g_{ik})|, \text{ for } k \neq j \quad (15)$$

Note that diagonal elements t_{jj} will be larger than the non-diagonals t_{ij} , so that after all, this Hypothesis H1 is quite reasonable. Then every element of the coupling matrix c_{ij} obeys the following Equation (16),

$$c_{ij} = g_{ij} \cdot (1 - d_{ij}) - t_{ji} \cdot (\hat{p}_{ij} + g_{ij}) \quad (16)$$

where δ_{ij} is 1 when i and j are equals. Otherwise, 0.

On the other hand, it is possible to approximate the diagonal elements t_{ij} of the transfer function matrix of the feedback loop as Equation (17).

$$t_{ij} = \frac{g_{ij} \cdot \hat{p}_{ij}^{-1}}{1 + g_{ij} \cdot \hat{p}_{ij}^{-1}} \quad (17)$$

Hence the elements c_{ij} of the coupling matrix can be written as,

$$c_{ij} = g_{ij} \cdot (1 - d_{ij}) - \frac{g_{ij} \cdot \hat{p}_{ij}^{-1}}{1 + g_{ij} \cdot \hat{p}_{ij}^{-1}} \cdot (\hat{p}_{ij} + g_{ij}) \quad (18)$$

It is important to emphasise that the non-diagonal elements of the controller G_b will be designed to reduce coupling interactions taking into account Equation (18).

Moreover, an optimum non-diagonal controller g_{ij}^{opt} was previously proposed in Egaña and García-Sanz (1999) defining the nominal plants \hat{p}_{ij}^N and \hat{p}_{ji}^N as those which minimise the non-parametric uncertainty radii $\Delta\hat{p}_{ij}$ and $\Delta\hat{p}_{ji}$ that comprise the plant templates,

$$g_{ij}^{\text{opt}} = g_{ij} \cdot \frac{\hat{p}_{ij}^N}{\hat{p}_{ji}^N}, \text{ for } i \neq j \quad (19)$$

Franchek *et al.* (1997) stated a multivariable technique to design fully populated controllers under the presence of uncertainty. As their work pointed out, for this purpose a *sufficient condition* to include non-diagonal elements is,

Condition C1: the plant P and its inverse \hat{P} are stable and do not have any hidden unstable mode.

This limitation is an inherent constraint for any similar technique, and therefore it is also an important remark to consider hereby. Note that the plant model described in Equations (3)-(7) achieve the above-mentioned condition.

The system is required for a last condition about the Relative Gain Analysis -denoted as RGA- proposed by Bristol (1966). Skogestad (1996) demonstrated that robustness could be only achieved for non-'ill-conditioned' multivariable uncertain plants. The relationship between condition number and RGA analysis was also included in the same paper, concluding that large RGA elements -above 10- lead to 'ill conditioned' plants. To summarise, the condition considered here can be expressed as follows,

Condition C2: The plant P is not 'ill-conditioned' for any of the possible plants in the whole set \mathbf{P} .

3. CONTROLLER DESIGN

In this Section, one controller system is tested on the Adept One SCARA robot arm: a controller designed by a non-diagonal technique (Egaña and García-Sanz, 1999; García-Sanz and Egaña, 2002).

The first step suggested by García-Sanz and Egaña (2002) is the RGA in order to pair input and output signals and to quantify *how much* coupled the system is.

Due to RGA properties, for 2×2 systems only one element of the RGA matrix Λ is necessary: the sum of the elements of every row or column is 1. Therefore, for a system like this, λ_{11} equals λ_{22} and λ_{12} equals λ_{21} . In addition, perfect decoupled systems yield diagonal elements equal to 1, and the rest of them equal to 0.

Figure 4 shows the first element λ_{11} for all the possible plants due to uncertainty. At low frequencies -below 0.06 rd/s- the coupled behaviour is very low, but as far as the frequency increases the system presents a more coupled dynamics. At a frequency of 0.2 rd/s the element λ_{11} reaches a maximum value of 1.8 that is rather high. The required bandwidth of the system derived from tracking specifications lies between approximately 2 and 3.5 rd/s. In those frequencies the maximum value of λ_{11} is greater than 4.5. Hence, the robot arm presents a very coupled behaviour.

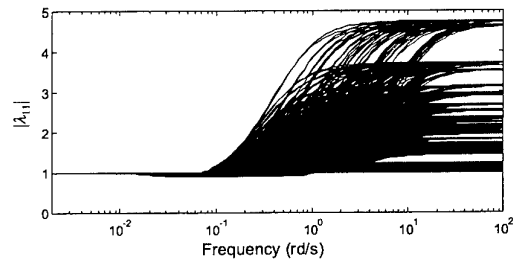


Figure 4. Element λ_{11} of the Relative Gain Analysis Matrix

This analysis also yields a very obvious result angle q_1 will be controlled by motor 1, and angle q_2 by motor 2. Thus the sequential technique may be applied as follows.

- *Step 1:* Design of the first loop controller, g_{11} .

Through standard loop-shaping the controller of Equation (19) is found, satisfying all the performance specifications.

$$g_{11} = \frac{1.65 \cdot 10^9 \cdot s^2 + 4.384 \cdot 10^9 \cdot s + 2.619 \cdot 10^9}{(s^2 + 829.2 \cdot s + 1.545 \cdot 10^5) \cdot s} \quad (20)$$

- *Step 2:* Design of the decoupling element of control effort u_1 on angle q_2 .

Taking into account the optimum controller of Equation (19), the controller g_{21} of Equation (21) is searched minimising the coupling effect c_{21} that can be obtained from Equation (18) for this case.

$$g_{21} = \frac{6.187 \cdot 10^{11} \cdot s^2 + 1.666 \cdot 10^{12} \cdot s + 9.815 \cdot 10^{11}}{1130 \cdot s^3 + 9.372 \cdot 10^5 \cdot s^2 + 1.748 \cdot 10^8 \cdot s + 3.461 \cdot 10^7} \quad (21)$$

- *Step 3:* Design of the second loop controller, g_{22} .

The controller of the second loop is to be designed. However, note that the dynamic behaviour that now can be observed acting on input u_2 and getting measures from angle q_2 is not the stand-alone plant M_{22} , but the following equivalent plant M_{22}^c ,

$$M_{22}^c = M_{22} - \frac{(M_{22} \cdot g_{21} + M_{21} \cdot g_{11}) \cdot M_{12}}{1 + M_{12} \cdot g_{21} + M_{11} \cdot g_{11}} \quad (22)$$

Then through a standard QFT loop-shaping the controller of Equation (23) is designed.

$$g_{22} = \frac{4.218 \cdot 10^{10} \cdot s^2 + 1.119 \cdot 10^{11} \cdot s + 6.3 \cdot 10^{10}}{(s^2 + 3870 \cdot s + 3.177 \cdot 10^6) \cdot s} \quad (23)$$

- *Step 4:* Shaping of the closed loop to satisfy tracking specifications.

Open loop prefilters of Equation (24) and Equation (25) are included in order to satisfy time domain specifications for reference tracking.

$$f_{11} = \frac{14.3}{s^2 + 7.5620 \cdot s + 14.3} \quad (24)$$

$$f_{22} = \frac{3.026}{s^2 + 6.355 \cdot s + 3.026} \quad (25)$$

The non-diagonal controller is composed of the feedback controller G -with the elements of Equations (20), (21) and (23)-, and the diagonal prefilter F -Equations (24) and (25)-.

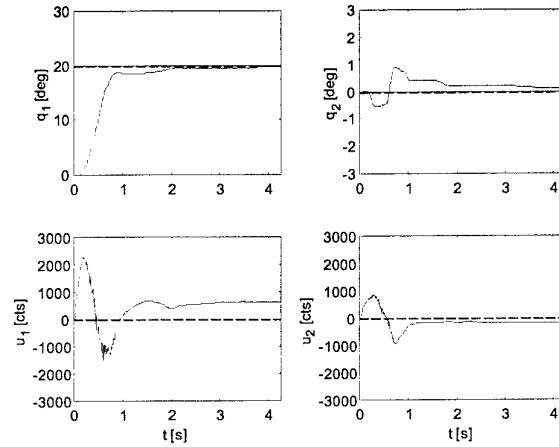


Figure 5: Experiment with the non-diagonal controller

The controller was implemented using a sampling time of 10 ms. One experiment is shown in Figure 5. The reference for angle q_1 is commanded from 0 up to 20 degrees, while the reference for angle q_2 is constant. The influence of the coupling effect with the non-diagonal controller is lower than 1 degree and the designed specifications are achieved.

Integral elements are included in both diagonal controllers in order to remove steady-state errors. These elements present a fairly good behaviour in spite of the Coulomb friction terms or the uncertainties.

4. CONCLUSIONS

This paper has demonstrated the use of the non-diagonal controllers for uncertain systems. In spite of some limitations on the use of those elements -with unstable or non-minimum phase elements-, if sufficient conditions are satisfied these techniques work perfectly even for uncertain systems, and robustness is not affected by uncertainty.

This controller design is the first approach to obtain a competitive control system for the reference tracking of a robot manipulator. A further goal subjected to the improvement of sampling time is force control.

ACKNOWLEDGEMENTS

The authors gratefully appreciate the support given by the Spanish 'Comisión Interministerial de Ciencia y Tecnología' (CICYT) under grant DPI'2000-0785.

REFERENCES

- Boje, E. and O.D.I.Nwokah (1997). Quantitative feedback design using forward path decoupling. *Symposium on Quantitative Feedback Theory and Other Frequency Domain Methods*; University of Strathclyde (United Kingdom); 185-191.
- Boje, E. and O.D.I.Nwokah (1999). Quantitative multivariable feedback design for a turbofan engine with forward path decoupling. *International Journal of Robust and Nonlinear Control*; **9** (12), pp. 857-882.
- Bristol, E.H. (1966). On a new measure of interactions for multivariable process control. *Transactions on Automatic Control*; **11**: 133-134.
- Egaña, I. and M.García-Sanz (1999). Quantitative Non-Diagonal MIMO Controller Design for Uncertain Systems. *4th International Symposium on Quantitative Feedback Theory QFT and Robust Frequency Domain Methods*; University of Durban, Durban (South Africa); 187-198.
- Egaña, I. and M.García-Sanz (2000). PID Tuning for Loop Decoupling of Multivariable Systems with Uncertainty. *IFAC Workshop on Digital Control*; Universitat Politècnica de Catalunya, Terrassa (Spain); 297-302.
- Franchek, M.A., P.Herman P and O.D.I.Nwokah (1997). Robust nondiagonal controller design for uncertain multivariable regulating systems. *ASME Journal of Dynamic Systems, Measurement and Control*; **119**: 80-85.
- García-Sanz, M. and I.Egaña (2002). Quantitative Non-Diagonal Controller Design For Multivariable Systems With Uncertainty. To appear on Part 2 of the Isaac Horowitz Special Issue, in the *International Journal of Robust and Nonlinear Control*.
- Horowitz, I. (1979). Quantitative synthesis of uncertain multiple input-output feedback systems, *International Journal of Control*; **30**: 81-106.
- Horowitz, I. (1982). Improved design technique for uncertain multiple input-output feedback systems. *International Journal of Control* 1982; **36**: 977-988.
- Horowitz, I and M.Sidi (1980). Practical design of feedback systems with uncertain multivariable plants. *International Journal of Systems Science*; **11**(7): 851-875.
- Kidd, (1984). Extension of the Direct Nyquist Array Technique to Uncertain Multivariable Systems Subjected to External Disturbances. *International Journal of Control*; **40**(5): 875-901.
- O'Reilly, J. and W.E.Leithead (1991). Multivariable control by 'individual channer design'. *International Journal of Control*; **54**: 1-46.
- Rosenbrock, H.H. (1970). *State space and multivariable theory*. Wiley: New York.
- Skogestad, S. and K. Havre (1996). The use of RGA and condition number as robustness measures. *Proceedings of the European Symposium of Computer-Aided Process Engineering*; Rodhes (Greece).
- Yaniv, O. (1995). MIMO QFT using non-diagonal controllers. *International Journal of Control* 1995; **61** (1), pp. 245-253.

IDENTIFICATION FOR ROBUST CONTROL OF A FAST FERRY

J. Aranda¹, J. M. de la Cruz², J.M. Díaz¹, P. Ruipérez¹

¹ Dpt. De Informática y Automática. Fac. Ciencias. UNED. Madrid. Spain

² Dpt. de Arquitectura de Ordenadores y Automática. Fac. Ciencias Físicas.

U. Complutense. Madrid. Spain

Fax: 34 91 398 66 97. Phone : 34 91 398 71 48. E-mail : jaranda □ dia.uned.es

Abstract: The interval transfer functions from wave height to pitch and heave movement described in this paper are interpreted as a family of transfer functions whose coefficients are bounded by some known intervals and centred at nominal values. The nominal model is obtained by a non-linear least square algorithm of identification applied in the frequency domain. Once the nominal model was obtained, then the tightest intervals around each coefficient of the nominal transfer functions was created while satisfying the membership and frequency response requirements. Different model validation tests were made (Bode plots and simulations). These tests show that the uncertainty model obtained is a valid interval model and it can be used for robust control design.

Keywords: Identification algorithms, Optimization problem, Robust performance.

1. INTRODUCTION

The main problem for the development of high speed ship is concerned with the passenger's comfort and the safety of the vehicles. The vertical acceleration associated with roll, pitch and heave motion is the cause of motion sickness. The roll control is the most attractive candidate for control since increasing roll damping can be obtained more easily. However, shipbuilders are also interested in increasing pitch and heave damping. In order to solve the problem antipitching devices and pitch control methods must be considered. Previously, models for the vertical ship dynamic must be developed for the design, evaluation and verification of the results.

The number of published investigations about ship modelling is immense. For example, non-linear models in 6 degrees of freedom are shown in Fossen (1994) and Lewis (1989). These models are theoretical and they are obtained from the equations of a rigid solid partially immersed in water.

Obtaining a very accurate mathematical model of a system is usually impossible and very costly. It also often increases the complexity of the control algorithm. A trend in the area of system identification is to try to model the system uncertainties (Bhattacharyya et al., 1995) to fit the available analysis and design tools of robust control.

The interval functions described in this paper are interpreted as a family of transfer functions from wave height to pitch and heave movement whose coefficients are bounded by some known intervals and centred at nominal values. The nominal model (Aranda et al., 1999b; Aranda et al., 2000) is obtained by a non-linear least square algorithm applied in the frequency domain. Once the nominal model is obtained, then the tightest intervals around each coefficient of the nominal transfer functions are created while satisfying the membership and frequency response requirements.

2. IDENTIFICATION METHODOLOGY

The method describes in this paper follows the steps of classical identification diagram (Ljung, 1989; Schoukens and Pintelon, 1991; Söderström and Stoica, 1989). A model test was carried out in the towing tank of CEHIPAR (Madrid, Spain). The model was free to move in heave direction and pitch angle. The wave surface elevation was measured at 68.75 m. forward from model bow. Different regular and irregular waves and ship speed were tested. A set of simulated data (Aranda et al., 1999a) has been generated by the program PRECAL (which uses a geometrical model of the ship to predict her dynamic behaviour), reproducing the same conditions of the experiments with regular waves.

Two transfer functions are identified (see Figure 1):

- $G_p(s)$: transfer function from wave height (m) to pitch movement ($^\circ$).
- $G_H(s)$: transfer function from wave height (m) to heave movement (m).

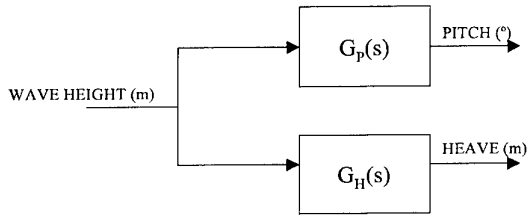


Fig. 1. Blocks diagram of the identified system

The identification is made in the frequency domain and uses the simulated data of magnitude and phase obtained by the program PRECAL in the encounter frequency ω_{ei} ($i=1,2,\dots,25$) for the transfer functions $G_p(j\omega_{ei})$ and $G_H(j\omega_{ei})$.

$$\begin{aligned} G_p(j\omega_{ei}) &= \text{Re}(G_p(j\omega_{ei})) + j \text{Im}(G_p(j\omega_{ei})) \\ G_H(j\omega_{ei}) &= \text{Re}(G_H(j\omega_{ei})) + j \text{Im}(G_H(j\omega_{ei})) \end{aligned} \quad (1)$$

In general, the estimated transfer functions $\hat{G}_p(s)$ and $\hat{G}_H(s)$ can be written in the following form:

$$\hat{G}(s) = \frac{x_{n+m+1}s^m + x_{n+m}s^{m-1} + \dots + x_{n+1}}{s^n + x_n s^{n-1} + \dots + x_1} \quad (2)$$

where m is the number of zeros and n is the total number of poles. The parameter vector is:

$$\bar{P} = (x_1, x_2, \dots, x_n, x_{n+1}, \dots, x_{n+m+1}) \quad (3)$$

The estimation of the parameter vector \bar{P} is made by a non-linear least squares procedure that uses the following cost function (Schoukens and Pintelon, 1989):

$$K(\bar{P}) = \sum_{k=1}^N |(\text{Re}(G(j\omega_{ek})) - \text{Re}(\hat{G}(j\omega_{ek})) + \dots + j(\text{Im}(G(j\omega_{ek})) - \text{Im}(\hat{G}(j\omega_{ek})))|^2 \quad (4)$$

A number of considerations need to be made based in a priori knowledge of the ship dynamics. So, there are three constraints in the identification process of the models:

- The models must be stables.
- The gain of $G_p(s)$ must tend to zero in low encounter frequencies.
- The gain of $G_H(s)$ must tend to one in low encounter frequencies

The solution to a non-linear least squares problem with constraints is described for example in Söderström and Stoica (1989), and can be programmed using MATLAB.

3. INTERVAL MODELLING

Bhattacharyya et al. (1995) describes a method to obtain the family of linear time invariant systems $\bar{G}(s)$ by letting the transfer function coefficients lie in intervals around those of the nominal $G(s)$. This method is adapted to our problem. Let

$$y(j\omega_{ei}) = D(j\omega_{ei})u(j\omega_{ei}) \quad i = 1, 2, \dots, N \quad (5)$$

where $\omega_{e1}, \omega_{e2}, \dots, \omega_{eN}$ are the test encounter frequencies and the complex number $u(j\omega_{ei})$ and $y(j\omega_{ei})$ denote in phasor notation the input-output pair at the frequency ω_{ei} generated from an identification experiment. Suppose that $G^l(s)$ is the transfer function of a linear time-invariant system which is such that $G^l(j\omega_{ei})$ is closest to $D(j\omega_{ei})$ in some norm sense. In general it is not possible to find a single rational function $G^l(s)$ for which $G^l(j\omega_{ei}) = D(j\omega_{ei})$ and the more realistic identification problem is to fact identify an entire family $\bar{G}(s)$ of transfer functions which is capable of validating the data in the sense that for each point $D(j\omega_{ei})$ there exists some transfer function $G_i \in \bar{G}(s)$ with the property that $G^l(j\omega_{ei}) = D(j\omega_{ei})$.

Let the nominal transfer function $G^l(s)$, which has been identified by a non-linear least squares procedure explained in the previous section, and the transfer function $G(s)$ with the form:

$$G(s) = \frac{\hat{x}_{n+m+1}s^m + \hat{x}_{n+m}s^{m-1} + \dots + \hat{x}_{n+1}}{s^n + \hat{x}_n s^{n-1} + \dots + \hat{x}_1} \quad (6)$$

The family of linear time-invariant systems $\bar{G}(s)$ is defined by :

$$\bar{G}(s) = \{G(s) : \hat{x}_i \in [x_i - w_{x_i} \cdot \varepsilon_{x_i}^-, x_i + w_{x_i} \cdot \varepsilon_{x_i}^+] \forall i\} \quad (7)$$

where w_{x_i} are to be regarded as *weights* chosen apriori whereas the ε 's are to be regarded as *dilation parameters* to be determined by the identification algorithm and the data $D(j\omega_{ei})$.

3.1 Weight selection

Suppose the test data consists of N data points obtained at corresponding frequencies,

$$D(j\omega_e) = \{D(j\omega_{ei}) = \alpha_i + j\beta_i, i = 1, 2, \dots, N\} \quad (8)$$

the 1st model is defined as:

$$G_l(j\omega_e) = \begin{cases} D(j\omega_{ei}) & i = l \\ G^l(j\omega_{ei}) & i = 1, 2, \dots, l-1, l+1, \dots, N \end{cases} \quad (9)$$

The model $G_l(j\omega_{ei})$ is identical to the nominal identified model $G^l(j\omega_{ei})$ with the 1st data point replaced by the 1st component of the test data $D(j\omega)$. Now the 1st identified model $G_1^l(s)$ is constructed, which is identified from the 1st data set $G_1(j\omega)$. Let

$$G_1^l(s) = \frac{x_{n+m+1}^l s^m + \dots + x_{n+1}^l}{s^n + x_n^l s^{n-1} + \dots + x_1^l} \quad (10)$$

The models $G_1^l(s)$ must be identified with the same method used to identify the nominal model $G^l(j\omega)$. The weight vector \bar{w} is :

$$\bar{w} = \left[\frac{1}{N} \sum_{l=1}^N |x_1 - x_1^l|, \dots, \frac{1}{N} \sum_{l=1}^N |x_{n+m+1} - x_{n+m+1}^l| \right] \quad (11)$$

$$\bar{w} = [w_{x_1}, \dots, w_{x_n}, w_{x_{n+1}}, \dots, w_{x_{n+m+1}}]$$

The weight selection is an important stage because an inappropriate selection may results in an unnecessarily large family.

3.2 Computation of the intervals of the transfer function coefficients.

Replacing $s=j\omega_{ei}$ in (6):

$$G(j\omega_{ei}) = \left(\frac{\hat{x}_{n+1}^2 - \omega_{ei}^2 \hat{x}_{n+3}^2 + \dots}{\hat{x}_1^2 - \omega_{ei}^2 \hat{x}_3^2 + \dots} + j \cdot \frac{\omega_{ei}^3 \hat{x}_{n+2}^3 - \omega_{ei}^3 \hat{x}_{n+4}^3 + \dots}{\omega_{ei}^3 \hat{x}_2^3 - \omega_{ei}^3 \hat{x}_4^3 + \dots} \right) \quad (12)$$

if $G(j\omega_{ei})$ is made equal to the data set $D(j\omega_{ei})$ for a particular encounter frequency ω_{ei} , then:

$$D(j\omega_{ei}) = \alpha_i + j\beta_i = \frac{n! + j \cdot n!}{d! + j \cdot d!} \quad (13)$$

Operating, the next pair of equations are obtained:

$$\begin{aligned} F_1(\alpha_i, \beta_i, x_1^i, \dots, x_{n+m+1}^i) &= (\alpha_i d! - \beta_i d!) - n! = 0 \\ F_2(\alpha_i, \beta_i, x_1^i, \dots, x_{n+m+1}^i) &= (\beta_i d! + \alpha_i d!) - n! = 0 \end{aligned} \quad (14)$$

\hat{x}_i for all i is defined by:

$$\hat{x}_i = x_i + w_{x_i} \varepsilon_{x_i}^l \begin{cases} i = 1, \dots, n+m+1 \\ l = 1, \dots, N \end{cases} \quad (15)$$

Rewrite (14) in terms of a matrix equations:

$$\begin{aligned} A \cdot \bar{x} + A \cdot W \cdot \bar{\varepsilon}_x^l &= -E \\ A \cdot W \cdot \bar{\varepsilon}_x^l &= -B - E \end{aligned} \quad (16)$$

where:

$$A = \begin{bmatrix} \alpha_i & -\beta_i \omega_{ei} & \alpha_i \omega_{ei}^2 & -\beta_i \omega_{ei}^3 & \dots & -1 & 0 & \omega_{ei}^2 & 0 & \omega_{ei}^4 & \dots \\ \beta_i & \alpha_i \omega_{ei} & -\beta_i \omega_{ei}^2 & \alpha_i \omega_{ei}^3 & \dots & 0 & \omega_{ei} & 0 & \omega_{ei}^3 & 0 & \dots \end{bmatrix}$$

$$E = \begin{bmatrix} k_1 \omega_{ei}^n \\ k_2 \omega_{ei}^n \end{bmatrix}$$

$$k_1 = \begin{cases} \alpha_i & \text{si } n = 0, 4, 8, \dots \\ -\beta_i & \text{si } n = 1, 5, 9, \dots \\ -\alpha_i & \text{si } n = 2, 6, 10, \dots \\ \beta_i & \text{si } n = 3, 7, 11, \dots \end{cases} \quad k_2 = \begin{cases} \beta_i & \text{si } n = 0, 4, 8, \dots \\ \alpha_i & \text{si } n = 1, 5, 9, \dots \\ -\beta_i & \text{si } n = 2, 6, 10, \dots \\ -\alpha_i & \text{si } n = 3, 7, 11, \dots \end{cases} \quad (17)$$

$$W = \begin{bmatrix} w_{x_1} & & 0 \\ & \ddots & \\ 0 & & w_{x_{n+m+1}} \end{bmatrix}$$

$$\bar{\varepsilon}_x^l = [\varepsilon_{x_1}^l, \dots, \varepsilon_{x_{n+m+1}}^l]^T$$

$$\bar{x} = [x_1, \dots, x_{n+m+1}]^T$$

$$B = A \cdot \bar{x}$$

$\bar{\varepsilon}_x^l$ is the vector of the dilation parameters obtained for the encounter frequency ω_{ei} . Here it is assumed without loss of generality that $A(\omega_{ei}, \alpha_i, \beta_i)$ has full rank. Then the minimum norm solution $\bar{\varepsilon}_x^l$ can be computed as:

$$\bar{\varepsilon}_x^l = -W^{-1} (A^T A)^{-1} A^T (B + E) \quad (18)$$

After finding $\bar{\varepsilon}_x^l$ for all $l=1,\dots,N$, the dilation parameters of the intervals of the transfer function coefficients are determined as follows:

$$\varepsilon_{x_k}^- = \min_l \{0, \varepsilon_{x_k}^l\} \quad \varepsilon_{x_k}^+ = \max_l \{0, \varepsilon_{x_k}^l\} \quad (19)$$

4. RESULTS

In Table 1 and Table 2 different model structures (where m is the number of zeros, n is the total number of poles and nps is the number of simple poles) are showed for heave and pitch movement, at several ship speed. The cost function and mean square error can be compared when the model structure is reduced.

Table 1: Model structures for heave movement

Ship speed (knots)	Model Structure (m,n,nps)	Value of the cost function	Mean square error (m ²)
20	(4,6,2)	0.0383	0.0143
20	(3,5,1)	0.0692	0.0141
20	(2,3,1)	0.0696	0.0138
30	(4,6,2)	0.0385	0.0111
30	(3,5,1)	0.1012	0.0115
30	(2,3,1)	0.2381	0.0170
40	(4,6,2)	0.0471	0.0112
40	(3,5,1)	0.1045	0.0113
40	(2,3,1)	0.4510	0.0125

Table 2: Model structures for pitch movement

Ship speed (knots)	Model Structure (m,n,nps)	Value of the cost function	Mean square error ((°) ²)
20	(4,6,2)	0.1213	0.1056
20	(3,5,1)	0.1228	0.1052
30	(4,6,2)	0.0938	0.0995
30	(3,5,1)	0.0946	0.0998
40	(4,6,2)	0.0942	0.1214
40	(3,5,1)	0.0989	0.1226

The model interval was obtained for each of model structures show in Table 1 and Table 2. For example, the transfer functions of model structure (4,6,2) for heave movement and pitch movement at 40 knots are:

$$G_H(s) = \frac{3.219s^4 - 0.9423s^3 + 26.03s^2 - 6.78s + 80.35}{s^6 + 16.43s^5 + 42.62s^4 + 106.6s^3 + 142.9s^2 + 142.6s + 80.35}$$

$$G_P(s) = \frac{0.5381s^4 - 6.051s^3 + 13.21s^2 - 52.28s}{s^6 + 16.43s^5 + 42.62s^4 + 106.6s^3 + 142.9s^2 + 142.6s + 80.35}$$

In Table 3 and Table 4 the model interval of $G_H(s)$ and $G_P(s)$ are showed.

Table 3: Model interval of $G_H(s)$

x	Lower Interval	Nominal value	Upper Interval
x ₁	79.95	80.35	83.50
x ₂	139.79	142.61	143.09
x ₃	139.63	142.94	144.56
x ₄	106.31	106.59	109.02
x ₅	35.88	42.62	43.09
x ₆	12.98	16.43	16.52
x ₈	-6.81	-6.78	-6.28
x ₉	25.99	26.02	26.35
x ₁₀	-5.14	-0.92	-0.81
x ₁₁	-0.14	3.21	3.28

Table 4: Model interval of $G_P(s)$

x	Lower Interval	Nominal value	Upper Interval
x ₁	49.71	50.08	50.87
x ₂	80.70	83.73	84.31
x ₃	91.03	91.84	92.42
x ₄	63.45	63.99	66.07
x ₅	28.31	28.73	28.95
x ₆	6.19	9.85	9.95
x ₈	-53.07	-52.57	-52.48
x ₉	12.55	13.21	13.47
x ₁₀	-6.79	-6.05	-4.59
x ₁₁	0.25	0.53	2.74

In Figure 2 Bode plot of $G_H(s)$ and data obtained by PRECAL are showed.

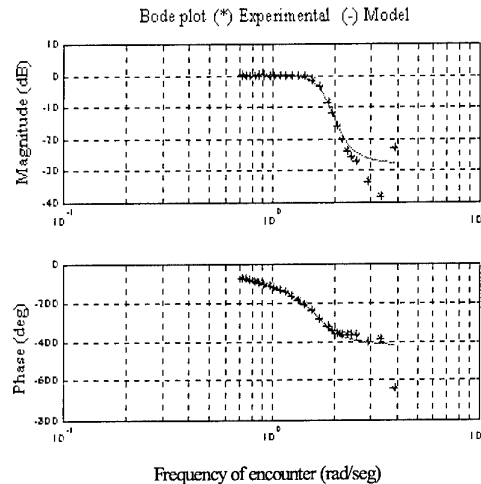


Fig. 2. Bode plot of $G_H(s)$ and data of PRECAL program.

In Figure 3 Bode plot of $G_P(s)$ and data obtained by PRECAL are showed.

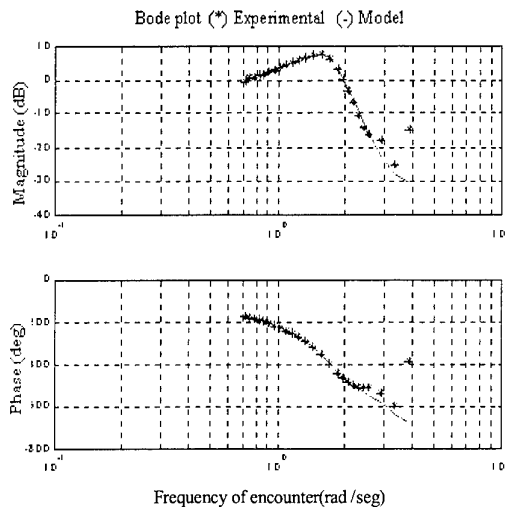


Fig. 3. Bode plot of $G_p(s)$ and data of PRECAL program.

Figure 4 shows the output of $G_H(s)$ and the measured heave in the CEHIPAR when the input was irregular waves at 40 knots and SSN=5.

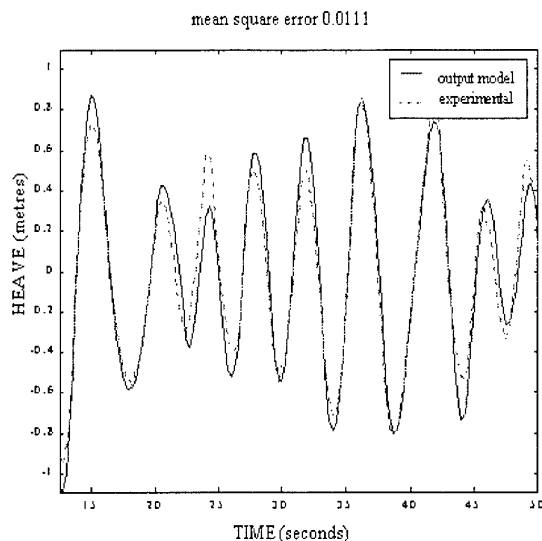


Fig. 4. Simulation of $G_H(s)$ and measured heave at 40 knots and sea state number (SSN) equal to 5.

Figure 5 shows the output of $G_p(s)$ and the measured pitch in the CEHIPAR when the input was irregular waves at 40 knots and SSN=5.

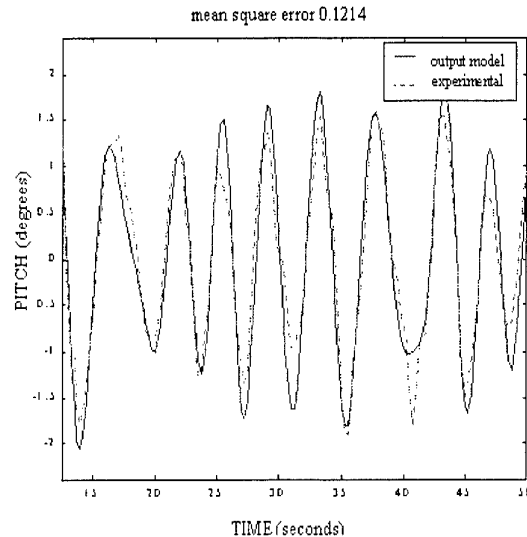


Fig. 5. Simulation of $G_p(s)$ and measured pitch at 40 knots and sea state number (SSN) equal to 5.

5. CONCLUSION

In this paper continuous linear models for vertical dynamics of a high speed ship has been showed. These models were identified by a non-linear least square algorithm applied in the frequency domain. Once the nominal model was obtained, tightest intervals around each coefficient of nominal transfer functions was created while satisfying the membership and frequency response requirements. Different model validation tests was made.

Acknowledgements: This development was supported by CICYT of Spain under contract TAP97-0607-C03-02.

REFERENCES

- Aranda, J., J.M De la Cruz, B. De Andres, J.M. Díaz, S. Estebán. and P. Ruipérez. (1999) Data used in the model identification of vertical dynamic of TF-120 ship. Technical report (in Spanish). CRIBAV-00-01 of project TAP97-0607-C03-01 (<http://ctb.dia.uned.es/cribav/>)
- Aranda, J., J.M. De la Cruz, J.M. Díaz and P. Ruipérez. (1999). Interval modelling for the vertical dynamics of TF-120 Ship. Technical report (in Spanish). CRIBAV-02-02 of project TAP97-0607-C03-01 (<http://ctb.dia.uned.es/cribav/>)
- Aranda, J., J.M. de la Cruz, J.M. Díaz, B. de Andrés, P. Ruipérez, S. Esteban and J.M. Girón. (2000) Modelling of a high speed ship by a non-linear least squares method with constraints. *Proceedings of 5th IFAC Conference on Manoeuvring and Control of Marine Ships MCMC2000*. Aalborg. pp. 227-232.

- Bhattacharyya, S., H. Chapellat and L. Keel. (1995) *Robust Control: The Parametric Approach*. Prentice Hall.
- De la Cruz, J.M., J. Aranda, J.M. Díaz, P. Ruipérez and A. Marón. (1998) Identification of the vertical plane motion model of a high speed ship by model testing in irregular waves. *Proceedings of IFAC Conference CAMS'98 Control Applications in Marine Systems*. Fukuoka. pp. 277-282.
- Fossen, T. I. (1994). *Guidance and Control of Ocean Vehicles*. John Wiley & sons.
- Lewis, E.V. (1989). *Principles of Naval Architecture. Second Revision. Volume III. Motions in Waves and Controllability*. Society of Naval Architects and Marine Engineers.
- Ljung, L. (1989). *System Identification: Theory for the User*. Prentice Hall.
- Schoukens, J. and R. Pintelon. (1991). *Identification of Linear Systems*. Pergamon Press.
- Söderström, T. and P. Stoica. (1989). *System Identification*. Prentice Hall.

ROBUST QFT CONTROLLER FOR MARINE COURSE-CHANGING CONTROL

Teresa M. Rueda Rodríguez*, Francisco J. Velasco González*, Emiliano
Moyano Pérez** and Eloy López García***

* *Dpto. Tecnología Electrónica, Ingeniería de Sistemas y Automática. Univ. de Cantabria
(Spain)*

** *Dpto. Matemática Aplicada y Ciencias de la Computación. Univ. de Cantabria (Spain)*

*** *Dpto. Ciencias y Técnicas de la Navegación, Máquinas y Construcciones Navales. Univ.
del País Vasco (Spain)*

Abstract: This paper describes the design of a robust QFT (Quantitative Feedback Theory) controller for the control of the changing of a ship's course in the presence of disturbances. A linear model is used with uncertainties in the parameters obtained from the non-linear model of the ship. The required performance specifications and the existing number of plants determine the bounds which the system must not violate. The results are compared with those obtained with a conventional PID controller by means of genetic algorithms.

Keywords: ship control, ship autopilots, marine systems, control systems, ship model, course-changing control, plant templates, bounds, QFT control.

1. INTRODUCTION

In any physical process which one aims to control, certain performance specifications must be fulfilled. If the mathematical model of the system is not exact or if there are external disturbances, that is, if the system presents uncertainties, it is then necessary to use robust control techniques in the design of the controller. Among the different techniques available, the QFT (Quantitative Feedback Theory) method developed by Horowitz (1992) has been chosen for this work. With this model, the physical dimension of the problem is maintained at all times and an adequate

balance is achieved between the structure level of the process and the complexity of the problem.

The above method is applied in this work for the course-changing control of the ship, the R.O.V. Zeefakkel (Fossen and Paulsen, 1992), using for the design of the QFT controller the first order Nomoto model (Nomoto, et al., 1957) which relates the heading angle with the rudder angle. Saturation effects have been taken into account in the design. The results are compared with those of a conventional autopilot.

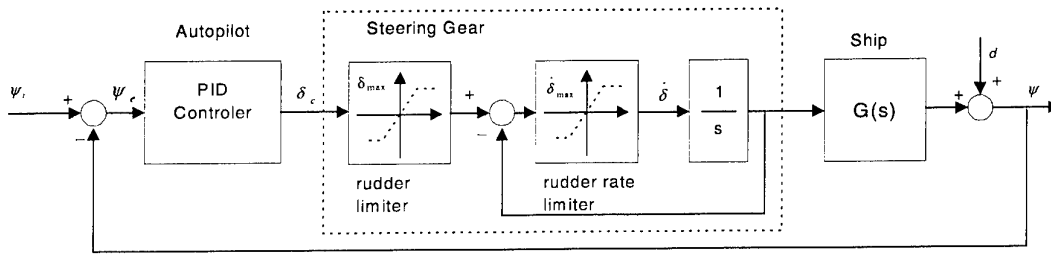


Fig. 1. Block diagram of a conventional steering system

2. MATHEMATICAL MODEL OF THE VESSEL

Figure 1 shows the block diagram of a ship steering system with a conventional autopilot (PID controller). Saturation effects have been taken into account both in the rudder angle and in the speed of change of this angle.

The command applied is ψ_r , which represents the desired heading and ψ_e is the heading error. The control signal of the controller which acts as a command to the steering gear is δ_e and represents the rudder angle required to correct the deviation from the heading. The actual value of the rudder angle is δ and ψ is the ship's course.

The mathematical model of the ship's dynamics between the rudder angle signal δ and that of the ship's course ψ assuming that the relation is linear (Van Amerongen and Udink Ten Cate, 1975), can be represented (Nomoto, et al., 1957) by the transfer function:

$$\frac{\psi}{\delta}(s) = \frac{K(1 + sT_3)}{s(1 + sT_1)(1 + sT_2)} \quad (1)$$

or equally by the differential equation:

$$T_1 T_2 \ddot{\psi} + (T_1 + T_2) \dot{\psi} + \psi = K(\delta + T_3 \dot{\delta}) \quad (2)$$

where K , T_1 , T_2 and T_3 are the parameters which represent the ship's dynamics. These parameters are basically determined by the dimensions and forms of the vessel and also depend on operating conditions such as ship speed, load or ballast situation, draft, trim and water depth.

Equation (1) is usually approximated by

$$\frac{\psi}{\delta}(s) = \frac{K}{s(1 + sT)} \quad (3)$$

with $T = T_1 + T_2 - T_3$.

Expressed as a differential equation:

$$T\ddot{\psi} + \dot{\psi} = K\delta \quad (4)$$

This attractively simple model provides a reasonably accurate representation of the performance of vessels when they keep a straight course or one with only slight changes. However, if the characteristics of the vessel's rotation are to be studied, a non-linear term (Van Amerongen and Udink Ten Cate, 1975) can be added to the linear model:

$$T_1 T_2 \ddot{\psi} + (T_1 + T_2) \dot{\psi} + K H_B(\psi) = K(\delta + T_3 \dot{\delta}) \quad (5)$$

where $H_B(\psi)$ is a non-linear function of ψ which is obtained from the relation between $\dot{\psi}$ and δ in the steady state by means of the spiral test. This can be approximated (Van Amerongen and Udink Ten Cate, 1975) by:

$$H_B(\psi) = b_3 \psi^3 + b_1 \psi \quad (6)$$

If equation (4) is used, we get

$$T\ddot{\psi} + H_N(\psi) = K\delta \quad (7)$$

with

$$H_N(\psi) = n_3 \psi^3 + n_1 \psi \quad (8)$$

3. CONTROL PROBLEM

An autopilot must fulfil two objectives: course keeping and course changing. In the first case, the control objective is to maintain the ship's heading following the desired course ($\psi(t) = \text{constant}$). In the second case, the aim is to implement the change of course without oscillations and in the shortest time possible. In both situations, the operability of the system must be independent of the disturbances produced by the wind, the waves and the currents.

The course followed by a vessel can be specified by means of a second order reference model (Fossen, 1994):

$$\ddot{\psi}(t) + 2\zeta\omega_n \dot{\psi}(t) + \omega_n^2 \psi(t) = \omega_n^2 \psi_r \quad (9)$$

where ω_n is the natural frequency and ζ ($0.8 \leq \zeta \leq 1$) is the desired damping coefficient of the closed loop system.

As an application of the proposed methodology, the simulation of the behaviour of a vessel of 45m in length, the R. O. V. Zeefakkel, is performed. The model's parameters at a speed of 10 knots are (Fossen and Paulsen, 1992):

$$K = 0.5 \text{ s}^{-1}, T = 31 \text{ s}, n_1 = 1, n_3 = 0.4 \text{ s}^2$$

4. DESIGN SPECIFICATIONS

The aim of the design of this work is that the vessel should make a fast change of course following, without oscillations, the course determined by the values $\zeta = 0.9$ and $\omega_n = 0.07 \text{ rad/s}$ and that this course should be maintained despite the effect of bow waves in the order of 1m in significant height. (Moyano, et al., 2000) It is considered that these may lead to variations in the course of up to 1° .

The non-linearities in the ship model mean that the performance in response to changes in course may vary. The prior study of this effect has led the authors to consider for the model design the vessel given by equation (3) with the following uncertainty in the K and T parameters (at a speed of 10 knots):

$$K \in [0.21, 0.5]$$

$$T \in [29.5, 31]$$

Despite the fact that the model is non-linear, the QFT model for linear SISO systems with parametric uncertainty will be used, incorporating the two-degrees-of-freedom control system shown in figure 2. This includes a cascade compensator, $G(s)$, and a prefilter $F(s)$ (both LTI) in order to reduce the variations in the output of the system caused by the uncertainties in the plant parameters and disturbances.

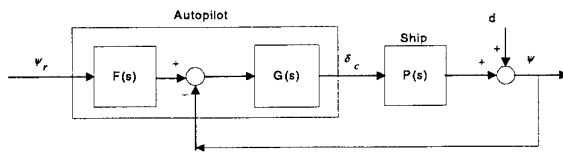


Fig. 2 Block diagram of the two degree-of-freedom control system

The system must fulfil robust stability and robust tracking specifications (Houpis and Rasmussen, 1999; Yaniv, 1999):

For the robust stability margins, the phase margin angle should be at least 45° and the gain margin 2 dB. Thus, the robust stability specification is defined by:

$$\left| \frac{P(j\omega) G(j\omega)}{1 + P(j\omega) G(j\omega)} \right| \leq \delta = 1.2 \quad (10)$$

Robust tracking: The change of course must be defined within an acceptable range of variation. This is generally defined in the time domain but is normally transformed to the frequency domain, being expressed by:

$$T_{RL}(j\omega) \leq T_R(j\omega) \leq T_{RU}(j\omega) \quad (11)$$

where $T_R(s)$ represents the closed loop transfer function and $T_{RL}(s)$ and $T_{RU}(s)$ the equivalent transfer functions of the lower and upper tracking bounds. In this case, the following is specified:

$$T_{RL}(s) = \frac{a}{s^3 + b s^2 + c s + a} \quad (12)$$

with $a = 269.5 \cdot 10^{-6}$, $b = 181 \cdot 10^{-3}$, $c = 118.3 \cdot 10^{-4}$

$$T_{RU}(s) = \frac{195 \cdot 10^{-4} s + 49 \cdot 10^{-4}}{s^2 + 112 \cdot 10^{-3} s + 49 \cdot 10^{-4}} \quad (13)$$

for $\omega \leq 0.4 \text{ rad/s}$, as shown in Figure 3.

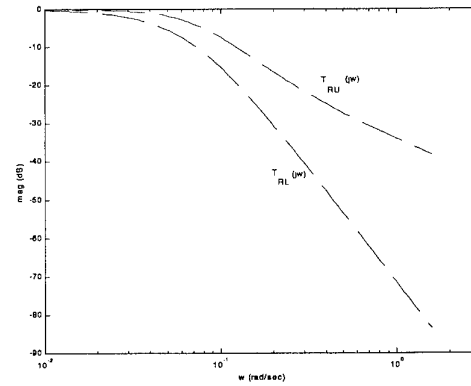


Fig. 3 Robust tracking specifications.

As mentioned above, the aim of the design is to maintain the course even when there are bow waves. No disturbance rejection restriction has been specified because the simulation considers only waves of a reasonable force.

5. SIMULATIONS

The following nominal plant has been chosen for the design:

$$P(s) = \frac{0.5}{s(31s + 1)} \quad (14)$$

and the following set of frequencies for the design has been established:

$$\Omega = \{0.03, 0.07, 0.1, 0.2, 0.4, 1, 1.2\} \quad (15)$$

Using the Matlab QFT Toolbox (Borguesani, et al., 1995) the plant templates are computed for each frequency, as shown in Figure 4.

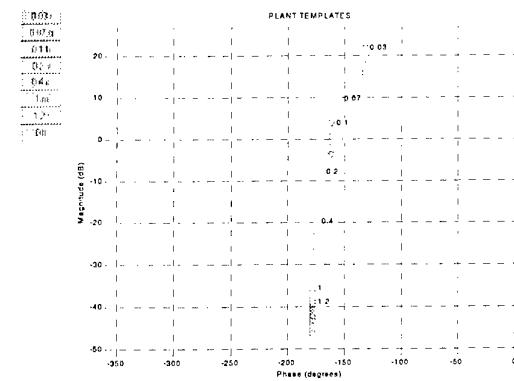


Fig. 4 Plant Templates.

On the basis of the performance specifications and the plant templates, the robust stability and robust tracking bounds are calculated. The intersection of all of the bounds at the various frequencies is shown in Figure 5.

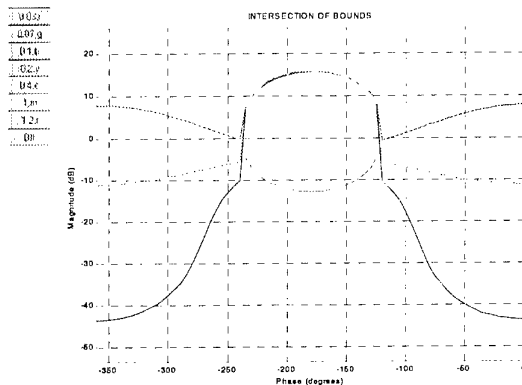


Fig. 5 Intersection of bounds.

For the design of the $G(s)$ controller, the Nichols Chart is used, adjusting the nominal open-loop transfer function $L_0 = P_0 G$ (P_0 is the nominal plant) in such a way that no bounds are violated, as shown in Figure 6.

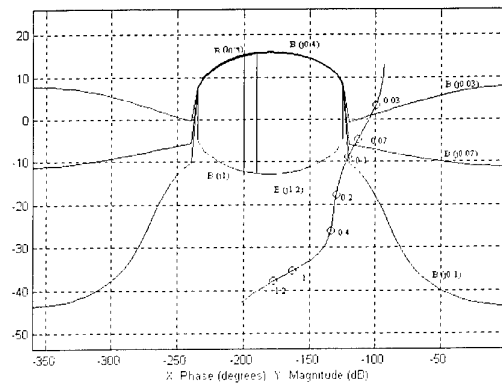


Fig. 6 Shaping of $L_0(j\omega)$ on the Nichols chart for the nominal plant.

The controller obtained is:

$$G(s) = \frac{180.45 \cdot 10^{-3} s^3 + 625.38 \cdot 10^{-3} s^2 + 16.57 \cdot 10^{-3} s + 36.92 \cdot 10^{-7}}{s^4 + 168.53 \cdot 10^{-2} s^3 + 203.23 \cdot 10^{-2} s^2 + 18.73 \cdot 10^{-2} s}$$

(16)

With this controller, the robust stability specification is fulfilled but not the robust tracking specification, as can be seen from Figures 7 and 8. The solid line shows the response of the system and the dashed line represents the specifications.

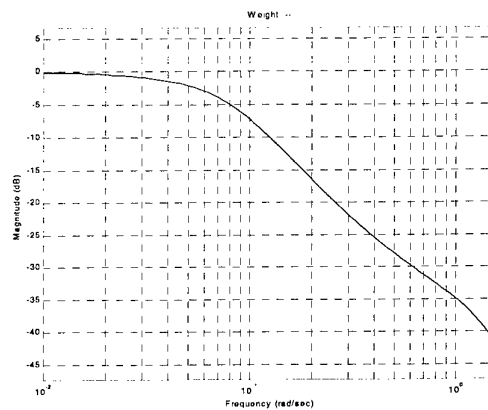


Fig. 7 Robust Stability

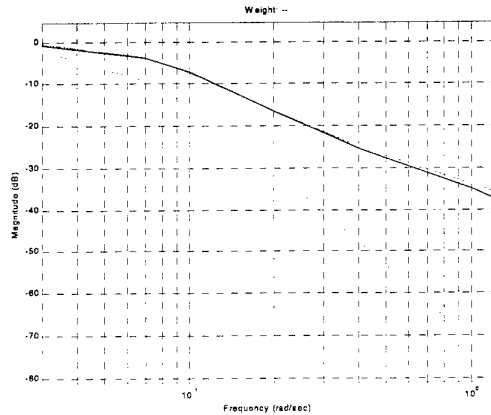


Fig. 8 Robust Tracking

By adjusting the prefilter:

$$F(s) = \frac{128.89 \cdot 10^{-3}}{s + 128.89 \cdot 10^{-3}} \quad (17)$$

a restriction on the frequency response of the system is obtained such that it is maintained within the limits imposed in the design. It is also verified that the control structure designed allows the ship's course to fit the specifications for various course changes. As examples, Figures 9 and 10 show the results for changes in course of 10° and 30° respectively.

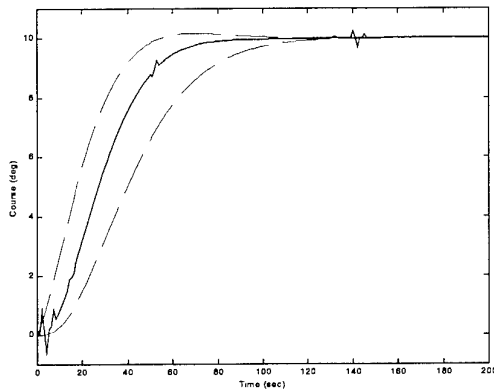


Fig. 9 Course changing manoeuvre. $\psi_r = 10^\circ$

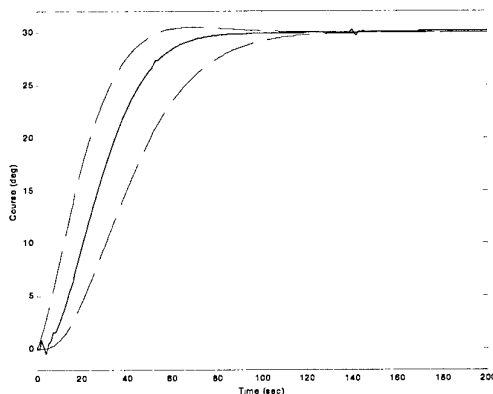


Fig. 10 Course changing manoeuvre. $\psi_r = 30^\circ$

The change of course manoeuvre obtained with QFT design has been compared with that of a vessel with a conventional PID controller which has been tuned by means of genetic algorithms:

$$G(s) = \frac{15523.7s^2 + 448.37s + 0.1}{44737s^2 + 4473.7s} \quad (18)$$

Figure 11 shows a change of course manoeuvre of 10° for the two controllers and Figure 12 illustrates the required variations in the rudder angle (control signal).

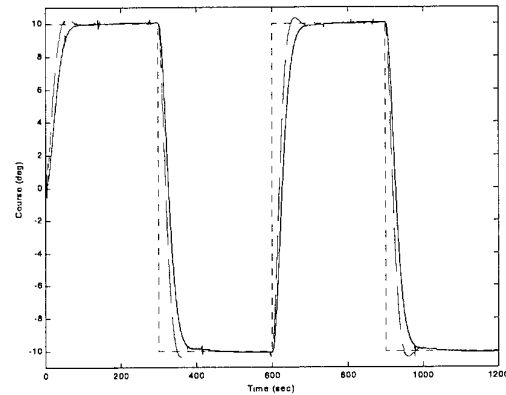


Fig. 11. Change of course manoeuvres for the QFT (solid line) and PID (dashed line) controllers. Reference heading (dotted line).

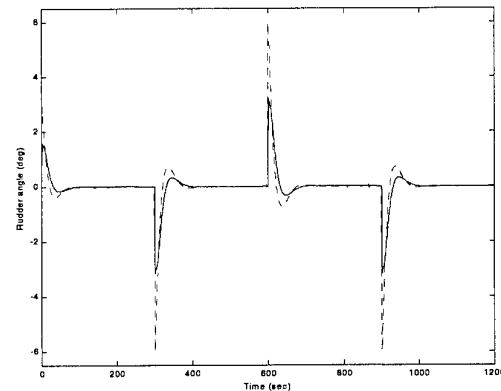


Fig. 12. Rudder Angle. QFT signal control (solid line), PID signal control (dotted line)

6. CONCLUSIONS

This paper describes the use of the QFT robust control technique which is highly suitable since the system presents uncertainties and disturbances. Robust stability and robust tracking specifications have been imposed. The results have been compared with those

obtained using a conventional PID controller. It can be observed that a more satisfactory result is obtained with the QFT controller in the response of the system at the expense of an increase in the complexity of the control.

7. ACKNOWLEDGEMENTS

This development was supported by CICYT of Spain under contract DPI2000-0386-C03-03.

8. REFERENCES

- Borguesani, C., Chait, Y., Yaniv, O. 1995. Quantitative Feedback Theory Toolbox – For use with MATLAB. *The MathWorks Inc.*
- Fossen T. I., Paulsen M. A. (1992) Adaptive Feedback Linearization Applied to Steering of Ships. 1st *IEEE Conference on Control Applications.*
- Fossen, T. I. (1994). *Guidance and Control of Ocean Vehicles.* John Wiley and Sons Ltd., England.
- Horowitz, I. M. (1992). *Quantitative Feedback Design Theory (QFT).* QFT Publications, Boulder, Colorado.
- Houpis, C. H., Rasmussen, S. J. (1999). *Quantitative Feedback Theory. Fundamentals and Applications.* Marcel Dekker, Inc., New York.
- Moyano, E., Velasco, F.J., Bravo, L. (2000). Obtaining Parametric Wave Models. 2nd *International Congress on Maritime Technological Innovations and Research*, vol.1, pages 394-401.
- Nomoto, K., Taguchi, T., Honda, K., Hirano S. (1957). On the steering qualities of Ships. *International Shipbuilding. Progreess.* Vol. 4.
- Van Amerongen, J., Udink Ten Cate A. J. (1975). Model Reference Adaptive Autopilots for Ships. *Automatica*, vol.11, no. 1
- Yaniv, O. (1999). *Quantitative Feedback Design of Linear and Nonlinear Control Systems.* Kluwer Academic Publishers. Norwell, Massachusetts.

MULTIVARIABLE CONTROL FOR COOLING MACHINES BASED ON VAPOR COMPRESSION

J.M. Galvez, L. Machado and A.G. da Silva.

*Department of Mechanical Engineering, Federal University of Minas Gerais, Brazil.
Av. Antonio Carlos 6627, Pampulha, 31.270-901 Belo Horizonte, MG, Brazil.
Phone: +55 31 3499-5236. Fax: +55 31 3443-3783. E-mail: jmgm@dedalus.lcc.ufmg.br.*

Abstract. Variable speed compressors and electronic expansion valves are among the most successful devices recently developed in the cooling systems control field. Currently, the researcher's expectancy points to new automatic control schemes for the next generation of cooling machines, however, some difficulties must be solved before new schemes can be used in practice. Multivariable output feedback control of cooling processes is a difficult task mainly due to the existing cross-coupling among inputs and outputs. This paper proposes a control scheme that allows the freezing power and the super heating to be independently controlled. It introduces a frequency domain based control design procedure that includes robustness analysis and controller validation. Finally, it presents simulation results.

Keywords: Cooling Systems, Multivariable Control, Frequency Domain.

1. INTRODUCTION

The improvement of power consumption efficiency of industrial devices is one of the main issues for the incoming decades. In the last century of the industrial age, the world population has virtually exploded, nature has been almost devastated and energy resources have been depleted. In spite of that, the human living comfort has become a priority for most of the whole world population, even for the third world people; and because of that, energy per-capita consumption should continuously increase in the future. It is a fact that the next decades are going to testify a continuous and strenuous search for new devices and technologies to save energy resources. The energy consumption by heating and cooling systems in commercial and industrial buildings corresponds to approximately 50% of the world energy consumption (Imbabi, 1990). Heating and cooling systems are high-energy consumption

processes and their operation in commercial and industrial buildings is still inefficient. The just arrived worldwide energy crisis has started a search for new energy-saving cooling systems.

It is already known that the solution for the poor operation of heating and cooling systems relies on the proper choice and design of automatic controllers. Low-cost controllers such as On/Off and SISO PID controllers are the standard ones in the heating, ventilation and air conditioning (HVAC) industry. However, their low energy efficiency causes an extra-undesired energy burning (Machado, 1996). Time varying thermal loads and time delays in the control loop are among the most challenging difficulties remaining to be solved for the next generation of cooling machines (Arguello et al, 1999).

Most today controllers are only capable of dealing with constant thermal loads, in practice, thermal loads are time varying. The temperature sensor location is another difficult in the control field of HVAC devices. The natural position for the sensor is close to or even

inside the target environment; currently, the sensor is usually located close to the freezing power source (to avoid time delays in the control loop).

Furthermore, to optimize energy efficiency, the generated freezing power must respond to thermal loads variations keeping the super heating as steady as possible. Conventional single-input single-output (SISO) control of cooling machines is not capable of independently control the freezing power and super-heating due to the existing inputs-outputs cross-coupling interactions.

Several control strategies to deal with the control problem of time varying processes, time delays and I/O cross coupling have been proposed by the control community. Among them, robust control, adaptive control and intelligent control are the most important. A drawback of these new sophisticated alternatives is that they are usually expensive and required advanced computational resources. To face time-varying thermal loads, time delays and I/O cross coupling; new low-cost multi-input multi-output (MIMO) control strategies must be explored.

This paper introduces a MIMO control scheme for a cooling machine based on the vapor compression cycle that permits the independent control of its output variables. It is shown that the proposed strategy permits to control the freezing power keeping the super heating almost unperturbed. Figure 1 shows the schematic diagram of a cooling machine of this type.

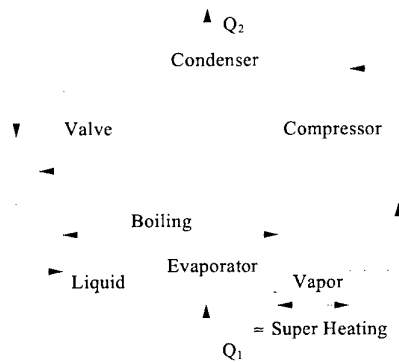


Figure 1. The Cooling System.

2. OUTPUT FEEDBACK CONTROL

Output feedback has been the industrial standard for control purposes not only to shape the plant response, fulfilling performance specifications, but mainly to deal with output disturbances and model uncertainties.

Traditionally, the industrial control community has relied on the intrinsic robustness of output feedback controllers to face the control design problem for SISO plants. A diversity of tuning algorithms has

been successfully developed and applied to SISO control of industrial plants. Behind this success there has always been a property that exists for all physical system, the dominance of the low-frequency poles in the system time response. This fact has been the background of nearly every robust control design technique. Considering this concept in the controller design, there is no need for solving the modeling problem as rigorously as it could be required without the pole dominance property.

Several attempts have been made to extend the SISO design techniques to the MIMO case. With some exceptions, the success of MIMO control design also depends on the pole dominance property. In this context, the size (order) of large-scale MIMO systems becomes less important when compared with the usually strong input-output cross-coupling existing in MIMO systems. In recent years, the research has been focused in new decoupling techniques. It is worth to mention the pioneer contributions from Bristol (1966), Kouvaritakis (1979), Mees (1981), McAvoy, (1983) and Grosdidier and Morari (1986). Characteristics of these techniques are: the control design procedure is usually carried out in the frequency domain; low frequency models are, in general, accurate enough for control design in this environment; model uncertainties are easily represented in the frequency domain; output disturbances are usually low frequency signals.

3. MIMO CONTROL – A BRIEF REVIEW

This section presents a brief review of the basic concepts on multivariable control systems. The following is based on the books from Maciejowski (1989) and Skogestad et al (1996).

The system output, $y(s)$, is given by

$$y(s) = T(s)P(s)r(s) + S(s)d(s) - T(s)m(s) \quad (1)$$

where $r(s)$ is the reference input, $d(s)$ represents the disturbances and $m(s)$ is the measurement noise.

In this case, $S(s)$ is known as the output sensitivity function and is defined as

$$S(s) = [I + G(s)K(s)]^{-1} \quad (2)$$

the system closed loop transfer function (or complementary sensitivity), $T(s)$, is then given by

$$T(s) = S(s)G(s)K(s) \quad (3)$$

The input sensitivity function is defined as

$$S_i(s) = [I + K(s)G(s)]^{-1} \quad (4)$$

and its corresponding complementary function as

$$T_i(s) = K(s)G(s)S_i(s) \quad (5)$$

A multiplicative model for plant uncertainty is

$$G(s) = G_0(s)[I + W_i(s)] \quad (6)$$

Hence, the following criteria to assess the system performance and stability can be established:

- a) The criterion for nominal performance is defined by

$$\|S(s)W_p(s)\|_\infty < 1 \Leftrightarrow \bar{\sigma}[S(s)] < \frac{1}{w_p(s)} \quad (7)$$

where $\bar{\sigma}[\cdot]$ is the greatest singular value of $[\cdot]$ and $W_p(s)$ is a performance weighting matrix given by

$$W_p(s) = w_p(s)[I] \quad (8)$$

- b) In the case of non structured uncertainty (NSU), the criterion for robust performance is given by

$$\gamma \bar{\sigma}(w_p(s)S_i(s)) + \bar{\sigma}(w_i(s)T_i(s)) \leq 1 \quad (9)$$

where $\gamma = \min(\text{plant condition number, controller condition number})$
and the criterion for robust stability (NSU) by

$$\|T(s)W_i(s)\|_\infty < 1 \Leftrightarrow \bar{\sigma}[T(s)] < \frac{1}{w_i(s)} \quad (10)$$

where $\bar{\sigma}[\cdot]$ is the greatest singular value of $[\cdot]$ and $W_i(s)$ is an uncertainty weighting matrix given by

$$W_i(s) = w_i(s)[I] \quad (11)$$

- c) In the case of structured uncertainty (SU), the robust performance condition is given by

$$\mu(Q(s)) < 1 \quad \forall \omega \quad (12)$$

where, the matrix $Q(s)$ is defined

$$Q(s) = \begin{bmatrix} Q_{11}(s) & Q_{12}(s) \\ Q_{21}(s) & Q_{22}(s) \end{bmatrix} \quad (13)$$

with

$$\begin{aligned} Q_{11}(s) &= w_p(s) S_0(s) \\ Q_{12}(s) &= w_p(s) S_0(s) G_0(s) \\ Q_{21}(s) &= -w_i(s) K(s) S_0(s) \\ Q_{22}(s) &= -w_i(s) K(s) S_0(s) G_0(s) \\ S_0(s) &= (I + G_0(s)K(s))^{-1} \end{aligned} \quad (14)$$

and the robust stability condition (SU) by

$$\mu(Q_{22}(s)) < 1 \quad \forall \omega \quad (15)$$

Equations from (7) to (15) are used in Section 6 to validate the controller design.

4. THE COOLING SYSTEM MODEL

This paper is concerned with the control of cooling systems based on vapor compressor. The system inputs are the expansion valve opening position, which defines the mass flow rate (MFR) and the compressor speed, which controls the volume flow rate (VFR). The system outputs are the super heating, ΔT , and the freezing power, Q_f , (Figure 2).

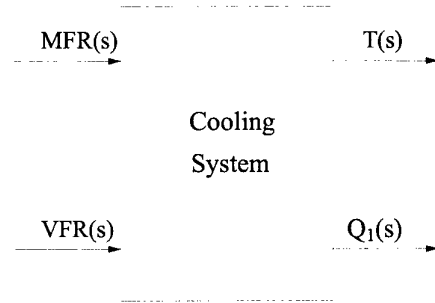


Figure 2. The Open Loop System.

Figure 3 shows the cross coupling between inputs and outputs. Ideally, only the expansion valve would be used to regulate the super heating and only the variable-speed compressor would be used to control the generation of freezing power. ($G_{12}(s) = G_{21}(s) = 0$ in Figure 3). Unfortunately, this is not the case. Actually, each of the outputs is a function of both inputs (the valve opening position and the compressor velocity). This means that $G_{12}(s)$ and $G_{21}(s)$ can not be neglected in practice.

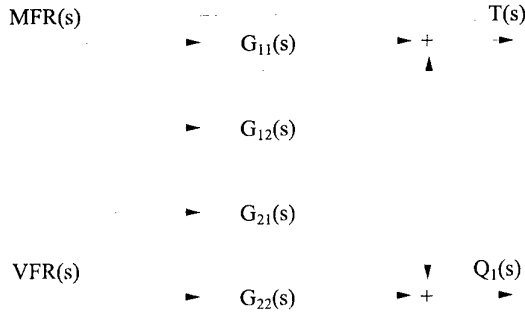


Figure 3. The Cooling System Cross Coupling.

In this case, the system dynamics can be defined by a matrix transfer function of the form:

$$\begin{bmatrix} \Delta T(s) \\ Q_1(s) \end{bmatrix} = \begin{bmatrix} G_{11}(s) & G_{12}(s) \\ G_{21}(s) & G_{22}(s) \end{bmatrix} \begin{bmatrix} MFR(s) \\ VFR(s) \end{bmatrix} \quad (16)$$

Equation 16 can be written as:

$$[Y(s)] = [G(s)][U(s)] \quad (17a)$$

with

$$\begin{aligned} [G(s)] &= \begin{bmatrix} G_{11}(s) & G_{12}(s) \\ G_{21}(s) & G_{22}(s) \end{bmatrix} \\ [Y(s)] &= \begin{bmatrix} Y_1(s) \\ Y_2(s) \end{bmatrix} = \begin{bmatrix} \Delta T(s) \\ Q_1(s) \end{bmatrix} \\ [U(s)] &= \begin{bmatrix} U_1(s) \\ U_2(s) \end{bmatrix} = \begin{bmatrix} MFR(s) \\ VFR(s) \end{bmatrix} \end{aligned} \quad (17b)$$

Several models for cooling systems can be found in the literature (Koury, 1998; Machado, 1996; Outtagarts, 1994). In this work, the cooling system model identified in Machado (1996) has been used throughout the analysis and simulation.

In this case,

$$\begin{aligned} G_{11}(s) &= \frac{-5.62}{(45s+1)} \\ G_{12}(s) &= \frac{2.49(-70s+1)}{(59.52s+1)} \\ G_{21}(s) &= \frac{33.89(-36.37s+1)}{(25.65s+1)(67.79s+1)} \\ G_{22}(s) &= \frac{22.20(630s+1)}{(80s+1)(90s+1)} \end{aligned} \quad (18)$$

Equation 18 shows that the plant is a non-minimal phase and a non-strictly proper system. Also, the conditioning numbers of the controllability and observability matrices of state space realizations of this plant are of the order of 10^4 showing that cooling systems are, in general, ill-conditioned plants.

5. THE 2x2 MIMO CONTROL LAW

In this work, the nominal performance criterion was specified as

$$\bar{\sigma}[S(s)] < \frac{1}{w_p(s)} = \frac{200s}{50s+1} \quad (19)$$

And the criterion for robust stability was chosen as

$$\bar{\sigma}[T(s)] < \frac{1}{w_i(s)} = \frac{10}{0.1s+1} \quad (20)$$

Equation 20 shows that to fulfill the robust stability criterion the plant should be made strictly proper. This can be achieved by the proper inclusion of a low-pass filter in the control loop of the form

$$[F(s)] = \begin{bmatrix} 1 & 0 \\ 0 & F_{22}(s) \end{bmatrix} \quad (21)$$

The practical consequence of this is that the compressor speed will change smoothly during the system transients. The proposed design strategy is basically a frequency-domain procedure. In this case, the MIMO controller design is carried out in two steps. First a MIMO pre-compensator, $K_1(s)$, is designed to scale the system and reach diagonal dominance at low frequency and then a MIMO controller, $K_2(s)$, is designed to meet performance specifications such that the controller will have the final form

$$[K_F(s)] = [F(s)][K_1(s)][K_2(s)] \quad (22)$$

Thus, the MIMO control law has the form:

$$\begin{aligned} [U(s)] &= [F(s)][K_1(s)][K_2(s)][R(s) - Y(s)] \\ &= [F(s)][K(s)][E(s)] \end{aligned} \quad (23a)$$

where

$$\begin{aligned} [R(s)] &= \begin{bmatrix} \Delta T(s) \text{ Setpoint} \\ Q_1(s) \text{ Setpoint} \end{bmatrix} \\ [E(s)] &= \begin{bmatrix} \Delta T(s) \text{ Error} \\ Q_1(s) \text{ Error} \end{bmatrix} \\ [K(s)] &= \begin{bmatrix} K_{11}(s) & K_{12}(s) \\ K_{21}(s) & K_{22}(s) \end{bmatrix} \end{aligned} \quad (23b)$$

and

$$[K_F(s)] = \begin{bmatrix} 1 & 0 \\ 0 & F_{22}(s) \end{bmatrix} \begin{bmatrix} K_{11}(s) & K_{12}(s) \\ K_{21}(s) & K_{22}(s) \end{bmatrix} \quad (24)$$

all entries of $K(s)$ have the general form of SISO PID controllers, thus, the MIMO PID controller is given by

$$K(s) = \begin{bmatrix} Kp_{11} + \frac{Ki_{11}}{s} + Kd_{11}s & Kp_{12} + \frac{Ki_{12}}{s} + Kd_{12}s \\ Kp_{21} + \frac{Ki_{21}}{s} + Kd_{21}s & Kp_{22} + \frac{Ki_{22}}{s} + Kd_{22}s \end{bmatrix} \quad (25)$$

Also, to have a proper controller a low-pass filter must be included in every single PID (omitted here for simplicity). Figure 4 shows the MIMO controller structure.

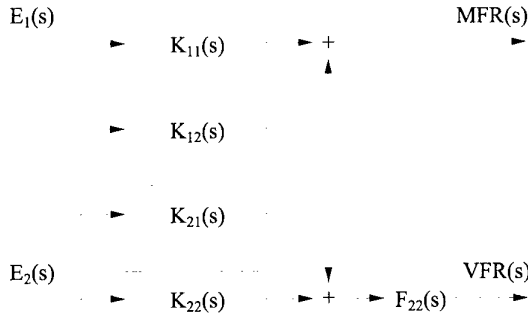


Figure 4. The MIMO PID Controller Implementation.

This leads to a closed loop matrix transfer function that can be approximated at low frequencies by

$$\begin{bmatrix} \Delta T(s) \\ Q_1(s) \end{bmatrix} \cong \begin{bmatrix} T_{11}(s) & 0 \\ 0 & T_{22}(s) \end{bmatrix} \begin{bmatrix} \Delta T(s) \text{ Setpoint} \\ Q_1(s) \text{ Setpoint} \end{bmatrix} \quad (26)$$

And since the closed loop system is diagonal dominant at low frequency, the independent control of superheating and freezing power is tangible as it is shown in the next section. Figure 5 shows the block diagram for the closed loop system.

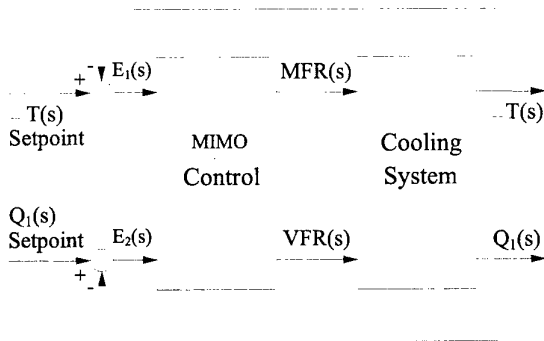


Figure 5. The Closed Loop System.

Several techniques for multivariable control design can be found in the literature (Maciejowski, 1989; Skogestad, 1996; Ho & Xu, 1998). An acceptable performance is reached with

$$\begin{aligned} F_{22}(s) &= \left[\frac{1}{80s+1} \right] \\ K_{11}(s) &= \left[\frac{-(0.2063s^2 + 0.1724s + 0.0106)}{s(1.3s+1)} \right] \\ K_{12}(s) &= \left[\frac{(0.5978s^2 + 0.0299s + 0.0005)}{s(1.3s+1)} \right] \\ K_{21}(s) &= \left[\frac{(0.3179s^2 + 0.2657s + 0.0163)}{s(1.3s+1)} \right] \\ K_{22}(s) &= \left[\frac{(1.3520s^2 + 0.0676s + 0.0011)}{s(1.3s+1)} \right] \end{aligned} \quad (27)$$

Finally, the closed loop transfer function has the form

$$T(s) = [I + G_0(s)K_F(s)]^{-1}G_0(s)K_F(s) \quad (28a)$$

with

$$[Y(s)] = [T(s)] [R(s)] \quad (28b)$$

6. SUMMARY OF THE DESIGN PROCEDURE

- Design a low-pass filter to compensate the plant for strict properness such that the open loop system be given by

$$[G(s)] = [G_0(s)][F(s)] \quad (29a)$$

- Design a pre-compensator to decouple the pre-filtered plant at low frequencies such that the open loop system be given by

$$[G(s)] = [G_0(s)][F(s)][K_1(s)] \quad (29b)$$

- Design a MIMO PID controller based on the decoupled pre-filtered plant such that the open loop system be given by

$$[G(s)] = [G_0(s)][F(s)][K_1(s)][K_2(s)] \quad (29c)$$

- Compute the MIMO controller MTF as

$$[K_F(s)] = [F(s)][K_1(s)][K_2(s)] \quad (29d)$$

7. EXPERIMENTAL RESULTS

Simulation results are presented here to illustrate and validate the controller performance.

Figure 6 presents the frequency response of the nominal plant $G_0(s)$; it shows the super-heating (quadrant II) and freezing power (quadrant IV) frequency responses; it also shows the strong effect of the I/O cross coupling (quadrants I and III). Figure 7 presents the frequency response of the plant with pre-filtering (Equation 29a); it shows the performance of the low-pass filter, $F(s)$, making the plant strictly proper (quadrant I). Figure 8 shows the plant frequency response with pre-filtering and pre-compensation (Equation 29b); it also shows (quadrants I and III) how the effects of the I/O cross coupling were eliminated by the pre-compensator $K_f(s)$.

Figures 9, 10 and 11 present the step responses of the nominal plant $G_0(s)$, the plant with pre-filtering and pre-compensation (Equation 29b) and the closed loop system (Equation 28), respectively.

Finally, Figures 12 and 13 show, graphically, the controller performance and validation and also the robustness analysis based on Equations 7 to 15.

8. FINAL COMMENTS

Classical on-off controllers for cooling machines have already shown to be inefficient for energy saving purposes. Variable compressor speed operation has recently emerged as the solution for the energy consumption minimization problem. The searching for an inexpensive compressor speed controller is currently on the focus of the attention of the control community and although some fine results can be found in the technical literature, the final solution is still under investigation.

This paper has introduced a designing procedure of MIMO controllers for cooling machines based on vapor compression. The proposed technique has been applied to an ill-conditioned, non-minimal phase and non-strictly proper model of an existing cooling machine showing excellent performance in analysis and simulation. The controller performance and stability robustness has been assessed and validated through well-known criteria. The results have shown that independent control of superheating and freezing power in cooling systems is a feasible task and that the proposed MIMO controller scheme has a unique potential for saving-energy-oriented control.

REFERENCES

- Arguello-Serrano, B. & Vélez-Reyes, A., "Nonlinear Control of a Heating, Ventilating, and Air Conditioning System with Thermal Load Estimation", IEEE Transactions on Control Systems Technology, vol. 7, pp. 56-63, January 1999.
- Bristol, E.H., "On a New Measure of Interaction for Multivariable Process Control", IEEE Transactions on Automatic Control, Vol. 11, pp.133-134, 1966.
- Grosdidier, P. and Morari, M., "Interactions Measurements for Systems under Decentralized Control", Automatica, vol. 22, pp. 309-319, 1986.
- Ho, W.K. and Xu, W., "Multivariable PID Controller Design Based on the Direct Nyquist Array Method", Proceedings of the American Control Conference, Philadelphia, Pennsylvania, pp. 3524-3528, 1998.
- Imbabi, M.S., "Computer Validation of Scale Model Test for Building Energy Simulations", International Journal on Energy Resources, Vol. 14, pp.727-736, 1990.
- Kouvaritakis, B., "Theory and Practice of the Characteristic-Locus Design Method", IEE Proceedings, Vol. 126, pp. 542-548, 1979.
- Machado, L., Modele de Simulation et Etude Experimentale d'un Evaporateur de Machine Frigorifique en Regime Transitoire, L'Institut National des Sciences Appliquees de Lyon, France, 1996.
- Maciejowski, J.M., "Multivariable Feedback Design", Addison-Wesley Publishing Company, 1989.
- McAvoy, T. J., "Interaction Analysis - Principles and Applications", Instrument Society of America, 1983.
- Mees, A.I., "Achieving Diagonal Dominance", Systems and Control Letters, vol. 1, pp. 155-158, 1981.
- Outtagarts, A., Comportement Dynamique d'un Evaporateur de Machine Frigorifique Alimente par un Detendeur Electronique, L'Institut National des Sciences Appliquees de Lyon, France, 1994.
- Skogestad, S. and Postlethwaite, I., "Multivariable Feedback Control - Analysis and Design", John Wiley & Sons, 1996.
- Stoecker, W.F. & Jones, J.W., Refrigeration and Air Conditioning, McGraw-Hill Book Company, 1982.

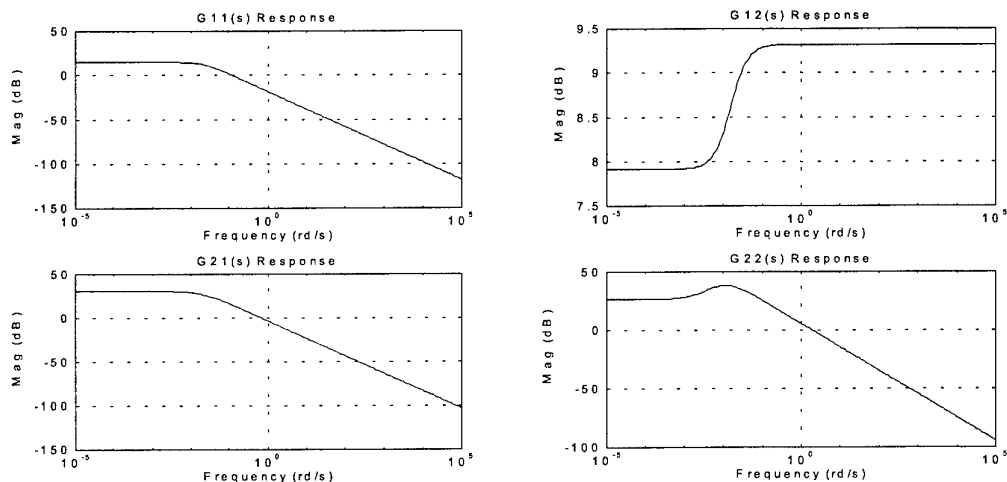


Figure 6. Nominal Plant Frequency Response $[G_0(s)]$ (Open Loop).

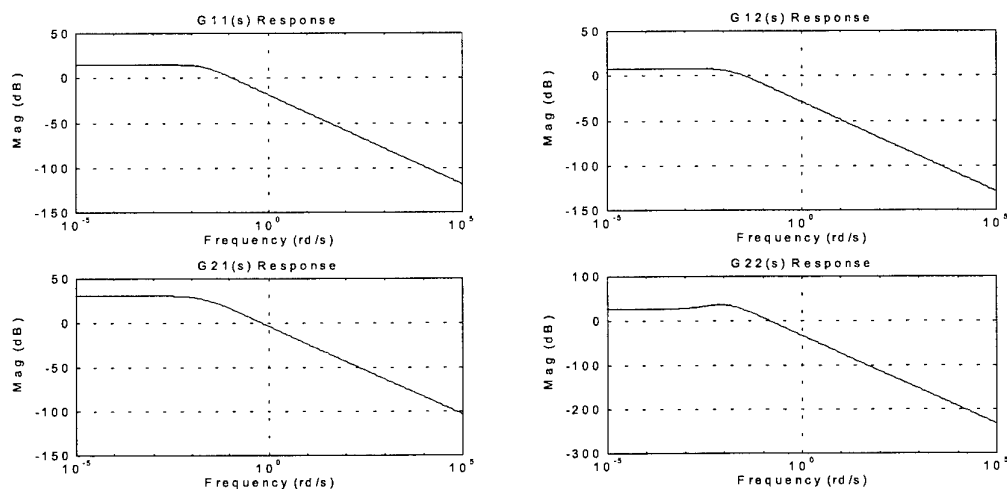


Figure 7. Pre-Filtered Nominal Plant Frequency Response $[G_0(s) F(s)]$ (Open Loop).

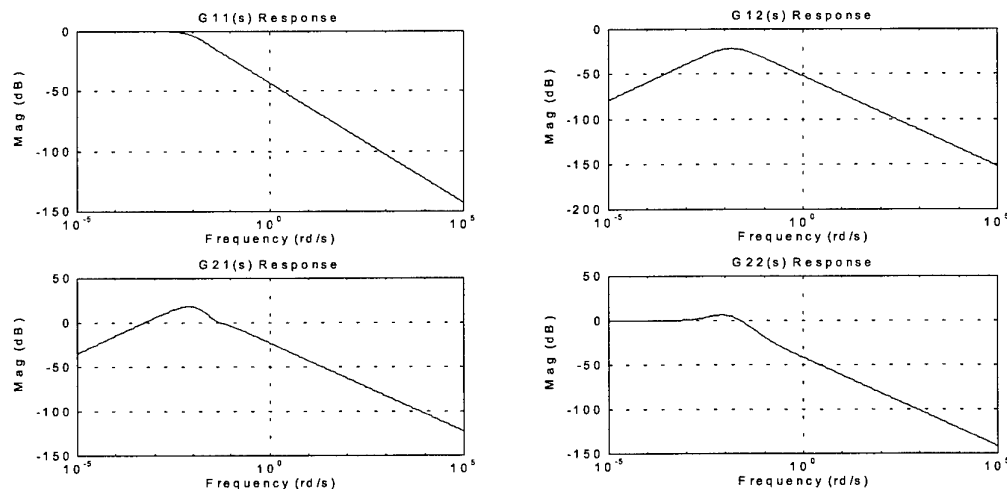


Figure 8. Pre-Compensated, Pre-Filtered Nominal Plant Frequency Response $[G_0(s) F(s) K_1(s)]$ (Open Loop).

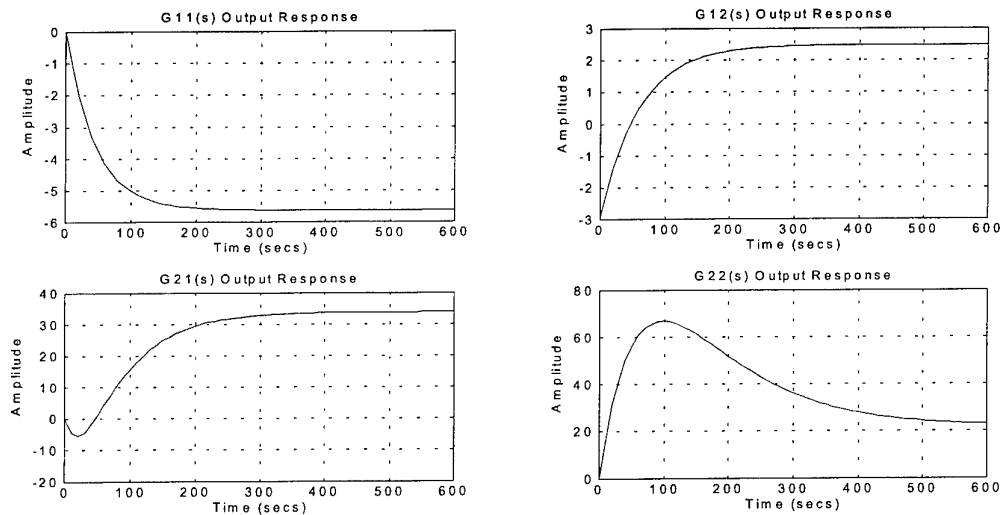


Figure 9. Nominal Plant Step Response $[G_0(s)]$ (Open Loop).

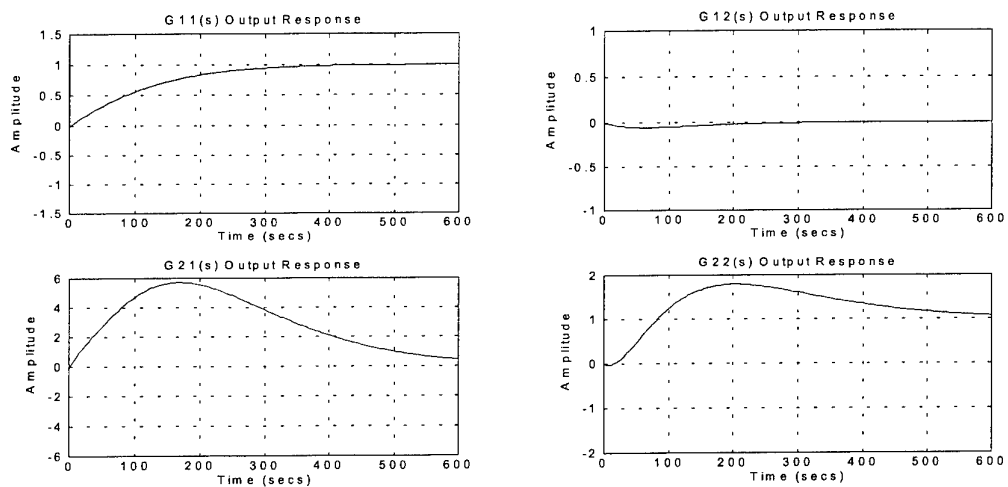


Figure 10. Pre-Compensated and Pre-Filtered Nominal Plant Step Response $[G_0(s) F(s) K_1(s)]$ (Open Loop)

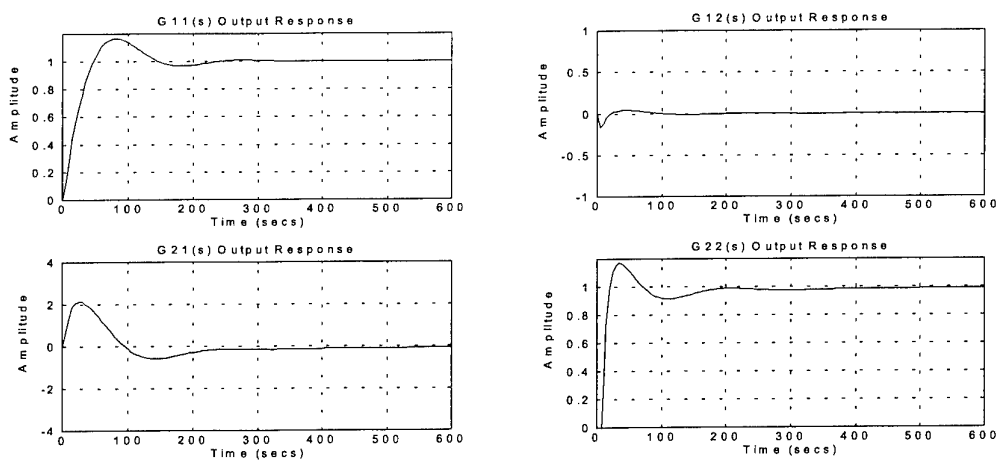


Figure 11. Closed Loop System Step Response $[Closed\ Loop\ of\ G_0(s) F(s) K_1(s) K_2(s)]$

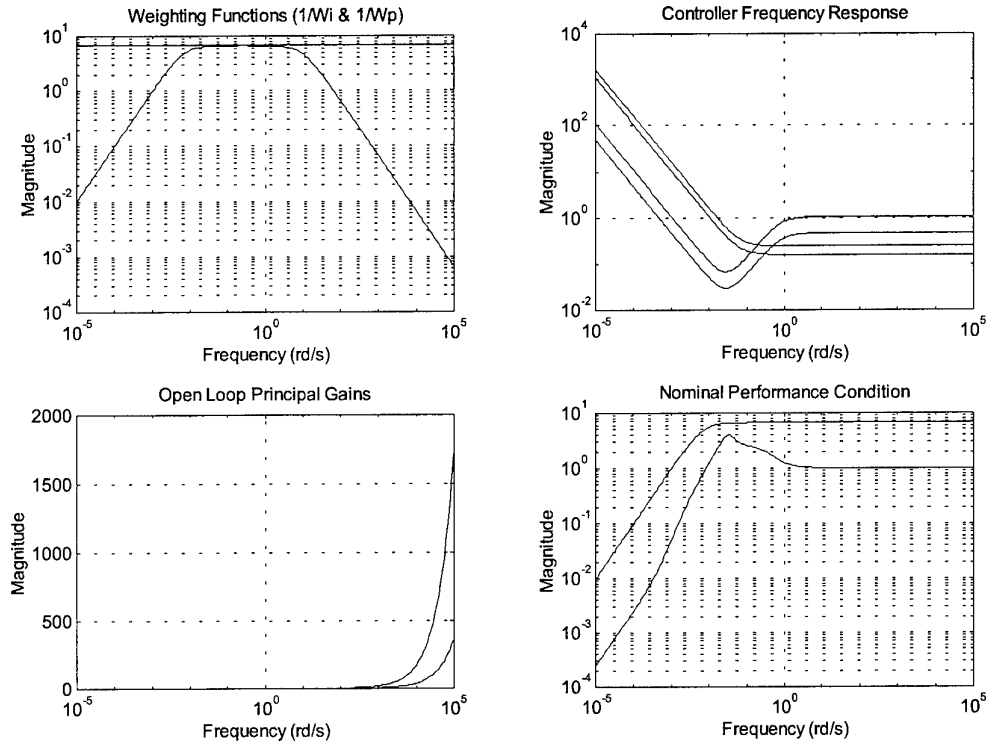


Figure 12. Controller Validation and Robustness Analysis.

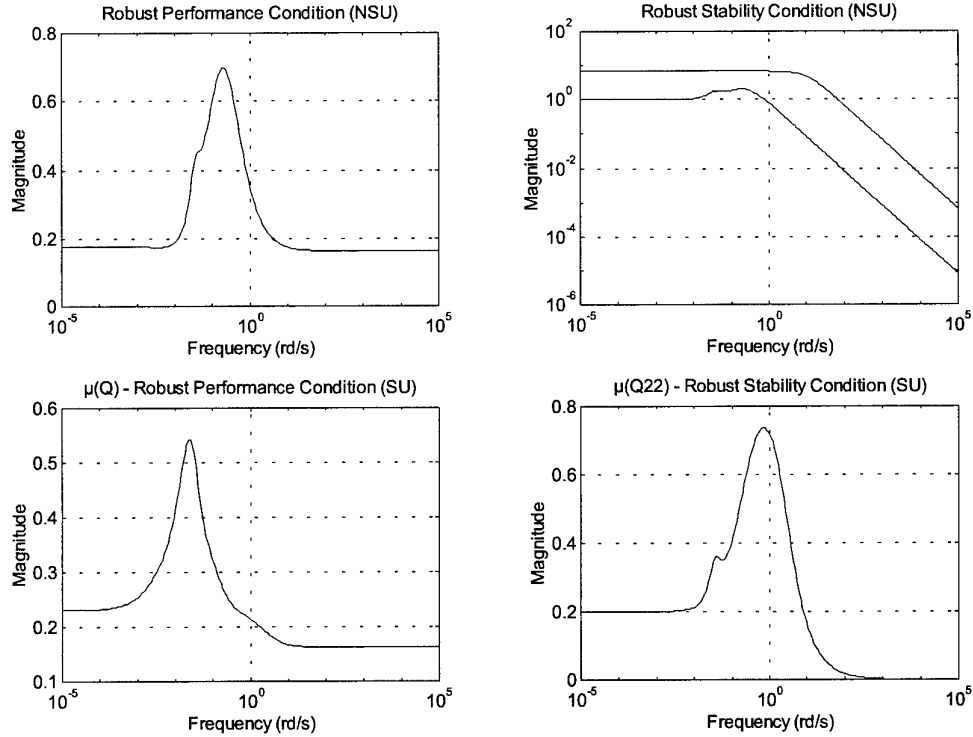


Figure 13. Controller Validation and Robustness Analysis.

QFT CONTROL DESIGN FOR AN APPROXIMATELY LINEARIZED PNEUMATIC POSITIONING SYSTEM

Fulin Xiang and Jan Wikander

*Mechatronics Research Group, Department of Machine Design
 Royal Institute of Technology, S-100 44 Stockholm, Sweden*

Abstract: In this work, a block-oriented approximate feedback linearization for control of a pneumatic cylinder positioning system is briefly introduced and a rather detailed discussion is presented on the uncertain linearization residual characterization based on the describing function technique. With the limitation of the Bode's gain-phase relationship, making use of the characterized gain-phase information leads to a good trade-off between performance and stability in the loopshaping, thus the conservativeness of the QFT robust control design is significantly reduced and high control performance is achieved. Simulation and experimental results are shown.

Keywords: feedback linearization, pneumatic systems, friction, robust control, uncertainty, position control, describing functions.

NOTATION

- D denotes Laplace or differential operator.
- The square bracket "[]" in the expressions, like $G(D)[q(u)]$ or $G^{-1}(D)[q(u)]$, is used to define that the bracketed component $[q(u)]$ is to be located on the input side of the linear dynamics $G(D)$ or $G^{-1}(D)$.
- The term with an over-head " $\hat{}$ " represents its corresponding estimate, e.g. $\hat{G}(D)$ is the estimate of $G(D)$ and in the perfect case $\hat{G}(D) = G(D)$.
- \bar{N} with its corresponding subscript represents a sinusoidal input describing function, SIDF.

the presence of high friction has long been a challenge topic, because of the substantial inherent nonlinearities within the system. Xiang (2001) proposed a block-oriented approximate feedback linearization technique for the control and modelling of pneumatic actuator systems. By this technique, a controlled pneumatic system can be considered to be composed by some series and parallel connections of blocks -- nonlinear elements and linear sub-systems. Feedback linearization is then implemented based on the block level units. It is shown that high control performance is achieved by this fairly straight forward approach. Due to the system uncertainties and constraints, there might be considerable uncertain linearization residuals left. In this case, if high robustness is pursued for the final pneumatic servo system, it is quite appropriate to select a robust control technique for the controller synthesis of the approximate linearized system.

1. INTRODUCTION

High precision positioning of a pneumatic actuator in

One of the rather attractive robust control techniques is the quantitative feedback theory (QFT) which has

been used effectively in a variety of control applications, such as flight control, Houpis (1995). Originally developed by Horowitz and Sidi (1972, 1978) and Horowitz (1973), it is aimed at designing a feedback controller so that pointwise frequency response specifications on closed loop tracking and disturbance rejection are met in spite of large parametric and/or unstructured plant uncertainty. Comparing to other robust control techniques, such as H_∞ control, QFT can take into account phase information in the design process. Thus it can provide a somewhat less conservative framework for making trade-off between performance and stability. But, as the linear time invariant control can not breakthrough the Bode's gain-phase relationship, large system uncertainty will exert even greater limitation on control system performance. To overcome the problem, nonlinear QFT and some other nonlinear techniques, such as the reset control and nonlinear lead compensator, have been explored in quite a few works, such as Glass and Franchek (2000), Banos and Barreiro (2000), and Zheng *et al* (2000). But as one would expect, there are still many open questions and techniques to be formalized in nonlinear QFT, Banos and Barreiro (2000).

Rather than seeking a nonlinear control algorithm, the work presented here focuses on characterization of the uncertain linearization residual or the linearized system, based on the sinusoidal input describing function, SIDF, technique, Taylor (1999). It is shown that the conservativeness of the QFT robust control design can be significantly reduced by making use of the characterized gain-phase information of the linearized (uncertain) system. With the limitation of the Bode's gain-phase relationship, making use of the possible gain-phase information leads to a good trade-off between performance and stability in the loopshaping, thus results in high control performance. A convincing demonstration of this, presented in this work, is the position control design for the friction compensated pneumatic system where there exists considerable linearization (friction compensation) residual due to the slow force generation dynamics.

The organization of the following sections is as: Section 2 gives a mathematical description of the concerned pneumatic system and a brief introduction of the block-oriented approximate feedback linearization; In section 3, a rather detailed discussion is presented on the uncertain linearization residuals characterization for both the inner force generation loop and outer motion control loop; Based on the characterization results, in section 4, QFT controller design is presented; Some experimental position control results are shown in section 5; The final section gives the conclusions and discussion.

2. CONSTITUTIVE EQUATIONS AND BLOCK-ORIENTED APPROXIMATE FEEDBACK LINEARIZATION

As shown in Fig. 1, the pneumatic system concerned in this work is made up of a horizontally mounted 0.032x0.4 rodless cylinder, two 3/2 way solenoid spool servo valves with a nominal flow rate of 500 l/min, two analog pressure sensors and an optical incremental position sensor with a resolution of 5 μ m.

The supply pressure is 7×10^5 Pa. The maximum static cylinder friction force is about 15-20% of the maximum static cylinder force. This means that the nonlinear friction force is so significant that it is taken as the main disturbance force.

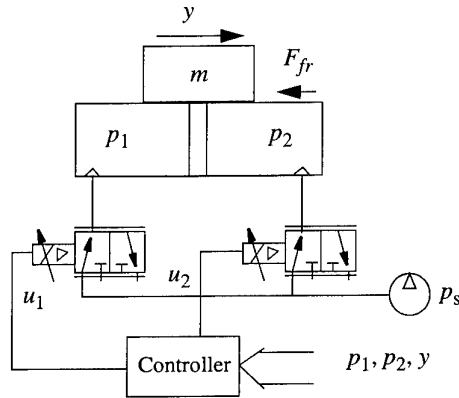


Figure 1: Rodless pneumatic cylinder positioning system

With the assumptions that the supply pressure p_s and the supply air temperature T are constants; temperatures are uniform throughout of the system; air can be considered as an ideal gas; the kinetic energy of the air is negligible; the flow force effect on the spool can be neglected; and the servo valve's model can be simplified as an input nonlinearity followed by a normalized Hurwitz dynamics, then the pneumatic actuator system can be described by the following equations.

- Motion equations

$$m\ddot{y} + f_v\dot{y} = F - F_{nfr}(\dot{y}) \quad 0 \leq y \leq l \quad (1)$$

$$F = A(p_1 - p_2) \quad 0 < p_{at} \leq p_i \leq p_s \quad (2)$$

where, for $i = 1, 2$, p_i represents the i th chamber's pressure; m , l , A , y , f_v , $F_{nfr}(\dot{y})$, p_{at} and p_s are the payload mass, cylinder stroke, piston area, displacement, viscous friction coefficient, nonlinear friction force, atmosphere and supply pressure respectively.

- Pressure build-up equation

$$\dot{p}_i = \left(\frac{RT}{A} Q_i - \dot{y}_i p_i \right) \frac{n}{y_i + y_0} \quad (3)$$

where $y_0 > 0$ is the effective initial displacement corresponding to the non-working volume; n, R, T are specific heat ratio, gas constant, and supply air temperature respectively; For $i = 1, 2$, Q_i and y_i represent the i th chamber's mass flow rate and corresponding displacement ($y_1 = l - y_2 = y$) respectively.

- Mass flow rate equations

$$Q_i = \frac{p_{ui} c_q}{\sqrt{T}} q_p(p_i) G_{v0}(D) [q_u(u_i)] \quad (4)$$

$$q_p(p_i) = \begin{cases} 1 & p_{ri} = \frac{p_{di}}{p_{ui}} \leq b \\ \sqrt{1 - \left(\frac{p_{ri} - b}{1 - b}\right)^2} & p_{ri} = \frac{p_{di}}{p_{ui}} > b \end{cases} \quad (5)$$

$$p_{di} = p_i, \quad p_{ui} = p_s \quad \text{while } G_{v0}(D) [q_u(u_i)] \geq 0$$

$$p_{di} = p_{at}, \quad p_{ui} = p_i \quad \text{while } G_{v0}(D) [q_u(u_i)] < 0$$

where for $i = 1, 2$, u_i, p_{ui} and p_{di} represent the i th chamber's corresponding valve input, up and down stream pressure respectively; b and c_q represent the critical pressure ratio and specific heat constant respectively; $G_{v0}(D)$ stands for the normalized Hurwitz valve dynamics; $q_u(u_i)$ represents the lumped effective valve nonlinearity which is supposed to be hysteresis-like as in Xiang and Wikander (2001). Eq. 4 and 5 originate from Sanville (1971), but the fixed effective orifice cross section area is replaced with $G_{v0}(D) [q_u(u_i)]$ and the discharge coefficient is neglected here.

From Eq. 1, 2 and 3 it can be seen that the coupling between the pressure build-up and piston motion is mainly defined by the measurable variables p, y and \dot{y} .

If y and \dot{y} are treated as two exogenous disturbance signals in the pressure build-up process, then the whole servo system can be decomposed into two cascaded, inner pressure and outer motion control, sub-systems. Let

$$L_p := c_q R \sqrt{T} / A \quad (6)$$

$$N_v(\dot{y}_i, p_i) := -\dot{y}_i p_i \quad (7)$$

$$N_y(y_i) := n / (y_i + y_0) \quad (8)$$

where L_p is a lumped constant; N_v and N_y represent the nonlinear blocks through which the two exogenous disturbance signals, y and \dot{y} , act on the inner pressure sub-system. With these notations, for $i = 1, 2$, the pressure build-up model can be re-expressed in the following block-oriented form.

$$\dot{p}_i = (L_p p_{ui} q_p(p_i) G_{v0}(D) [q_u(u_i)] + N_v(\dot{y}_i, p_i)) N_y(y_i) \quad (9)$$

Now select the valve input signal u_i as

$$u_i = \hat{q}_u^{-1} (\hat{G}_{v0}^{-1}(D) [\hat{p}_{ui} \hat{q}_p^{-1}(p_i) \hat{N}_y^{-1}(y_i)] v_{pi} - \hat{L}_p \hat{G}_{v0}^{-1}(D) [\hat{p}_{ui} \hat{q}_p^{-1}(p_i) \hat{N}_v(\dot{y}_i, p_i)]) \quad (10)$$

where v_{pi} is the introduced equivalent linear pressure control signal. By substituting Eq. 10 into 9, it is evident that when the estimates tend to be their corresponding true values and if all the inverse functions can be exactly realized, the pressure build-up system is reduced to the linear subsystem

$$\dot{p}_i = G_v(D) [v_{pi}] \quad (11)$$

where $G_v(D) := L_p G_{v0}(D)$.

Based on this linearized pressure build-up model, an inner pressure controller can be designed with just some linear feedback control law. Let $G_F(D)$ represent the i th chamber's closed pressure control loop dynamics, with the presented symmetric or asymmetric pressure control strategy given in Xiang (2001), the force response can be expressed as

$$F = G_F(D) [F_{ref}] \quad (12)$$

Assuming $G_F(D)$ is of minimum phase, the force reference can be chosen as

$$F_{ref} = v_m + \hat{G}_F^{-1}(D) [\hat{F}_{nfr}] \quad (13)$$

where v_m is the introduced equivalent linear motion control signal. Substituting Eq. 13 into 12 and then the result into Eq. 1, gives

$$m\ddot{y} + f_v \dot{y} = G_F(D) [v_m] - \delta_{fr}(\dot{y}, D) \quad (14)$$

where

$$\delta_{fr}(\dot{y}, D) = F_{nfr}(\dot{y}) - G_F(D) \hat{G}_F^{-1}(D) [\hat{F}_{nfr}(\dot{y})] \quad (15)$$

represents the nonlinear friction compensation residual. If the inverse of $G_F(D)$ can be exactly realized and the estimate of the nonlinear friction tends to be its true value, then $\delta_{fr} \rightarrow 0$, and the linearized motion control system is reduced to

$$m\ddot{y} + f_v \dot{y} = G_F(D) [v_m] \quad (16)$$

3. CHARACTERIZATION OF THE LINEARIZATION RESIDUALS

Due to the system uncertainties and limitations, perfect cancellation of all the nonlinear effects is impossible, which means that the existence of linearization residual is unavoidable. So, how to

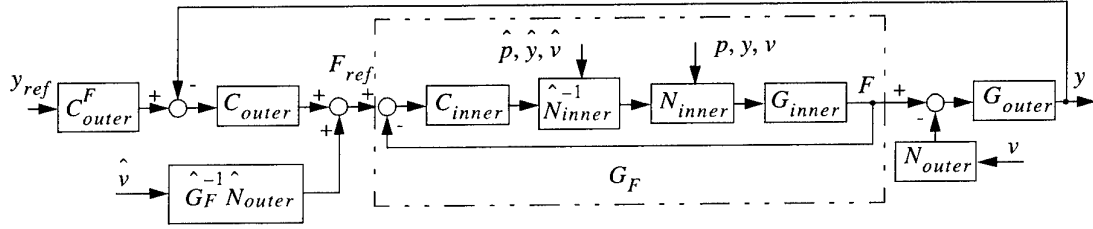


Figure 2: Linearization and inner-outer cascaded control design

characterize the linearization residual, to reduce its adverse effects on the overall system and how to design a high performance control system despite the existence of considerable linearization residual will be the main QFT control design problems. Moreover, solving these problems will relax the requirement on modelling and linearization accuracy. Since the pressure p , corresponding to the force F measurement, is introduced for the linearization, a cascaded feedback control structure shown in Fig. 2 seems to be a superior choice. In the figure, the inner and outer loop nonlinearities N_{inner} , N_{outer} (the nonlinear friction) and their corresponding compensators \hat{N}_{inner}^{-1} and $\hat{G}_F \hat{N}_{outer}^{-1}$ are shown conceptually. The controllers to be designed include the inner feedback controller C_{inner} , outer feedback controller C_{outer} and outer feed forward controller C_{outer}^F . Even though QFT is a well established robust control technique, a good characterization of the approximate linearization residual will definitely facilitate the trade-off making between the performance and stability in the loop shaping of the QFT control design, thus result in high control performance. In characterizing the inner-outer linearization residuals, \hat{N}_{inner}^{-1} vs N_{inner} and $\hat{G}_F \hat{N}_{outer}^{-1}$ vs N_{outer} , the following facts and assumptions are admitted.

- a1) In both inner and outer loop feedback linearization, “under” nonlinearity compensation strategy is employed, which means that after the linearization the nonlinear effect is either totally removed or considerably reduced but the residual possesses its original nonlinearity’s characteristics and does not lead to an unstable plant.
- a2) Considering the input constraint, sensor noise and the limited compensation improvement effect, the linear dynamics inverse \hat{G}_F^{-1} is not implemented, Xiang (2001).
- a3) The two chamber pressures, p_1 and p_2 , are controlled symmetrically, and are kept varying around a selected base pressure such that in most cases $q_p \approx 1$.

- a4) The estimation (measurement) errors of y, \dot{y} , p_1 and p_2 are negligible.

Consequently, it is supposed that the linearization residuals can be described in a structure of their original form, but with less nonlinear effects, especially in low frequency range. In accordance with frequency domain QFT control design, all the linearization residuals will be characterized with the describing function technique, one of the approximate ways of representing the frequency response of a nonlinear system.

3.1 Inner Loop Linearization Residuals

Except for the nonlinear friction force, i.e. the outer loop nonlinearity N_{outer} , all other nonlinearities are supposed to be in the inner loop. The inner loop nonlinearity N_{inner} mainly consists of valve nonlinearity $q_u(u)$, flow rate related nonlinearity $q_p(p)$ and p_u , as well as piston motion coupling N_y and N_v . Substitute Eq. 10 into 9. Let

$$\alpha := p_{ui} q_p N_y G_{v0} [\hat{q}_u^{-1} (\hat{G}_{v0}^{-1} [\hat{p}_{ui} \hat{q}_p^{-1} \hat{N}_y^{-1}])] \quad (17)$$

$$\begin{aligned} \beta_0 &:= (\beta_{00} + N_v) N_y \\ &= -(\dot{y}_i - \beta_{00}/p_i) N_y p_i = -\beta p_i \end{aligned} \quad (18)$$

where

$$\begin{aligned} \beta_{00} &:= L_p p_{ui} q_p G_{v0} \left[q_u \left(\hat{q}_u^{-1} \left(-L_p \hat{G}_{v0}^{-1} [\hat{p}_{ui} \hat{q}_p^{-1} \hat{N}_y^{-1}] \right) \right) \right] \\ \beta &:= (\dot{y}_i - \beta_{00}/p_i) N_y \end{aligned} \quad (19)$$

Then, the pressure build-up system can be represented as

$$\begin{aligned} \dot{p}_i &= \alpha L_p G_{v0} [q_u(\hat{q}_u^{-1}(v_{pi}))] + \beta_0 \\ &= \alpha L_p G_{v0} [q_u(\hat{q}_u^{-1}(v_{pi}))] - \beta p_i \end{aligned} \quad (20)$$

With \bar{N}_{qu} representing the valve nonlinearity compensation residual’s SIDF, then from Eq. 20, the linearized pressure build-up system plant transfer function can be expressed as

$$G_v(s) = \frac{L_p \alpha}{s + \beta} G_{v0}(s) \bar{N}_{qu} \quad (21)$$

In this way the linearization residuals in the inner pressure build-up system are lumped in three terms, i.e. α , β and \bar{N}_{qu} . When all the estimations tend to be their corresponding true values and when all the inverse functions can be exactly realized, $\alpha \rightarrow 1$, $\beta \rightarrow 0$ and $\bar{N}_{qu} \rightarrow 1$. Now, characterization of the inner loop linearization residuals is reduced to characterization of these three terms.

Valve nonlinearity residual \bar{N}_{qu} . The valve nonlinearity $q_u(u)$ is a lumped hysteresis-like input nonlinearity. It represents the integrated effects of all the nonlinear elements from valve input to valve effective opening. In Xiang and Wikander (2001), experimental results show that with either dead-zone inverse or backlash inverse the hysteresis-like nonlinear effect, in frequency response (describing function), can be considerably reduced. By assumption a1), the linearization residual is still a hysteresis-like nonlinearity and can be simplified as a backlash hysteresis -- the simplest representation of hysteresis. The backlash SDF shows that when the input amplitude decreases lower than certain value both gain and phase will decrease greatly, Slotine and Li (1992). With small amplitude input, considerable phase lag may cause control problem, such as limit cycles. The condition for a limit cycle occurrence is when the loop transfer function $C(s)G(s)$ is intersected with the negative inverse of the nonlinearity, backlash, describing function $-1/\bar{N}_{qu}$. To avoid limit cycle, the controller $C(s)$ must be designed such that the intersection can not occur.

Flow rate related nonlinearity compensation residual -- the α term. By assumption a1) and a3), the flow rate related nonlinearity compensation residual α has a similar but less effect on the inner system than its original nonlinearity $p_u q_p$. This means that the effect of the compensation residual α is between the two extremes, totally un-compensated and compensated, cases. Supposing the effect of \bar{N}_y in α term can be negligible, then the investigation can be carried on in a fixed cylinder piston case e.g. $0 < y = y_{fix} < l$ and y_{fix} is a constant. Referring to Eq. 9, to characterise the α term, a simulation model as depicted in Fig. 3 is used, where u represent the valve opening. The SDF

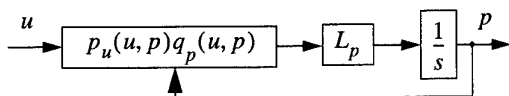


Figure 3: \bar{N}_p in un-compensated case

simulation on this model is conducted with the method

given in Xiang and Wikander (2001). With \bar{N}_p representing its simulated SDF, the gain and phase plots of \bar{N}_p are shown in Fig. 4 and Fig. 5, where the

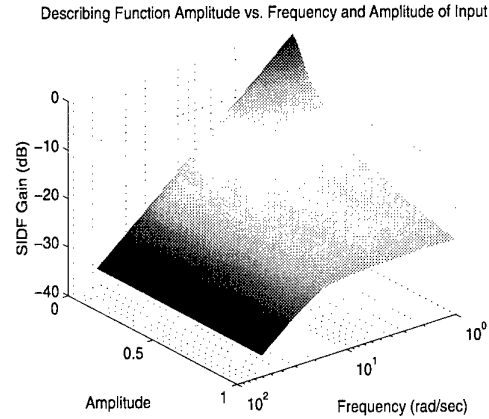


Figure 4: \bar{N}_p gain plot

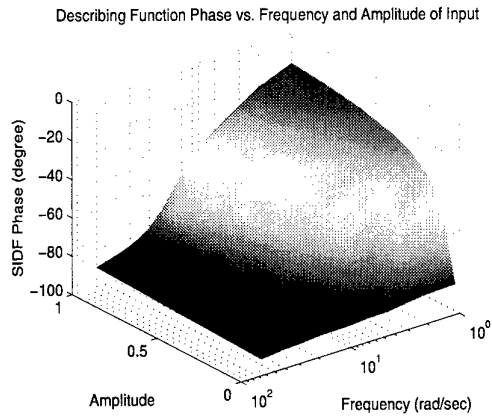


Figure 5: \bar{N}_p phase plot

input and output have been normalized. From these figures it can be seen that

- When the input sinusoid's frequency is high, the output signal p is small due to the integrator effect, and thus the $p_u q_p$'s effect is small. Otherwise, $p_u q_p$'s effect will become more and more significant with the increase of input amplitude. At the maximum input amplitude point, $p_u q_p$'s effect will get most serious while when the input amplitude tends to be zero, the system tends to be a pure linear integrator system.
- $p_u q_p$'s nonlinear effect results in a considerable drop in the SDF gain, but also considerable reduction of phase lag. The later feature, in fact, is favourable for the servo control.

Fig. 6 shows both the linear case and the most seriously nonlinear case of \bar{N}_p . For the system

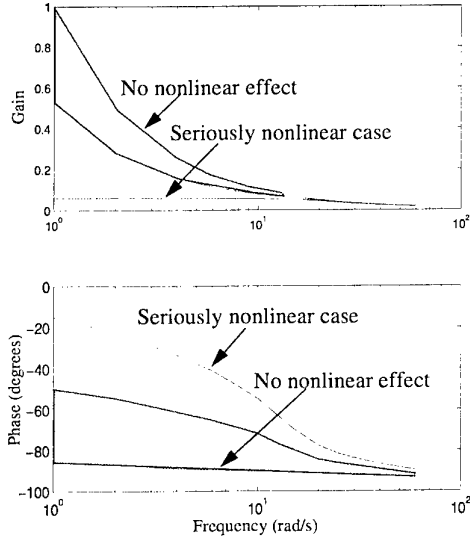


Figure 6: the system of \bar{N}_p followed by an integrator

depicted in Fig. 3, when $p_u q_p$ is replaced with α , it is reasonable to suppose that the system's frequency response is located in the shadowed area of Fig. 6, which represents the equivalent family of linear time invariant plants (ELF) corresponding to the compensation residual α . Its area and shape depend on the flow rate related nonlinearity compensation quality. In the perfect case of flow rate related nonlinearity compensation, $\alpha = 1$, the 'no nonlinear effect' case indicated in Fig. 6. So the main characteristics of the flow rate related nonlinearity compensation residual is to result in gain decreasing and phase 'lead'. Since the phase 'lead' caused by the flow rate related nonlinearity compensation residual is beneficial, and since normally this effect occurs with large input amplitude and low frequency, the phase problem is believed to be not crucial. So, for controller synthesis simplicity, the phase effect of the α term can be neglected. In this way, α can be taken as a bounded scalar, i.e. $\alpha \in [\alpha_l, \alpha_u]$. The value of the lower bound α_l and upper bound α_u should be positive and around the ideal value $\alpha_{ideal} = 1$.

Motion coupling nonlinearity compensation residual-the β term. Referring to Eq. 3, when the displacement y and velocity \dot{y} are taken as an external signal, the system from flow rate to pressure can be considered as a first order system. Furthermore, for the i th chamber, when $\dot{y}_i \geq 0$, it is a stable plant. By assumption a1), the linearization is supposed to be realized in the way such that $\beta \geq 0$. From Eq. 19, it can be seen that the amplitude of β is also dependent on the displacement. With the decreasing of the corresponding chamber

volume, the amplitude of β will increase. The β term, here, is supposed can be characterized as a scalar varying in the range of $[0, \beta_u]$. The specification of the upper bound depends on the compensation quality and displacement range.

3.2 Friction Compensation Residual

When the force loop dynamics is not fast enough and when the nonlinear friction effect (especially the stiction effect) is significant, like the case in the presented pneumatic positioning system, friction compensation is difficult and the compensation residual is considerable. There are quite many aspects that affect the residual. But first of all, a friction model which can give a more explicit description of the friction behaviour in low velocity and at velocity reversal is desired. Among the so many friction models, the LuGre dynamic friction model proposed in Canudas de Wit *et al* (1995) is considered here to be a satisfactory one, and it is used in this work. It can be expressed as

$$F_{fr} = F_{nfr} + f_v v = \sigma_0 z + \sigma_1 \dot{z} + f_v v$$

$$\dot{z} = v - \frac{|v|}{g(v)} z \quad (22)$$

$$g(v) = \frac{1}{\sigma_0} \left(F_c + (F_s - F_c) e^{-(v/v_s)^2} \right)$$

where $v = \dot{y}$ is the velocity, z the virtual friction state, σ_0 stiffness coefficient, σ_1 internal damping coefficient, F_c Coulomb friction, F_s static friction and v_s Stribeck velocity. Detailed discussion on nonlinear friction compensation is presented in Xiang (2001). For the friction compensated positioning system, careful characterization of the compensation residual will facilitate the controller synthesis to achieve high positioning performance.

As discussed in Xiang (2001), the dynamics inverse effect, the $\hat{G}_F^{-1}(D)$ term in Eq. 13, for output nonlinearities compensation would be limited by the control input constraint and sampling frequency. By making a trade-off between the compensation effort and the compensation effect improvement, $G_F(D)$ inverse is not used in the friction compensation. So Equation 13, in fact, is reduced to

$$F_{ref} = v_m + \hat{F}_{nfr} \quad (23)$$

As a result, Eq. 15 can be represented as

$$\delta_{fr}(\dot{y}, D) = F_{nfr}(\dot{y}) - G_F(D)[\hat{F}_{nfr}(\dot{y})] \quad (24)$$

In characterization of the friction compensation residual $\delta_{fr}(\dot{y}, D)$, supposing that the friction estimation error can be neglected, Eq. 24 is reduced to

$$\delta_{fr}(\dot{y}, D) = (1 - G_F(D))[F_{nfr}(\dot{y})] \quad (25)$$

Since the behaviour of nonlinear friction and the behaviour of the friction affected system are interacting with each other, an investigation on the integrated system is more appreciated. Accordingly a simulation model presented in Fig. 7 is used for this

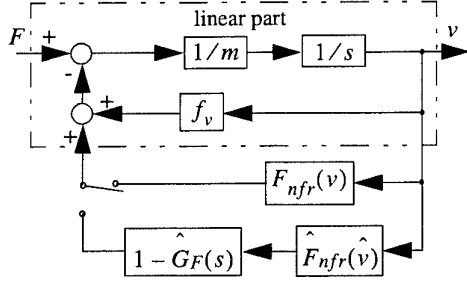


Figure 7: Simulation model for the characterization of friction and friction compensation residual effect

investigation. In this simulation, $G_F(D)$ is a second order linear dynamics characterised with $\omega_F = 78$ rad/s and $\xi_F = 0.65$; The payload mass $m = 5.5$ kg; The force input signal F is a sinusoidal signal with amplitude of $a = [0.012, 0.015, 0.02, 0.03, 0.04, 0.05, 0.06, 0.08, 0.09, 0.1, 0.13, 0.15, 0.2, 0.3, 0.4, 0.5] \times 600$ N, and frequency of $\omega = [1, 2, 4, 6, 8, 10, 12, 20, 30, 40, 60, 80, 100, 150, 200]$ rad/s; The LuGre friction model parameter values used in the simulation are

σ_0 (N/m)	σ_1 (Ns/m)	v_s (m/s)	F_c (N)	F_s (N)	f_v (Ns/m)
1.15e5	1500	0.01	60	80	95

When there is no nonlinear friction, the system from F to v is linear and its SIDF, represented with \bar{N}_l , is equal to its frequency response function, i.e.

$$\bar{N}_l(a, \omega) = 1/(m \cdot j\omega + f_v) \quad (26)$$

To check how the nonlinear friction F_{nfr} and friction compensation residual δ_{fr} affect the linear system of \bar{N}_l , two cases are considered. First, the no compensation case, i.e. the system defined by Eq. 1; The simulated SIDF is represented with \bar{N}_{nfr} . And the last, the compensated case, i.e. the system defined by Eq. 1 but with F_{nfr} term replaced by δ_{fr} of Eq. 25; The simulated SIDF is represented with \bar{N}_δ .

Fig. 8 and Fig. 9 show the gain and phases change of the linear system \bar{N}_l caused by the nonlinear friction F_{nfr} . Some facts can be seen From the plots. First, with

the increase of frequency, the nonlinear friction's

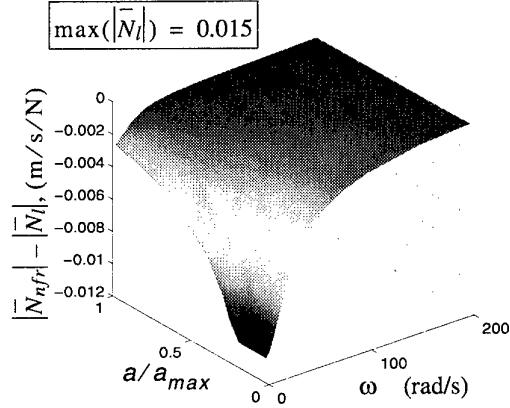


Figure 8: Gain change caused by the nonlinear friction

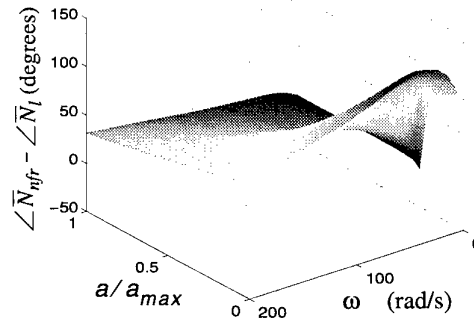


Figure 9: Phase change caused by the nonlinear friction

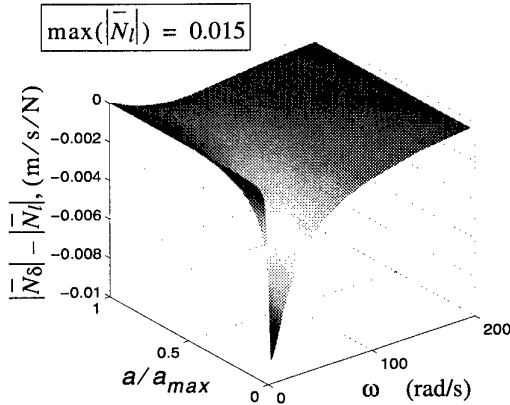


Figure 10: Gain change caused by friction compensation residual

effect will decrease very much. This phenomenon can also be seen in Gäfvert (1997). Second, at low

frequency and small input amplitude range the nonlinear friction causes a considerable gain drop. When the input amplitude and frequency tends to zero the gain almost drops to zero. And the last, the nonlinear friction has the effect of reducing phase lag (a nonlinear damping effect), but in the near zero frequency range this effect tends to zero. The characteristics of the nonlinear friction effect can also be seen in the solid lines of Fig. 12 and Fig. 13.

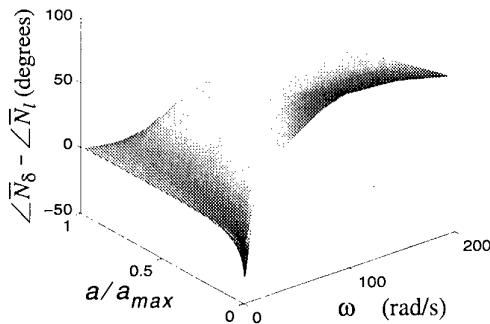


Figure 11: Phase change caused by friction compensation residual

Fig. 10 and Fig. 11 show the nonlinear friction compensation effect for the system that has a considerable force generation dynamics. In other words, they show how the liner system is affected by the nonlinear friction compensation residual. From the plots, it can be seen that even though there is a considerable force generation dynamics, the nonlinear friction compensation is still quite effective especially in the low frequency range. The friction compensation effect can be seen more clearly by comparisons of the gain and phase changes before and after the compensation in 2D plots as shown in Fig. 12 and Fig. 13. It is noted that gain drop caused by the nonlinear

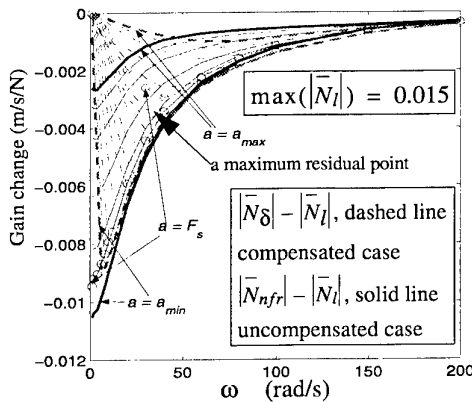


Figure 12: Comparison of the gain changes caused by F_{nfr} and δ_{fr}

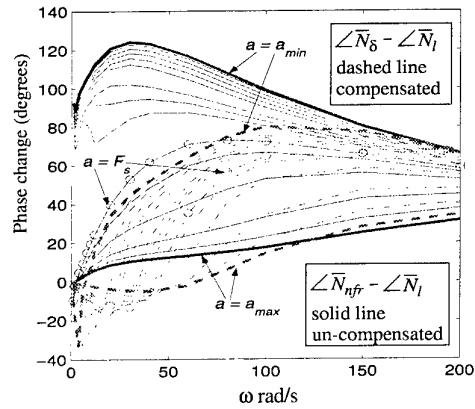


Figure 13: Comparison of the phase changes caused by F_{nfr} and δ_{fr}

friction can be compensated effectively. But this effect depends on the sinusoid's input amplitude and frequency. The smaller the input amplitude the larger the residual (amplitude) left and at a certain frequency point the residual reaches its maximum value for a given input amplitude. This maximum residual frequency will increase with the increase of sinusoidal input amplitude. From Fig. 13, it is also noted that the increase in SIDF gain by the compensation is at the cost of phase loss (see the dashed line). In characterization of the friction compensated system, it is important that the main features, in the most frequently appeared cases, can be captured such that with the limited system capacity, high control performance can be achieved, while a relatively large uncertainty can be tolerated. From Fig. 12 and Fig. 13, it can be seen that the envelope formed by the four lines, the un-compensated $a = F_s$ and $a = a_{max}$ lines, and the compensated $a = F_s$ and $a = a_{max}$ lines, includes almost all the compensated case gain lines and phase lines, except the compensated case

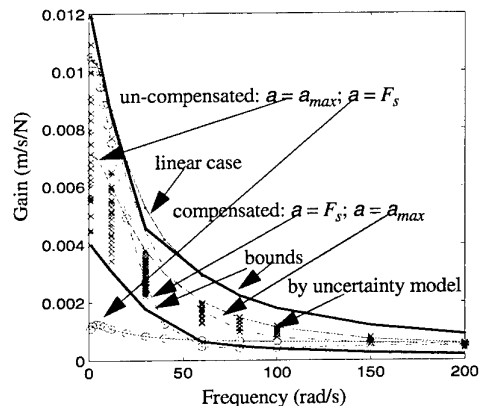


Figure 14: Uncertainty (residual) gain modelling

phase lines corresponding to $a < F_s$. The main purpose to characterize a uncertainty or a uncertain system is to determine its upper and lower bounds. To do so, in Fig. 14 and Fig. 15, the nonlinear friction and

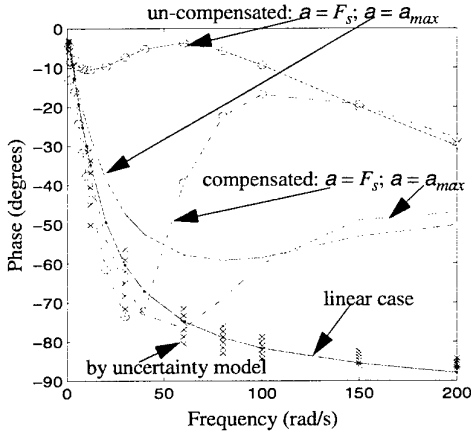


Figure 15: Uncertainty (residual) phase modelling

friction compensation residual effects on the linear system from force to velocity are depicted in the gain and phase plots (not the above 'gain change' and 'phase change' plots). With the under compensation assumption a1), an uncertainty gain model shown by the area between the two thick solid lines in Fig. 14 and phase model shown by the "x" marked clusters in Fig. 15 seems reasonable. The two thick lines represent the upper and lower bounds which include most of the area of the mentioned envelope and the linear case. The lower bound in low frequency range is higher than the un-compensated case $a = F_s$ line. It is used to indicate the friction compensation effect. The better compensation, the closer to the upper bound. To characterize the uncertain system from force to velocity, the uncertain model structure is selected as

$$G_{vl}(s) = \frac{k_y}{s + a_y} (1 + \Delta_y(s)) \quad (27)$$

$$k_y \in [k_{yd}, k_{yu}], a_y \in [a_{yd}, a_{yu}]$$

where k_y and a_y represent the two uncertain parameters of the structured model, they are bounded by their corresponding upper and lower bounds of k_{yd} , k_{yu} , a_{yd} and a_{yu} respectively; $\Delta_y(s)$ represents the additive unstructured uncertainty. The structured model parameters, k_y and a_y , and $\Delta_y(s)$ values are obtained through manual fitting. For the cases of $k_y = 0.08:0.01:0.12$ and $a_y = 10:2:20$, the structured model's gain and phase distribution are shown with the "x" marked clusters in Fig. 14 and Fig. 15. Most of the phase 'lead' (nonlinear damping, friction, caused phase lag reduction) cases are not included in the structured model. But this phase 'lead' information

will be used to decide the phase margin selection in the following outer loop controller synthesis. The gain distribution by the structured model is assigned in a way such that it is located in the middle of the target area and that it covers most of the area, except for some area in the high frequency range which is difficult to fit with the structured model. The next step is to select $|\Delta_y(s)|$ values such that the envelope formed by the upper and lower bounds described by

$$|G_{vl}(s)|_{upper} = \max \left| \frac{k_y}{s + a_y} \right| (1 + |\Delta_y(s)|)$$

$$|G_{vl}(s)|_{lower} = \min \left| \frac{k_y}{s + a_y} \right| (1 - |\Delta_y(s)|) \quad (28)$$

$$k_y \in [0.08, 0.12], a_y \in [10, 20]$$

will cover almost all the target area. For the interested frequency points $|\Delta_y(\omega)|$ is selected as

$$|\Delta_y(\omega)| = [0, 0, 0, 0, 0, 0, 0.1, 0.1, 0.2, 0.3, 0.5, 0.5, 0.5, 0.5]$$

$$\omega = [1, 2, 4, 6, 8, 10, 12, 20, 30, 40, 60, 80, 100, 150, 200] \quad (29)$$

As a result, the uncertain (linearized but with linearization residual) system from force F to position y can be represented as

$$G_y(s) = \frac{k_y}{(s + a_y)s} (1 + \Delta_y(s)) \quad (30)$$

$$k_y \in [k_{yd}, k_{yu}], a_y \in [a_{yd}, a_{yu}]$$

It should be noted that the $a < F_s$ compensated cases are not included in the outer loop plant model, but the phase lag in the low frequency range (refer to Fig. 13) will be considered in the controller synthesis.

4. CONTROLLER DESIGN

It is well known that to increase feedback controller amplitude will increase the system's input and output disturbances rejection capability, and is one of the main ways to improve tracking performance for an uncertain system. But for a real system, feedback controller amplitude will be limited by many other factors, such as input constraint, sampling frequency, sensor noise, un-modelled dynamics and/or nonlinearities, especially in high frequency range. With a limited bandwidth or loop cross-over frequency, the loop's gain-phase relationship is limited. How to utilize the above characterized gain-phase information to make trade-off between performance and stability in the loopshaping will be the main problem in the presented QFT controller design work.

4.1 Inner Loop Controller Design

For the inner controller design, the valve nonlinearity compensation residual, \bar{N}_{qu} , will not be involved in the plant. Its effect will be considered in the Nichols chart. Referring to Eq. 21, the inner loop plant can be given as

$$G_v(s) = \frac{L_p \alpha}{(s + \beta)(s/\omega_v^2 + 2\zeta_v/\omega_v + 1)} \quad (31)$$

$\beta \in [0, 0.15], \alpha \in [0.9, 1.1]$

$\omega_v = 310, \zeta_v = 0.7, L_p = 2.4 \times 10^6$

The control design objective for the inner loop is to design a controller such that, without causing limit cycles and within the given bandwidth, the loop gain should be as high as possible in the interested frequency range, e.g. low frequency range, while keeping enough phase and gain margin. Fig. 16 shows

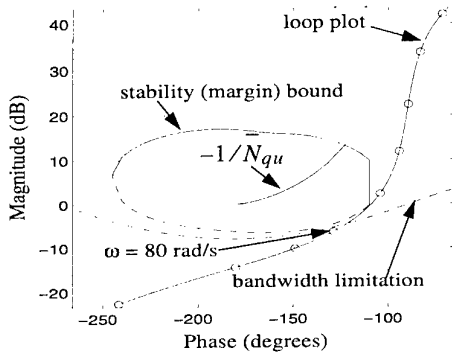


Figure 16: Inner loop QFT controller design

the inner loop design. The bandwidth of the closed loop is selected to be 80 rad/s. So the loop amplitude, at 80 rad/s frequency point, must be lower than the bound. The margin bound is calculated such that the amplitude of the closed inner loop, $G_{2clp}(j\omega)$, satisfies

$$|G_{2clp}(j\omega)| = \left| \frac{C_{inner}(j\omega)G_v(j\omega)}{1 + C_{inner}(j\omega)G_v(j\omega)} \right| \leq \mu, \omega \in [0, \infty) \quad (32)$$

Here and in the following μ is decided according to the algorithm given in Borghesani *et al* (1994). For the inner loop, $\mu = 1.2$. This corresponds to at least 49.2° phase margin and at least 1.83 dB gain margin. In the controller synthesis, it is also important to make the loop plot and the $-1/\bar{N}_{qu}$ plot as parallel as possible so that the possibility of generating limit cycles can be reduced to the lowest level. The designed inner controller is

$$C_{inner}(s) = \frac{0.0003s^2 + 2.3s + 299}{s^3 + 844s^2 + 231856s + 17920144} \quad (33)$$

4.2 Outer Loop Controller Design

The outer loop motion part plant is already defined by Eq. 30 and 29, where $k_{yd} = 0.08$, $k_{yu} = 0.12$, $a_{yd} = 10$ and $a_{yu} = 20$. So the overall outer loop plant can be given by

$$G_1(s) = G_{2clp}(s)G_y(s) \quad (34)$$

The outer loop controller design task is to design a controller for $G_1(s)$, such that within the limited bandwidth, the positioning accuracy can be as high as possible. Two important facts, which can be seen in Fig. 13, Fig. 14 and Fig. 15, which have not been considered in Eq. 30 and 29, are

- In low frequency and small input amplitude cases, the friction compensation residual will cause relatively large phase lag. This implies that these cases are phase critical.
- In the high frequency range, the friction effect has in fact almost not been compensated due to the considerable dynamics of the force generation loop. As a result, there are small gain and large phase 'lead' in this frequency range.

These two facts implies that to get a high positioning accuracy, especially high steady-state positioning accuracy, the only possible way is to considerably reduce the phase and gain margin so that in the low frequency range the loop's gain can be higher and the phase lag is small. In this work, $\mu = 7$ is selected. This corresponds to at least 8.2° phase margin and at least 1.14 dB gain margin. Fig. 17 shows the design of the

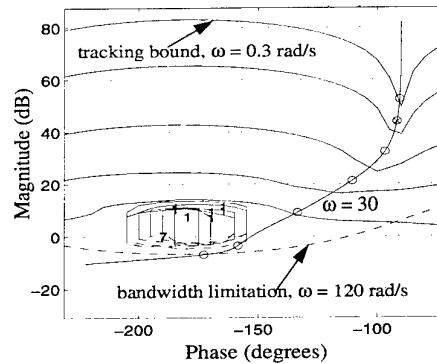


Figure 17: Outer loop QFT controller design

outer loop controller. The designed feedback and feed forward controllers are

$$C_{outer}(s) = \frac{6.7e9s^3 + 8.4e11s^2 + 7.4e13s + 1.4e15}{s^4 + 3334s^3 + 2.4e6s^2 + 7.5e8s + 1e11} \quad (35)$$

$$C_{outer}^F(s) = \frac{1}{s^2/50^2 + 2s/50 + 1} \quad (36)$$

5. EXPERIMENTAL POSITIONING RESULTS

Experiments are conducted with the pneumatic rodless cylinder positioning system presented in section 2. To test the robust performance and robust stability, system and experimental parameters are changed from test to test, but with no controller parameter modification. The default payload is 5.5 kg and the default friction compensator parameters are

	σ_0	σ_1	v_s	F_c	F_s	f_v
	(N/m)	(Ns/m)	(m/s)	(N)	(N)	(Ns/m)
Chamber1	1e5	1500	0.016	26	65	95
Chamber1	1e5	1500	0.01	26	95	125

Inertia force forward and viscous force forward are involved, in order to reduce tracking error. In every figure, there are two rows; The upper one shows the comparisons of different positioning with their corresponding references; All the references are after the low-pass filter, $C_{outer}^F(s)$, which is designed to be one part of the reference generator; The lower one shows the closed-up positioning error, and the transit behaviour can be seen more clearly there. All the positioning experiments show a $\leq 5 \mu\text{m}$ (sensor's resolution) steady-state positioning error. Fig. 18

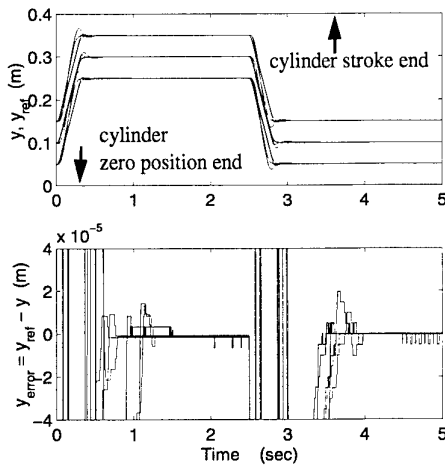


Figure 18: Normal positioning for payload of 5.5 kg and 15.5 kg

shows some normal positioning cases with payload changed from 5.5 kg to 15.5 kg. With this change of payload, only the overshoot is seen to be increased a

little bit. Fig. 19 shows the 0.5 mm small positioning

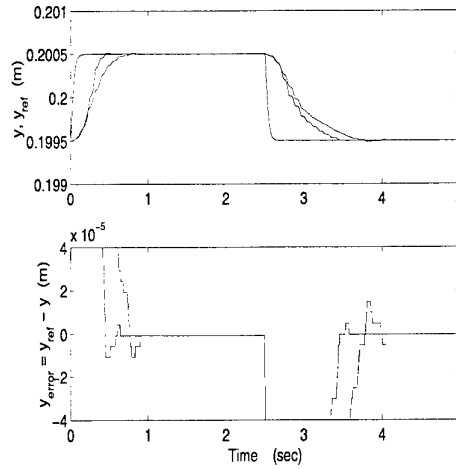


Figure 19: 0.5 mm small positioning for payload of 5.5 kg and 15.5 kg

cases with payload changed from 5.5 kg to 15.5 kg. Small positioning means small displacement, small pressure reference and thus small control input. In this case, the uncertainty is substantial. With the change of payload, only a little bit slower response is seen. Fig. 20 shows four cases: change and without change of

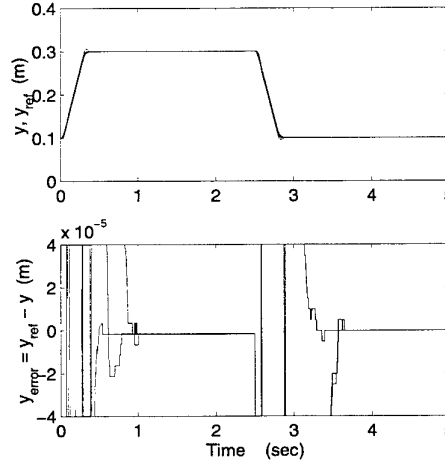


Figure 20: Change and without change of friction parameter; With and without velocity de-coupling

friction parameter, with and without velocity de-coupling. For both chambers, the friction compensator parameters are changed simultaneously as: $F_{c|default} - 13$ and $F_{s|default} - 20$. The without velocity

de-coupling case is to set $\hat{N}_v = 0$ in Eq. 10. From the figure, it can be seen that all the changes in the compensator parameter cause no obvious deviation in

positioning performance. Fig. 21 shows the position

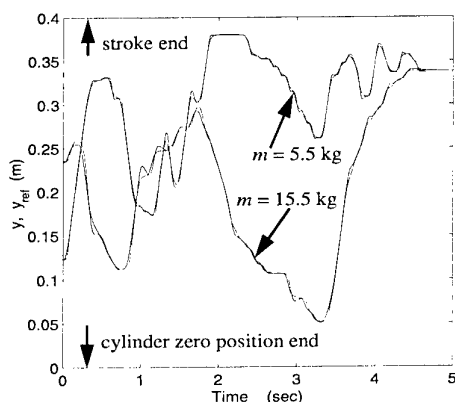


Figure 21: Position tracking for payload of 5.5 kg and 15.5 kg

tracking control results for random tracking references. For payload $m = 15.5$ kg the tracking error is seen somewhat larger than for payload $m = 5.5$ kg in the high frequency range (fast reference change).

6. CONCLUSIONS

With the introduced block-oriented feedback linearization technique, the nonlinearity compensation is fairly effective. The linearization residual and finally the linearized system are characterized with the presented method. The conservativeness of the QFT robust control design can be significantly reduced by making use of the characterized gain-phase information of the linearized (uncertain) system. With the limitation of the Bode's gain-phase relationship, making use of the possible gain-phase information leads to a good trade-off between performance and stability in the loopshaping, thus results in high control performance. For further reduction of the conservativeness of QFT robust control design, some other frequency domain nonlinearity modelling techniques, such as the general describing function method, may be worth exploring. For a high accuracy positioning, it is required that the overall closed loop system amplitude frequency response should be unit from the DC case to a quite large frequency range, and with no or only small peaks. Efficiently creating such a result by the interaction of feedback and feed forward loop shaping is worth further investigating.

REFERENCES

- Banos, A., and Barreiro, A. (2000). Stability of non-linear QFT designs based on robust absolute stability criteria. *International Journal of Control*, Vol. 73, No. 1, pp 74 - 88.
- Borghesani, C., Chait, Y. and Yaniv, O. (1994). *Quantitative Feedback Theory Toolbox for Use with MATLAB*. The MathWorks, Inc.
- Canudas de Wit, C., Olsson, H., Åström, K.J. and Lischinsky, P. (1995). A new model for control of systems with friction. *IEEE transactions on Automatic Control*, 40(3), March 1995.
- Glass, J.W., and Franchek, M.A. (2000). Frequency-based nonlinear controller design for regulating systems subjected to time-domain constraints. *International Journal of Robust and Nonlinear Control*, Vol. 10, p 39-57.
- Gäfvert, M. (1997). Comparison of two dynamic friction model. *Proceedings of IEEE International Conference on Control Applications*. p 386-391.
- Horowitz, I.M. (1973). Optimum loop transfer function in single-loop, minimum phase feedback systems. *International Journal of Control*, Vol. 22, pp 97-113.
- Horowitz, I.M. and Sidi, M. (1972). Synthesis of feedback systems with large plant ignorance for prescribed time domain tolerance. *International Journal of Control*, Vol. 16, pp 287-309.
- Horowitz, I.M. and Sidi, M. (1978). Optimum synthesis of nonminimum-phase feedback systems with parameter uncertainty. *International Journal of Control*, Vol. 27, pp 361-386.
- Houpis, C.H. (1995). Quantitative feedback theory (QFT) for engineer, WL-TR-95-3061, Flight Dynamics Directorate, Wright Laboratory, Wright-Patterson AFB, OH, USA.
- Sanville, F.E. (1971). A new method of specifying the flow capacity of pneumatic fluid power valves. *Hydraulic Pneumatic Power*, Vol. 17, No. 195, March 1971.
- Slotine, J. and Li, W. (1991). *Applied Nonlinear Control*. Prentice-Hall, Inc.
- Taylor, J. (1999). Describing functions. In: *Electrical Engineering Encyclopedia*. John Wiley & Sons, Inc., New York.
- Xiang, F. and Wikander, J. (2001). Experimental nonlinear modelling of a pneumatic analog solenoid valve -- a describing function approach. *Proceedings of The Seventh Scandinavian International Conference on Fluid Power, SICFP'01*, Linköping, Sweden.
- Xiang, F. (2001). Block-oriented nonlinear control of pneumatic actuator systems. *Doctoral Thesis*, TRITA-MMK 2001:9, ISSN 1400-1179, ISRN KTH/MMK/R--01/9--SE, Royal Institute of Technology, Sweden.
- Zheng, Y., Chait, Y., Hollot, C.V., Steinbuch, M. and Norg, M. (2000). Experimental demonstration of reset control design. *Journal of Control Engineering Practice*, Vol. 8, pp 113 - 120.

A NOTE ON THE USE OF THE STRUCTURED SINGULAR VALUE IN DECENTRALISED CONTROL

P. S. Rao, E. S. Boje

*Electrical and Electronic Engineering,
University of Natal, Durban, 4041, South Africa.
boje@nu.ac.za*

Abstract: This paper presents a method of computing frequency response bounds on the elements of a decentralised controller for a MIMO system for guaranteed closed loop stability. The proposed technique uses the structured singular value. It generates stability bounds that can be plotted on the Nichols chart and incorporated into the QFT loop shaping procedure.

Keywords: Decentralised control, structured singular value (SSV), quantitative feedback theory (QFT).

1. INTRODUCTION

Grosdidier and Morari (1986) have derived some techniques of using the structured singular value for computing stability bounds on the diagonal closed loop elements which can be used in an independent design for decentralised control systems. We note here that the same approach can be extended to find frequency response bounds on the elements of a diagonal controller. The main idea is to associate an uncertainty with the (structured) controller for a fixed plant model and use the SSV to analyse the stability of the closed-loop system. The bounds obtained impose both magnitude and phase constraints on the controller and are expected to be useful in a QFT type loop shaping synthesis procedure.

Matrices are represented here by upper case bold face letters while scalars are in lower case. Subscript ij refers to the ij^{th} element of a matrix. \mathbf{I}_n is the identity matrix of order n . The frequency argument (s or $j\omega$) is omitted in most expressions.

Consider first the feedback system comprising of an $n \times n$ plant \mathbf{P} , with a diagonal feedback controller \mathbf{K} =

$\text{diag}(k_{ii})$. If \mathbf{P} is stable, then the loop shown in figure 1 is stable for all stable \mathbf{K} satisfying

$$|k_{ii}| < \frac{1}{\mu(\mathbf{P})}, i=1..n \quad \forall \omega \quad (1)$$

where $\mu(\cdot)$ is the structured singular value corresponding to the diagonal structure of \mathbf{K} . This follows directly from the definition of the structured singular value and the fact that the spectral norm of a diagonal matrix $\bar{\sigma}(\mathbf{K})$ is the magnitude of its largest element ($\max_i |k_{ii}|$).

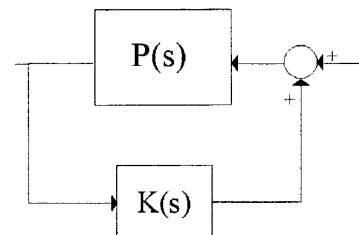


Figure 1: Plant and diagonal controller.

Inequality (1) gives a magnitude bound on the elements of \mathbf{K} or in other words restricts them to lie within a circle of radius $1/\mu(\mathbf{P})$ centred at the origin. It is possible to numerically optimise such bounds so as to obtain larger regions within which the elements of $\mathbf{K}(s)$ are constrained to lie. Further, this development does

not require any additional assumptions on the unstable plant poles.

The next section presents the method of doing this. A simple 2x2 example is then given. Extension of the principle to deal with uncertain plant models is also discussed.

2. STABILITY BOUNDS FOR CONTROLLER ELEMENTS

Consider a $n \times n$ plant P . Let $K(s) = k(s)I_n$ (where $k(s)$ is a scalar transfer function) be a diagonal controller that stabilises P .

Though the existence of a rational stabilising $k(s)$ cannot be proved, it is generally not difficult to find a real rational $k(s)$ such that $k(s)I_n$ stabilises a given unstable plant. Since $k(s)$ multiplies each of the characteristic gain loci of $P(s)$ ($K(s)$ is trivially commutative) one can shape the frequency response $k(j\omega)$ such that the loci of $k(j\omega)\lambda_i(P(j\omega))$, taken together, encircle the point $(-1,0)$ the required number of times (Maciejowski, 1989).

Now, it is expected that there exists a perturbation of the frequency responses of the controller elements around $k(j\omega)$ for which the closed-loop remains stable. Let Δ be an additive perturbation with the same diagonal structure as the controller. The perturbed controller can be represented as

$$K(s) = k(s)I_n + \Delta$$

where Δ is a diagonal perturbation matrix. The structured singular value can be used to obtain bounds on $|\Delta_{ii}|$.

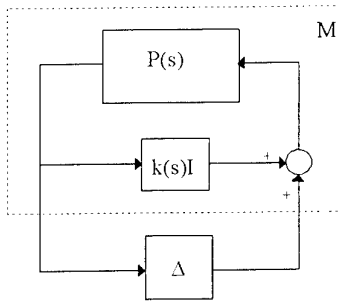


Figure 2. Schematic 2

The block diagram of the corresponding μ -test is shown

in figure 2. The part in the dotted line $M = P(I - kP)^{-1}$ is identified with the stable plant of (1).

The system is stable if

$$|\Delta_{ii}| < \frac{1}{\mu(M)}, \quad i = 1..n \quad \forall \omega \quad (2)$$

This bound can be very small especially at frequencies where the compensated characteristic gain loci

$k(j\omega)\lambda_i(P(j\omega))$ pass close to the point $(-1,0)$.

We now replace $k(j\omega)$ by a complex number z , which can be optimised to obtain a larger perturbation radius than that obtained from (2).

As is well known, the computation of $\mu(M)$ is a non-convex problem and so is replaced by a tight upper bound, $\bar{\mu}(M)$, (for instance the Perron root $\lambda_p(M)$) the computation of which is a convex problem. This upper bound is a smooth function of the elements of the matrix. Hence given $M = P(I - zP)^{-1}$, $\bar{\mu}(M)$ is a well-behaved function of z . It is therefore possible to use numerical (gradient based) search techniques to find a (locally) optimal z such that $\bar{\mu}(M)$ is minimised. This in turn maximises the perturbation radius $1/\mu(M)$ on the elements K_{ii} when applied to (2). The controller $k(s)$ no longer lies at the centre of the allowed perturbation sets of $K_{ii}(s)$.

We further add the constraint

$$|z(\omega) - k(j\omega)| < \frac{1}{\bar{\mu}(M)} \quad (3)$$

This ensures that the original nominal controller $k(s)I_n$ lies within the optimised bounds.

Now by using a connectedness argument, it is possible to deduce that the loop remains stable for all controllers K , such that each of the elements $K_{ii}(j\omega)$ lies within a circle defined by the optimised $z(\omega)$ and $1/\bar{\mu}(M)$ values above.

Fact: Given a stabilising controller $k(s)I_n$, and complex valued function $z(\omega)$ such that (3) holds, the closed loop system of figure 1 is stable for all diagonal K such that,

$$|K_{ii}(j\omega) - z(\omega)| < \frac{1}{\mu(P(j\omega)(I_n - z(\omega)P(j\omega))^{-1})} \quad \forall i \quad \forall \omega \quad (4)$$

i.e. each element of K lies within a circle centred at z and with a radius $1/\mu(P(I_n - zP))^{-1}$ at the frequency ω .

Proof: From the definition of μ , (4) implies

$$\begin{aligned} \det(I_n - (K - zI_n)(P(I_n - zP)^{-1})) &\neq 0 \\ \Rightarrow \det((I_n - zP) - (K - zI_n)P) \det((I_n - zP)^{-1}) &\neq 0 \\ \Rightarrow \det(I_n - KP) &\neq 0 \end{aligned}$$

The closed loop characteristic polynomial of figure 1, $\det(I_n - KP)$ is non-zero for all controllers satisfying (4). Hence, the number of encirclements of the origin by $\det(I_n - KP)$ does not change for this entire set of controllers satisfying (4).

Further, since one controller in the set, $k(s)I_n$, gives a stable closed loop, the entire set represented by (4) gives a stable closed loop. •

The circles obtained from the above formulation at any specified frequencies can be transferred onto the Nichols chart and used in conjunction with other bounds (derived from performance requirements) in a QFT type design procedure. Such bounds are expected to prove particularly useful for non-diagonally dominant systems for which stability cannot be easily addressed in the framework of classical frequency response methods.

For specific problems, it might be possible to further improve the bounds by having different centres and perturbation radii for each of the loops. The former can be achieved by replacing $z\mathbf{I}_n$ by $\mathbf{Z} = \text{diag}(z_i)$, the z_i s being the centres of the discs for each of the loops. A diagonal scaling factor can also be introduced to have different perturbation radii in each of the loops if required.

3. AN EXAMPLE

Consider the simple 2x2 plant model taken from Maciejowski (1989).

$$\mathbf{P} = \frac{1}{1.25(s+1)(s+2)} \begin{bmatrix} (s-1) & s \\ -6 & (s-2) \end{bmatrix} \quad (5)$$

Since the plant is stable, we first compute the unoptimised bound on the controller elements resulting from (1). The plot of $1/\mu(\mathbf{P})$ is shown in figure 3.

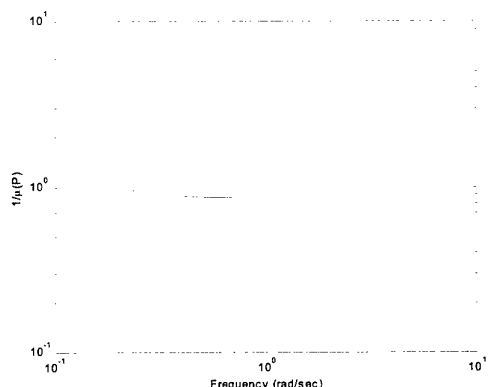
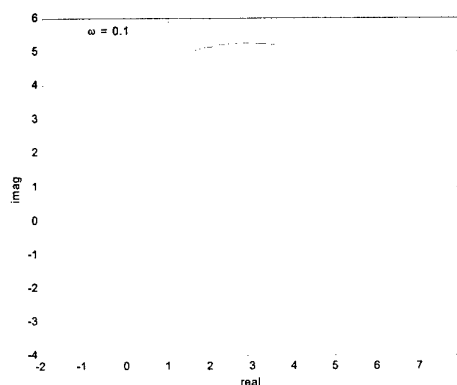


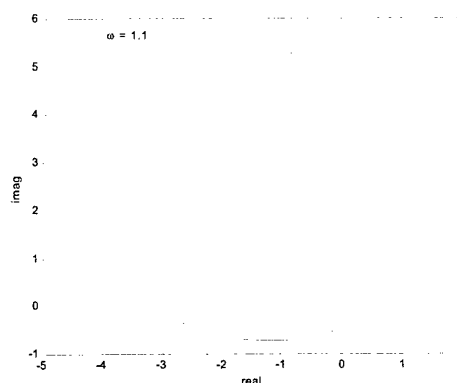
Figure 3: Unoptimised magnitude bound on the controller elements

The corresponding circles representing the bounds on the controller elements in the complex plane are shown (dotted) in figures 4 a-c for 3 frequency points ($\omega = 0.1, 1.12$ and 7.0 rad/sec) lying below, approximately at and above crossover respectively.

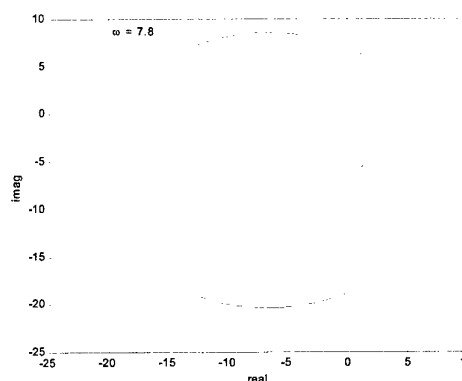
Since the plant is stable, we can choose the initial stabilising controller $k(s)=0$ and optimise the bounds.



(a) Bounds on K_{ii} at $\omega = 0.1$ rad/sec



(b) Bounds on K_{ii} at $\omega = 1.1$ rad/sec



(c) Bounds on K_{ii} at $\omega = 7.8$ rad/sec

Figure 4: Initial (dotted) and improved (solid) bounds on the controller elements at 3 frequency points.

The optimised bounds (on K_{ii} , $i=1,2$) obtained after 15 iterations of an optimisation routine based on sequential quadratic programming are also shown (solid) in figures 4 a - c. If the optimisation is continued further, the bounds at some frequencies expand further and tend towards half planes.

The circles shown in figure 4 can easily be transferred onto the Nichols chart to generate quadratic bounds that can be incorporated into a sequential or independent design procedure based on QFT.

3. EXTENSION TO UNCERTAIN PLANTS

3.1 Norm bounded uncertainty

The above idea can be easily extended to incorporate plant model uncertainty if the uncertainty is modelled as a norm bounded structured perturbation as in conventional μ theory.

Figure 5 shows the block diagram of the plant \mathbf{P} with a structured uncertainty Δ_p wrapped around it. The additive perturbation of the controller is denoted by Δ_k . The initial stabilising controller $\mathbf{K}(s)=k(s)\mathbf{I}_n$ is to be chosen so as to robustly stabilise the nominal as well as perturbed plants.

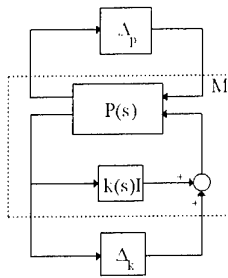


Figure 5: Plant with norm bounded uncertainty

This nominal $\mathbf{K}(s)$ can be designed by plotting the n plant eigenvalue templates and shaping $k(s)$ such that the compensated characteristic loci of the nominal plant have the required number of encirclements and in addition the compensated eigenvalue templates at a chosen set of frequency points avoid the critical point, $(-180^\circ, 0\text{dB})$, on the Nichols chart.

Without loss of generality let Δ_p be scaled such that $\bar{\sigma}(\Delta_p) \leq 1$. Also introduce a scaling factor $\mathbf{D} = d\mathbf{I}_n$ ($d \in \mathcal{R}$) into the Δ_k loop as shown in figure 6.

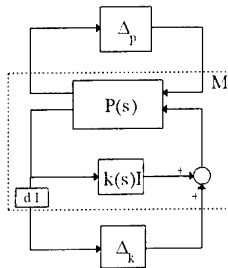


Figure 6: Block diagram for equation (6).

Now invoking the main loop theorem (Doyle and Packard, 1993), we have an extended μ test for the system of figure 6.

The system in figure 6 is stable if

$$|\Delta_{kii}| < d \quad \forall i \quad \forall \omega \quad (6)$$

where d is chosen such that

$$\mu(\mathbf{M}) < 1$$

(μ here being with respect to the augmented structure of Δ_p and Δ_k appended together). A formal proof of this follows from Skogestad and Morari (Theorem 1, Appendix). In this formulation, d is the radius of perturbation and should be maximised.

Again, $k(j\omega)$ can be replaced by a complex number z which is optimised such that d is maximised subject to the constraint $\mu(\mathbf{M}) < 1$.

3.2 Enumerated plant set

When a finite set of linear models for the plant are available, a common stability constraint on the controller frequency response can be obtained by using an augmented matrix $\tilde{\mathbf{M}}$.

Given m plant models, the matrices \mathbf{M}_i , $i=1..m$ are defined as (refer figure 2.)

$$\mathbf{M}_i = \mathbf{P}_i (\mathbf{I}_n - k\mathbf{P}_i)^{-1} \quad i=1..m$$

We then define the augmented matrix

$$\tilde{\mathbf{M}} = \text{diag}(\mathbf{M}_1 \mathbf{M}_2 \dots \mathbf{M}_m),$$

generating the block diagram shown in figure 7.

Inequality (2) can then be applied (replacing \mathbf{M} by $\tilde{\mathbf{M}}$) to compute the required controller bounds.

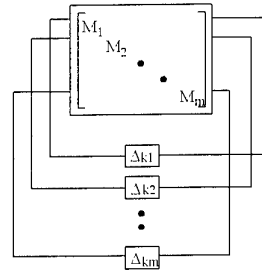


Figure 7: Block diagram for the augmented system for an enumerated plant set.

5. CONCLUSIONS

A technique based on the numerical optimisation of the SSV for computation of stability bounds in decentralised control has been discussed. The presentation addresses only diagonal controllers and cannot handle other general decentralised control structures. However, the method is expected to be potentially useful in applying quantitative techniques to non-diagonally-dominant systems.

REFERENCES

- Grosdidier, P., and M. Morari, (1986) 'Interaction measures for systems under decentralised control', *Automatica*, **Vol. 22(3)**, pp.309-319.
- Maciejowski, J. M., (1989) *Multivariable Feedback Design*, Prentice Hall International, U.K.
- Doyle, J., and A. Packard, (1993) 'The complex structured singular value' *Automatica*, **Vol. 29(1)**, pp. 71-109.
- Skogestad, S., and M. Morari, (1989) 'Robust performance of decentralised control by independent designs', *Automatica*, **Vol. 25(1)**, pp.119-125.

COMPENSATOR SELECTION USING QFT FOR H_∞ LOOPSHAPING WITH COPRIME UNCERTAINTIES

Francisco del Valle¹, Fernando Tadeo^{1*}, Omar Pérez²

¹*Departamento de Ingeniería de Sistemas y Automática
Facultad de Ciencias, Universidad de Valladolid, 47011 Valladolid, Spain
fernando@autom.uva.es*

²*Departamento de Procesos y Sistemas
Universidad Simón Bolívar, Sartenejas, Baruta, Estado Miranda, Caracas 1081-A, Venezuela
operez@usb.ve*

Abstract: This paper presents a method that uses QFT for choosing the initial open-loop transfer function and the using a robust loopshaping approach to consider unknown coprime uncertainties. Thus, this methodology considers not only the robustness properties of the shaped plant, but also those of the real plant. This technique is presented by way of an example using a model of a Neutralization process. Simulation results show the benefit of using this technique: the plant is controlled in a range of pH values, despite variations of the plant parameters, obtaining good performance at the desired working points. To apply the methodology presented in this paper it is only necessary to consider the possible uncertainty in the nominal model and using available software to design the controller.

1. INTRODUCTION

As it is well known, the essence of robust control is to model the uncertainties themselves and to incorporate them in the design procedure of the control system, with the aim of ensuring stability and performance at all working points. Usually it is possible to identify multiple local linear models at different operating regions, which can be used to evaluate the expected uncertainty of the nominal model. Then this uncertainty information is used to design a controller that ensures robust stability and performance.

Among all the available Robust Control techniques the H_∞ Loop Shaping (H_∞ LS) procedure (McFarlane and Glover, 1990) has been chosen, because it has been proved to be efficient to solve realistic problems. The approach involves the robust stabilization to additive perturbations of normalized coprime factors of a shaped plant. Prior to robust stabilization, the open-loop singular values are shaped using pre- and post- compensators. Then, the resulting shaped plant

is robustly stabilized with respect to coprime factor uncertainty using H_∞ optimization.

One difficulty of the H_∞ LS design method is that it does not directly address the robustness properties of the real plant, but rather it is concerned with the shaped plant, and, unfortunately, there is no direct connection between the robustness of the shaped and unshaped plant. This paper shows a methodology that solves this problem by considering the robustness properties of the real plant in the selection of the weights of the shaped plant. This selection is done using ideas from Quantitative Feedback Theory (Horowitz, 1962, 1992; Yaniv, 1999; Houpis and Rasmussen, 1999). Once selected a robust shaped plant the controller is designed by application of the H_∞ LS design method.

This technique is presented showing an example of designing a controller for a pH neutralization processes. This process plays an important role in chemical plants, such as biological, wastewater

Author to whom correspondence should be addressed. This work was supported by the CYTED (Proyecto Precompetitivo VII-5) and CICYT (Proyecto TAP97-1144)

treatment, electrochemistry and precipitation plants. However, it is difficult to control a pH process with adequate performance due to its nonlinearities, time-varying properties and sensibility to small perturbations when working near the equivalence point (Palancar et al., 1996).

2. H_∞ LOOP SHAPING

H_∞ LS, as introduced and solved in [5], considers the stabilization of a plant which has a normalized left coprime factorization: $\tilde{G} = D^{-1}N$. That is, N and D are stable transfer function matrices ($N, D \in RH^\infty$) such that there exists $X, Y \in RH^\infty$ which fulfils the identities $NX + DY = I$ and $NN^* + DD^* = I$ (Where H^* denotes $H^T(-\bar{s})$).

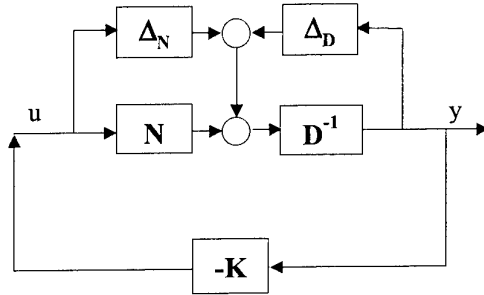


Figure 1: Coprime perturbed plant

In this technique two uncertainty blocks are used, as depicted in Figure 1, one on each of the factors in the coprime factorization: $G = (D + \Delta_D)^{-1}(N + \Delta_N)$, where $\Delta_D, \Delta_N \in RH^\infty$. The objective of robust stabilization is to stabilize the nominal plant \tilde{G} and the family of perturbed plants defined by

$$G = \{ (D + \Delta_D)^{-1}(N + \Delta_N) / \|\begin{bmatrix} \Delta_D & \Delta_N \end{bmatrix}\|_\infty < \varepsilon \}$$

where ε is the Stability Margin. Objectives of H_∞ LS are the maximization of this Stability Margin and achieving good input-output performance. It can be shown that this is equivalent to find a stabilizing K that minimizes $\gamma = \left\| \begin{bmatrix} K \\ I \end{bmatrix} (I + \tilde{G}K)^{-1} \tilde{D}^{-1} \right\|_\infty$, which can be calculated by solving an Algebraic Riccati Equation, as shown by [12].

Compared with other H_∞ design methods, the main advantage of the H_∞ LS method is that it does not require the so-called γ -iteration to calculate the optimal controller. Also there are available relatively

simple formulas to calculate the controller. On the other hand it does not (directly) include any closed-loop specification, which must be included by considering, instead of the nominal plant, a shaped plant. In practical designs, the Loop Shaping Design Procedure (LSDP) can be applied (McFarlane and Glover, 1990). The complete design procedure is the following:

1. Using pre- and post-compensators (W_1 and W_2) the singular values of the nominal plant \tilde{G} are modified to give a desired loop shape: $G_S = W_1 \tilde{G} W_2$, which should not contain unstable hidden modes.
2. G_S is considered to be perturbed by normalized coprime uncertainties, and an optimal feedback controller K_S is then synthesized using the H_∞ LS approach.
3. The combination of the H_∞ LS controller and the compensators gives the final controller: $K = W_2 K_S W_1$

Different methods to select the compensators have been studied:

- Wright and Kravaris (1991) propose the use of the Inequalities Method
- Pantas and Walsh (1996) the use of the Phase Crossover Frequency
- Tang et al. (1996) the use of Genetic Algorithms
- Tadeo et al (2000) show the use of graphical loopshaping techniques for designing a controller for a laboratory plant

In order to consider the robustness properties of the real plant in the design, this paper shows a methodology that solves this problem by considering the robustness properties of the real plant in the selection of the weights of the shaped plant, using QFT.

Following similar ideas as those in (Tadeo et al. 2000), the QFT GLS method is applied to obtain an open-loop transfer function L_G , which then is robustly stabilized by application of the H_∞ LS approach, obtaining a robust open-loop transfer function L_{H_∞} . It is important to notice that the available information about uncertainties in the model and performance specifications is considered when applying the QFT method to design $L(s)$. When applying the H_∞ LS method the uncertainty is considered unknown and coprime.

3. USING QFT FOR ROBUST LOOPSHAPING

The Quantitative Feedback Theory (QFT) is a well-known controller design technique, introduced by

Horowitz (1962), to solve the problem of designing controllers in the frequency domain. The main advantages of using this technique are the possibility of including performance and robustness specifications in the design, without losing the physical insight of the problem. The design methodology is presented in Horowitz (1992), Yaniv (1999), Houpis and Rasmussen (1999). Short overviews can be found in Horowitz (1991) and Niksefat and Sepehri (2001). Roughly speaking it consists of two main steps:

- First, design a controller using the Nichols Chart to meet the robustness specifications, taking into account the physical properties of the system and the performance requirements.
- Second, designing a prefilter to meet the performance specification.

This paper proposes to combine this QFT technique with the H_∞ LS technique to include the maximization of the Stability Margin for Coprime Uncertainties in the QFT design. The basic steps proposed are:

1. Use QFT to design an initial open-loop transfer function, with minimal robustness characteristics, taking into account the physical properties of the system and the performance requirements. This open loop transfer function is designed by manually adding poles and zeroes, to yield a stable nominal closed loop, while at the same time satisfying all bounds.
2. Use H_∞ LS to augment the QFT controller for increasing the Stability Margin for Coprime Uncertainties.
3. Design a prefilter to meet the performance specification. This prefilter is required to bring the response withing the robust tracking specifications.

Steps 1 and 3 use standard QFT, with the only modification that, as the controller will be augmented to increase its robustness, the robustness characteristics are relaxed using a less restrictive stability bound. That is, instead of using a robustness parameter of $\rho=1.2$ or 1.3 we propose to use $\rho \approx 1.5$, as the robustness of the controller will be taken care of in the second step.

The technique is now presented by way of an example in process control.

4. EXAMPLE: PH CONTROL PROCESS

4.1. The Plant

The process under study is the neutralization of an aqueous solution with Hydrochloric Acid (HCl) in a Continuous Stirred Tank Reactor (CSTR). The experimental setup (described in detail in Tadeo et al,

1996 and Tadeo et al., 2000) is shown in Figure 2. It consists of a CSTR where a liquid of variable pH is mixed with a solution of high concentration of HCl. This liquid is fed from the tank using a pump, which produces a variable flow depending on the level of liquid in the tank. The liquid in the mixing tank overflows (outlet not shown), so the volume of liquid in the tank can be considered constant. The control variable u is the flowrate of the titrating stream. The output variable y is the hydrogen ion concentration in the effluent stream.

Due to the nonlinear dependence of the pH value on the amount of titrated agent the process will be inherently nonlinear. Moreover, variations of the buffering effects could make the process time-varying. Both effects make the process difficult to control with classical process control techniques (Palancar et al., 1996).

Although the modeling of pH-control processes has been well studied (Gustafsson et al, 1995), in this case it is only necessary to have a simplified model, because when designing the controller the available information on plant uncertainty can be considered. This model was obtained based on first principles, and then validated in the real plant, by carrying out experiments at different working points. Also experiments were carried out by eliminating one of the streams, to check the shape of the titration curve. The experimental results were consistent with the non-linear model. Details on the experimental setup and the model can be seen in (Tadeo et al, 2000)

Assuming the input liquid is pure water, that the HCl has constant concentration, and there is perfect solution, mixing, and no buffering, the following model can be obtained:

$$\begin{aligned}\frac{dN_d}{dt} &= -\frac{q_0 N_d}{M} - \frac{q_a N_d}{M} + \frac{q_a N_a}{M} \\ \tau \frac{dN_d^*}{dt} &= N_d - N_d^* \\ pH &= -10 \log(N_d^*)\end{aligned}$$

Here, τ is the sensor time constant, M the mass of liquid in the tank, q_a is the acid mass flow, q_0 is the liquid mass flow, N_d is the acid concentration in the tank, N_d^m is the measured concentration and N_a is the input acid concentration. The model parameters were estimated using measured data.

It can be seen that this simplified model corresponds to an static logarithmic non-linearity and a dynamic model which is bilinear in one of the states. To reduce the number of non-linearities in the model, it was

decided to do the calculations working with concentrations, taking the antilogarithm of the measured pH, which is a common practice in industrial pH control:

$$N_d^m = 10^{-pH}$$

Observe that although the assumptions looks quite restrictive, deviations from the assumptions in the real system can be considered in the robust control design as unmodelled dynamics. This is one of the advantages of using a robust control approach.

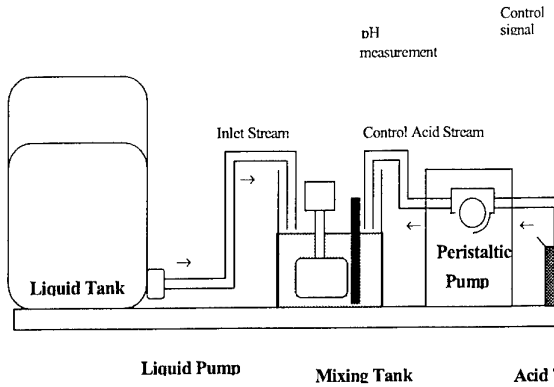


Figure 2: Laboratory Plant

4.2. Controller Design

First the effect of parameter variation on the transfer function was studied. The uncertain non-linear model was approximated by a set of local linear approximations. Assuming the parameter variations uncorrelated, the non-linear model was linearized considering the extreme values of each uncertain parameter. This approximation is suitable for slowly varying parameters.

First Step: Design using QFT

For QFT design the plant is modelled as the second order transfer function, with two real poles: the faster pole given by the sensor dynamics and the slower pole from the pH dynamics:

$$G(s) = \frac{k}{(s+a)(s+b)}$$

where the sensor pole is supposed constant:

$$b = 0.012725$$

and the following parametric variations have been measured:

$$K \in [-0.000004649, -0.00007469]$$

$$a \in [0.25, 2]$$

It can be seen that there are important parametric variations, as the dominant pole position varies 800% times, and the gain 1600%.

To design the initial controller usign QFT we consider two kind of design specifications:

- Minimum Phase and Gain Margins (type 1). Design parameter: $\rho=1.5$. (This value is selected so big, as the unmodelled dynamics will be taken care of in the second step by the H_∞ LS process)

- Tracking Properties (type 7):

$$\text{Upper limit: } G_U(s) = \frac{0.0013}{s^2 + 0.04s + 0.0013}$$

$$\text{Lower limit:}$$

$$G_L(s) = \frac{1}{5 \cdot 10^{10} s^3 + 4.2510^7 s^2 + 1.1510^4 + 1}$$

The design was carried out using QFT Toolbox in Matlab (Borghesani et al., 1995), as is now described:

First, the set of plants and templates were calculated: a set of 80 plants were obtained by parameter sweeping (their frequency responses are shown in Figure 3), and the corresponding templates (shown in Figure 4) calculated at the following frequencies:

$$w = [0.00001, 0.0001, 0.001, 0.01, 0.1, 0.5, 1]$$

In the next steps the robust stability and tracking bounds (shown in Figures 5 and 6) were calculated using the Matlab QFT Toolbox. Based on these bounds a controller was design for the nominal plant (see Figure 7). The selected controller was:

$$K_{QFT}(s) = \frac{3.901(s^{0.05289} + 1)(s^{0.00301} + 1)}{s(s^{3.839} + 1)(s^{0.00301} + 1)}$$

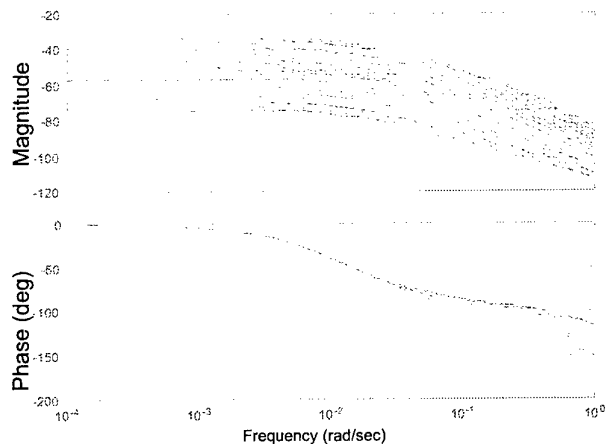


Figure 3: frequency response of linearized plants

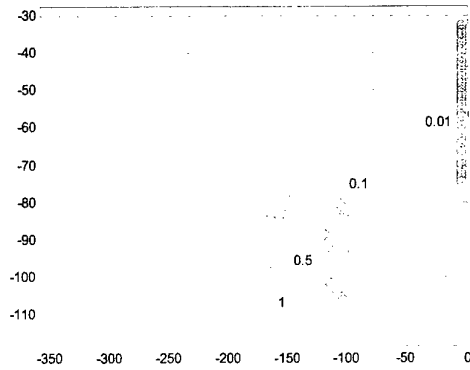


Figure 4: Templates

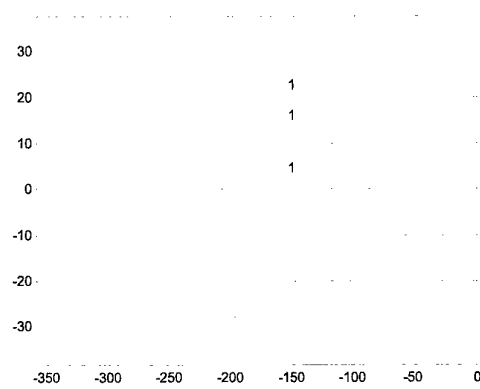


Figure 5: Robust Stability Bounds

Figure 8 shows the open loop transfer functions for this controller with the worst-case plants: the fastest and the slowest plants. Figures 9 and 10 show the corresponding closed-loop transfer functions, and figure 11 the step responses.

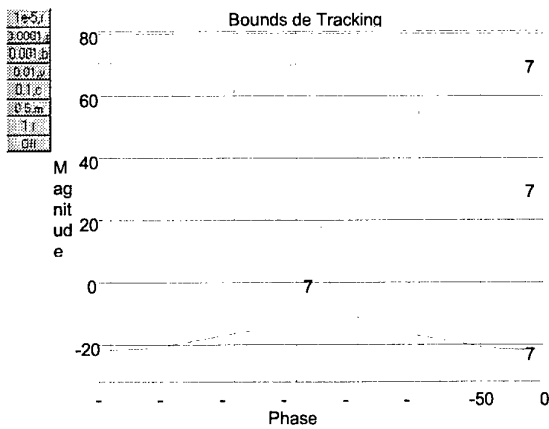


Figure 6: Tracking Bounds

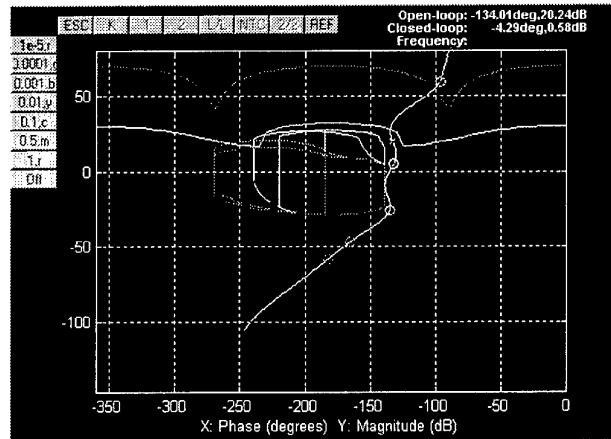


Figure 7: QFT Design

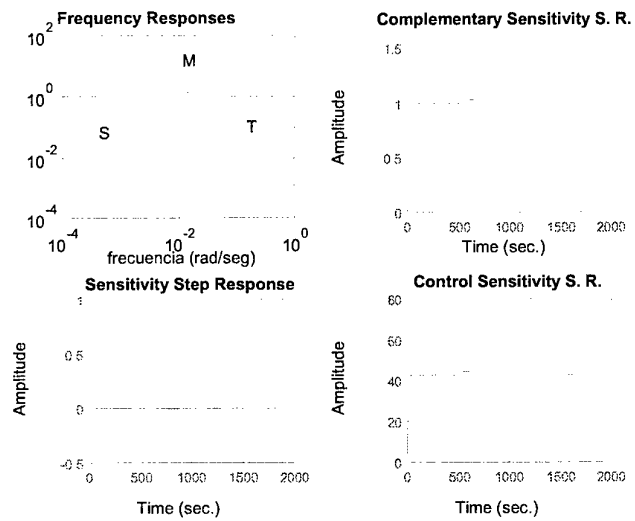


Figure 8: Characteristic Transfer Functions with QFT Controller

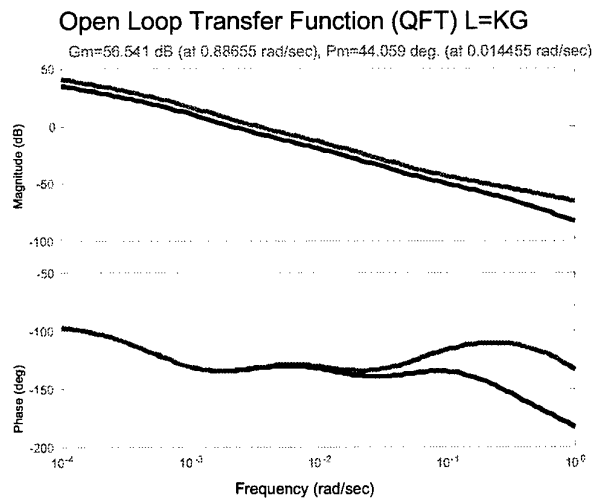


Figure 9: Open Loop Transfer Functions

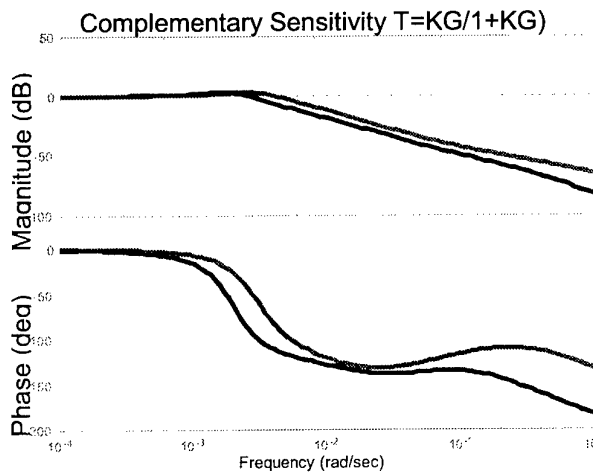


Figure 10: Complementary Sensitivity frequency response

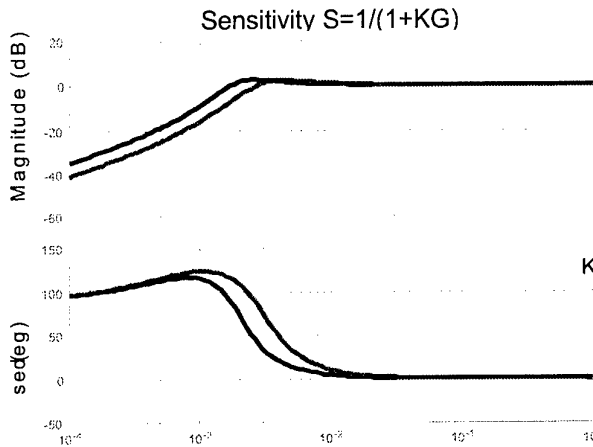


Figure 11: Sensitivity frequency response

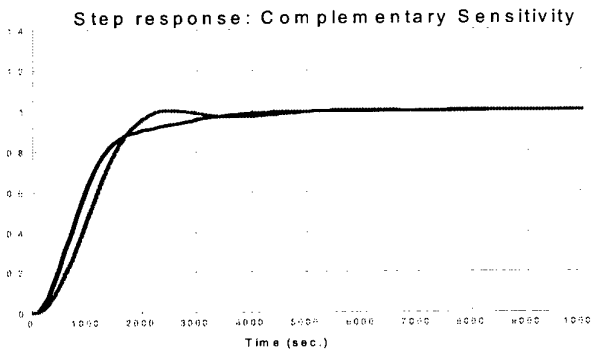


Figure 12: Command Step Response

Second Step: H_∞ Loop Shaping for the pH plant

Once an adequate open-loop transfer function $L_{QFT}(s)$ have been selected, the design can be made more robust by considering additional coprime uncertainties of $L_{QFT} = D^{-1}N$. These uncertainties include additional unmodelled dynamics, giving additional robustness. The resulting compensator K_G can be included in the feedback controller block by augmenting the controller designed using the GLS method. K_S is a stabilizing compensator of L_G and of the set of uncertain plants such that

$$G = \{ (D + \Delta_D)^{-1}(N + \Delta_N) / \| [\Delta_D \quad \Delta_N] \|_\infty < \epsilon \}.$$

Therefore, the robust controller can be calculated as follows:

$$K_{H_\infty} = K_{QFT} K_S$$

This method was applied to design a controller for the pH control plant. The obtained Algebraic Riccati Equation was solved using the Matlab Robust Control Toolbox (Chiang and Safonov). Considering the desired loop-shape the one calculated using QFT, the H_∞ LS method was applied, and an optimal compensator calculated. Before reduction, the controller was:

$$K_{H_\infty} = \frac{8.619s^4 + 2.757s^3 + 0.1586s^2 + 0.002028s + 0.000004097}{14.2029s^4 + 1.4293s^3 + 0.12423s^2 + 0.002830s + 0.000001870}$$

The characteristics transfer functions are shown in Figure 13 for the nominal plant. It can be seen that the shapes are adequate, and improved from the QFT design.

The open-loop shape when this compensator is included ($L_{H_\infty} = L_{QFT} K_S$) is shown in Figure 14 for the worst-case plants. It can be seen that the overall effect of the compensator is a gain reduction, especially at high frequencies. The open-loop cut-off frequency is decreased, so a reduction on the speed of response of the closed-loop system is achieved. The feedback system with the designed open-loop transfer function presents good robustness characteristics: With the nominal plant, the Gain Margin is 27.7dBs and the Phase Margin is 59.9°. Also there are good disturbance rejection properties, as can be seen from the Sensitivity Frequency Response in Figure 15.

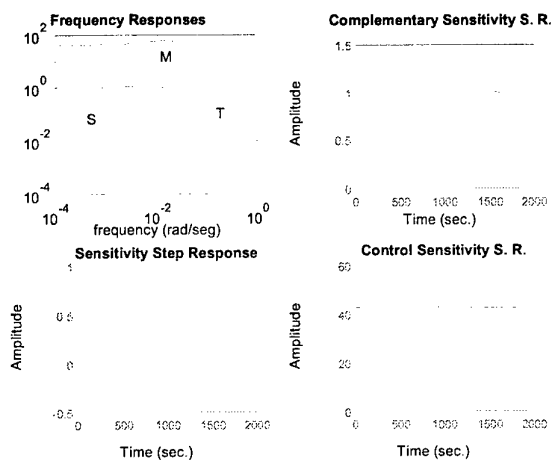


Figure 13: Nominal Characteristic Transfer Function with the final controller

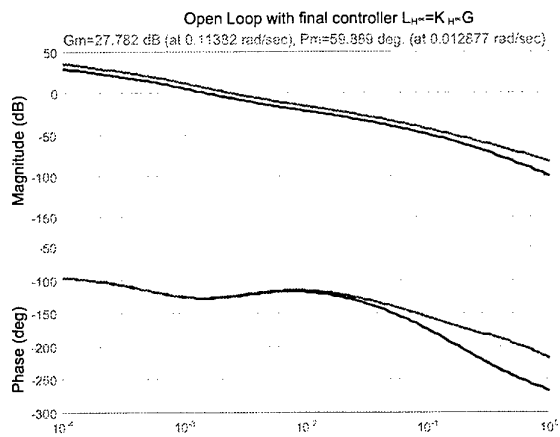


Figure 14: Open Loop frequency response

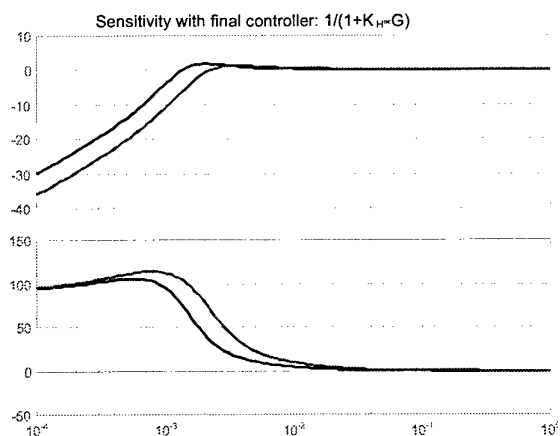


Figure 15: Sensitivity Frequency response

The order of the controller was further reduced using the balanced truncation method (Green and Limebeer, 1995).

Third Step: Prefilter Design

The final step of the technique proposed in this paper is the design of a prefilter using standard QFT. This method was applied to our case study, selecting the following Prefilter that fulfills the specifications:

$$F = \frac{(s/0.002767 + 1)(s/0.005882 + 1)}{(s/0.001212 + 1)(s/0.03323 + 1)}$$

It can be seen in Figures 16 and 17 that the transfer function from the reference to the output fulfills the stability and tracking specifications.

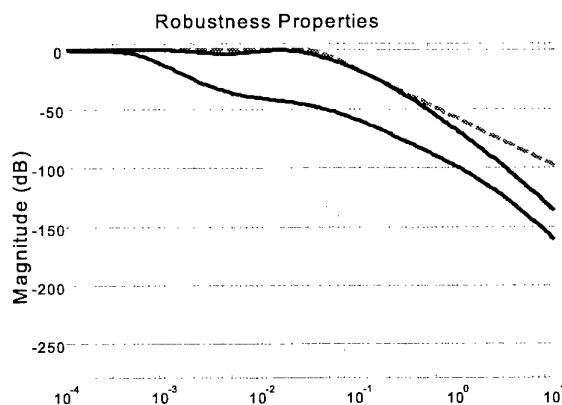


Figure 16: Prefilter Design- Robustness Check

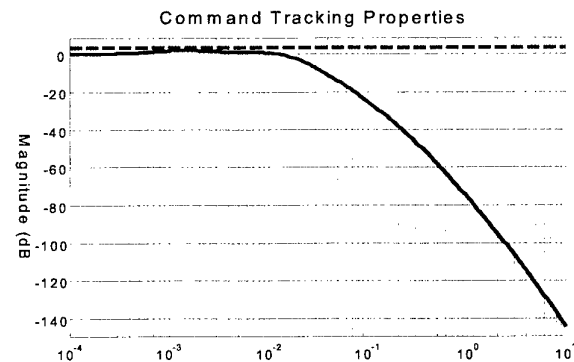


Figure 17: Prefilter Design- Tracking Check

Finally, the characteristic transfer functions were calculated for the feedback system with the final controller and the designed prefilter: the frequency and time responses of the command tracking properties are shown in Figures 18 to 20. It can be seen that using the technique presented in this paper, good command tracking and robustness properties are obtained: With the nominal plant, the Gain Margin is 27.7dBs and the Phase Margin is 59.9°, there are good command tracking and disturbance rejection properties.

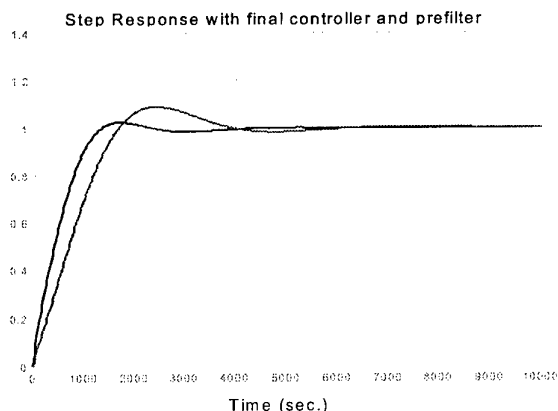


Figure 18: Command Step Response with prefilter

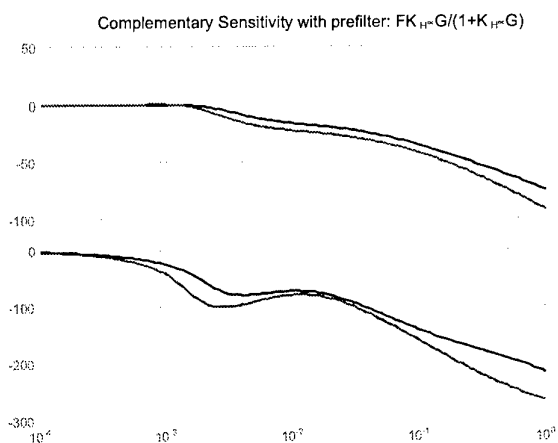


Figure 19: Complementary Sensitivity frequency response with Prefilter

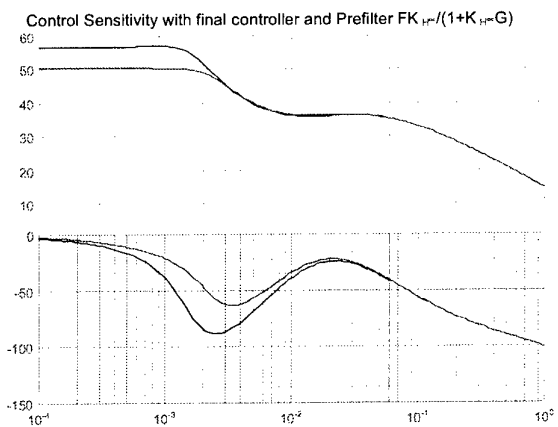


Figure 20: Control Sensitivity Response with Prefilter

5. CONCLUSIONS

H_∞ loopshaping is an appealing approach for controller design, as it addresses explicitly the problem of model uncertainty. However this design

method does not directly address the robustness properties of the real plant, but rather it is concerned with the shaped plant.

This paper has discussed a methodology that solves this problem by considering the robustness properties of the real plant in the selection of the weights of the shaped plant. Then a shaped plant is selected following the Quantitative Feedback Theory ideas. Once selected a robust shaped plant the controller is designed by application of the H_∞ loopshaping design method, following McFarlane/Glover ideas.

This three step design methodology makes possible to take advantage of the positive properties of the H_∞ loopshaping design method, but considering at the same time the robustness properties of the real plant. Also it is a natural way of considering two-degrees-of-freedom control systems. The application of this technique in a case study has shown its advantages for designing controllers for a real plant. It must be pointed out that it may be necessary to re-examine the robust stability and robust performance conditions with the final controller, as there is not guarantee on robust performance for the final controller. If these robustness are too strict, it may be necessary to relax them and repeat the design.

The idea shown in this paper of combining graphical and robust loopshaping has been shown to be promising. Compared with other robust control approaches this technique is more intuitive to the control engineer, thanks to the fact that the design parameter is the open-loop transfer function itself. Further work must be done to extend the proposed technique to multivariable systems and to ensure that the final controller fulfills the robustness conditions stated in the first step of the design.

ACKNOWLEDGMENTS

The authors are thankful to Mario Garcia and Isaac Horowitz for some helpful discussions. They also want to thank William Colmenares, Pastora Vega, and César de Prada, for their support during this work. Finally the first author would like to thank Ana Tadeo for modelling the system.

REFERENCES

- Borghesani, C., Chait, Y., Yaniv, O. (1995), *Quantitative Feedback Theory Toolbox*, The Mathworks, Inc.
- Chiang, R.Y.; Safonov, M.G. (1992), *Robust Control Toolbox*, The Mathworks Inc.
- Glover, K.; McFarlane, D. (1989) Robust stabilization of normalized coprime factor plant descriptions with H_∞ bounded uncertainty, *IEEE Trans. Automat. Contr.*, 34, 821-830

- Gustafsson, T.K et al. (1995) Modeling of pH for Control, *Ind. Eng. Chem. Res.*, 34, 820-827
- Horowitz, I.M (1963), Synthesis of Feedback Systems, New York, Academic Press
- Horowitz, I.M., (1992), Quantitative Feedback Design Theory (QFT). QFT Publishers, 660 South Monaco Parkway, Denver, Colorado 80224-1229
- Houpis, C.H., Rasmussen, S.J., (1999), Quantitative Feedback Theory. Fundamentals and Applications. Marcel Dekker
- McFarlane, D.C.; Glover, K., (1990), *Robust Controller Design Using Normalized Coprime Factor Plant Descriptions*, Lecture Notes Control & Information Sciences. Springer Verlag
- Niksefat N., Sepehri, N. (2001), Designing Robust Force Control of Hydraulic Actuators despite System and Environmental Uncertainties, *IEEE Control Systems Magazine*, 21, 2, pp.66-77
- Palancar, M.C., Aragon, J.M.; Miguens, J.A.; Torrecilla, J.S. (1996), Application of a Model Reference Adaptive Control System to pH Control. Effects of Lag and Delay Time, *Ind. Eng. Chem. Res.*, 35, 4100-4110
- Pantas, A.; Walsh, S., (1996) Evaluation of H_∞ Loop Shaping Controller Design on a Process Control Problem, *UKACC Control'96*, Exeter, UK
- Skogestad, S.; Postlethwaite, I., (1996) *Multivariable Feedback Control, Analysis and Design*, John Wiley & Sons
- Tadeo, F.; Holohan, A.; Vega, P. (1998) l_1 -Optimal Regulation of a pH Control Plant, *Computers chem. Eng.*, 22, S459-466
- Tadeo, F.; Pérez, O.; Alvarez, T. (2000), Control of Neutralization Processes by Robust Loopshaping, *IEEE Trans. Contr. Syst. Technol.*, 8, 236-246
- Tang, K.S.; Man, K.F.; Gu, D.W. (1996) Structured Genetic Algorithm for Robust H_∞ Control Systems Design, *IEEE Trans. on Industrial Electronics*, 43, 575-582
- Whidborne, J.F.; Postlethwaite, I.; Gu, D.W. (1994) Robust Controller Design using H_∞ loop-shaping and the method of inequalities, *IEEE Trans. Contr. Syst. Technol.*, 2, 455-461
- Yaniv, O., (1999) Quantitative Feedback Design of Linear and Non-linear Control Systems. Kluwer Academic Publishers.
- Zhou, K.; Doyle, J.C.; Glover, K. (1996) *Robust and Optimal Control*, Prentice Hall: New Jersey

QFT DESIGN WITH PHASE SPECIFICATIONS

José C. Moreno[†], Alfonso Baños[‡], and Manuel Berenguel[†]

[†]Dpto. Lenguajes y Computación, Escuela Politécnica Superior
 Universidad de Almería, 04120 Almería, Spain
 e-mails: jcmoreno@ual.es, beren@ual.es

[‡]Dpto. Informática y Sistemas, Facultad de Informática
 Universidad de Murcia, 30071 Murcia, Spain
 e-mail: abanos@dif.um.es

Abstract: This paper analyses the phase specifications problem in QFT. An algorithm is proposed aimed at achieving pre-specified closed loop transfer function phase and magnitude variations taking into account the plant uncertainty. A two-degrees of freedom feedback control structure is used and a new type of boundary is included to satisfy these objectives. As the control effort heavily depends on a good estimation of these boundaries, the proposed algorithm allows avoiding over-design. Copyright© 2001 IFAC

Keywords: phase characteristics, phase contours, control system synthesis.

1. INTRODUCTION

Quantitative Feedback Theory (QFT) is a robust control design method where system uncertainty is typically of parametric nature, commonly given in the form of *templates* (see Horowitz (1982) for a survey of the technique). QFT uses a two-degrees of freedom (2DoF) feedback scheme (Fig. 1), where it is assumed that the uncertain system is represented by a transfer function $P(s)$ belonging to a set of plants \mathbf{P} , while $G(s)$ and $F(s)$ are respectively the compensator and pre-compensator to be synthesised in order to meet robust stability and performance specifications.

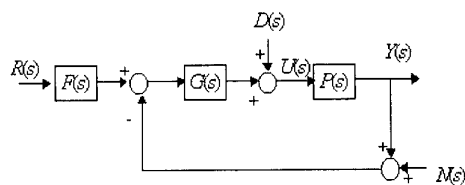


Fig. 1. A 2DoF feedback system

In QFT, closed loop specifications are given in the frequency domain, in terms of admissible bounds on closed loop transfer functions. Then, specifications are combined with the uncertainty of the system (given in the form of *templates*) to obtain limits or *boundaries* on the frequency shape of the compensator $G(s)$. In addition, nominal specifications are used to shape the pre-compensator $F(s)$. This paper focuses in the analysis of the problems associated with the simultaneous consideration of magnitude and phase specifications for the closed loop transfer function (which can be of interest, for instance, in problems dealing with co-ordinated movement in robotics).

Few works about phase specifications and their applications can be found in the QFT literature (Bailey and Kallel, 1992; Holt and Lee, 1989). The way in which these papers address the problem differs from the approach used in this paper, which mainly consists of shaping $F(s)$ and $G(s)$ to achieve some nominal phase and magnitude specifications using a new set of boundaries. Another important point not

previously considered is the computation of multi-valued boundaries. For instance, the algorithm proposed by Bailey and Kallel (1992) to compute the phase tracking boundaries did not exploit the fact that boundaries can be multiple-valued.

The consideration of multiple-valued boundaries may have an important practical relevance, as the control effort is directly related with them. This fact was pointed out in (Bailey *et al.*, 1988) and considered in the subsequent works, but general solutions to this problem have not been found. The computation of multiple-valued tracking boundaries has been analysed in (Moreno *et al.*, 1997) and extended (Moreno, 2001) to include also phase tracking boundaries to guarantee certain closed loop transfer function phase variations (from reference input to system output). The consideration of phase specifications results in new type of boundary (the *nominal phase tracking boundary*), which is developed in this work.

The paper is organised as follows. After some preliminaries in Section 2, the subsequent Sections show different approaches for solving the phase specification problem. Section 3 considers a first algorithm using a design viewpoint. In Section 4 a much less conservative solution is investigated. An example is developed in Section 5.

2. PRELIMINARIES

The problem that will be considered in this work is the design of a control system (Fig. 1) to satisfy tracking specifications, considering a nominal value of the closed loop transfer function $T = FGP/(1+GP)$ and allowed deviations. P is any element of a set of plants \mathcal{P} . For the nominal value and allowed variations, the specifications are given for both magnitude and phase.

G can be designed to meet variations over both magnitude and phase of the closed loop transfer function $T(s)$. The role of the pre-compensator $F(s)$ is to fix the nominal value of $T(s)$, but due to the fact that phase and magnitude of $T(s)$ are related, by the Bode's Integral assuming minimum phase systems, or analogous constraints for unstable and nonminimum phase systems, phase and magnitude can not be independently manipulated in design.

Usually, F and G are designed without taking into account the phase specifications in the design process, then a satisfactory design can be obtained meeting variations over the nominal magnitude of $T(s)$ and variations over the nominal phase of $T(s)$, but this is not the general case.

In robotics, the robot motion control problems can be separated into two categories: positioning and contouring. In contouring problems, the robot tool tip

is commanded to follow a specific path. Here the spatial contour tracking accuracy of the robot is of paramount concern since it directly influences the quality of the final product. These cases can be handled using phase specifications. In (Eitelberg, 2000) this problem is solved using tracking error magnitude specifications.

Throughout the paper the following notation will be used:

\mathcal{P} : A set of plants.

\mathcal{W} : A finite set of frequencies.

$L(s): G(s) \cdot P(s)$ with $P \in \mathcal{P}$

\mathcal{L} -template(ω): $\{L(j\omega): P \in \mathcal{P}\}$ with $\omega \in \mathcal{W}$

$X(s): \frac{L(s)}{1+L(s)}$

$T(s): F(s) \cdot X(s)$

$\mathcal{N} = \{X(s): P \in \mathcal{P}\}$

It will be said that \mathcal{N} is a crossing set of transfer functions if $\exists X_1, X_2 \in \mathcal{N}: |X_1(j\omega)| = |X_2(j\omega)|$ for some $\omega > 0$. The set of frequencies in which there are crossings is noted by $Lf(\mathcal{N}) = \{0 \leq \omega \leq \omega_s\}$, where

$$\omega_s = \text{Sup}\{\omega > 0: |X_i(j\omega)| = |X_j(j\omega)|, i \neq j, X_i, X_j \in \mathcal{N}\}$$

For this type of set \mathcal{N} , $M_D(\mathcal{N})$ is defined as

$$\text{Max} \left\{ \text{abs} \left(|X_i(j\omega)|_{dB} - |X_j(j\omega)|_{dB} \right): X_i \text{ and } X_j \in \mathcal{N} \ i \neq j, \right. \\ \left. \omega \in Lf(\mathcal{N}) \right\}$$

the maximum difference between the magnitude of transfer functions belonging to \mathcal{N} for all frequencies in $Lf(\mathcal{N})$.

3 A SOLUTION FROM THE DESIGN VIEWPOINT

Given design specifications over a frequency set \mathcal{W} (Fig. 2a), the problem is to find $G(s)$ to satisfy them (satisfying a set of boundaries). Once G has been obtained, F has to be designed to achieve nominal specifications (Fig. 2b). In Moreno *et al.* (1997) an algorithm to compute the boundaries over the nominal open loop transfer function (equivalently over $G(s)$) is presented. This algorithm is based on the construction of a 3D surface, where the boundaries are simply contour lines. Here, to compute a new set of boundaries the same idea is used.

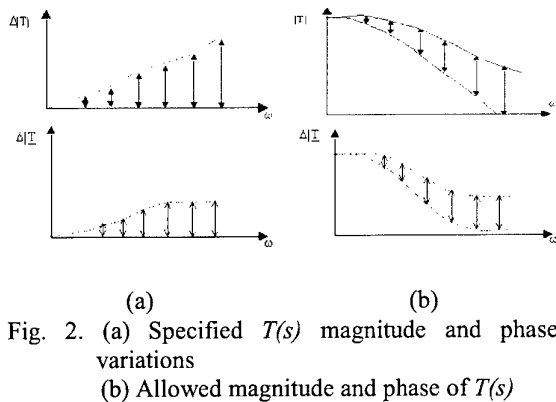


Fig. 2. (a) Specified $T(s)$ magnitude and phase variations
(b) Allowed magnitude and phase of $T(s)$

The main problem is that two objectives (phase and magnitude specifications) have to be met with only one degree of freedom, F . The $G(s)$ degree of freedom will be used too, in order to satisfy a new set of boundaries which guarantee that finally, using F , both objectives can be met.

A sketch of the algorithm is:

Algorithm 1

1. Compute $P_m \in \mathcal{O}$ such that

$$X_{\text{sup}}(\omega) = \left| \frac{P_m(j\omega) \cdot G(j\omega)}{1 + P_m(j\omega) \cdot G(j\omega)} \right| = \max_{P \in \mathcal{O}} \left| \frac{L(j\omega)}{1 + L(j\omega)} \right|$$

where $P \in \mathcal{O}$ and $\omega \in W$.

2. Choose $F = \frac{B_u}{X_{\text{sup}}}$.

In step #1, the point P_m has been calculated for each \mathcal{L} -template(ω) in such a way that the M-contour passing through the point P_m is the maximum M-contour passing through the \mathcal{L} -template(ω). The algorithm guarantees the achievement of a desired shape of the nominal magnitude but not necessarily the shape of the nominal phase (in general, the maximum N-contour passing through the shifted template does not pass through the point P_m). It can be demonstrated (Moreno, 2001) that by using this algorithm, the phase specifications shown in Fig. 3 can be met, in which the upper phase bound for each frequency in W is modified such that the phase band for each frequency is the double of the original specification. In order to guarantee a proper $F(s)$, the pole-zero excess of X_{sup} must be less or equal than the pole-zero excess of B_u .

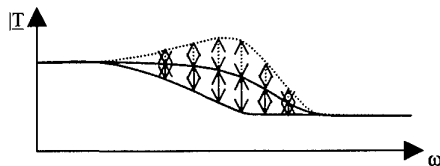


Fig. 3. Phase specifications that can be fulfilled using the algorithm

Thus, allowing a (conservative) modification of the original phase specification (Fig. 4), the previous algorithm gives a solution to the problem.

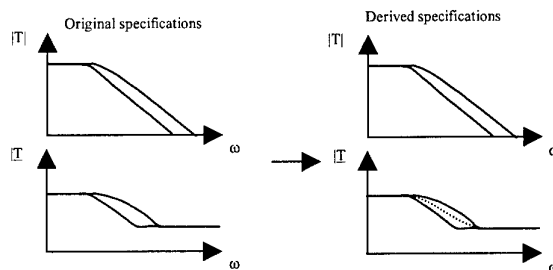


Fig. 4. Transformation of the original specifications

The computation of $X_{\text{sup}}(\omega)$ is very easy to implement if \mathcal{R} is not a crossing set of transfer functions. The maximum M-contour passes through the same point L_m ($P_m \cdot G$) for all the \mathcal{L} -templates, so

$$X_{\text{sup}}(s) = \frac{L_m(s)}{1 + L_m(s)}.$$

From the design viewpoint, this algorithm is a conservative solution to the phase specification problem, because the derived specifications are more restrictive than the original ones. Obviously, if the plant is a single integrator with uncertain gain and a 0dB robust stability specification is used, the transformation shown in Fig. 4 is not needed, as the maximum M and N contours pass through the same point of each template. In this particular case the above algorithm is not conservative. For example, if the uncertain plant and the compensator are given by

$$P(s) \in \mathcal{O} = \left\{ \frac{k}{s} : k = 0.01, 0.05, 0.1, 0.5, 1 \right\} \quad (2)$$

$$G(s) = \frac{6s + 5}{s}$$

a set of non-crossing open loop transfer functions (Fig. 5a) and a crossing set \mathcal{R} in Fig. 5(b) are obtained. There exists a maximum in the set of open loop transfer functions but this is not the case when obtaining $X(s)$, due to the location of open loop transfer functions on the Nichols Chart, as can be seen in Fig. 6.

The original specifications in this example are given by the following transfer functions (corresponding to the curves shown in Fig. 7):

$$B_u(s) = \frac{1.2 \cdot 10^9}{(s+10)(s+10^4)(s+1.2 \cdot 10^4)}$$

$$B_l(s) = \frac{5 \cdot 10^9}{(s+10)(s+5)(s+10^4)^2}$$

ω (r/s)	$\Delta T $ (dB)	$\Delta\angle T$ (°)
0.1	0.0017	1.1458
1	0.1703	11.3099
10	6.9897	63.4349
100	26.0314	87.1376
1000	46.0207	89.7135

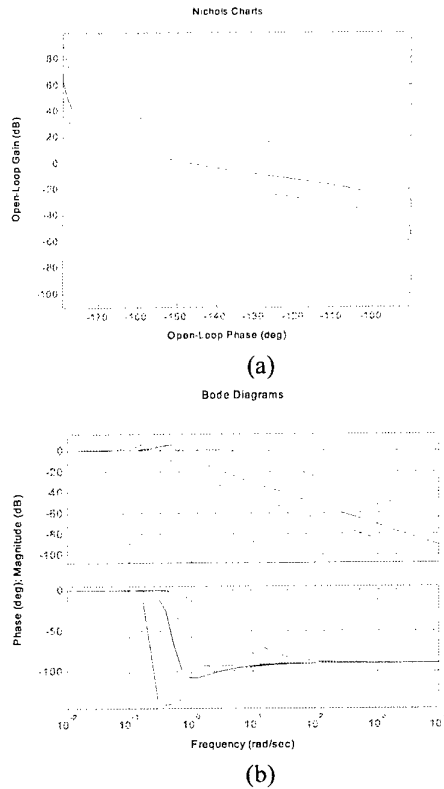


Fig. 5. (a) Set of open loop transfer functions.
(b) Set of $X(s)$ transfer functions

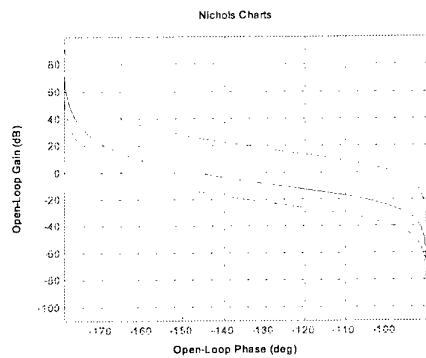


Fig. 6. Situation of the set of open loop transfer functions on the Nichols Chart

Using the algorithm in (Moreno *et al.*, 1997), the magnitude and phase tracking boundaries can be computed (Fig. 8). The nominal open loop transfer function (Fig. 9) can be obtained using computer tools (Borguesani *et al.*, 1995). The result is

$$G(s) = \frac{4336s^4 + 230880s^3 + 726610s^2 + 297840s + 1.952}{0.000125s^5 + 1.25s^4 + 46.82s^3 + 100.7s^2 + 19.6s + 1}$$

Fig.10 shows the magnitude and phase plots of X in the set \mathcal{N} .

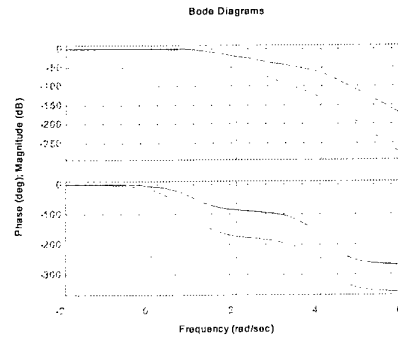


Fig. 7. Original specifications

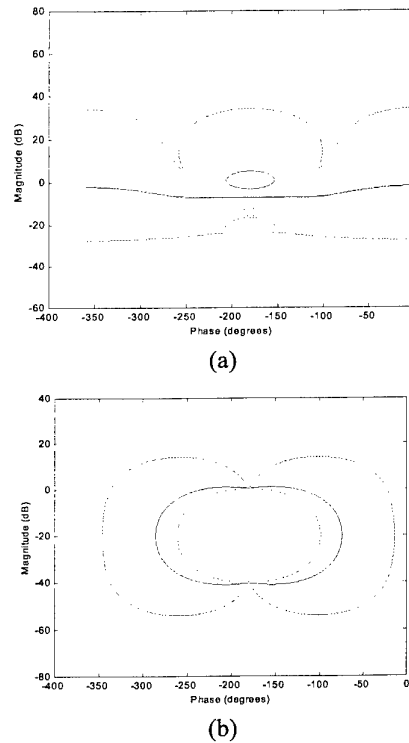


Fig. 8. (a) Magnitude tracking boundaries.
(b) Phase tracking boundaries

Then, the proposed algorithm can be applied to obtain

$F(s)$, given as result

$$F(s) = \frac{150000s^6 + 1.506 \cdot 10^9 s^5 + 5.259 \cdot 10^{12} s^4 + 2.772 \cdot 10^{14} s^3 + 4336s^7 + 9.566 \cdot 10^7 s^6 + 5.263 \cdot 10^{11} s^5 + 3.298 \cdot 10^{13} s^4 + 8.72 \cdot 10^{14} s^3 + 3.574 \cdot 10^{14} s + 2.342 \cdot 10^9}{3.644 \cdot 10^{14} s^3 + 9.077 \cdot 10^{14} s^2 + 3.574 \cdot 10^{14} s + 2.342 \cdot 10^9}$$

In Fig. 11, both magnitude and phase of the closed loop transfer functions $T(s)$ are shown.

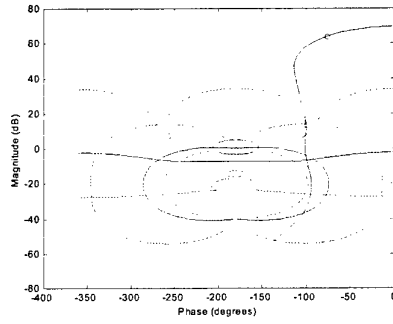


Fig. 9. Nominal open loop transfer function

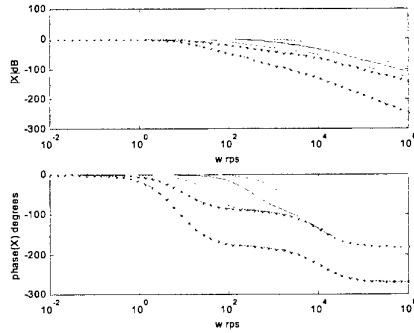


Fig. 10. $X(s)$ transfer functions and specifications.

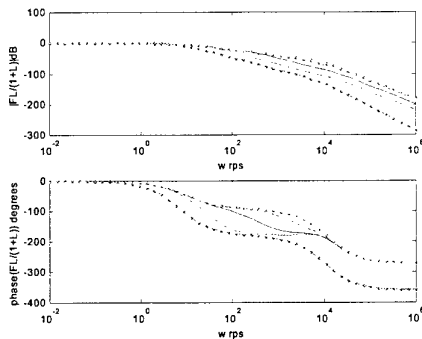


Fig. 11. $T(s)$ transfer functions and specifications

X_{sup} has been selected belonging to the set \mathfrak{N} , but it can be observed in Fig. 12 that this selection is incorrect, because \mathfrak{N} is a crossing set of transfer functions. The approximation in this case has provided good results because $M_D(\mathfrak{N})$ is small. Obviously, there exists a relation between $M_D(\mathfrak{N})$ and the situation of nominal open loop transfer function in Nichols Chart. So, when the \mathcal{L} -template is near of point $(-180^\circ, 0\text{dB})$ $M_D(\mathfrak{N})$ is higher.

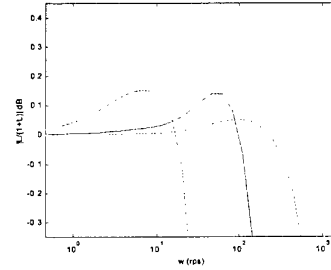


Fig. 12. Set of $X(s)$ transfer functions at low frequency

In this example, a robust stability specification of 0.2 dB has been used, this being related with the approximation error incurred when selecting X_{sup} belonging to the set \mathfrak{N} .

This example has shown that the computation of X_{sup} can be performed by defining an approximation error, using a robust stability specification. The difficulty in computing X_{sup} is another of the main drawbacks of the algorithm.

4. A NEW TYPE OF BOUNDARY

The idea developed in this Section is based on using the 2DoF scheme to satisfy the shape of both the nominal magnitude and phase specifications instead of using only the $F(s)$ pre-compensator for these purposes.

In the loop shaping, the allowed region of the Nichols Chart has to be restricted to a zone such that the maximum M and N contours passing through the template cross the same point. This is possible only for a template with all its points lying at the same phase (an integrator with uncertain gain). In general, a new specification has to be defined directly related with the approximation error. A new type of boundary is proposed to satisfy these objectives, which is called the *Nominal Phase Shaping Boundary*. This boundary provides an allowed region $C(\omega)$ of the Nichols Chart given by the following expressions:

$$C(\omega) = \left\{ (x, y) \in \text{Nichols Chart} : \right. \\ \left. \max_{P \in \wp} \text{Angle} \left(\frac{P(j\omega) \cdot G(j\omega)}{1 + P(j\omega) \cdot G(j\omega)} \right) - \text{Angle} \left(\frac{P_m(j\omega) \cdot G(j\omega)}{1 + P_m(j\omega) \cdot G(j\omega)} \right) \leq \delta(\omega) \right\} \\ \text{with } x = P_0(j\omega) \cdot G(j\omega)_{\text{dB}} \text{ and } y = \text{Angle}(P_0(j\omega) \cdot G(j\omega))$$

$$\text{with } \frac{P_m(j\omega) \cdot G(j\omega)}{1 + P_m(j\omega) \cdot G(j\omega)} = \max_{P \in \wp} \frac{P(j\omega) \cdot G(j\omega)}{1 + P(j\omega) \cdot G(j\omega)} \quad \text{and}$$

$P_0 \in \wp$ being the nominal plant.

In order to compute this region, the next algorithm (based on Moreno *et al.* (1997)) is used. For each frequency ω , the template is shifted over the Nichols

Chart and, for each phase and each magnitude, the difference between the maximum N-contour passing through the template and the N-contour passing through the point P_m (the maximum M-contour passes through this point) is computed. This generates a surface in a three-dimensional space, in such a way that the new boundary at frequency ω can be computed by taking a section of this surface corresponding to a constant value $\delta(\omega)$.

In the following we use the notation:

$$L_0 = l e^{-j\phi}$$

Algorithm 2

1. Choose a phase vector and a magnitude vector
2. For each phase ϕ and each magnitude l
If $(-180^\circ, 0\text{dB}) \notin \text{Template}$, then

$$S(\phi, l) = \max_{P \in \phi} \text{Angle} \left(\frac{L_0(j\omega)}{P_0(j\omega) / P(j\omega) + L_0(j\omega)} \right) - \text{Angle} \left(\frac{L_0(j\omega)}{P_0(j\omega) / P_m(j\omega) + L_0(j\omega)} \right)$$

else

$$S(\phi, l) = 360^\circ$$

end

end

3. Boundary = contour line of S for the height $\delta(\omega)$

The region of Nichols Chart above this boundary is the allowed zone. Due to the shape of the N-contour in the Nichols Chart, it can be asserted that the satisfaction of this restriction is compatible with the satisfaction of the magnitude and phase tracking boundaries.

Furthermore, the shape of this new type of boundary can be characterised from the shape of the templates, which can be typified within three types T_1 , T_2 , and T_3 (Fig. 13)

- T_1 : The largest magnitude points are situated at the greatest phase (right part of the template).
- T_2 : The largest magnitude points are situated at the smallest phase (left part of the template).
- T_3 : There exist more than one point corresponding to the largest magnitude.

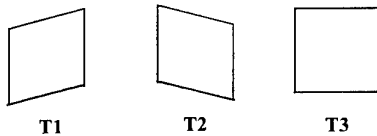


Fig. 13. Examples of the three types of templates \mathcal{Y}

- Closed (the allowed region is the exterior of the boundary) in the case T_1 and T_3 . Due to the fact that at small magnitudes, the phase of the template points is the same that the N-contours passing through these points.
- Open (the allowed region is above the boundary) in the case T_2 .

In addition, $\delta(\omega)$ can be used in the algorithm as a parameter to obtain less conservative results (restrictiveless boundaries for greater values of $\delta(\omega)$).

5. AN EXAMPLE

Consider the uncertain plant (taken from Horowitz and Sidi (1972))

$$P(s) = \frac{ka}{s(s+a)} \quad \text{with } k \in [1, 10] \text{ and } a \in [1, 10]$$

The working frequencies are $W = \{1, 2, 10\}$ rad/s, the nominal point is $k = a = 1$, and the specifications given by

$$B_u(s) = \frac{5 \cdot 10^{10}}{(s+10)(s+10^3)(s+5 \cdot 10^3)(s+10^3)}$$

$$B_l(s) = \frac{10^{10}}{(s+10)(s+1)(s+10^3)^3}$$

Tracking specifications (allowed magnitude variations) are given by 3.01, 6.99 and 20.04 dB for $W = 1, 2$ and 10 rad/s respectively. The phase tracking specifications (allowed phase variations) are 45° , 63.44° and 84.29° for the same W . Finally, 0.1° is used as a nominal phase shaping specification for all $\omega \in W$. In Fig. 15, the magnitude tracking boundaries (a), the phase tracking boundaries (b), and the nominal phase shaping boundaries (c) are shown.

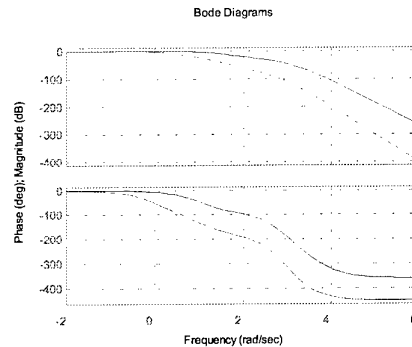
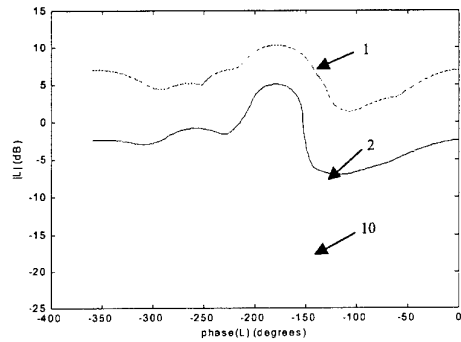
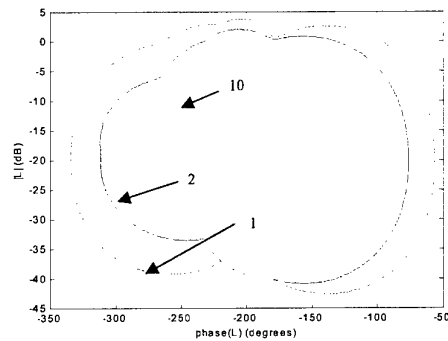


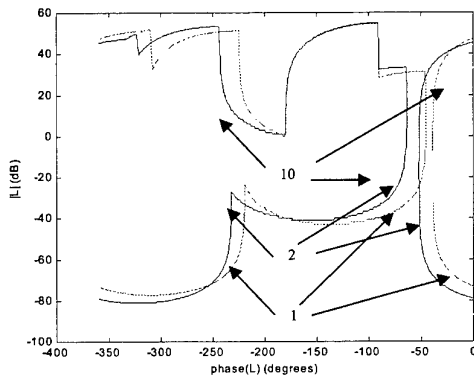
Fig. 14. Phase and magnitude specifications for $T(s)$



(a)



(b)



(c)

Fig. 15. (a) Magnitude tracking boundaries.
(b) Phase tracking boundaries.
(c) Nominal phase shaping boundaries

As done in the previous algorithm, using computer tools (Borguesani *et al.*, 1995) the nominal open loop transfer function can be designed (Fig. 17). The obtained $G(s)$ compensator is given by

$$G(s) = 0.028 \frac{\left(\frac{s}{0.01} + 1\right)}{\left(\frac{s}{10000} + 1\right)}$$

Before computing $F(s)$, it is important to check if specification are satisfied for other frequencies which are not considered in the initial working set W . In our case, at low frequencies the specifications are violated (Fig. 17).

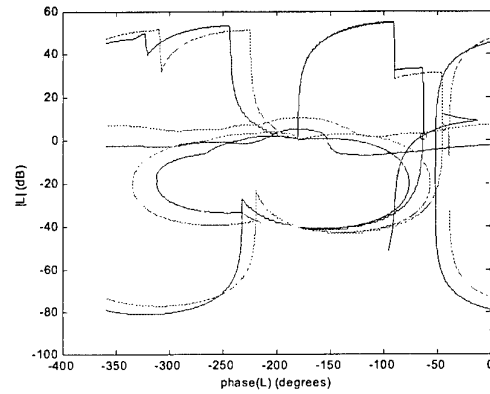


Fig. 16. Loop-shaping of nominal open loop transfer function

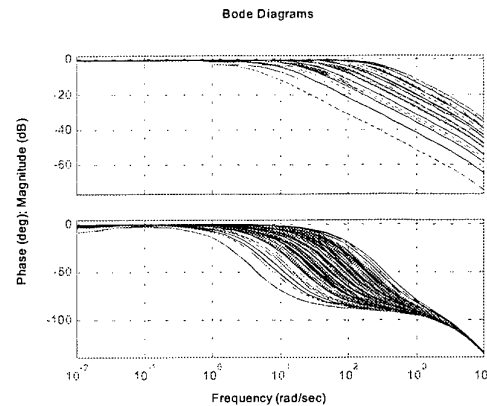
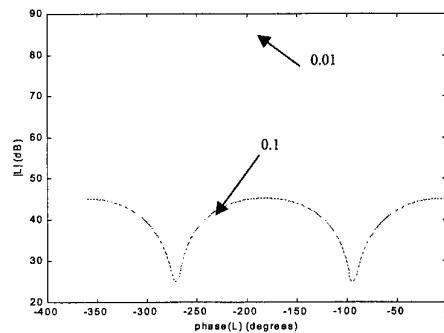


Fig. 17. $X(s)$ transfer

Thus, two new frequencies 0.01 and 0.1 rad/s are included in W . In this way, the next set of specifications is given by:

ω (rps)	$\Delta T $ (dB)	$\Delta\angle T$ (deg.)
0.01	0.0004	0.5729
0.1	0.0432	5.7106
1	3.0103	45.0000
2	6.9897	63.4349
10	20.0432	84.2894

The boundaries corresponding to these new two frequencies are included in Fig. 18.



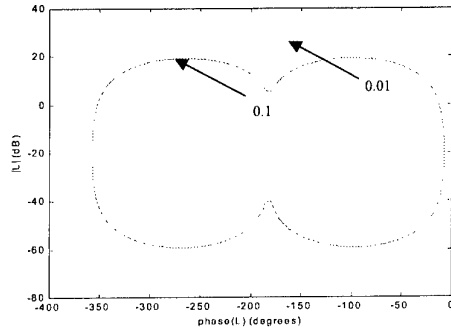


Fig. 18. (a) Magnitude tracking boundaries.
(b) Phase tracking boundaries.

The nominal open loop transfer function is now (Fig. 19)

$$G(s) = 9.544 \cdot \frac{(s + 0.1101)(s + 0.01072)(s + 0.08572)}{(s + 10000)(s + 0.00933)(s + 0.1167)(s + 5000)}$$

Fig. 20 shows how specifications are satisfied over the whole frequency axis. The selected precompensator is given by:

$$F(s) = \frac{918400s^6 + 1.379 \cdot 10^{10}s^5 + 4.606 \cdot 10^{13}s^4 + 4.721 \cdot 10^{17}s^3 + 9433000s^7 + 6.613 \cdot 10^{10}s^6 + 1.044 \cdot 10^{14}s^5 + 4.823 \cdot 10^{16}s^4 + 9.748 \cdot 10^{16}s^3 + 5.442 \cdot 10^{15}s^2 + 4.772 \cdot 10^{13}s + 4.816 \cdot 10^{17}s^3 + 9.797 \cdot 10^{16}s^2 + 5.446 \cdot 10^{15}s + 4.772 \cdot 10^{13}}{s^7 + 6.613 \cdot 10^{10}s^6 + 1.044 \cdot 10^{14}s^5 + 4.823 \cdot 10^{16}s^4 + 9.748 \cdot 10^{16}s^3 + 5.442 \cdot 10^{15}s^2 + 4.772 \cdot 10^{13}s + 4.816 \cdot 10^{17}}$$

Fig. 21 contains the final result of the design stage using the proposed algorithm.

6. CONCLUSIONS

In this paper, the problem of dealing with phase specifications in QFT has been studied and two algorithms have been proposed to solve it. The first algorithm (a sketch has been included in the text) is based in the transformation of the original specifications, often leading to a conservative solution from the design viewpoint. The second algorithm is based in the inclusion of a new type of boundary in the loop-shaping stage. Both algorithms use the 2DoF controller to solve the phase nominal shaping problem.

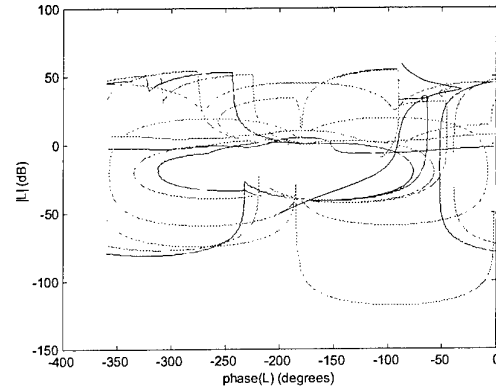


Fig. 19. Loop-shaping of nominal open loop transfer function

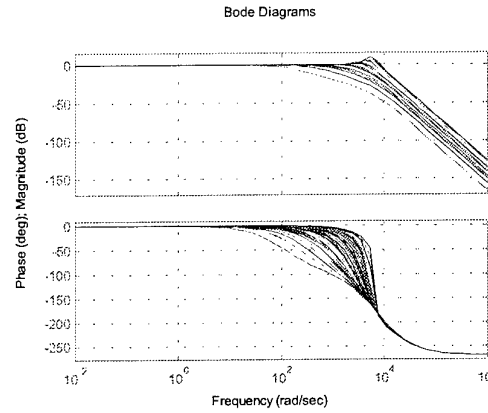
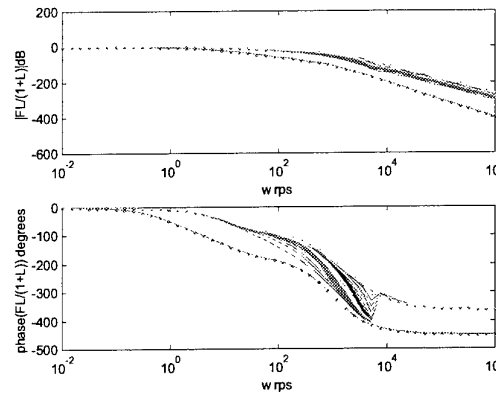


Fig. 20. $X(s)$ transfer functions



ACKNOWLEDGEMENTS

The authors would like to thank the Spanish Comisión Interministerial de Ciencia y Tecnología (CICYT) for partially funding this work under grants QUI99-0663-C02-02 and DP2000-1218-C04-03.

REFERENCES

- Bailey, F. N., D. Panzer and G. Gu (1988). Two algorithms for frequency domain design of robust control systems. *Int. J. Control*, **48**, 1787-1806.
- Bailey, F. N. and M. Kallel (1992). Loop Gain-Phase Shaping Techniques for Robust Multi-Axis Coordination Motion Control. In: *Proc. ACC*, June 1992.
- Borguesani, C., Y. Chait and O. Yaniv (1995). *The Quantitative Feedback Theory Toolbox for MATLAB*. The MathWorks, MA.
- Eitelberg, E. (2000). Quantitative Feedback Design for Tracking Error Tolerance. *Automatica*, **36**(2), 319-326.
- Holt, T. and M. Y. Lee (1989). A Control Strategy for Multi-Axis Robot Contouring Accuracy Enhancement. In: *Proc. of First National Conference on Applied Mechanism and Robotics*, Cincinnati OH.
- Horowitz, I. and M. Sidi, (1972). Synthesis of feedback systems with large plant ignorance for prescribed time-domain tolerances. *Int. J. Control*, **16**(2), 287-309.
- Horowitz, I. (1982). Quantitative feedback theory. *IEEE Proc.*, **129** (D-6), 215-226.
- Moreno, J.C., A. Baños, and F.J. Montoya (1997). An Algorithm for Computing QFT Multiple-valued Performance Bounds. In: *Proc. Symp. on QFT and other Frequency Domain Methods and Applications*, pp. 29-32. Univ. Strathclyde (Scotland).
- Moreno, J.C. (2001). *An Algorithm for dealing with phase specifications in QFT*. Internal Report. Universidad de Almería, Spain.

Fig. 21. Variations over the magnitude and the phase of $T(s)$ due to uncertainty in plant

A GEOMETRIC APPROACH TO ROBUST PERFORMANCE OF PARAMETRIC UNCERTAIN SYSTEMS

Bondia, J., Picó, J.

*Dept. Systems Engineering & Control
 Technical University of Valencia
 e-mail: jbondia@isa.upv.es, jpico@isa.upv.es*

Abstract: Based on the observation that inclusion of a system in a family of Bode diagrams implies inclusion on the respective family of step responses, some ideas about a new geometric approach for the robust performance problem for interval systems are presented. This approach allows to deal with classical time specifications such as overshoot, settling time and steady state error. Two examples are presented with remarkable results.

Keywords: Parametric uncertainty, interval systems, robust performance

1. INTRODUCTION.

Given the parametric uncertain plant

$$P(s, \tilde{\mathbf{q}}) = \frac{b(s, \tilde{\mathbf{q}})}{a(s, \tilde{\mathbf{q}})} \quad (1)$$

where $\tilde{\mathbf{q}} = (\tilde{q}_1, \dots, \tilde{q}_p)$, $\tilde{q}_i = [q_i^-, q_i^+]$, robust performance problem consists on finding a controller so that the closed loop response at each instant $t^* \in [0, \infty[$ belongs to the interval $[m^-(t^*), m^+(t^*)]$. Functions $m^-(t)$ and $m^+(t)$ denote the lower and upper bounds on the closed loop output. Usually, the kind of bounds one looks for is that of a low order system (first or second order). In this case, bounding functions will be derived from bounds on time domain specifications such as overshoot, settling time and steady state error. These control specifications can be easily mapped to an *uncertain reference model*. For instance, if a "second order response" is desired with overshoot $\delta \in [0\%, 10\%]$, settling time $t_e \in [1s, 4s]$ and steady state error $\pm 1\%$, then control specifications can be given by means of the reference model

$$M(s, \tilde{\mathbf{r}}) = \frac{\tilde{K}}{1 + 2\tilde{\xi} \frac{s}{\tilde{\omega}_n} + \left(\frac{s}{\tilde{\omega}_n}\right)^2} \quad (2)$$

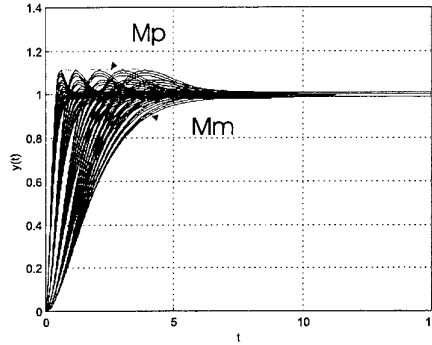


Fig. 1. Unit step response of the reference model (2).

where $\tilde{\mathbf{r}} = (\tilde{K}, \tilde{\xi}, \tilde{\omega}_n)$ and $\tilde{K} = [0.99, 1.01]$, $\tilde{\xi} = [0.5912, 1]$, $\tilde{\omega}_n = [1, 6.7664]$. Bounding functions $m^-(t)$, $m^+(t)$ correspond, thus, to the lower and upper envelope of the response of the uncertain reference model (figure 1). In general, the uncertain reference model will consist on a set of first and second order terms shaping the desired bounding functions.

Definition 1.1. Given an uncertain system $G(s, \tilde{\mathbf{q}})$, with output envelopes $g^-(t)$, $g^+(t)$, a trajectory $y(t)$ is said to belong to the *output space*

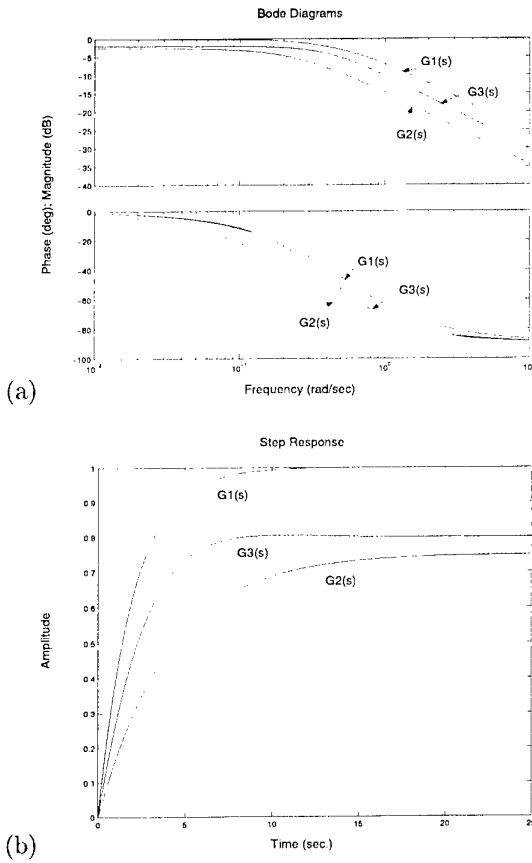


Fig. 2. (a) Frequency envelopes (b) Unit step output envelopes.

of $G(s, \tilde{\mathbf{q}})$, denoted by \mathcal{Y}_G , if $g^-(t) \leq y(t) \leq g^+(t)$, $\forall t \in [0, \infty[$. The output space is then the functional interval $[g^-(t), g^+(t)]$ (Bondia and Picó, 2001).

Consider a first order uncertain system, for instance:

$$G(s, \tilde{\mathbf{q}}) = \frac{[0.75, 1]}{1 + [2, 4]s} \quad (3)$$

In this case, the output envelopes are generated by two members of the family, in particular:

$$g^+(t) \rightarrow \frac{1}{1 + 2s} \stackrel{\text{def}}{=} G_1(s) \quad (4)$$

$$g^-(t) \rightarrow \frac{0.75}{1 + 4s} \stackrel{\text{def}}{=} G_2(s) \quad (5)$$

These members also define the envelopes of the Bode diagrams of the family (frequency envelopes). Any member with a Bode diagram within the frequency envelopes will have an output within the output envelopes. This can be generalized for any system of relative degree one, for instance:

$$G_3(s) = \frac{1.538s + 0.8}{4.938s^2 + 4s + 1} \quad (6)$$

as shown in figure 2.

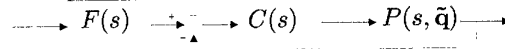


Fig. 3. TDF control structure.

Based on this observation some ideas about a new geometric approach for the robust performance problem for interval systems are presented. The use of an uncertain reference model as shown above allows to deal with classical time specifications such as overshoot, settling time and steady state error in opposition to current methodologies (Zhou, 1998; Bhattacharyya *et al.*, 1995; Barmish, 1994; Ackermann, 1993). Two examples are presented with remarkable results.

2. MAIN RESULT.

From the above observation the following is conjectured.

Lemma 2.1. Given a reference model $M(s, \tilde{\mathbf{r}})$ and an uncertain plant $G(s, \tilde{\mathbf{q}})$, let $\mathcal{M}(j\omega^*)$ and $\mathcal{G}(j\omega^*)$ be their images in the complex plane for $s = j\omega^*$, respectively. If $\mathcal{G}(j\omega^*) \subseteq \mathcal{M}(j\omega^*)$, $\forall \omega^* \in [0, \infty[$ then $\mathcal{Y}_G \subseteq \mathcal{Y}_M$.

If a two degrees of freedom (TDF) control structure is considered (figure 3), the resulting closed loop system is:

$$G_{lc}(s, \tilde{\mathbf{q}}) = \frac{F(s)C(s)P(s, \tilde{\mathbf{q}})}{1 + C(s)P(s, \tilde{\mathbf{q}})} \quad (7)$$

where $F(s)$ is the prefilter and $C(s)$ the loop controller. By lemma 2.1, the system will fulfill the specifications whenever

$$\mathcal{G}_{lc}(j\omega^*) \subseteq \mathcal{M}(j\omega^*), \quad \forall \omega^* \in [0, \infty[\quad (8)$$

Denoting by $H(s)$ the inverse of the loop controller, $H(s) \stackrel{\text{def}}{=} 1/C(s)$, the following result holds.

Theorem 2.1. $\mathcal{G}_{lc}(j\omega^*) \subseteq \mathcal{M}(j\omega^*)$ if and only if $H(j\omega^*) \frac{1}{\mathcal{P}(j\omega^*)} \subseteq F(j\omega^*) \frac{1}{\mathcal{M}(j\omega^*)} - 1$, $\forall \omega^* \in [0, \infty[$.

Proof: (sufficiency) By (7),

$$\frac{F(j\omega^*)C(j\omega^*)P(j\omega^*)}{1 + C(j\omega^*)P(j\omega^*)} \subseteq \mathcal{M}(j\omega^*) \quad (9)$$

must hold, for all $\omega^* \in [0, \infty[$. Operating, to get a unique instance of $\mathcal{P}(j\omega^*)$,

$$\frac{F(j\omega^*)}{\frac{1}{C(j\omega^*)P(j\omega^*)} + 1} \subseteq \mathcal{M}(j\omega^*) \quad (10)$$

$$\frac{F(j\omega^*)}{H(j\omega^*) \frac{1}{\mathcal{P}(j\omega^*)} + 1} \subseteq \mathcal{M}(j\omega^*) \quad (11)$$

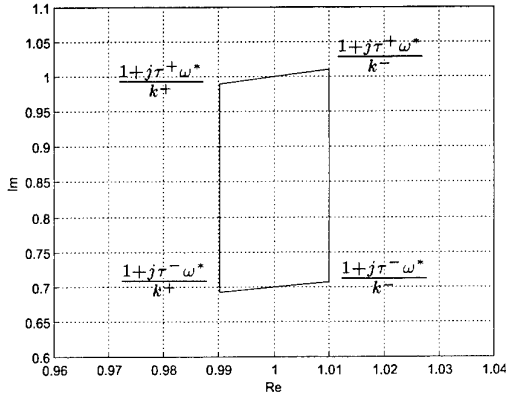


Fig. 4. Image of the inverse of a first order system.

Set inclusion is invariant under division by $F(j\omega^*)$, thus

$$\frac{1}{H(j\omega^*)\frac{1}{\mathcal{P}(j\omega^*)} + 1} \subseteq \frac{1}{F(j\omega^*)\frac{1}{\mathcal{M}(j\omega^*)}} \quad (12)$$

The above condition will hold whenever set inclusion holds for the denominators. Therefore,

$$H(j\omega^*)\frac{1}{\mathcal{P}(j\omega^*)} + 1 \subseteq F(j\omega^*)\frac{1}{\mathcal{M}(j\omega^*)} \quad (13)$$

$$H(j\omega^*)\frac{1}{\mathcal{P}(j\omega^*)} \subseteq F(j\omega^*)\frac{1}{\mathcal{M}(j\omega^*)} - 1 \quad (14)$$

Necessity is proved using similar arguments. ■

The control synthesis problem for robust performance consists on finding a prefilter $F(s)$ and a loop controller $C(s) = 1/H(s)$ so that theorem 2.1 holds. It is, thus, a set inclusion problem.

2.1 Inverse reference model image set.

The reference model $M(s, \tilde{r})$ will usually be an uncertain system of first or second order. In this case, an analytic description of $1/\mathcal{M}(j\omega^*)$ can be obtained.

First order reference model. Let

$$M(s, \tilde{r}) = \frac{\tilde{k}}{1 + \tilde{\tau}s} \quad (15)$$

with $\tilde{k} = [k^-, k^+]$ and $\tilde{\tau} = [\tau^-, \tau^+]$. For a fixed frequency ω^* ,

$$\frac{1}{M(j\omega^*, \tilde{r})} = \frac{1}{\tilde{k}} (1 + j\tilde{\tau}\omega^*) \quad (16)$$

The image of $1 + j\tilde{\tau}\omega^*$ is a vertical line with endpoints $1 + j\tau^-\omega^*$ and $1 + j\tau^+\omega^*$. Considering without loss of generality positive gain, multiplication by $1/\tilde{k}$ expands or contracts this vertical line without changing the phase. Thus, the resulting image set is the polytope shown in figure 4.

Second order reference model. Let

$$M(s, \tilde{r}) = \frac{\tilde{k}}{1 + 2\tilde{\xi}\frac{s}{\tilde{\omega}_n} + \left(\frac{s}{\tilde{\omega}_n}\right)^2} \quad (17)$$

with $\tilde{k} = [k^-, k^+]$, $\tilde{\xi} = [\xi^-, \xi^+]$, $\tilde{\omega}_n = [\omega_n^-, \omega_n^+]$. For a fixed frequency ω^* ,

$$\frac{1}{M(j\omega^*, \tilde{r})} = \frac{1}{\tilde{k}} \left(1 - \left(\frac{\omega^*}{\tilde{\omega}_n}\right)^2 + 2\tilde{\xi}j\frac{\omega^*}{\tilde{\omega}_n} \right) \quad (18)$$

$$\stackrel{\text{def}}{=} \frac{1}{\tilde{k}} S(\omega^*, \tilde{r}) \quad (19)$$

The image of $S(\omega^*, \tilde{r})$ consists on a union of vertical lines. For $\bar{\omega} = \omega^*/\tilde{\omega}_n$,

$$S(\bar{\omega}, \tilde{r}) = 1 - \bar{\omega}^2 + j2\tilde{\xi}\bar{\omega} \quad (20)$$

which corresponds to a vertical line with endpoints $1 - \bar{\omega}^2 + j2\xi^-\bar{\omega}$ and $1 - \bar{\omega}^2 + j2\xi^+\bar{\omega}$. As $\bar{\omega}_n = [\omega_n^-, \omega_n^+]$, then $\bar{\omega} = [\omega^*/\omega_n^+, \omega^*/\omega_n^-]$, producing a sweep of the vertical line on the complex plane. Multiplication by $1/\tilde{k}$ converts this vertical line into a polytope, as for a first order reference model. Therefore, $1/\mathcal{M}(j\omega^*)$ will result from a sweep of polytopes on the complex plane (figure 5). Vertices A to F will depend on ω^* and can be obtained evaluating (18) for the following values of the uncertain parameters:

- $\omega^* < \omega_n^-$

$$A \rightarrow (k^-, \xi^+, \omega_n^-) \quad D \rightarrow (k^-, \xi^+, \omega_n^+)$$

$$B \rightarrow (k^+, \xi^+, \omega_n^-) \quad E \rightarrow (k^-, \xi^-, \omega_n^+)$$

$$C \rightarrow (k^+, \xi^-, \omega_n^-) \quad F \rightarrow (k^+, \xi^-, \omega_n^+)$$

- $\omega_n^- \leq \omega^* < \omega_n^+$

$$A \rightarrow (k^-, \xi^+, \omega_n^-) \quad D \rightarrow (k^-, \xi^+, \omega_n^+)$$

$$B \rightarrow (k^-, \xi^-, \omega_n^-) \quad E \rightarrow (k^-, \xi^-, \omega_n^+)$$

$$C \rightarrow (k^+, \xi^-, \omega_n^-) \quad F \rightarrow (k^+, \xi^-, \omega_n^+)$$

- $\omega^* \geq \omega_n^+$

$$A \rightarrow (k^-, \xi^+, \omega_n^-) \quad D \rightarrow (k^-, \xi^+, \omega_n^+)$$

$$B \rightarrow (k^-, \xi^-, \omega_n^-) \quad E \rightarrow (k^+, \xi^+, \omega_n^+)$$

$$C \rightarrow (k^+, \xi^-, \omega_n^-) \quad F \rightarrow (k^+, \xi^-, \omega_n^+)$$

The arcs AD , CF obey the expression:

$$\begin{aligned} AD &= \frac{1}{k^-} (1 - \bar{\omega}^2 + 2\xi^+ j\bar{\omega}) \\ CF &= \frac{1}{k^+} (1 - \bar{\omega}^2 + 2\xi^- j\bar{\omega}) \\ \frac{\omega^*}{\omega_n^+} &\leq \bar{\omega} \leq \frac{\omega^*}{\omega_n^-} \end{aligned} \quad (21)$$

For $\omega^* = 0$ the image set is the interval $[1/k^+, 1/k^-]$.

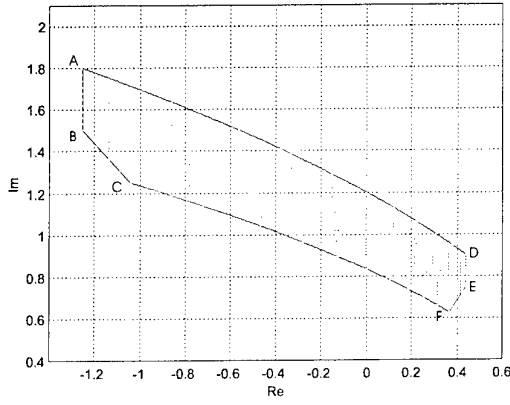


Fig. 5. Image of the inverse of a second order system.

2.2 Inverse plant image set.

The image set $1/\mathcal{P}(\omega^*)$ will depend on the way the uncertain parameters appear in the transfer function of the plant. Considering independent uncertainty structure, the image of $b(j\omega^*, \tilde{\mathbf{q}})$ and $a(j\omega^*, \tilde{\mathbf{q}})$ are both rectangles, thus, $1/\mathcal{P}(\omega^*)$ results from the quotient of two polytopes (in particular, rectangles). As the next lemma shows, this can be obtained by quotients of edge-vertex pairs.

Lemma 2.2. Let Q_1 and Q_2 be two complex plane polytopes with vertex sets V_1 and V_2 and edge sets E_1 and E_2 , respectively. Then,

$$\partial \left(\frac{Q_1}{Q_2} \right) \subset \frac{E_1}{V_2} \cup \frac{V_1}{E_2} \quad (22)$$

where $\partial(\cdot)$ denotes the border of the complex plane set (\cdot) .

Proof: See (Bhattacharyya *et al.*, 1995). ■

E_1/V_2 is the quotient of the rectangle $a(j\omega^*, \tilde{\mathbf{q}})$ by each vertex of $b(j\omega^*, \tilde{\mathbf{q}})$, resulting four rectangles scaled and rotated. V_1/E_2 is the quotient of each vertex of $a(j\omega^*, \tilde{\mathbf{q}})$ by the rectangle $b(j\omega^*, \tilde{\mathbf{q}})$. As the inverse of a line segment is an arc of a circle crossing the origin, this will lead to a set of convex and concave arcs (figure 6).

In the case there is no independent uncertainty structure, more complex image sets will result. In this case, their convex hull can be used instead, although this will lead to conservativeness.

2.3 A geometric interpretation.

Condition (14) has a natural geometric interpretation (figure 7). $H(j\omega^*)$ is a complex number multiplying the image set $1/\mathcal{P}(j\omega^*)$. Therefore $H(j\omega^*)$ expands (or contracts) this set by $|H(j\omega^*)|$ and rotates it with respect to the origin by $\angle H(j\omega^*)$. Sweeping on $|H(j\omega^*)|$ from 0 to

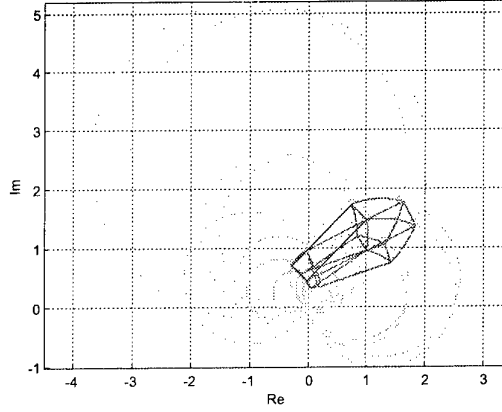


Fig. 6. Quotient of two rectangles.

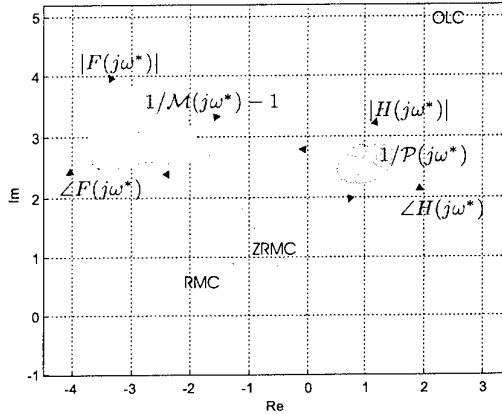


Fig. 7. Geometric interpretation of theorem 2.1.

∞ , $H(j\omega^*)/\mathcal{P}(j\omega^*)$ describes a cone with origin at $(0,0)$ (*open loop cone*, OLC). On the other hand, $\angle H(j\omega^*)$ determines the orientation of this cone. Similarly, $F(j\omega^*)$ expands (or contracts) the image set $1/\mathcal{M}(j\omega^*) - 1$ by $|F(j\omega^*)|$ and rotates it with respect to the point $(-1,0)$ by $\angle F(j\omega^*)$. Sweeping on $|F(j\omega^*)|$ from 0 to ∞ , $F(j\omega^*)/\mathcal{M}(j\omega^*) - 1$ describes a cone with origin at $(-1,0)$ and orientation determined by $\angle F(j\omega^*)$ (*reference model cone*, RMC). Given $F(j\omega^*)$, the cone with origin $(0,0)$ and minimum width which inscribes to $F(j\omega^*)/\mathcal{M}(j\omega^*) - 1$ will be denoted as *zero reference model cone*, ZRMC.

Sweeping on the frequency from 0 to ∞ , $|F(j\omega^*)|$, $\angle F(j\omega^*)$, $|H(j\omega^*)|$ and $\angle H(j\omega^*)$, must be chosen so that theorem 2.1 holds.

Let \mathcal{S}_C^+ and \mathcal{S}_C^- be the left and right side of the cone C and ϕ_C^+ , ϕ_C^- their angles with respect to the real axis for a fixed frequency ω^* (to ease notation this dependency will not be denoted explicitly).

Definition 2.1. The width of the cone C is defined as follows:

$$\text{width}(C) \stackrel{\text{def}}{=} \phi_C^+ - \phi_C^- \quad (23)$$

Proposition 2.1. If there exist $F(j\omega^*)$, and $H(j\omega^*)$ so that (14) holds, then

$$\text{width}(\text{ZMRC}) \geq \text{width}(\text{OLC}) \quad (24)$$

Proof: As $H(j\omega^*)/\mathcal{P}(j\omega^*)$ moves along the OLC, if (14) holds, then OLC must necessarily be contained in ZMRC, yielding (24). ■

Proposition 2.2. $\text{width}(\text{ZMRC}) \geq \text{width}(\text{OLC})$ if and only if

$$\phi_{\text{ZMRC}}^+ - \phi_{\text{OLC}}^+ \geq \phi_{\text{ZMRC}}^- - \phi_{\text{OLC}}^- \quad (25)$$

Proof: (refer to figure 7) $\phi_{\text{ZMRC}}^+ - \phi_{\text{OLC}}^+$ represents the angle OLC must be rotated with respect to the origin to overlap the left side of both cones ($\mathcal{S}_{\text{ZMRC}}^+ = \mathcal{S}_{\text{OLC}}^+$). Respectively, $\phi_{\text{ZMRC}}^- - \phi_{\text{OLC}}^-$ represents the angle OLC must be rotated with respect to the origin to overlap the right side of both cones ($\mathcal{S}_{\text{ZMRC}}^- = \mathcal{S}_{\text{OLC}}^-$). Therefore,

- (a) if $\phi_{\text{ZMRC}}^+ - \phi_{\text{OLC}}^+ < \phi_{\text{ZMRC}}^- - \phi_{\text{OLC}}^-$ then when the right side of both cones overlap, the left side of OLC has already overpassed the left side of ZMRC. Thus, $\text{width}(\text{OLC}) > \text{width}(\text{ZMRC})$,
- (b) if $\phi_{\text{ZMRC}}^+ - \phi_{\text{OLC}}^+ > \phi_{\text{ZMRC}}^- - \phi_{\text{OLC}}^-$ then when the right side of both cones overlap, the left side of OLC is in the interior of ZMRC. Thus, $\text{width}(\text{OLC}) < \text{width}(\text{ZMRC})$,
- (c) if $\phi_{\text{ZMRC}}^+ - \phi_{\text{OLC}}^+ = \phi_{\text{ZMRC}}^- - \phi_{\text{OLC}}^-$ the same angle will produce overlapping of the left and right side simultaneously. Thus, $\text{width}(\text{OLC}) = \text{width}(\text{ZMRC})$.

■

Let $F(s)$ be considered a gain: $\angle F(j\omega^*) = 0$, $\forall \omega^* \in [0, \infty[$. Then, ZMRC will remain fixed and OLC will be rotated by $\angle H(j\omega^*)$. In this case, $\phi_{\text{ZMRC}}^{-(+)} - \phi_{\text{OLC}}^{-(+)}$ correspond to the bounds on $\angle H(j\omega^*)$ which will lead to a solution of the problem.

Corollary 2.1. Let

$$\angle H^+(j\omega) = \phi_{\text{ZMRC}}^+(\omega) - \phi_{\text{OLC}}^+(\omega) \quad (26)$$

$$\angle H^-(j\omega) = \phi_{\text{ZMRC}}^-(\omega) - \phi_{\text{OLC}}^-(\omega) \quad (27)$$

If $F(s)$ is constant then

- (a) if $\forall \omega \in [0, \infty[\angle H^-(j\omega) \leq 0 \leq \angle H^+(j\omega)$ then robust performance can be obtained with $H(s) = K$.
- (b) if $\forall \omega \in [0, \infty[\angle H^+(j\omega) > H^-(j\omega)$, then robust performance can be obtained with a dynamic loop controller. An analysis of $\angle H^+(j\omega)$ and $\angle H^-(j\omega)$ gives us the structure of $H(s)$.

The problem of controller synthesis can be addressed by an iterative process. From $\angle H^-(j\omega)$

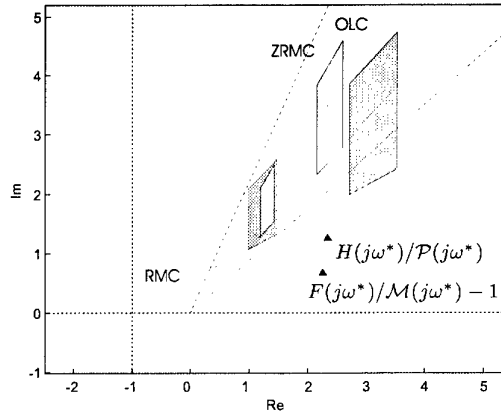


Fig. 8. Proportional controller design for first order systems.

and $\angle H^+(j\omega)$ the poles and zeros of $C(s) = 1/H(s)$ are selected (phase shaping). Then, $F(s)$ and the gain of $H(s)$ are changed until theorem 2.1 holds.

3. EXAMPLES.

3.1 First order

Let the uncertain plant

$$P(s, \tilde{\mathbf{q}}) = \frac{\tilde{K}_p}{1 + \tilde{\tau}_p s} \quad (28)$$

with $\tilde{K}_p = [20, 50]$ and $\tilde{\tau}_p = [10, 40]$. A time constant between 0.1 and 1.5 seconds and a steady state error of 1% is desired. This specification is matched to the reference uncertain model

$$M(s, \tilde{\mathbf{r}}) = \frac{\tilde{K}}{1 + \tilde{\tau} s} \quad (29)$$

with $\tilde{K} = [0.99, 1.01]$ and $\tilde{\tau} = [0.1, 1.5]$. The images of $1/\mathcal{M}(j\omega^*) - 1$ and $1/\mathcal{P}(j\omega^*)$ correspond to polytopes of the form shown in figure 4. These polytopes will move along the cones RMC and OLC, respectively, due to $|F(j\omega^*)|$ and $|H(j\omega^*)|$. If $F(s)$ and $H(s)$ are considered gains (a proportional controller is sought) the orientation of RMC and OLC will remain constant with frequency and the value of their modules must be found so that situation in figure 8 holds for every frequency.

A point $p = x + jy$ belongs to $F(j\omega^*)/\mathcal{M}(j\omega^*) - 1$ if

$$\tau^+ \omega^* x - y \leq -\tau^+ \omega^* \quad x \leq \frac{F(j\omega^*)}{K^-} - 1 \quad (30)$$

$$\tau^- \omega^* x - y \geq -\tau^- \omega^* \quad x \geq \frac{F(j\omega^*)}{K^+} - 1 \quad (31)$$

Making the change of variables $x = \bar{x}$, $y = \omega^* \bar{y}$, dependency with frequency can be avoided simplifying to a great extent the design. A point

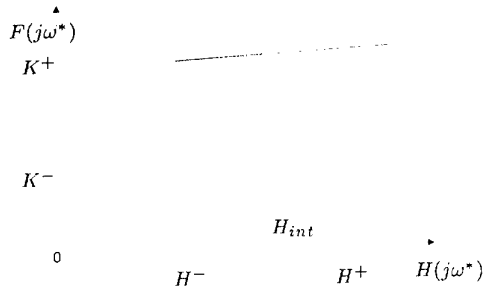


Fig. 9. Solution space.

$p = \bar{x} + j\omega^* \bar{y}$ belongs then to $F(j\omega^*)/\mathcal{M}(j\omega^*) - 1$ if

$$\tau^+ \bar{x} - \bar{y} \leq -\tau^+ \quad \bar{x} \leq \frac{F(j\omega^*)}{K^-} - 1 \quad (32)$$

$$\tau^- \bar{x} - \bar{y} \geq -\tau^- \quad \bar{x} \geq \frac{F(j\omega^*)}{K^+} - 1 \quad (33)$$

Due to convexity of both image sets, condition (14) will hold whenever the four vertices of $H(j\omega^*)/\mathcal{P}(j\omega^*)$ belong to $F(j\omega^*)/\mathcal{M}(j\omega^*) - 1$. This leads to the following equations¹

$$\frac{-\tau^- K_p^+}{\tau^- - \tau_p^+} \leq H(j\omega^*) \leq \frac{-\tau^+ K_p^-}{\tau^+ - \tau_p^+} \quad (34)$$

$$H(j\omega^*) \frac{K^-}{K_p} + K^- \leq F(j\omega^*) \leq H(j\omega^*) \frac{K^+}{K_p} + K^+ \quad (35)$$

Bounds on $F(j\omega^*)$ are affine functions on $H(j\omega^*)$. The maximum value admissible for $F(j\omega^*)$ is that given by

$$H(j\omega^*) = \frac{K_p^- K_p^+ (K^+ - K^-)}{K_p^+ K^- - K_p^- K^+} \stackrel{\text{def}}{=} H_{int}$$

which correspond to the intersection of the bounds in (35). Thus, the pairs $(H(j\omega^*), F(j\omega^*))$ leading to a solution of the problem are given by

$$\begin{aligned} F(j\omega^*) &\in \left[H(j\omega^*) \frac{K^-}{K_p} + K^-, H(j\omega^*) \frac{K^+}{K_p} + K^+ \right] \\ H(j\omega^*) &\in [H^-, \min\{H^+, H_{int}\}] \\ H^- &\stackrel{\text{def}}{=} \frac{-\tau^- K_p^+}{\tau^- - \tau_p^+} \quad H^+ \stackrel{\text{def}}{=} \frac{-\tau^+ K_p^-}{\tau^+ - \tau_p^+} \end{aligned} \quad (36)$$

whenever $H_{int} \geq H^-$ (figure 9).

For the plant (28) and the model reference (29) the solution space is given in figure 10(a). For $H(s) = 0.6826$ ($C(s) = 1/0.6826 = 1.4650$) and $F(s) = 1.0238$ inclusion (14) holds (figure 10(b)). In figure 10(c) a simulation of the closed loop system is shown. As it can be seen, specifications are fulfilled.

¹ $\tilde{K}_p > 0$ has been considered here. Similar expressions are derived for negative gain.

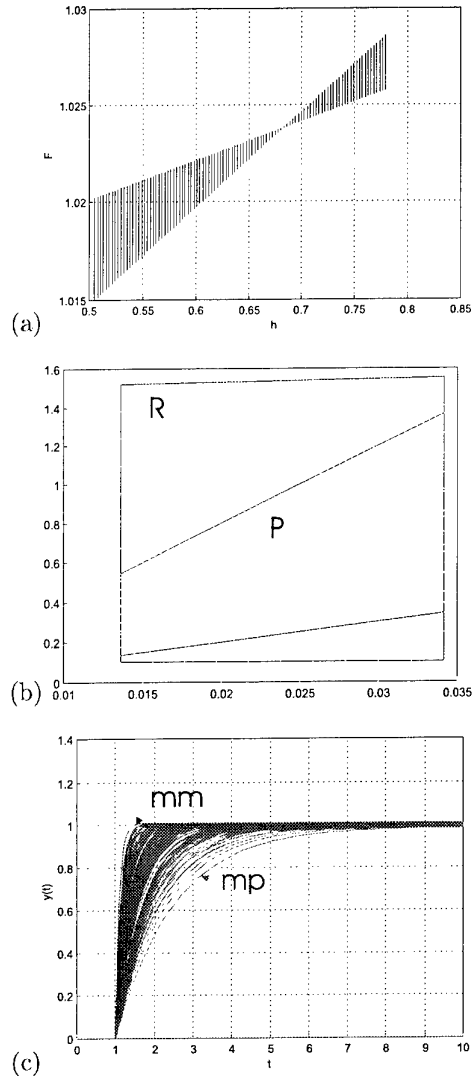


Fig. 10. (a) Solution space for $H(s)$ and $F(s)$ (b) Inclusion of image sets for $\omega^* = 1$ (c) Closed loop response.

3.2 Second order

Let the uncertain plant

$$P(s, \tilde{\mathbf{q}}) = \frac{\tilde{K}_p}{1 + 2\tilde{\xi}_p \frac{s}{\tilde{\omega}_{n,p}} + \left(\frac{s}{\tilde{\omega}_{n,p}}\right)^2} \quad (37)$$

with $\tilde{K}_p = [0.3, 0.5]$, $\tilde{\xi}_p = [0.4, 0.5]$ and $\tilde{\omega}_{n,p} = [1, 1]$ and the reference model

$$M(s, \tilde{\mathbf{r}}) = \frac{\tilde{K}}{1 + 2\tilde{\xi} \frac{s}{\tilde{\omega}_n} + \left(\frac{s}{\tilde{\omega}_n}\right)^2} \quad (38)$$

with $\tilde{K} = [0.99, 1.01]$, $\tilde{\xi} = [0.7, 1]$ and $\tilde{\omega}_n = [10, 15]$.

Considering $F(s) = 1$, bounds on $\angle H(s)$ are obtained applying corollary 2.1. These bounds determine the structure of the controller. For

$$H(s) = \frac{s(1/24s + 1)}{s^2 + 0.9s + 1} \quad (39)$$

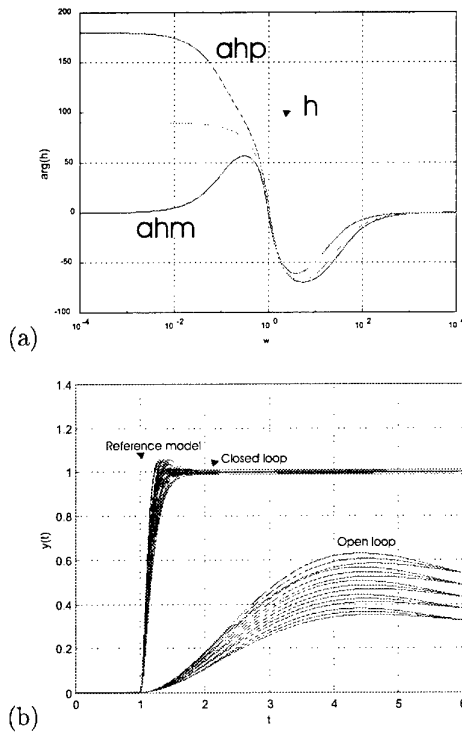


Fig. 11. (a) angle bounds (b) Open loop vs. closed loop response.

the angle bounds hold (figure 11(a)). Sweeping on the frequency, the gain of $H(s)$ must now be found so that theorem 2.1 holds. For a gain of 0.055 specifications are fulfilled (figure 11(b)), although a complete inclusion of the image set does not hold for every frequency (lemma 2.1 is sufficient, but not necessary). The resulting controllers are

$$F(s) = 1 \quad (40)$$

$$C(s) = \frac{18.1818(s^2 + 0.9s + 1)}{s(1/24s + 1)} \quad (41)$$

4. CONCLUSIONS.

A new geometric approach for the robust performance problem for interval systems has been introduced. It arises from the observation that inclusion of a system in a family of Bode diagrams implies inclusion on the respective family of step responses. On the contrary to current approaches which deal with frequency domain specifications, this new approach allows to deal directly with classical time domain specifications, such as overshoot, settling time and steady state error by means of an uncertain reference model. The remarkable results obtained in the examples presented here motivate a further study on the methodology. A deeper study must still be done concerning lemma 2.1.

5. REFERENCES

- Ackermann, J. (1993). *Robust Control. Systems with Uncertain Physical Parameters*. Springer-Verlag.
- Barmish, B. R. (1994). *New Tools for Robustness of Linear Systems*. Macmillan Publishing Company.
- Bhattacharyya, S.P., H. Chapellat and L.H. Keel (1995). *Robust Control. The Parametric Approach*. Prentice Hall.
- Bondia, J. and J. Picó (2001). Application of functional intervals to the stability analysis of fuzzy linear systems. *Proceedings of the Joint 9th IFSA World Congress and 20th NAFIPS International Conference, Vancouver, Canada*.
- Zhou, K. (1998). *Essentials of Robust Control*. Prentice Hall.

DIGITAL IMPLEMENTATION OF CONTROLLERS

Eduard Eitelberg

NOY Business, 58 Baines Road, Durban 4001, South Africa
e-mail: controle@pixie.udw.ac.za

Abstract: A competent quantitative feedback control system design must not ignore the effects of digital implementation of the designed analog controller. Two of the most important and significantly quantifiable effects are: the **loop effect** that reduces stability margins; and the **signal effect** that refers to both, aliasing at the ADC and reverse aliasing at the DAC. The often observed huge sensitivity to control algorithm evaluation accuracy is not a control system design issue — it need not arise if the controller is implemented in the form of a **velocity algorithm**.

Keywords: *digital control, loop effect, signal effect, velocity algorithms.*

1. PROBLEM STATEMENT

All real systems ($P_s(s)$ in Figure 1) and most of their (engineering) performance specifications are in continuous-time. Hence, it is most natural to carry out the control system design in continuous-time. However, it must yield all relevant data for the digital control system implementation as well — including the sampling parameters. The effect of sampling (if any) must be visible in the continuous-time design.

On the other hand, generally and unfortunately, there can be no one-to-one correspondence between a continuous-time design and its (partial) discrete-time implementation. The control engineer must learn to live with a certain amount of ambiguity.

The following philosophy is followed in the recently published book “Control Engineering Course Notes” by Ed. Eitelberg (2000).

Approximate the designed continuous-time **controller** by using, for example, one of the suitable simulation methods. Simulation methods, in general, yield sufficiently good approximation at 'low frequency' where the performance is specified. Then analyse the stability of the resulting closed loop system. This can be done by transforming the **whole sampled control loop** into a form where the stability is determined on the imaginary axis. This process is significantly simplified and can lead to very useful design procedures when the last transform is the inverse of the above controller approximation (simulation) method.

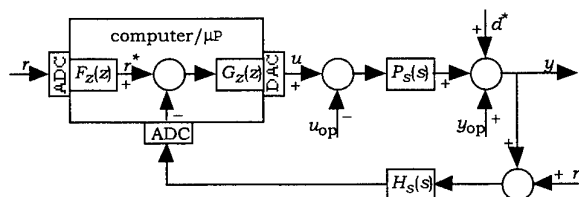


Figure 1: Simple SISO feedback system with digital controller. $H(s)$ may contain an anti-alias filter.

This basic philosophy is illustrated schematically in Figure 2. The implicit and (especially) the explicit Euler methods, with the step-size of T , would be very simple to use for the controller approximation stage. Indeed, much attention has been given to the explicit Euler method ($s = (z - 1)/T$) by Middleton and Goodwin (1990), who use

the corresponding inverse transformation $z = 1 + wT$ in Figure 2. They actually use ' δ ' instead of ' w ', but the method is the same. Both of these Euler methods lead to the system stability boundary approaching the imaginary axis only for (very) small T relative to *all* system time-constants. Therefore, neither of these two methods can be generally recommended for quantitative control system design, as the stability cannot be judged along the w -plane imaginary axis. Nevertheless, explicit or implicit Euler methods can be used for the controller approximation in many cases — even though they are not good enough for stability analysis.

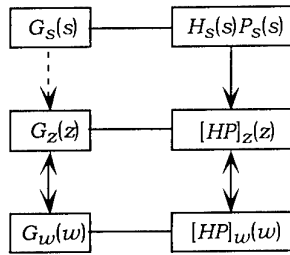


Figure 2: Philosophy of control system design with digital equipment in the loop. Dashed arrow indicates approximation and solid arrows indicate exact correspondence. (Here: $G_w(w) = G_s(w)$, $w = (2/T)(z-1)/(z+1)$ and $1/T$ is the sampling rate.)

The simplest rational transformation into the w -plane with the stability boundary on the imaginary axis is based on the trapezoidal rule — the **T-transform**:

$$z = \frac{1 + wT/2}{1 - wT/2} \Leftrightarrow w = \frac{2}{T} \frac{z-1}{z+1} \quad (1)$$

2. SAMPLING EFFECT ON CONTROL SYSTEMS

We follow the philosophy of Figure 2 and assume that some continuous-time controller transfer functions $F_s(s)$ and $G_s(s)$ have been designed, yielding the loop transfer function

$$L_s(s) = G_s(s)H_s(s)P_s(s) \quad (2)$$

The 'simulation/approximation' controller algorithms are obtained as

$$G_z(z) = G_s\left(\frac{2}{T} \frac{z-1}{z+1}\right); F_z(z) = F_s\left(\frac{2}{T} \frac{z-1}{z+1}\right) \quad (3)$$

For the pre-filter $F_s(s)$ other approximations can be used without any effect on the following analysis of the feedback loop performance.

Now the inverse T-transform is used, yielding

$$G_w(w) = G_s(w) \quad (4)$$

and

$$[HP]_w(w) = [HP]_z\left(\frac{1 + wT/2}{1 - wT/2}\right) \quad (5)$$

with

$$\begin{aligned} L_w(w) &= G_w(w)[HP]_w(w) \\ &= G_s(w)[HP]_w(w) \end{aligned} \quad (6)$$

The first term $G_s(w)$ of $L_w(w)$ is formally equal to the first term $G_s(s)$ of $L_s(s)$ when we set $w = s$. It would be useful for the continuous-time design if, similarly, we could somehow relate the entire loop transfer function $L_w(w)$ to $L_s(s)$. There is indeed a very useful approximate relationship which was originally derived by Eitelberg (1988), see also (Eitelberg, 2000).

We assume that $H_s(s)P_s(s)$ is composed of a strictly proper rational part $[HP]_s(s)$ and a dead-time term e^{-sT_d} as

$$H_s(s)P_s(s) = [HP]_s(s)e^{-sT_d} \quad (7)$$

Under some realistic conditions (see Eitelberg, 2000) we obtain

$$\begin{aligned} [HP]_w(w) &\approx [HP]_s(w) \left(1 + w \frac{2\Delta - T}{2}\right) \left(\frac{1 - wT/2}{1 + wT/2}\right)^k \\ k &= \text{ceil}(T_d/T) \quad \Delta = kT - T_d \end{aligned} \quad (8)$$

It is convenient to define $T_d = kT - \Delta$ ($0 \leq \Delta < T$) as the loop dead-time which includes any delays caused by the digital equipment.

Even when the continuous-time system has no dead-time or non-minimum phase-lag zeros, the digital equipment in the loop

always introduces the *non-minimum phase-lag* term $(1 - \omega T/2)$ into the feedback loop $L_w(\omega)$. For $\Delta \neq 0$, the zero of $(1 + \omega(2\Delta - T)/2)$ is further from the complex plane origin than the zeros of the all-pass term that result from the analog dead-time or digital implementation delays. Hence, for any Δ , **the dominant non-minimum phase-lag term is always $(1 - \omega T/2)$** . Because of the multiplicity of these non-minimum phase-lag zeros, the *loop gain cross-over frequency* can be limited to much less than the $1/T$ from a single right half-plane zero.

A control system designer must not ignore the effect of digital equipment on analog signals — aliasing by the analog to digital converter (ADC) and reverse aliasing by the digital to analog converter (DAC) — as distinct from the above described loop effect. The corresponding expertise is assumed for the purpose of this presentation.

3. CONTROLLER DESIGN PROCEDURE WITH '1-sT/2'

The previous section characterised the sampling effect in the ω -domain. Strictly speaking, a design specification should be translated from the s -, or ω -domain to the ω -domain as well, before a controller design can be executed. However, it can be suggested that there is no practical control engineering need for the proliferation of complex domains: s , z , ω , δ , and who knows what else. In particular, replace the variable ω in eq. (8) with s . That means, formally,

$$[HP]_w(s) \approx [HP]_s(s) \left(1 + s \frac{2\Delta - T}{2} \right) \left(\frac{1 - sT/2}{1 + sT/2} \right)^k \quad (9)$$

Since $G_w(s) = G_s(s)$, we can design in the s -domain by using '1-sT/2' with appropriate multiplicity (alone and in the all-pass term of eq. (9)) as the only (dominant) effect of the digital equipment in the loop — the '**loop effect**'. It is true, that the frequency values around $2\pi/T$ and above lose some of their usual meaning (they cannot get through the digital equipment without being aliased into the Nyquist frequency band), but this is beyond the loop gain cross-over where only the stability margins

are specified (the Nyquist stability criterion remains valid). Furthermore, this approach makes it easier to simultaneously visualise the '**signal effects**' — aliasing and reverse aliasing in the feedback loop — in Figure 3.

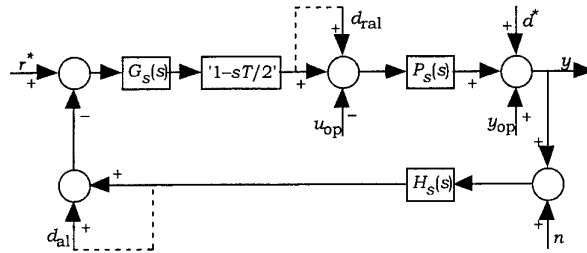


Figure 3: Loop and signal effects of digital control equipment. '1-sT/2' indicates the dominant 'loop effect'. Dashed lines indicate non-linear formation of effective low-frequency aliased disturbance d_{al} in the ADC and high-frequency reverse-aliased disturbance d_{ral} in the DAC.

This design philosophy is demonstrated with the following simple example.

Example 1: Digital controller in the loop.

Let the plant, performance, and stability specifications be given as

$$P_s(s) = \frac{1 + s/10}{s(1 + s/0.1)}, \quad H_s(s) = 1 \quad (10)$$

$$|S(j\omega)| = \left| \frac{1}{1 + L(j\omega)} \right| \leq \frac{1}{100} = -40 \text{ dB}, \quad (11)$$

$$\omega \leq 0.03$$

$$|S(j\omega)| = \left| \frac{1}{1 + L(j\omega)} \right| < 3 \text{ dB}, \quad \forall \omega \quad (12)$$

Due to considerations of computing time, only first-order difference equations are allowed as control algorithms and it takes one sampling interval to evaluate the algorithm. Figure 4 shows the plant frequency response $P_s(j\omega)$ on the sensitivity chart background. A loop $L_s(j\omega) = P_s(j\omega)G_s(j\omega)$ is (over-) designed so that it satisfies the low frequency specification in eq. (11) and leaves phase reserve for the stability margin in eq. (12):

$$G_s(s) = 3 \frac{1 + s/0.3}{1 + s/7} \quad (13)$$

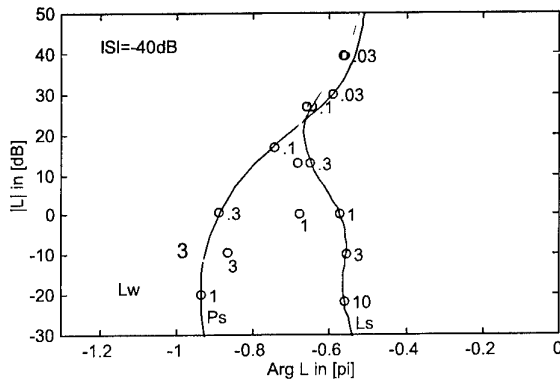


Figure 4: Feedback loop design. Ls indicates continuous design and Lw indicates digital implementation.

With this phase reserve, a lower sampling rate can be tolerated than with a smaller phase reserve. In this example, because of the algorithm evaluation delay (dead-time) of T , the loop effect is $(1-sT/2)^2/(1+sT/2)$. This would limit the loop gain cross-over frequency to about $0.5/T$, when 0.2π phase margin is allowed (cf. Eitelberg, 2000). Equation (12) is equivalent to at least 0.25π phase margin and leads to a lower gain cross-over frequency limit. The corresponding $L_w(j\omega) = P_s(j\omega)G_s(j\omega) (1-j\omega T/2)^2/(1+j\omega T/2)$ is shown in Figure 4 with the lowest possible sampling rate

$$1/T = 4.5 \quad (14)$$

The control algorithm is found from eq. (13) by substituting $s = (2/T)(z-1)/(z+1)$. The discrete-time transfer function is

$$G_z(z) = \frac{\frac{21T+140}{7T+2} z + \frac{21T-140}{7T+2}}{z + \frac{7T-2}{7T+2}} \quad (15)$$

The corresponding algorithm is

$$\begin{aligned} u_i^* &= \frac{7T-2}{7T+2} u_{i-1}^* + \frac{21T+140}{7T+2} e_i + \frac{21T-140}{7T+2} e_{i-1} \\ &= 0.125 u_{i-1}^* + 40.69 e_i - 38.06 e_{i-1} \end{aligned} \quad (16)$$

u_i^* denotes the computer internal sequence of the control values. Due to the mentioned delay, the physical computer output (plant input) is defined by

$$u_i = u_{i-1}^* = 0.125 u_{i-1}^* + 40.69 e_{i-1} - 38.06 e_{i-2} \quad (17)$$

Nevertheless, eq. (16) is programmed in the computer and not eq. (17). This example with PAM-DAC (pulse amplitude modulated digital to analog converter) was originally implemented with analog and digital electronic components, see (Eitelberg, 1988). A Simulink implementation is shown in Figure 5. Input limits had to be included so that a (fair) comparison with a PWM-DAC (pulse width modulated digital to analog converter) implementation is possible.

Figure 6 shows the system's ability to reduce sinusoidal output disturbances and to alias high frequency noise. Notice, that only frequencies above $2\pi f_s/2 = \pi/T = 14.137 \text{ rad/[time-unit]}$ — far beyond the loop gain and phase cross-over frequencies — will be aliased. The aliased frequency in d_{al} is $2\pi/T - 28.244 = 0.03 \text{ rad/[time-unit]}$ for the dashed line and $2\pi/T - 28.24 = 0.034 \text{ rad/[time-unit]}$ for the dash-dotted line. d_{al} amplitude is transferred to the output without change because $|L/(1+L)| = 1$ at these frequencies. In real systems, one is very unlikely to see such clean sinusoidal aliasing.

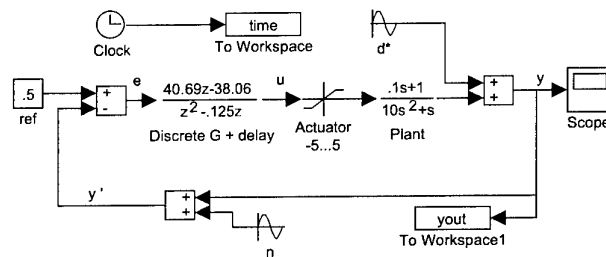


Figure 5: Simulink block diagram with PAM-DAC (Pulse Amplitude Modulated Digital to Analog Converter).

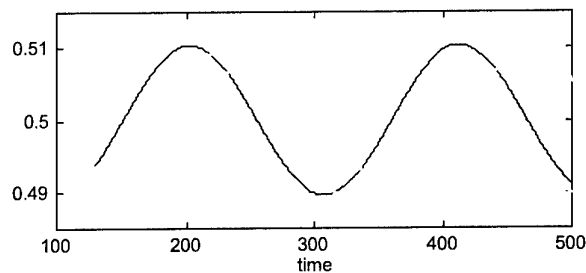


Figure 6: Disturbance rejection with PAM-DAC. Solid line shows the y response to $d^* = \sin(0.03t)$ with $n = 0$. The dashed and dash-dotted lines show the y responses to a 100 times smaller sensor noise, $n = 0.01 \sin(28.244t)$ and $n = 0.01 \sin(28.24t)$ respectively while $d^* = 0$.

The PWM-DAC (Pulse Width Modulated Digital to Analog Converter) Simulink implementation is shown in Figure 7 and Figure 8 shows this system's ability to reduce sinusoidal output disturbances and to alias high frequency noise.

Figure 8 illustrates the role of the signal d_{ral} in Figure 3 — the dominant conversion frequency of 4.5 Hz is clearly visible. In this example, no anti-alias filters are implemented. This causes a slight problem, because the PWM-generated reverse-aliased frequencies in d_{ral} are aliased back into the system bandwidth via d_{al} and the result is sensitive to the relative offset between ADC and DAC. In particular, the conversion frequency f_h (and its harmonics) alias precisely into a constant bias — this is clearly visible in Figure 8. This can happen with PAM-DAC only if the converted signal is held for lesser duration than the conversion interval.

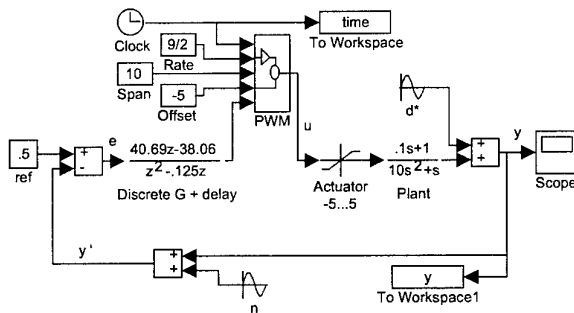


Figure 7: Simulink block diagram with PWM-DAC. The block PWM evaluates $(u[3]*\text{rem}(u[1]*u[2],1) < (u[5]-u[4]))*u[3]+u[4]$.

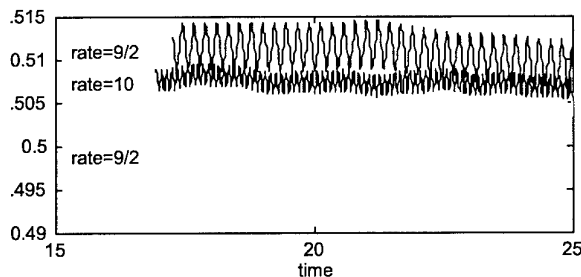


Figure 8: Disturbance rejection with PWM-DAC. Solid lines show the y response to $d^* = \sin(0.03t)$ with $n = 0$. Dashed line shows the y response to $n = 0.01 \sin(25.3t)$ while $d^* = 0$. The sampling rate is $9/2$, but the PWM rate is varied as indicated in the figure.

Figure 4 indicates a theoretical gain margin of about 12 dB = 4 and a limit cycling frequency of about 4 rad/[time-unit]. This is confirmed experimentally for both, PAM and PWM, implementations.

This example can be made more practical with an anti-alias filter $1/(1+sT/2)$. The digital equipment together with this simplest of filters yields a modified equivalent $(1-sT/2)^2/(1+sT/2)^2$. The improvement in high frequency noise transfer properties, especially with the PWM implementation, would be significant. There is an additional way to reduce the PWM-induced reverse aliased d_{ral} . In Figure 7, the PWM rate can be set independently of the sampling frequency in the block 'Discrete G + delay'. For example, Figure 8 illustrates the effect of changing 9/2 to 10 in the block 'Rate'.

End of Example 1.

For plant modes and disturbances above the sampling rate, additional filtering may be necessary — see (Eitelberg and Boje, 1991) or (Eitelberg, 2000) for some suitable design procedures.

4. IMPLEMENTATION WITH VELOCITY ALGORITHMS

Direct implementations of the control algorithms tend to calculate very small differences between large numbers. This is only mildly visible in eq. (17) because of the slow sampling rate relative to the controller corner frequencies. These numerical problems are strongly compounded in direct implementations of high order control algorithms. One of the remedies can be an implementation of the algorithm in the FSR form (incorrectly called FIR). However, this tends to require summing very many small numbers.

Here, the often recommended remedy of splitting the discrete transfer function (and the corresponding algorithm) into series- or parallel-connected sections of maximum second order is followed (Phillips and Nagle, 1984; Middleton and Goodwin, 1990). Consider the second order controller section:

$$G_s(s) = \frac{U(s)}{E(s)} = \frac{b_0 s^2 + b_1 s + b_2}{s^2 + a_1 s + a_2} \quad (18)$$

The algorithm is defined by $G_z(z) = G_s((z/T)(z-1)/(z+1))$ and can be written as

$$G_z(z) = \frac{b_{z0} z^2 + b_{z1} z + b_{z2}}{z^2 + a_{z1} z + a_{z2}} \quad (19)$$

Assume now, that the a_{zi} and b_{zi} are implemented with some small errors Δa_{zi} and Δb_{zi} . These implemented $\hat{a}_{zi} = a_{zi} + \Delta a_{zi}$ and $\hat{b}_{zi} = b_{zi} + \Delta b_{zi}$ correspond to a different continuous-time controller

$$\hat{G}_s(s) = \frac{\hat{b}_0 s^2 + \hat{b}_1 s + \hat{b}_2}{s^2 + \hat{a}_1 s + \hat{a}_2} \quad (20)$$

The continuous-time coefficients relate to the discrete-time implementation errors as

$$\begin{aligned} \hat{b}_0 &\approx b_0 + \Delta b_{z0} - \Delta b_{z1} + \Delta b_{z2}, \\ \hat{b}_1 &\approx b_1 + \frac{\Delta b_{z0} - \Delta b_{z2}}{T}, \\ \hat{b}_2 &\approx b_2 + \frac{\Delta b_{z0} + \Delta b_{z1} + \Delta b_{z2}}{T^2}, \\ \hat{a}_1 &\approx a_1 - \frac{\Delta a_{z2}}{T}, \\ \hat{a}_2 &\approx a_2 + \frac{\Delta a_{z1} + \Delta a_{z2}}{T^2} \end{aligned} \quad (21)$$

See (Eitelberg, 2000) for the derivation of eq. (21). Clearly, small T leads to extreme sensitivity in the actually implemented control system — even for very small implementation errors of the algorithm coefficients. Consider, for example, the coefficient a_2 which is equal to the square of a second order controller denominator corner frequency. For example, if the sampling rate is 100 times the corner frequency then $a_2 T^2 = 10^{-4}$. Let the 'other' denominator coefficient a_{z1} ($a_{z1} \rightarrow -2$ for small T) be implemented with a 12-bit mantissa, then the 0.5LSB round-off error of a_{z1} is a clearly very small $2^{-12} = 0.00024$ (0.012% of $|a_{z1}| = 2$) — but the relative error of a_2 due to Δa_{z1} is $0.00024/10^{-4} = 2.4$ (240% of a_2)!

Now, never mind how exact the implemented algorithm coefficients a_{zi} and

b_{zi} are, we still have the problem of working with very small differences of large numbers in the direct implementation of even first order algorithms. This phenomenon is somewhat easier to analyse in any of the equivalent (canonical) state-space formats, some of which are recommended for digital filter implementation (Phillips and Nagle, 1984). Any rational proper SISO controller transfer function (such as in eq. (18)) can be modelled in the time-domain by state equations

$$\begin{aligned} \dot{\mathbf{x}} &= \mathbf{A}\mathbf{x} + \mathbf{B}e \\ u &= \mathbf{C}\mathbf{x} + b_0 e \end{aligned} \quad (22)$$

Application of the Laplace, T-, and inverse z-transforms yields directly an explicit (state space) controller implementation algorithm

$$\begin{aligned} \mathbf{x}_i &= \left[\mathbf{I} - \frac{T}{2} \mathbf{A} \right]^{-1} \left\{ \left[\mathbf{I} + \frac{T}{2} \mathbf{A} \right] \mathbf{x}_{i-1} + T\mathbf{B} \frac{e_i + e_{i-1}}{2} \right\} \\ u_i &= \mathbf{C}\mathbf{x}_i + b_0 e_i \end{aligned} \quad (23)$$

For small T , the recursion equation for \mathbf{x}_i has the same coefficient precision problem as the above analysed direct implementation. However, here it is easy to modify the algorithm by first evaluating the state increment and then adding this increment to \mathbf{x}_{i-1} . Add and subtract \mathbf{x}_{i-1} from the right-hand side of the difference equation in eq. (23). After simplification, the algorithm is now evaluated in the numerically well-conditioned sequence

$$\begin{aligned} \Delta \mathbf{x}_i &= T \left[\mathbf{I} - \frac{T}{2} \mathbf{A} \right]^{-1} \left\{ \mathbf{A}\mathbf{x}_{i-1} + \mathbf{B} \frac{e_i + e_{i-1}}{2} \right\} \\ \mathbf{x}_i &= \mathbf{x}_{i-1} + \Delta \mathbf{x}_i \\ u_i &= \mathbf{C}\mathbf{x}_i + b_0 e_i \end{aligned} \quad (24)$$

There is one slightly arguable problem with this algorithm — $\Delta \mathbf{x}_i$ can only be evaluated *after* the ADC releases the new measured e_i . In order to avoid this, a linearly transformed state vector \mathbf{v}_i is introduced with yet to be defined transformation matrices \mathbf{M} and \mathbf{N} so that $\mathbf{x}_i = \mathbf{M}\mathbf{v}_i + \mathbf{N}e_i$. Two specific choices that were derived by Eitelberg (2000) yield

$$\begin{aligned}\Delta \mathbf{v}_i &= T \left[\mathbf{I} - \frac{T}{2} \mathbf{A} \right]^{-1} \left\{ \mathbf{A} \mathbf{v}_{i-1} + \left[\mathbf{I} - \frac{T}{2} \mathbf{A} \right]^{-1} \mathbf{B} e_{i-1} \right\} \\ \mathbf{v}_i &= \mathbf{v}_{i-1} + \Delta \mathbf{v}_i \\ u_{vi} &= \mathbf{C} \mathbf{v}_i \\ u_i &= u_{vi} + G_s \left(\frac{2}{T} \right) e_i\end{aligned}\quad (25)$$

or

$$\begin{aligned}\Delta \mathbf{v}_i &= T \left[\mathbf{I} - \frac{T}{2} \mathbf{A} \right]^{-1} \left\{ \mathbf{A} \mathbf{v}_{i-1} + \mathbf{B} e_{i-1} \right\} \\ \mathbf{v}_i &= \mathbf{v}_{i-1} + \Delta \mathbf{v}_i \\ u_{vi} &= \mathbf{C} \left[\mathbf{I} - \frac{T}{2} \mathbf{A} \right]^{-1} \mathbf{v}_i \\ u_i &= u_{vi} + G_s \left(\frac{2}{T} \right) e_i\end{aligned}\quad (26)$$

Both algorithms can be called the (generalised) **velocity algorithms**, because the increment $\Delta \mathbf{v}_i$ is exactly, or approximately, a scaled rate of the continuous-time controller state \mathbf{v} at t_{i-1} . This is most clearly visible in eq. (26), where $\mathbf{A} \mathbf{v}_{i-1} + \mathbf{B} e_{i-1} = \dot{\mathbf{v}}_{i-1}$. In both algorithms, the first three equations can be evaluated in the given order *before* the new measurement e_i is available. After the ADC releases this e_i , only a single multiplication with $G_s(2/T)$ and a single addition to u_{vi} need to be carried out in the last equation of the algorithm, before u_i can be passed on to the DAC of the controller. Thus, the computation delay can be practically eliminated — depending on the operation of the entire control software.

It is an additional advantage of velocity algorithms in general, that $\Delta \mathbf{v}_i$ can be accumulated separately over many time-steps, if necessary. Thus, at every step, the greatest possible portion of the accumulated increment can be transferred to (the finite precision mantissa of) \mathbf{v}_i and the remainder is retained in the increment accumulator without any loss of precision. This trick is even more crucial in the (generally cheaper or faster) *fixed-point* controller implementations.

For a second order controller section in eq. (18), eq. (25) can be written explicitly as (Eitelberg, 2000)

$$\begin{aligned}\Delta v_{1,i} &= a_{\Delta 11} v_{1,i-1} + a_{\Delta 12} v_{2,i-1} + b_{\Delta 1} e_{i-1} \\ \Delta v_{2,i} &= a_{\Delta 21} v_{1,i-1} + a_{\Delta 22} v_{2,i-1} + b_{\Delta 2} e_{i-1} \\ v_{1,i} &= v_{1,i-1} + \Delta v_{1,i} \\ v_{2,i} &= v_{2,i-1} + \Delta v_{2,i} \\ u_i &= v_{1,i} + G_s(2/T) e_i\end{aligned}\quad (27)$$

where

$$\begin{aligned}D^*(2/T) &= 1 + a_1(T/2) + a_2(T/2)^2 \\ a_{\Delta 11} &= \frac{-T(a_1 + a_2(T/2))}{D^*(2/T)}; \quad a_{\Delta 12} = \frac{T}{D^*(2/T)} \\ a_{\Delta 21} &= \frac{-Ta_2}{D^*(2/T)}; \quad a_{\Delta 22} = \frac{-Ta_2(T/2)}{D^*(2/T)} \\ b_{\Delta 1} &= \frac{T[(b_1 - b_0 a_1) + (b_2 - b_0 a_2)T + (a_1 b_2 - a_2 b_1)(T/2)^2]}{[D^*(2/T)]^2} \\ b_{\Delta 2} &= \frac{T}{[D^*(2/T)]^2} [(b_2 - b_0 a_2) + (a_1 b_2 - a_2 b_1)T \\ &\quad + ((a_1^2 - a_2)(b_2 - b_0 a_2) - a_1 a_2(b_1 - b_0 a_1))(T/2)^2] \\ G_s(2/T) &= \frac{b_0 + b_1(T/2) + b_2(T/2)^2}{D^*(2/T)}\end{aligned}\quad (28)$$

Equation (26) can be written in a very similar form.

The following example demonstrates the implementation of the above ideas for a not particularly simple controller.

Example 2: Series connection of controller terms.

In (Eitelberg, 2000), a marine stabilisation system design is reported. The following controller transfer function was derived:

$$\begin{aligned}G_s(s) &= \frac{\left(1 + \frac{6.25}{s}\right) \left(1 + \frac{s}{10}\right)}{\left(1 + 1.2 \frac{s}{50} + \left(\frac{s}{50}\right)^2\right) \left(1 + \frac{s}{300}\right)} \\ &\quad \times \frac{\left(1 + 0.2 \frac{s}{17} + \left(\frac{s}{17}\right)^2\right)}{\left(1 + 1.4 \frac{s}{17} + \left(\frac{s}{17}\right)^2\right)}\end{aligned}\quad (29)$$

One can utilise $1/(1 + s/300)$ as the analog anti-alias filter. The rest of G_s can be split into two second order sections and the first order PI section:

$$G_{s1}(s) = \frac{1 + \frac{s}{10}}{1 + 1.2 \frac{s}{50} + \left(\frac{s}{50}\right)^2};$$

$$G_{snotch}(s) = \frac{1 + 0.2 \frac{s}{17} + \left(\frac{s}{17}\right)^2}{1 + 1.4 \frac{s}{17} + \left(\frac{s}{17}\right)^2}; \quad (30)$$

$$G_{sPI}(s) = \left(1 + \frac{6.25}{s}\right)$$

The corresponding digital implementation can be represented in a block diagram form as in Figure 10.

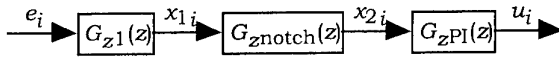


Figure 10: Digital controller implementation in series form.

The transfer functions G_{z1} , G_{znotch} , and G_{zPI} in Figure 10 represent the equivalent velocity algorithms. Since $1/(1 + s/300)$ is now the highest frequency component of the analog part of the feedback loop, a suitable sampling rate would be about 300 samples/second. Let us choose $T = 2$ ms, on the safe side. Eitelberg (2000) has shown that 10 ms would be possible. Nevertheless, here the algorithm's ability to perform sufficiently accurately with a 'very high' sampling rate of 500 samples-per-second is demonstrated.

The low-passing block G_{z1} is obtained from $G_{s1}(s) = (250s + 2500) / (s^2 + 60s + 2500)$.

Therefore, $b_0 = 0$, $b_1 = 250$, $b_2 = 2500$ and $a_1 = 60$, $a_2 = 2500$. Using $T/2 = 0.001$ in eq. (28) yields $D^* = 1.0625$ and hence,

$$a_{\Delta 11} = -0.11765; \quad a_{\Delta 12} = 0.0018824$$

$$a_{\Delta 21} = -4.7059; \quad a_{\Delta 22} = -0.0047059$$

$$b_{\Delta 1} = 0.45092$$

$$b_{\Delta 2} = 2.68446 \quad (31)$$

$$G_s(2/T) = 0.23765$$

The algorithm can be written with an 'outrageous' 1-digit coefficient precision as

$$u_{1,i} = v_{1,i-1} - 0.1v_{1,i-1} + 0.002v_{2,i-1} + 0.5e_{i-1}$$

$$v_{2,i} = v_{2,i-1} - 5v_{1,i-1} - 0.005v_{2,i-1} + 3e_{i-1} \quad (32)$$

$$x_{1,i} = v_{1,i} + 0.2e_i$$

The notch-filter block G_{znotch} is obtained from $G_{snotch} = (s^2 + 3.4s + 289) / (s^2 + 23.8s + 289)$. Therefore, $b_0 = 1$, $b_1 = 3.4$, $b_2 = 289$ and $a_1 = 23.8$, $a_2 = 289$. Using $T/2 = 0.001$ in eq. (28) yields $D^* = 1.024089$ and hence,

$$a_{\Delta 11} = -0.047045; \quad a_{\Delta 12} = 0.0019530$$

$$a_{\Delta 21} = -0.56441; \quad a_{\Delta 22} = -0.00056441$$

$$b_{\Delta 1} = -0.038892$$

$$b_{\Delta 2} = 0.022754 \quad (33)$$

$$G_s(2/T) = 0.98008$$

The algorithm can be written with an 'outrageous' 1-digit coefficient precision as

$$v_{3,i} = v_{3,i-1} - 0.05v_{3,i-1} + 0.002v_{4,i-1} - 0.04x_{1,i-1}$$

$$v_{4,i} = v_{4,i-1} - 0.6v_{3,i-1} - 0.0006v_{4,i-1} + 0.02x_{1,i-1}$$

$$x_{2,i} = v_{3,i} + x_{1,i} \quad (34)$$

Notice that the states v_3 and v_4 are allocated to G_{znotch} , since v_1 and v_2 are already in use for G_{z1} . The PI controller block G_{zPI} can be obtained from $G_{sPI}(s) = (1 + 6.25/s)$ by setting $a_1 = a_2 = b_2 = 0$ in eq. (28), but here a direct route is taken. Application of the inverse T-transform yields

$$\frac{U}{X_2} = G_{zPI}(z) = \left(1 + \frac{6.25}{T} \frac{z-1}{z+1}\right) = \left(1 + 0.00625 \frac{z+1}{z-1}\right) \quad (35)$$

It is convenient to use the following trick. Substitute $(z+1)/(z-1) = 1 + 2/(z-1)$ into eq. (35) and solve for the controller output U :

$$U = \left(1.00625 X_2 + \frac{0.0125}{z-1} X_2\right) \quad (36)$$

Introduce the new variable $V_5 = [0.0125/(z-1)]X_2$ into eq. (36). Then

$$zV_5 = V_5 + 0.0125 X_2$$

$$U = (1.00625 X_2 + V_5) \quad (37)$$

Inverse z -transform yields (with an 'outrageous' 1-digit precision)

$$\begin{aligned} v_{5,i} &= v_{5,i-1} + 0.01(x_{2,i-1}) \\ u_i &= v_{5,i} + x_{2,i} \end{aligned} \quad (38)$$

In Chapter VII of (Eitelberg, 2000), some equivalent but much more practical PI controller implementations with reset wind-up protection are derived. This is not shown here.

Notice that the individual section outputs x_1 and x_2 are not needed outside the controller. Yet their values have to be stored for the evaluation of the follow-on algorithms and the overall controller output u . All three sections can be combined into one fifth-order algorithm by eliminating these 'unnecessary' variables x_1 and x_2 — see (Eitelberg, 2000).

The above velocity algorithm is implemented in the Simulink diagram in Figure 11. The controller sections are implemented individually — for physical clarity and for relative ease of 'debugging' (or delousing?).

The individual controller sections are implemented with the Simulink blocks as is shown in Figure 12. The step responses of these digital filters are compared individually and collectively to their continuous-time counterparts — this leads quickly to finding the almost inevitable errors. A few typing errors in the preceding equations were found this way. After all small differences are plausibly explainable with the digital implementation effects or with the used numerical precision, these controller blocks are inserted in the (continuous-time) feedback loop of Figure 11.

Incidentally, during this debugging activity, one can try setting small coefficients to 0, or 1, and thus optimise the number of arithmetic operations. The debugging is very much more difficult in the combined controller implementation. In the experience of the author, the principle of 'divide-and-conquer' is extremely useful in software development and in many other activities. Many 'modern' control methods may be aesthetically pleasing but make 'dividing and conquering' difficult.

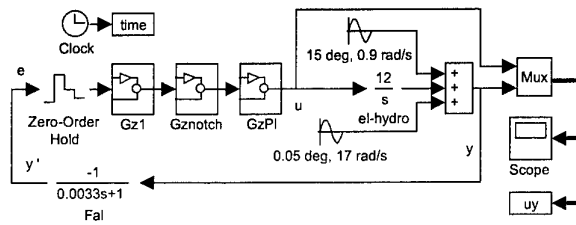


Figure 11: Control system with velocity algorithm in series form.

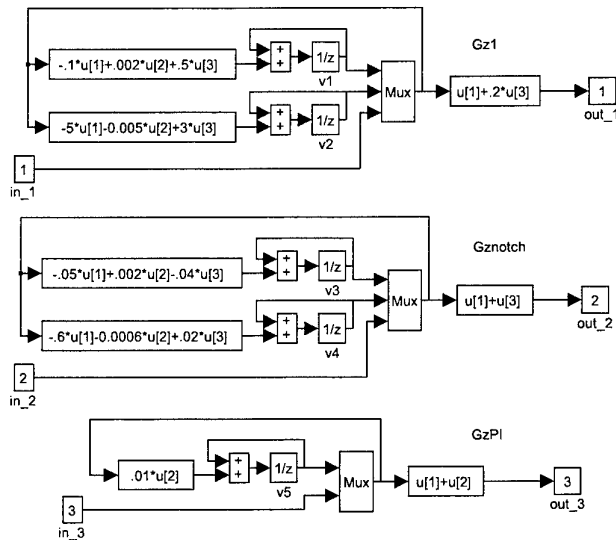


Figure 12: Simulink implementation of the individual controller sections.

Figure 13 indicates achievement of performance that was originally specified in section IV-6.2 of (Eitelberg, 2000), despite only single-digit coefficient precision in this case.

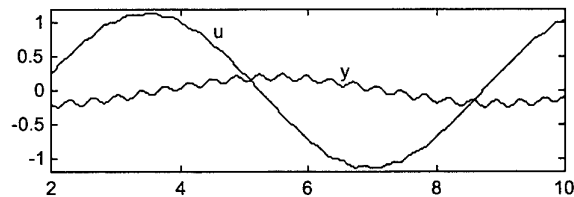


Figure 13: Performance of the feedback loop of Figure 11 with 1-digit coefficient precision in the velocity algorithm. The 17 rad/s vibration transfer to the actuator (from y to u) is significantly reduced by the notch filter.

To prove the advantage of the above velocity algorithms, the identically sectioned direct (position) algorithms are calculated as follows.

$$G_{z1}(z) = G_{sl} \left(\frac{2}{T} \frac{z-1}{z+1} \right) = \frac{0.238z^2 + 0.00471z - 0.233}{z^2 - 1.88z + 0.887} \quad (39)$$

$$G_{znotch}(z) = G_{snotch} \left(\frac{2}{T} \frac{z-1}{z+1} \right) = \frac{0.980z^2 - 1.95z + 0.973}{z^2 - 1.95z + 0.954} \quad (40)$$

$$G_{zPI}(z) = G_{zPI} \left(\frac{2}{T} \frac{z-1}{z+1} \right) = \frac{1.01z - 0.994}{z-1} \quad (41)$$

The given 3-digit coefficient accuracy leads to good closed-loop performance despite very wrong individual section step responses. When they are implemented, however, with still a comparatively generous 2-digit accuracy then the closed loop system is unstable.

End of Example 2.

5. CONCLUSION

A competent quantitative feedback control system design must not ignore the effects of digital implementation of the designed analog controller. Two of the most important and significantly quantifiable effects are: the **loop effect** that reduces stability margins; and the **signal effect** that refers to both, aliasing at the ADC and reverse aliasing at the DAC. The loop effect and some examples of the signal effect were analysed and demonstrated in an example.

The often observed huge sensitivity to control algorithm evaluation accuracy can be avoided by **velocity algorithms**, two of which were shown in this paper. The benefits of a velocity algorithm were demonstrated in an example from a real design.

More details and the very important digital implementation of industrial PID controllers can be found in (Eitelberg, 2000).

REFERENCES

- Eitelberg, Ed. (1988): Sampling rate design based on $(1-sT/2)$. *Int. J. Control*, Vol. 48, No. 4, pp. 1423–1432.
- Eitelberg, Ed. (2000): *Control Engineering Course Notes*. Durban: NOYB Press, ISBN 0-620-26359-8.
- Eitelberg, Ed. and Boje, E. (1991): Feedback controller design for plants with modes and disturbances above the sampling frequency. *Int. J. Systems Sci.*, Vol. 22, No. 9, pp. 1553–1562.
- Middleton, R. H. and Goodwin, G. C. (1990): *Digital Control and Estimation*. Prentice-Hall, Englewood Cliffs.
- Phillips, C. L. and Nagle, H. T. (1984): *Digital Control System Analysis and Design*. Prentice-Hall, Englewood Cliffs.

OPTIMAL IMPLEMENTATION OF A MULTIVARIABLE CONTROLLER IN A FIXED POINT DSP

Luis A. Gonzalez[†], and Luis A. Salas[‡]

[†]*Centro de Investigación y Desarrollo de Tecnología Digital
Ave. Del Parque # 1310, Mesa de Otay, CP 22510 Tijuana, Baja Ca. México*

[‡]*Universidad Autónoma de Baja California
Calzada Tecnológico s/n, Mesa de Otay, Tijuana, Baja Ca. México
e-mail: lgonzal@citedi.mx and lsalas@citedi.mx*

[†]*IEEE Member*

Abstract: Digital Signal Processors (DSP) are excellent candidates for the implementation of multivariable complex control fast systems. This paper reports the application of fixed point DSP in the control of a multivariable mechanical system, a 3 DOF robot manipulator. Results from analysis of the effects of controller's coefficient wordlength on the robustness of the system allows the choice of the most suitable DSP. Then, an optimal realization was computed using a method based on the worst-case criterion for the minimization of the effects of error quantization noise at the output while avoiding overflow of the internal signals of the controller. The implemented controller behaves excellent without not much change in the robustness characteristics of the system.

Keywords: Fixed Point Arithmetics, quantization error, robust control, Optimal realization.

1. INTRODUCTION

Implementation of complex controllers using fixed point arithmetic processors has become very important in the industrial applications due to the low cost, portability, and high speed of this type of processors. Application to disc drive servos see Hanselmann, et al., (1987), Silvinski, et al., (1985), and robotics see Henrichfreise, (1988), can be found in the literature. Implementation of a controller in fixed point processors, bear many problems not found in its floating point counterpart. See Hanselmann, (1987) for an account of the kind of problems we can met when dealing with this type of processors. Briefly, working with fixed point arithmetic may present problems of numerical representation of signal

and coefficients and overflow. These two only problems can induce instability or deviate the performance of the close loop system from specifications. Reduction of the effects above mentioned depends, among other things, heavily on the structure we chose to implement our controller. Here, we worked with the problem of computing an optimal structure for a controller of a three degrees of freedom robot manipulator. But, before we went into this problem, analytical and simulation analysis were carried out to find the 'best' wordlength of the controller coefficients that did not deteriorate the robustness of the close loop system. To do this we obtained the upper bounds of the singular value for stability and nominal performance for different wordlength values, and finally, carried out an

analytical test proposed by Fialho and Georgiou (1994). There exist many structures for a single controller for been implemented, see Neuman, et al., (1979), Williamson, (1985). Our aim was to derive a structure such that the controlled system robustness remains as close as possible to the 'ideal'. Hence, we opted for using a structure or realization derived under an optimal criterion, where some design conditions were similar to the conditions taken during the design process of our controller, as for example the condition to consider the exogenous inputs to have unknown but bounded power density spectrum. Robert & Mullis, (1978), worked out an optimal realization base on a quadratic criterion for digital filter implementation. A new approach to this problem by Rotea-Williamson (1995) considers the H_2 and H_∞ norm minimization that cover both, the case when the power density spectrums of the quantization error and/or the exogenous inputs to the close loop system, are known, and the case when they are unknown but bounded. Using the computational procedure proposed by Viassolo (1996), we derived several optimal realizations from where the 'best' was chosen. The paper is divided as follows: Section II gives a brief introduction to the problems found when using fixed point processors. Section III presents the theory of the method to derived the optimal $2/\infty$ realization and the computational procedure. Section IV, shows the analytical, and the experimental results obtained from the close loop system for different optimal realization of the controller implemented in a DSP. Finally, in Section V we present the conclusions of this work.

2. PROBLEMS ON USING FIXED-POINT PROCESSORS.

In this section we specify briefly many of the characteristic problems found when fixed-point processors with a limited resolution on the representation of signals and coefficients are used to implement a controller.

Arithmetics.-Problems we can find when using fixed-point arithmetics data are: overflow due to the fixed wordlength range, and quantization effects due to roundoff or truncation. These two effects are a constant source of error that we need to be aware of. Therefore, we need to know the different techniques and methods of analysis to work with these two sources of error in order to diminish their effects on the system performance. On this design digital representation in two's complement was used. Any number in two's complement is written as:

$$d = 2^{-\alpha} \left[\sum_{j=0}^{p-1} b_j 2^{-j} + \sum_{j=1}^{p-2} b_j 2^{-j} \right] \quad b_j \in \{0, 1\} \quad (1)$$

where $b_j, j=0,1,\dots,p-2$ represents the bits (0 or 1), b_{p-1} carries the sign information p is the total wordlength and α determines the location of the binary point. If

$\alpha=0$, then d is an integer, and if $\alpha=1$, d is a fractional number. Number format can be a source of error due to overflow. Usually, in point fixed arithmetic, fractional format is chosen since that facilitates the operations as products or accumulated products with scalar product computations that can easily be truncated or rounded-off to the size of the factors for storage and further processing by simply dropping the least significant $p-1$ bits. Hence, we can say that fractional fixed-point arithmetics trade off precision for number size.

But, use of fractional arithmetics did not save us from the overflow problem which possible occurs in add and subtraction operations, but not with multiplications. Overflow is due to the limited number range of wordlength so, controller signals and coefficients must fit well into the wordlength range if quantization effects are to be minimized. The DSP used in this application incorporates optional saturation by code when an overflow happens. Finally, quantization error results when scalar multiplications must be roundedoff or truncated to the size of the fraction. There exist an ample literature on the subject of the influence of the quantization error in the performance of digital filters and close loop controls. See Katz, (1981), and Franklin et al., (1990). Quantization error is introduced through roundoff error of controller internal signals and coefficients that may produce bias, noise, and limit cycles at the output of the close loop system. On a robust close-loop control system these effects are primarily reflected in the loss of robustness for performance or in more critical cases the system could be taken into instability. Analysis of the effects of the quantization noise depends on the model taken for the quantization error. Usually, analysis of quantization of the internal signals of the controller is taken separately from the analysis of quantization of coefficients. As sensitivity analysis of eigenvalues which is one of the methods to find the best representation of the controller that minimize the effects due to coefficient quantization.

Structures.- The numerical performance of the controller implemented in fixed-point processors depends greatly in the structure used for the controller with respect to: number storage elements, number of non-zero non-unity coefficients, coefficient range, and roundoff noise. For SISO transfer functions, parallel, and cascade structures are a correct choice. Both, offer a spread of poles and zeros between blocks. In the other hand state space structures offer an infinity number of possible realizations. Not without surprise, the companion structures that only have a minimum number of coefficients, are not good candidates, since they suffer from ill-conditioning and high coefficient sensitivity. Mullis, et al., (1976), has shown that parallel realizations (block diagonal state matrix), can be taken as a good suboptimal realization.

Optimal realizations that minimize roundoff noise while scaling the internal signals to avoid overflow, have received a lot of attention. Solution to these problems has been proved to be feasible and a similar transformation T can be constructed.

While the above criteria of selection are generally for open systems without much considerations for the close-loop behaviour, there are methods to obtain a realization based on close loop performance. Monroney, et al., (1980), and Sasahara, et al., (1984), have considered the minimization effects of noise quantization for a SISO system under an LQG criteria. More recently Rotea, and Williamson (1995), worked the MIMO case with a worst-case criteria.

A more detailed explanation of this last method along with the computational procedure to derive an optimal realization will be shown in Section 2, and 3.

Scaling.- The operation of scaling when fixed-point processor is used is generally necessary. The objective of the scaling is to fit data into the number range to avoid overflow without provoking too much quantization noise. Scaling must be carried out on the inputs, outputs, states, and scalar products.

3. OPTIMAL REALIZATION

Here, is given a brief description of the method used to derive an optimal realization. As mentioned in Section I, there exist a good number of works on the computation of optimal realizations which minimize the quantization noise on signals at the output while kept the word range as to avoid overflow. Rotea and Williamson (1995), proposed a model to describe how the internal signals of a fixed point implementation are quantized. Based on this framework they posed and solve four optimal realization problems in a close loop context. These realizations are based on either H_2 and H_∞ norms of the quantization noise gain subject to either H_2 and H_∞ scaling constraints. Assume a controller $K(z)$ with state space representation $(\Phi_c, \Gamma_c, C_c, D_c)$ connected to an augmented open loop transfer matrix $P(z) = [P_{ij}(z)]_{i,j=1,2}$ as shown in Fig (1),

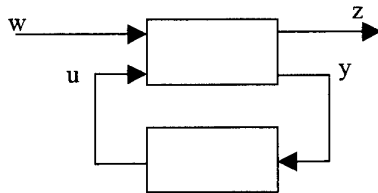


Fig. 1.- Discrete close loop system

From an adequate partition of the plant, the input output equations of the close loop system will be:

$$z = P_{11}(z)w + P_{12}(z)u \quad (2)$$

$$y = P_{21}(z)w + P_{22}(z)u$$

$$u = K(z)y$$

where u is the control input to the plant, y is the measurement output with purpose of feedback, w is the exogenous input, and z the output of interest of the closed loop system.

The general scheme for the controller implementation to describe the internal signal quantization is given as:

$$x_{k+1} = \Phi_c x_k + B_c(\Phi_c)\epsilon_k + \Gamma_c y_k \quad (3)$$

$$\zeta_k = C_o(\Phi_c)x_k + D_o(\Gamma_c)y_k$$

$$u_k = C_c x_k + D_i(C)\epsilon_k + D_c y_k$$

where x , u , and y denote the state, output and input of the fixed point implementation of the controller, respectively. ζ is the quantized internal signal of the implementation, the model input ϵ represents the quantization error or quantization noise. The signals ζ , and ϵ are related via the nonlinear equation $\epsilon(k) = (N(\zeta))(k)$; $N := Q - I$, where $Q(*)$ is a nonlinear memoryless operator to implement roundoff quantization on each entry of vector $\zeta(k)$, to β fractional bits; that is $|\epsilon(k)| < 2^{-(\beta+1)}$ for all k . The functions B_o , C_o , D_o , and C_i are linear on its argument. Due to the problem posed by the presence of the nonlinearities, the quantization noise ϵ was taken as an exogenous signal, that for purpose of analysis can be taken as zero mean white noise signal, coming into the controller. From the general scheme different quantization schemes can be derived as: Quantization Before Multiplication, and Quantization After Multiplication with or without Error Feedback.

Different from the infinity wordlength realizations, in finite wordlength realizations the output of the system due to a given input, depends on the state space structure used to implement the controller. Therefore, if any other realization of the controller is of the form $(T^{-1}\Phi_c T, T^{-1}\Gamma_c, C_c T, D_c)$, for a nonsingular transformation T it can easily be found that the quantization error and the quantized signal will be affected by this transformation. Let $L(z)$ be the quantization scheme for the controller, then the close loop controlled system will look as shown in Fig. 2

to determine the least upper value of the wordlength which will guarantee robust stability and nominal performance. The controller for the robot manipulator was designed using μ -synthesis technique, see Gonzalez, et al., (1999), for specific details. A controller of order 43 was obtained, then it was reduced to a more manageable 10 order balanced realization by a truncation technique. It was found by μ -analysis that the close loop ten order system kept its robustness to stability and performance. Here, the same analysis is worked out on the same system, but, for different coefficient wordlength of the controller in order to ascertain the effects of finite wordlength on the robustness of our design. From a μ -analysis of the weighted sensitivity function, curves of the structural value for robust stability were obtained for different wordlength and are shown in Fig. 4

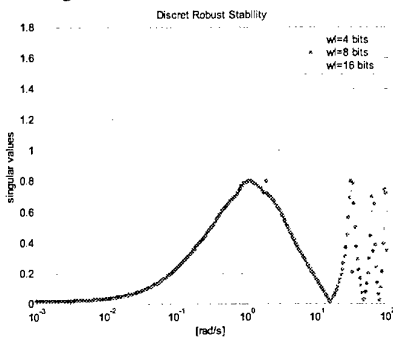


Fig.4. Robust stability analysis for different wordlength.

From the theory of μ -analysis the system will be robust stable if the upper bound of the structural value is less than one, clearly, this is satisfied for infinite wordlength, but amazingly for this case, robust stability is maintained even for a 4 bits wordlength. A similar simulation experiment was carried out on the nominal performance of the system. The results of this simulation are shown in Fig.5.

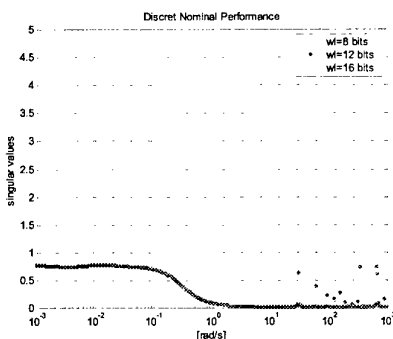


Fig.5.-Nominal performance for different wordlength.

From Fig.5, clearly, close loop nominal performance will be violated if a 4 bits word processor is used. The above experiments show, the well known fact, that performance is harder to achieve than stability. We also obtained the step response of the first joint of the

robot for different wordlength values. This result is shown in Fig. 6. A very impressive result from this simulation is to find out that the balanced realization worked well even for a 4 bits wordlength. We can see that for 4 bits wordlength the system's response becomes more sluggish and noisy, as compared with the longest wordlength, but with a similar settling time. On the other hand the 8 bits wordlength has no overshoot and shorter settling time hence, it could be considered as the best option. Similar analysis were also made for other controller realizations but, they did not behave as well as the balanced realization.

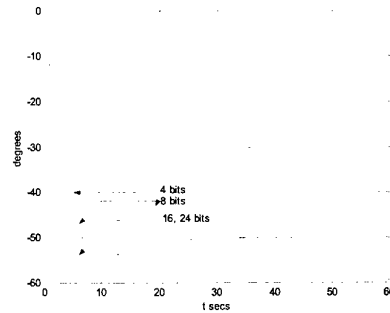


Fig.6.-Coefficient wordlength effect on time responses.

Also, by applying a result given by Fialho, et al., (1994), it was found the least value of the size of the wordlength for this problem, that kept robust stability. Briefly, is presented the problem of analysis of sensitivity of a sampled data control system to the effects due to the quantization error on system's coefficient representation. Assume a sampled-data control system with a plant in state space discrete form (Φ, Γ, C, D) and a digital controller $(\Phi_c, \Gamma_c, C_c, D_c)$. Then, the state coefficient matrix of the corresponding close-loop realization is of the form:

$$\Phi_{cl} = \begin{bmatrix} \Phi - \Gamma D_c C & \Gamma C \\ -\Gamma_c D_c & \Phi_c \end{bmatrix} = \begin{bmatrix} \Phi & 0 \\ 0 & 0 \end{bmatrix} + \begin{bmatrix} -\Gamma & 0 \\ 0 & I \end{bmatrix} \begin{bmatrix} D_c & -C_c \\ -\Gamma_c & \Phi_c \end{bmatrix} \begin{bmatrix} C & 0 \\ 0 & I \end{bmatrix} \quad (14)$$

or

$$\Phi_{cl} = \Phi_o + \Gamma_o M_o C_o \quad (15)$$

where M_o is the system matrix of the digital controller. Therefore, the feedback system will be stable if and only if all the eigenvalues of Φ_{cl} are in the interior of the unit circle.

Say, due to finite precision arithmetic the actual system matrix implemented may take the value $M_o + \Delta$ where Δ will contain all the coefficient quantization errors. For a given realization of the controller the problem is to compute the minimum value of $\|\Delta\|$ respect to an induced norm that guarantee stability of the close loop system. Fialho et al. (1994), based on

an statistical point of view behavior of the quantization error, derived an approximate expression for the wordlength of least size that guarantee robust stability as:

$$W_r = \log_2 \left(2 \frac{N}{2} + \frac{N}{45} * \left(\frac{1}{\eta} \right) \right) \quad (16)$$

in bits. N is the number of nonzero random entries in Δ , and η is the least upper bound defined as:

$$\eta = \inf \{ \Delta : \Phi_c + \Gamma_o \Delta C_o \text{ is unstable} \} \quad (17)$$

where $\|\cdot\|$ is the infinity norm. η is the so called complex or real stability radius depending if Δ is complex or real and has already been computed.

The computed value of the limit wordlength for the balanced realization using Eq.(16) for our case was 12 that is greater than the value obtained from the simulation. Being too conservative we took this result to chose an appropriate DSP for our implementation. Specifically, we worked with a 16 bits DSP TMS320F240 of Texas Instrument [15].

4.2.- Optimal Implementation and Experimental Results.

As was mentioned above we worked with fractional arithmetic format for coefficients and with a DSP with an overflow mode of operation. Here, we presents the process to compute the optimal realization derived by Rotea et al. (1994), for our fixed point application The first and important step is to choose the quantization scheme. Here, we worked with the Quantization Before Multiplication with Error Feedback scheme or model which is described as :

$$\begin{aligned} \alpha x &= \Phi_c + (I - \Phi_c)T\epsilon + \Gamma_c y \\ T\zeta &= x \\ u &= C_c x + C_c T\epsilon + D_c y \end{aligned} \quad (18)$$

Hence, for the representation of Eq.(5), we have:

$$\begin{aligned} L_{11}(z) &= (zI - \Phi_c)^{-1} (\Phi_c - I) \\ L_{12}(z) &= (zI - \Phi_c)^{-1} \Gamma_c \\ L_{21}(z) &= C_c (zI - \Phi_c)^{-1} (\Phi_c - I) + C_c \\ L_{22}(z) &= K(z) = C_c (zI - \Phi)^{-1} \Gamma + D \end{aligned} \quad (19)$$

The close loop system with the quantization model for our application looks as shown in Fig. 7.

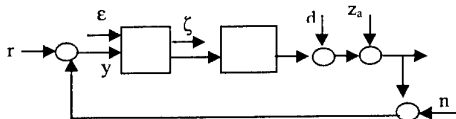


Fig. 7.- Close loop system with quantization controller scheme

Where $G_n(z)$ is the nominal plant, the exogenous input vector considered for this design is $w = [r^T d^T n^T z_a^T]^T$ where r , d , n , and z_a are the command or reference, disturbance at the output, noise in the sensors, and modeled uncertainty respectively. The output vector was taken as $z = [u^T y^T]^T$ where u is the output of the controller, and y is the close loop error. It is also included the quantization noise $T\epsilon$ taken as an exogenous signal, and the scaled internal signal vector $T\zeta$. The open loop plant $P(z)$ for this system is given as:

$$\begin{bmatrix} y \\ z \end{bmatrix} = \begin{bmatrix} -G_n(z) & I_3 & -I_3 & -I_3 & -I_3 \\ I_3 & 0 & 0 & 0 & 0 \\ -G_n(z) & I_3 & -I_3 & 0 & -I_3 \end{bmatrix} \begin{bmatrix} u \\ w \end{bmatrix} \quad (20)$$

where

$$\begin{aligned} P_{11}(z) &= -G_n(z) \\ P_{12}(z) &= [I_3 \quad -I_3 \quad -I_3 \quad -I_3] \\ P_{21}(z) &= \begin{bmatrix} I_3 \\ -G_n(z) \end{bmatrix} \\ P_{22}(z) &= \begin{bmatrix} 0 & 0 & 0 & 0 \\ I_3 & -I_3 & 0 & -I_3 \end{bmatrix} \end{aligned} \quad (21)$$

From Fig.7, the transfer matrix functions, that relates the quantized noise $T\epsilon$, and the exogenous inputs w with the output difference $z-z_d$, and the scaled signal $T\zeta$, respectively are given as:

$$\begin{aligned} H_{12}(z) &= L_{12}(z)S_i(z)P_{12}(z) \\ H_{21}(z) &= P_{21}(z)S_o(z)L_{21}(z) \end{aligned} \quad (22)$$

where $S_i(z) = (I + G_n(z)K_c(z))^{-1}$,

and $S_o(z) = (I + K_c(z)G_n(z))^{-1}$.

Once the quantization noise and scaling transfer matrix have been defined the next step is to derive the optimal realization. This computation depends on an initial realization, a positive number and the norms to work with the quantized error gain and the scaling constraint, (2/oo). Viassolo, (1996), one of MC. Rotea's student propose the following procedure to compute the optimal realization:

- Select an initial realization for the controller, here given by its system matrix M_i , the scaling norm, and the upper bound γ for the scaling norm
- Compute the transformation:

$$T_{ic} = \frac{1}{\gamma} \begin{bmatrix} C_{iq}(M_i) & 0 & \dots & 0 \\ 0 & C_{2q}(M_i) & \dots & 0 \\ \vdots & \vdots & \vdots & y;n \\ 0 & 0 & \dots & C_{in}(M_i) \end{bmatrix} \quad (23)$$

hence, the new realization will be

$$M_{sc} = \begin{bmatrix} I & 0 \\ 0 & T_{sc}^{-1} \end{bmatrix} M_i \begin{bmatrix} I & 0 \\ 0 & T_{sc} \end{bmatrix} \quad (24)$$

that will be written as $M_{sc} = (T_{sc}, M_i)$, and satisfies $C_{1q}(M_{sc}) = \dots = C_{nq}(M_{sc}) = \gamma$.

- Starting from M_{sc} , solve the optimal realization problem to obtain the transformation T_{op} that yields the optimal realization $M_{op} = (T_{op}, M_{sc})$
- Using M_{op} and γ compute the transformation

$$T_{scop} = \frac{1}{\gamma} \begin{bmatrix} C_{1q}(M_{op}) & 0 & \dots & 0 \\ 0 & C_{2q}(M_{op}) & \dots & 0 \\ \vdots & \vdots & \ddots & \vdots \\ 0 & 0 & \dots & C_{nq}(M_{op}) \end{bmatrix} \quad (25)$$

and obtain the realization $M_{scop} = (T_{scop}, M_{op})$ that satisfies $C_{1q}(M_{scop}) = \dots = C_{nq}(M_{scop}) = \gamma$.

For this experiment we try as initial realizations:

- The balanced realization obtained direct from the design
- The Schur form of the realization.
- The realization for $q = 2$, $p = 2$ that was derived by applying Viassolo's procedure.

During the experiments the power density spectrum of the exogenous input vector w was also considered unknown but bounded, therefore, the norm $q = \infty$ for the scaling constraint C_{1q} was used. For each trial the quantization noise gain for norm 2 and ∞ was calculated, as well as the max $C_{i,2}$. The results of the computation are shown in Table I Table II, and Table III.

From these results it is found that the realization derived from an initial optimal realization (Op22), is the best if the power density spectrum of the exogenous input is known ($p = 2$, $J_2 = 3.59$).

Table I ($q = \infty$)

	Bal. Scal.	p=2		p= ∞	
		BaScOp	BaScOp Sc	BaScOp	BaScOp Sc
J_{∞}	25.78	30.20	20.28	1.51×10^4	18.38
J_2	20.97	5.51	4.05	1.26×10^4	11.53
Max $C_{i,2}$	0.5479	0.58	0.6521	0.0853	0.4998

Table II ($q = \infty$)

	Schur Sca	p=2		p= ∞	
		SchScOp	Op22OpSc	SchScOp	SchScOpSc
J_{∞}	21.076	29.86	19.96	19.964	17.02
J_2	6.1582	5.511	4.247	4.247	7.827
Max $C_{i,2}$	0.648	0.39	0.6536	0.6536	0.6488

Table III ($q = \infty$)

	Op22 In	p=2		p= ∞	
		Op22Op	Op22OpSc	Op22Op	Op22OpSc
J_{∞}	17.318	29.67	18.73	1.54×10^4	71.193
J_2	3.5554	5.456	3.59	1.32×10^4	52.7
Max $C_{i,2}$	0.4533	0.5765	0.6538	0.0708	0.444

For the case when the power density spectrum is unknown but bounded, the best realization was the one derived using the Schur realization as initial ($p = \infty$, $J_{\infty} = 17.02$). A point of interest of the above results is that the realization derived from Op22 as initial deteriorates with respect to the quantization error gain for $p = \infty$, and does not show significant improvement for $p = 2$. For these two realizations the maximum overflow gain is almost the same (0.6538 and 0.6488) respectively. An analysis of variance of the output for the three realizations for different wordlength size was done as well. The result of this analysis is shown in Table IV

Table IV

Wordlength	Init. Balanced	Init. Schur	Init. Op22
8	4.6891×10^{-5}	1.1771×10^{-5}	3.4559×10^{-6}
12	1.9477×10^{-7}	4.5982×10^{-8}	1.35×10^{-8}
16	7.6082×10^{-10}	1.7962×10^{-10}	5.2733×10^{-11}
24	1.1609×10^{-14}	2.7408×10^{-17}	8.0464×10^{-18}
32	1.7714×10^{-19}	4.1821×10^{-20}	1.2278×10^{-20}

The results of Table IV are also presented in graphical form in Fig.8 below: It is clear from the graphs, that the realization derived from the OP22 initial realization causes the least variance at the output due to quantization error for any wordlength.

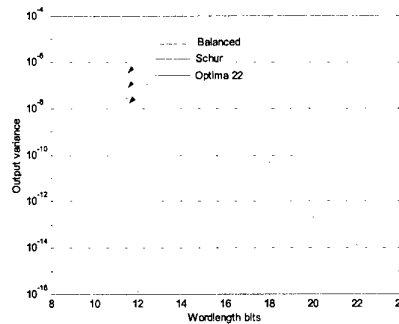


Fig. 8.- Variance at the output for different wordlength.

The realization derived from the Schur initial realization also show a small value for the variance of the output. Due to this small difference on the variance, and because the exogenous inputs characteristics were not known exactly this last realization was chosen for implementation in the DSP.

Then, the controller was implemented using two different structures: A balanced realization derived direct from the design in floating point arithmetics (here we used a 486 computer to implement the controller), that was noted as the 'ideal ', and the optimal realization derived from an Schur initial realization implemented in the 16 bits DSP processor. Below, Fig.(9), and Fig (10) show the joint time responses of the close loop controlled system for a step input of $(-50, -20, 40)$ degrees on the first, second, and third joints for the ideal and optimal realization, respectively.

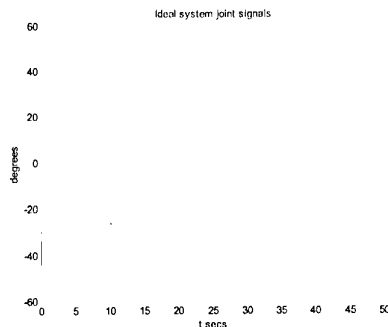


Fig. 9.- Step responses of the robot with the ideal implementation.

The two controlled systems show a good performance on tracking of the reference signals, but not without surprise, the optimal realization, clearly outperforms the ideal realization, since it is almost four times faster, show no overshoot, and filtered the oscillations present at the third joint.

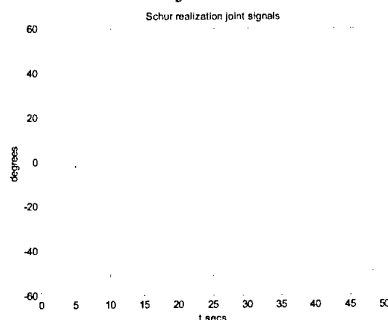


Fig. 10.- Step responses of the robot for the optimal Schur implementation.

In order to see the effects of the scaling constraints on the internal signals of the controller Fig. (11), and Fig. (12) also show the time responses of three of these signals for the ideal and the optimal realizations respectively.

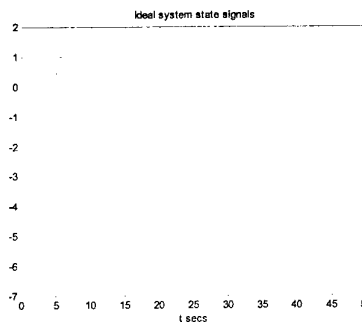


Fig. 11.- State dynamics of the close loop system for the ideal implementation.

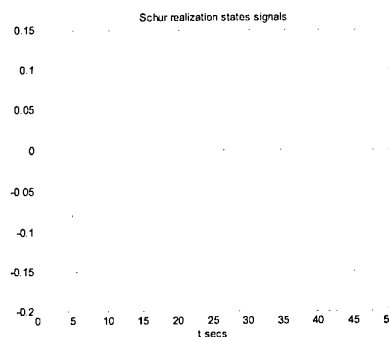


Fig. 12.- State dynamics of the close loop for the optimal Schur implementation

The optimal realization clearly shows the effects of the constraint to keep in range (< 1) , the size of the internal signals of the controller. For this experiment the maximum size of the signals was less than 0.26 that is well inside the working range. In the other hand the ideal without this constraint produced signals almost thirty times greater in instantaneous magnitude than the optimal realization. This difference on performance was simple due to the structure of the controller since the input control signals were almost the same for both realizations as proved by the RMS value of the difference between the two control vectors $U_{id}-U_{op}$ equal to 1.1 degrees. A significant advantage of the optimal realization derived from a Schur initial realization with respect to the other analysed realizations is that the number of coefficients equal to zero is larger in the Schur than in the other realizations something that will lessen the effects produce by the time delay due to the computation time on the close loop stability and performance.

5. CONCLUSIONS

Here, was presented the process of implementation of a complex controller, derived for a three degree of freedom robot manipulator, using fixed point arithmetic processors. The controller was of order

ten, with three inputs and three outputs. Analysis of coefficient wordlength effects on stability and nominal performance, analytical and from simulation, were carried out to arrive at an assessment of the choice for the more suitable DSP. Based on a quantization noise model, and on an optimal technique where minimization of the quantization error gain is achieved subject to scaling of the internal signal constraints, and under matrix 2/00 norm, different optimal realization were computed for the controller. The computation of the optimal realization depends greatly on the initial realization taken at the start of the computation. Six different initial realizations were try of which the two derived from the Schur and Optimal Cuadratic realizations were the best with respect to the 'size' of the quantization error gain, and output variance. The resultant optimal realizations obtained with Viasolo's computational procedure based on Rotea-Williamson method, worked very well for our case obtaining excellent results on the performance of the robot on tracking of command signals as well as on regulation to constant disturbance, and noise rejection as compared with other realizations. But, most important is the suitability of the controller to be implemented in a 16 digits fixed point DSP processor without causing deterioration on the stability, and/or performance of the close loop system. One problem to observe of the method was the lack of a criterion to propose an initial realization. The optimal realization derived from a balanced initial realization, also produced good practical results in its implementation in the DSP.

REFERENCES

- [1] I. J. Fialho and T. T. Georgiou, "On Stability and Performance of sample-data systems subject to word length constraint", IEEE Trans. Automat. Contr., Vol.39, pp. 2476-2481, Dec. 1994.
- [2] Silvinski, Ch. And J. Borniski, "Control system compensation and implementation with the TMS32010, Texas Instrument Applications Report, 1985.
- [3] H. Hanselmann and W. Moritz, "High Bandwith Control of the Head Positioning Mechanism ina Winchester Disc Drive", IEEE Control System Magazine, pp. 15-19, Oct., 1987.
- [4] H. Henrichfreise, "The control of an elastic manipulation devise using DSP", American Control Conf. ACC, Atlanta, Ge., June 15-17, 1988.
- [5] Williamson, D. "Finite wordlength design of digital Kalman filters for state estimation", IEEE Trans. Aut. Contr., AC-30, 930, 1985.
- [6] H. Hanselmann, "Implementation of Digital Controllers - A Survey", Automatica, Vol. 23, pp. 7-32, January 1987.
- [7] Neuman, C. P. and C. S. Baradello, "Digital Transfer Functions for microcomputer contrl", IEEE Trans. Sys. Man Cyber., SMC-9, 856, 1979.
- [8] Mills W. L., C. T. Mullis and R. A. Roberts, "Digital filter realizations without overflow oscillations", Proc. IEEE Int. Conf. Acoust. Speech Sig. Process., Tulsa Oklahoma, 1978.
- [9] Mullis C. T. and R. A. Roberts, "Synthesis of minimum roundoff noise fixed point digital filters", IEEE Trans. Cts. Syst., CAS-23, 551, 1976.
- [10] Sasahara H., M. Kawamata and T. Higuchi, "Design of microprocessor-based LQG control systems with minimum quantization error", Proc. IECON-84, Tokyo.
- [11] M. A. Rotea and D. Williamson, "Optimal realization of finite wordlength digital filters and controllers", IEEE Trans. Circ. Sys., Vol. 42, No.2, Feb. 1995.
- [12] D. E. Viassolo, M.Sc. Thesis, "Implementation of Digital Controllers", Engineering, Purdue University, Aug. 1996.
- [13] P. Moroney, A. S. Willsky, and P. K. Houpt, "The digital implementation of control compensators: the coefficient wordlength issue", IEEE Trans. Aut. Contr., AC-25, No. 4, Aug. 1980.

ROBUST FEEDBACK SYNTHESIS FOR NARMAX MODELS USING GENERALIZED DESCRIBING FUNCTIONS

P. S. V. Nataraj and K. Kotecha

*Systems and Control Engineering Group,
Department of Electrical Engg.,
IIT Bombay 400 076, India.
Email: nataraj@ee.iitb.ernet.in*

Abstract: In this paper, a technique is proposed for synthesizing robust sampled-data feedback systems for plants described by polynomial NARMAX models. The technique is based on the concept of generalized frequency response functions, and exploits recent results that enable derivation of these directly from the NARX description of the plant. A nonlinear chemical reactor example is solved using the procedure and found to yield satisfactory results.

Keywords: NARMAX model, Nonlinear System Identification, Nonlinear Control, Robust Control, Quantitative Feedback Theory (QFT)

1. INTRODUCTION

Sampling of real finitely realizable continuous-time nonlinear systems naturally produces NARMAX (Nonlinear AutoRegressive Moving Average with eXogenous inputs) models, as demonstrated by Chen and Billings (1989). The NARMAX model provides a unified representation for a wide class of discrete-time nonlinear stochastic systems, and includes several known nonlinear input-output models, such as Hammerstein, Weiner bilinear, and state-affine, as special cases. The chief advantages of the NARMAX model over functional series representations such as the Volterra series, are that for identification the former requires a reduced

number of parameters, smaller data sets, and there is no need for special input signals. With the identification results also being easier to analyze for NARMAX models, these are certainly more convenient to use than the Volterra series.

Of the various forms of NARMAX models the polynomial NARMAX model is perhaps the most suitable in practical applications, because it is linear in the parameters. Many linear identification results have been extended to the polynomial NARMAX model, and several combined routines of intelligent structure determination and parameter estimation are available, see Korenberg, *et al.* (1988). Indeed, practical identification of sev-

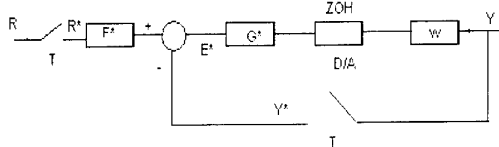


Fig. 1. The nonlinear sampled-data system.

eral industrial systems has established that most practical systems can be satisfactorily modeled by polynomial NARMAX models.

Quantitative Feedback Theory (QFT) of Horowitz (1993) is a well-established body of robust control synthesis techniques. A QFT technique for sampled-data systems comprising of a nonlinear continuous time plant modeled by differential equations has been outlined by Horowitz and Liao (1986). However there are no QFT techniques to handle systems described by polynomial NARMAX models. In view of the popularity and widespread use of these models, it is very desirable to have such a QFT technique. In this work, we propose a QFT technique for systems described by polynomial NARMAX models.

Further, in the nonlinear QFT procedures of Horowitz (1976) and Ioinovici (1987), a major computational difficulty arises while generating templates of the so-called 'LTIE plant' set. Our proposed technique is also based on the LTIE plant approach. However, in our technique a new method of computing the LTIE plant templates based on generalized describing functions is introduced. In the new method, the LTIE plant templates are generated easily and efficiently, *directly* from the coefficients of the nonlinear model. Thereby, the computational difficulties inherent in the existing methods of LTIE plant template generation are solved.

To implement the proposed procedure on nonlinear systems, an integrated package has been developed (cf. sec. 4.3). Initial experience with this package in the area of chemical process control has been encouraging (a simulated chemical reactor

examples is given in sec. 5). It is hoped that the developments and software tools reported here make it possible to use QFT *on-line* in nonlinear robust control, in the not too distant future.

It is assumed in this paper that the reader is familiar with the ideas and results concerning nonlinear frequency response functions as given by Jones and Billings (1991), and with those of QFT methods as given by Horowitz (1976; 1993) and Horowitz and Liao (1986).

2. BACKGROUND

Consider a nonlinear SISO plant in a two degree of freedom structure. Suppose the plant is given by nonlinear continuous mapping $w : u(t) \rightarrow y(t)$, with unique continuous inverse w^{-1} . Due to the uncertainty in physical parameters, there is a denumerable set of nonlinear plants $\mathbb{W} = \{w\}$. The given finite set of deterministic inputs I to the system consists of the set of possible setpoint signals $\mathbb{R} = \{r\}$ and disturbances $\mathbb{D} = \{d\}$. For each $i_\alpha \in I$, there is a specified set of acceptable plant outputs \mathbb{A}_α . The design problem is to find strictly proper LTI operators F (the prefilter) and G (the controller), such that for each $i_\alpha \in I$, the system output $y \in \mathbb{A}_\alpha, \forall w \in \mathbb{W}$.

For nonlinear continuous-time plants, a QFT synthesis technique to solve the above problem has been presented by Horowitz (1976). The technique, based on Schauder's fixed point theorem and valid for zero-initial conditions, is basically a two-step procedure: The first step is to find a set \mathbb{P}_{eq} of what are known as LTI 'equivalent' (LTIE) plants. The second step is to solve the synthesis problem with \mathbb{P}_{eq} replacing \mathbb{W} . It has been shown by Horowitz (1976) that for a large nonlinear problem class, the prefilter F and controller G which solve this 'equivalent' LTI problem, also solve the original nonlinear problem (i.e., for the set \mathbb{W}).

Next consider a nonlinear sampled-data system shown in Fig. 1. Assume that a fixed sampling period T is used, giving sampling frequency $\omega_s = \frac{2\pi}{T}$. As is customary, let $f^*(t)$ denote the impulse-

sampled signal, $F^*(s)$ denote the Laplace transform of $f^*(t)$, and $F(z)$ denote $[F^*(s)]_{z=e^{sT}}$.

A QFT approach similar to the nonlinear continuous-time case has been suggested by Horowitz and Liao (1986). In the sampled-data case, the actual plant input is of a staircase form (as a ZOH is used), and therefore the acceptable output set must be carefully formulated so that the $w^{-1}(a)$ indeed emerges as a staircase signal. Once this has been done, the designer can proceed by obtaining the 'equivalent' LTI set \mathbb{P}_{eq} , exactly as in the nonlinear continuous-time case, and apply linear sampled-data QFT techniques to the set \mathbb{P}_{eq} .

An improved algorithm to find the LTIE plant set has been given by Ioinovici (1987). This method does not require w^{-1} to exist, which is a constraint inherent in Horowitz's LTIE method. Further, Ioinovici demonstrated through several examples that his algorithm gives superior results to the earlier LTIE method, in terms of reduced overdesign. However, certain difficulties are found in Ioinovici's LTIE algorithm:

1. Finding *analytically* the solution of nonlinear differential equation describing the plant, for each member of I .
2. Obtaining the expressions for Laplace-transforms of each of these time-domain solutions.
3. As discussed earlier, it is very desirable in practice to have polynomial NARMAX representations for nonlinear plants. However, Ioinovici algorithm does not address plants represented as NARMAX models - in polynomial or other forms (the same is true for Horowitz's algorithm.)

A method to directly find (i.e. without solving differential equations or Laplace-transforming) the LTIE plant templates from the given Polynomial NARMAX model and the set I is described in the following section.

3. THE NARMAX MODEL AND ITS LTIE PLANT

Suppose that the nonlinear plant is represented by the model

$$\begin{aligned} y(k) = & F[y(k-1), \dots, y(k-n_y), \\ & u(k-1), \dots, u(k-n_u), \\ & \zeta(k-1), \dots, \zeta(k-n_\zeta)] + \zeta(k) \end{aligned} \quad (1)$$

where F is some nonlinear function of lagged input signals $u(k-n_u)$, outputs $y(k-n_y)$, and noise $\zeta(k-n_\zeta)$, with k denoting the sampling intervals and n the lags. The model in (1) is referred to as the NARMAX model. Chen and Billings (1989) rigorously proved that a nonlinear discrete-time-invariant system can always be represented by the NARMAX model in a region around an equilibrium point, subject to two sufficient conditions: (1) The response function of the system is finitely realizable (which means that distributed-parameter systems are excluded) (2) A linearized model exists if the system is operated close to the chosen equilibrium point. Further, the model can also be shown to be valid for the non-zero initial state response case.

If the nonlinear function $F(\cdot)$ is continuous, it can always be arbitrarily closely approximated by a polynomial function. For practical purposes, therefore, we may choose $F(\cdot)$ as a finite polynomial function, giving us a polynomial NARMAX model.

Once a polynomial NARMAX model of the plant has been estimated, we can discard the moving average noise terms in (1) to get a polynomial NARX (Nonlinear AutoRegressive with exogenous inputs) model. This is justified, as the moving average noise terms were originally included to ensure unbiased estimation, and therefore can be dispensed with once estimation is over.

The output $y(t)$ of NARX model is expressed as

$$y(t) = \sum_{m=1}^M y_m(t) \quad (2)$$

where $y_m(t)$ is m -th order output of system, given by

$$\begin{aligned} y_m(t) = & \sum_{p=0}^m \sum_{k_1, k_2=1}^K c_{p,q}(k_1, \dots, k_{p+q}) \\ & \times \prod_{i=1}^p y(t-k_i) \prod_{i=p+1}^{p+q} u(t-k_i) \end{aligned} \quad (3)$$

with $p + q = m$, $k = 1, \dots, K$ and $\sum_{a=1}^K \dots \sum_{b=1}^K =$

>From a polynomial NARX model description of the plant, the n -th order GFRFs (Generalized Frequency Response Functions) can be computed using the recursive probing algorithm of Jones and Billings (1989). The algorithm yields the n -th order frequency responses to be found, without restriction on the order n . Further, this method also exposes the structure of $H_n(\cdot)$, and enables the GFRFs to be related to the structure and coefficients of the nonlinear difference equation model of the plant. These GFRFs can be subsequently used to evaluate the GDFs (Generalized Describing Function), giving us a unidimensional frequency domain representation of the nonlinear plant.

Using the recursive probing input method, the n -th order GFRFs for the NARX model (2), (3) are computed as follows:

$$\begin{aligned} & \left(1 - \sum_{k_1=1}^K c_{1,0}(k_1) \exp(-j(\omega_1 + \dots + \omega_n)k_1) \right) \\ & \times H_n(j\omega_1, \dots, j\omega_n) \\ & = \sum_{k_1, k_n=1}^K c_{0,n}(k_1, \dots, k_n) \\ & \times \exp(-j(\omega_1 k_1 + \dots + \omega_n k_n)) \\ & + \sum_{q=1}^{n-1} \sum_{p=1}^{n-q} \sum_{k_1, k_n=1}^K c_{p,q}(k_1, \dots, k_{p+q}) \\ & * \exp(-j(\omega_{n-q+1} k_{n-q+1} + \dots + \omega_{p+q} k_{p+q})) \\ & \times H_{n-q,p}(j\omega_1, \dots, j\omega_n) \\ & + \sum_{p=2}^n \sum_{k_1, k_p=1}^K c_{p,0}(k_1, \dots, k_p) \times \\ & H_{n,p}(j\omega_1, \dots, j\omega_n) \end{aligned} \quad (4)$$

where $H_{n,p}(\cdot)$ is generated by the recursion

$$\begin{aligned} H_{n,p}(\cdot) &= \sum_{i=1}^{n-p+1} H_i(j\omega_1, \dots, j\omega_i) \times \\ & H_{n-i,p-i}(j\omega_{i+1}, \dots, j\omega_n) \times \\ & \exp(-j(\omega_1 + \dots + \omega_i)k_p) \end{aligned} \quad (5)$$

The recursion finishes at $p = 1$ and

$$\begin{aligned} H_1(j\omega_1, \dots, j\omega_n) &= H_n(j\omega_1, \dots, j\omega_n) \\ &\times \exp(-j(\omega_1 + \omega_n)k_1) \end{aligned} \quad (6)$$

Next, the n -th order multidimensional output spectrum is found:

$$\begin{aligned} Y(j\omega_1, \dots, j\omega_n) &= H_n(j\omega_1, \dots, j\omega_n) \\ &\times \prod_{i=1}^n U(j\omega_i) \end{aligned} \quad (7)$$

where $U(j\omega)$ represents the normalized input spectrum. Then, the unidimensional output spectrum is obtained:

$$\begin{aligned} Y_n(j\omega) &= \frac{1}{(2\pi)^{n-1}} \int_{-\infty}^{\infty} \dots \int_{-\infty}^{\infty} \\ & Y_n(j\omega_1, j(\omega_2 - \omega_1), \dots, j(\omega_n - \omega_{n-1})) \\ & \times d\omega_1 \dots d\omega_{n-1} \end{aligned} \quad (8)$$

The total unidimensional output spectrum is given by summation of all the n -th order unidimensional output spectrums:

$$Y(j\omega) = \sum_{n=1}^N Y_n(j\omega) \quad (9)$$

Finally, this output response is used to evaluate the GDF:

$$N(A, j\omega) = \frac{Y(j\omega)}{AU(j\omega)} \quad (10)$$

where A denotes the input amplitude or waveform scaling factor. Note that $N(A, j\omega)$ is considered undefined whenever $U(j\omega) = 0$.

It is easily seen that the GDF characterizes precisely Ioinovici's LTIE plant that corresponds to the given polynomial NARMAX model and the input signal considered in (7).

Thus, the GDF provides a new and powerful frequency domain representation of a wide class of nonlinear systems. This characterization is subsequently used in the proposed procedure as a basis for controller synthesis using the principles of sampled-data QFT.

4. A QFT PROCEDURE FOR POLYNOMIAL NARMAX MODELS

4.1 The Basic Idea

Suppose that a polynomial NARMAX model description of the nonlinear plant is available. From this model, a NARX model is extracted, and the n -th order GFRFs generated using (4)-(6). For any particular input signal $i_\alpha \in I$, the corresponding GDF is obtained by finding the total output frequency response and then dividing it by the input signal spectrum, as given in (7)-(10). Now, the GDF is unidimensional in frequency, so a single magnitude and phase (Bode) response is got at each frequency. By repeating the procedure over I , a band of (instead of a single) magnitude and phase plots is obtained at each frequency. This response band forms the template of the LTIE plant at each frequency.

These LTIE plant templates are next used for feedback synthesis using linear sampled-data QFT methods. The resulting controller and prefilter when used on the original nonlinear plant, are guaranteed to achieve the given specs. This has been shown in general for a large class of nonlinear systems using fixed-point theorems of nonlinear function analysis by Horowitz (1993).

4.2 The Proposed Procedure

We now give the complete synthesis procedure.

- (1) For the considered plant, formulate the set I of signals for which the design is to be performed, and the set A of acceptable output responses.
- (2) Generate appropriate input-output data set for experimental (or simulated) identification of the non-linear plant. Using an integrated structure determination and parameter estimation algorithm of Korenberg, *et al.* (1988), identify a parsimonious model in the polynomial NARMAX form from these data sets. Validate the model using model validation methods for nonlinear systems.
- (3) From the identified NARMAX model, obtain the NARX model (2)-(3) by discarding the moving average noise terms.
- (4) From the obtained NARX model, find GFRFs $H_1(j\omega_1), H_2(j\omega_1, j\omega_2), \dots, H_n(j\omega_1, \dots, j\omega_n)$ using (4)-(6) where the highest order n is commensurate with the nonlinearity of the model. Evaluate these functions in the output frequency domain, and use the same domain for all further work.
- (5) Pick any input signal $i_\alpha \in I$, and find its input spectrum $U(j\omega)$.
- (6) Find the n -th order output frequency response $Y_n(j\omega_1, j(\omega_2 - \omega_1), \dots, j(\omega_n - \omega_{n-1}))$ using (7), the unidimensional output frequency response $Y_n(j\omega)$ using (8), the total unidimensional frequency response $Y(j\omega)$ using (9), and the GDF $N(A, j\omega)$ using (10).
- (7) Repeat steps (5)-(6) over the set I (and/or over set W), to get magnitude and phase response bands at each frequency. These bands form the template of the LTIE plants at each frequency.
- (8) Using the LTIE plant templates generated at the design frequencies, synthesize a controller $G(z)$ and a prefilter $F(z)$ using linear sampled-data QFT methods. The steps in sampled-data controller design using QFT are detailed by Horowitz (1993).
- (9) Design verification: The performance of the closed loop system with the synthesized prefilter $F(z)$ and controller $G(z)$, and the original nonlinear plant model needs to be checked in the time domain. This can be accomplished using simulation packages such as SIMULINK (2001).

4.3 Software Aspects

To implement the proposed procedure, a suite of MATLAB-based program has been developed at IIT, Bombay. This suite can be categorized in terms of the following sets of programs:

1. NLID: Performs automatic structure detection, parameter estimation and model validation of multivariable nonlinear systems, see Makwana (1995).

The underlying algorithms are based on the works of Billings and co-workers (see the references).

2. NLMIMO: Finds GFRFs and GDFs for multivariable NARX models identified using NLID, with at most second order terms, see Date (1995). Program handles step command inputs for a range of amplitudes, and up to three uncertain model coefficients. The LTIE templates generated are readily usable by QFT_IIT.

3. QFT_IIT: Performs robust feedback synthesis using QFT principles, see Nataraj (1994). A recent version incorporates a fully automated controller synthesis routine based on the numerous suggestions given by Horowitz (1993).

Using the integrated software package, the overall design cycle for the problem example given in sec. 5 took about 3 min. on a PC/Pentium-I 133 MHz. A major portion of this time was taken up by the MATLAB-based numerical integration routine QUAD8 called upon by NLMIMO. A more efficient numerical integration routine should considerably reduce the computation time, enabling the procedure to be executed fast enough for on-line QFT-based control of nonlinear processes.

5. SIMULATION EXAMPLE

5.1 Problem Description

We test our design algorithm on a nonlinear differential equation model of an isothermal CSTR described by Eaton and Rawlings (1990). The reaction occurring in CSTR is $2A \xrightarrow{k} B$ with (reaction rate) \propto (concentration of A)². Assuming that volume of liquid is constant, the mass balance equation is

$$V \frac{dC_A}{dt} = F_{in} [C_{Ain}(t) - C_A(t)] - KVC_A^2(t) \quad (11)$$

where K is related to the reactor temperature by $K = K_0 e^{-E/R_g T}$. Here, C_A is the concentration of reactant A , mol/lit., C_{Ain} is inlet concentration of A , mol/lit., F_{in} is the inlet flow, in mols/hr., T is reactor temperature, Kelvin, V is the volume of

vessel, liters, and E and R_g are physical constants. The input and output variables of CSTR are F_{in} and C_A , respectively. The reactor parameter values are $K = 0.972$ mol lit/hr., and $V = 10.0$ liters. The initial steady-state concentration of reactant A is 0.5 mol/lit., with the inlet concentration $C_{Ain} = 3.6$, and $F_{in} = 0.784$.

(11) is rewritten in terms of deviation variables with respect to the initial steady state values:

$$\frac{dy}{dt} = \frac{C_{Ain} - C_{A,s}}{V} u - \frac{F_{in,s} + 2KVC_{A,s}}{V} y - Ky^2 - \frac{1}{V} uy \quad (12)$$

where $y(t)$ and $u(t)$ are the deviations in C_A and F_{in} from their respective steady states $C_{A,s}$ and $F_{in,s}$. The reactor model (12) is used to generate input-output data set for identification purposes. The sampling time is taken as 0.01 hours. From this data set, a NARMAX model is first identified using program NLID described in sec. 4.3 and then a NARX model is extracted as

$$y(k) = \alpha y(k-1) + \beta u(k-1) - 0.0031u(k-1)y(k-1) \quad (13)$$

where $\alpha = 0.8858, \beta = 0.0156$.

Next, uncertainty is introduced into the reactor parameter values, which leads to the following bounds on the estimated NARX parameter values: $\alpha \in [0.7, 0.9], \beta \in [0.012, 0.018]$.

Based on the open loop responses, for a unit step in setpoint of C_A the closed loop specs are set as follows. Steady state offset at most 2%; Maximum overshoot: 10%; Minimum and maximum 2% settling times: 0.53 and 0.65 hours, respectively. These figures of merit are translated into the frequency domain via transfer function models. The translated frequency domain specs and the original time domain ones are shown as dotted lines in Figs. 2 and 3. Moreover, a gain margin of 5 dB and a phase margin of 45° are sought.

5.2 Design Execution

The design is executed as follows.

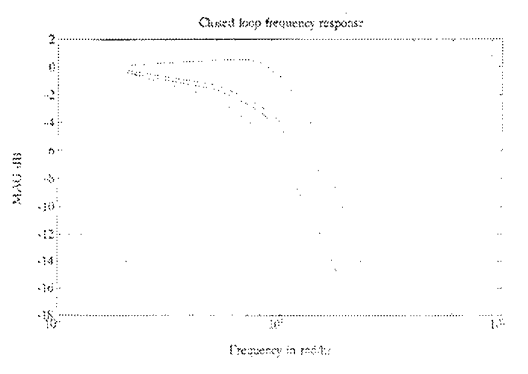


Fig. 2. The closed loop frequency responses

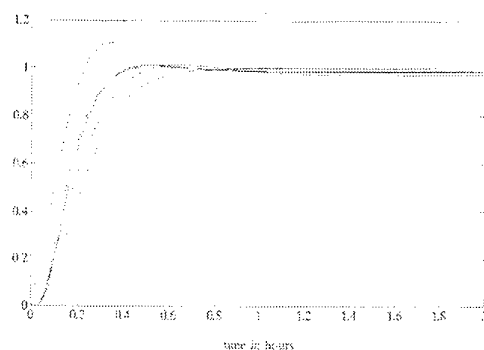


Fig. 3. The closed loop time responses obtained for the original reactor system.

1. For generating the LTIE templates corresponding to the obtained NARX model, first and second order GFRFs are used. Following step 4 of our procedure, the first two GFRFs are derived from (12) as

$$H_1(\exp(j\omega)) = \frac{\beta}{1 - \alpha \exp(-j\omega)}$$

$$H_2(\exp(j\omega_1), \exp(j\omega_2 - \omega_1)) = \frac{0.0031 \exp(-j\omega_2) H_1(\exp(j\omega_2))}{1 - \alpha \exp(-j\omega_2)} \quad (14)$$

Continuing the procedure until step 6 and using the equation

$$N(j\omega) = \frac{1}{U(j\omega)} [Y_1(j\omega) + Y_2(j\omega)]$$

the GDF is evaluated over the design frequency range. At each frequency, $N(j\omega)$ is a function of uncertain parameters α and β . Thus, by evaluating $N(j\omega)$ at different value sets of the reactor parameters, the LTIE plant template at each frequency

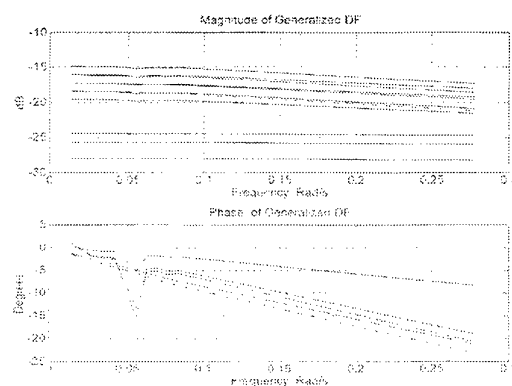


Fig. 4. Frequency responses of some LTIE plants. Dotted lines is for the linear transfer function H_1 .

is got (cf. step 7). Program NLMIMO describe in sec. 4.3 is used to automate these computations. The frequency responses of the LTIE plants are plotted in Fig. 4.

An important condition to be satisfied by the plant family is that the plant templates must be topologically path connected, see Nwokah and Thompson (1989).

This condition is checked for our example as follows: From the expressions for H_1 , H_2 in (14), and from (7), (8), it is seen that the domains of $Y_1(j\omega)$ and $Y_2(j\omega)$ are path connected sets, and that $Y_1(j\omega)$, $Y_2(j\omega)$ are continuous functions. Since a continuous image of a path connected set is path connected, it follows that the templates generated from (10) are indeed path connected.

For further work, the nominal plant is arbitrarily taken as the linear transfer function $H_1(\cdot)$ with $\alpha = 0.8858$, $\beta = 0.0156$.

2. The robust margin bounds and the discrete-time tracking bounds on a nominal loop transmission $L_0^*(s)$ are derived from the specs stated in sec. 5.1.

3. The synthesis of a $G(z)$ that satisfies these bounds and of an appropriate prefilter $F(z)$ is carried out using the QFT_IIT toolbox. Using the QFT_IIT tool box, a controller is obtained as

$$G_{num}(z) = 1.52z^6 + 3.29z^5 - 0.72z^4 - 5.50z^3 - 1.98z^2 + 2.29z + 1.26$$

$$\begin{aligned}
G_{den}(z) &= z^6 - 1.49z^5 - 0.20z^4 + 1.21z^3 \\
&\quad - 0.8z^2 + 0.28z - 0.00015 \\
G(z) &= G_{num}(z) / G_{den}(z)
\end{aligned} \tag{15}$$

and a prefilter as

$$\begin{aligned}
F_{num}(z) &= 0.00472z^2 + 0.0094z + 0.0047 \\
F_{den}(z) &= z^2 - 1.71z + 7.25 \\
F(z) &= F_{num}(z) / F_{den}(z)
\end{aligned} \tag{16}$$

5.3 Design Verification

Since our proposed method is based on GDFs an error analysis for the validity of the describing function approximation is necessary, see Bergen, *et al.* (1982) and Mees and Bergen (1975). The analysis is carried out as given by Nataraj, *et al.* (1997), and verifies closed loop stability.

Before proceeding to time domain design verifications with the $G(z)$ and $F(z)$ obtained above, the closed loop frequency responses are first checked. Fig. 2 (dotted lines are the specs) shows that, over the entire range of NARX model parameters α, β , these specs are satisfactorily met in the frequency domain.

Closed loop time domain simulation studies on the nonlinear reactor model are performed using the simulation package SIMULINK. The setpoint on C_A is changed by a step of unit magnitude, and the closed loop time responses for different reactor parameter values are obtained (see Fig. 3). Over the entire range of parameter uncertainty, the reactor concentration responses (solid line figure, nearly single) are seen to be well within the time domain specs.

6. CONCLUSIONS

A new synthesis procedure for robust control of nonlinear sampled-data systems has been proposed. This procedure uses generalized describing function to characterize a given NARX model. Robust controller design is carried out using principles of nonlinear QFT. The proposed procedure enables one to apply QFT methods to the widely

used polynomial NARMAX models. A simulation example of a nonlinear reactor model has been solved using the proposed procedure. The results have been found to be quite satisfactory.

REFERENCES

- Chen, S. and S. A. Billings (1989). Representation of nonlinear systems: the NARMAX model. *International Journal of Control*, **49**, 1013-1032.
- Date P. (1995). *Robust control of nonlinear chemical processes*. M.Tech Thesis, Indian Institute of Technology, Bombay, India.
- Eaton J. and J. Rawlings (1990). Feedback control of chemical process using on-line optimization techniques. *Computers and Chemical Engineering*, **14**, pp. 469-49.
- Horowitz, I. (1976). Synthesis of feedback systems with nonlinear time-varying uncertain plants to satisfy quantitative performance specifications. *Proc. IEEE*, **64**, pp. 123-130.
- Horowitz, I. (1993). *Quantitative feedback design theory, Vol. 1*. QFT publications, Boulder, Colorado, U.S.A.
- Horowitz, I. and Y. K. Liao (1986). Quantitative feedback design for sampled-data systems. *International Journal of Control*, **44**, pp. 665-675.
- Ioinovici, A. (1987). Application of the quantitative synthesis of feedback systems with uncertain nonlinear plants, *International Journal of Control*, **45**.
- Jones, J. C. and S. A. Billings (1989). Recursive algorithm for computing the frequency response of a class of nonlinear difference equation models. *International Journal of Control*, **50**, pp. 1925-1940.
- Jones, J. C. and S. A. Billings (1991). Describing functions, Volterra series and the analysis of nonlinear systems in frequency domain. *International Journal of Control*, **53**, pp. 871-887.
- Korenberg, M., S. A. Billings, Y. P. Liu, and P. J. McElroy (1988). Orthogonal parameter estimation

algorithm for nonlinear stochastic systems. *International Journal of Control*, **48**, pp. 193-210.

Makwana, K.G. (1995). *A MATLAB-based nonlinear systems identification toolbox*, M. Tech Thesis, Indian Institute of Technology, Bombay, India.

Mees, A. I. and A. R. Bergen (1975). Describing functions revisited, *IEEE Trans. Autom. Control*, **20**, pp. 473-478.

Nataraj, P. S. V. (1994). A MATLAB-based toolbox for synthesis of lumped linear and nonlinear and linear distributed systems. *Proc. IEEE/IFAC symposium on Computer aided Control System Design*, Tucson, Arizona.

Nataraj, P. S. V., P. Date, and A. Umrani (1997). Robust feedback synthesis for nonlinear integrodifferential equation models using generalized describing functions. *Automatica*, **33**, pp. 959-962.

Nwokah, O. D. I. and D. F. Thompson (1989), Algebraic and topological aspects of quantitative feedback theory, *International Journal of Control*, **50**, pp. 1057-1069.

Simulink (2001). *Simulink User's Guide*. The MathWorks Inc., Massachusetts, U. S. A.

Permission granted by John Wiley & Sons for the publication of this article in the Symposium
Proceedings. This article will be published in THE INTERNATIONAL JOURNAL OF ROBUST
and NONLINEAR CONTROL 2002 Issue

HOROWITZ: BRIDGING THE GAP

Constantine H. Houpis, Professor Emeritus

*Air Force Institute of Technology
Wright-Patterson AFB, OH, U.S.A.*

Abstract: This paper illustrates how Professor Horowitz's continual stress of his phrase "the transparency of QFT" is the foundation of what is felt by many to be a requirement in the enhancement of the future progress of the state-of-the-art developments for the 21st century, that is: "Bridging the gap between theory and the real-world."

Keywords: Quantitative Feedback Theory; Transparency of QFT; Bridging the Gap; robust multivariable control theory; structured and unstructured parametric uncertainty.

1. INTRODUCTION

As control theory was being developed in late 1940 through the '50's one of the many items of concern was how to design control systems for plants that are strongly nonlinear. Since then, many design methods have been developed for such plants. The principal features of Quantitative Feedback Theory (QFT) appeared in an article by Professor Isaac Horowitz in 1959. In developing QFT, Professor Horowitz felt that there was a need for a control system design technique that control system design engineers could readily understand and apply. Also, for a technique that a control system design engineer would be able to have a "handle on the patient's pulse" throughout each step of the design process, and be able to handle structured plant parameter uncertainty as well as unstructured plant uncertainty. Thus, along with his graduate students, since 1959, he has developed such a technique: QFT.

Through these past many years Horowitz has continually stressed the *transparency of QFT*; that is the ability to visually relate the implementation of the design parameters to the real-world problem, from the *onset* of the design, and throughout the individual design steps.

During the '70's Professor Horowitz received U. S. Air Force contracts that brought him in contact with the control community at Wright-Patterson Air Force Base. One of these contracts was with the Air Force Wright Laboratory (AFWL) Flight Dynamics Directorate's Control System Development Branch (AFWL/FIGL). By 1981 the Branch Chief, Mr. Evard H. Flinn, and his control system engineers, Mr. Duane Rubertus and Mr. Phil Chandler, all felt that QFT was a powerful multivariable nonlinear control system design technique for plants having structured parameter uncertainties. Mr. Flinn asked Professor Houpis, a Senior Research Associate to his Branch, and as a Professor at the Air Force Institute of

Technology (AFIT), that he, along with his graduate students, become involved with Professor Horowitz in applying QFT to flight control problems. Also, to assist Horowitz in expanding his technique. He felt that the publication of the results of these theses in technical journals and in textbooks would help to further elucidate and expand the utilization of this nonlinear design technique.

2. JOINT AFWL/FIGL-AFIT HOROWITZ YEARS

The years of 1982-1992 were a very productive QFT period. The first few years Professor Horowitz, under AFWL/FIGL contract, annually taught an AFIT course on QFT and was a co-thesis advisor with Houppis to M.S. thesis students. During the latter part of this period, with the suggestion to look into state-of-the-art topics proposed by individuals in the aerospace industry, the QFT technique was applied by Horowitz and Houppis and by their theses students to the design of flight control systems. These topics involved the utilization of thrust vectoring and high angle-of-attack flight.

During this period Horowitz amazed all those who were closely involved with him with the breadth and knowledge that he had, not only in control theory but in the field of mathematics. During one of the weekly thesis committee meetings with a thesis student he said "out of the clear blue sky" to the student "use the Binet-Cauchy theorem." Nowhere in his QFT publications had he made any reference to this theorem. In searching through countless linear algebra texts and inquires, no one was aware of this theorem. After prodding Isaac he finally remembered the text that discussed this theorem.

The European control community is a strong advocate of the frequency domain approach for control system analysis and synthesis. Thus, they recognized the potential of applying QFT, a frequency domain technique, to nonlinear control systems containing structured and unstructured parametric uncertainty. As a consequence, a QFT paper was presented at the International Control Conference 88 at Oxford University, Oxford, England (Horowitz, *et al*, 1988)

The productive association of AFWL/FIGL and AFIT with Professor Horowitz attracted the attention of the late Professor Osita D. I. Nwokah and his doctoral student David Thompson starting in the summer of 1988. Through Professor Nwokah's efforts the first QFT session at a technical conference was held at the 1990 CDC held in San Diego, CA. Since then QFT sessions have been held at other technical conferences.

A heightened awareness of Professor Horowitz's contributions to the state-of-the art of control theory

resulted through this association and the presentation of numerous papers by QFT researchers at technical conferences. With support of AFWL the first QFT symposium was held at Wright-Patterson AFB, OH. The purpose of this QFT symposium was a testimonial to the founder of QFT and to the numerous QFT researchers. Many of their results were transferred to the general public (Houppis, *et al*, 1992). Throughout this period of association Professor Horowitz exemplified the essence of the following anonymous quote:

"In **THEORY** (scientist)

There is no difference between theory and practice.

In **PRACTICE** (engineer)

There is a difference between practice and theory."

Thus, an engineer who has a firm understanding of the results of the "scientific method" and has a firm understanding of the nature and characteristics of the plant to be controlled must be able to *Bridge the Gap* between theory and practice. The essence of *Bridging the Gap* is brought out in the following sections (see Houppis and Rasmussen, 1999).

3. UNMANNED RESEARCH VEHICLE (URV)

During the latter part of the 20th century the Control System Development Branch of the Air Force Research Laboratory (AFRL/VACC) was responsible for the design, simulation, and flight testing of digital flight control systems for Uninhabited Research Vehicles (URV). Because of the close R&D collaboration of the Branch with AFIT faculty, a number of AFIT M.S. thesis students were involved in the QFT design of digital flight control systems for the Lambda URV shown in Fig. 1 (Houppis, *et al*, 1992). The objectives of the project described in this section were as follows:

1. To design robust flight control systems using the QFT design technique to satisfy the desired performance specifications.
2. To flight test these designs.
3. To implement an inner loop flight control system (FCS) on the Lambda URV that would be part of an autonomous flight control system.
4. To illustrate some of the real-world problems that are encountered in performing the control system design process.

Accomplishing this design project required four cycles around the control design process loop. These four design cycles were:

Cycle 1 – This cycle involved the satisfaction of only the first two of the project objectives.

Cycle 2 – Cycle 1 was repeated but involved the design of an improved integrator wind-up limiter.

Cycle 3 – A redesign of the FCS was accomplished to satisfy requirements 1 through 3.

Cycle 4 – A refinement of the plant model was made in order to take into account a bending mode that was neglected in the previous designs.

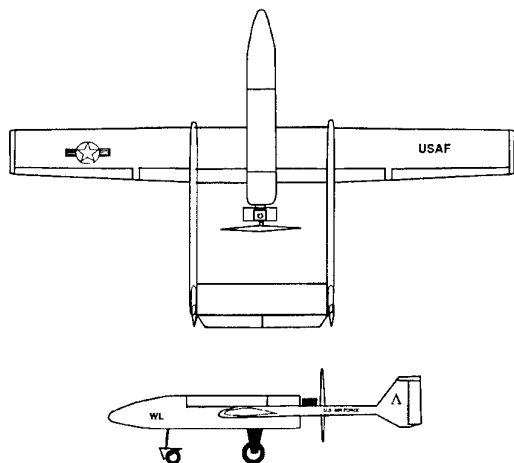


Fig. 1 Lambda Uninhabited Research Vehicle (URV).

Cycles 1 and 3 were unsuccessful and cycles 2 and 4 produced successful flight tests.

This R&D effort involved the following design steps (Houpis and Rasmussen, 1999):

- (1) Prescribing the desired flight scenario.
- (2) Prescribing the desired performance specifications
- (3) Obtaining the required number of plant models
- (4) The QFT design of the digital flight control system
- (5) The linear off-line design simulation
- (6) The nonlinear off-line simulation
- (7) The hardware-in-the-loop simulation/implementation in the laboratory
- (8) Flight testing

Two QFT designs for Cycle 1 were required to satisfy design objectives 1 and 2. The nonlinear and hardware-in-the-loop simulations of the first design revealed that system noise needed to be minimized and the accuracy of the software implementation design needed to be improved. Thus, the second QFT design involved in achieving a lower gain (see Sec. 9-3.7: Houpis and Rasmussen, 1999) and the utilization of an improved software algorithm implementation (see Sec. 9-3.12: Houpis and Rasmussen, 1999) in order to enhance the controller's numerical accuracy. The flight test of the second QFT URV flight control system design revealed that there existed a reversed polarity on an angle sensor and the integrator wind-up limiter design that was implemented did not work. Cycle 2, utilizing the second QFT design of Cycle 1, involved an improved wind-up limiter design and the correction to the sensor polarity. With these

improvements a successful second flight test was achieved

For Cycle 3 a new QFT design was accomplished that involved the use of a hardware noise filter and its implementation to minimize system noise and to satisfy design objective 3. Based upon satisfactory simulations a third flight test was made that revealed that an unmodeled longitudinal bending mode existed - thus the flight was aborted. Because the bandwidth requirement of the first two QFT designs was low enough, the bending mode did not affect the second flight test.

Based on test data from the third flight test, the bending mode was modelled and incorporated in the fourth QFT design process of Cycle 4. The fourth flight test of the final URV flight control system design that was implemented met all requirements. All of these four QFT design cycles demonstrated what Horowitz has continually stressed: the *transparency of QFT*; that is the ability to visually relate the implementation of the design parameters to the real-world problem, from the *onset* of the design and throughout the individual design steps.

4. VISTA F-16 SUBSONIC ENVELOPE DESIGN

This QFT design example, as did the previous example, exemplifies two important features: *transparency of QFT* and *Bridging the Gap*. Throughout his years of exposing QFT, Horowitz always stressed the former; that is, the ability to visually relate the implementation of the design parameters to the real-world problem, from the onset of the design and throughout the individual design steps. Both of these features were involved in the design of a flight control system for the UAV and for the VISTA F-16 shown in Fig. 2 (Phillips, *et al*, 1995).

At the *onset* of the student's (Major Scott Phillips, an F-16 pilot) VISTA F-16 QFT design, he determined from the size of his QFT templates that a robust design with a fixed set of controllers could *not* be achieved thanks to *the transparency of QFT*. As a consequence, he proceeded to achieve a gain scheduling QFT design. This design required the determination of the manner in which the gain scheduling was to be accomplished. During the process of achieving this design Major Phillips told his thesis committee the following:

"I can tell from the feeling at the seat of my pants, as a pilot, when the gain must be changed."

Based upon *this feel of the seat of his pants* he developed a graph that determined at what point during the flight scenario a gain change needed to be

done. Thus, he was able to utilize his real-world knowledge of the aircraft and its handling qualities to achieve the desired robust FCS. This situation typifies the second feature *Bridging the Gap*.

The design of this FCS involved the six design steps listed in Sec. III. Based upon the successful computer simulations the design was implemented and flown by Major Phillips on AFRL/VACC Lamars flight test facility. The flight test results verified that the performance specifications were met and the flying qualities were to Major Phillips' satisfaction. Based upon the results of this thesis a follow-on full envelope QFT FCS design was satisfactorily achieved by another graduate student (Reynolds, *et al*, 1996).

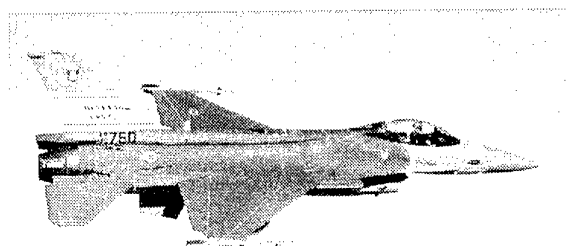


Fig. 2 VISTA F-16

5. UNSTRUCTURED PLANT PARAMETER UNCERTAINTY

The previous examples have dealt with QFT designs dealing with structured plant parameter uncertainty. Dr. Anthony Bentley illustrated in his article (Houpis, *et al*, 1992) how Horowitz's QFT technique can be applied to nonlinear SISO systems having unstructured plant parameter uncertainty.

6. HOROWITZ'S QFT TRANSPARENCY AND BRIDGING THE GAP

The impetus of the QFT R&D that was achieved through the AFWL/FIGL-AFIT association was continued through the association with AFIT Professor Meir Pachter (a flight control specialist and a colleague of Houpis) with AFRL/VACC since 1992. In a student's QFT flight control system design the student brought to the attention of his thesis committee that in his Bode plots of his t_{ij} control ratios spikes occurred which penetrated the upper specified τ_{ij} control ratio bound in the low frequency range of the desired loop bandwidth. Professor Pachter, because of his aeronautical background, exemplified Horowitz's exposition of the *transparency of QFT*. His immediate response was: "the spikes are

due to the phugoid mode of the aircraft and will note effect the aircraft's desired response." Naturally, the student was greatly relieved!

As stated in Section 2, an engineer who has a firm understanding of the results of the "scientific method" and has a firm understanding of the nature and characteristics of the plant to be controlled must be able to *Bridge the Gap* between theory and practice. This concept led to the development of QFT Engineering Rules (E.R.s) (Houpis and Rasmussen, 1999). This "*Bridging the Gap*" was also demonstrated by Major Phillips as noted in the previous section.

7. SUMMARY

The anonymous quotation, given in Section 2, during the 1990's, was best illustrated by the thoughts of control system design engineers and educators throughout the international control community. They strongly believed that in facing the technological problems of the 21st century, it is necessary that engineers of the future must be able to *bridge the gap* between the scientific and engineering methods. As indicated in the previous sections, Professor Horowitz exemplified this concept by his development of QFT.

Horowitz's *transparency of QFT* and his QFT technique exemplified the concept of "*Bridging the Gap*" which are the essential aspects of the QFT control system design process illustrated in Fig. 3. The intent of this figure is to give the control system design engineer an overview of what is involved in achieving a successful and practical control system design. The aspects of this figure present the factors that help in *bridging the gap* between theory and the real-world. While accomplishing a practical control system design, the designer must keep in mind that the goal of the design process, besides achieving a satisfactory theoretical robust design, is to implement a control system which meets the functional requirements. In other words, during the design process one must keep the real world in mind. For instance, in performing the simulations, one must be able to interpret the results obtained, based upon a knowledge of what can be reasonably expected of the plant that is being controlled. For example, in performing a time simulation of an aircraft's transient response to a pilot's maneuvering command to the flight control system, the *simulation run time* may need to be only 5 s since by that time a pilot would have instituted a new command signal. If within this 5 s window the performance specifications are satisfied, then it will be deemed that a successful design has been achieved. However, if the performance of interest is the steady-state response, then the simulation run-time must be considerably longer.

Achieving a satisfactory multivariable robust control system design for a nonlinear system is a difficult problem. There are a number of nonlinear control system design techniques for handling nonlinear control systems, many of which are highly mathematical. Professor Horowitz developed a control system QFT design technique that control system design engineers could readily understand and apply. Also a technique that a control system

designengineer would be able to have a "handle on the patient's pulse" throughout each step of the design process, and be able to handle structured plant parameter uncertainty. The contributions (Horowitz, 1991) of Professor Horowitz led to the development of the "QFT control system design process of bridging the gap."

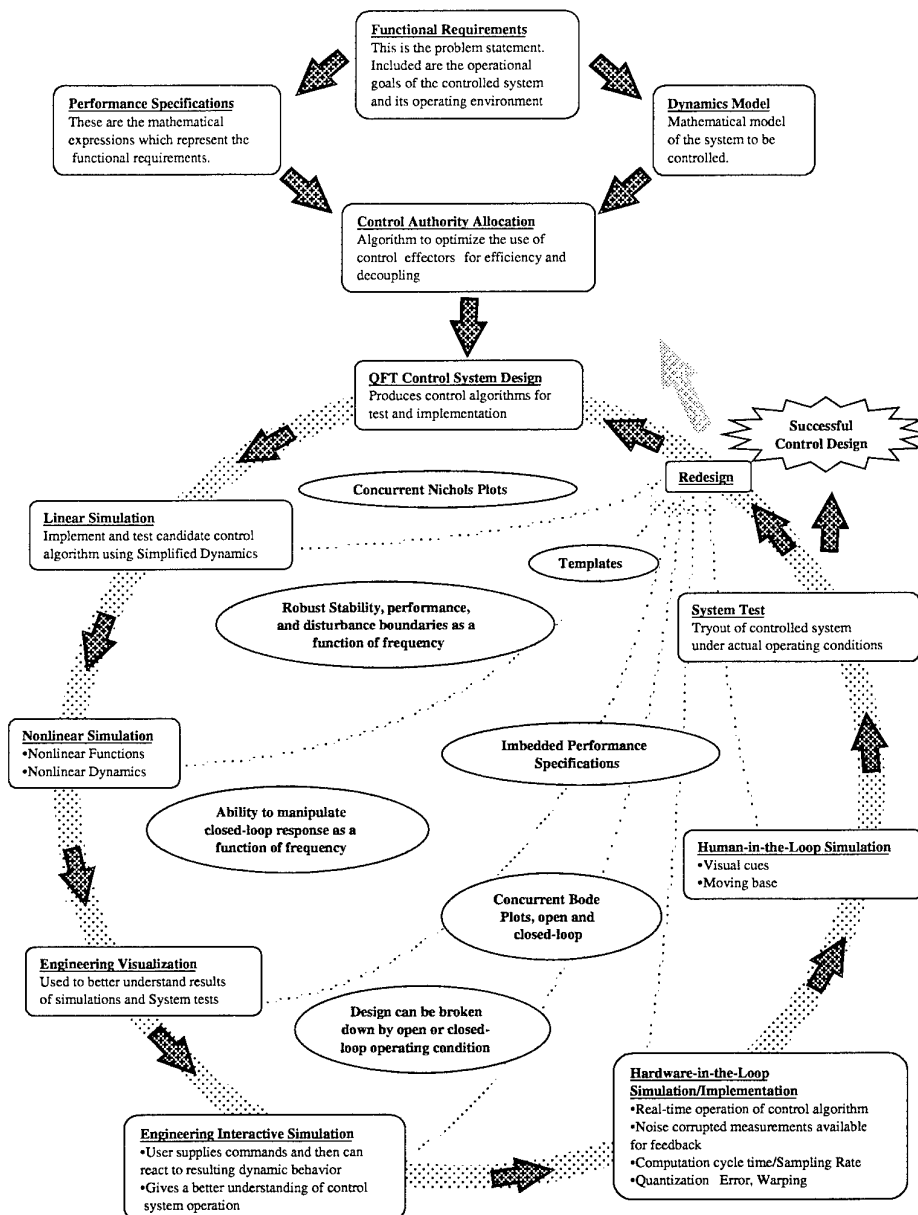


Fig. 3 The QFT control system design process: bridging the gap.

REFERENCES

- Horowitz, I. M. (Dec. 1959). Fundamental Theory of Linear Feedback Control Systems, *Trans. IRE*, AC-4
- Horowitz, I. M., S. H. Wang, and C. H. Houpis (1988). Quantitative Design for Systems with Uncertainty and Control Failures, *Proceedings of the Int. Control Conference 88*, Oxford University, Oxford, England.
- Horowitz, I. M. (1991). Survey of Quantitative Feedback Theory (QFT), *Int. J. of Control*, vol. **53**, No. 2, pp. 255-291.
- Houpis, C. H. and P. R. Chandler, Editors (1992). *Quantitative Feedback Theory Symposium Proceedings*, WL-TR-92-3063, Wright Laboratories, Wright-Patterson AFB, OH.
- Houpis, C. H. and S. J. Rasmussen (1999). *QUANTITATIVE FEEDBACK THEORY Fundamentals and Applications*, Marcel Dekker, NY.
- Phillips, S., M. Pachter, and C. H. Houpis (May 1995). A QFT Subsonic Envelope Flight Control System Design, *National Aerospace Electronics Conference (NAECON)*, Dayton, OH.
- Reynolds, O., C. H. Houpis, and M. Pachter (1996). Full Envelope Flight Control System Design Using QFT, *AIAA J. of Guidance, Control and Dynamics*, Vol. **19**, No. 1.

INTERVAL QFT: A MATHEMATICAL AND COMPUTATIONAL ENHANCEMENT OF QFT

P. S. V. Nataraj, S. Sheela, and A. K. Prakash

*Systems and Control Engineering, Dept. of Electrical Engineering,
Indian Institute of Technology, Bombay, India. 400 076
Email: nataraj@ee.iitb.ernet.in*

Abstract: The paper presents an overview of a mathematical and computational enhancement of Horowitz's QFT design procedure. The enhancement uses methods of interval analysis and is called as interval QFT, or IQFT. IQFT addresses and solves some of the fundamental issues in QFT, concerning selection of design frequencies, selection of controller phases in bound generation, approximation of plant templates with finite plant sets, and generation of plant templates and controller bounds with reliability and to a prescribed accuracy. Several examples are presented to illustrate the key features of IQFT.

Keywords: Interval Analysis, Quantitative Feedback Theory, Robust Control.

1. INTRODUCTION

Over the last few decades, the quantitative feedback theory (QFT) approach of Horowitz (1993) to robust control system design has been gaining popularity among control researchers. The QFT approach comprises of a collection of techniques for dealing with several classes of uncertain plants: linear and nonlinear, time-invariant and time-varying, lumped and distributed, single input-output and multi input-output, single-loop and multiple-loop, etc. Recently, several researchers have shown that the QFT technique is more general and powerful than other robust control approaches, see for example, (Chait and Holot, 1990; Jayasuriya, 1993; Nwokah *et al.*, 1992; Yaniv and Horowitz, 1987; Zhao and Jaisuriya, 1998).

The QFT approach (like all other robust control approaches) is based on mappings involving *point* numbers. It is the thesis of this paper that several key

enhancements to the *point* QFT approach can be obtained by adopting a fundamentally different approach based on mappings involving *intervals*. The interval based QFT (IQFT) approach provides guarantees on the reliability and accuracy of the generated plant templates and controller bounds, and automatically produces error estimates. Further, the key issues of finite frequency selection in design frequency set formulation, finite plant approximation in template generation, and finite phase selection in bound generation are resolved in the IQFT approach.

The idea behind the interval analysis (IA) methods is to design algorithms, which in a single computation, do the approximation and a rigorous error analysis. With interval methods, one can directly deal with interval sets containing infinitely many points, and perform set operations such as subdivisions, unions, intersections, finding convex hulls, testing for set inclusion, testing for disjointedness of sets, etc. The

basis for the systematic approach of IA methods is to combine computer arithmetic with order relations. For details of IA and its methods, the reader is referred to the book of Moore (1979).

The IA approach to QFT, or IQFT, is being pursued in the interval mathematics - QFT group at IIT Bombay. IQFT can be applied to (perhaps) any problem that can be solved with point QFT methods, but is surprisingly richer in its consequences. These are summarized below.

Interval Analysis based Template Generation (IATG) algorithms provide several guarantees: the templates are (a) guaranteed to be of prescribed accuracy, (b) guaranteed to be reliable, despite all kinds of computational errors such as round-off, truncation, and approximation, (c) guaranteed to enclose all actual template points, thereby avoiding any loss of robustness due to template approximation errors.

Interval Analysis based Bound Generation (IABG) algorithms also provide several guarantees: the bounds are (a) guaranteed to be robust against template inaccuracies, in the sense that regardless of the accuracy of the interval plant template used these can never lead to violation of the specifications, (b) guaranteed to be robust against phase discretization, so that no blip in the bounds can lead to violation of the specifications, (c) guaranteed to be reliable, despite all kinds of computational errors, such as round off, truncation, and approximation; the algorithms also offer key improvements: (d) the bounds are obtainable usually in much less time, and (e) a *posteriori* error estimates are readily available from the bounds.

Before proceeding to describe IQFT methods, the various ways in which the design problems can be posed in QFT are first categorized.

1.1 Classes of QFT Design Problems

Class A problem: "Suppose the design frequency is given. Then, how may the QFT designer generate the plant template and compute the controller bounds so that the latter are guaranteed to be reliable over designer-selected controller phase intervals?"

On the other hand, at the given frequency, the QFT designer may wish to specify *a priori* the desired accuracy of the controller bounds, and leave it to the algorithm to automatically arrive at the appropriate controller phase intervals. This situation leads to the following problem class:

Class B problem: "Suppose the design frequency is given. Then, how may the QFT designer generate the plant template, and determine the controller phase

intervals with their corresponding controller bounds, so that the bounds are guaranteed to be reliable and have a prescribed accuracy?"

At an even more advanced level, the designer may wish to specify only the desired accuracy of the controller bounds, the range of design frequencies along with the desired spacing between the bounds, and leave it to the algorithm to automatically determine whatever frequency and controller phase intervals are appropriate. This situation leads to the following problem:

Class C problem: "Suppose the design frequency range is given. Then, how may the QFT designer determine the frequency intervals, the controller phase intervals, and generate the plant templates, so that the bounds are guaranteed to be reliable, have a prescribed accuracy, and be spaced apart as desired?"

As described in the sequel, to solve problems of class A, the QFT designer can execute an IATG algorithm for generating the interval plant template and then apply an IABG algorithm to compute the controller bounds over designer-selected phase intervals (cf. section 4). To solve problems of classes B and C, the QFT designer can execute the appropriate *unified* procedure (cf. sections 5 and 6). The unified procedures combine template and bound generation steps for generating bounds of prescribed accuracy, and appropriate controller phase and design frequency intervals are determined automatically in the procedures. The issues of finite frequency and finite phase selection in point QFT are resolved in the unified procedures, along with the issue of finite plant approximation that troubles all point-based QFT methods of template and bound generation.

It is pertinent to note here why these issues (or difficulties) arise in the first place in QFT. According to Moore (1991, section 5), "Point methods and computations with ordinary *floating-point* numbers have no direct way of dealing with sets containing infinitely many or uncountably many points". Further, "using *point* methods, there may be no indication, let alone guarantee, of the accuracy or completeness of the results". As stated earlier, it is the thesis of this paper that the above mentioned issues in the *point* QFT approach can be resolved by adopting a fundamentally different approach to QFT using *interval-mappings* (rather than point-mappings).

The rest of this paper is organized as follows. In sections 2 and 3, an overview of the various IATG and IABG algorithms is given. In sections 4 through 6, procedures to solve design problems of class A, B, and C are outlined. In section 7, concluding remarks on IQFT are given.

All computations in this work are done on a PC / Pentium III 550 MHz machine using the interval arithmetic toolbox INTLAB of Rump (1999) that runs under MATLAB.

2. INTERVAL TEMPLATE GENERATION

Consider a plant represented by the transfer function $g(s, \lambda)$, where $\lambda = \{\lambda_1, \dots, \lambda_n\}$ is a real vector of the plant parameters and s is the Laplace variable. Suppose the parameters λ_i vary independently over given real intervals Λ_i^0 so that we have a box $\Lambda^0 = \{\Lambda_1^0 \dots \Lambda_n^0\}$ of plant parameters.

Denote the phase angle and magnitude functions of $g(s, \lambda)$ as $f_{\text{ang}}(\omega, \lambda) = \arg g(\omega, \lambda)$; $f_{\text{mag}}(\omega, \lambda) = |g(\omega, \lambda)|$, where ω is a given frequency. Define the angle - magnitude function f as $f(\omega, \lambda) = (f_{\text{ang}}(\omega, \lambda), f_{\text{mag}}(\omega, \lambda))$. Then, the set $G := \{f(\omega, \lambda), \lambda \in \Lambda^0\}$ defines a region in the angle-magnitude plane (i.e., in the Nichols chart), called the template of $g(s, \lambda)$ at the given ω .

Definition 2.1. *The expression which arises if each occurrence of λ in $f(\omega, \lambda)$ is replaced by Λ , if each occurrence of a pre-declared function (like \sin , \cos , \exp , etc.) is replaced by the corresponding pre-declared interval function, and if the arithmetic operations in $f(\omega, \lambda)$ are replaced by the corresponding interval arithmetic operations, is called the natural interval extension of $f(\omega, \lambda)$ to Λ . The natural interval extension of f to Λ is denoted as $F(\omega, \Lambda)$.*

One can compute $F(\omega, \Lambda)$ and obtain, with a single evaluation of F , a template comprising of a single angle-magnitude rectangle. By inclusion property of natural interval extensions (Moore, 1979, Theorem 3.1) encloses the actual template $G(\omega)$. However, this angle-magnitude rectangle $F(\omega, \Lambda)$ usually has a width that considerably exceeds the specified width ϵ . Therefore, one may repeatedly subdivide (or partition) the parameter box, find the evaluations of F over the sub-boxes using interval arithmetic, and take the union of the results to get templates comprising of smaller and smaller angle-magnitude rectangles which give increasingly accurate information about the actual phase-magnitude values. It is a fundamental result in interval analysis that as the partition of the parameter box is refined, these templates will converge to the actual template. The partition or subdivision process can be stopped when the widths of all the angle-magnitude rectangles is less than ϵ .

Depending on the way the subdivision is done, IATG algorithms can be cast into three categories, as follows.

2.1. IATG using Uniform Subdivision

The uniform subdivision process has been originally suggested by Moore (1979, sec. 4.1) in a general setting of finding the range of a function, and for QFT template generation by Sardar and Nataraj (1997), as follows.

First, find a uniform subdivision factor N for all parameter intervals, making use of an inequality relation in (Moore, 1979, equation 4.5). Then, subdivide each parameter interval into N equal subintervals with this subdivision factor, and create a so-called *uniform* subdivision partition. Lastly, evaluate $F(\omega, \Lambda)$ over the sub-boxes of the uniform partition, in a *parallel* manner, using vectorized operations. It can be shown from the work of Moore (1979, sec. 4.1) that every resulting angle-magnitude rectangle is of width at most ϵ , and that the collection of all these rectangles constitutes the required template, which necessarily contains the actual one.

The advantage of this algorithm is that it is a single step algorithm – the template can be generated with a single interval evaluation of F for each sub-box of the partition, and moreover, this can be done in a *parallel* manner for all the sub-boxes using vectorized interval arithmetic operations. The disadvantage of this algorithm is that N is usually heavily overestimated, due to overestimation in the Lipschitz constant calculation (Rall, 1981) and in Moore's inequality referred above. Consequently, a much larger number of sub-boxes than required will be generated with such a N . Therefore, it is clear that the amount of computational effort may be rather large in this algorithm, which may lead in turn to correspondingly large computation times.

2.2. IATG using Adaptive Subdivision

The adaptive subdivision process is also well-known in general setting of range finding in IA literature, see, for example, Kearfott (1987). Nataraj and Sardar (2000b) have also recently used it, together with the interval Gauss-Seidel method, for template generation as follows.

First, evaluate F over the current parameter box, and check the width of the resulting angle-magnitude rectangle against the specified maximum width. If the specified width is exceeded, then bisect the box into two sub-boxes by cutting in the coordinate direction in which the box is longest. Discard the original box. Pick any one of the two sub-boxes, and put the other sub-box in a processing list. Successively subdivide the picked (current) sub-box till the width of the resulting angle-magnitude rectangle is at most ϵ . Then, write the angle-magnitude information to a solution list, and discard the current sub-box. Repeat the above for all sub-boxes created in this process.

Finally, output the generated template as the collection of all angle-magnitude rectangles present in the solution list.

The advantage of this algorithm is that it generates a considerably much smaller number of angle-magnitude rectangles in the template, because a sub-box is successively subdivided into smaller sub-boxes only as long as the angle-magnitude rectangle width is unacceptable. This can therefore be viewed as an adaptive subdivision process. However, each sub-box is processed *sequentially*. Therefore, the algorithm generally takes considerably more time than the above one involving parallel computations.

2.3. IATG using Parallel-Adaptive Subdivision

The attractive feature of the uniform subdivision based approach is parallel evaluation of F over all sub-boxes of a partition; while that of the adaptive subdivision based approach is adaptive subdivision. An algorithm that combines these two advantageous features i.e., *parallel* functional evaluation and *adaptive* subdivision is the so-called parallel-adaptive (PA) algorithm by Nataraj and Sheela (2001b). The PA algorithm for template generation runs as follows.

In the first or initial iteration, create a partition by subdividing all parameter intervals into subintervals of nearly equal width. Then, perform parallel evaluation of F over the sub-boxes of the partition, and save all angle-magnitude rectangles, whose widths are less than ϵ in a solution list, discarding the corresponding sub-boxes from any further consideration. In the second and succeeding iterations (only those sub-boxes for which the corresponding angle-magnitude rectangles have unacceptable widths are left), cut simultaneously all sub-boxes in the *longest* direction, discard the original sub-boxes used for cutting, and perform parallel evaluation of F over the sub-boxes resulting from cutting. Save all angle-magnitude rectangles whose widths are less than ϵ in the solution list, discarding the corresponding parameter sub-boxes from any further consideration. Terminate the iterations when there are no more sub-boxes to deal with.

The advantage of the PA algorithm over the uniform subdivision algorithm is that the former usually generates a much smaller number of angle-magnitude rectangles. This is due to the usage of adaptive subdivision process in the former algorithm, which keeps the amount of computations to reasonable limits, and in turn results in significant reductions in computation times. In contrast, a much large number of sub-boxes are typically created in the uniform subdivision partition, due to heavy overestimation in the subdivision factor. This thereby leads to large execution times. The advantage of the PA algorithm

over the adaptive subdivision algorithm is that the former usually executes much faster since all sub-boxes under consideration are cut in parallel (i.e., simultaneously), F is evaluated in parallel over all the resulting sub-boxes. Recall that in the adaptive subdivision algorithm, the sub-boxes are adaptively cut and processed sequentially, which slows down the processing due to its sequential nature.

In several examples, the PA algorithm is found to be faster than the above two categories by 1-2 orders of magnitude, see Nataraj and Sheela (2001b). The efficiency of the PA algorithm, in terms of the final number of template rectangles generated and the algorithm execution time, is greatly influenced by the selection of the co-ordinate direction along which boxes are subdivided in each iteration. In the version of the PA algorithm just described, the rule of subdivision is to cut each box along its longest direction. However, in many examples it is observed that this subdivision rule merely increases the number of template rectangles without yielding any significant reduction in their widths. Therefore, to further improve upon the efficiency of the PA algorithm, more efficient subdivision rules need to be explored. These are next described.

2.4. IATG using Parallel-Adaptive with Other Subdivision Rules

In the so-called parallel-adaptive with back-tracking algorithm proposed by Sheela and Nataraj (2001b), the subdivision rule is to adaptively cut the boxes along a *favorable* direction, i.e., in a direction along which the width of F over the sub-boxes of partition is reduced at least by some acceptable percentage.

In the so-called parallel-adaptive with first-box algorithm proposed by Nataraj and Prakash (2001), the subdivision rule is as follows. In a given iteration, pick the first box from the list of parameter boxes to be processed and bisect it along the first co-ordinate direction to get two sub-boxes. Then, evaluate F over these sub-boxes, and find the maximum width of F . Repeat the process in all other co-ordinate directions, and determine the co-ordinate direction in which the corresponding maximum width of F is the least. This co-ordinate direction is then used as the direction for subdividing all boxes in the current iteration. The parallel-adaptive algorithm can also be based on other subdivision rules found in the literature on interval branch and bound algorithms for global optimization, see, for instance, Ratz and Csendes (1995).

2.5. Illustrative Examples

The PA algorithm with the various subdivision rules is applied to generate the interval plant templates on a suite of eleven transfer function examples listed in the Appendix. The templates of all transfer functions are generated to an accuracy of 1 deg. and 1 dB. The findings of this study are summarized in Table 1. In this Table, Rule A is the rule of subdivision along the longest co-ordinate direction used in the basic version of the PA algorithm. Rule B is the maximum smear rule in Ratz and Csendes (1995), and commonly used for global optimization. The number of uncertain parameters is given as n . A “-” in the Table indicates that the computer runs out of memory.

The performances with the various subdivision rules are compared, in terms of solution boxes and the execution time in seconds taken to generate these boxes. Summarizing the first-box subdivision rule is seen to be the best choice overall, in terms of consistency, number of template rectangles, and time taken

Table 1. Performances of Parallel-adaptive IATG and boundary extraction algorithms

	Example	n	Soln	Rule A	Rule B
1	Under damped	2	boxes time(s)	30,223 7.24	281,814 109
2	DC Motor	2	boxes time(s)	- -	3,048 4.11
3	Simple poles	3	boxes time(s)	7,712 3.27	627 1.88
4	Non-minimum phase	3	boxes time(s)	512 1.33	808 1.59
5	Non-rational	3	boxes time(s)	6,759 7.69	35,404 35.23
6	Electro-Mechanical	3	boxes time(s)	- -	- -
7	Vehicle clutch	3	boxes time(s)	30,424 6.09	3,109 2.15
8	Multiple lags	4	boxes time(s)	235,139 1.23e3	411,118 1.27e3
9	Mechanical	5	boxes time(s)	17,320 10.89	- -
10	Aircraft	5	boxes time(s)	40,002 10.73	966 1.92
11	Inv. pendulum	7	boxes time(s)	- -	208 1.312

Table 1 (Contd)

Ex.	Soln	Back-tracking	First-box	Boundary extraction
1	boxes time(s)	25,526 3.5	32,201 4.86	1,053 16
2	boxes time(s)	2,451 1.5	2,860 1.11	285 0.4
3	boxes time(s)	459 0.74	627 0.46	128 0.08
4	boxes time(s)	504 0.3	512 0.4	138 0.08
5	boxes time(s)	6,759 3	6,891 3.55	436 2.9
6	boxes time(s)	84,466 16	92,608 21.99	1,604 84
7	boxes time(s)	2,644 0.79	2,844 1.81	319 0.6
8	boxes time(s)	170,448 633	189,903 10 ³	2369 70
9	boxes time(s)	1,751 1	1,981 0.99	579 0.8
10	boxes time(s)	642 1	1,508 1.06	131 0.1
11	boxes time(s)	194 0.7	208 0.64	101 0.05

2.6. Properties of IATG Algorithms

Mathematical reliability of the IATG algorithms readily follows from the existence of well-known theorems in interval analysis and usage of exact interval arithmetic in all computations. For instance, it follows immediately from the inclusion property of natural interval extensions (Moore, 1979, Theorem 3.1) that, for any $\epsilon > 0$, the generated templates indeed enclose the exact templates. Moreover, it is a fundamental result in interval analysis (Moore, 1979, Theorem 4.1) that as the partitions are refined, the enclosures will converge to the actual ranges of the values over the given domain sets. From this property, it follows that in the limiting case of the specified width equal to zero, IATG algorithms yield templates that converge to the exact templates. Further, for any finite $\epsilon > 0$, IATG algorithms generate the required templates in a *finite* number of steps. This can be shown by proceeding on similar lines to Kearfott (1987, Theorem 2.10). Lastly, rigorous justification of the subdivision processes in a general setting are given by Moore (1979) and Kearfott (1987).

Computational reliability of the IATG algorithms means that the algorithms are stable when implemented on floating-point systems. The IATG algorithms can be made computationally reliable by implementing them in any interval arithmetic compiler. An interval arithmetic compiler uses machine interval arithmetic (MIA) in all computations, see, for instance, (Klatte *et al.*, 1993).

Efficiency of implementation. IATG algorithms are efficient to implement as they are simple from a computer programmer's point of view, and as their performances are not sensitive to details of implementation or to any "tuning".

Range of application of IATG algorithms is very vast, as the algorithms are applicable to any programmable transfer function that is continuous in its parameters.

2.7. Boundary Extraction

Similar to the case of the point template, it can be shown that for a simply connected interval plant template only the boundary template rectangles need to be considered in designs. Now, the set of boundary rectangles of an interval plant template is obtainable as the union of upper, lower, left and right boundary rectangles in the Nichols chart (by upper boundary rectangles we mean the template rectangles with the maximum magnitude at each phase, and so on).

Nataraj and Sheela (2001a) present an algorithm to extract all the boundary rectangles from a given interval template, without introducing any kind of boundary approximations. The procedure given therein to extract upper boundary rectangles from an interval template is as follows: Start always by marking the rectangle forming the left end of the template as a boundary rectangle, and set it as *current* rectangle. Then, journey along the top edge of the current rectangle towards the right end, checking if any upward jump to a higher magnitude occurs on this journey. **IF yes**, mark the rectangle associated with the jump as a boundary rectangle, set it as *current* rectangle, and take the jump along the left side of the current rectangle to reach its top edge. Next, continue the journey along the top edge of the current rectangle towards the right end, and so on, as before. **IF no**, complete the journey to reach the right end of the top edge, and when the right end of the entire template itself is thereby reached, print out all the boundary rectangles and exit the procedure; otherwise, journey downwards along the right side of current rectangle to the next lower magnitude rectangle, mark the latter rectangle as a boundary rectangle, set it as *current* rectangle, and journey along the top edge of the current rectangle towards the right end, and so on, as before.

The procedure to extract lower boundary rectangles is the same as to that for upper boundary rectangles, except for a few obvious modifications, such as journeying along the bottom (instead of top) edge of each current rectangle, and checking for any downward (instead of upward) jumps to a lower (instead of upper) magnitude on the journey. The procedure to extract left and right boundary rectangles is derived by simply interchanging the roles of

magnitude and phase in the above procedures. Finally, the set of all boundary rectangles of the interval template is obtained by taking the union of the upper, lower, left and right boundary rectangles.

The results of boundary extraction obtained on the suite of eleven transfer function examples referred to earlier, are given in Table 1 in the last column. The Table shows that the proposed algorithm extracts the boundary rectangles quite efficiently in terms of computational time. Typically, the algorithm takes about 10-40 milliseconds to extract the boundary rectangles from a set of 100 interval template rectangles - indicating the efficiency of the boundary extraction algorithm.

3. INTERVAL BOUND GENERATION

In this section, IABG algorithms for the various specifications are described. The robust sensitivity reduction case is first taken up.

3.1 Robust sensitivity reduction

Consider the plant family $\{g(s, \lambda), \lambda \in \Lambda^0\}$ embedded into a single-loop system with controller $\kappa(s)$. Then, the robust sensitivity reduction specification (spec) at a given frequency ω is

$$|1 + \kappa(j\omega) \cdot g(j\omega, \lambda)|^{-1} \leq w_s(\omega), \quad \forall \lambda \in \Lambda^0$$

The quadratic constraints algorithm in (Chait and Yaniv, 1993) computes the bounds at ω as follows. Substituting the polar forms $\kappa = k e^{j\theta}$ and $g = g e^{j\phi}$ in the above spec and simplifying gives the quadratic inequality (dropping the argument $j\omega$),

$$g^2 k^2 + 2 g k \cos(x) + z_s \geq 0$$

where $z_s := 1 - 1/w_s^2$, $x := \theta + \phi$. The quantity x is the phase of the loop transmission function. Setting the LHS of above inequality to zero and solving for the roots gives

$$(1) \quad k_{root}^u, k_{root}^l := \left\{ \cos x + \sqrt{\cos^2 x - z_s} \right\} / g$$

Thus, for the plant g , the allowable magnitude range of the controller for satisfying the sensitivity reduction spec at θ is $[0, k_{root}^l] \cup [k_{root}^u, \infty)$. Then, for the entire template G the allowable magnitude range of the controller at θ $[0, k_{bound}^l] \cup [k_{bound}^u, \infty)$, where $k_{bound}^u = \max\{k_{root}^u\}$; $k_{bound}^l = \min\{k_{root}^l\}$. The quantities k_{bound}^u , k_{bound}^l are called as the upper and lower bounds on the controller magnitude at θ . The procedure can be repeated for all $\theta \in [-2\pi, 0]$ to obtain the bounds over the entire controller phase range.

The quadratic constraints approach generates bounds at point values of controller phase and frequencies, and is based on point plant templates. The quadratic constraints approach can be extended for generating bounds at interval values of controller phase, and even for interval frequencies, using interval templates, as described below.

It is assumed that in the sequel that all interval templates are closed and simply connected.

3.1.1. Computing the root intervals. Consider a template rectangle picked from the interval plant template at a given frequency ω , and denote its magnitude interval as G and phase interval as Φ . Let the controller phase be also an interval Θ . Then, substituting all these interval quantities in the RHS of (1) gives

$$(2) \quad K_{root}^u := \frac{Q_+}{G} := \frac{-\cos X + \sqrt{\cos^2 X - z_s}}{G}$$

$$K_{root}^l := \frac{Q_-}{G} := \frac{-\cos X - \sqrt{\cos^2 X - z_s}}{G}$$

where ,

$$(3) \quad X = \Theta + \Phi$$

By analogy with the point case, X is the phase interval of the loop transmission function, and K_{root}^u , K_{root}^l are the upper and lower root intervals at phase interval X for the considered template rectangle.

Computation of these root intervals directly from (2) using interval arithmetic produces overestimation, due to multiple occurrences of the intervals Θ and Φ in the functional expressions and the interval dependency effect. However, if the computations are done as per Theorem 2.2 in Nataraj and Sardar (2000a), then the exact values of the root intervals are obtained.

3.1.2. Computing the working phase interval. It is shown by Nataraj and Sardar (2000a) that any bound computations for this spec need to be performed only for those X belonging to the so-called working phase interval Y defined as

$$(4) \quad Y := -(\arccos(-\sqrt{z_s}), \arccos(\sqrt{z_s}) + \pi)$$

Elsewhere in the range $[-2\pi, 0]$, any controller magnitude is satisfactory to achieve the spec, so there is no need to compute the bounds at such phases.

3.1.3. Composing the bound intervals. Consider a template rectangle in the interval template. Using (2), the root intervals are computed at various X in the working phase range Y . From these X and using the phase interval Φ of template rectangle, the

corresponding controller phase intervals Θ are back-calculated from (3) and the root intervals at X are reassigned to the respective Θ . The obtained results are plotted in the Nichols chart as 2-dim interval vectors or rectangles given by (Θ, K_{root}^u) and (Θ, K_{root}^l) , with the controller phase intervals Θ on the x-axis and the root intervals on the y-axis.

The procedure is repeated for all template rectangles, to obtain a Nichols plot of the upper and lower root intervals versus controller phase intervals for the entire interval template.

At each Θ , the uppermost and lowermost root intervals are picked from this plot and designated as the upper and lower bound intervals. The remaining root intervals are discarded.

3.1.4. Composing bounds from bound intervals. At each Θ the upper and lower bounds are obtained as the maximum and minimum of the upper and lower bound intervals. Now, for any interval, the maximum and minimum occur at the right and left endpoints of the interval. Hence, the upper and lower bounds are simply the left and right endpoints of the respective bound intervals at each Θ .

3.1.5. Computational reliability. All computations described in this section (as elsewhere in this paper) are done using machine interval arithmetic, which automatically takes care of all kinds of computational errors, such as round off, truncation, and approximation. This produces bound values that are not only exact for the given interval plant template, but are also reliable.

3.1.6. IABG algorithm for robust sensitivity reduction specification. The main steps of the IABG algorithm in Nataraj and Sardar (2000a), called as Algorithm SRI, can now be outlined.

First, any of the IATG algorithms described in section 2 is used to generate the interval template at the given frequency, and the set of boundary template rectangles extracted from the template using the boundary extraction algorithm of Nataraj and Sheela (2001a).

Then, the working phase interval Y is found as per section 3.1.2, and subdivided into several phase subintervals of say, 5deg. phase widths.

Next, the root intervals are computed as per section 3.1.1 at each of these subintervals, and the bound intervals composed as per section 3.1.3.

Lastly, the bounds are composed from these bound intervals as per section 3.1.4.

3.2. Robust gain-phase margin specification

At a given frequency ω , the robust gain-phase margin specification can be written as

$$\kappa(j\omega).g(j\omega,\lambda) / (1+\kappa(j\omega).g(j\omega,\lambda)) \leq w_m(\omega), \forall \lambda \in \Lambda^0$$

The IABG algorithm for this spec, called as Algorithm RSBI in Nataraj and Sardar (2000a), is identical to the one in the preceding subsection, except for very some minor changes in the RHS expressions in (2).

3.3. Robust tracking specification

At a given frequency ω , the robust tracking specification can be written as

(5)

$$\frac{|\kappa(j\omega).g_i(j\omega,\lambda) / (1+\kappa(j\omega).g_i(j\omega,\lambda))|}{|\kappa(j\omega).g_k(j\omega,\lambda) / (1+\kappa(j\omega).g_k(j\omega,\lambda))|} \leq \delta(\omega),$$

for all pairs of plant elements g_i, g_k in the plant family. Consider an arbitrary but fixed pair of boundary rectangles and recall that G denotes the magnitude interval and Φ the phase interval of a template rectangle. Then, by substituting these quantities in (5) squaring both sides, and simplifying gives the quadratic inequality

$$\begin{aligned} & \left\{ G_i^2 G_k^2 \left(1 - \frac{1}{\delta^2} \right) \right\} k^2 + \\ & 2 \left\{ G_i^2 G_k \cos(\Phi_i + \Theta) - \frac{G_k G_i^2}{\delta^2} \cos(\Phi_k + \Theta) \right\} k + \\ & \left\{ G_k^2 - \frac{G_i^2}{\delta^2} \right\} \geq 0 \end{aligned}$$

Making the substitutions $X_1 = 1/G_i, X_2 = 1/G_k, X_3 = \Phi_i + \Theta, X_4 = \Phi_k + \Theta$ and solving the above with equality sign gives

(6)

$$K_{root}^u, K_{root}^l = ((X_2 \cos X_4 / \delta^2 - X_1 \cos X_3) \pm \text{Sqrt}((X_2 \cos X_4 / \delta^2 - X_1 \cos X_3)^2 - (1 - 1/\delta^2)(X_1^2 - X_2^2 / \delta^2))) / (1 - 1/\delta^2)$$

Thus, for the considered pair of boundary template rectangles, the allowable magnitude range of the controller at Θ is $[0, \min\{K_{root}^l\}] \cup [\max\{K_{root}^u\}, \infty)$. The allowable magnitude range of the controller at Θ for the entire interval plant template is obtained by taking the

intersection of the magnitude ranges over all pairs of boundary template rectangles.

Just as is the case with (2), direct interval arithmetic evaluation of (6) produces overestimated values of K_{root}^u and K_{root}^l , due to multiple occurrences of the intervals X_1, \dots, X_4 in the functional expressions and the interval dependency effect. However, by combining the concept of *monotonicity* with the tool of *subdivision*, the root intervals can be obtained directly and exactly, with no need for any initial guess values or algorithmic iterations (as in classical optimization methods). Then, the computed bounds also turn out to be exact for the given interval template. These ideas form the basis of the IABG algorithm in Nataraj (2001), called as Algorithm TSI that generates tracking bounds.

The procedures to solve various classes of QFT design problems are next given.

4. PROCEDURE FOR CLASS A PROBLEMS

At a given design frequency, any of the IATG algorithms mentioned in section 2 can be applied to generate the interval plant template, reliably and to a prescribed accuracy. The respective IABG algorithm in section 3 can then be applied to this interval plant template to compute the controller bounds over designer-selected phase intervals. This approach provides a solution to QFT design problems of class A.

4.1. Illustrative Example

Algorithm TSI mentioned in section 3.3 is illustrated on an aircraft example. At a given frequency ω , the interval template and the tracking bounds are generated to satisfy the robust tracking specification.

Example 4.1. The transfer function for the longitudinal motion of an aircraft in open-loop is given as Example 10 in the Appendix. The nominal values are as follows: $k_0=2, z_0=0.5, p_0=10, \omega_{n0}=6, \xi_0=0.8$. The tracking bounds for the above plant at $\omega=0.1$ with the tracking specification as $\delta=1.03$ are required. The controller phase intervals are to span the range $[-2\pi, 0]$ with a width of 5 deg.

Notes: The design frequency is selected as $\omega=0.1$. The controller phases at which bounds are to be generated are also selected (spaced 5deg. apart) as is usually done in point QFT methods. The accuracy of the bounds is not prescribed (only reliable bound values are wanted by the designer). This puts the design problem in class A.

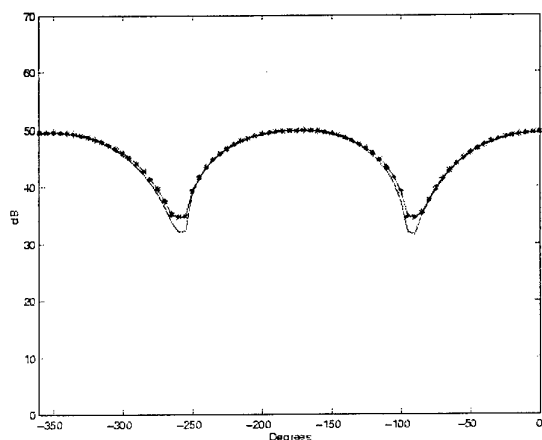


Figure 1. Inner (upper solid line) and outer (lower solid line) tracking bounds generated by IABG Algorithm TSI for the aircraft example at $\omega=0.1$. The stars denote the tracking bounds generated using the QFT toolbox. The QFT design problem is of class A.

Solution: The various steps of the solution are as follows. The interval template is generated at $\omega=0.1$ using the IATG algorithm of Sheela and Nataraj (2001b). This gives an interval plant template comprising of 70 rectangles, and takes 0.82 seconds and 85,480 *flops*. From the interval plant template, the set of boundary template rectangles is extracted using the algorithm in Nataraj and Sheela (2001a). This gives a set of 47 boundary template rectangles, and takes just 0.02 seconds and 88 *flops*. Algorithm TSI is applied to this set of boundary rectangles to generate the tracking bounds on the nominal loop transmission function $L_0(0.1j)=\kappa(0.1j) g_0(0.1j)$, as the plots on L_0 are usually preferred to those on $\kappa(\cdot)$ in QFT designs. Algorithm TSI takes 7.58 seconds and 5,817,592 *flops* and the resulting plot of tracking bounds on $L_0(0.1j)$ is shown in Figure 1 as the upper solid line.

For comparison, the algorithm available in the QFT toolbox is also applied. Each uncertain parameter is rastered at the minimum, mean and maximum values, as is the common practice in QFT. With such a rastering, the QFT toolbox gives a template consisting of $3^5=243$ plants. The bound generation algorithm in the QFT toolbox takes 234 seconds and 5,817,592 *flops*. Thus, the IABG algorithm TSI requires about 46 times less *flops* than the QFT toolbox algorithm, and executes about 31 times faster than the latter.

Comments on the error estimates: The lower solid line in Figure 1 is the so-called *outer* estimate of the tracking bounds. Using the outer and inner estimates, the maximum possible error at any particular phase is obtained as the difference between the corresponding inner and outer values.

The maximum possible error in the generated tracking bounds is the maximum of these differences over the entire phase range. From Figure 1, this is seen to be about 1.5 dB.

5. PROCEDURE FOR CLASS B PROBLEMS

IATG and IABG algorithms can be combined to form a unified procedure that solves QFT design problems of class B. The unified procedure in Nataraj and Sheela (2001c) produces controller bounds of prescribed accuracy, for the robust sensitivity reduction and robust gain-phase margin specification problems. Moreover, the proposed procedure also completely solves the problem of phase selection inherent in point QFT procedures.

To solve problems in this class, firstly an acceptable size of template rectangles needs to be determined and specified to the IATG algorithms, as follows.

5.1. Size of Template Rectangles for Class B

Let ϵ denote the desired accuracy of the bounds in dB, and let ϵ be split into two positive quantities ϵ_Q and ϵ_G such that their sum equals ϵ . Further, let the working phase interval Y be subdivided such that width of Q_{\pm} in (2) is at most ϵ_Q on every subdivision. Let \hat{w} denote the smallest width of these subdivisions.

Then, it is shown by Nataraj and Sheela (2001c) that an acceptable size of the interval plant template (for specifying to the IATG algorithms) is as follows: the magnitude and phase sides of each template rectangle have lengths at most ϵ_G and \hat{w} , respectively.

5.2. The Unified Procedure

The steps of the unified procedure for robust sensitivity reduction specification are

1. *Split the accuracy:* The accuracy ϵ is split into two positive quantities ϵ_Q and ϵ_G such that their sum equals ϵ .
2. *Subdivide working phase interval:* The working phase interval Y in (4) is successively bisected till over every subdivision of Y , the width (in dB) of function Q_{\pm} in (2) is at most ϵ_Q , where X denotes a subdivision. The smallest width of these subdivisions is denoted as \hat{w} .
3. *IATG Step:* Using any IATG algorithm mentioned in section 2 an interval plant template comprising of template rectangles

of prescribed size is generated: each template rectangle should have its magnitude side of length at most ϵ_G dB, and phase side of length at most \hat{w} . Then, the boundary template rectangles are extracted, while the rest are discarded.

4. *IABG Step* : Using the X intervals obtained above, the bound intervals are composed as in section 3.1.3, and then the bounds are composed from these bound intervals as in section 3.1.4.

The procedure is identical for the robust gain-phase margin specification, except that the respective algorithm is used in the IABG step above.

5.3. Illustrative Example for Class B Problems

The unified procedure is illustrated on a mechanical system, for generation of robust gain-phase margin bounds to a prescribed accuracy.

Example 5.1. The transfer function of a mechanical system is given as Example 9 in the Appendix. The design frequency is $\omega=8$, and the gain-phase margin spec is $w_m=2.3$ dB. The prescribed accuracy on the robust gain-phase margin bounds is $\epsilon=2.57$ dB.

Notes: The design frequency is selected as $\omega=8$. The controller phases at which bounds are to be generated, however, are not selected, but are rather left to be appropriately determined by the procedure. The accuracy of the bounds is, however, prescribed. This puts the design problem in class B.

Solution: The unified procedure is used to generate the gain-phase margin bounds of prescribed accuracy. Some details of the procedure are given below. The prescribed accuracy $\epsilon=2.57$ dB is split as $\epsilon_Q=1.57$, and $\epsilon_G=1$ dB, so that $\epsilon=\epsilon_Q+\epsilon_G$. The working phase interval is successively bisected into smaller intervals till the width of Q_{\pm} functions over each of these intervals does not exceed $\epsilon_Q=1.57$. The subdivision process takes about 0.3 seconds, and 15 subintervals are generated. The minimum width of the intervals is found as $\hat{w}=0.0137$ rads. Next, the interval plant template is generated using the parallel-adaptive with back-tracking algorithm given by Sheela and Nataraj (2001b). The acceptable size of each template rectangle is specified to this algorithm: each template rectangle should have its magnitude side of length at most equal $\epsilon_G=1$ dB, and its phase side of length at most equal to $\hat{w}=0.0137$ rads. The interval template is generated in about 1 second, as a collection of 1751 template rectangles. The boundary extraction algorithm of Nataraj and Sheela (2001a) extracts 579 boundary template rectangles, and takes about 0.8 seconds. IABG algorithm RSBI in Nataraj and Sardar (2000a) is executed to generate the controller bounds.

The time required for executing this step is about 3 seconds, and the total *flops* is 50,675. The results are plotted in Figure 2. (For comparison, the results of the QFT toolbox using a phase grid spaced 5deg apart are also plotted in the same figure, with marking '*').

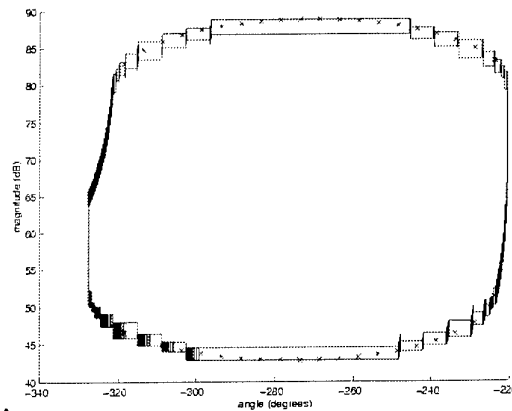


Figure 1. Robust gain-phase margin bounds for the mechanical system obtained using the Unified procedure. The specified bound accuracy is 2.57 dB, which is almost exactly achieved. Note that the phase intervals are of varying widths. The QFT design problem is of class B, with the frequency given as $\omega=0.8$.

Comments on the accuracy of the bounds: The maximum possible error in the generated bounds is readily obtainable from the widths of the plotted intervals in Figure 2. From Theorem A.1 in Nataraj and Sheela (2001c), the error in the generated bounds is no greater than the maximum width (measured along the y-axis) of the bound intervals. This maximum width is found to be 2.564 dB, and occurs for the upper bound interval [70.2686,72.8320] over the phase interval [-323.6288,-323.5905] deg, and for lower bound interval [56.6548,59.2187] over the phase interval [-221.5007,-221.4489] deg. Hence, the maximum error in the generated bounds does not exceed 2.564 dB. This maximum error is less than the prescribed accuracy of $\epsilon=2.57$ dB, confirming that the generated bounds are indeed of prescribed accuracy.

Comments on the automatic selection of phase intervals: The controller phase intervals plotted in Figure 2 are found to have varying widths, with the maximum width as 50 deg and the minimum width as 0.0002deg. The widths vary because the phase intervals are adaptively and automatically found in the unified procedure (in the subdivision step), so that bounds of prescribed accuracy can be generated. In contrast, in the point QFT procedures, the designer arbitrarily selects the controller phase points at which the bound values are to be generated. Thus, the unified procedure completely solves the problem associated with phase selection in the point QFT procedures.

6. PROCEDURE FOR CLASS C PROBLEMS

The developments given above for the point frequency case can be extended to the interval frequency case. Extensions of some key concepts are first outlined, followed by the procedure to solve class C problems.

Let Ω^0 denote the given design frequency range, and Ω denote a fixed but arbitrary frequency interval in Ω^0 .

Natural interval extensions. The natural interval extension in Definition 2.1 is extended for the interval frequency case as follows: The expression which arises if each occurrence of λ and ω in $f_{\text{mag}}(\omega, \lambda)$ is replaced by Λ and Ω , if each occurrence of a pre-declared function (like sin, cos, exp, etc.) is replaced by the corresponding pre-declared interval function, and if the arithmetic operations in $f_{\text{mag}}(\omega, \lambda)$ are replaced by the corresponding interval arithmetic operations, is called as the natural interval extension of $f_{\text{mag}}(\omega, \lambda)$ to Ω and Λ . The natural interval extension of f_{mag} is denoted as $F_{\text{mag}}(\Omega, \Lambda)$. Similarly for $F_{\text{ang}}(\Omega, \Lambda)$ and $F(\Omega, \Lambda)$.

Interval frequency plant template. By extension of the definition for the point frequency case, the plant template at frequency interval Ω can be defined as $G(\Omega) = \{f(\omega, \lambda), \lambda \in \Lambda^0, \omega \in \Omega\}$.

The plant template for the case of frequency interval can also be generated using any of the IATG algorithms in section 2, by considering Ω as just another interval parameter for purposes of subdivision. The resulting template is called as an interval frequency plant template. An interval frequency plant template also comprises of one or more phase-magnitude rectangles, called as template rectangles, just as for the point frequency case. A key property of the interval frequency plant template at Ω is that it always encloses the exact template $G(\Omega)$. That is, the interval frequency plant template at Ω contains all the points in the usual (point frequency) templates generated at all $\omega \in \Omega$.

Working phase interval. The working phase interval Y is now a function of frequency, as z_s depends on frequency through the spec. The working phase interval Y corresponding to the Ω under consideration can be found from (4).

Spacing the frequency intervals and the bounds. The designer can choose among various criteria for obtaining frequency intervals from the given design frequency range. The following criterion is chosen here. Let Ω' be an adjacent frequency interval to Ω . Then, the maximum of the upper bound at Ω and maximum of the upper bound at Ω' should be within

some specified distance or spacing, denoted T dB (note that the maximums of the bounds need not occur at the same Θ). This criterion can be written as (with all quantities in dB)

$$(7) \quad |\min F_{\text{mag}}(\Omega, \Lambda) - \min F_{\text{mag}}(\Omega', \Lambda)| \leq T - \beta$$

where F_{mag} is the natural interval extension of the plant magnitude function (cf. section 6.1), and β is the overestimation in F_{mag} . Similarly for the spacing between the minimums of the lower bounds at Ω and Ω' .

The above criterion is chosen just to illustrate the methodology of the proposed procedure. Other criteria can be specified by the designer to suit the needs of the problem, and the proposed procedure can be suitably adapted to achieve the ends.

6.1 The procedure

A unified procedure for obtaining gain-phase margin bounds is outlined below. The procedure generates bounds that are of prescribed accuracy ϵ dB, and spaced such that bounds of adjacent frequency intervals have their maximum magnitudes within T dB, and similarly for the minimum magnitudes.

The steps of the unified procedure for robust gain-phase margin specification are

1. *Split the accuracy:* The accuracy ϵ is split into two positive quantities ϵ_Q and ϵ_G such that their sum equals ϵ .
2. *Subdivide the design frequency range:* The design frequency range is successively bisected till (7) is achieved at each frequency interval Ω .
3. *Subdivide the working phase intervals:* At each frequency interval Ω , the following is done. The working phase interval Y in (4) is first computed. Then, Y is successively bisected till over each subdivision X , the width (in dB) of function Q_{\pm} in (2) is at most ϵ_Q . Lastly, the smallest width of these subdivisions is found and denoted as \hat{w} .
4. *IATG at each frequency interval:* For each frequency interval Ω , using any IATG algorithm an interval frequency plant template comprising of template rectangles of prescribed size is generated: each template rectangle should have its magnitude side of length at most ϵ_Q dB, and phase side of length at most \hat{w} . Then, the boundary template rectangles are extracted, while the rest are discarded from each interval frequency plant template.

5. *IABG at each frequency interval:* At each frequency interval Ω , using the X intervals obtained in step 3 above, the bound intervals are composed as in section 3.1.3 and then the bounds are composed from these bound intervals as in section 3.1.4.

6.2. Illustrative Example for class C problem

Example 6.1. The transfer function of a system found in active noise and vibration control is given as Example 1 in the Appendix. The system has highly under-damped resonance. The nominal parameters are $\omega_{n0}=0.75$ and $\zeta_0=0.02$. The robust gain-phase margin specification is $w_m=1.2$ dB. The design frequency range is $\Omega^0 = [0.5, 1.5]$. The objective is to generate the bounds with an accuracy $\epsilon=2.5$ dB and spacing $\Gamma=7.5$ dB (cf. equation 7) over the given design frequency range.

Notes: The design frequencies (as points or as intervals) and the controller phases at which bounds are to be generated are not selected here, but are rather left to be appropriately determined by the procedure. However, the design frequency range, the accuracy of the bounds, and the spacing between them are prescribed. This puts the design problem in class C.

The above unified procedure is applied to generate the robust stability bounds of prescribed accuracy and spacing. In Step 1, the prescribed accuracy $\epsilon=2.5$ dB is split as $\epsilon_Q=2.1$, $\epsilon_G=0.4$ dB, so that $\epsilon=\epsilon_Q + \epsilon_G$. In step 2, the given design frequency interval $\Omega^0 = [0.5, 1.5]$ is successively bisected till the spacing inequality in (7) is achieved at each frequency interval Ω . This step gave 17 frequency intervals listed in Table 2. Then, steps 3 and 4 are executed at each frequency interval to generate the interval frequency template and extract the boundary rectangles, as detailed in the earlier example. Lastly, the IABG algorithm for the robust gain-phase margin specification, Algorithm RSBI in Nataraj and Sardar (2000a), is applied to the boundary rectangles of the templates to generate the bounds at each frequency interval. The total time for these steps is about 300 seconds. For plotting purposes, the controller bounds are converted to those on the nominal loop transmission function $L_o(s)$. Figure 3 shows the plots of these bounds at selected frequency intervals Ω_4 , Ω_5 and Ω_6 (bounds only for selected frequencies are plotted, to avoid cluttering the figure).

Table 2. Design frequency intervals obtained by subdividing the given design frequency range in Example 6.1

$\Omega_1=[0.50,0.56]$	$\Omega_2=[0.56,0.62]$
$\Omega_3=[0.62,0.65]$	$\Omega_4=[0.65,0.68]$
$\Omega_5=[0.68,0.75]$	$\Omega_6=[0.75,0.78]$
$\Omega_7=[0.78,0.81]$	$\Omega_8=[0.81,0.84]$
$\Omega_9=[0.84,0.87]$	$\Omega_{10}=[0.87,0.90]$
$\Omega_{11}=[0.90,0.93]$	$\Omega_{12}=[0.93,1.00]$
$\Omega_{13}=[1.00,1.06]$	$\Omega_{14}=[1.06,1.12]$
$\Omega_{15}=[1.12,1.25]$	$\Omega_{16}=[1.24,1.37]$
$\Omega_{17}=[1.37,1.50]$	

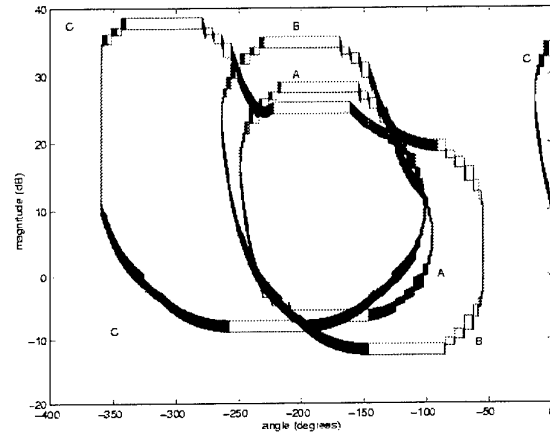


Figure 2. Robust gain-phase margin bounds for the under-damped system in Example 6.1. The bounds are generated by the unified procedure for class C problems. Seventeen design frequency intervals are automatically generated, but bounds for only 3 frequency intervals are plotted and marked as A - Ω_4 , B - Ω_5 , C - Ω_6 . The specified bound accuracy is 2.5 dB.

Comments on the automatic selection of frequency intervals: It is seen in Figure 3 that the frequency intervals are such that the spacing between the bounds (in the sense of section 6.4) is at most $\Gamma=7.5$ dB. Further, it is seen in Table 2 that the frequency intervals have different widths, with the maximum width as 0.13 and the minimum width as 0.03. The widths vary because the frequency intervals are automatically found in the unified procedure (in the subdivision Step 2), so that bounds of prescribed accuracy are generated.

In contrast, in the point QFT procedures, the designer (usually arbitrarily) selects the frequency values at which the design is to be performed. The unified procedure completely solves the difficulty of carefully analyzing and selecting design frequencies with the point QFT procedures. To emphasize this capability, note in Figure 3 that while proceeding from Ω_4

through Ω_6 , the bounds shift considerably rightward at Ω_5 . This phenomenon is important for loop-shaping, and the unified procedure captures it automatically. However, it is quite likely that this phenomenon would be missed in a designer-selected frequency set.

Comments on the accuracy of the bounds: The maximum possible error in the generated bounds is readily obtainable from the widths of the plotted intervals in Figure 3. It is seen from the figure that this maximum error is less than the prescribed accuracy of $\epsilon=2.5$ dB.

Comments on the automatic selection of phase intervals: The phase intervals plotted in Figure 3 have different widths at a given frequency interval. Further, the widths also vary with the frequency interval. The widths vary in this manner because they are adaptively and automatically found in the unified procedure (in the subdivision step 3), so that bounds of prescribed accuracy can be generated. In contrast, in the point QFT procedures, the designer arbitrarily selects the phase values at which the bounds are to be generated.

7. CONCLUDING REMARKS

It has been shown in this paper how IQFT lends rigor and reliability to Horowitz's basic QFT design technique. Several fundamental issues that have been so far treated in a rather ad-hoc manner in QFT, such as selection of design frequencies, phases, and plant parameter combinations, are treated in a systematic fashion in IQFT.

Much, however, remains to be added to the baggage of IQFT tools, even for the basic single input-output linear plant case. Preliminary work done by Vamsikrishna (2000) on loop-shaping using global optimization tools of IA has met with some success, but needs to be made computationally more efficient and tested on more examples. The computational verification of existence of a solution to the basic QFT design problem seems to be possible, and is an exciting prospect in IQFT. Further, the cases of multivariable and nonlinear plants are as yet untouched in IQFT.

REFERENCES

F. N. Bailey, D. Panzer, and G. Gu. (1988). Two algorithms for frequency domain design of control systems. *International Journal of Control*, **48**, 1787-1806.

C. Borghesani, Y. Chait and O. Yaniv. (1995). The quantitative feedback theory toolbox for Matlab, The MathWorks Inc., MA, USA.

Y. Chait, C. Borghesani and Y. Zheng. (1995). Single loop QFT design for robust performance in the presence of nonparametric uncertainties. *Trans. of the ASME Journal of Dynamic Systems, Measurement and Control*, **117**, 420-424.

Y. Chait and C. V. Hollot. (1990). A comparison between H-infinity methods and QFT for a SISO plant with both parametric uncertainty and performance specifications. In O.D.I. Nwokah, editor, *Recent developments in quantitative feedback theory*, 33-40.

Y. Chait and O. Yaniv. (1993). Multi-input /single-output computer-aided control design using quantitative feedback theory. *International Journal of Robust and Nonlinear Control*, **3**, 47-54.

W. Chen and D.J. Balance. (1999). Plant Template Generation for Uncertain Plants in QFT. *Trans. of the ASME Journal of Dynamic Systems, Measurement and Control*, **121**, 359-364.

B. Cohen, M. Nordin and P.O. Gutman. (1995). Recursive grid methods to compute value sets of transfer functions with parametric uncertainty. In *Proc. Of ACC*, 3861-3865.

I. M. Horowitz. (1991). Survey of quantitative feedback theory (QFT). *International Journal of Control*, **53**, 255-291.

I. M. Horowitz. (1993). *Quantitative feedback design theory (QFT)*. QFT Publications, Boulder, Colorado, USA.

S. Jayasuriya. (1993). Frequency domain design for robust performance under parametric, unstructured, or mixed uncertainties. *Trans. of the ASME journal of Dynamic Systems, Measurement and Control*, **115**, 439-451.

R. B. Kearfott. (1987). Abstract generalized bisection and cost bound. *Mathematics of computation*, **49**, 187-202.

R. B. Kearfott. (1987). Some tests of generalized bisection. *ACM Transactions on Mathematical Software*, **13**, 197-220.

R. Klatte, U.Kullisch, M. Neaga *et.al.* (1993). *PASCAL-XSC language reference with examples*. Springer-Verlag, Berlin.

R. E. Moore. (1979). *Methods and applications of interval analysis*. SIAM, Philadelphia.

R. E. Moore. (1991). Global optimization to prescribed accuracy. *Computers Math. Appl.*, **21**, 25-39.

- P. S. V. Nataraj (2001). Computation of QFT bounds for robust tracking specifications. *Automatica*, accepted.
- P. S. V. Nataraj and A. K. Prakash. (2001). On subdivision direction selection for QFT template generation. *In preparation*.
- P.S.V.Nataraj and G.Sardar. (2000a). Computation of QFT bounds for robust sensitivity and gain-phase margin. *Trans. of the ASME Journal of Dynamic Systems, Measurement and Control*, **36**, 111-119.
- P. S. V. Nataraj and G. Sardar. (2000b). Template generation for continuous transfer functions using interval analysis, *Automatica*, **122**, 528-534.
- P. S. V. Nataraj and S. Sheela. (2001a). An algorithm for extraction of boundary rectangles from interval QFT templates. *Submitted*.
- P. S. V. Nataraj and S. Sheela. (2001b). A template generation algorithm using parallel function evaluations and adaptive subdivisions. *Submitted*.
- P. S. V. Nataraj and S. Sheela. (2001c). A Unified procedure for generation of QFT bounds to prescribed accuracy. *Submitted*.
- O.D.I.Nwokah, S.Jayasuriya and Y.Chait. (1992). Parametric robust control by quantitative feedback theory. *AIAA Journal of Guidance and Control*, **5**, 207-214.
- L. B. Rall. (1981). Automatic differentiation, techniques and applications. *Lecture Notes in Computer Science*, **120**, Springer-Verlag, Berlin.
- D. Ratz and T. Csendes. (1995). On the selection of subdivision directions in interval branch-and-bound methods for global optimization. *Journal of Global Optimization*, **7**, 183-207.
- J. M. Rodrigues, Y.Chait and C.V. Holot. (1997). An efficient algorithm for computing QFT bounds. *Trans. of the ASME Journal of Dynamic Systems, Measurement and Control*, **119**, 548-552.
- S. M. Rump. (1999). INTLAB - Interval laboratory. In T. Csendes, Editor, *Developments in reliable computing*. Kluwer Academic Publishers.
- G. Sardar and P. S. V. Nataraj. (1997). A template generation algorithm for non-rational transfer functions in QFT designs. *In Proc. 36th IEEE Conf. Decision and Control*, 2684-2689, San Diego, USA.
- S. Sheela and P. S. V. Nataraj. (2001a). A new subdivision strategy for range computations. *Reliable Computing*, to appear.
- S. Sheela and P. S. V. Nataraj. (2001b). A reliable parallel - adaptive algorithm with back-tracking for QFT template generation. *IETE Jl. Technical Review*. To appear.
- M. Sidi. (1976). Feedback synthesis with plant ignorance, non-minimum phase and time domain tolerances. *Automatica*, **12**, 265-271.
- D. F. Thompson and O.D.I.Nwokah. (1994). Analytical loop shaping methods in quantitative feedback theory. *Trans. of the ASME Journal of Dynamic Systems, Measurement and Control*, **116**, 169-177.
- P. Vamsikrishna. (2000). Design of controllers using global optimization techniques. M. Tech thesis, Systems and Control Engg. Group, IIT Bombay, India.
- O. Yaniv and I. Horowitz. (1987). Quantitative feedback theory- reply to criticisms. *International Journal of Control*, **40**, 945-962.
- Y. Zhao and S. Jayasuriya. (1998). An H-infinity formulation of quantitative feedback theory. *Trans. of the ASME Journal of Dynamic Systems, Measurement and Control*, **120**, 305-313.

APPENDIX A. LIST OF EXAMPLES

The following is a suite of transfer function examples used in this work. The test problems are taken from the QFT literature. The problem names reflect the general type of the system.

Example 1. Under-damped Second Order System (Rodrigues *et. al.*, 1997): The transfer function for a system occurring in active noise and vibration control with highly underdamped resonances is

$$g(s) = \frac{\omega_n^2}{s^2 + 2\xi\omega_n s + \omega_n^2}$$

$$\omega_n \in [0.75, 1.25], \xi \in [0.02, 0.06], \omega = 1.$$

Example 2. DC Motor (Bailey *et.al.*, 1988): The DC Motor drives a viscously damped inertial load. The transfer function between the torque and armature voltage is

$$g(s) = \frac{K(J_i s + B_i)}{(Ls + R)(J_m s + J_i s + B_m + B_i) + K^2}$$

$$K \in [0.2, 0.6], J_i \in [10^{-5}, 3 \cdot 10^{-5}], J_m = 2 \cdot 10^{-3}$$

$$B_m = 2 \cdot 10^{-5}, L = 10^{-2} H,$$

$$R = 1\Omega, B_i = B_m, \omega = 20.$$

Example 3. Simple poles (Nataraj and Sardar, 2000a): The transfer function for a stable second order system with real poles is

$$g(s) = \frac{k}{(s+a)(s+b)}$$

$$a \in [1,5], b \in [20,30], k \in [1,10], \omega = 1.$$

Example 4. Non-minimum phase (Sidi, 1976): The transfer function for a non-minimum phase system with real poles and zeros is

$$g(s) = \frac{K(1-Ds)}{s(1+Bs)}, B \in [0.3,1]$$

$$D \in [0.05,0.1], K \in [1,3], \omega = 1.$$

Example 5. Non-rational (Horowitz, 1993, pp.129): The transfer function for a non-rational system is

$$g(s) = \frac{e^{-sT}}{1+be^{-as}}, a \in [1,2]$$

$$b \in [0.4,0.6], T \in [0.01,0.02], \omega = 2.$$

Example 6. Electro-Mechanical (Cohen et. al., 1995): The transfer function between control torque to motor speed of an electro-mechanical system is

$$g(s) = \frac{J_l s^2 + ds + k}{J_l J_m s^3 + (J_l + J_m)ds^2 + (J_l + J_m)ks}$$

$$J_m = 0.4, J_l \in [5.6,8], d \in [30,300],$$

$$k \in [5880,5900], \omega = 10\pi.$$

Example 7. Vehicle clutch system (Chen and Balance, 1999): The transfer function between the input clutch position to the output transmission speed is

$$g(s) = \frac{k_c(s^2 + \frac{c_s}{j_v} + \frac{k_s}{j_v})}{j_e s \left\{ s^2 + \left(\frac{c_s}{j_v} + \frac{c_s}{g_r^2 j_c} \right) s + \frac{k_s}{j_v} + \frac{k_s}{g_r^2 j_c} \right\}}$$

$$j_v = [1400,11000], k_s = [5800,115000], k_c = [100,800],$$

$$j_e = 0.09, j_c = 3.07, c_s = 377, g_r = 27.0, \omega = 10.$$

Example 8. Multiple transport lags (Nataraj and Sardar, 2000b): The transfer function for a system with multiple transport lags is

$$g(s) = \frac{(T+\tau_1)e^{-sT_1}}{\log_{10} T_1 - \frac{e^{-sT}}{(1+\cos \tau_1 s)}} + \frac{1-e^{-sT_r}}{sT_r \left[1 + \left(\frac{sT_r}{4\pi} \right)^2 \right]}$$

$$T_1 \in [3,5], T_r \in [0.5,0.7], T \in [9.25,9.35],$$

$$\tau_1 \in [0.49,0.5], \omega = 0.5.$$

Example 9. Mechanical system ((Horowitz, 1993, pp. 222) : The transfer function for a mechanical system is

$$g(s) = \frac{km}{s(s^2 fm^2 + bms + c)}, f \in [1,2]$$

$$m^2 \in [1,10], b \in [0.5,1], c \in [2,3]$$

$$k \in [0.5,2], \omega = 8.$$

Example 10. Aircraft, longitudinal Motion (Thomson and Nwokah, 1994): The transfer function for the longitudinal motion of an aircraft is (from aerodynamic data, the ranges for the uncertain parameters are identified)

$$g(s) = \frac{k(1+\frac{s}{z})}{s(1+\frac{s}{p})(1+2\frac{\xi}{\omega_n}s+\frac{s^2}{\omega_n^2})}$$

$$z \in [0.5,0.75], p \in [1,10], \xi \in [0.8,0.9]$$

$$\omega_n \in [5,6], k \in [0.2,2], \omega = 0.1.$$

Example 11. Inverted pendulum (Borghesani et. al, 1995): The transfer function between pendulum angle to the cart's motor current is

$$g(s) = \frac{K\alpha\omega_n^2(1/L)s^2e^{-s\tau}}{\left\{ \frac{(s(s+\alpha)-K_{gr}K\alpha)(s^2+2\xi\omega_n s+\omega_n^2)}{(s^2-g/L)} \right\}}$$

$$L \in [0.3,0.45], K \in [1.5,1.7], \xi \in [0.001,0.02],$$

$$\tau \in [0.014,0.015], \alpha \in [15,17], \omega_n \in [50,70],$$

$$K_{gr} \in [0.005,0.15], g = 9.81, \omega = 10.$$

SIMULTANEOUS MEETING OF CONTROL SPECIFICATIONS IN QFT

M. Gil-Martínez¹ and M. García-Sanz²

¹Electrical Engineering Department, University of La Rioja. Luis de Ulloa, 20, 26004 Logroño, SPAIN

²Automatic Control and Computer Science Department, Public University of Navarra. Campus Arrosadía, 31006 Pamplona, SPAIN

Abstract: Given a linear uncertain plant, a feedback two degrees of freedom control must be designed to satisfied specified tolerances on general performance and stability robust behaviours: gain and phase margins, appropriate response to command and disturbance inputs and control effort limitation. Solution existence mathematical theories developed until the moment in QFT, have only cared *implicitly* for the cost of feedback. So under certain constraints on the plant and on the rest of tolerances, they can infer necessary and sufficient conditions for the existence of an optimum open loop transmission function that lies on its bounds at each frequency. This remains an unresolved problem when control effort constraints are *explicitly* included. This paper dealt with it more than a loop shaping challenge, as a question of achieving a feasible set of bounds, i.e. gaining a non- empty QFT bound intersection at each frequency. Bound formulation based on quadratic inequalities is the foundation of the study. This permits to set up certain rules amongst the different specification tolerances as a function of the plant uncertainty to guarantee the simultaneous meeting of feedback requirements.

Keywords: Quantitative Feedback Theory, Robust Control, Uncertain Systems.

1. INTRODUCTION

Quantitative Feedback Theory (QFT), (Horowitz, 1991; Houpis, and Rassmussen, 1999; Yaniv, 1999), has proven to be a very effective design methodology of feedback control. However, it has often been criticised for lack of a rigorous mathematical theory to support its claims. The trouble arises on whether an open loop transfer function $L_o=GP_o$ satisfying the various frequency *bounds* can be found, labelling this the solution existence problem. The bounds represent robust performance and robust stability requirements in QFT domain.

Feedback tolerances in early QFT works included *explicitly* specifications on the uncertain system response to command and disturbance inputs (robust performance specifications) and robust stability. Attending to robust

performance specifications, as the amplitude of the controller increases, the plant output response to disturbances decreases and the sensitivity of the plant output to tracking commands decreases. In turns, it also implies a larger open loop $L=GP$, and hence a larger cross-over frequency or larger bandwidth, so it also increases the plant output response to sensor noise on a wider bandwidth. Hence, the bound outlook must permit reducing the high frequency open loop gain $|L|$, reaching its high frequency asymptote as fast as possible to reduce the cost of feedback (Horowitz, 1972, 1973). As long as, tolerances on control effort are only *implicitly* considered, i.e. any bound represents them, some constraints must be imposed on the uncertain plant and on the rest of performance tolerances *explicitly* cared about, to guarantee solution existence to the feedback problem, (Horowitz, 1979 App.1). Under these premises,

several researchers have developed theorems with necessary and sufficient conditions for solution existence in minimum phase systems: Horowitz (1979, App.1), Nowokah and Thompson (1989), Nowokah et al. (1990), Thompson and Nowokah (1989, 1994), Jayasuriya and Zhao (1994a,b), Nordgren et al. (1994).

In recent QFT works, more general performance specifications, including also the cost of feedback, have been formulated in terms of QFT bounds, Chait and Yaniv, (1993), Borghesani et al. (1994), Yaniv (1999). Unfortunately, in this case the solution existence question remains an unresolved problem.

This paper dealt with this problem, more than if a L function exists given certain bounds, as a question of defining a feasible set of bounds. Taking advantage of bound formulation developed by Chait and Yaniv (1993) for automatic bound computation, it is going to be used to find out whether the set of algebraic bound inequalities must be met simultaneously, i.e. if there exist a non-empty bound intersection at each frequency of interest. System uncertainty and specification figures of merit are immersed in the bound formulas, so the trade-offs between arbitrarily small feedback requirements and arbitrarily large uncertainties can be algebraically arranged.

This paper is made up of seven sections. Section 2 expresses the closed loop requirements on robust performance and robust stability. Bound formulation through quadratic inequalities is revised in Section 3. Section 4 examines bound formulation of each feedback problem classifying them in typologies of bounds. The simultaneous meeting of feedback requirements is dealt with in Section 5. Firstly, general rules are given, and following, the most frequent tolerance values in practical systems are discussed. An example in Section 6 illustrates the methodology for a particular control design. The conclusions are given in Section 7.

2. ROBUST FEEDBACK PROBLEM STATEMENT

Consider the plant $P(s)$ with structured parametric uncertainty $\{P\}$ in Figure 1. A SISO feedback loop with a controller $G(s)$ and a pre-filter $F(s)$ is the design objective in order to meet robust stability and robust performance specifications despite plant uncertainty and plant disturbances. Assume the responses of all $L(j\omega) = G(j\omega)P(j\omega)$ form a convex set on the complex plane. Assuming also unity-feedback $H(s)=1$ for simplicity, the closed loop specifications δ_k of the system are described in the frequency domain in terms of inequalities on the system's transfer functions $|T_k|$, $k=1, \dots, 5$, from some inputs to some outputs (Table 1): $k=1$, robust stability (Y/R), robust control effort for the rejection of system

input disturbances (U/D_1) and robust sensor noise attenuation (Y/N); $k=2$, robust rejection of system output disturbances (Y/D_2); $k=3$, robust rejection of system input disturbances (Y/D_1); $k=4$, robust control effort: for the system output disturbance rejection (U/D_2), for the noise attenuation (U/N) and for the tracking of reference signals (U/R); $k=5$, robust tracking of reference signals (Y/R).

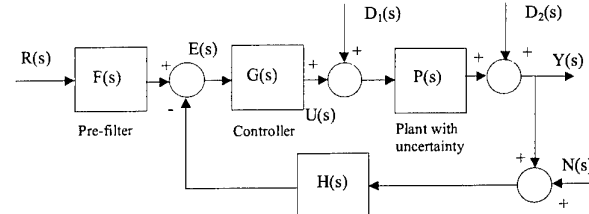


Figure 1: SISO Feedback System

Table 1: Feedback problems

Transfer functions and specifications				Eq.
$ T_1(j\omega) = \left \frac{Y(j\omega)}{R(j\omega)F(j\omega)} \right = \left \frac{U(j\omega)}{D_1(j\omega)} \right = \left \frac{Y(j\omega)}{N(j\omega)} \right = \left \frac{P(j\omega)G(j\omega)}{1 + P(j\omega)G(j\omega)} \right \leq \delta_1(\omega), \omega \in \Omega_1$				(1)
$ T_2(j\omega) = \left \frac{Y(j\omega)}{D_2(j\omega)} \right = \left \frac{1}{1 + P(j\omega)G(j\omega)} \right \leq \delta_2(\omega), \omega \in \Omega_2$				(2)
$ T_3(j\omega) = \left \frac{Y(j\omega)}{D_1(j\omega)} \right = \left \frac{P(j\omega)}{1 + P(j\omega)G(j\omega)} \right \leq \delta_3(\omega), \omega \in \Omega_3$				(3)
$ T_4(j\omega) = \left \frac{U(j\omega)}{D_2(j\omega)} \right = \left \frac{U(j\omega)}{N(j\omega)} \right = \left \frac{U(j\omega)}{R(j\omega)F(j\omega)} \right = \left \frac{G(j\omega)}{1 + P(j\omega)G(j\omega)} \right \leq \delta_4(\omega), \omega \in \Omega_4$				(4)
$\delta_{5inf}(\omega) < T_5(j\omega) = \left \frac{Y(j\omega)}{R(j\omega)} \right = \left F(j\omega) \frac{P(j\omega)G(j\omega)}{1 + P(j\omega)G(j\omega)} \right \leq \delta_{5sup}(\omega), \omega \in \Omega_5$				(5)

3. QUADRATIC INEQUALITIES IN QFT BOUND FORMULATION

In the bound generation step of the QFT design procedure, tolerances on the closed-loop system frequency response $\delta_k(\omega)$, in combination with plant uncertainty *templates* (set of complex numbers on phase/log-magnitude axis) representing the frequency response of an uncertain plant at a fixed frequency ω_i , are translated into ω_i -bounds on the controller $G(j\omega_i)$. Logarithmic complex plane, the Nichols Chart (NC), is the domain used in QFT from Horowitz and Sidi (1972).

Various approaches to the bound generation problem exist. Traditionally, QFT bounds have been computed using manual graphical manipulations of the plant templates on the NC. The necessity of alleviating much of the manual work required in the graphical procedure has led to several researchers to develop different algorithms for automatic computation of these bounds. For the general case, early bound generation algorithms used geometrical and/or search-based CAD techniques, (Longdon and East, 1978; Houppis and Lamont, 1988; Thompson and Nwokah 1989; Bailey and Hul, 1989;

Jayasuriya, 1990; Wang et al., 1991; Yaniv, 1992. Recently, more efficient numerical algorithms based on quadratic inequalities have been proposed. Chait and Yaniv (1993), Yaniv and Chait (1991, 1992, 1993), and Chait et al. (1995) developed quadratic inequalities for general settings including continuous and discrete-time systems, as well as for parametric and non-parametric uncertain models. These algorithms establish a formal process of mapping the plant uncertainty and the feedback specifications into the bound formulas through quadratic inequalities. They also form the basis of bound computation in the QFT Toolbox of MATLAB (Borghesani et al., 1994). Being this procedure the starting point of the work developed in this paper, next paragraphs summarise it. Other works improving the efficiency and accuracy of algorithms for computing bounds are in Zhao and Jayasuriya (1994), Rodrigues et al. (1997), Nataraj and Sardar (2000).

For many practical problems, it is difficult if not impossible to analytically describe the plant templates. Consequently, algorithms for computing QFT bounds choose a set of discrete frequencies $\{\omega_i\}=\{\cap\Omega_k, k=1,\dots,5\}$ and approximate the ω_i plant template by a finite m -point set of plants. This approximation should trade-off between computational complexity and the accuracy of the bound computed, (Rodrigues et al., 1997). Each of the $r=1,\dots,m$ plants in the ω_i -template can be expressed in its polar form as $P_r(j\omega_i)=p_r(\omega_i)\cdot e^{j\theta_r(\omega_i)}=p\angle\theta$, and equally the controller polar form is $G(j\omega_i)=g(\omega_i)\cdot e^{j\phi}=g\angle\phi$ (phase controller dependence on frequency has been suppressed considering ϕ range is the same for all the ω_i -bounds). Substituting them into any of the $k=1,\dots,5$ feedback problems (Equations (1) to (5) in Table 1) and simplifying, results in quadratic inequalities, that follow the general form:

$$I_{\omega_i}^k(p, \theta, \delta_k, \phi) = a \cdot g^2 + b \cdot g + c \geq 0 \quad (6)$$

where the coefficients a, b, c depends on: $p=p_r(\omega_i)$, $\theta=\theta_r(\omega_i)$, $\delta_k=\delta_k(\omega_i)$ and ϕ . For a particular frequency ω_i , a fixed plant $p\angle\theta$ in the ω_i -template and a fixed controller phase ϕ in the range $[-360^\circ, 0^\circ]$, the coefficients a, b and c take discrete values. Thus, the unknown parameter in (6) is the controller magnitude g .

Feedback problems (1) to (5) are now reformulated in Inequalities (7) to (11) as Table 2 shows. Note that the tracking problem in (5) is a two degrees of freedom design (F and G). G design aims to reduce the variation in $|T|=|T_s|/|F|$, under the limit $\delta_s=\delta_{sup}/\delta_{inf}$, implying a double valued problem. Due to it, two arbitrarily plants $p_d\angle\theta_d$ and $p_e\angle\theta_e$ in the ω_i -template $\{P_r(j\omega_i), r=1,\dots,m\}$ appear in Equation (11), instead of a single plant $p\angle\theta$ as for the rest of feedback problems; Chait and Yaniv

(1993). After the G -design, the F -design is accomplished such that $\delta_{sin}<|F||T|<\delta_{sup}$. This last step is straightforward and its details are omitted in this paper.

The quadratic equation $I_{\omega_i}^k(p, \theta, \delta_k, \phi) = 0$, associated to (6) has two solutions: g_1 (negative square-root) and g_2 (positive square-root). Computing them for all the plants $r=1,\dots,m$ in the ω_i -template, the most restrictive $g_1\angle\phi$ and/or $g_2\angle\phi$ solutions determine the boundaries of a region on the NC that can not be penetrated by $g\angle\phi$ (see Section 4). Furthermore, they constitute the restrictions or bounds on G at the frequency ω_i to achieve the specification $\delta_k(\omega_i)$. This procedure is carried out for all the frequencies of interest $\omega_i \in \Omega_k$ and all the specifications $\delta_k(\omega_i)$, $k=1,\dots,5$.

Table 2: Bound quadratic inequalities

k	Bound Quadratic Inequality	Eq.
1	$p^2 \cdot \left(1 - \frac{1}{\delta_1^2}\right) \cdot g^2 + 2 \cdot p \cdot \cos(\phi + \theta) \cdot g + 1 \geq 0$	(7)
2	$p^2 \cdot g^2 + 2 \cdot p \cdot \cos(\phi + \theta) \cdot g + \left(1 - \frac{1}{\delta_2^2}\right) \geq 0$	(8)
3	$p^2 \cdot g^2 + 2 \cdot p \cdot \cos(\phi + \theta) \cdot g + \left(1 - \frac{p^2}{\delta_3^2}\right) \geq 0$	(9)
4	$\left(p^2 - \frac{1}{\delta_4^2}\right) \cdot g^2 + 2 \cdot p \cdot \cos(\phi + \theta) \cdot g + 1 \geq 0$	(10)
5	$p_e^2 p_d^2 \left(1 - \frac{1}{\delta_5^2}\right) \cdot g^2 + 2 p_e p_d \left(p_e \cos(\phi + \theta_d) - \frac{p_d}{\delta_5^2} \cos(\phi + \theta_e)\right) \cdot g + \left(p_e^2 - \frac{p_d^2}{\delta_5^2}\right) \geq 0$	(11)

Setting the bounds on the nominal loop transmission $L_0=P_0 \cdot G$ for a particular nominal plant P_0 from $\{P\}$, rather than on G , is more natural for loop shaping. Then, being $L_0(j\omega_i)=l_0\angle\psi_0$, the L_0 -bounds are simply computed by translating the G -bounds vertically by $|P_0(j\omega_i)|=p_0$ and horizontally by $\angle P_0(j\omega_i)=\theta_0$, where $P_0(j\omega_i)=p_0\angle\theta_0$, is the nominal plant of the ω_i -template. The results given for the G -bounds along the paper are also applicable to the L_0 -bounds.

4. BOUND FORMULATION AND TYPOLOGIES

g denotes the controller magnitude. Thus, from the g_1 and/or g_2 computed for each plant in the ω_i -template at each ϕ in $[-360^\circ, 0^\circ]$, only the positive real ones give real constraints. As described in Thompson and Nowokah (1994), this leads to single-valued bounds when only one root is real and positive in the whole compensator phase range, $\phi \in [-360^\circ, 0]$, or to multi-valued bounds if there are either no positive real roots or two positive real roots depending on the phase angle ϕ . Thompson (1998) establishes three bound categories, distinguishing between upper and lower single valued bounds, apart from the multi-valued bounds. The present work extends these conclusions formulating four bound categories in

terms of the open loop transmission, much more sensitive to the cost of feedback than the sensitivity function (Horowitz, 1991). Four classes of solutions to the general feedback problem expressed in the quadratic inequalities (7) to (11) can be found, giving four categories of bounds labelled as typologies A, B, C and D.

4.1 Bound typology description

- **Typology A.** $\{g_2, g_1\} > 0$ and real for $\phi \in [-180^\circ \mp \varepsilon]$, $0^\circ < \varepsilon < 180^\circ$, and $a > 0$. Then to meet (6):

$$g \angle \phi \geq g_2 \angle \phi \text{ and } g \angle \phi \leq g_1 \angle \phi \quad (12)$$

$g_2 \angle \phi$ and $g_1 \angle \phi$ are two ω_i -bounds joint at their ends. They only exist over a particular phase range wherein g_{12} are no complex. According to the requirement expressed in (12), from the $g_{12} \angle \phi$ computed for all the plants $p \angle \theta$ in the ω_i -template, the most severe ones are the largest g_2 and the smallest g_1 for each ϕ . This selection of $g_{12} \angle \phi$ constitutes the G -bound formulas at the frequency ω_i and the specification $\delta_k(\omega_i)$. Their graphical representation looks like Figure 2(a), blurred by the particular ω_i -template shape. The stripped area is the allowed region for $g \angle \phi$.

- **Typology B.** $g_2 > 0$ and real, $g_1 < 0$ and real, for each $\phi \in [-360^\circ, 0^\circ]$; and $a > 0$. Then to comply with (6):

$$g \angle \phi \geq g_2 \angle \phi \quad (13)$$

$g_2 \angle \phi$ is the single ω_i -bound for $g \angle \phi$ over the whole phase range. Keeping with the condition in (13), from the g_2 computed for all the plants $p \angle \theta$ in the ω_i -template at fixed ϕ , the most stringent one is the largest g_2 . Extending for all the $\phi \in [-360^\circ, 0^\circ]$, those $g_2 \angle \phi$ computed constitute the G -bound formula at the frequency ω_i and the specification $\delta_k(\omega_i)$. Their graphical representation looks like Figure 2(b).

- **Typology C.** $\{g_2, g_1\} > 0$ and real for $\phi \in [-180^\circ \mp \varepsilon]$, $0^\circ < \varepsilon < 180^\circ$, and $a < 0$. Then, to meet (6):

$$g_2 \angle \phi \leq g \angle \phi \leq g_1 \angle \phi \quad (14)$$

Figure 2(c) shows these results. This kind of solutions does not appear for the most common realistic systems. Nevertheless, this possibility is considered, for the sake of generality.

- **Typology D.** $g_1 > 0$ and real, $g_2 < 0$ and real, for each $\phi \in [-360^\circ, 0^\circ]$; and $a < 0$. Then to comply with (6):

$$g \angle \phi \leq g_1 \angle \phi \quad (15)$$

$g_1 \angle \phi$ is the single ω_i -bound for $g \angle \phi$ over the whole phase range. See Figure 2(d). Keeping with the condition in (15), from the $g_1 \angle \phi$ computed for all the plants in the ω_i -template at a fixed ϕ , the toughest one is the smallest

g_1 . Repeating for each $\phi \in [-360^\circ, 0^\circ]$, $g_1 \angle \phi$ constitutes the G -bound formula at the frequency ω_i and the specification $\delta_k(\omega_i)$.

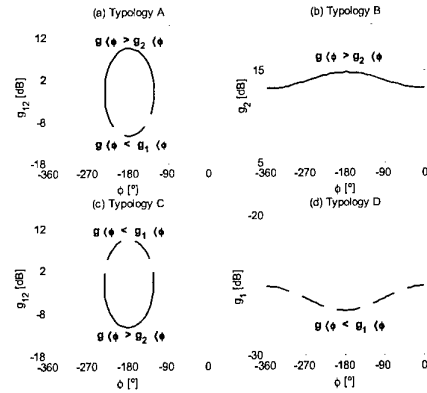


Figure 2: Bound typologies

The bound graphical notation for the whole document is that a bound plotted with a *solid line* implies that $G(j\omega)$ (or $L_0(j\omega)$) must lie above or on it in order to meet the particular specification, while a bound plotted with a *dashed line* implies that $G(j\omega)$ (or $L_0(j\omega)$) must lie below or on it. Optimum $L_0(j\omega)$ (or $G(j\omega)$) lies on the associated boundary at each value of ω (Horowitz, 1973) in the sense that, this $L_0(j\omega)$ always meets the required specification, despite the inherent uncertainty in $P(j\omega)$, with the minimum 'cost of feedback'.

4.2 Bounds for the $k=1, \dots, 5$ feedback problems

Table 3: $g_{1,2}$ solutions of the quadratic inequalities

k	$g_{1,2}$	Eq.
1	$g_{1,2} = \frac{1}{p \cdot \left(1 - \frac{1}{\delta_1^2}\right)} \left(-\cos(\phi + \theta) \mp \sqrt{\cos^2(\phi + \theta) - \left(1 - \frac{1}{\delta_1^2}\right)} \right)$	(16)
2	$g_{1,2} = \frac{1}{p} \cdot \left(-\cos(\phi + \theta) \mp \sqrt{\cos^2(\phi + \theta) - \left(1 - \frac{1}{\delta_2^2}\right)} \right)$	(17)
3	$g_{1,2} = \frac{1}{p} \cdot \left(-\cos(\phi + \theta) \mp \sqrt{\cos^2(\phi + \theta) - \left(1 - \frac{p^2}{\delta_3^2}\right)} \right)$	(18)
4	$g_{1,2} = \frac{1}{p \cdot \left(1 - \frac{1}{p^2 \delta_4^2}\right)} \cdot \left(-\cos(\phi + \theta) \mp \sqrt{\cos^2(\phi + \theta) - \left(1 - \frac{1}{p^2 \delta_4^2}\right)} \right)$	(19)
5	$g_{1,2} = \frac{1}{p_e p_d \left(1 - \frac{1}{\delta_5^2}\right)} \cdot \left(p_e \cos(\phi + \theta_d) - \frac{p_d}{\delta_5^2} \cos(\phi + \theta_e) \right) \mp \sqrt{\left(p_e \cos(\phi + \theta_d) - \frac{p_d}{\delta_5^2} \cos(\phi + \theta_e) \right)^2 - \left(1 - \frac{1}{\delta_5^2}\right) \left(p_e^2 - \frac{p_d^2}{\delta_5^2} \right)}$	(20)

Solving the quadratic equations $I_{\omega_i}^k(p, \theta, \delta_k, \phi) = 0$ for the k -feedback problems, $k=1, \dots, 5$, expressed in (7) to

(11), g_1 and g_2 solutions are presented in Equations (16) to (20) in Table 3.

Attending to mathematical behaviour of (16) to (20), some conclusions about the bound typologies and bound formulas for the different performance and stability problems are summarised in Table 4. From this point, the constraints to design a solvable feedback problem can be studied.

Table 4: Bound formulations and their typology

k	δ_k	typol	G-bounds
1	$0 < \delta_1 < 1$	D	$g \angle \phi \leq g_1 \angle \phi ; \phi \in [-360^\circ, 0^\circ], g_1$ in (16)
	$\delta_1 > 1$	A	$g \angle \phi \geq g_2 \angle \phi, g \angle \phi \leq g_1 \angle \phi ; \phi \in [-180^\circ \mp \varepsilon], g_{12}$ (16)
2	$0 < \delta_2 < 1$	B	$g \angle \phi \geq g_2 \angle \phi ; \phi \in [-360^\circ, 0^\circ], g_2$ in (17)
	$\delta_2 > 1$	A	$g \angle \phi \geq g_2 \angle \phi, g \angle \phi \leq g_1 \angle \phi ; \phi \in [-180^\circ \mp \varepsilon], g_{12}$ (17)
3	$p > \delta_3$	B	$g \angle \phi \geq g_2 \angle \phi ; \phi \in [-360^\circ, 0^\circ], g_2$ in (18)
	$p < \delta_3$	A	$g \angle \phi \geq g_2 \angle \phi, g \angle \phi \leq g_1 \angle \phi ; \phi \in [-180^\circ \mp \varepsilon], g_{12}$ (18)
4	$p < 1/\delta_4$	D	$g \angle \phi \leq g_1 \angle \phi ; \phi \in [-360^\circ, 0^\circ], g_1$ in (19)
	$p > 1/\delta_4$	A	$g \angle \phi \geq g_2 \angle \phi, g \angle \phi \leq g_1 \angle \phi ; \phi \in [-180^\circ \mp \varepsilon], g_{12}$ (19)
5	$\frac{p_{\max}}{p_{\min}} > \delta_5$	B	$g \angle \phi \geq g_2 \angle \phi ; \phi \in [-360^\circ, 0^\circ], g_2$ (20)
	$\frac{p_{\max}}{p_{\min}} < \delta_5$	A	$g \angle \phi \geq g_2 \angle \phi, g \angle \phi \leq g_1 \angle \phi ; \phi \in [-180^\circ \mp \varepsilon], g_{12}$ (20)

5. SIMULTANEOUS MEETING OF FEEDBACK REQUIREMENTS

Checking G-bound formulas and typologies in Table 3 and Table 4, notice that for a specific compensator phase ϕ , the typology and the magnitudes g_1, g_2 depend on the closed loop tolerances δ_k and on the open loop plant uncertainty in magnitude p and phase θ . Considering the plant uncertainty (p and θ) a parameter arbitrarily large and inherent to the plant nature, the specification figures of merit (δ_k) are the design parameters for the simultaneous meeting of all the specifications. Following, some general guidelines on this matter are given in Section 5.1. Sections 5.2 to 5.5 discuss the more frequent tolerances in practical systems. In general, the simultaneous meeting of all the specifications, or in case the best performance achievable, is highly dependent on the application, as an example shows in Section 6.

5.1 General rules for solution existence

The simultaneous meeting of bounds is checked for each particular frequency and there is a particular set of specifications to achieve at each frequency. Hence, from the point of a non-empty bound intersection, only for

those frequencies where the specifications can conflict, trade-off solutions should be adopted for δ_k .

Single-valued bounds (typologies B and D) are more aggressive than double-valued bounds (typologies A and C) because they must be satisfied for the whole phase range $[-360^\circ, 0^\circ]$. A requirement more stringent for upper bounds (single or double valued) means a higher g_2 magnitude, and for lower bounds (single or double valued) a smaller g_1 magnitude, at each phase angle ϕ . Double-valued bounds severity also increases when their phase range of existence ($\mp \varepsilon$ around -180°) increases. Harder δ_k figures of merit lead to more severe bounds as described.

Type A bounds of any magnitude $g_{1,2}$ can coexist with type B or D bounds allowing a simultaneous fulfilment. If type B and D bounds coexist, g_1 bound D magnitudes should be higher than g_2 bound B magnitudes for some ϕ , relaxing δ_k when necessary.

5.2 Stability problem

Robust stability is the main requirement in any practical design. QFT cared for it through a δ_1 constraint, that is a constant value for all the frequencies, see Equations (1), (7) and (16). Robust gain and phase margins can be obtained from δ_1 by simple arithmetic, (Yaniv and Chait, 1993). δ_1 requirement yields a single dominant high frequency bound, also labelled universal high-frequency contour or simply U-contour.

Even in the absence of significant disturbances (no necessity of constraints δ_2 and/or δ_3) the latter should not be entirely ignored. If it is, very large peaks of $|L/(1+L)|$ will result at high frequencies. Such peaking does not violate tracking constraints δ_5 since the pre-filter F attenuate the higher frequencies of the command input. However, a large peak produces due to $D_{1,2}$ if there is not a constraint on the damping factor of the complex pole nearest to the $j\omega$ axis. To cope with it apart from stability purposes, a restriction δ_1 of the form (1) should always be added, (Horowitz and Sidi, 1972,1978).

Characterising stability constraint, δ_1 is a constant value independent of the frequency. For reasonable gain and phase margins (or disturbance peak limitation), Biernson (1988) advises $\delta_1 \leq 1.3$ ($MF \geq 45^\circ$ and $MG \geq 5\text{dB}$). δ_1 much larger than 1 implies too conservative margins, what amplifies high frequency noise. According to Table 4, stability requirements (δ_1 moderately greater than 1) always yields typology A bounds, that can coexist (simultaneous solution) with any other type of bounds. See Figure 3, for a plant $P(j\omega)=k/j\omega$ with uncertainty $k \in [1, 3]$, and nominal plant for $k=1$.

5.3 Disturbance rejection problem

According to Table 4, disturbance requirements are expressed in QFT as upper single-valued bounds (typology B) and/or double-valued bounds (typology A). For disturbances at the system output, the bound typology at ω depends exclusively on the constraint value $\delta_2(\omega)$. However, the typology of input disturbance bounds depends on $\delta_3(\omega)$ and the plant magnitude p (that takes a set of values for the ω template). Both constraints δ_2 and δ_3 can be rewritten as a single restriction δ_D on the sensitivity function $S=1/(1+L)$: $\delta_D(\omega)=\min\{\delta_2(\omega), \min(\delta_3(\omega)/|P(j\omega)|)\}$. Being $|P(j\omega)|$ a set of plant magnitudes for each particular ω -frequency.

The specification figures of merit $\delta_D(\omega)$ usually take values below zero at the frequencies of interest in the disturbance problem, assuring appropriated attenuation levels. These, $0 < \delta_D(\omega) < 1$ for $\omega < \omega_D$ yield upper single bounds (typology B). However, there is also a constraint on the δ_D -specification values at high frequencies for gaining solution existence: $\delta_D(\omega) > 1$, (Horowitz 1979, App.1). Then, $\delta_D(\omega) > 1$ for $\omega > \omega_D$ yield double valued bounds (typology A), allowing the reduction of the open-loop gain at high frequencies. Check it in Figure 3, for $\delta_D = \delta_2$. δ_D values at high frequencies ($\omega = 90$ rad/sec. in the example) are considerably greater than 1 ($\delta_D = \delta_2 = 9$ in Figure 3). Thus, typology A bounds due to δ_1 are dominant (more restrictive) than typology A bounds due to δ_D , as Figure 3 shows.

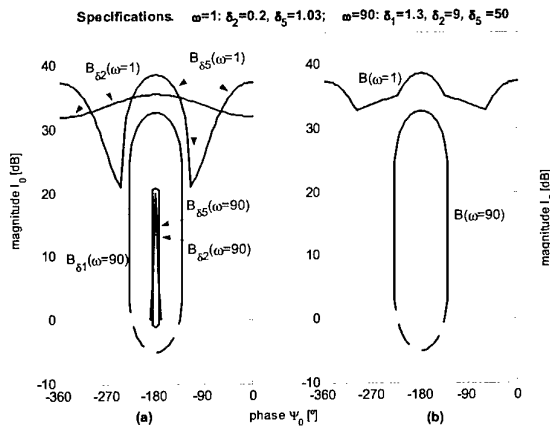


Figure 3. (a) Bounds for δ_1 , δ_2 , δ_3 at $\omega=[1, 90]$; (b) Bound solution.

5.4 Tracking problem

In a two degrees of freedom feedback problem, the controller G aims to reduce the variation in $|T|=|T_3|/|F|=|L/(1+L)|$ under the limit $\delta_5 = \delta_{5sup}/\delta_{5inf}$ due to the uncertainty in P . The pre-filter F positions $|T_3|=|F \cdot T|$

within the frequency domain desired models, δ_{5sup} (upper model) and δ_{5inf} (lower model).

At large frequencies any rational function $P(s)=K \cdot \Pi(s+z_i)/\Pi(s+p_j)$ degenerates into Ks^{-e} , where e is the excess of poles over zeros of P . Also, at large frequencies $|L| \ll 1$. Thus, $\Delta \ln|T| \approx \Delta \ln|L| = \Delta \ln|P| \approx \Delta \ln K$. Hence, the acceptable variation in $|T(j\omega)|$, i.e. $\delta_5(\omega)$, can spread at these frequencies exceeding the actual variation in $|P(j\omega)|$, and there is then no need of feedback in this frequency range, (Horowitz and Sidi, 1972). The same idea is also expressed in Horowitz (1979 App.1). So solution existence theorem for single loop design requires certain tolerances on $|T(j\omega)|$. For $\omega < \omega_5$, $\delta_5(\omega) = \delta_{5sup}(\omega)/\delta_{5inf}(\omega)$ is greater than 1, but as close to it as the sensitivity reduction required due to parameter variation. However, in the high ω range, $\omega > \omega_5$, the feedback is allowed to increase the sensitivity $S = (\partial T(j\omega)/T(j\omega))/(\partial P(j\omega)/P(j\omega))$ rather than decrease it (increase the spread between $\delta_{5sup}(\omega)$ and $\delta_{5inf}(\omega)$). In fact, as noted by Bode (1945): $\int_0^\infty \ln |S| d\omega = 0$, in any practical system; so the decrease in sensitivity ($|S| < 1$) achieved in the control bandwidth range, must be balanced by $|S| > 1$ in another range. This is achieved by $\delta_{5sup}(\omega)/\delta_{5inf}(\omega)$ considerably greater than 1 in the high frequency range. Anyway, it is easy to live with this constraint because at sufficient large ω , $|T|$ is negligible small, so that large relative changes in $|T|$ are inconsistent, (Horowitz, 1973).

Considering all this, tracking bounds are single valued upper bound (typology B) at $\omega < \omega_5$, where the specification closed loop tolerances are smaller than the open loop uncertainty, i.e. $p_{max}/p_{min} > \delta_5$ in Table 4. However, $\forall \omega > \omega_5$, the tracking bounds are double valued (typology A), being $p_{max}/p_{min} < \delta_5$, and so the sensitivity is allowed to increase. A continuous increment δ_5 at high frequencies, yields type A bounds due to δ_1 become dominant respect to type A bounds due to δ_5 . Check all in Figure 3.

When the feedback requirements impose restrictions on the response to command and disturbance inputs, δ_5 and δ_D , the composite (intersection) bound of those typology B bounds of each problem must be fulfilled in the frequency range $[0, \min(\omega_5, \omega_D)]$. This unavoidable means overdesign respect to the non-dominant specification, i.e. that with lower bound magnitude at each ϕ . See Figure 3.

5.5 Control effort and Cost of feedback

To cope with the global feedback problem with tracking, disturbance and stability constraints in presence of

uncertainty, the composite QFT bound at each ω must be inviolate by $L_0(j\omega)$. Besides, as the early QFT works describe (Horowitz 1972, 1973), $L_0(j\omega)$ magnitude as a function of frequency must decrease as fast as possible. The main reasons are the unmodelled high order dynamics joint to the great uncertainty in using a linear plant model at high frequencies, and the main price paid for feedback: the excess bandwidth, (Bode, 1945).

The benefit of feedback requires $|L(j\omega)|$ significant larger than 1 over a certain ω range. The larger the range, the larger also that over which $|L(j\omega)| > |P(j\omega)|$. Besides, any practical design requires $|L| \rightarrow 0$ when $\omega \rightarrow \infty$. The problem arises at intermediate frequencies where $|L(j\omega)| \ll 1$ but $|L/P| > 1$, because stability requires $|L(j\omega)|$ decreases comparatively slowly with ω , (Bode, 1945). In this range, $|U/N| \approx |L/P| > 1$, what means a noise amplification at the plant input. Hence, $|L|$ must decrease as quickly as possible but without violate the single high frequency bound due to stability requirements, (Horowitz, 1972).

For arbitrarily large feedback benefits (arbitrarily large plant uncertainty and arbitrarily small performance requirements) there will be typology B bounds (upper single valued bounds) due to δ_s , δ_D , $\forall \omega < \omega_p$, $\omega_p = \max(\omega_s, \omega_D)$. However, $\forall \omega > \omega_p$, as long as δ_s and δ_D tolerances should be relaxed (take values much larger than 1), the stability requirement becomes dominant, $\delta_1 \approx 1.3$. Then, the single effective bound for $\omega > \omega_p$ is of typology A (double valued bound), allowing $|L(j\omega)| \rightarrow 0$ when $\omega \rightarrow \infty$. See Figure 3.

However, arbitrarily large feedback benefits can imply an excessive cost of feedback. A ω range several times the system bandwidth, where $|U/N| \approx |L/P| > 1$, produces large $|L/P|$ peak values. As N is generally stochastic, this large amplification over a large bandwidth causes elements G and P to be saturated for most of the time, so that the useful signal components due to R cannot get through, (Horowitz, 1973).

To economy in bandwidth avoiding overdesign and its negative effects, leads to include *explicitly* constraints on the control effort. In the present paper cost of feedback bounds are born from δ_4 specification in (4). As long as, the cost of feedback usually yields a limit on the open loop gain $|L|$ at moderately high frequencies, there will probably exist plants with magnitudes $0 < p < 1$ in those frequency templates. Thus, relatively small values of $\delta_4(\omega)$ in this ω range means $p\delta_4 < 1$, giving typology D bounds (lower single valued bounds), see Table 4. That constitutes the main reason of non-solution existence, at the frequencies where typology D and B bounds coexist and at the phases where the type D bound is lower than

the type B bound. In this case, performance severity in tracking and/or disturbance rejection should be relaxed. An example is provided in Section 6.

At large high frequencies the control effort does not need to be limited. What is more, there is no point in considering any feedback requirement at frequencies where the linear models do not fit the real behaviour and physical constraints do not allow any kind of control.

Control effort limitation is not restricted to the moderately high frequencies, e.g. due to excessive ambitious performance required and/or presence of large uncertainties. Actuators a priori not well designed can also saturate in response to predicted commands and disturbances inputs. This can also be taken into account in a 'quantitative' control theory as QFT. In this sense, tolerances on $|T_4| = |G/(1+L)| < \delta_4$, (see Table 1), not only bound to $|U/N|$ but also to $|U/D_2|$, to $|U/RF|$, and extensively to $|U/D_1|$ tailoring δ_u as follows. $\delta_u(\omega) = \min\{\delta_4(\omega), \min(\delta_1(\omega)/|P(j\omega)|)\}$, being $\delta_1(\omega)$ the real tolerance on $|U/D_1|$ and $|P(j\omega)|$ the set of plant magnitudes of the ω -template. In these cases, at frequencies with moderate small δ_u and small plant magnitudes p , there will be typology D bounds. Thus, this can be inconsistent with other typology B bounds at the same frequencies. Undoubtedly, this effect get worse with increasing frequencies where for practical strictly proper plants p reduces, if δ_4 requirements exist and remain moderate small.

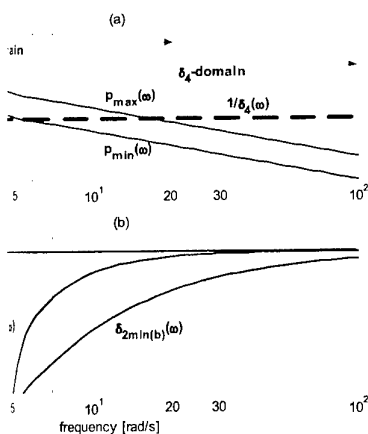
6. APPLICATION EXAMPLE

Given the plant $P(j\omega) = k/j\omega$, where $k \in [1, 3]$, the goal is to design a controller G such that for any plant in $\{P\}$: (i) the closed loop is stable, with $|PG/(1+PG)| < \delta_1 = 1.3$ at all frequencies; (ii) the sensitivity reduction meets $|1+PG|^{-1} < \delta_2(\omega)$, $\omega \in \Omega_2 = [0, \omega_2]$ and (iii) the control effort is limited to $|G/(1+PG)| < \delta_4(\omega) = 5$, $\omega \in \Omega_4 = [\omega_{4inf}, \omega_{4sup}]$. Frequency values are particularised as: $\omega_2 = 20$, $\omega_{4inf} = 4$, $\omega_{4sup} = 100$ (rad/s).

The stability requirement $\delta_1 = 1.3$ yields minimum gain and phase margins of 5dB and 45°, respectively (Yaniv and Chait, 1993). As discussed before, it produces doubled valued bounds (typology A in Figure 2) in a phase range around -180° , according to formulas in Tables 3 and 4.

Tolerances on $\delta_2(\omega)$, $\omega \in \Omega_2$, aim disturbance attenuation ($|Y/D_2| < \delta_2$). Thus, $0 < \delta_2(\omega) < 1 \quad \forall \omega < \omega_2$, giving single valued upper bounds (typology B in Figure 2) that extend on $\phi \in [-360^\circ, 0]$. Disturbances $\forall \omega > \omega_2$ are neglected dynamically (peak values due to them are limited by δ_1). A constant tolerance $\delta_4(\omega) = 5$ in $\omega \in \Omega_4$ limits the control

frequency range $\omega \in [\omega_{inf}, \omega_2]$ this limits the effort in disturbance $[\omega_2, \omega_{sup}]$ its main target is to bound the i.e. the excess of $|L|$ over $|P|$. This can amplify noises (U/N) or even disturbances (U/D_2).



uncertainty and δ_4 -specification; (b)

compares $1/\delta_4(\omega)$ with plant uncertainty. Note that for $\omega > \omega^* = 5$ rad/s, there is (a). Thus, the bounds to meet δ_4 will be typology D (single-valued lower bound). So at frequencies $\omega < \omega^*$ type B and D bounds. Assuming $\delta_4(\omega)$ is tailored at these frequencies for non-intersection. Restrictions on $\delta_2(\omega)$ are

$$0 < \delta_2(\omega) < 1, \omega < \omega^* \quad (21)$$

$$1(\omega) < \delta_2(\omega) < 1, \omega^* < \omega < \omega_2$$

in (19) must be greater than $g_2 \angle \phi(\delta_2)$ in a certain ϕ range. Taking (a) $\phi + \theta = 0^\circ$ and substituting in (17) and (19), results in constraints on δ_2 , i.e. $\delta_{2min}(a)$ and (b) as Figure 4b):

$$\delta_2 = \sqrt{1 - p_{min}^2(\omega) \cdot \delta_4^2(\omega)} \quad (22)$$

$$\delta_2 = 1 - p_{min}(\omega) \cdot \delta_4(\omega) \quad (23)$$

marker constraint on δ_2 . From it, $g_1 \angle \phi(\delta_4)$ is less than $g_2 \angle \phi(\delta_2)$ at ϕ close to 0° (and $\phi \rightarrow -360^\circ$). To guarantee reasonable ϕ condition $\delta_{2min(a)}$ should be adopted. In the range of solution widens, tougher the δ_4 larger plant uncertainty exists.

As guidelines, Figure 5 plots L_0 -bounds on plant $P(j\omega)$, taking as nominal plant

$P_0(j\omega) = 1/j\omega$. Figure 5(a) and Figure 5(b) shows L_0 -bounds at $\omega = 2$ and 30 rad/s. At the lower frequencies, disturbance and stability requirements, e.g. $\delta_1 = 1.3$ and $\delta_2 = 0.1$, are achievable simultaneously (more stringent values of δ_2 could be even taken). At the higher frequencies, control effort constraints dominate over stability tolerances, being both met at once. However, Figure 5(c) and (d) show the necessary trade-offs at mid frequencies, e.g. $\omega = 6$ rad/s. In Figure 5(c), $\delta_1 = 1.3$, $\delta_2 = 0.6$ and $\delta_4 = 5$ satisfy the constraint $\delta_{2min(a)}$. On the contrary, Figure 5(d) shows a case of no solution existence because both $\delta_{2min(a)}$ and $\delta_{2min(b)}$ are violated with $\delta_2 = 0.1$. Note that Figures 4 and 5 depict bounds on $l_0 \angle \psi_0$ not on $g \angle \phi$. After loop-shaping, $L_0 = GP_0$ should remain inside the striped area.

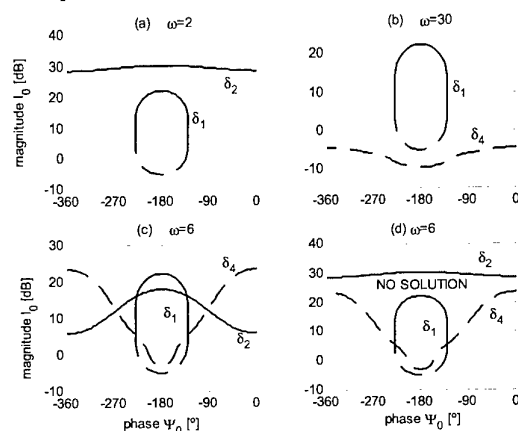


Figure 5: L_0 -bounds, $\delta_1 = 1.3$, (a) $\omega = 2$, $\delta_2 = 0.1$; (b) $\omega = 30$, $\delta_4 = 5$; (c) $\omega = 6$, $\delta_2 = 0.6$, $\delta_4 = 5$; (d) $\omega = 6$, $\delta_2 = 0.1$, $\delta_4 = 5$.

7. CONCLUSIONS

The solution existence problem for a wide range of robust performance and robust stability requirements has been dealt with. Feedback tolerances are explicitly imposed not only on the response to commands and disturbances but also on the control effort, which includes the cost of feedback. The simultaneous meeting of them was translated into the QFT loop shaping domain as the non-empty bound intersection of bounds at each frequency. The bound typology and bound aggressiveness were found the issues to concern. To guarantee bound solution in presence of arbitrarily large uncertainties inherent to the system nature, constraints on the specification tolerances were studied.

ACKNOWLEDGEMENTS

The authors gratefully appreciate the support given by the Spanish 'Comisión Interministerial de Ciencia y Tecnología (CICYT)' under grant DPI2000-0785.

REFERENCES

- Bailey, F.N. and C.-H. Hul (1989). CACSD tools for loop gain-phase shaping design of SISO robust controllers. *Proc. IEEE Control System Society Workshop on Computer Aided Control System*, 151-157.
- Biernson G. (1988). *Principles of Feedback Control*. Vol(1), Wiley.
- Bode H.W. (1945). *Network Analysis and Feedback Amplifier Design*, Van Nostrand, New York, USA.
- Borghesani C., Y. Chait O. and Yaniv (1994). *Quantitative Feedback Theory Toolbox User's Guide*. The Math Works Inc., USA.
- Chait, Y., C. Borghesani, and O.Yaniv (1995). Single-loop QFT design for robust performance in the presence of non-parametric uncertainties. *ASME J. of Dyn. Syst., Meas., Control*, 117, 420-424.
- Chait Y. and O. Yaniv (1993). Multi-input/single-output computer-aided control design using the Quantitative Feedback Theory. *Int. J. Robust & Non-linear Control*, 3, 47-54.
- Horowitz I.M. (1973). Optimum loop transfer function in single-loop minimum-phase feedback systems. *Int. J. Control*, 18 (1), 97-113.
- Horowitz I.M. (1979). Quantitative synthesis of uncertain multiple input-output feedback systems. *Int. J. Control*, 30 (1), 81-106.
- Horowitz I.M. (1991). Survey of quantitative feedback theory (QFT). *Int. J. Control*, 53 (2), 255-291.
- Horowitz I.M, and M Sidi, (1972). Synthesis of feedback systems with large plant ignorance for prescribed time-domain tolerances. *Int. J. Control*, 16 (2), 287-309.
- Horowitz I.M, and M Sidi. (1978). Optimum synthesis of nonminimum-phase feedback systems with parameter uncertainty. *Int. J. Control*, Vol. 27, pp.361-386
- Houpis, C.H., and G.B. Lamont (1988). *ICECAP-QFT Users Manual*, Air Force Institute of Technology, Electrical and Computer Department, Wright-Patterson AFB.
- Houpis C.H. and S.J. Rassmussen (1999). *Quantitative Feedback Theory. Fundamentals and Applications*. Marcel Dekker, New York, USA.
- Jayasuriya, S. (1990). QFT type design for maximizing tolerable disturbances in structured uncertain systems. *Recent Developments in QFT*, O.D.I. Nowokah ed., ASME Pubs., 51-58.
- Jayasuriya, S. and Y. Zhao (1994a). Stability of quantitative feedback designs and the existence of robust QFT controllers. *Int. J. Robust and Non-Linear Control*, 4, 21-46.
- Jayasuriya, S. and Y. Zhao (1994b). Robust stability of plant with mixed uncertainties and quantitative feedback theory. *ASME J. of Dyn. Syst., Meas., Control*, 116, 10-16.
- Longdon, L., and D.J. East (1978). A simple geometrical technique for determining loop frequency bounds which achieve prescribed sensitivity specifications. *Int. J. Control*, 30 (1), 153-158.
- Nataraj, P.S.V., and G. Sardar (2000). Computation of QFT bounds for robust sensitivity and gain-phase margin specifications. *ASME J. of Dyn. Syst., Meas., Control*, 122, 528-534.
- Nordgren, R.E., O.D.I. Nowokah and M.A. Franchek (1994). New formulations for quantitative feedback theory. *Int. J. Robust & Non-linear Control*, 4, 47-64.
- Nowokah, O.D.I and D.F. Thompson (1989). Algebraic and topological aspects of quantitative feedback theory. *Int. J. Control*, 50 (4), 1057-1069.
- Nowokah, O.D.I., D.F. Thompson and R.A. Perez (1990). On some existence conditions for QFT controllers. *Recent developments in QFT*. ODI Nowokah (Ed.), DSC, 24, 1-10.
- Rodrigues, J.M., Y. Chait, and C.V. Hollot, (1997). An efficient algorithm for computing QFT bounds. *ASME J. of Dyn. Syst., Meas., Control*, 119 (3), 548-552.
- Thompson D.F. (1998). Gain bandwidth optimal design for the new formulation quantitative feedback theory. *ASME J. of Dyn. Syst., Meas., Control*, 120, 401-404.
- Thompson D.F., and O.D.I. Nowokah (1989). Stability and optimal design in quantitative feedback theory. *Proc. ASME Winter Annual Meeting Conf.*, ASME Paper No. 89-WA/DSC-39.
- Thompson D.F., and O.D.I. Nowokah (1994). Analytic loop shaping methods in quantitative feedback theory. *ASME J. of Dyn. Syst., Meas., Control*, 116, 169-177.
- Wang, G.C., C.W. Chen, and S.H. Wang (1991). Equation for loop bound in quantitative feedback theory. *Proc. Conf. on Decision and Control*, 2968-2969.
- Yaniv O. (1992). *MISO QFT CAD Package*. Tel-aviv University, Israel.
- Yaniv O. (1999). *Quantitative Feedback Design of Linear and Non-linear Control Systems*. Kluwer Academic Publishers, Massachusetts, USA.
- Yaniv, O., and Y. Chait (1991). Direct robust control of uncertain sampled-data systems using the quantitative feedback theory. *Proc. ACC Conf.*, 1987-1988;
- Yaniv, O., and Y. Chait (1992). A simplified multi input/output formulation for the Quantitative Feedback Theory. *J. of Dyn. Syst., Meas., Control*, 114, 179-185.
- Yaniv and Chait (1993). Direct control design in sampled-data uncertain systems. *Automatica*, 29 (2), 365-372.
- Zhao, Y., and S.Jayasuriya (1994). On the generation of QFT bounds for general interval plants. *ASME J. of Dyn. Syst., Meas., Control*, 116, 618-627.

COMPARING ROBUST CONTROL DESIGN STRATEGIES FOR PRACTICAL IMPLEMENTATION IN AUTONOMOUS VEHICLES

L. Ganzelmeier, J. Helbig, E. Schnieder
Institute of Control and Automation Engineering
Technical University of Braunschweig
Germany

Langer Kamp 8
38106 Braunschweig
Germany

j.helbig@tu-bs.de

Abstract--In this paper a robust controller design task for the lateral dynamics of non-identical autonomous road vehicles is considered. The focus lies on the comparison of different design strategies for robust lateral control: H_∞ - control with unstructured uncertainties on the one side and QFT-Design with structured parameter uncertainties on the other side. It is shown that through the appropriate choice of design parameters, varying vehicle dynamics can be taken into account without substantial losses regarding accuracy and dynamics. Both design strategies are discussed in detail. The evaluation of both design strategies takes place using practical implementation results from the lateral control of autonomous vehicles.

Index Terms--robust control, autonomous non-identical vehicles, combustion engine, lateral dynamics, practical results

I. INTRODUCTION

During the last decades the subject of design and analysis of various longitudinal and lateral control laws has been studied extensively. Throughout the literature numerous topics such as sliding mode control, parameter scheduling, nonlinear vehicle dynamics, look-ahead curvature processing and automated highway systems have been reported [Byr98], [Ger96], [Man93], [Söh99]. Even though much effort have been spent on various control laws for longitudinal and lateral control of autonomous vehicles this paper presents a mostly neglected aspect of autonomous vehicle control.

The main task of the presented project is to drive non-identical customary cars completely autonomously. With varying vehicle parameters like the velocity or mass the dynamic of one vehicle is

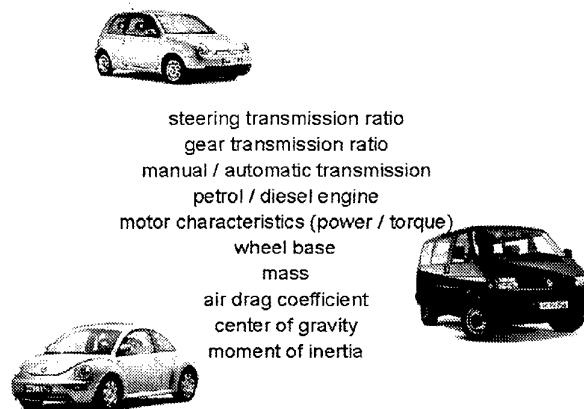


Fig. 1: Influence parameters on vehicle dynamics

continuously changing. In addition much larger influences exist from different dynamics of non-identical vehicles like shown in figure 1. For this reason it is a large challenge for every control task to operate appropriate under such a wide variety of vehicle dynamics. The basic idea is to take full advantage of recent robust controller design methodologies and using these advantages for longitudinal and lateral control of autonomous vehicles. This paper focuses on the different design strategies for robust lateral control. The studied cars are equipped with actuators that are able to turn the steering wheel, to press the clutch, brake, accelerator and to change the gears in cars with manual shift. Therefore the controllers have the full range to affect the vehicle in the way a human driver operates a car. In order to get sufficient information about the state of the vehicle an additional sensor is fixed to the car.

II. MODELLING OF LATERAL DYNAMICS

The design objective of lateral control of an autonomous vehicle is to ensure accurate tracking of a desired path. In previous research works the robust design objective is mainly to cover a wide range of longitudinal velocity without getting stability problems of the closed loop system [Byr98],[Man93],[Söh99]. This work goes a step beyond this point and presents a controller that covers not only broad changes in longitudinal velocity but also various types of cars. To illustrate the differences and with that the challenge for the robust design procedure two extremely different cars are shown in figure 2: A small passenger car (VW Lupo) and a bus (VW T4).



Fig. 2: Range of automatically driven cars

For the description of lateral vehicle dynamics the Single-Track Model [Mit90] is used. Certain simplifications are made: linear tire characteristics, both wheels of an axle merged together in a virtual center line and coupling of horizontal and vertical dynamics is not considered. This approach yields to a fourth order degree state-space representation which depends on all vehicle parameters and the longitudinal velocity:

$$\begin{aligned}\dot{x} &= Ax + Bu \\ y &= Cx\end{aligned}\quad (1)$$

III. ROBUST CONTROL OBJECTIVES

Classical controller design strategies base on the assumption that the nominal plant model equals the real plant. For various reasons this never emerge in practice.

Norm-based robust control

With the introduction of (unstructured) model uncertainties the described deviations can be handled. Unstructured model uncertainties are used if there are no information about the specific character of the uncertainties. Only an upper limit of the uncertainties can be given. Although the uncertainties are not known in detail it is possible to give an adequate condition for stability. This condition generally can be described with the aid of singular values respectively the H_∞ -norm and is known from common literature [Doy89] as Small-Gain-Theorem.

$$\bar{\sigma}[\Delta_A KS] = \|\Delta_A KS\|_\infty < 1 \quad \forall \omega \quad (2)$$

$$\bar{\sigma}[\Delta_M T] = \|\Delta_M T\|_\infty < 1 \quad \forall \omega \quad (3)$$

The Small-Gain-Theorem shows that stability with unstructured model uncertainties can be achieved by restricting the H_∞ -norm of certain closed loop transfer functions with a suitable controller K . Since the late eighties an algorithm for computing H_∞ -optimal controller in state space representation is known [Doy89]. The controller is calculated by solving two algebraic Riccati equations and consists of a combination of observer and state feedback control. The controller is called optimal as the H_∞ -norm and with that the largest singular value of the respective transfer function is getting minimal.

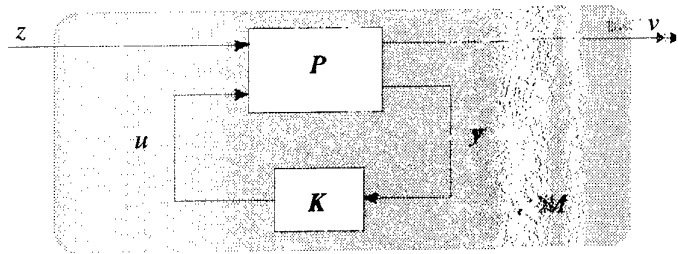


Fig. 3: Structure of the controller design task for robust stability

In consideration of figure 4 block P includes the mechanical plant model, the description of the model uncertainties in the frequency domain and the specifications for robust control performance by weighting the sensitivity function S . The controller K is designed in order to minimize the effects of the input signal z on the output signal v with regard to the H_∞ -norm for the generalized plant model. With

$$P = \begin{bmatrix} P_{11} & P_{12} \\ P_{21} & P_{22} \end{bmatrix} = \begin{bmatrix} A & B_1 & B_2 \\ C_1 & D_{11} & D_{12} \\ C_2 & D_{21} & D_{22} \end{bmatrix} \quad (4)$$

the transfer behavior from z to v is derived with the linear fractional transformation (LFT)

$$M = T_{vz} = LFT(P, K) = P_{11} + P_{12} K (I + P_{22} K)^{-1} P_{21} \quad (5)$$

The H_∞ -optimal controller K_∞ leads to

$$\|M\|_\infty = \|LFT(P, K_\infty)\|_\infty \rightarrow \min \quad (6)$$

Guaranteed stability for closed loop systems for plants with model uncertainties is called robust stability. The H_∞ -controller design leads to a controller that guarantees the best possible robust stability for models with unstructured uncertainties.

The controller in state-space representation is [Doy89]

$$K_x = [A + \gamma^{-2} B_1 B_1^T X_x + B_2 F_x + Z_x H_x C_2; Z_x H_x; F_x F_1]; 0] \quad (7)$$

with X_z and Y_z solutions of two algebraic riccati equations and F_z, H_z, Z_z as

$$\begin{aligned} F_z &= -B_z^T X_z \\ H_z &= -Y_z C_z^T \\ Z_z &= (I - \gamma^{-2} Y_z X_z)^{-1} \end{aligned} \quad (8)$$

Robust Control Design Using Quantitative Feedback Theory

Quantitative Feedback Theory is a frequency domain technique for robust controller design. In contrary to the H_∞ - design both unstructured and structured parameter uncertainties are considered [Bai91]. The frequency response is visualized with the Nichols plot (magnitude versus phase). For the nominal transfer function of the lateral dynamics for a passenger car travelling at $v=8\text{m/s}$ the nichols plot is shown in figure 4.

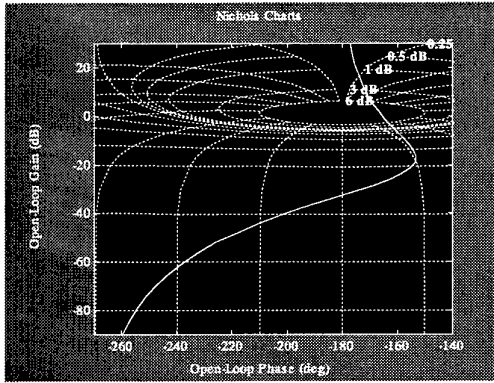


Fig. 4: Nichols Plot nominal plant

The plant uncertainties are the longitudinal velocity and the type of the car. Following the QFT-Design the plant templates for the described perturbations are shown in figure 5.

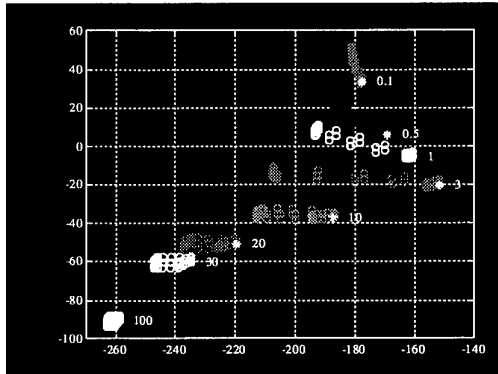


Fig. 5: Nichols Plot perturbed plant

The frequency domain specifications are given by certain transfer functions.

Sensitivity function / plant output disturbance rejection:

$$\left| \frac{1}{1+G_K} \right| < \delta_s \quad (9)$$

Plant input disturbance rejection:

$$\left| \frac{G}{1+G_K} \right| < \delta_G \quad (10)$$

Tracking boundaries (prefilter V):

$$\alpha < \left| \frac{V \cdot G_K}{1+G_K} \right| < \beta \quad (11)$$

With these frequency domain specifications the controller design via loop-shaping can be executed. The design objective is to find a controller K that satisfies all given frequency specifications. The loop-shaping is carried out regarding equally specifications and plant perturbations.

Loop-shaping:

$$|G_K(j\omega_i)| = |K(j\omega_i)| + |G_0(j\omega_i)| + \Delta(j\omega_i) \quad (12)$$

IV. PRACTICAL RESULTS

With both controller design strategies it is possible to cover the uncertainties resulting from all varying parameters and especially from the change in velocity. Figure 6 shows the results of a respective autonomous driving experiment: the vehicle starts in first gear switches to second gear and reaches its maximum velocity at 15m/s . To concentrate on the lateral dynamics only the tracking error between the desired path and the vehicles lateral position and the corresponding longitudinal velocity is plotted. The controller works without any stability or damping problems over the whole velocity range.

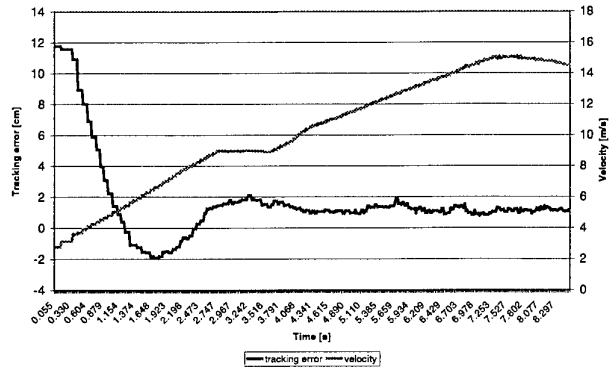


Fig. 6: Tracking error of lateral controlled vehicle over a wide velocity range

Figure 7 shows the respective picture series of this ride. To underline the achieved high accuracy of the lateral control the track was marked with guidance cones standing only a few centimeters on each side of the car.

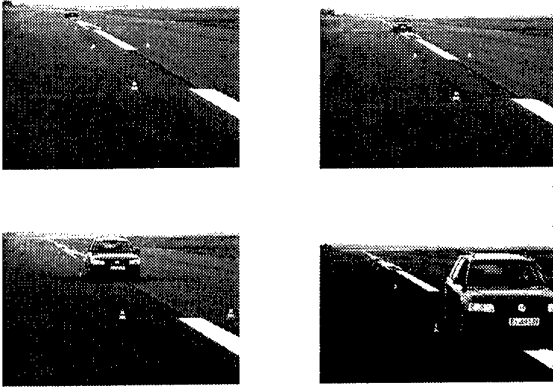


Fig. 7: Picture series of a completely autonomous driven vehicle

Even more interesting are the achieved results in the lateral control of different cars. The chosen cars represent the maximum possible range in passenger cars: A very small, short and lightweight car (VW Lupo - fig. 2), a middle class car (VW Passat - fig.) and a long and heavy van (VW T4 - fig. 2).

The specifications for the robust design cycle cover all differences between the various cars. To get comparable data the control task was the alignment of the car during accelerating up to 10m/s. The initial conditions of the tracking error between desired path and the vehicles lateral position were chosen between 6 and 9cm. Furthermore all cars were placed with distinct orientation regarding

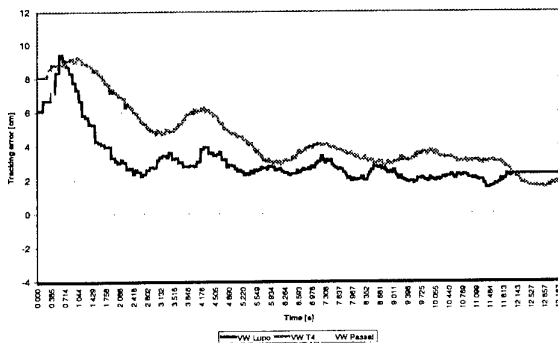


Fig. 8: Tracking error of various lateral controlled vehicles

the straight line. Experimental results for three different cars are shown in figure 8. The substantial differences between these cars in steering transmission ratio, wheel base, mass, center of gravity and moment of inertia are covered perfectly by the robust controllers (the results in fig. 6 and 8 are achieved with H_∞ - design).

V. CONCLUSION

In this paper we presented lateral control laws for non-identical autonomous road vehicles. The main scope was to extend previous approaches for autonomous vehicles. In previous research works the robust design objective was mainly to cover changes in the longitudinal velocity. This work goes a step beyond this point and presents a lateral controller that covers not only broad changes in longitudinal velocity but also various types of cars. The used controller designs for all lateral specifications are described. The first practical results for lateral robust control of non-identical autonomous vehicles are presented.

REFERENCES

- [Bai91] Bailey, F.N. and C.H. Hui: Loop Gain-Phase Shaping For Single-Input-Single-Output Robust Controllers. IEEE Control Systems, Vol. 15(1), p. 93-101, 1991
- [Byr98] Byrne, R.H., C.T. Abdallah and P. Dorato: Experimental Results in Robust Lateral Control of Highway Vehicles. IEEE Control Systems, Vol. 18(2), p. 70-76, 1998
- [Doy89] Doyle, J., K. Glover, P. Khargonekar and B.A. Francis: State Space Solution to Standard H_2 and H_∞ Control Problems. IEEE Transactions on Automatic Control, Vol. AC-34, No. 8, 1989
- [Ger96] Germann, S.: Modellbildung und modellgestützte Regelung der Fahrzeuglängsdynamik. VDI-Verlag, Reihe 12, Nr. 309, Düsseldorf, 1996
- [Hou99] Houppis, C.H. and S.J. Rasmussen: Quantitative Feedback Theory Fundamentals and Applications. Marcel Dekker, New York/Basel, 1999
- [Man93] Manigel, J.: Autonome Fahrzeugführung durch Rechnersehen. Dissertation, Technische Universität Braunschweig, 1993
- [Mit90] Mitschke, M.: Dynamik der Kraftfahrzeuge, vol. C, Berlin, Springer, 1990
- [Söh99] Söhnitz, I. and K. Schwarze: Control of an autonomous vehicle: design and first practical results. IEEE International Conference on Intelligent Transportation Systems 1999, Tokyo
- [Yan99] Yaniv, O.: Quantitative Feedback Design of Linear and Nonlinear Control Systems. Kluwer Academic Publishers, Boston/Dordrecht/London, 1999

ONE-DIMENSIONAL ACTIVE NOISE CONTROL USING THE INTERNAL MODEL PRINCIPLE

Michael O' Brien
Patrick Pratt
C.J. Downing

Abstract: With increasingly stringent E.U. regulations on the allowable decibel levels in the working environment, the requirement for active noise control solutions is becoming more important to the industrialist. Much of the unwanted sound that occurs in industry tends to be of a tonal nature. This paper outlines a technique that uses classical control structures coupled with the internal model principle and H_∞ optimization theory to suppress such acoustic disturbances. Furthermore, a discussion on the application and limitations of this technique to disturbances that contain multiple tones and, in particular, harmonics of a fundamental frequency will be presented.

Keywords: Robust Stability and Performance, Robust Control Applications, Uncertain Dynamic Systems.

1. INTRODUCTION

Traditionally, unwanted acoustic disturbances were suppressed using passive mufflers and dampers. This technique is applied where the target disturbance frequencies lie approximately above 500Hz. However, for frequencies below this value, the space required to physically implement such solutions becomes extremely cumbersome. Consequently, active noise control is becoming progressively more important to the industrialist as a substitute for these passive solutions.

The concept of active noise control is illustrated in figure 1. It may be seen that a spatial superposition occurs between the primary unwanted signal and secondary signal from the cancellation loudspeaker. In effect, destructive interference occurs, causing a localized zone of silence.

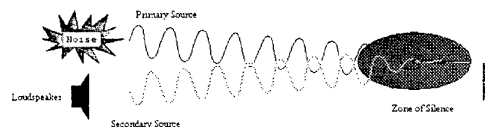


Figure 1. Fundamentals of Active Noise Control

In the past two decades, several successful active noise control applications have been reported, mainly in systems with one-dimensional properties. In particular, Eriksson (1985), Elliot (Elliot and Nelson, 1984) and Morgan (1980) contributed significantly to the initial developments in this area. The most common reported active noise control applications are one-dimensional acoustic ducts such as in heat-ventilation and air-conditioning systems.

Inherent in acoustic plants is a high level of uncertainty and considerable time variance. For this reason, much of the earlier work in this field suggested that adaptive feedforward solutions were the most viable. However, in the late 1970s Zames (1979) developed a new

feedback strategy, referred to as H_∞ control, which allowed the design of controllers specifically for uncertain plants. It took almost fifteen years before this design strategy found application in active noise control. Early work by Nakai *et al.* (1994), suggested robust techniques as an alternative to the adaptive strategy, but it was not until the latter half of the 1990s that Hu (1996, 1998) and Rafaely (1997) reported successful applications. However, much of this work, though non-adaptive in nature, remained feedforward in structure. Moreover, much of the literature neglected the practical issues of implementing feedback techniques for active noise control. O' Brien and Pratt (2001c) identify many of the theoretical and practical implications of implementing robust active noise control. Furthermore, O' Brien and Pratt (2001b) outline a reasonably extensive comparison between the adaptive and the robust active noise control strategies.

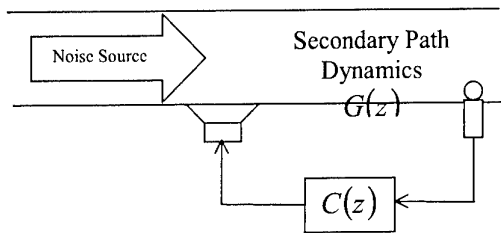


Figure 2. Feedback active noise controller applied to a one-dimensional acoustic duct

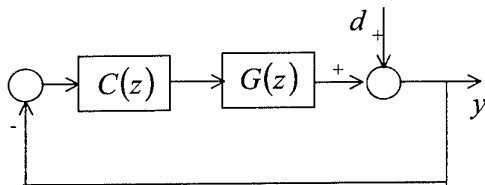


Figure 3. Classical feedback controller

Figure 2 illustrates the basic one-dimensional SISO robust active noise control solution. This can be easily reconciled with the classical feedback structure of figure 3. It may be shown that noise attenuation in the acoustic duct is equivalent to disturbance rejection in the classical sense. Moreover, Kuo and Morgan (1996) showed that the secondary path plant is time variant and thus any model acquired for $G(z)$ will invariably be uncertain. Therefore, the main requirements of the controller, $C(z)$, are internal stability and good disturbance rejection in the presence of an uncertain secondary path.

Central to the robust performance of any closed loop system is the *sensitivity function*, which is given by $S(z) = 1/(1 + C(z)G(z))$. It may be shown that a small value of sensitivity at certain frequencies is equivalent to good disturbance rejection at those frequencies.

Equally important is the *complementary sensitivity function* $T(z) = C(z)G(z)/(1 + C(z)G(z))$, which may be interpreted as a set point tracking metric.

2. INTERNAL MODEL PRINCIPLE

In many classical feedback structures, similar to figure 3, the unwanted disturbance d is tonal in nature. The *internal model principle* is a technique used in feedback systems to reject tonal disturbances at the output. If we assume that the tonal disturbance d in figure 3 has a frequency of ω_n rad/s, then the requirement of the internal model principle is that the closed loop system contain an internal model of the tonal disturbance in the forward path. Thus, the product $C(z)G(z)$ must contain the factor $Z\{s^2 + \omega_n^2\} = 1 - 2\cos(j\omega_n T_s)z^{-1} + z^{-2}$ in the denominator, where T_s is the sample time and $Z\{\}$ denotes the z-transform. Francis and Wonham (1976) provide a comprehensive analysis of the internal model principle.

2.1 Application of the Internal Model Principle to Active Noise Control Applications

As previously observed, much of the unwanted acoustic noise that occurs in practice tends to be tonal in nature. Consequently, the internal model principle may be satisfactorily applied to reject such deterministic disturbances. The application of the internal model principle is demonstrated in figure 4, which, in effect, is a modification of figure 3. Due to the fact that an internal model of the disturbance is now present in the forward path, the modified requirement is to design a controller that is robustly stable for the modified plant $G'(z)$, where $G'(z)$ is given by

$$G'(z) = \frac{G(z)}{Z\{s^2 + \omega_n^2\}} \quad (1)$$

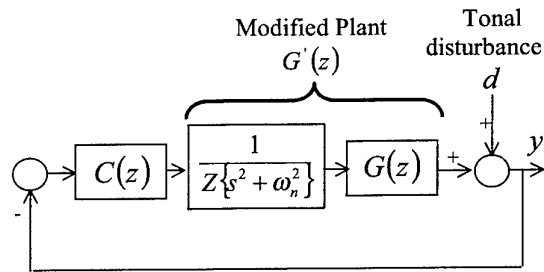


Figure 4. Classical feedback controller incorporating the internal model principle for rejection of tonal disturbance with frequency ω_n rad/s

2.2 Tonal Disturbance Propagation in the Prototype Acoustic Plant

The prototype plant used for all experiments was a one-dimensional acoustic duct approximately 10cm in diameter and 1m in length. A noise source was placed upstream within the duct which produced a tonal disturbance of 230Hz. The cancellation speaker and the feedback microphone were mounted on the wall of the duct approximately 30cm and 10cm respectively from the mouth.

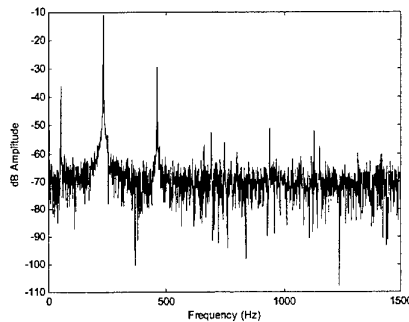


Figure 5. Existence of downstream fundamental and induced harmonics in the acoustic duct

Figure 5 depicts the disturbance signal detected by the feedback microphone without cancellation being employed. Initially, it may be observed that the 230Hz tone is present, but harmonics of this frequency are also induced. It is surmised (O' Brien and Pratt, 2000) that the presence of these harmonics is due to the existence of non-linearities in the source and in the plant. More importantly, it must be noted that successful active noise control within the duct requires the cancellation of both the fundamental and the induced harmonics. The cancellation of the fundamental is discussed in section 4.1, while sections 5 and 6 outline the issues involved in canceling the first and any higher harmonics. Also present, but not considered, is an unwanted 50Hz hum that is due to the transformer driving the power amplifiers. It is important to note that the existence of non-linearly induced harmonics is not limited to this prototype duct, but will be present to varying degrees in most acoustic systems.

3. PARAMETERIZATION OF PLANT UNCERTAINTY

One of the key advantages of employing H_∞ control for closed loop systems is the method by which plant uncertainty is defined. Due to its extensive analysis in the literature, plants are often defined with a *multiplicative disk-like uncertainty*

$$G(z) = \{G_0(z)(1 + W_2(z)\Delta)\} \quad \|\Delta\|_\infty < 1 \quad (2)$$

where Δ is the structured plant perturbation.

Dropping the dependence on z for the purpose of convenience, G_0 is the nominal plant, and W_2 is a frequency dependent function that places a bound on the maximum allowable uncertainty. O' Brien and Pratt (2001c) offer guidelines for the selection of this perturbation bound in typical acoustic plants. Indeed, it is generally accepted that plants are well modelled at lower frequencies with the uncertainty increasing at higher frequencies. For the prototype duct, it was found that uncertainty becomes significant above 250Hz. Consequently, W_2 was chosen to be small below this frequency and large at frequencies higher than 250Hz. An appropriate weighting function was found to be

$$W_2 = Z \left\{ \frac{0.09s}{s + 250(2\pi)} \right\} \quad (3)$$

Doyle *et al.* (1992) show that robust stability is maintained *iff* the following condition is met

$$\|W_2 T\|_\infty < 1 \quad (4)$$

In summary, if a controller can be designed to meet (4) for the modified uncertain plant $G'(z)$ in figure 4, then good tonal attenuation is achievable within the duct.

3.1 Estimating the Plant Model

Central to the H_∞ design methodology is the requirement for a nominal plant model. Hu (1995, 1996) derived a mathematical model of a typical acoustic duct; however, due to their relative complexity, mathematical models of acoustic systems are difficult to obtain and consequently models are generally estimated empirically. In this case, the methodology for acquiring a plant model is given in figure 6.

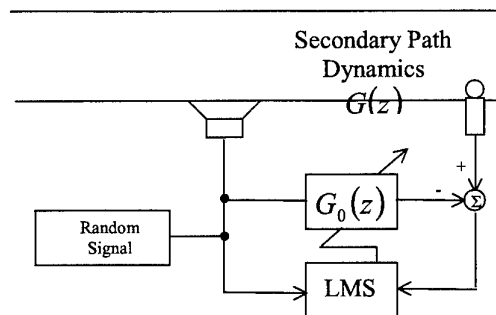


Figure 6. Estimation of the secondary path

It should be noted that switching off the unwanted disturbance while estimation is being performed yields a more accurate plant model. Following this, a persistently exciting signal is injected through the cancellation speaker (in this instance a random signal was used). The LMS algorithm was then used to adaptively estimate an FIR model of the secondary path. Kuo and Morgan (1996) exhaustively discuss this estimation technique.

It was found that a more accurate model was achieved as the number of FIR filter taps was increased. It is particularly obvious from figure 7 that low order models cannot model high frequency pole and zero dynamics. However, for reasons outlined by O'Brien and Pratt (2001b), an FIR filter with 16 taps was chosen to model the secondary path.

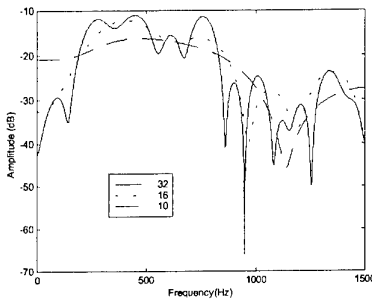


Figure 7. Spectral plots of the acoustic plant model for filter lengths of 32, 16 and 10.

3.2 Failure of H_∞ Control and the Internal Model Principle

The calculation of a H_∞ optimal controller is a non-trivial exercise, with some numerical techniques available in the literature. In particular, Grimble (1994) proposes a polynomial solution, but a state-space solution outlined by Safonov *et al.* (1989) is generally favoured. For this application, all of the controllers were evaluated using the Mathworks Inc. (1998) MATLAB *dhinf* command, which employs the latter technique as its solver. A plant model was estimated as an FIR filter of length 16 using the technique given in section 3.1. The target disturbance signal to be cancelled was a 230Hz tone. Following this, the plant was modified by including the factor $Z\{s^2 + (2\pi 230)^2\}$ in the denominator of the plant model. Note that a sample frequency of 3kHz was chosen, which met Nyquist's criterion and was still within the processing capabilities of the controller. With this established, and the uncertainty bound defined in (3), a robustly stabilizing controller was designed. However, when this controller was implemented on the prototype system, robust stability was maintained but no cancellation of the 230Hz disturbance occurred.

Careful scrutiny of the designed controller $C(z)$ indicated that the factor $Z\{s^2 + (2\pi 230)^2\}$ was contained in its numerator. In effect, this cancelled the factor $Z\{s^2 + (2\pi 230)^2\}$ in the denominator of the modified plant within the forward path $C(z)G'(z)$. This invalidated the internal model principle, even though robust internal stability was being maintained. Because of this, an alternative method had to be pursued to implement the internal model principle in the acoustic system. Note that the ineffectiveness of the internal model principle may be a general problem with H_∞ design for closed loop plants. However, this requires further investigation.

4. THE SENSITIVITY FUNCTION BOUND

Inherent in the H_∞ design technique is the ability to shape the sensitivity function, i.e. to specify at the design phase a bound on the disturbance rejection capabilities for the closed loop system in figure 3. Thus, a second frequency dependent weighting

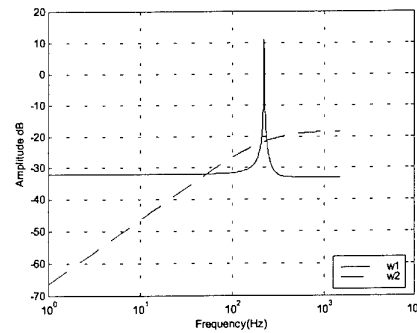


Figure 8. Frequency plots of the uncertainty perturbation bound W_2 and the sensitivity bound W_1

function W_1 is introduced that places a bound on the sensitivity function as follows

$$S < 1/W_1 \quad \forall \omega \quad (5)$$

This may be written in terms of ∞ -norms as

$$\|W_1 S\|_\infty < 1 \quad (6)$$

Therefore, if rejection over a specific frequency band is required, W_1 must be made large over that band.

Doyle *et al.* (1992) show that satisfactory disturbance rejection, while maintaining robust stability in the presence of plant uncertainty, requires that the following condition be met.

$$\|W_1 S\| + \|W_2 T\|_\infty < 1 \quad (7)$$

4.1 Using the Sensitivity Bound to Implement the Internal Model Principle

From the discussion in the previous sub-section it may be deduced that if cancellation of a tone of frequency ω_n rad/s is required, then W_1 must be large at this frequency. This is achieved by ensuring that the factor $Z\{s^2 + \omega_n^2\}$ exists in the denominator of W_1 . Thus, for cancellation of a 230Hz tonal disturbance, the following weighting function was used (which is a first order band-pass Butterworth filter whose pass-band lies in the region of 230Hz)

$$W_1 = Z\left\{0.025 \frac{s^2 + 628.3s + [230(2\pi)]^2}{s^2 + [230(2\pi)]^2}\right\} \quad (8)$$

Frequency plots of W_1 and W_2 are given in figure 8. Once again, the MATLAB *dhinf* command was used to calculate the controller and upon implementation it was found that robust stability was maintained. Moreover, as may be observed from figure 9, 28dB reduction of the 230Hz tone was achieved.

On analysing the controller it was observed that its denominator contained the factor $z^2 - 1.772z + 1$, which may be shown to be $Z\{s^2 + (2\pi 230)^2\}$ for a sampling frequency of 3kHz. In effect, the internal model principle is being implemented to reject the unwanted 230Hz acoustic disturbance.

5. CANCELLATION OF THE FIRST HARMONIC

Careful scrutiny of figure 9 indicates the existence of the uncanceled 460Hz first harmonic. Not included in figure 9 but significantly present are uncanceled second and third harmonics. O'Brien and Pratt (2000) outline an adaptive solution to cancel these harmonics. However, the internal model principle can be extended to deal with multiple tonal frequencies. The uncertainty bound weighting function in (3) is used to calculate the final controller and once again the factor $Z\{s^2 + (2\pi 230)^2\}$ must be present in the denominator of the controller to ensure cancellation of the fundamental. Furthermore, if the first harmonic is also to be cancelled, then the factor $Z\{s^2 + (2\pi 460)^2\}$ must also be present in the denominator of the controller. From this discussion, the disturbance rejection weighting function, W_1 , was chosen to be

$$W_1 = W_{1a} W_{1b} \quad (9)$$

where W_{1a} and W_{1b} are given by

$$W_{1a} = Z\left\{0.025 \frac{s^2 + 628.3s + [230(2\pi)]^2}{s^2 + [230(2\pi)]^2}\right\} \quad (10.a)$$

and

$$W_{1b} = Z\left\{\frac{s^2 + 502.7s + [460(2\pi)]^2}{s^2 + [460(2\pi)]^2}\right\} \quad (10.b)$$

respectively.

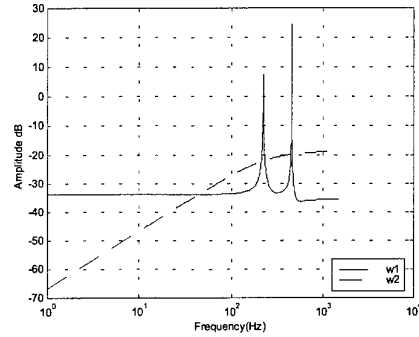


Figure 10. Frequency plots of the uncertainty perturbation bound W_2 and the modified sensitivity bound W_1

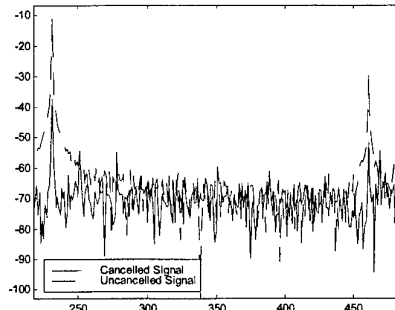


Figure 11. Cancellation of a 230Hz fundamental and its first harmonic at 460Hz using the internal model principle

Frequency plots of the modified weighting functions are given in figure 10. Upon calculation of the controller it was found that its denominator contained the factors $z^2 - 1.772z + 1$ and $z^2 - 1.141z + 1$. These may be shown to be $Z\{s^2 + (2\pi 230)^2\}$ and $Z\{s^2 + (2\pi 460)^2\}$ respectively for a sampling frequency of 3kHz. Initially it was observed that robust stability was once again maintained with the calculated controller. In addition, it may be seen from

figure 11 that 28dB cancellation of the fundamental is maintained, with a further 20dB reduction of the first harmonic being achieved.

6. CANCELLATION OF THE HIGHER HARMONICS

With cancellation being realized for the fundamental and the first harmonic, the obvious progression is to design a controller that achieves cancellation for the second and higher harmonics. To include the second harmonic at 690Hz, the weighting function W_1 must now include W_{1a} and W_{1b} in cascade, along with the factor $Z\{s^2 + (2\pi 690)^2\}$ in its denominator. However, experimentation indicated that a robustly stabilizing controller could not now be found with the MATLAB solver. The rationale for this will duly be explained.

Due to their inherent acoustic propagation delay, acoustic systems contain the dynamic equivalent of non-minimum phase zeros. Bosgra and Kwakernaak (1999) outline the implications of non-minimum phase dynamics for a feedback system, with O'Brien and Pratt (2001a) indicating their specific significance to acoustic systems. The findings of these authors may be summarized as follows: -

- The waterbed effect is a phenomenon that occurs only in non-minimum phase systems. This states that an improvement in sensitivity at any frequency must be coupled with degradation in performance at some other frequency. This is stated more definitively in (11) where it is assumed that the system contains non-minimum-phase zeros but no unstable poles (which is typical of acoustic plants).

$$\int_0^\infty \log|S(j\omega)|d\omega = 0 \quad (11)$$

The sensitivity function must be less than unity at the position of non-minimum phase zeros.

- When this is coupled with the waterbed effect, it is found that the disturbance amplification at some other frequencies becomes far more pronounced.
- The bandwidth over which sensitivity reduction can occur is limited by the lowest non-minimum phase zero.

It is clear that these observations may compromise the performance of robust active noise control solutions. In particular, it was found from the plant model that the lowest non-minimum phase zero was located at approximately 50Hz. With considerable bandwidth already sacrificed in cancelling the fundamental 230Hz tone and the first harmonic at 460Hz,

experimentation indicated that insufficient bandwidth was available to cancel the second and any higher harmonics.

7. CONCLUSION

It was shown that successful active noise control of tonal disturbances could be implemented via the internal model principle and a H_∞ optimal controller. In noise control applications, the target acoustic plant is highly uncertain and time variant. Thus, careful selection of an uncertainty bound is required for a successful solution. It was found that plant models were generally accurate at lower frequencies, with uncertainty increasing at higher frequencies.

A difficulty arose when the controller produced by the MATLAB solver possessed inverse marginally stable dynamics, which cancelled the dynamics introduced by virtue of the internal model principle. As a result, no cancellation of the tonal disturbance occurred.

Nevertheless, an appropriate selection of the sensitivity bound, also inherent in the H_∞ cost formulation, can make the closed loop system implicitly contain the internal model principle. For the prototype system, it was found that successful attenuation of 28dB of the 230Hz fundamental and 20dB of its first harmonic could be achieved. However, the physical properties of the duct prohibited any attenuation of the second and higher harmonics.

8. REFERENCES

- Bosgra, O. and Kwakernaak, H., (1999). *Design Methods for Control Systems* Notes for a course of the Dutch Institute of Systems and Control Winter term 1999-2000
- Doyle J., Francis B., Tattenbaum A., (1992). *Feedback Control Theory*, Macmillan Publishing Company, NY.
- Elliot, S.J. and Nelson, P.A., (1984). Models for Describing Active Noise Control in Ducts *I.S.V.R Technical Report No. 127*, NTIS PB85-189777
- Eriksson, L.J., (1985). *Active Sound Attenuation Using Adaptive Signal Processing Techniques* Ph.D Thesis, University of Wisconsin-Madison
- Francis, B.A., Wonham, W.M. (1976) The Internal Model Principle of Control Theory *Automatica* Vol. 12 pp. 457-465
- Grimble, M.J., (1994). *Robust Industrial Control – Optimal Design Approach for Polynomial Systems*, Prentice Hall Inc., Englewood Cliffs, NJ
- Hu, J. (1995). Active Sound Cancellation in Finite-Length Ducts Using Closed Form Transfer

- Function Models, *ASME J. Dynamics Syst., Measurement, Contr.*, **Vol. 117, No. 2**, pp. 143-154,
- Hu, J.S., (1996). Active Noise Cancellation in Ducts Using Internal Model Based Control *IEEE Trans on Contr Sys Tech*, **Vol. 4 No. 2**
- Hu J. S., (1998). Application of Model Matching Techniques to Feedforward Active Noise Controller Design, *IEEE Trans on Contr Sys Tech*, **Vol. 6 No. 1**
- Kuo, S.M. and Morgan, D. R., (1996). *Active Noise Control Systems: Algorithms and DSP Implementation*, John Wiley & Sons, Inc. NY
- Mathworks Inc., (1998), *Robust Control Systems Toolbox User's Guide*. Natick, MA.
- Morgan, D.R., (1980). An Analysis of Multiple Correlation Cancellation Loops with a Filter in the Auxiliary Path' *IEEE Trans. Acoust., Speech, Signal Processing*, **ASSP-28**, 454-467
- Nakai H, Amano Y, Kimura T and Nagano M, (1994). 2-Degree-of-Freedom Control Approach to Active Noise Control, *Proc. Inter-Noise 94*
- O' Brien M. and Pratt P. (2000). Non-Linear Active Noise Control for Poorly Correlated References, *Presented at ISSC-2000*
- O' Brien, M. and Pratt, P., (2001a). Active Noise Control Using Robust Feedback Techniques *IEEE International Conference on Acoustics, Speech and Signal Processing - ICASSP 01*
- O' Brien M. and Pratt P. (2001b). A Comparison Between Adaptive and Robust Active Noise Control Strategies, *ISSC 2001 (To be Published)*
- O' Brien M. and Pratt P. (2001c). On the Selection of Weighting Functions for Robust Active Noise Control Applications, *(Unpublished Work)*
- Rafaely, B., (1997). *Feedback Control of Sound*, PhD Thesis, University of Southampton
- Safonov, M.G., Limebeer, D.J.N and Chiang, R. Y., (1989). Simplifying the H_∞ Theory via loop-shifting, matrix-pencil and descriptor concepts, *Int. J. Control*, **Vol. 50, No. 6**, 2467-2488
- Zames G., (1979). Feedback and Optimal Sensitivity: Model Reference Transformations, weighted Seminorms and Approximate Inverses, *Proc. 17th Allerton Conf.*, pp. 744-752

APPLICATION OF A ROBUST FAULT-TOLERANT CONTROL SCHEME TO A NONLINEAR SYSTEM

Alberto Cardoso*, António Dourado**

*CISUC- Centre for Informatics and Systems of the University of Coimbra
Dep. de Engenharia Informática, Pólo II da UC, 3030 Coimbra, Portugal
e-mail: *alberto@dei.uc and **dourado@dei.uc.pt*

Abstract: This paper investigates the application of a robust FDI (fault detection and isolation) and control strategy for a non-linear system. This strategy considers (i) an observer-based approach to estimate the state variables of the system and (ii) the integration of the control design and the fault diagnosis in an H_∞ framework. The main purposes are to obtain a controller with robustness against uncertainty and with insensitivity to faults, and a fault detection filter to generate residual signals, which are used to isolate and identify the faults. This approach is applied to a non-linear system, a laboratory inverted pendulum.

Keywords: Fault-tolerant systems, uncertain dynamic systems, robust control, fault detection and diagnosis, non-linear systems.

1. INTRODUCTION

Growing demands on reliability and safety have increased the use of fault tolerant control approaches to design process control systems. A common approach considers a fault diagnosis module, which includes the detection, isolation and identification actions, followed by the reconfiguration of the control system in case of a fault is detected. That module considers a fault detection filter to generate residual signals in order to detect and isolate the faults. To obtain an optimal design in the case of process uncertainty, the design of the controller and FDI (fault detection and isolation) filter should not be separated (Niemann and Stoustrup, 1997).

Considering a model-based FDI approach, the robust control techniques and the H_∞ framework can be used to design the fault tolerant control system, integrating the controller and the fault detection filter.

The control system obtained with this methodology should improve the plant efficiency and the closed loop

performance in presence of faults, disturbances and uncertainty.

The approach considered in this work, uses the generalised setup for robust control to integrate the uncertainty, controller and fault diagnosis specifications in the same framework. The fault tolerant control system is obtained using a μ synthesis method and the D - K iterative technique, followed by the optimal Hankel norm approximation (Anderson and Liu, 1989) for controller order reduction. The model-based FDI approach considers an observer-based method to estimate the state variables of the process.

This methodology was initially presented in (Nett, *et al.*, 1988) and further developed in (Tyler and Morari, 1994), (Isermann, 1994) and (Niemann and Stoustrup, 1997).

The model-based fault detection filter considers the analytical redundancy inherent in the dynamic relationships between inputs and outputs of a system.

Usually, a mathematical model is used to derive a residual quantity, which is supposed to be "small" for an unfaulty plant and "large" whenever a fault occurs. Faults could then be detected if the residual exceeds a given threshold. In order to achieve fault isolation, a set of residuals could be used, each one indicating a different fault. Surveys can be found for instance in (Frank and Ding, 1997), (Patton, 1997), (Chen and Patton, 1999) and (Frank, *et al.*, 2000).

This work claims to give a contribution for the robustness analysis of the control and fault diagnosis system with respect to abrupt faults in actuators and sensors of a non-linear system. The generalised controller, including the robust controller and fault detection filter, is designed using the robust control framework and the frequency domain representation of the design objectives, and was successfully applied to an inverted pendulum system.

The fault detection filter is designed to generate a set of residuals corresponding to the expected faults in the system. The residual signals can be used to identify an occurred fault and then as input of a supervisory system to generate alarm signals and to monitor the closed loop system's performance. The diagram of a fault tolerant control system considering fault diagnosis and supervision is represented in Figure 1.

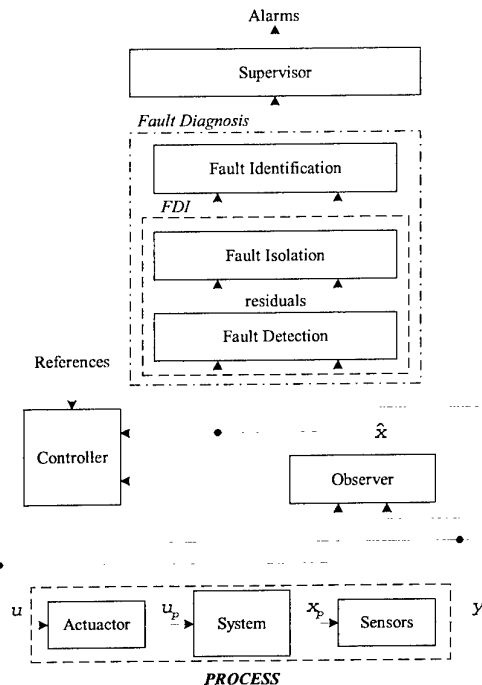


Fig. 1. Diagram of the fault tolerant control system considering fault diagnosis and supervision to generate alarm signals.

2. DESIGN FORMULATION

Considering the model-based approach, a mathematical model is built and in a non-linear system case, a model linearisation around an operating point is performed. The deviations between the linear model and the real plant will be considered as uncertainties in the control system formulation. For fault diagnosis purposes, the system is described including actuator and sensor faults, which are represented by additive signals as illustrated in Figure 2. The system dynamics can be described by the state space model (1):

$$\begin{aligned} \dot{x}(t) &= Ax(t) + Bu_R(t) & y_R(t) &= Cx(t) + Du_R(t) \\ y(t) &= y_R(t) + f_s(t) & u_R(t) &= u(t) + f_a(t) \end{aligned} \quad (1)$$

Concerning the control system formulation, instead of using a standard one parameter controller, a two parameter generalised controller (controller and fault detection filter), given by (2), will be considered to integrate the control design (control action $u(t)$) and the fault detection filter (residual signal $r(t)$).

$$\begin{bmatrix} u(t) \\ r(t) \end{bmatrix} = Ky(t) = \begin{bmatrix} K_1 \\ K_2 \end{bmatrix} y(t) \quad (2)$$

The design setup uses a generalisation of the standard configuration for robust control (Zhou *et al.*, 1996; Niemann and Stoustrup, 1997) as illustrated in Figure 3.

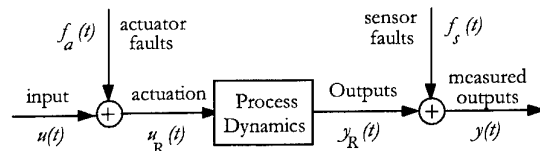


Fig. 2. System description with actuator and sensor faults.

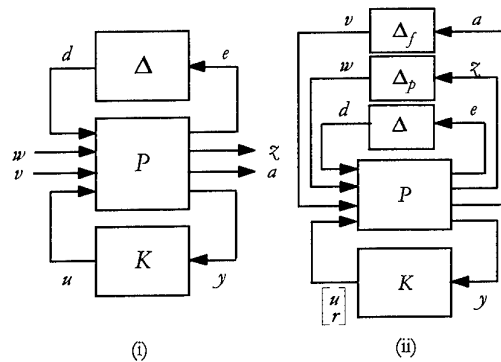


Fig. 3. (i) Generalised setup for robust control. (ii) Setup with performance and fault detection specifications, represented by fictitious perturbations blocks.

In this generalised setup, the model uncertainty is represented by Δ , and the fault detection and the performance specifications by fictitious perturbations blocks Δ_f and Δ_p , respectively. It is assumed that each block is scaled such that $\|\Delta\| \leq 1, \forall \omega$.

The block P is an augmented plant, including the nominal plant model and the uncertainty description, fault detection and performance weighting functions (Lundström *et al.*, 1991). To achieve fault isolation, the fault detection weighting functions must represent the expected behaviour of each fault. In this work, the effects of abrupt faults are investigated.

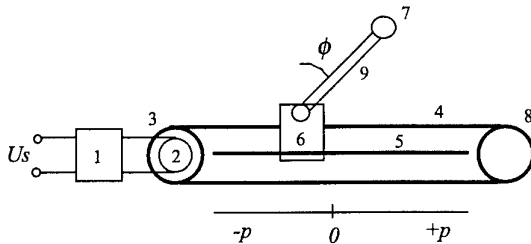
The generalised controller, to be designed using the μ synthesis, must achieve nominal and robust stability and nominal and robust performance. For the purpose of analysis, the controller K is combined with the augmented plant P using a lower linear fractional transformation (LFT) to obtain a $M-\Delta$ structure (Balas, *et al.*, 1993; Postlethwaite and Skogstad, 1993).

To obtain a robust controller and a robust fault detection filter, the $D-K$ iterative procedure, initially proposed by Doyle and Stein (1981), is applied using the Matlab[®] μ Analysis and Synthesis Toolbox (Balas, *et al.*, 1993).

3. THE INVERTED PENDULUM

The Inverted Pendulum consists of a cart and an aluminium rod with a cylindrical weight (pendulum) fixed to the cart by an axis. The cart, which can be moved along a guiding bar, is connected by a transmission belt to a drive wheel.

The wheel is driven by a current controlled motor, which delivers a torque proportional to the acting control voltage (U_s) such that the cart is accelerated. A scheme of the plant is illustrated in Figure 4.



1- Servo-amplifier 2- Motor 3- Drive wheel
4- Transmission Belt 5- Metal guiding bar 6- Cart
7- Pendulum weight 8- Guide roll 9- Pendulum rod

Fig. 4. Scheme of the Inverted Pendulum.

Two output variables are measured:

- i) the cart position by means of an incremental encoder which is fixed to the driving shaft of the motor;
- ii) the angle of the pendulum rod by means of an incremental encoder which is fixed to the pivot of the pendulum.

The inverted pendulum system can be described by a mathematical model as a system of coupled differential equations. These equations have been derived using the equation of motion for the cart and the angular momentum conservation law for the rotary motion of the rod about the centre of gravity.

This model is non-linear with some uncertain factors as the dry friction (Coulomb friction) and the static friction acting on the cart. In order to obtain a suitable linear model a linearisation is performed around the main operating point of the plant.

However, in the linear model is not possible to consider the effects of the non-linearities. To reduce the effects of the dry and static frictions (main non-linearities), a compensator was introduced. This compensator has a constant value obtained experimentally.

The linear model is valid as long the following conditions are satisfied:

- i) a limitation of the control force F ($|F| \leq 20N$);
- ii) a limitation of the guiding bar ($|\text{cart position}| \leq 0.5m$);
- iii) a limitation of the angle ϕ ($|\phi| \leq 10^\circ$).

The state and output equations, describing the system, are given by:

$$\dot{x} = Ax + bu \quad \text{and} \quad y = Cx \quad (3)$$

with

$$x = \begin{bmatrix} x_1 \\ x_2 \\ x_3 \\ x_4 \end{bmatrix} = \begin{bmatrix} \Delta p \\ \phi \\ \dot{r} \\ \dot{\phi} \end{bmatrix} = \begin{bmatrix} \text{cart position perturbation} \\ \text{pendulum angle} \\ \text{cart velocity} \\ \text{pendulum angular velocity} \end{bmatrix} \quad (4)$$

and

$$u = [\text{Force acting via the transmission belt}] \quad (5)$$

The main operating point is defined by (6):

$$x_0 = [x_1 = p \quad x_2 = 0 \quad x_3 = 0 \quad x_4 = 0]^T \quad (6)$$

The state matrices are given by (7):

$$A = \begin{bmatrix} 0 & 0 & 1 & 0 \\ 0 & 0 & 0 & 1 \\ 0 & -0.757 & -2.47 & 0.00068 \\ 0 & 20.346 & 4.7569 & -0.0185 \end{bmatrix} \quad b = \begin{bmatrix} 0 \\ 0 \\ 0.247 \\ -0.475 \end{bmatrix} \quad (7)$$

$$C = \begin{bmatrix} 1 & 0 & 0 & 0 \\ 0 & 1 & 0 & 0 \end{bmatrix}$$

The obtained system is unstable and the controller must guarantee the stability of the closed loop system, even if noise, disturbances or faults, limited to a given range, are present.

4. THE ROBUST CONTROL FRAMEWORK

To design a robust controller for the inverted pendulum system, the framework of the control system with uncertainties, which will allow the application of the μ -synthesis and analysis, is shown in Figure 5.

In this figure the structure of the augmented plant P is built using the weighting transfer functions to describe the objectives and to weight the input signals. In the framework, the external input w includes the measurement noise in each sensor and the cart position reference. The three considered faults (f_a , f_{s1} , f_{s2}) are represented by the input variable v . The performance and the fault detection objectives are represented by the external outputs z and a , respectively.

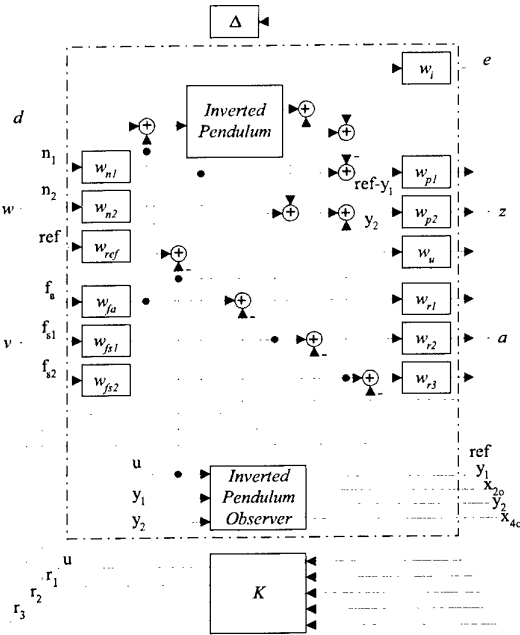


Fig. 5. Setup for robust control and fault detection for the inverted pendulum plant.

The inputs of the generalised controller are the cart position reference, the two plant's measured outputs (the

cart position and the pendulum angle) and the other two state variables (cart and pendulum angular velocities), which are generated by an observer system. Concerning the outputs, the control action is generated by the controller and the residual signals are obtained by the fault detection filter.

To approximate the control problem into a μ problem suitable for D - K iteration, the uncertainty is represented by a norm-bounded perturbation and a weighting transfer function, and the specifications for the closed loop system are expressed in the frequency domain as weighting transfer functions.

The design objectives for the closed loop system can be formulated as:

- i) the output signal y_1 should track the cart position reference, ref , and the output signal y_2 should tend towards zero;
- ii) the two outputs should be insensitive to noise and faults;
- iii) the control action at high frequencies should be restricted, avoiding rapid variations;
- iv) the residual signals, r_1 , r_2 and r_3 , should be large only when a fault has occurred, f_a , f_{s1} and f_{s2} , respectively;
- v) these objectives should hold in the presence of a bounded uncertainty, Δ .

To achieve these objectives, the weighting transfer functions of the augmented plant P must be chosen appropriately. The selection of these transfer functions is a fundamental task to address the trade-offs between control and fault detection.

4.1 Uncertainty description

The inverted pendulum plant is represented by the nominal plant model, $G_{nom}(s)$, with an uncertainty description defining the set of all possible plant variations. In this case, the plant uncertainty is described by structured multiplicative input uncertainty. The set of all possible plants $G(s)$ is then described by equation (8).

$$G(s) := \left\{ \begin{array}{l} G_{nom}(s)(1 + \Delta(s)w_i(s)) : \\ \Delta(s) \text{ stable, } \|\Delta(s)\|_\infty \leq 1 \end{array} \right\} \quad (8)$$

Essentially, the plant uncertainty is due to modelling errors and non-linear effects that are not compensated. Therefore, the plant uncertainty is obtained experimentally and is described by the following weighting transfer function:

$$w_i(s) = \frac{0.05(s + 0.2)}{s^2 + 0.07s + 0.49} \quad (9)$$

4.2 Performance specifications

To achieve the performance objectives (i, ii, and iii design objectives) the transfer functions from the inputs w and v to the output z are shaped using the weighting transfer functions w_{p1} , w_{p2} and w_u .

The transfer functions w_{n1} , w_{n2} , w_{ref} , w_{fa} , w_{fs1} and w_{fs2} are chosen to express the knowledge about the measurement noise in each sensor, reference and faults, respectively. Therefore, the weighting transfer functions are chosen in order to achieve:

$$\|w_{out} T_{out,in} w_{in}\|_{\infty} \leq 1, \text{ for all } \Delta \text{ satisfying } \|\Delta\|_{\infty} \leq 1 \quad (10)$$

It is assumed that the input signals are bounded according to:

- i) the measurement noise is white noise with low power;
- ii) the reference signal satisfies $|\text{ref}| \leq 0.3m$;
- iii) the fault on the control action satisfies $|f_a| \leq 2N$;
- iv) the faults on the measurements are given by $|f_{s1}| \leq 0.2m$ and $|f_{s2}| \leq 2^\circ$.

Given these bounds, the weighted transfer functions for the inputs are given by:

$$\begin{aligned} w_{n1}(s) &= \frac{0.005(s+1)}{0.5s+1} & w_{n2}(s) &= \frac{0.0025(2s+1)}{s+1} \\ w_{ref}(s) &= 0.3 & w_{fa}(s) &= 2 \\ w_{fs1}(s) &= 0.2 & w_{fs2}(s) &= 0.035 \end{aligned} \quad (11)$$

To attain to the performance objectives the following requirements can be assumed in terms of:

- i) the error signal given by $(\text{ref} - y_1)$: steady-state error lower than 8%; amplification at high-frequencies lower than 4dB; closed-loop bandwidth higher than 0.2rad/s;
- ii) the output signal y_2 : steady-state error lower than 0.036rad; attenuation at high-frequencies lower than -20dB; closed-loop bandwidth higher than 0.3rad/s;
- iii) the control action u : control action at low frequencies should be lower than 10N; action for frequencies higher than 0.05rad/s should be lower than 2N.

Given these performance requirements, the corresponding weighted transfer functions are given by:

$$\begin{aligned} w_{p1}(s) &= \frac{12.5(5s+1)}{100s+1} & w_{p2}(s) &= \frac{27.8(3.3s+1)}{10s+1} \\ w_u(s) &= \frac{10s+1}{20s+10} \end{aligned} \quad (12)$$

4.3 Fault detection specifications

In order to achieve the diagnosis performance objectives (iv design objective), the transfer functions from the inputs w and v to the residual output r are shaped using w_{r1} , w_{r2} and w_{r3} .

Assuming the boundaries defined above for the input signals and expressing the desire of good diagnostic performance at low frequencies, the weighted transfer functions for the residual signals are given by:

$$\begin{aligned} w_{r1}(s) &= \frac{10(s+1)}{10s+1} & w_{r3}(s) &= \frac{10(0.5s+1)}{s+1} \\ w_{r2}(s) &= \frac{4(0.2s+1)}{2s+1} \end{aligned} \quad (13)$$

4.4 Controller Design

The desired generalised controller for the inverted pendulum, satisfying the design objectives, is obtained using the μ synthesis method. Applying this method, and considering the $M-\Delta$ structure ($M = F(P, K)$) and the structured singular value, the generalised controller must satisfy condition (14).

$$\|F_{\mu}(M, \Delta)\|_{\infty} = \mu(M) \leq 1 \quad (14)$$

Applying the $D-K$ iterative procedure, and after two iterations, a generalised controller K of 15th order is found, giving $\mu=0.9804$. Using the optimal Hankel norm technique, the controller order is then reduced to a seven-order state-space representation. To implement this controller, a discrete-time representation of the controller is obtained considering a zero order sampling with a sampling time of 30ms.

5. RESULTS

The generalised controller was tested in an inverted pendulum laboratory environment, considering periodic step changes in the cart position reference (at $t=0s$, $t=30s$ and $t=60s$). In order to analyse the responses of the system in presence of faults, three different faults have been applied on the plant, from $t=40s$ to $t=70s$. The responses to the fault on the control action ($f_a=-2N$) are represented in Figure 6.

The responses to faults on the cart position measurement ($f_{s1}=0.2m$) and on the pendulum angle measurement ($f_{s2}=2^\circ$) are represented in Figures 7 and 8, respectively. These responses shown that the closed loop system has a satisfactory behaviour even if faults are present.

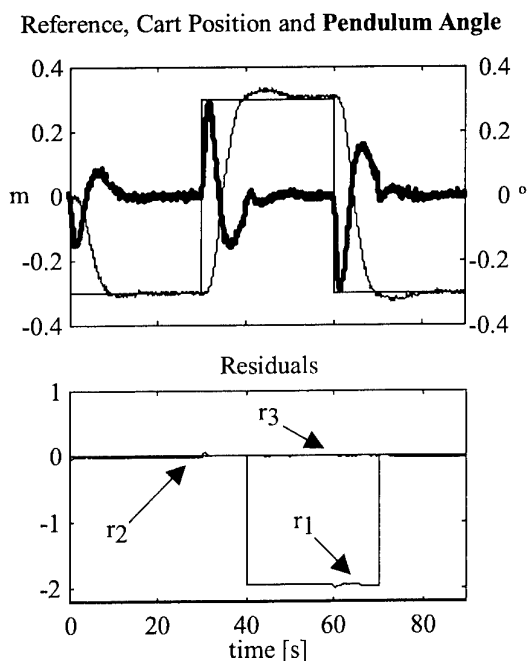


Fig. 6. Closed loop responses to step changes in the cart position reference and a step fault ($f_s = -2N$) in the control action, from $t=40s$ to $t=70s$.

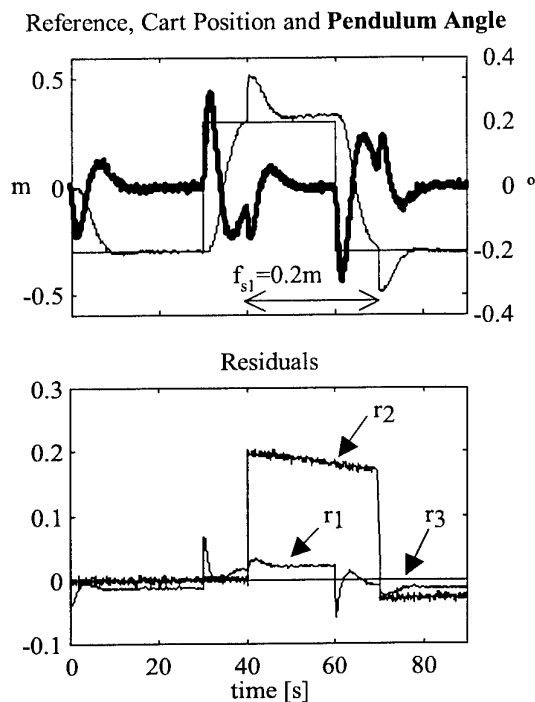


Fig. 7. Closed loop responses to step changes in the cart position reference and a step fault ($f_{s1} = 0.2m$) in the cart position sensor, from $t=40s$ to $t=70s$.

Concerning the residual signals, generated by the fault detection filter, they present a clear response to the representative fault and might be used to detect and to isolate each occurred fault.

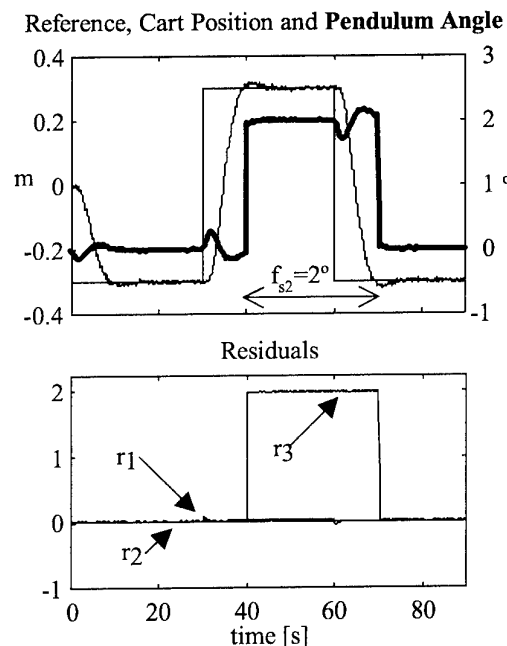


Fig. 8. Closed loop responses to step changes in the cart position reference and a step fault ($f_{s2} = 2^\circ$) in the pendulum angle sensor, from $t=40s$ to $t=70s$.

6. CONCLUSIONS

Control and fault detection systems for dynamic processes are often designed independently. This methodology may lead to unnecessarily poor diagnosis performance due to interaction between the controller and the fault detection filter, especially in the case of uncertain plants.

To address this problem, the design of the controller and the fault detection filter should be integrated into the same framework. An approach relying on robust control methods has been studied in this paper, to achieve a robust fault tolerant control system for the inverted pendulum plant. The simultaneous design of the control system and a model based fault detection filter has been converted into a robust control problem.

The inverted pendulum is described by a state space representation and a norm-bounded transfer function is used to represent knowledge about process uncertainty. The performance and fault detection specifications are expressed using weighting transfer functions. A generalised controller, integrating the controller and the fault detection filter, has been obtained using the μ synthesis.

The results show a good performance of the controller and the generalised controller ability's to diagnose and isolate abrupt faults on the control action and on the measurement signals.

Acknowledgments

This work was partially financed by FCT / PRAXIS XXI Program (Alcine Project) and by POSI Program supported by European Union.

REFERENCES

- Anderson, B. D. O. and Liu, Y. (1989). Controller Reduction: Concepts and Approaches. *IEEE Transactions on Automatic Control*, **34**, 802-812.
- Balas, G. J., J. C. Doyle, K. Glover, A. Packard and R. Smith (1993). *μ -Analysis and Synthesis Toolbox*. The MathWorks and MUSYN, USA.
- Chen, J. and Patton, R. J. (1999). *Robust Model-Based Fault Diagnosis for Dynamic Systems*. Kluwer Academic Publishers.
- Doyle, J. C., and G. Stein (1981). Multivariable Feedback Design: Concepts for a Classical/Modern Synthesis. *IEEE Transactions Automatic Control*, **AC-26**, 4.
- Frank, P. M. and Ding, X. (1997). Survey of robust residual generation and evaluation methods in observer-based fault detection systems. *Journal of Process Control*, **7** (6), 403-424.
- Frank, P. M., Ding, S. X. and Köppen-Seliger B. (2000). Current developments in the theory of FDI. *Proceedings of SAFEPROCESS'2000, the IFAC Symposium on Fault Detection, Supervision and Safety for Technical Processes*. Budapest, Hungary, 16-27.
- Isermann, R. (1994). Integration of fault detection and diagnosis methods. *Proceedings of IFAC Symposium on Fault Detection, Supervision and Safety for Technical Processes*. Helsinki, Finland, 597-612.
- Lundström, P., S. Skogestad and Z. Q. Wang (1991). Performance Weight Selection for H-infinity and Mu-Control Methods. *IEEE Trans. Inst. of Measurement and Control*, **13**.
- Nett, C. N., Jacobson, C. A. and Miller, A. T. (1988). An integrated approach to controls and diagnostics: The 4-parameter controller. *Proceedings of the 1988 American Control Conference*, Atlanta, USA. 824-835.
- Niemann, H. and Stoustrup, J. (1997). Integration of Control and Fault Detection: Nominal and Robust Design. *Proceedings of IFAC Symposium on Fault Detection, Supervision and Safety for Technical Processes*, Univ. of Hull, UK, 341-346.
- Patton, R. J., (1997). Fault-Tolerant Control: The 1997 Situation. *Proceedings of IFAC Symposium on Fault Detection, Supervision and Safety for Technical Processes*, Univ. of Hull, UK, 1033-1055.
- Postlethwaite, I. and S. Skogestad (1993). Robust Multivariable Control using H_∞ Methods: Analysis, Design and Industrial Applications, "Essays on Control: Perspectives in the Theory and its Applications" (Editors: H. L. Trentelman e J. C. Willems), Birkhäuser.
- Tyler, M. L. and Morari, M. (1994). Optimal and robust design of integrated control and diagnostic modules. *Proceedings of the 1994 American Control Conference*, 2060-2064.
- Zhou, K., J.C. Doyle and K. Glover (1996), *Robust and Optimal Control*, Prentice Hall.

INTERACTIVE EDUCATIONAL ENVIRONMENT FOR DESIGN BY QFT METHODOLOGY

S. Dormido, J. Aranda, J.M. Díaz, S. Dormido Canto

*Dpt. de Informática y Automática. Fac. Ciencias. UNED. c/Senda del Rey n° 9.
28040 - Madrid. Spain. Fax: 34 91 398 66 97. Phone : 34 91 398 71 48.
E-mail: jaranda@dia.uned.es*

Abstract: For students that begin the learning in control engineering many concepts are not very intuitive at first, due their properties are expressed in two different domains: the time and the frequency domains. Transient behaviour, such as settling time, overshoot and the risk of saturation is analysed typically in the time domain; while concepts like stability, noise rejection and robustness are expressed more easily in the frequency domain. In loop shaping on Nichols chart, the designer must to have enough skill to add necessary elements (gain, poles and zeros) to the controller until the nominal loop lies near its bound. This aspect of the QFT design is usually the most difficult for students. This paper discusses an interactive environment in Sysquake for the design by QFT methodology, where the student can be see immediate the effect of modifying the parameters.

Keywords : Educational aids, QFT, Interactive, Loop shaping

1. INTRODUCTION

To design technical systems or simply to understand the physical laws that describe their behaviour, scientists and engineers often use computers to calculate and represent graphically different magnitudes. In control engineering, these quantities include among others: time and frequency responses, poles and zeros in the complex plane, Bode, Nyquist and Nichols diagrams, phase plane, etc. Frequently, these magnitudes are closely related; they constitute different visions of the same reality. The understanding of these relationships is one of the keys to achieve a good learning of the basic concepts and allows the student to carry out control systems designs with sound sense.

Traditionally, the design of the systems is carried out following an iterative process. Specifications of the problem are not normally directly used to calculate the value of the system parameters because there is not an

explicit formula that relates them directly. This is the reason for dividing each iteration into two phases. The first one, often called synthesis consists on calculating the unknown parameters of the system. These parameters are based on a group of design variables that are related with the specifications. During the second phase, called analysis, the performance of the system is evaluated and compared to the specifications. If they do not agree, the design variables are modified and a new iteration is performed again.

It is possible however to merge both phases into one where the result of modifying the parameters produces an immediate effect. In this way the design procedure becomes really dynamic and the student feels the gradient of the change of the performance criteria with regard to the elements that manipulates. This interactive capacity allows to identify much more easily the compromises that can be achieved.

At the present time a new generation of software packages have allowed the arising of an interesting alternative for the interactive learning of the automatic control. These tools are based on objects that admit a direct graphic manipulation. During these manipulations, the objects immediately are updated, so that the relationship among the objects is maintained at all moments. Ictools and CCSdemo, developed in the Department of Automatic Control at Lund Institute of Technology and Sysquake (Piguet, 1999) and in the Institute d'Automatique of the Federal Polytechnic School of Lausanne are good examples of this new educational philosophy for teaching automatic control. For those that begin the learning in this field many concepts are not very intuitive at first, due to the fact that their properties are expressed in two different domains: the time and the frequency domains. Transient behaviour, such as settling time, overshoot and the risk of saturation are analysed typically in the time domain; while concepts like stability, noise rejection and robustness are expressed more easily in the frequency domain. The basic mechanisms that relate them and other phenomena as for example the effects of the sampling and the non-linear elements, to mention just a few, can be illustrated in a very effective way using these tools.

Taking into account this philosophy this paper discusses an interactive environment in Sysquake for the design by using QFT methodology, where the student can see immediately the effect of modifying the parameters. Several graphics are displayed simultaneously, and some elements can be manipulated with the mouse. During the manipulation, all the graphics are updated in a coherent way to reflect the changes.

This application is used in the design of an academic example and in the design of a controller for a real plant.

2. INTERACTIVITY IN DESIGN BY USING QUANTITATIVE FEEDBACK THEORY

Figure 1 shows a general diagram for a feedback control system. Where F is the pre-filter, G is the controller, P is the plant and H is the sensor. R is the reference signal and Y is the output. It can be subjected to reference disturbances W , input plant disturbances V and output plant disturbances D . Besides the sensor has a noise N .

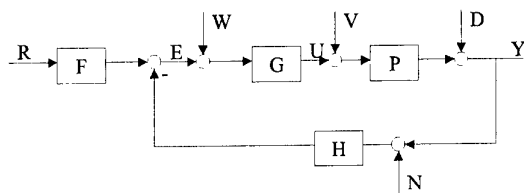


Fig. 1. Feedback Control System

The main goal is to design a robust controller that considers parametric uncertainty of plant P . The design must carry out several performance specifications: Tracking of a reference R , control effort limits and disturbances rejection.

The shaping of the loop gain in order to obtain the desired specifications is really at the heart of what is now called "classical methods". Bode, Nichols and many other control practitioners developed graphical methods and special diagrams to obtain this in a simple way for *siso* systems. The basic elements for manipulating the loop gain directly are the well known pure gain, lead and lag compensation.

QFT introduced by Horowitz (1963, 1972) was developed with the same philosophy in mind. The goal of QFT is to ascertain in an explicit way that the loop gain specifications are maintained under the given model uncertainty.

The basic principle is to describe the controller system by a set of transfer functions which define a set in a Nichols chart at each frequency. These sets are called templates in the QFT terminology. The requirement is that, at each frequency, the specifications for the closed loop system must be fulfilled for all elements in the template.

The aim is to impose some constraints in the controller's frequency response which can be related in a simple way to the restrictions in the nominal loop gain. This mechanism transforms the design procedure from a simultaneous and very difficult synthesis problem into a classical control problem with one nominal process model with constraints.

By using Quantitative Feedback Theory a robust controller can be designed. This technique looks for a design that combines the following requirements:

- Obtaining the performance specifications.
- Plant variations inside uncertainty regions (Robustness).

QFT methodology has several stages:

- Synthesis of tracking models.
- Modelling disturbances
- Obtaining plant templates.
- Choosing the nominal plant.
- Generating stability bounds.
- Generating performance bounds.
- Intersection of all bounds.
- Loop shaping (Synthesis of controller G).
- Pre-Filter shaping
- Analysis, simulation and validation.

Obtaining plant templates and generating different bounds usually needs a demanding computational work. In this stages the designer must program algorithms and wait for results.

In the loop shaping phase on Nichols chart, the designer must have enough skill to add necessary elements (gain, poles and zeros) to the controller G until the nominal loop satisfies the specifications and results in closed-loop stability.

This aspect of QFT design is usually the most difficult for beginners. For them, it is sometimes easier to design a controller G by using root locus plot, Bode diagrams or step response plot.

The interactive design environment in Sysquake for loop shaping (IDESQLS) shows the following in an only window: Nichols chart, Bode and root locus diagrams and the step response plot of the closed-loop transfer function.

Therefore IDESQLS provides the designer with other well-know tools for analysis in order to verify the results of modifications that he inserts into nominal open-loop in Nichols chart.

3. DESCRIPTION OF THE INTERACTIVE DESIGN ENVIRONMENT

Sysquake (Piguet, 1999) is an interactive design CAD tool for automatic control and signal processing. It was developed in the Institut d'Automatique of the Federal Polytechnic School of Lausanne.

Sysquake's window can simultaneously display several interactive figures. So IDESQLS shows the following in an only window: Nichols chart, Bode and root locus diagrams and the step response plot of the closed-loop transfer function. The user can select the figures that he wants to display and it is possible to resize all the figures.

Sysquake allows the user to interact some elements of its figures by using the mouse. During the manipulation, all the graphics are updated in a coherent way in order to reflect the changes. The user can select the element (gain, pole or zero) that he wants to add to the controller G , in order to place the mouse over nominal open-loop on Nichols chart and drag it in order to set the value of the added element. The modifications introduced in the Nichols chart are displayed simultaneously in the other figures.

Sysquake has a setting menu where the user can set the value of different parameters of the displayed figures. In IDESQLS the user can define the transfer function of the controller G and the type of element that will be added to the present controller when he

drags the nominal open-loop in Nichols chart. IDESQLS also allows the user to select a data file to draw stability and performance bounds in Nichols chart.

Sysquake displays different information in a messages bar as the user places the mouse over the different elements of the figures. For example, in IDESQLS as the mouse is placed over a bound, the bound generation frequency is displayed in the messages bar. Whereas if the mouse is placed over a point of the nominal open-loop plot, frequency, magnitude and phase are displayed in the messages bar.

4. EXAMPLES

4.1 A classic example of loop shaping.

In this section a classic example (Borghesani et al, 1995) of loop shaping is done using IDESQLS.

Let the uncertain plant, $P(s)$, described by the following parametric family \bar{P}

$$\bar{P} = \left\{ P(s) = \frac{k}{(s+a)(s+b)} : k \in [1,10], a \in [1,5], b \in [20,30] \right\} \quad (1)$$

The feedback problem is to design a controller, $G(s)$, such that the closed-loop system verifies the following specifications:

1) Robust stability with at least 50° phase margin for all $P(s) \in \bar{P}$.

$$\left| \frac{P(j\omega)G_c(j\omega)}{1+P(j\omega)G_c(j\omega)} \right| \leq 1.2, \text{ for all } P \in \bar{P}, \omega \in [0, \infty) \quad (2)$$

2) Reject plant output disturbance according to:

$$\left| \frac{Y(j\omega)}{D(j\omega)} \right| \leq \left| 0.02 \frac{(j\omega)^3 + 64(j\omega)^2 + 748(j\omega) + 2400}{(j\omega)^2 + 14.4(j\omega) + 169} \right|, \quad (3)$$

for all $P \in \bar{P}$, $\omega \in [0,10]$

3) Reject plant input disturbance according to:

$$\left| \frac{Y(j\omega)}{D(j\omega)} \right| \leq 0.01, \text{ for all } P \in \bar{P}, \omega \in [0,50] \quad (4)$$

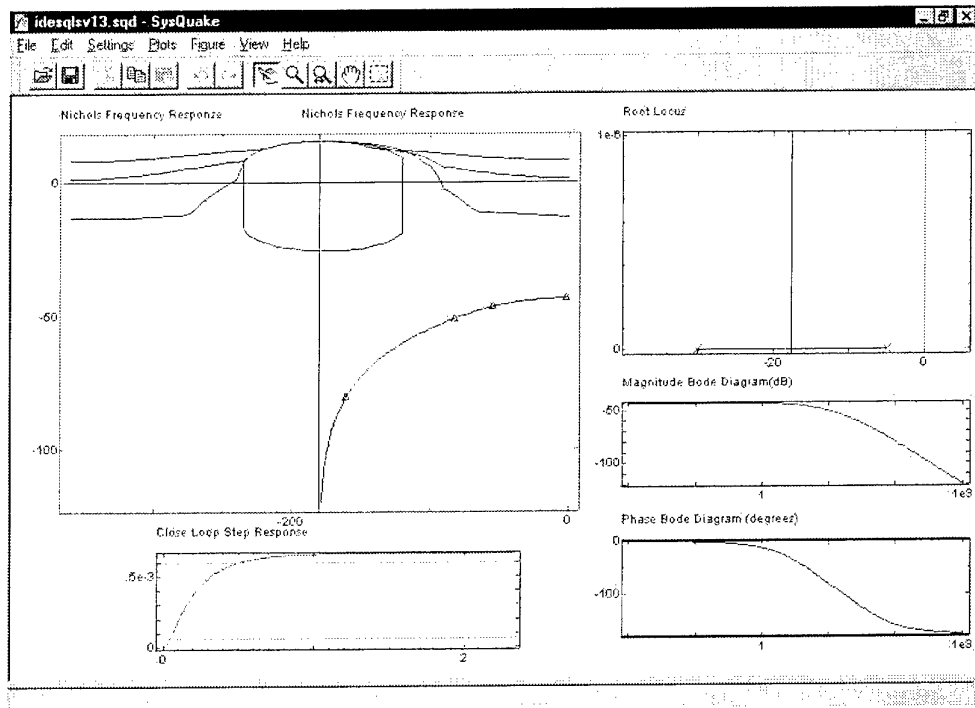


Fig 2. Window of IDESQLS in the beginning of the example.

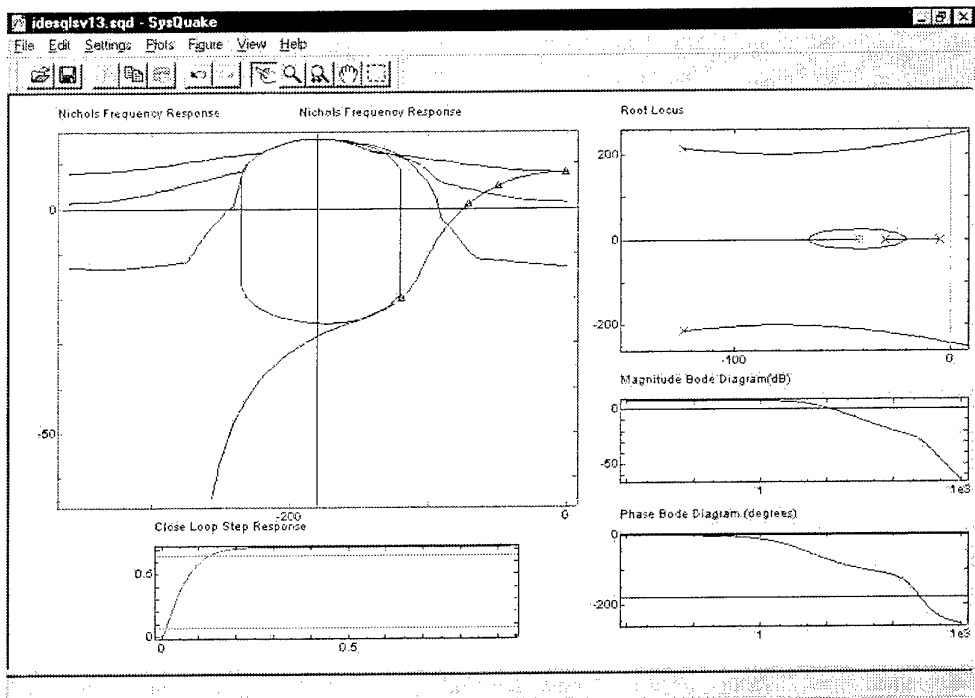


Fig 3. Window of IDESQLS in the end of the example.

Templates and stability and performance bounds have been calculated in the following frequencies:

$$\omega = [0.1, 5, 10, 100] \text{ (rad / seg)} \quad (5)$$

The nominal plant is:

$$P_0 = \frac{1}{s^2 + 35s + 150} \quad (6)$$

Initially, the controller G is a simple unit gain. Figure 2 shows the IDESQLS window for this example. To carry out the performance bound at $\omega=0.1$ rad/seg it is necessary to increase the gain of the controller.

The type of block *Gain'* is selected by default in the Settings menu. The evaluated nominal open-loop at the frequency ω is represented by a triangle in Nichols chart. The user must drag up the nominal open-loop plot till the first triangle on the right-hand side is over the upper bound.

The user can observe that a phase lead is necessary because the nominal loop lies inside the stability bounds at frequencies higher than $\omega=100$ rad/seg. It is necessary to add a real zero. So, by selecting *Real Zero* in the Settings menu, the user must place the mouse at $\omega=60$ rad/seg and drag the nominal loop till obtaining $z=42$.

Finally the controller design involves shaping the high frequency response of the nominal loop with the objective that its magnitude falls as fast as possible. A strictly proper controller is obtained by adding a pair of complex poles. So, by selecting *Complex Pole* in the Settings menu, the user must place the mouse over the nominal loop and drag the nominal loop till obtaining $\delta=0.5$ y $\omega_n=248$. The final controller is

$$G = \frac{380 \left(1 + \frac{s}{42} \right)}{\left(\frac{s^2}{248^2} + \frac{s}{248} + 1 \right)} \quad (7)$$

The modifications introduced in Nichols chart are immediately updated in the remaining figures of the window (see Figure 3).

4.2 A real example of loop shaping.

The main problem for the development of high speed craft is concerned with the passenger's comfort and the safety of the vehicles. The vertical acceleration associated with roll, pitch and heave is the main cause of motion sickness. The roll control is the most attractive candidate for control since damping can be increased more easily. However, shipbuilders are also interested in increasing pitch and heave damping. In order to solve the problem, antipitching devices and pitch control methods must be considered. Previously, models for the vertical ship

dynamics must be developed for design, evaluation and verification of the results.

Once the modelling phase of the vertical dynamics of a high speed ferry (De la Cruz, et al., 1998; Aranda, et al., 2000) and actuators (Esteban, et al., 2000) is completed then the next stage is to design a controller on heave and pitch motions in order to command the positions of the actuators. The final goal is to decrease the vertical accelerations to reduce motion sickness. The feedback system under consideration is schematically described in Figure 4.

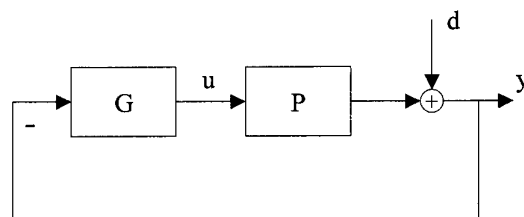


Fig. 4. Feedback system under considerations

The model of the plant P is the model of the vertical dynamics of a high speed ferry properly connected to the model of the actuators. The input plant u is the position of the actuator (T- Foil) and the output plant y is the pitch motion that is subjected to one perturbation: wave height (d).

P is an uncertain plant, described by the parametric family \bar{P} :

$$\bar{P} = \left\{ \begin{aligned} P(s) &= K \frac{(s+a)(s+b)}{(s+100)(s+1.8)(s+0.4915)(s^2+cs+d)}; \\ K &= [-0.87, -0.34], a = [-7.85, -5.79], \\ b &= [0.016, 0.041], c = [0.86, 1.16], d = [2.27, 2.80] \end{aligned} \right\} \quad (8)$$

The feedback problem is to design a controller, $G(s)$, such that the closed-loop system verifies the following specifications:

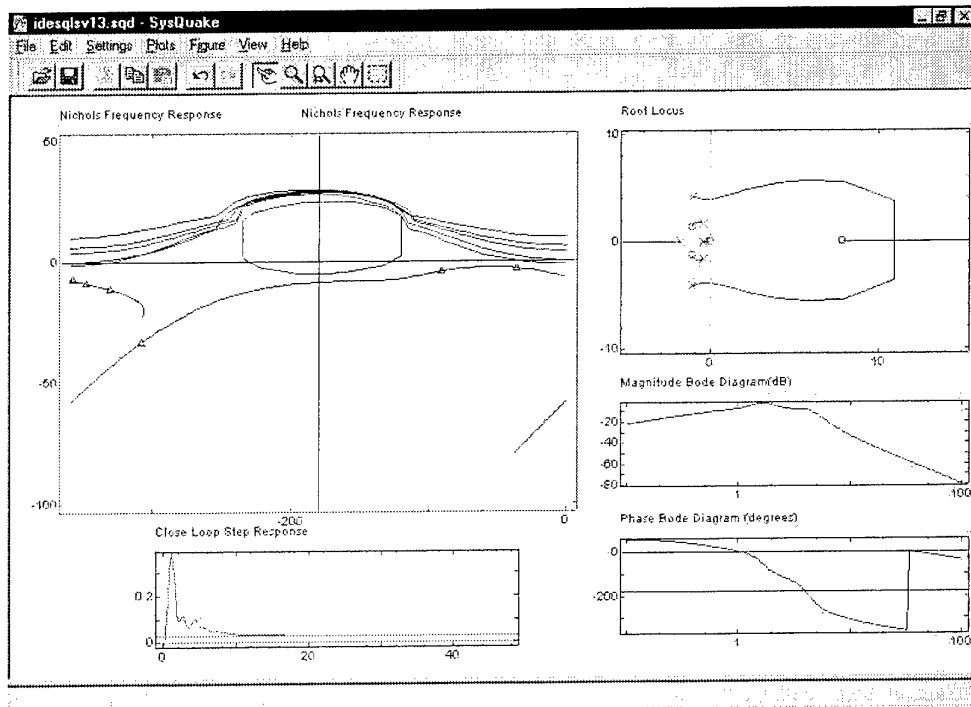


Fig.5. Window of IDESQLS in the beginning of the example.

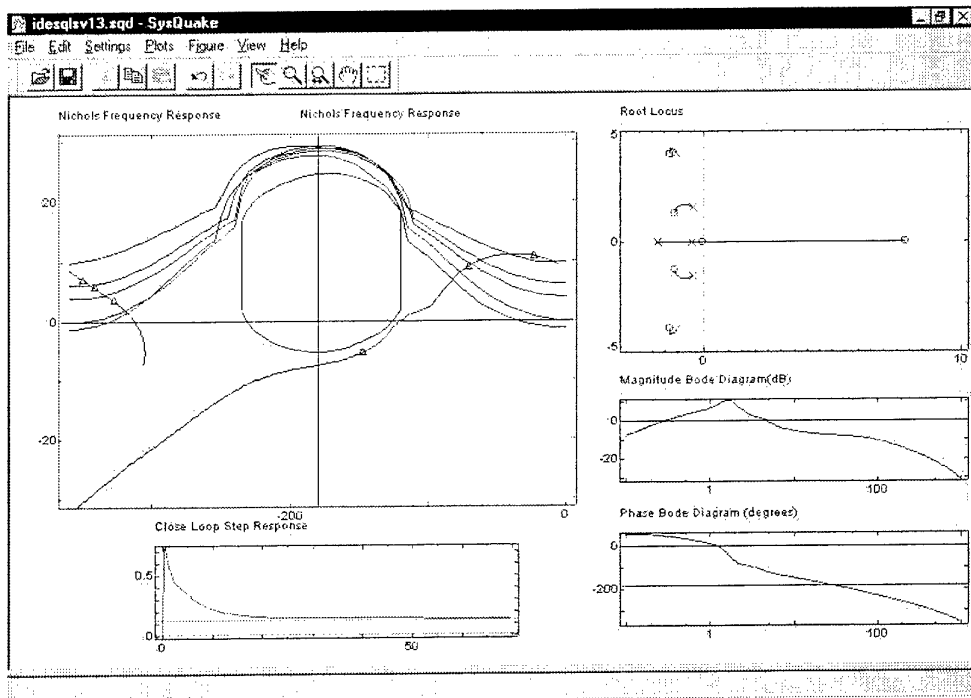


Fig. 6. Window of IDESQLS in the end of the example.

1) Robust stability with at least 50° phase margin for all $P(s) \in \bar{P}$.

$$\left| \frac{P(j\omega)G_c(j\omega)}{1+P(j\omega)G_c(j\omega)} \right| \leq 1.2, \text{ for all } P \in \bar{P}, \omega \in [0, \infty) \quad (9)$$

2) Plant output disturbance rejection (sensitivity) for any $P \in \bar{P}$, $\omega \in [0.5, 2]$. The transfer function from the plant output disturbance to the plant output is bounded by:

$$\left| \frac{Y(j\omega)}{D(j\omega)} \right| \leq \left| \frac{1.15(j\omega)^4 + 3.626(j\omega)^3 + 6.515(j\omega)^2 + 8.273(j\omega) + 2.856}{(j\omega)^4 + 3.96(j\omega)^3 + 7.793(j\omega)^2 + 10.43(j\omega) + 2.914} \right| \quad (10)$$

Templates and stability and performance bounds have been computed at the frequencies

$$\omega = [0.5, 0.8, 1, 1.5, 2, 10] \text{ (rad / seg)} \quad (11)$$

The nominal plant is:

$$P_0 = \frac{-0.87s^2 + 6.798s + 0.2855}{s^5 + 107s^4 + 333.1s^3 + 595.7s^2 + 749.7s + 257.9} \quad (12)$$

A classical controller was designed for this plant. The nominal controller G_0 is a second order filter that was tuned for the nominal plant solving a non linear optimization problem (Aranda et al., 2001).

$$G_0 = \frac{170.3s^2 + 385.6s + 518.7}{s^2 + 2.172s + 18.47} \quad (13)$$

Figure 5 shows the IDESQLS window for this loop shaping problem when $G=G_0$. G_0 is a good controller for the nominal plant, but the previous specification of plant output disturbance rejection is not verified.

To satisfy the performance bounds it is necessary to increase the gain controller. The user must drag up the nominal open-loop plot till the first triangle on the right-hand side is over the upper bound. It can be observed that a phase lead is necessary because the nominal loop lies inside the stability bounds. It is necessary to add a pair of complex zeros; the user must drag the nominal loop till obtaining a natural frequency $\omega_n=4.32$ rad/seg and a damping factor $\delta=0.31$. The final step to design the controller involves shaping the high frequency response of the nominal loop with the aim that its magnitude falls as fast as possible. The user must place the mouse over the nominal loop and drag the nominal loop till obtaining $\delta=0.8$ y $\omega_n=1000$. The final controller is

$$G_c = \frac{1.67 \cdot 10^5 \left(\frac{s^2}{1.74^2} + \frac{2 \cdot 0.65 \cdot s}{1.74} + 1 \right) \left(\frac{s^2}{4.32^2} + \frac{2 \cdot 0.31 \cdot s}{4.32} + 1 \right)}{\left(\frac{s^2}{4.3^2} + \frac{2 \cdot 0.25 \cdot s}{4.3} + 1 \right) \left(\frac{s^2}{1000^2} + \frac{2 \cdot 0.8 \cdot s}{1000} + 1 \right)} \quad (14)$$

These modifications in Nichols frequency response are updates in the remaining figures of the window (see Figure 6). We can see that all specifications are satisfied.

5. CONCLUSION

An interactive design environment for loop shaping was built in Sysquake. This application allows our students to understand more quickly and better the synthesis of controllers using QFT methodology. IDESQLS provides the designer with other well-know tools for analysis in order to verify the results of modifications that he inserts into nominal open-loop in Nichols chart. So the design and analysis phases are merged into one, and the student can see immediately the effect of modifying the parameters.

This paper shows how IDESQLS is used in an academic example, appropriate for teaching. Also IDESQLS is used in the design of a controller to solve a practical problem. This design is compared with a previously classical controller.

Acknowledgements: This research has been supported by CICYT in Spain under contract DPI2000 - 0386 - C03 - 01.

REFERENCES

- Aranda, J., J.M. de la Cruz, J.M. Díaz, B. de Andrés, P. Ruipérez, S. Esteban, J.M. Girón. (2000) Modelling of a High Speed Craft by a Non-Linear Least Squares Method with Constraints. *Proceedings of 5th IFAC Conference on Manoeuvring and Control of Marine Crafts MCMC2000*. Aalborg. pp. 227-232.
- Aranda, J., J.M. Díaz, P. Ruipérez, T.M. Rueda, E. López. (2001). Decreasing of the motion sickness incidence by a multivariable classic control for a high speed ferry. *Proceedings of IFAC Conference on Control Applications in Marine Systems*. CAMS2001. Glasgow. UK. 18th-20th July.
- Borghesani, C., Y. Chait and O. Yaniv. (1994). *Quantitative Feedback Theory Toolbox - For use with MATLAB*. 1st Edition. The Math Works. Inc.
- De la Cruz, J.M., J. Aranda, J.M. Díaz, P. Ruipérez, A. Marón. (1998). Identification of the vertical plane motion model of a high speed craft by model testing in irregular waves. *Proceedings of IFAC Conference CAMS'98 Control Applications in Marine Systems*. Fukuoka. pp. 277-282.
- Esteban, S., J.M. Girón-Sierra, J.M. de la Cruz, B. de Andrés, J.M. Díaz, J. Aranda. (2000). Fast Ferry Vertical Accelerations Reduction with Active Flaps and T-Foil. *Proceedings of 5th IFAC Conference on Manoeuvring and Control of*

- Marine Crafts MCMC2000*. Aalborg. pp. 233-238.
- Horowitz, I. M. (1963). *Synthesis of Feedback Systems*. Academy Press, New York.
- Horowitz, I. M. (1972). *Synthesis of Feedback Systems with large plant ignorance for prescribed time-domain tolerance*. Int. J. Control, 16(2), pp. 287-309
- Piguet, Y. (1999). *Sysquake User Manual, version 1.0*. Calerga. Lausanne (Switzerland)

HIGH-ORDER CONTROLLERS MODEL REDUCTION USING QFT TOOLS

Javier Castillejo
Marta Barreras
Pablo Vital
Mario García-Sanz

Automatic Control and Computer Science Department
Public University of Navarre
31006, Pamplona
SPAIN
E-mail: mgsanz@unavarra.es

Abstract: Certain robust control design techniques, like H_∞ - H_2 methodologies, usually obtain controllers with a high order mathematical expression that may cause some robustness problems. To reduce this disadvantage there are several order-reduction techniques. However, sometimes these techniques do not guarantee the required design specifications. In this context, the present paper uses Quantitative Feedback Theory (QFT) tools to search for a low-order controller that accomplishes design objectives. This article describes this method and presents two examples.

Key-Words: Order Reduction, QFT, Robust Control.

1. INTRODUCTION

H_∞ - H_2 and μ -synthesis robust control techniques are useful to find controllers for systems with plant uncertainty, satisfying both reference-tracking and disturbance rejection specifications (Skogestad, 1996). The main advantage of these methods lies in the fact that once the problem is stated, the controller is found with an iterative process.

However, these techniques generally result in a high order controller. Practical implementation of this kind of controllers may be difficult, because the order is related to the number of samples that the controller needs to be fully operative. Moreover, a great number of elements involves a great number of previous values to operate with. So the higher the controller order is, the faster and more accurate the microprocessor must be.

For this purpose, one can use several order reduction techniques, and the three main methods are:

truncation, residualization and optimal Hankel norm approximation.

Truncation technique takes some elements of the original model and the rest –generally corresponding to the fastest modes– are removed. It usually obtains a good approximation at high frequencies. Residualization process sets derivatives to zero in the space-state equations, and gets a system similar to initial at low frequencies (Skogestad, 1996).

Optimal Hankel norm techniques find a reduced order model such that the Hankel norm of the approximation error is minimized. A complete analysis of this technique was done by Glover in (Glover, 1984). Enns (Enns, 1984) and Anderson (Anderson, 1986) proved that trying to get a better fit in a frequency range caused great errors out of this range.

All of these techniques share the same basis: obtaining a model with similar dynamics to the initial one. But this is not the goal when designing a controller. If a suitable compensator has been found, the real objective is finding a reduced order model

which accomplishes –or tries to accomplish- the same specifications than the high order controller.

In order to overcome this problem, a simple and new method based in QFT (Quantitative Feedback Theory), (Horowitz, 1992) is introduced in this paper. This technique uses the QFT toolbox for Matlab® (Borghesani et al., 1995) which provides an interactive and friendly environment with a graphical interface which lets the designer analyse in an easy way the controller behaviour.

The method is aimed to find a controller that maintains the design specifications, without any considerations of the original structure of the high-order controller.

Section 2 describes the steps followed to achieve the reduction using several methodologies. Section 3 presents two practical examples.

2. METHODOLOGY

2.1 Overview

The starting point is the controller obtained through the classical robust control techniques. If the resulting order is too high, these steps are followed:

The controller, together with the plant, is taken to Nichols chart. The plant under consideration $P(s)$ is a member of a family \wp , exhibiting a parametric and a bounded non-parametric uncertainty with the following structure,

$$\wp = \{P(\alpha)[1 + \Delta_n] : \alpha \in \Omega, \Delta_n \in \Delta\} \quad (1)$$

where, $|\Delta_n(j\omega)| < m(\omega)$.

And the controller to be obtained can be written in the form,

$$G(x, j\omega) = k_c \frac{\prod_{i=1}^{n_z} (j\omega + z_i)}{\prod_{i=1}^{n_p} (j\omega + p_i)} \quad (2)$$

A representative set of frequencies -in which the behaviour of the system is to be evaluated- are chosen.

$$I = [\omega_1, \omega_2, \dots, \omega_n] \quad (3)$$

For these frequencies, the magnitude of $L=G_{11\infty}P$ must be found. With these values it is possible to obtain the exclusion areas (bounds) of the design. A generalised bound can be represented as a function q of phase and frequency, composed of upper and lower parts, q_u and q_l , respectively, such that,

$$\begin{aligned} q_u(\angle L_0(x, j\omega_i), \omega_i) &\leq L_0(x, j\omega_i) \\ L_0(x, j\omega_i) &\leq q_l(\angle L_0(x, j\omega_i), \omega_i) \\ i &\in I \end{aligned} \quad (4)$$

In this context, an automatic or manual reduction of the terms of the controller is done. Three design possibilities are proposed:

- Beginning a classic QFT loop-shaping, starting from plant templates and bounds, discarding the original controller. This process is carried out manually, and the success depends on the experience of the designer.
- Beginning a classic QFT design, but this time using automatic loop-shaping tools. Genetic algorithms have proved to be successful considering the loop-shaping procedure like a nonlinear, non-convex optimisation problem. Section 3.1 shows an example based in a QFT adaptation for the algorithm designed by Goldberg in (Goldberg, 1989) presented in (García-Sanz and Guillén, 2000).
- Reducing the original controller using the classical techniques, and then adjusting manually controller elements, until a suitable fit is found. Section 3.2 presents an example illustrating this possibility.

Figure 1 shows a graphical representation of the process followed.

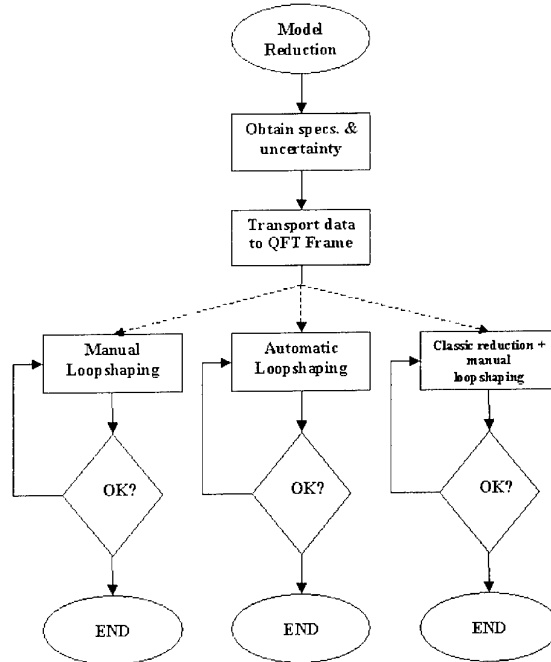


Figure 1: Reduction process.

2.2 QFT Specifications

In order to cope with the controller in the QFT environment, it is first necessary to obtain the specifications to be satisfied.

The general diagram in which QFT theory is based can be seen in figure 2.

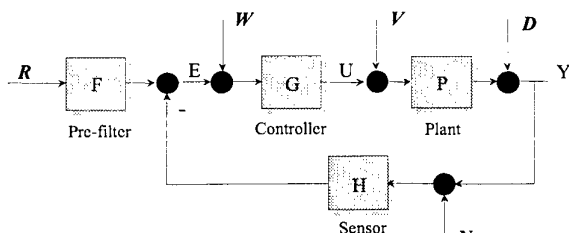


Figure 2: General diagram for a two degree-of-freedom control system.

If initial regulator has been designed using any control technique where prefilter is not considered, the resulting QFT controller properties must be similar to the initial ones. Hence, in this case the use of the prefilter is, in general, not necessary because the controller itself obtains a suitable tracking.

The QFT specifications to be considered in controllers design are shown in table 1.

Table 1: QFT Specifications.

Type	Specification	Name
1	$\left \frac{PGH}{1+PGH} \right \leq W_{S_1}$	Gain and phase margins (with sensor dynamics)
2	$\left \frac{1}{1+PGH} \right \leq W_{S_2}$	Sensitivity reduction
3	$\left \frac{P}{1+PGH} \right \leq W_{S_3}$	Rejection of disturbances at plant input
4	$\left \frac{G}{1+PGH} \right \leq W_{S_4}$	Control effort
5	$\left \frac{GH}{1+PGH} \right \leq W_{S_5}$	Control effort (with sensor dynamics)
6	$\left \frac{PG}{1+PGH} \right \leq W_{S_6}$	Tracking bandwidth
7	$W_{S_{7a}} \leq \left \frac{PG}{1+PGH} \right \leq W_{S_{7b}}$	Tracking
8	$\left \frac{H}{1+PGH} \right \leq W_{S_8}$	Rejection of disturbances at plant output (with sensor dynamics)

9	$\left \frac{PH}{1+PGH} \right \leq W_{S_9}$	Rejection of plant input disturbances (with sensor dynamics)
---	--	--

Depending on plant characteristics (existence and kind of associate uncertainty) and design requirements, it will be necessary to use a bigger or smaller number of specifications. Although it will always be necessary to define at least the values corresponding to sensibility and complementary sensibility functions.

If controllers are calculated neglecting sensor dynamics ($H = 1$), the specifications used for a typical design will be Type 1 and Type 2. For certain patterns of uncertainty, Type 3 can also be considered.

For each one of the selected frequencies it is necessary to find the specifications that the controller-plant group meets. With this procedure, a set of bounds in Nichols chart are obtained. These bounds represent the exclusion areas for the open loop systems.

2.3 Including uncertainty

There are several uncertainty models which can be introduced in different ways, taking into account that these kinds of uncertainty may appear simultaneously.

2.3.1 Unstructured uncertainty

Introducing available information about unstructured uncertainty usually involves calculating a radius of uncertainty for each design frequency. The value of this radius is obtained using the plant uncertain parameters. In those cases where uncertainty is modelled as simple plant input or output noise (additive or multiplicative), it is possible to consider this noise as a disturbance, including it in specifications Type 2 or Type 3, with a plant without uncertainty.

2.3.2 Structured uncertainty

Structured or parametric uncertainty is represented as one or several variable parameters inside the transfer function that defines the plant model. Some robust control techniques, like H_∞ , cannot handle this kind of uncertainty, but there is not any inconvenient in QFT to be considered.

3. EXAMPLE 1

The following example shows a detailed description of the procedure used to find a low order controller starting from an H_∞ compensator. Genetic Algorithms are used to fit the system behaviour to specifications.

3.1 Model reduction

This example uses the H_∞ controller showed in Figueres (Figueres). The plant is a DC-DC converter which has the polynomial model of the transfer function (5).

$$P(s) = \frac{2.59 \cdot 10^{10} s^3 + 1.1 \cdot 10^{16} s^2 + 5.2 \cdot 10^{20} s + 2.6 \cdot 10^{23}}{4.17 \cdot 10^6 s^4 + 4.56 \cdot 10^{11} s^3 + 2 \cdot 10^{16} s^2 + 7.1 \cdot 10^{16} s + 3.3 \cdot 10^{22}} \quad (5)$$

The initial controller, described in (Glover, 1984) is shown in the equation 6.

$$G_{H_\infty}(s) = \frac{a_5 s^5 + a_4 s^4 + a_3 s^3 + a_2 s^2 + a_1 s + a_0}{s^6 + b_5 s^5 + b_4 s^4 + b_3 s^3 + b_2 s^2 + b_1 s + b_0} \quad (6)$$

$$\begin{aligned} a_0 &= 1.2 \cdot 10^{26} & b_0 &= 5.1 \cdot 10^{23} \\ a_1 &= 10^{24} & b_1 &= 4 \cdot 10^{21} \\ a_2 &= 1.1 \cdot 10^{21} & b_2 &= 10^{19} \\ a_3 &= 2.2 \cdot 10^{17} & b_3 &= 8.2 \cdot 10^{15} \\ a_4 &= 4.7 \cdot 10^{12} & b_4 &= 3.2 \cdot 10^{11} \\ a_5 &= 4.3 \cdot 10^7 & b_5 &= 3.1 \cdot 10^6 \end{aligned}$$

Table 2: H_∞ Controller- Plant Specifications.

$\omega(\text{rad/s})$	Type 1	Type 2
250	0.9996	$4.37 \cdot 10^{-4}$
1000	0.9998	0.001
4000	1.0009	0.0049
16000	1.009	0.0241
64000	1.1208	0.178
256000	0.8804	1.48
750000	0.138	1.076

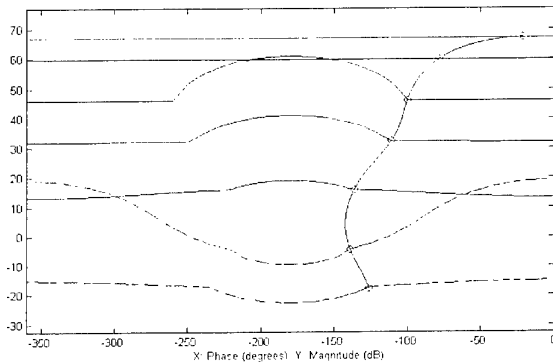


Figure 3: Open-loop transmission function with restriction bounds. $P(s) G_{H_\infty}(s)$

Controller and plant data are taken to the QFT frame. The selected frequencies, as well as the resulting specifications can be seen in table 2. The representation of the controller and the plant transfer function in Nichols chart, as well as the bounds corresponding to table 2 are shown in figure 3.

At this point the order reduction is to be done. Using a C++ adaptation -designed in (García-Sanz and Guillén, 2000)- of the Simple Genetic Algorithm proposed in (Goldberg, 1989), it is possible to find with a minimum effort a suitable controller. The second order controller found is shown in (3), and

was obtained in ten minutes in a Pentium-500 computer, while advanced QFT designers could not find a suitable controller using manual loopshaping. Nichols chart of the corresponding system can be seen in figure 4.

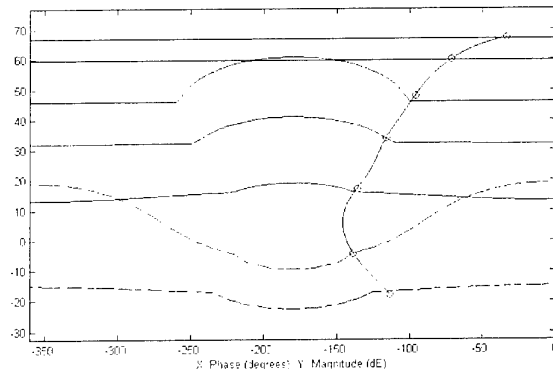


Figure 4: $P(s) G_{QFT}(s)$

The transfer function of the reduced controller is:

$$G_{QFT} = \frac{13.8s^2 + 6.21 \cdot 10^5 s + 2.08 \cdot 10^9}{s^2 + 1.65 \cdot 10^4 s + 6 \cdot 10^6} \quad (7)$$

The specifications achieved by the plant-reduced controller are shown in table 3.

Table 3: QFT controller-Plant specifications.

$\omega(\text{rad/s})$	Type 1	Type 2
250	0.9996	$4.33 \cdot 10^{-4}$
1000	0.9997	0.001
4000	1.0004	0.0039
16000	1.009	0.0206
64000	1.105	0.1535
256000	0.8804	1.480
750000	0.1341	1.048

3.2 Comparison between controllers

3.2.1 QFT vs. Reduced H_∞ -Controller

The reduced order controller proposed in (Figueres) is shown in figure 5. This model was obtained using the order reduction techniques found in Matlab's Robust Control Toolbox (Borguesani et al., 1995).

Table 4 shows the specifications of the H_∞ reduced controller.

Table 4: Reduced order H_∞ controller-plant specifications.

$\omega(\text{rad/s})$	Type 1	Type 2
250	1.0232	$4.4 \cdot 10^{-4}$
1000	1.0009	0.001
4000	1.2923	0.0053
16000	1.72	0.0355
64000	1.2351	0.1723
256000	1.1092	1.8622
750000	0.1386	1.087

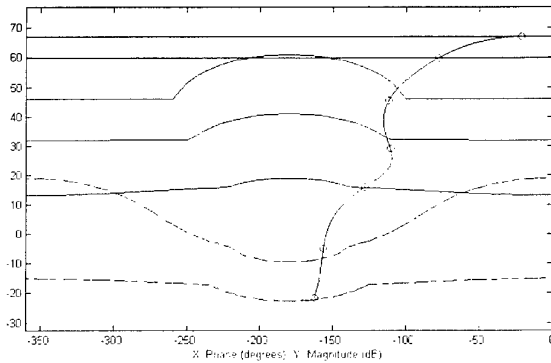


Figure 5: Reduced order H_∞ controller-Plant. $P(s)$
 $\tilde{G}_{H_\infty}(s)$

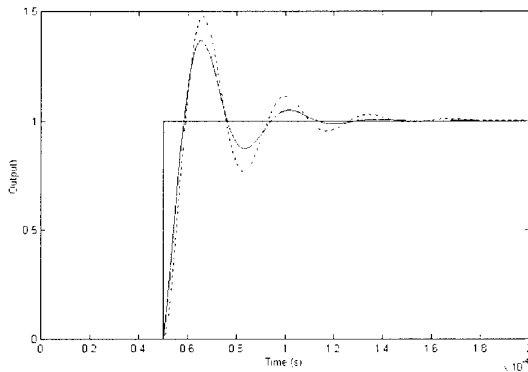


Figure 6. H_∞ and QFT controllers comparison. Solid line: G_{QFT} , dashed line: G_{H_∞}

It can be seen that none of the Type 1 specifications are accomplished, and Type 2 are only accomplished at $\omega=1000$ rad/s and $\omega=64000$ rad/s. A time-domain response with a unit step input can be seen in figure 6, and the corresponding control action is shown in figure 7.

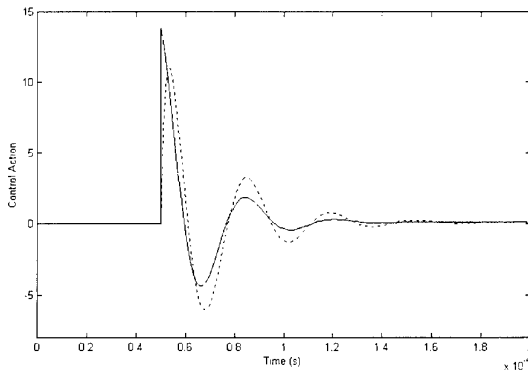


Figure 7. H_∞ and QFT controllers comparison. Solid line: G_{QFT} , dashed line: G_{H_∞}

3.2.2 QFT vs. Original H_∞ Controller

If a unit step input is introduced, the response of the system with the initial H_∞ controller and the final QFT-controller as well as the control order in both

cases, are shown in figures 8 and 9. The similarity between both controllers can be checked.

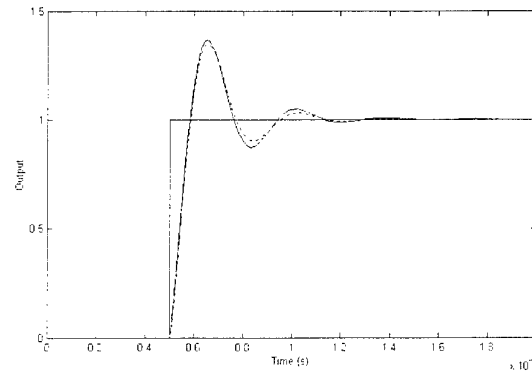


Figure 8. H_∞ and QFT controllers comparison.
Solid line: G_{QFT} , dashed line: G_{H_∞}

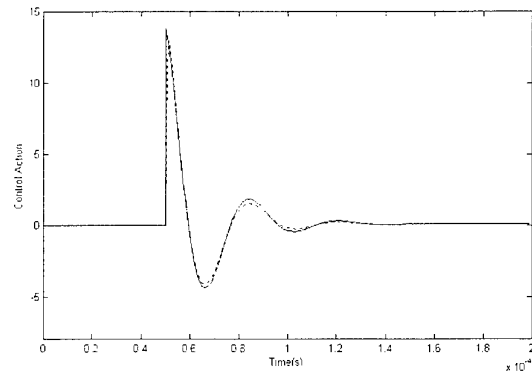


Figure 9. Control action. Solid line: G_{QFT} , dashed line: G_{H_∞}

4. EXAMPLE 2

The next example has been taken from (Doyle, 1992). It is a controller for a flexible beam. The simplified model for the plant and the proposed controller are shown in equation 8 and 9, respectively.

$$P(s) = \frac{-6.475s^2 + 4.03s + 175.8}{5s^4 + 3.568s^3 + 139.5s^2 + 0.0929s} \quad (8)$$

$$G_{H_\infty}(s) = \frac{a_7s^7 + a_6s^6 + a_5s^5 + a_4s^4 + a_3s^3 + a_2s^2 + a_1s + a_0}{s^8 + b_7s^7 + b_6s^6 + b_5s^5 + b_4s^4 + b_3s^3 + b_2s^2 + b_1s + b_0} \quad (9)$$

$a_0 = 0.01406$	$b_0 = 3435$
$a_1 = 1036$	$b_1 = 3.44 \cdot 10^6$
$a_2 = 1.961 \cdot 10^6$	$b_2 = 4.94 \cdot 10^6$
$a_3 = 907300$	$b_3 = 2.348 \cdot 10^6$
$a_4 = 111700$	$b_4 = 632600$
$a_5 = 31410$	$b_5 = 112900$
$a_6 = 907.6$	$b_6 = 13260$
$a_7 = 1.424$	$b_7 = 1013$

The specifications for this design can be seen in table 5. Plant and controller models are taken to QFT design environment, together with specifications. Figure 12 shows initial system.

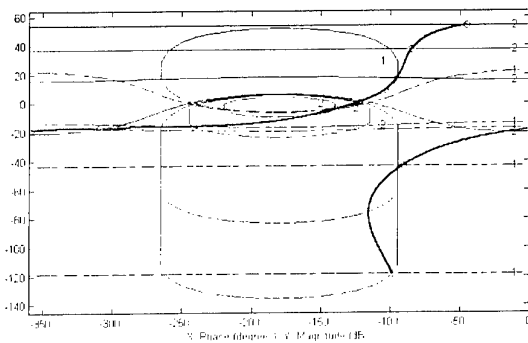


Figure 12: Open-loop transmission function with restriction bounds. $P(s) G_{H\infty}(s)$

Reducing the order using both mathematical and manual methods, it is possible to obtain the system shown in figure 13.

The mathematical expression for the reduced order controller is:

$$G_{QFT}(s) = \frac{1.549s + 1.695 \cdot 10^{-5}}{s^2 + 3.362s + 4.141} \quad (10)$$

This controller does not accomplish design specifications in certain frequencies. It could be possible to improve the proximity to lower frequencies bounds, but it yields a worse performance.

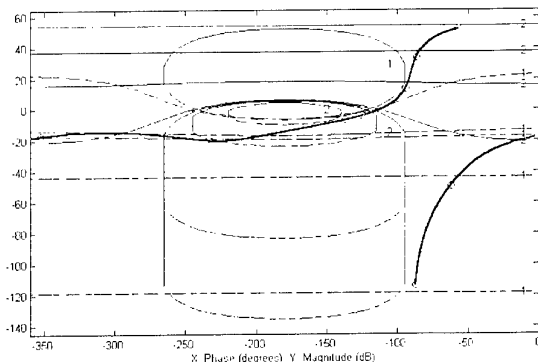


Figure 13: $P(s) G_{QFT}(s)$

Figure 14 and 15 show the effects of a step input and a disturbance at the plant output in both H_∞ and QFT systems.

Reduced model shows a better response with a lower control action. Obviously, the reason for this enhancement is not in the order reduction. Looking figure 12 and table 5 it can be seen that low frequency specifications are not accomplished, and QFT controller is similar to H_∞ controller with a lower gain. A better performance is obtained decreasing gain for H_∞ controller. Therefore, the conclusion is that the chosen weight functions were not the most suitable.

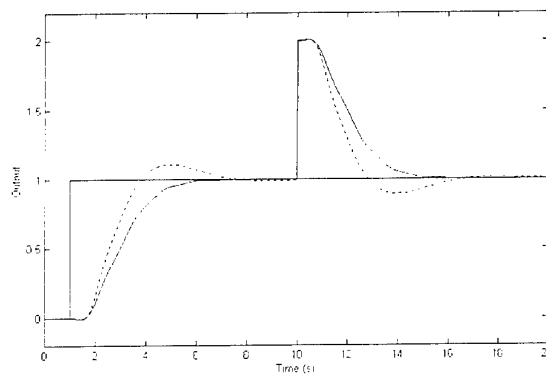


Figure 14: H_∞ and QFT controllers comparison. Solid line: G_{QFT} , dashed line: $G_{H\infty}$

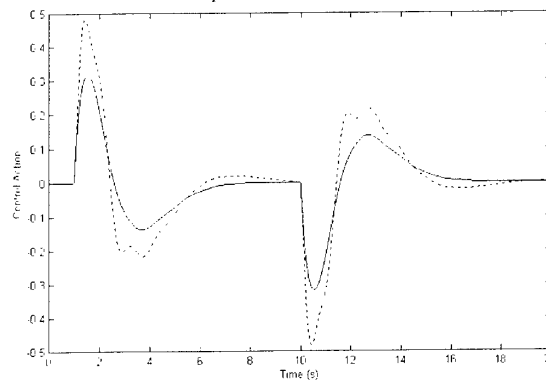


Figure 15: Control action. Solid line: G_{QFT} , dashed line: $G_{H\infty}$

Table 5. Initial and final systems specifications.

$\omega(\text{rad/s})$	H_∞ system		QFT system	
	Type 1	Type 2	Type 1	Type 2
0.001	0.9986	0.002	0.9986	0.00255
0.01	0.9986	0.014	0.9986	0.02124
0.1	1.002	0.1397	0.9934	0.2109
1	0.9282	1.5	0.621	1.3618
4	0.1733	1.0706	0.1049	1.062
5.5	0.1237	0.916	0.1255	0.8755
10	0.00680	1.00007	0.00346	0.9984
100	1.18e-6	1.0000002	2.016e-6	0.9999999

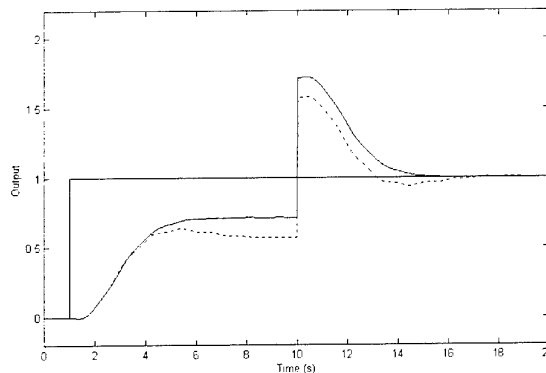


Figure 16: H_∞ and QFT controllers comparison. Solid line: G_{QFT} , dashed line: $G_{H\infty}$

Another interesting test consists in simulating with a saturation at controller output. Figure 16 and figure 17 show the simulated output signal using the same saturation for both controllers, with the previous input and disturbance. QFT controller has not such a bad performance. However, both controllers show the same problem: the lack of a suitable integral action. It would be desirable to correct this, to avoid problems with real actuators.

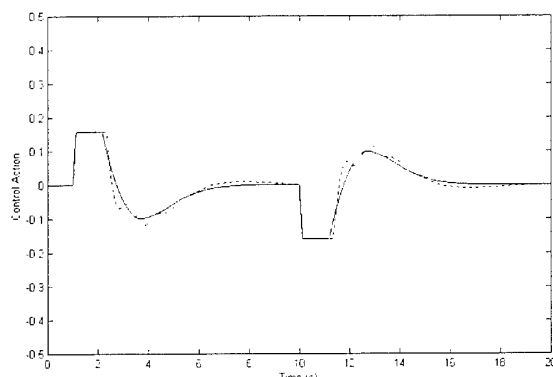


Figure 17. Control action. Solid line: G_{QFT} , dashed line: G_{H_∞}

5. CONCLUSIONS

The present paper has introduced a new technique for order reduction based on the combined use of traditional methods and QFT tools. The main advantage of this new method, in comparison with the ones in the bibliography, is that the reduced order controller is designed to accomplish the specifications of the initial system, while other methods generally try to obtain a dynamic behaviour similar to the original one, which does not actually guarantees the achievement of these specifications.

Another advantage of this method is its visual character, and its transparency. It gives the designer the possibility to observe in a graphic and easy way either the characteristics of the controller and the effects of changes in the parameters. Hence, the control engineer is able to decide in a moment whether certain limitations in certain frequencies can be relaxed, in benefit of a bigger simplicity in the controller.

ACKNOWLEDGEMENTS

The authors gratefully appreciate the support given by the Spanish 'Comisión Interministerial de Ciencia y Tecnología' (CICYT) under grant DPI2000-0785.

REFERENCES

- Anderson, B. D. O. (1986). *Weighted Hankel-norm approximation: Calculation of bounds*, Systems & Control Letters 7(4): 247-255.
- Borghesani, C., Chait, Y. and Yaniv, O. (1995). *Quantitative Feedback Theory Toolbox – For use with Matlab*. 1st Edition. The Mathworks Inc.
- Chiang, R. Y. and Safonov, M. G. (1992). *Robust Control Toolbox Users Guide*, Mathworks, South Natick.
- Doyle, J. C. (1992). *Feedback Control Theory*, Macmillan Publishing Company.
- Enns, D. (1984). *Model reduction with balanced realizations: An error bound and a frequency weighted generalization*, Proceedings of the 23th IEEE Conference on Decision and Control, Las Vegas, NV, USA, pp. 127-32.
- Figueres, E. *Teoría de control H_∞ aplicada al diseño de lazos ACC de convertidores DC-DC conmutados*. Industrial Electronic Subject, Politechnique University of Valencia.
- García-Sanz, M., Guillén, J.C. (2000). *Automatic Loop-Shaping of QFT Robust Controllers Via Genetic Algorithms*, 3rd IFAC Symposium on Robust Control Design, ROCOND00, F3A/107, June 2000, Praha, Czech Republic.
- Glover, K. (1984). *All optimal Hankel-norm approximations of linear multivariable systems and their L^∞ -error bounds*, International Journal of Control 39(6): 1115-93.
- Goldberg, D. E. (1989). *Genetic Algorithms in Search, Optimization and Machine Learning*. Reading, MA: Addison-Wesley.
- Horowitz, I. (1992). *Quantitative Feedback Design Theory (QFT)*, QFT Publications, Boulder.
- Skogestad, S. and Postlethwaite, I. (1996). *Multivariable Feedback Control*, Wiley & Sons, England.

GENERATION OF FREQUENCY RESPONSE TEMPLATES FOR LINEAR SYSTEMS WITH AN UNCERTAIN TIME DELAY AND MULTILINEARLY CORRELATED PARAMETER PERTURBATIONS

Chyi Hwang^{*,1} and Shih-Feng Yang^{**}

^{*}*Department of Chemical Engineering National Chung
 Cheng University Chia-Yi 621 TAIWAN
 E-mail: chmch@ccu.edu.tw
 Fax: 886-5-272-1206*

^{**}*Department of Information Management Transworld Institute
 of Technology Douliu 640 TAIWAN
 E-mail: ysf@tit.edu.tw*

Abstract: A simplicial algorithm is applied in this paper to generate frequency response templates for a class of transfer functions having an uncertain time delay and multilinearly correlated parameter perturbations. It relies on developing a new zero inclusion test algorithm for checking whether the origin is included in the image of a box $\mathbf{T} \times \mathbf{Q} = [\tau^-, \tau^+] \times \prod_{i=1}^{m-1} [q_i^-, q_i^+]$ under a mapping of the form $f(\tau, \mathbf{q}) = g(\mathbf{q}) + h(\mathbf{q})e^{-j\omega\tau}$, where $g(\mathbf{q})$ and $h(\mathbf{q})$ are multilinear complex-valued functions of $\mathbf{q} \in \mathbf{Q}$. We present easy-to-check sufficient conditions for the zero inclusion and exclusion of the value set $f(\mathbf{T}, \mathbf{Q})$. Using these sufficient conditions on subdivisions in the parameter box $\mathbf{T} \times \mathbf{Q}$, we implement a branch-and-bound zero inclusion test algorithm. To illustrate the proposed algorithm, we provide a numerical example.

Keywords: Frequency responses, time delay, uncertainty

1. INTRODUCTION

Classical methods of analysis and synthesis for feedback control systems rely heavily on the information derived from frequency responses. Frequency domain properties of families of polynomials and transfer functions are also very important in the area of robust feedback control against parametric perturbations. For example, the feedback control design method of using Horowitz's quantitative feedback theory is based on using frequency response templates (or value sets) of the uncertain plant's transfer function at various

frequencies of interest. Here, the frequency response template denotes the smallest region in the complex plane within which the values of the parametric transfer function $G(s; \mathbf{q})$ evaluated at $s = j\omega$ for all parameter vector \mathbf{q} in a prescribed domain \mathbf{Q} lie.

The problem of generating frequency-response templates for a transfer function under parametric perturbations has been studied as early as 1950s (Steward, 1951). In recent years, as motivated by such basic results as the Kharitonov and Edge theorems (Kharitonov, 1978; Bartlett *et al.*, 1988) in the parametric robustness area, there has been renewed interest in developing efficient techniques for computing frequency response templates for families of transfer functions with various forms of parameter dependence. Instead of using a brute-force parameter gridding approach, most of the developed template generation techniques are based on characterizing a small subset \mathbf{E} of the parameter domain \mathbf{Q} whose

¹Author to whom all correspondence should be addressed.

image under the mapping $G(j\omega; \mathbf{q})$ covers the boundary of the template

$$G(j\omega; \mathbf{Q}) = \{G(j\omega; \mathbf{q}) : \mathbf{q} \in \mathbf{Q}\}.$$

For an interval plant whose transfer function coefficients are defined on intervals of the real axis, the subset \mathbf{E} consists of 32 one-parameter plants. With this characterization, Bailey *et al.* (1988) proposed a phase-angle sweeping technique for computing the template boundaries. For the exact computation of the template boundary of an interval plant, Karamancioglu *et al.* (1996) have recently proposed criteria for eliminating the generation of interior points of the template. Based on testing the intersection of two rectangles in the plane with a modified Cohen-Sutherland algorithm, Hwang and Chen (1996) applied a pivoting procedure to trace the template boundaries.

In the feedback control of an interval plant, the closed-loop transfer function's numerator and denominator would be linear combinations of two independent interval polynomials. For this case, Bartlett *et al.* (1993) has shown that a frequency-response template is bounded by the templates corresponding to 32 Kharitonov plant segments. In a more general case where the uncertain parameters enter the coefficients of both the numerator and denominator polynomials of a transfer function $G(s; \mathbf{q})$ in an affine manner and the uncertainty domain is a box \mathbf{Q} , Fu (1990) has shown that the template boundary is included in the image of the edge set of the box \mathbf{Q} , i.e., $\partial G(j\omega; \mathbf{Q}) \subset G(j\omega; E(\mathbf{Q}))$, where ∂ denotes the boundary and $E(\mathbf{Q})$ the set of edges of \mathbf{Q} . With this elegant characterization, the boundary of a frequency response template for a family of linear-polytopic uncertain systems can be obtained by a finite number sets of one-dimensional parameter sweeping. However, this approach to template generation often wastes time in calculating interior points of the template. To overcome this shortcoming, Chen and Hwang (1998a) have applied a pivoting procedure along with a zero-inclusion test algorithm to trace out the approximate template boundaries.

Based on exploiting the notion of principal points associated with nonlinear differentiable complex-valued mappings, several authors (Kiselev *et al.*, 1997) have recently proposed technique for generating frequency-response templates for families of transfer functions with nonlinear parameter dependence. The set of principal points \mathbf{P} associated with the mapping $G(j\omega; \mathbf{q})$ is the smallest analytically characterizable subset of the box \mathbf{Q} whose image $G(j\omega; \mathbf{P})$ covers the template boundary $\partial G(j\omega; \mathbf{Q})$. To facilitate obtaining

the set of principal points, Hwang and Chen (1999) have generalized the notion of principal points and characterized the set of generalized principal points \mathbf{G} , which is the smallest superset of \mathbf{P} admitting a fully analytical characterization. They showed that the set of generalized principal points (GPPs) \mathbf{G} consists of all the edges of the box and connected and/or isolated one-dimensional manifolds on the faces and/or in the interior of the box. Chen and Hwang (1998b) further showed that in the special case where $G(j\omega; \mathbf{q})$ depends multilinearly on the parameter vector \mathbf{q} all the GPP manifolds possesses connectedness properties. They also presented a pivoting procedure with integer labelling to trace out all connected GPP manifolds. However, there still lack an effective method to detect the existence of isolated GPP manifolds.

In this paper, we are concerned with the generation of frequency-response templates for a class of transfer functions $G(s; e^{-\tau s}, \mathbf{q})$ having an uncertain time delay and multilinearly correlated parameter perturbations. Due to the fact that for a fixed frequency ω , $G(j\omega; e^{-j\tau\omega}, \mathbf{q})$ is a nonlinear function of \mathbf{q} and τ and the uncertain delay term $e^{-j\tau\omega}$ is a periodic function, the potential existence of isolated GPP manifolds makes it unreliable to generate template boundaries via tracing GPP manifolds. Instead, we apply a simplicial algorithm to trace out the boundary of the template $G(j\omega; \mathbf{T}, \mathbf{Q})$. The main contribution of the paper lies in developing a new branch-and-bound zero inclusion/exclusion test algorithm for checking if the origin is contained in the image of the parameter box $\mathbf{T} \times \mathbf{Q}$ under the mapping $f(\tau, \mathbf{q}) = g(\mathbf{q}) + h(\mathbf{q})e^{-j\tau\omega}$, where both $g(\mathbf{q})$ and $h(\mathbf{q})$ are multilinear functions of the parameter vector \mathbf{q} . More precisely, we present an easy-to-check sufficient condition for the zero inclusion of the value set $f(\mathbf{T}, \mathbf{Q})$. Moreover, we adapt the Mapping Theorem (Zadeh and Desoer, 1963), which is a sufficient condition for the zero exclusion of the value set corresponding to a multilinear mapping, to check the zero exclusion of the value set $f(\mathbf{T}, \mathbf{Q})$. The adaptation is achieved through overbounding the arc $e^{-j[\tau^-, \tau^+]\omega}$ due to an interval time delay by a two-dimensional box such that the modified mapping is multilinear.

The paper is organized as follows. In Section 2, sufficient conditions of zero inclusion and exclusion for the value set $f(\mathbf{T}, \mathbf{Q})$ are presented. With these sufficient conditions, in Section 3, a branch-and-bound zero inclusion test algorithm for the value set $f(\mathbf{T}, \mathbf{Q})$ is developed. In Section 4, the frequency-response template associated with a transfer function is characterized with the notion of zero inclusion for the value set with a quasi-polynomial. Based on this

characterization of frequency-response template, we describe a simplicial algorithm for tracing out the template boundary. In Section 5, a numerical example is provided to illustrate the efficiency of proposed zero inclusion test algorithm and the application of pivoting procedure for generating frequency response template boundaries. Finally, some conclusions are drawn in Section 6.

2. SUFFICIENT CONDITIONS FOR ZERO INCLUSION AND EXCLUSION

Consider the function of the form

$$f(\tau, \mathbf{q}) = g(\mathbf{q}) + h(\mathbf{q})e^{-j\tau\omega}, \quad j = \sqrt{-1} \quad (1)$$

where $\mathbf{q} = (q_0, q_1, \dots, q_{m-1})$ is an m -dimensional (m -D) real vector, both $g(\mathbf{q})$ and $h(\mathbf{q})$ are complex-valued multilinear functions of \mathbf{q} , and ω is a constant real number. Let $\mathbf{T} = [\tau^-, \tau^+]$ and \mathbf{Q} denotes the m -D box

$$\mathbf{Q} = \{\mathbf{q} : q_k \in [q_k^-, q_k^+], k = 0, 1, \dots, m-1\} \quad (2)$$

The image of the $(m+1)$ -D box $\mathbf{T} \times \mathbf{Q}$ under the mapping $f(\tau, \mathbf{q})$ is denoted by

$$f(\mathbf{T}, \mathbf{Q}) = \{f(\tau, \mathbf{q}) : \tau \in \mathbf{T}, \mathbf{q} \in \mathbf{Q}\} \quad (3)$$

The image $f(\mathbf{T} \times \mathbf{Q})$ is a subset of the complex plane \mathbf{C} and is often referred to as the value set. The purpose of this section is to develop an algorithm for checking if the value set $f(\mathbf{T}, \mathbf{Q})$ includes the origin.

To facilitate presenting the algorithm, we put τ and \mathbf{q} in an $(m+1)$ -dimensional vector as

$$\mathbf{b} := (b_0, b_1, b_2, \dots, b_m) = (\tau, q_0, q_1, \dots, q_{m-1}) \quad (4)$$

and write $f(\mathbf{b}) = f(\tau, \mathbf{q})$. Hence, $\mathbf{B} = \mathbf{T} \times \mathbf{Q}$ is an $(m+1)$ -D box and $f(\mathbf{B}) = f(\mathbf{T}, \mathbf{Q})$. The $(m+1)$ -D box \mathbf{B} has 2^{m+1} vertices and $m(m+1)2^{m-2}$ 2-D faces. Let the set of $n_v = 2^{m+1}$ vertices of the box \mathbf{B} be denoted by

$$\mathbf{B}_v := \{\mathbf{b} : b_k = b_k^- \text{ or } b_k = b_k^+, k = 0, 1, \dots, m\} \quad (5)$$

and the set of $n_f = m(m+1)2^{m-2}$ 2-D faces by

$$\begin{aligned} \mathbf{B}_s &:= \{\mathbf{q} : b_\mu \in [b_\mu^-, b_\mu^+], b_\nu \in [b_\nu^-, b_\nu^+], \mu \neq \nu; \\ &b_k = b_k^- \text{ or } b_k = b_k^+, \text{ for } b \in \mathbf{I}_{m+1} \setminus \{\mu, \nu\}\} \end{aligned} \quad (6)$$

where $\mathbf{I}_{m+1} = \{0, 1, \dots, m\}$. Then the set of images of the vertices of the box \mathbf{B} is denoted by

$$\begin{aligned} f(\mathbf{B}_v) &:= \{f(\mathbf{q}) : \mathbf{b} \in \mathbf{B}_v\} \\ &:= \{\hat{f}_0, \hat{f}_1, \dots, \hat{f}_{2^{m+1}-1}\} \end{aligned} \quad (7)$$

2.1 A sufficient condition for zero inclusion.

We are now ready to present sufficient conditions for the zero inclusion of the value set $f(\mathbf{T}, \mathbf{Q})$. The following theorem is a sufficient condition for the zero inclusion of the value set.

Theorem 1: If the manifold $\mathbf{M} \subset \mathbf{R}^{m+1}$ defined by

$$f(\tau, \mathbf{q}) = 0 \quad (8)$$

has an intersection with the box $\mathbf{T} \times \mathbf{Q}$, then $0 \in f(\mathbf{T}, \mathbf{Q})$.

This theorem implies that if there exists at least one $\tau^* \in \mathbf{T}$ and $\mathbf{q}^* \in \mathbf{Q}$ such that $f(\tau^*, \mathbf{q}^*) = 0$ then the value set $f(\mathbf{T}, \mathbf{Q})$ includes the origin. However, it is too general to be useful for checking the zero inclusion of $f(\mathbf{T}, \mathbf{Q})$. However, based on the above theorem, an easy-to-check sufficient condition for the zero inclusion of $f(\mathbf{T}, \mathbf{Q})$ reads as

Theorem 2: If the manifold \mathbf{M} defined by (8) has an intersection with at least one of the 2-D faces of the box $\mathbf{T} \times \mathbf{Q}$, then $0 \in f(\mathbf{T}, \mathbf{Q})$.

It is noted that the intersection of the manifold \mathbf{M} with a 2-D face of the box $\mathbf{T} \times \mathbf{Q}$ can be easily achieved through finding the real roots of a 2nd-degree polynomial. To see this, we first consider a 2-D face involving the edge $\tau \in [\tau^-, \tau^+]$ as follows:

$$\begin{aligned} \mathbf{F}_2(\tau, g_i) &:= \{(\tau, q_0, \dots, q_{i-1}, q_i, q_{i+1}, \dots, q_{m-1}) : \tau \in [\tau^-, \tau^+], \\ &q_i \in [q_i^-, q_i^+], q_k = q_k^- \text{ or } q_k^+, \text{ for } k \in \{0, 1, \dots, m-1\} \setminus \{i\}\} \end{aligned} \quad (9)$$

On this face, the manifold \mathbf{M} defined by (8) satisfies an equation of the form

$$g_i(q_i) + h_i(q_i)e^{-j\tau\omega} = 0 \quad (10)$$

where $g_i(q_i)$ and $h_i(q_i)$ are both first-degree complex polynomials in q_i . To test if there exist a solution $(\tau^*, q_i^*) \in [\tau^-, \tau^+] \times [q_i^-, q_i^+]$ to the above equation, we first solve the quadratic equation

$$|g_i(q_i)|^2 - |h_i(q_i)|^2 = 0 \quad (11)$$

for q_i^* . If a solution q_i^* to (11) exists and lies in the interval $[q_i^-, q_i^+]$, then we know that the complex number $-g_i(q_i^*)/h_i(q_i^*)$ is of unity length. Hence, if there is a $\tau^* \in [\tau^-, \tau^+]$ such that

$-g_i(q_i^*)/h_i(q_i^*) = e^{-j\tau^*\omega}$, then the manifold \mathbf{M} has an intersection with the 2-D face $\mathbf{F}_2(\tau, q_i)$ defined in (9).

On the other hand, if a 2-D face $\mathbf{F}_2(q_i, q_k)$ includes the edges $q_i \in [q_i^-, q_i^+]$ and $q_k \in [q_k^-, q_k^+]$, then it is easy to see that on this face, the manifold \mathbf{M} is described by the equations of the form

$$g_2(q_i, q_k) = a_{1,1}q_iq_k + a_{1,0}q_i + a_{0,1}q_k + a_{0,0} = 0 \quad (12a)$$

$$h_2(q_i, q_k) = b_{1,1}q_iq_k + b_{1,0}q_i + b_{0,1}q_k + b_{0,0} = 0 \quad (12b)$$

The solution to the above equations can be easily obtained via solving a quadratic equation. If a solution exists and lies in the domain $[q_i^-, q_i^+] \times [q_k^-, q_k^+]$, then

the manifold \mathbf{M} intersects the 2-D face $\mathbf{F}_2(q_i, q_k)$ being tested.

2.2 A sufficient condition for zero exclusion.

To authors' best knowledge, there has no effective zero exclusion test algorithm appeared in the control literature for the value set $f(\mathbf{T}, \mathbf{Q})$ with the mapping f given in (1). However, if f is a multilinear function, then a sufficient condition for the zero exclusion can be derived from the following theorem.

Theorem 3: (Mapping Theorem (Zadeh and Desoer, 1963)): Let $f(\mathbf{b})$ be a multilinear complex-valued function of \mathbf{b} . Then the image of an $(m+1)$ -box \mathbf{B} under the mapping f is a subset of the convex hull of the images of the vertices of \mathbf{B} , i.e.,

$$f(\mathbf{B}) \subset \text{conv}\{f(\mathbf{B}_v)\} \quad (13)$$

where

$$\text{conv}\{f(\mathbf{B}_v)\} := \left\{ \sum_{i=0}^{2^{m+1}-1} \lambda_i \hat{f}_i : 0 \leq \lambda_i \leq 1, i = 0, 1, \dots, 2^{m+1}-1 \right\} \quad (14)$$

In view of this theorem, a sufficient condition for the zero exclusion of the image of a multilinear function f over a box \mathbf{B} can be stated as follows:

Theorem 4: Let $f(\mathbf{b})$ be a multilinear complex-valued function. If the convex hull of the images of the vertices of the box \mathbf{B} under the mapping f does not contain the origin, then the value set $f(\mathbf{B})$ does not include the origin, i.e.,

$$0 \notin \text{conv}\{f(\mathbf{B}_v)\} \rightarrow 0 \notin f(\mathbf{B}) \quad (15)$$

It is noted that the mapping f given in (1) is multilinear in \mathbf{q} and nonlinear in the variable τ . This special form of f motivates us to construct a multilinear function \tilde{f} and an $(m+2)$ -D box $\tilde{\mathbf{Q}}$ such that $f(\mathbf{T}, \mathbf{Q}) \subset \tilde{f}(\tilde{\mathbf{Q}})$. The underlying idea is to replace the delay term $e^{-j\tau\omega} = \cos\tau\omega - j\sin\tau\omega$ by a two-variable expression $q_m - jq_{m+1}$ so that the modified mapping

$$\tilde{f}(\tilde{\mathbf{q}}) = g(\mathbf{q}) + h(\mathbf{q})(q_m - jq_{m+1}) \quad (16)$$

is multilinear, where $\tilde{\mathbf{q}} = (q_0, q_1, \dots, q_{m+1})$. The augmented variables q_m and q_{m+1} lie in the intervals $[q_m^-, q_m^+]$ and $[q_{m+1}^-, q_{m+1}^+]$, respectively, where

$$q_m^- = \min_{\tau \in [\tau^-, \tau^+]} \cos(\tau\omega) \quad (17a)$$

$$q_m^+ = \max_{\tau \in [\tau^-, \tau^+]} \cos(\tau\omega) \quad (17b)$$

$$q_{m+1}^- = \min_{\tau \in [\tau^-, \tau^+]} \sin(\tau\omega) \quad (17c)$$

$$q_{m+1}^+ = \max_{\tau \in [\tau^-, \tau^+]} \sin(\tau\omega) \quad (17d)$$

Since the arc or unit circle given by

$\{e^{-j\tau\omega} : \tau \in [\tau^-, \tau^+]\}$ is bounded by the rectangle $\mathbf{Q}_2 = [q_m^-, q_m^+] \times [q_{m+1}^-, q_{m+1}^+]$, it is obvious that

$$f(\mathbf{T}, \mathbf{Q}) \subset \tilde{f}(\tilde{\mathbf{Q}}) \quad (18)$$

where $\tilde{\mathbf{Q}} = \mathbf{Q} \times \mathbf{Q}_2$. In view of this set inclusion property, we can test the zero exclusion for the value set $f(\mathbf{T}, \mathbf{Q})$ by constructing the convex hull of the images of the vertices of the box $\tilde{\mathbf{Q}}$ and checking if it excludes the origin. Hence, we have the following sufficient condition for the zero exclusion of the value set $f(\mathbf{T}, \mathbf{Q})$.

Theorem 5: Let $g(\mathbf{q})$ and $h(\mathbf{q})$ be both multilinear functions of \mathbf{q} and let the function \tilde{f} be defined in (16). Then

$$0 \notin \text{conv}\{\tilde{f}(\tilde{\mathbf{Q}}_v)\} \quad (19)$$

implies $0 \notin f(\mathbf{T}, \mathbf{Q})$, where $\tilde{\mathbf{Q}}$ is a $(m+2)$ -D box given in (18b).

3. A ZERO INCLUSION TEST ALGORITHM

By the test procedure a box $\mathbf{B} = \mathbf{T} \times \mathbf{Q}$ is checked for the zero exclusion of the convex hull of $\tilde{f}(\tilde{\mathbf{Q}}_v)$ and/or the intersection of the manifold \mathbf{M} with the exposed 2-D faces \mathbf{B}_s of the box \mathbf{B} . Since the conditions presented in Theorem 2 and Theorem 5 are sufficient for the zero inclusion and exclusion of the value set $f(\mathbf{B}) = f(\mathbf{T}, \mathbf{Q})$, an undecidable case occurs when both conditions do not hold. Hence, if the convex hull of $\tilde{f}(\tilde{\mathbf{Q}}_v)$ includes the origin and that all 2-D faces of the box \mathbf{B} do not intersect \mathbf{M} , the test procedure returns undecidable:

$$\text{Test}(\mathbf{B}) = \begin{cases} \text{IN: } \mathbf{B}_s \cap \mathbf{M} \neq \emptyset \\ \text{EX: } 0 \notin \text{conv}\{\tilde{f}(\tilde{\mathbf{Q}}_v)\} \\ \text{UD: otherwise} \end{cases} \quad (20)$$

If an undecidable case occurs in the zero inclusion/exclusion test for the value set $f(\mathbf{B}_0)$ of a box \mathbf{B}_0 , we have to subdivide the box \mathbf{B}_0 into two smaller ones, say $\mathbf{B}_0 = \mathbf{B}_1 \cup \mathbf{B}_2$, and perform the zero exclusion and/or inclusion tests for the value sets $f(\mathbf{B}_1)$ and $f(\mathbf{B}_2)$. Let the $(m+1)$ -D box

$$\mathbf{B}_0 = [b_0^-, b_0^+] \times \dots \times [b_m^-, b_m^+] \quad (21)$$

be partitioned on the variable b_i with the partition point b_i^* into \mathbf{B}_1 and \mathbf{B}_2 . Then, we have

$$\mathbf{B}_1 = [b_0^-, b_0^+] \times \dots \times [b_{i-1}^-, b_{i-1}^+] \times [b_i^-, b_i^*] \times [b_{i+1}^-, b_{i+1}^+] \times \dots \times [b_m^-, b_m^+] \quad (22a)$$

$$\mathbf{B}_2 = [b_0^-, b_0^+] \times \dots \times [b_{i-1}^-, b_{i-1}^+] \times [b_i^*, b_i^+] \times [b_{i+1}^-, b_{i+1}^+] \times \dots \times [b_m^-, b_m^+] \quad (22b)$$

For each partition of a box \mathbf{B}_0 into two sub-boxes \mathbf{B}_1 and \mathbf{B}_2 , there are 2^m newly generated vertices and $m(m-1)2^{m-3}$ newly generated 2-D faces, which are the common vertices and 2-D faces of the sub-boxes \mathbf{B}_1 and \mathbf{B}_2 . It is obvious that if one of the common 2-D faces of \mathbf{B}_1 and \mathbf{B}_2 has an intersection with the manifold \mathbf{M} , we can conclude from Theorem 2 that the value set $f(\mathbf{B}_0)$ includes the origin. For the zero exclusion test, according to (16)-(18), the two boxes $\tilde{\mathbf{Q}}_1$ and $\tilde{\mathbf{Q}}_2$ are constructed and the zero exclusion of the convex hulls of $\tilde{f}(\tilde{\mathbf{Q}}_{1v})$ and $\tilde{f}(\tilde{\mathbf{Q}}_{2v})$ are checked.

For each box subdivision, the zero inclusion/exclusion status for the value set $f(\mathbf{B}_0)$ is given by

$$Test(\mathbf{B}_0) = \begin{cases} \text{IN: if } Test(\mathbf{B}_1) = \text{IN or } Test(\mathbf{B}_2) = \text{IN} \\ \text{EX: if } Test(\mathbf{B}_1) = \text{EX or } Test(\mathbf{B}_2) = \text{EX} \\ \text{UD: otherwise} \end{cases} \quad (23)$$

In the case that $Test(\mathbf{B}_0) = \text{UD}$ and $Test(\mathbf{B}_i) = \text{UD}$ for $i=1$ and/or 2, the box \mathbf{B}_i has to be subdivide iteratively until the zero inclusion/exclusion status of the value set $f(\mathbf{B}_i)$ is determined.

Based on the sufficient inclusion/exclusion conditions and the iterative box partitions, we develop an algorithm for the zero inclusion test. The algorithm uses the depth-first strategy and works with a stack. The standard stack operations to be implemented are *MakeStack*, *Push*, *Pop*, and *IsEmpty*. The operation $(\mathbf{B}_1, \mathbf{B}_2) = \text{Subdivision}(\mathbf{B}_0, r)$ partitions \mathbf{B}_0 on direction r with the partition point $b_r^* = (b_r^- + b_r^+)/2$ into \mathbf{B}_1 and \mathbf{B}_2 . The function *NextDirection*(r, m) works as

$$\text{NextDirection}(r, m) = \begin{cases} 0, & \text{if } r = m \\ r+1, & \text{if } r < m \end{cases} \quad (24)$$

The function $d(\tilde{f}(\tilde{\mathbf{Q}}_v))$ returns the distance between the origin and the center of $\text{conv}\{\tilde{f}(\tilde{\mathbf{Q}}_v)\}$, i.e.,

$$d(\tilde{f}(\tilde{\mathbf{Q}}_v)) = \left| \frac{1}{N_v} \sum_{k=1}^{N_v} V_k \right| \quad (25)$$

where $V_k, k=1, \dots, N_v$ are the vertices of the convex hull $\text{conv}\{\tilde{f}(\tilde{\mathbf{Q}}_v)\}$ and N_v is the number of these vertices. The zero inclusion test algorithm reads as follows:

```
begin procedure
  t = Test(B);
  if (t=IN) return IN;
  if (t=EX) return EX;
  if (t=UD) then
    B0 = B ; r=0;
    S=MakeStack();
    Push(S, B, r);
```

```
do while (¬ IsEmpty(S))
  (B1, B2) = Subdivision(B0, r);
  t1 = Test(B1); t2 = Test(B2);
  r = NextDirection(r, m);
  if (t1 = IN ∨ t2 = IN) return IN;
  else if (t1 = UD ∧ t2 = UD) then
    d1 = d(̃f(̃Q1v)); d2 = d(̃f(̃Q2v));
    if (d1 > d2) then
      Push(S, B1, r); Push(S, B2, r);
    else
      Push(S, B2, r); Push(S, B1, r);
    end if
  else if (t1 = UD) Push(S, B1, r);
  else if (t2 = UD) Push(S, B2, r);
  end if
  if (¬ IsEmpty(S)) (B0, r) = Pop(S)
end do
if (t1 = EX ∧ t2 = EX) return EX;
end if
end procedure
```

4. GENERATION OF FREQUENCY-RESPONSE TEMPLATES

In this section, we consider the problem of generating frequency response templates for a class of transfer functions given below:

$$G(s; \tau, \mathbf{q}) = \frac{N_0(s; \mathbf{q}) + N_1(s; \mathbf{q})e^{-\tau s}}{D_0(s; \mathbf{q}) + D_1(s; \mathbf{q})e^{-\tau s}}, \quad (26)$$

$$\tau \in \mathbf{T} = [\tau^-, \tau^+], \mathbf{q} = (q_0, q_1, \dots, q_{m-1}) \in \mathbf{Q}$$

where $N_i(s; \mathbf{q})$ and $D_i(s; \mathbf{q})$ for $i=1, 2$ are polynomials in s with coefficients being multilinear functions of \mathbf{q} . More precisely, we show that the zero inclusion test algorithm for the value set $f(\mathbf{T}, \mathbf{Q})$ can be applied, together with a pivoting method (Nishioka *et al.*, 1991), to trace the outer boundary of the frequency response template

$$G(j\omega; \mathbf{T}, \mathbf{Q}) = \{G(j\omega; \tau, \mathbf{q}) : \tau \in \mathbf{T}, \mathbf{q} \in \mathbf{Q}\} \quad (27)$$

where ω is a fixed frequency.

To test whether a point z in the complex plane is in the frequency response template $G(j\omega; \mathbf{T}, \mathbf{Q})$ or not we have to check if there exist a $\tau^* \in \mathbf{T}$ and a $\mathbf{q}^* \in \mathbf{Q}$ such that $G(j\omega; \tau^*, \mathbf{q}^*) = z$. Let $G(j\omega; \tau, \mathbf{q}) = z$, then we have from (26)

$$p(z; \tau, \mathbf{q}) = p_0(z; \mathbf{q}) + p_1(z; \mathbf{q})e^{-j\tau\omega} = 0 \quad (28a)$$

$$p_0(z; \mathbf{q}) = N_0(j\omega; \mathbf{q}) - zD_0(j\omega; \mathbf{q}) \quad (28b)$$

$$p_1(z; \mathbf{q}) = N_1(j\omega; \mathbf{q}) - zD_1(j\omega; \mathbf{q}) \quad (28c)$$

If the value set $p(z; \mathbf{T}, \mathbf{Q})$ includes the origin we can conclude that there exist a $\tau^* \in \mathbf{T}$ and a $\mathbf{q}^* \in \mathbf{Q}$ such

that $G(j\omega; \tau^*, \mathbf{q}^*) = z$, i.e., z is in the frequency response template $G(j\omega; \mathbf{T}, \mathbf{Q})$. This allows one to apply the zero inclusion test algorithm developed in the previous section to check if a point z in the complex plane belongs to the frequency response template $G(j\omega; \mathbf{T}, \mathbf{Q})$.

In using the pivoting method to trace the outer boundary of the template $G(j\omega; \mathbf{T}, \mathbf{Q})$, it is required first to divide complex plane into triangles as shown in Fig. 1. Then we assign to each triangle vertex a label 1 if it belongs to the template and otherwise a label 0, or equivalently,

$$L(v_i) = \begin{cases} 1, & \text{if } 0 \in p(v_i; \mathbf{T}, \mathbf{Q}) \\ 0, & \text{if } 0 \notin p(v_i; \mathbf{T}, \mathbf{Q}) \end{cases} \quad (29)$$

Based on the triangulation in Fig. 1 and the vertex labelling shown above, the following pivoting procedure finds a sequence of adjacent boundary triangles with each having vertices of different memberships in the template.

Pivoting Procedure:

Step 1. Choose $h_1 > 0$ and $h_2 > 0$ and divide the complex plane into triangles as shown in Fig. 1.

Step 2. Choose a $\tau_0 \in \mathbf{T}$ and a $\mathbf{q}_0 \in \mathbf{Q}$ and compute $z_0 = G(j\omega; \tau_0, \mathbf{q}_0)$

Step 3. Searching rightward from z_0 for a pair of triangle vertices $v_1^{(0)}$ and $v_2^{(0)} = v_1^{(0)} + h_1$ such that $L(v_1^{(0)}) = 1$ and $L(v_2^{(0)}) = 0$.

Step 4. Set the initial vertex moving directions d_1 and $d_2 = j = \sqrt{-1}$.

Step 5. Set $v = 3$, $\rho = 0$, and $v_v^{(\rho)} = v_2^{(0)} + jh_2$

Step 6. Perform zero inclusion/exclusion test for value set $p(v_v^{(\rho)}; \mathbf{T}, \mathbf{Q})$ and assign according to (29) a label to the vertex $v_v^{(\rho)}$.

Step 7. Find the index $\mu \neq v$ such that $L(v_\mu^{(\rho)}) = L(v_v^{(\rho)})$.

Step 8. If $v_1^{(\rho)} + v_2^{(\rho)} + v_3^{(\rho)} - v_\mu^{(\rho)} = v_1^{(0)} + v_2^{(0)}$, go to Step 12.

Step 9. Swap d_1 and d_2 , h_1 and h_2 .

Step 10. Find the vertices of next boundary triangle by the rule:

$$(v_1^{(\rho+1)}, v_2^{(\rho+1)}, v_3^{(\rho+1)}, v) = \begin{cases} (v_2^{(\rho)}, v_3^{(\rho)}, v_3^{(\rho)} + h_2 d_2, 3), & \text{if } \mu=1 \\ (v_1^{(\rho)}, v_1^{(\rho)} + h_1 d_1, v_3^{(\rho)}, 2), & \text{if } \mu=2 \\ (v_1^{(\rho)} - h_1 d_1, v_1^{(\rho)}, v_2^{(\rho)}, 1), & \text{if } \mu=3 \end{cases}$$

Step 11. Set $\rho := \rho + 1$, go to Step 6.

Step 12. Stop.

5. A NUMERICAL EXAMPLE

Consider the feedback control system shown in Fig. 2. The controller $G_c(s)$ and the two plants $G_{p1}(s; \mathbf{q})$ and $G_{p2}(s; \mathbf{q})$ are as follows (Bhattacharyya *et al.*, 1995):

$$G_c(s) = \frac{s+1}{s+2}$$

$$G_{p1}(s; \mathbf{q}) = \frac{s+q_0}{s^2+q_1s+4}$$

$$G_{p2}(s; \mathbf{q}) = \frac{s+q_2}{s^3+3s^2+q_3s+0.1}$$

The uncertain parameter vector $\mathbf{q} = (q_0, q_1, q_2, q_3)$ lies in the box

$\mathbf{Q} = [2.9, 3.1] \times [1.9, 2.1] \times [4.9, 5.1] \times [1.9, 2.1]$ and the uncertain time delay τ is set to lie in the interval $\mathbf{T} = [0.1, 0.3]$.

The transfer function from disturbance $D(s)$ to output $Y(s)$ is

$$G_d(s; \tau, \mathbf{q}) = \frac{N_1(s; \mathbf{q})e^{-\tau s}}{D_0(s; \mathbf{q}) + D_1(s; \mathbf{q})e^{-\tau s}}$$

where

$$N_1(s; \mathbf{q}) = (s+2)(s+q_0)(s+q_2)$$

$$D_0(s; \mathbf{q}) = (s+2)(s^2+q_1s+4)(s^3+3s^2+q_3s+0.1)$$

$$D_1(s; \mathbf{q}) = (s+1)(s+q_0)(s+q_2)$$

First, we consider the construction of the value set $G(j0.6; \mathbf{T}, \mathbf{Q})$. For a given $\omega = 0.6$ and a point z in the complex plane, the relation $G(j0.6; \tau, \mathbf{q}) = z$ is equivalent to

$$p(z; \tau, \mathbf{q}) = p_0(z; \mathbf{q}) + p_1(z; \mathbf{q})e^{-j0.6\tau}$$

$$p_0(z; \mathbf{q}) = -zD_0(j0.6; \mathbf{q})$$

$$p_1(z; \mathbf{q}) = N_1(j0.6; \mathbf{q}) - zD_1(j0.6; \mathbf{q})$$

For the zero exclusion test of the value set $p(z; \mathbf{T}, \mathbf{Q})$, we construct the multilinear mapping

$$\tilde{p}(z; \tau, \tilde{\mathbf{q}}) = p_0(z; \mathbf{q}) + p_1(z; \mathbf{q})(q_4 - jq_5)$$

where $\tilde{\mathbf{q}} = (q_0, q_1, \dots, q_5)$.

In performing the pivoting algorithm to trace the template boundary, the parameters $h_1 = h_2 = 10^{-4}$ are

used. Choose $\tau_0 = 0.1$, and $\mathbf{q}_0 = (2.9, 1.9, 4.9, 1.9)$ then the value of the frequency response $G_d(j\omega; \tau_0, \mathbf{q}_0)$ at $\omega = 0.6$ is evaluated to be $z_0 = 1.30119 - j1.73478$. Searching rightward from z_0 , we obtained the first triangle vertices $v_1^{(0)}$ and $v_2^{(0)}$ such that $L(v_1^{(0)}) = 1$ and $L(v_2^{(0)}) = 0$ as follows:

$$v_1^{(0)} = 1.5252 - j1.7347$$

$$v_2^{(0)} = 1.5253 - j1.7347$$

In testing the zero inclusion of the value set $p(v_1^{(0)}; \mathbf{T}, \mathbf{Q})$, the nineteenth box partition gave the sub-box $\mathbf{T}_0 \times \mathbf{Q}_0 = [0.2, 0.225] \times [3.0875, 3.1] \times [1.9, 1.9125] \times [5.0875, 5.1] \times [1.9, 1.9125]$. Partition $\mathbf{T}_0 \times \mathbf{Q}_0$ on the variable τ with the partition point $\tau^* = (\tau^- + \tau^+)/2$, we obtain the following two sub-boxes

$$\mathbf{T}_1 \times \mathbf{Q}_1 = [0.2, 0.2125] \times [3.0875, 3.1] \times [1.9, 1.9125] \times [5.0875, 5.1] \times [1.9, 1.9125]$$

$$\mathbf{T}_2 \times \mathbf{Q}_2 = [0.2125, 0.225] \times [3.0875, 3.1] \times [1.9, 1.9125] \times [5.0875, 5.1] \times [1.9, 1.9125]$$

By the zero inclusion test algorithm, it is found that on the 2-D face $\mathbf{F} = \{(0.2125, q_0, q_1, 5.1, 1.9)\}$:

$q_0 \in [3.0875, 3.1]$, $q_1 \in [1.9, 1.9125]$ the set of manifold defining equations

$$-2.83070q_0 + 3.77009q_1 + 1.61148 = 0$$

$$7.31960q_0 + 0.98954q_1 - 24.57030 = 0$$

has a solution $(q_0, q_1) = (3.09991, 1.90007)$. Thus by Theorem 2, we conclude that $p(v_1^{(0)}; \mathbf{T}_0, \mathbf{Q}_0)$ includes the origin, which implies that $0 \in p(v_1^{(0)}; \mathbf{T}, \mathbf{Q})$ and, therefore, $L(v_1^{(0)}) = 1$.

In performing the zero inclusion test for the second vertex $v_2^{(0)} = 1.5253 - j1.7347$, 95 box partition operations have been performed to reach the conclusion that $0 \notin p(v_2^{(0)}; \mathbf{T}, \mathbf{Q})$, i.e., the manifold \mathbf{M} does not intersect with the box $\mathbf{T} \times \mathbf{Q}$. Hence, the vertex $v_2^{(0)}$ is not in the template $G(j0.6; \mathbf{T}, \mathbf{Q})$ and, therefore, $L(v_2^{(0)}) = 0$.

By the pivoting procedure described in the previous section, the boundary curve of the frequency response template $G_d(j0.6; \mathbf{T}, \mathbf{Q})$ are traced out as shown in Fig. 3. To confirm the result, frequency response values of $G_d(j0.6; \tau, \mathbf{q})$ of 10000 randomly selected members of $G_d(s; \mathbf{T}, \mathbf{Q})$ are also shown in Fig. 3. It is noted that none of these frequency response points lies outside the closed boundary traced.

6. CONCLUSIONS

In this paper we have developed an efficient branch-and-bound zero inclusion test algorithm for the image of a box $\mathbf{T} \times \mathbf{Q}$ under the complex-valued mapping of the form $f(\tau, \mathbf{q}) = g(\mathbf{q}) + h(\mathbf{q})e^{-j\tau\omega}$, where

$(\tau, \mathbf{q}) \in \mathbf{T} \times \mathbf{Q}$, and $g(\mathbf{q})$ and $h(\mathbf{q})$ are multilinear functions of \mathbf{q} . To facilitate using the Mapping Theorem (Zadeh and Desoer, 1963) for the zero exclusion test, the arc or circle due to the uncertain delay term $e^{-j\tau\omega}$ for $\tau \in \mathbf{T}$ is overbounded by a box. On the other hand, we present an easy-to-check sufficient condition for the zero inclusion of the value set $f(\mathbf{T}, \mathbf{Q})$. The zero inclusion test algorithm is thus based on the proposed sufficient conditions for checking the zero inclusion and exclusion of the value sets on subdivided box domain. As an application, the developed zero inclusion test algorithm is applied along with a pivoting procedure to trace out the frequency response templates for a class of uncertain systems having an uncertain time delay and multiaffine parameter perturbations in the coefficients of transfer functions. This frequency response template generation technique indeed enhances the accuracy of plant template generation for the control design of uncertain time delay systems having the multiaffine parametric perturbations using quantitative feedback theory.

7. ACKNOWLEDGMENT

This work was supported by the National Science Council of Republic of China under Grant NSC86-2214-E-194-001.

REFERENCES

- Bailey, F. N., D. Panzer and G. Gu (1988). Two algorithms for frequency domain design of robust control systems. *Int. J. Control*, **48**, 1787-1806.
- Bartlett, A. C., A. Tesi and A. Vicino (1993). Frequency response of uncertain systems with interval plants. *IEEE Trans. Automat. Contr.*, **38**, 929-933.
- Bartlett, A. C., C. V. Hollot and L. Huang (1988). Root locations of an entire polytope of polynomials: it suffices to check the edges. *Math. Contr., Signals Syst.*, **1**, 61-77.
- Bhattacharyya, S. P., H. Chapellat and L. H. Keel (1995). *Robust Control: The Parametric Approach*. Prentice Hall PTR, New Jersey.
- Chen, J. J. and C. Hwang (1998a). Computing frequency responses of uncertain systems. *IEEE Trans. Circuits Syst. I*, **45**, 304-307.
- Chen, J. J. and C. Hwang (1998b). Robust d-stability analysis of polynomial families with coefficients depending nonlinearly on perturbed parameters. *IEE Proc. Part D*, **145**, 73-82.

- Fu, M. (1990). Computing the frequency response of linear systems with parametric perturbation. *Syst. & Contr. Lett.*, **15**, 45-52.
- Hwang, C. and J. J. Chen (1996). Computation of the frequency response of interval systems. *Circuits, Syst., Signal Processing*, **15**, 1-12.
- Hwang, C. and J. J. Chen (1999). Plotting robust root loci for linear systems with multilinearly parametric uncertainties. *Int. J. Control*, **72**, 501-511.
- Karamancioglu, A., V. Dzhafarov and C. Ozemir (1996). Frequency response of pid-controlled linear interval systems. *Circuits, Syst., Signal Processing*, **15**, 735-748.
- Kharitonov, V. L. (1978). Asymptotic stability of an equilibrium position of a family of systems of linear differential equations. *Differential Equations*, **14**, 1483-1485.
- Kiselev, O. N., H. L. Le and B. T. Polyak (1997). Frequency responses under parametric uncertainty. *Autom. Remote Control*, **58**, 645-661.
- Nishioka, K., N. Adachi and K. Takeuchi (1991). Simple pivoting algorithm for root-locus method of linear systems with delay. *Int. J. Control*, **53**, 951-966.
- Steward, R. M. (1951). A simple graphical method for constructing families of Nyquist diagrams. *Journal of the Aeronautical Sciences*, **18**, 767-768, 1951.
- Zadeh, L. and C. A. Desoer (1963). *Linear System Theory*. McGraw Hill. New York.

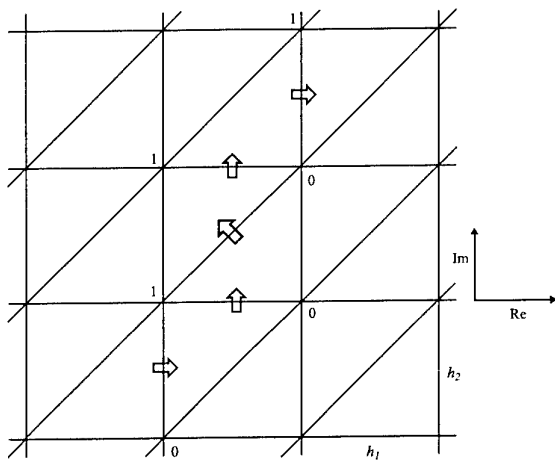


Fig. 1. Triangulation of the complex plane for the pivoting method

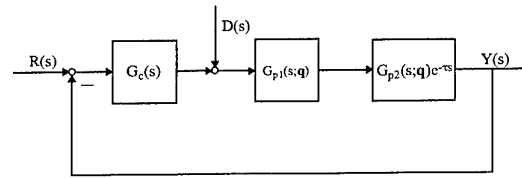


Fig. 2. The feedback control system for the example.

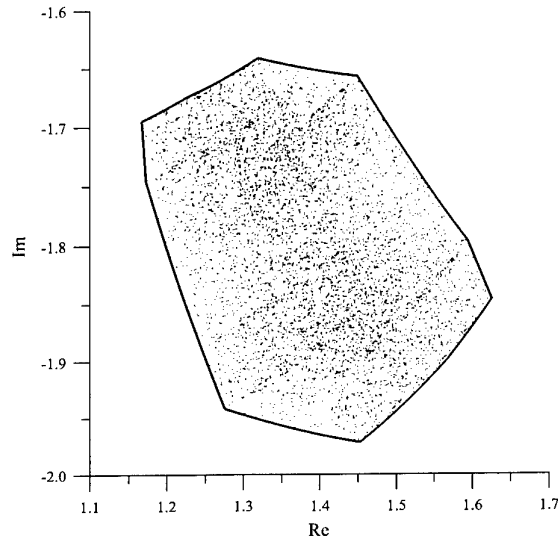


Fig. 3. Frequency response template $G_d(j0.6; T, Q)$ and frequency responses $G_d(j0.6; \tau, q)$ of 10000 randomly selected members of $G_d(j0.6; T, Q)$.

COMPUTATION OF SISO GENERAL PLANT TEMPLATES

Joaquín Cervera^{*}, Alfonso Baños^{*}, and Isaac M. Horowitz^{**}

^{*} *Departamento de Informática y Sistemas, Universidad de Murcia,
 Campus de Espinardo, 30071 Murcia, Spain,
 jcervera@um.es, abanos@dif.um.es*

^{**} *Prof. Emeritus, Dept. Applied Mathematics, Weizmann Institute of Science, Rehovot, Israel,
 and Dept. of Electrical and Computer Engineering, University of California, Davis, U.S.A.*

Abstract: in this work the problem of computing general SISO plant templates from the templates of the single plants involved is considered. Some important aspects of the problem are remarked, especially the potential loss of information in the template melting process when a single plant can intervene in different locations in the general plant expression. After this considerations a general algorithm is developed to avoid this information loss effect.

Keywords: multiloop control, value sets (templates) computation

1. INTRODUCTION

The computation of templates is an important question in QFT by itself. The single plant case has already been studied in the literature, for instance in (Bailey and Hui, 1989), (Nordin, 1993) and (Ballance and Cheng, 1998). A *general SISO plant* is defined in the context of this work as a plant which is composed by the interconnection of several single plants. This definition includes the possibility of series, parallel and feedback interconnection, even with plants in a feedback loop. Plant P in fig. 1 is an example of a general plant including all these possibilities.

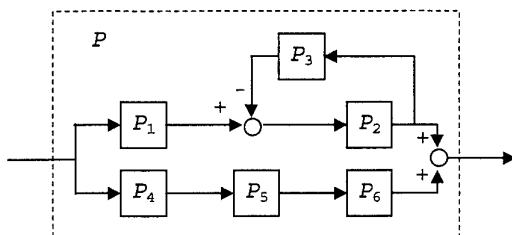


Fig. 1. General plant example.

Throughout this work only the case of parametric uncertainty will be considered, and it will be assumed that there are no uncertain parameters affecting more than one plant. This work has been motivated by the problem of QFT control systems design in the multiloop case, in particular in the non plant modifying case, topic in which the authors are doing some research and which has already been treated in the literature, (Horowitz and Sidi, 1973), (Horowitz and Wang, 1979), (Horowitz, 1993). In this framework the need for a tool for the computation of general SISO plant templates emerges in a natural way.

In the general plant case, the development of a refined template computation procedure is even more important than in the single plant case. The reason is that the number of combinations of uncertain parameters values choices, each parameter taking values from a discrete set, is an exponential function of the number of single plants involved. This fact makes especially impractical the application of a brute force method, that is, the computation of the plant frequency response for every possible combination of individual parameters values choices.

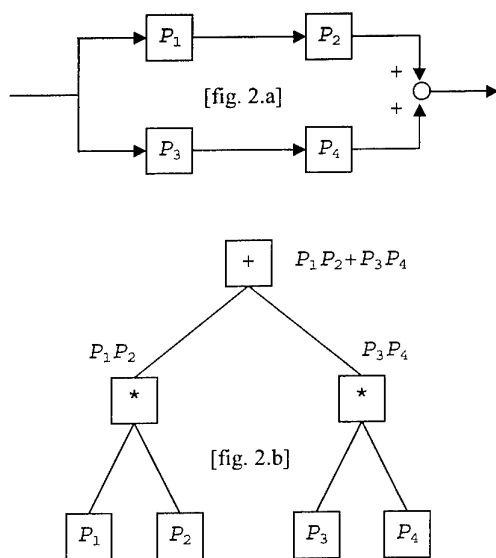


Fig. 2. Example of a general plant tree representation

This brute force approach can be refined using templates contours as a set of representative elements of the templates, instead of the whole set of plant points corresponding to the complete l -dimensional grid in the l -dimensional space of uncertain parameters (being l the number of uncertain parameters). The global plant P is represented by means of a binary tree structure whose leaves are individual plants in P . Each non leaf node n_c , with son nodes n_a and n_b , represent the general plant $P_c = P_a \text{ op}_c P_b$, where P_a and P_b are the plants represented by n_a and n_b , and $\text{op}_c \in \{+, *, /\}$ is an operator associated with n_c . The root node of the tree corresponds to P , the global plant. An example of this decomposition is shown in fig. 2, where the tree representation of the general plant in fig. 2.a is given in fig 2.b. Templates contours for leaf nodes (leaf plants) are supposed to be given. For each non leaf node n_c the template contour of its associated plant P_c , $C(P_c)$, can be obtained by combination of $C(P_a)$ and $C(P_b)$, template contours of plants P_a and P_b , associated with n_c 's son nodes n_a and n_b . This combination consists of computing $c = a \text{ op}_c b$ for every (a, b) pair where $a \in C(P_a)$ and $b \in C(P_b)$ and then obtaining the contour of the set of resulting c 's, which means dropping some of these points. This way, computing every node contour in a bottom-up order in the tree, i.e., from leaf nodes towards the root node, the template contour of P can be obtained from the individual plants contours.

This contours combination procedure can be even improved by the use of interpolation in a given computed contour before using it for computing its father node contour. The idea is filling with new points those zones of the contour where the density of

points is too low. Otherwise this zones with few points tend to expand in subsequently calculated contours. The effect is accumulative.

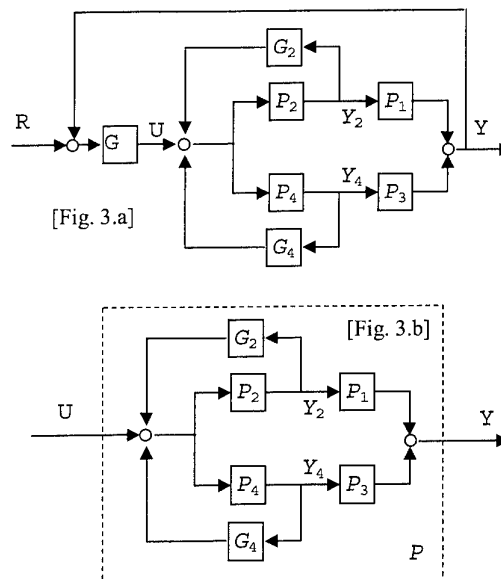


Fig. 3. Example of equivalent plant in a multiloop system

But when there is one (or more) individual plant P_k appearing in various locations in the expression of the global plant P , that is, acting as leaf node in the tree representing P in more than one leaf, some difficulties arise that oblige to modify the application of the described contours procedure and that even prevent us from using the interpolation improvement. The problem is located in the calculation of P_c contour for any given n_c node where P_a and P_b plants, associated with n_c 's sons n_a and n_b , are such that $P_k \subset P_a$ and $P_k \subset P_b$. This $P_i \subset P_j$ inclusion means ' P_i corresponds to n_i , which is a node included in the subtree under n_j , the node associated to P_j '. To compute this P_c contour it is necessary to take into account that not every $c = a \text{ op}_c b$ with (a, b) pair satisfying $a \in C(P_a)$ and $b \in C(P_b)$ is really a point of P_c template. Only (a, b) pairs in which P_k 's uncertain parameters have been instanciated with the same values produce a valid point of the template. Otherwise there would be at least one uncertain parameter taking different values for the same point of a template, which is incorrect.

The fact that the same plant appears in various locations in the same global plant expression happens of course when feedback paths are allowed into the plant structure, but not only in this situation. Even if this structure is not permitted, we can have such a situation when dealing with multiloop design. For instance, for the cascaded multiloop system in fig. 3.a, in a certain stage of the design process the equivalent

plant of fig. 3.b is considered, whose transfer function is

$$\frac{Y}{U} = \frac{P_1 P_2 + P_3 P_4}{1 + G_2 P_2 + G_4 P_4}$$

The fact that for every (a,b) pair P_k has to be instantiated with the same values in a and b can cause an undesired effect, that is, that the important information of a significant point $b \in C(P_b)$ is lost in the combination of both contours because there is no point $a \in C(P_a)$ with the same instantiation of P_k (and vice versa). Every a point with this same instantiation was dropped, whether directly in the computation of P_a contour, or indirectly in the computation of the contour of plants 'included' in P_a , i.e., with associated nodes in the subtree below P_a 's node.

In the case in which interpolation is not used, every point in every contour comes from the combination of leaf node plants instantiated with values in the original grid in the space of uncertain parameters. In this case at least there is a reasonable probability for b to find an a with the same P_k instantiation than it has, and so to avoid the loss of its information. It is a matter of combinations of a discrete number of elements. But this is much more difficult, almost impossible, if b has been obtained by interpolation or in the chain of combinations through n_b subtree which lead to b there was an element obtained by interpolation. In this situation b would need an a obtained from a direct or indirect interpolation which would have yielded the same uncertain parameters choices.

As a first approach to face these difficulties we have developed the algorithm described in next section. In this algorithm we have used for the calculation of the contour of a set of points the ϵ -hull algorithm described in (Nordin, 1993), in particular the implementation developed in (Montoya, 1998).

2. ALGORITHM

The attention has been centred in saving the lost information in the melting of two contours due to the lack of an a for a certain b (and vice versa) in the sense described previously.

For this purpose it will be kept a record of the particular uncertain parameters instantiation of each point of each contour considered in the process. This information provides the knowledge that a certain $b \in C(P_b)$ 'needs' a certain $a \in C(P_a)$ to combine with, having a a certain instantiation I_S of the uncertain parameters of the set of individual plants $S = P_a \cap P_b$. The intersection is here defined as the biggest set of individual plants such that $S \subset P_a$ and $S \subset P_b$, using the inclusion concept defined before. This record also

lets know whether such an a exists in $C(P_a)$ or not. Moreover, if it does not exist, it allows 'creating' such a point in $C(P_a)$ repeating the chain of combinations in the subtree under n_a which lead to $C(P_a)$, but now taking into account that this particular instantiation I_S of S must be respected after every melting of a couple of contours. That is, a point resulting from any melting in that subtree and whose uncertain parameters instantiation fits in I_S , will not be affected by the contour computation algorithm, which drops points from the set resulting from the combination of every point in $C(P_i)$ with everyone in $C(P_j)$ if they are not considered part of the contour of this set.

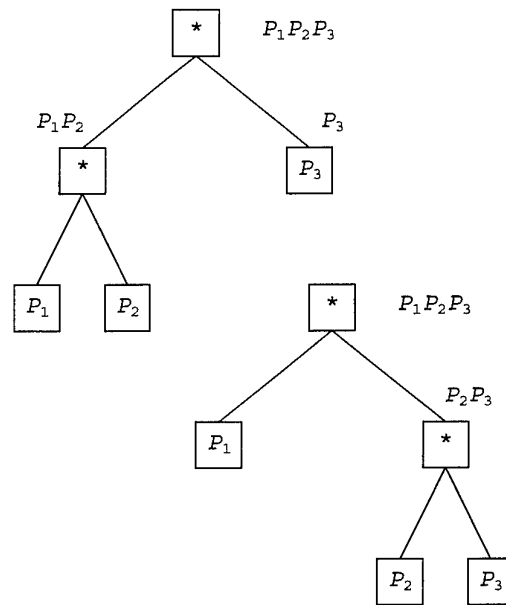


Fig. 4. Possible tree representations for $P=P_1P_2P_3$

For the use of interpolation, the procedure would be the same, but the reconstruction of such an $a \in C(P_a)$ could imply the addition of new uncertain parameter choices for leaf plants, not included in the original grid in the space of uncertain parameters. This is so because maybe none of the original choices combinations would produce the interpolated point we are interested in. This is just a detail to take into account, but there is a great problem about the use of interpolation: given a point $b = p_z = \text{interp}(p_x, p_y)$, where $p_x = p_{x1} \text{ op } p_{x2}$, and $p_y = p_{y1} \text{ op } p_{y2}$, the pair (p_{z1}, p_{z2}) such that $b = p_z = p_{z1} \text{ op } p_{z2}$ is not uniquely defined, consequently neither are the choices of uncertain parameters values for the individual plants in $S = P_a \cap P_b$. And so the way to construct a point a adequate to combine with b is neither uniquely defined. We have not dealt with this problem in the present work, but restricted to the case without interpolation.

The developed algorithm receives as its input the tree representing the global plant P whose template contour is to be calculated, in the way it was described in Section 1. This tree representation is not unique. For instance, for $P = P_1 P_2 P_3$, both representations in fig. 4 are valid. Its choice determines the order in which the contours will be combined. So when various choices are available it is important in terms of efficiency and accuracy to choose that that minimizes the total number of combinations (intermediate nodes) and the number of different locations in the expression of the global plant for any given leaf node plant (points in which loss of information may occur). A planned improvement of the presented algorithm in the future is a grammatical analyser for plant expressions that makes this choices by itself with optimizing criteria. The algorithm also receives as input the template contour for each of the leaf node plants involved. For instance, the algorithm input for the plant in fig. 2.a would be the grammatical tree in fig. 2.b together with $C(P_i)$, $i \in \{1, 2, 3, 4\}$. Its output will be the contour for the global plant P .

The algorithm, named *contour*, is executed in a recursive way, corresponding the first recursive call to the root node of the tree. The basic structure of this recursive procedure is as follows:

```
contour(father_node) ←
  ls = contour(left_son(father_node));
  rs = contour(right_son(father_node));
  result = combine(ls, rs);
```

Function *combine* takes care of constructing necessary points in ls and rs so as to remedy the loss of information we are trying to avoid. Its basic structure is:

```
combine(ls, rs, father_node) ←
  miss_in_ls =
    = missing_A_to_combine_with_B(ls, rs);
  miss_in_rs =
    = missing_A_to_combine_with_B(rs, ls);
  comp_ls = complete(miss_in_ls,
    left_son(father_node));
  comp_rs = complete(miss_in_rs,
    right_son(father_node));
  ls = ls ∪ comp_ls;
  rs = rs ∪ comp_rs;
  result = really_combine(ls, rs);
```

Function *complete*, which as *contour* is also recursive, takes care of constructing points in xs (ls/rs) compatible with those in ys (rs/ls) which were unpaired. There are many possible choices in the way to perform this task.

The securest one in the sense of preserving information is to construct for every unpaired point in ys every compatible point in xs , that is, if compatibility is determined by a set of common

individual plants, say again S , and a particular choice of uncertain parameters, say I_S , this would imply the calculation of every possible point in xs with choice I_S with respect to leaf node plants in S , and with every possible choice in the remaining leaf node plants. This could mean, in terms of computational complexity, getting too near the brute force approach, so this choice has not been taken.

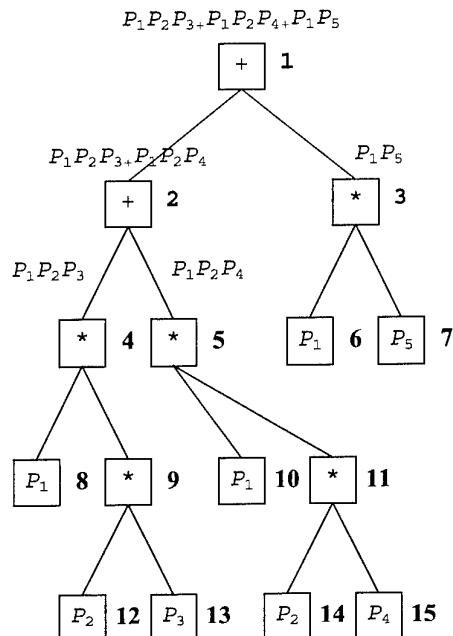


Fig. 5. Tree representation for $P = P_1 P_2 P_3 + P_1 P_2 P_4 + P_1 P_5$

Instead, it has been tried to find a trade-off between brute force and information loss by means of the following criterion about leaf node plants not belonging to S : the points constructed for a particular choice in S leaf node plants will be those formed by leaf node non S plants instantiations which are found in a contour in the downwards path followed by the recursive execution of *complete*. In particular, this contour could be each non leaf plant contour if no higher level contour is found before.

In the execution of *complete* it is taken into account the possible situation in which for a certain node a set of non S plants, say NS , belongs to both sons of the node. This situation is the same in the sense of information loss than the one taking place in *combine* that lead us to the development of *complete* and *missing_A_to_combine_with_B*. But in this occasion the problem is already solved by this couple of functions. So, *complete* not only calls itself in its normal recursive execution constructing points compatible with a particular choice in S , but also begins a new search for points compatible with $S \cup NS$ if this situation occurs. This point is explained with an example.

Consider plant $P = (P_1P_2P_3) + (P_1P_2P_4) + (P_1P_5)$. The chosen tree representation is given in fig. 5. Nodes are numbered with bold typeface numbers on their right. Imagine we are in the execution of *contour* function on the root node, after getting both son contours. *Combine* is called with this contours as parameters. The set of common leaf plant between nodes 2 and 3, S , is P_1 . *Combine* will detect some points *miss_in_ls* in the contour of node 3 with S uncertain parameters choices with no compatible point in the contour of node 2, so *complete* will be called with

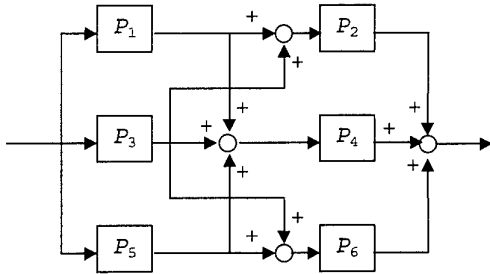


Fig. 6. Plant for example of algorithm execution.

node 2 and I_S . And here is where the consideration made has to be applied. In node 2 *complete* detects a leaf plant belonging to NS , P_2 , because this plant is in both son nodes of node 2 but is not in S . It was said that any combination of parameters of non S plants appearing in a contour in the downwards execution of *complete* should be taken into account. For P_2 there is a contour through node 4 and a different one through node 5. In the melting of both contours in node 3 some P_2 points will be lost. This is the same effect occurring in *combine* and that motivated the development of *complete*. So the same function can be used again to remedy the same problem. The initial result that *complete* would give back to *combine*, that would have lost some P_2 combinations, will be completed with the result of call to itself, this time asking for completing points which are unpaired in terms of P_2 when points from nodes 4 and 5 are put together.

3. EXAMPLE.

In this section a simple academic example will be examined with the objective of observing the information recovery achieved by the algorithm. The time spent by the execution of the algorithm using *complete* scheme, using $k = 8$ points per parameter to obtain individual plants templates, was 220 seconds over a PC with a 750 MHz Pentium III processor and 128 Mb RAM, using Matlab 5.2 running on Windows 2000. The brute force method run out computer memory for the same k , even for $k=4$. For $k=3$, we stopped execution after more than half an hour.

The plant structure for the example is shown in fig. 6. For $i=1...6$, $P_i=k_i/(s+a_i)$, and $k_1, k_6 \in [1,200]$,

$k_2, k_4 \in [1,50]$, $k_3, k_5 \in [10,30]$; $a_1, a_6 \in [1.5,3]$, $a_2, a_4 \in [1,4]$ and $a_3, a_5 \in [1.5,3]$ (12 uncertain parameters). The chosen tree is shown in fig. 7.

In fig. 8 and it is shown the execution of the algorithm *contour* with use of the *complete* routine, for the $\omega=1$ rad/s template. For each numbered node in the tree in fig. 7 in fig. 8 there are two template plots: before and after contour calculation. In fig. 9 it is shown the same execution but without *complete* routine in order to

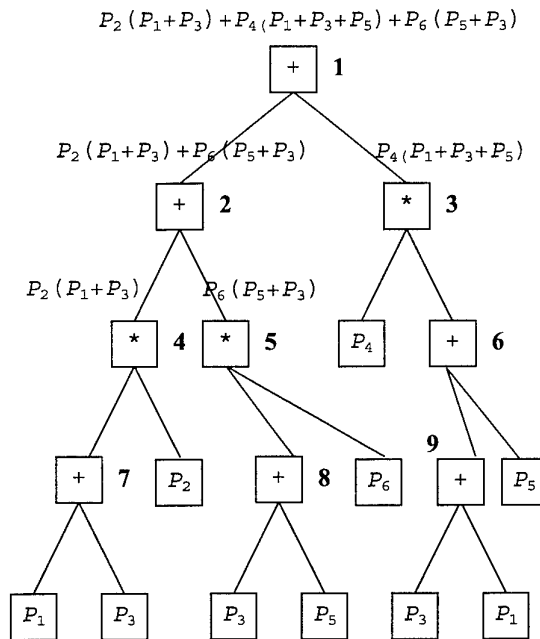


Fig. 7. Tree structure for plant example in fig. 6.

compare the information loss respect to execution without *complete*.

For the second case better results could be achieved if at every stage no point is dropped from the template. But this would lead to an exponential growth of the number of points involved, which has to be avoided by means of some prune strategy. As it can be seen, this prune does not affect the execution with *complete* routine.

4. CONCLUSIONS

The problem of the computation of general SISO plants templates once single plants involved templates are known has been considered. It has been shown the need for a non brute force method in the general case. Some points to be considered in the design of such a method have been remarked, with emphasis on the topic of information loss in templates melting. A strategy to avoid this phenomenon has been designed and implemented in an algorithm. This algorithm is a first approach to the problem which the authors plan

to refine in the future, applied as a part of the design of multiloop control systems. One of the points to be developed, already mentioned in this work, is the addition of a grammatical analyser for general SISO plants expressions that chooses the best tree representation, in terms of commented criteria. Also allowing the same parameter appearing in various plants is planned. Another important related topic to be developed, not treated in this work, is the use of knowledge of the significant parts of the templates obtained from practical experience.

ACKNOWLEDGEMENTS

This work has been supported by *Fundación Séneca, Centro de Coordinación de la Investigación* (Región de Murcia, Spain) by means of a *Programa Séneca de Formación del Personal Investigador* grant, and CICYT under project DPI2000-1218-C04-03.

REFERENCES

- Bailey, F. N. And Hui, C. H. (1989). A fast algorithm for computing rational functions. *IEEE transactions on automatic control*. **34**, 1209-1212.
- Ballance, D.J., and Chen, W. (1998). Symbolic computation in value sets of plants with uncertain parameters. *UKACC International conference on control '98*, 1322-1327.
- Horowitz, I. (1993). *Quantitative Feedback Design Theory-QFT (Vol. 1)*. QFT Press, 4470 Grinnell, Boulder, Colorado 80305, USA. This is available (in America) from I. Horowitz: O132012@aol.com, and elsewhere from A. Baños: abanos@dif.um.es
- Horowitz, I. and T. S. Wang (1979). Synthesis of a class of uncertain multiple loop feedback systems. *International Journal of Control*. **29**, 645-668.
- Horowitz, I. and M. Sidi (1973). Synthesis of cascaded multiple-loop feedback systems with large plant parameters ignorance. *Automatica*. **9**, 589-600.
- Montoya, F.J. (1998). Nonlinear control tools design by means of QFT: computational analysis and development of a CACSD tool (original in Spanish). Doctoral thesis. Universidad de Murcia, Spain.
- Nordin, M. (1993). Uncertain systems with backlash: modeling, identification and synthesis. Licenciate thesis, Royal Institute of Technology, Sweden.

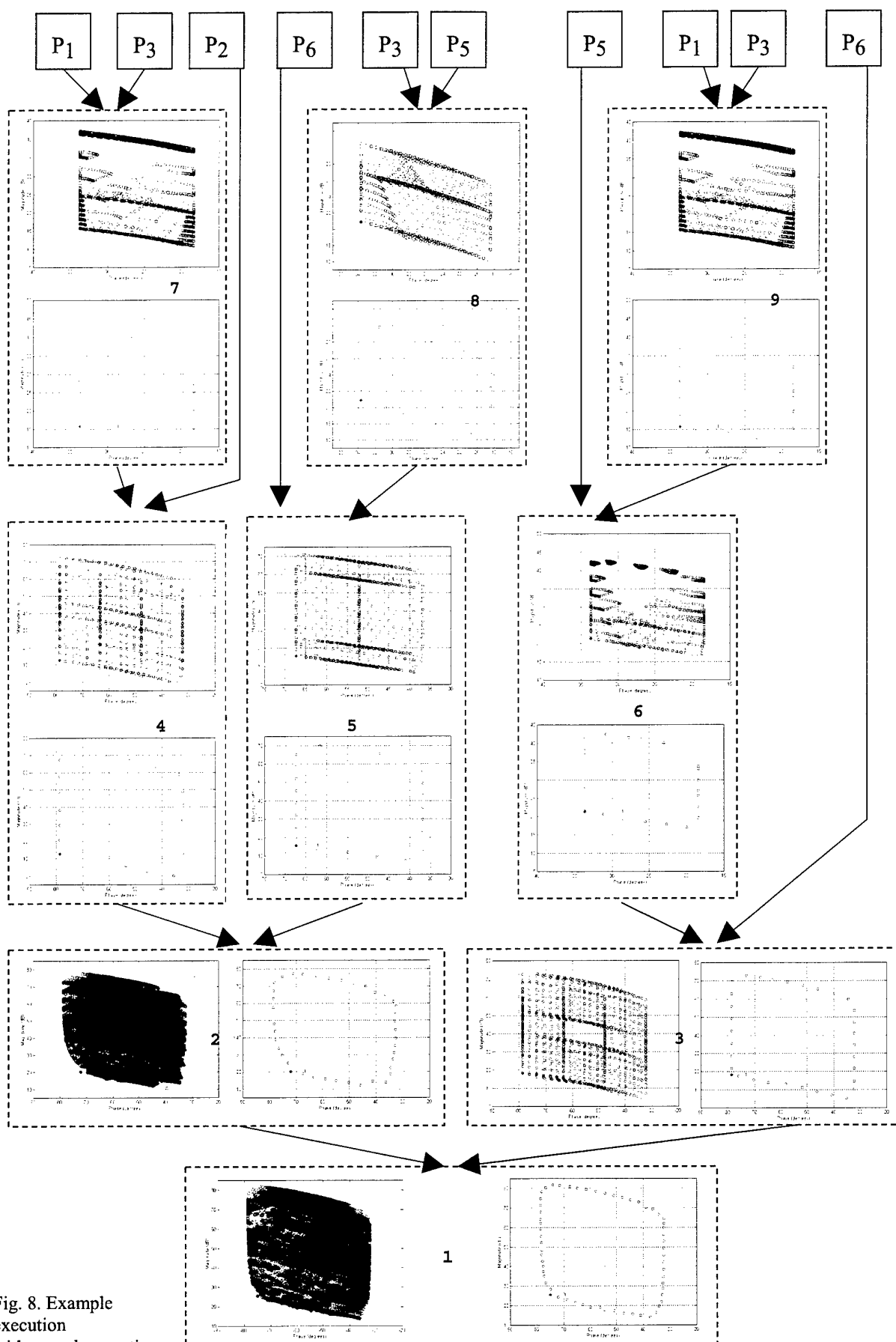


Fig. 8. Example execution with *complete* routine.

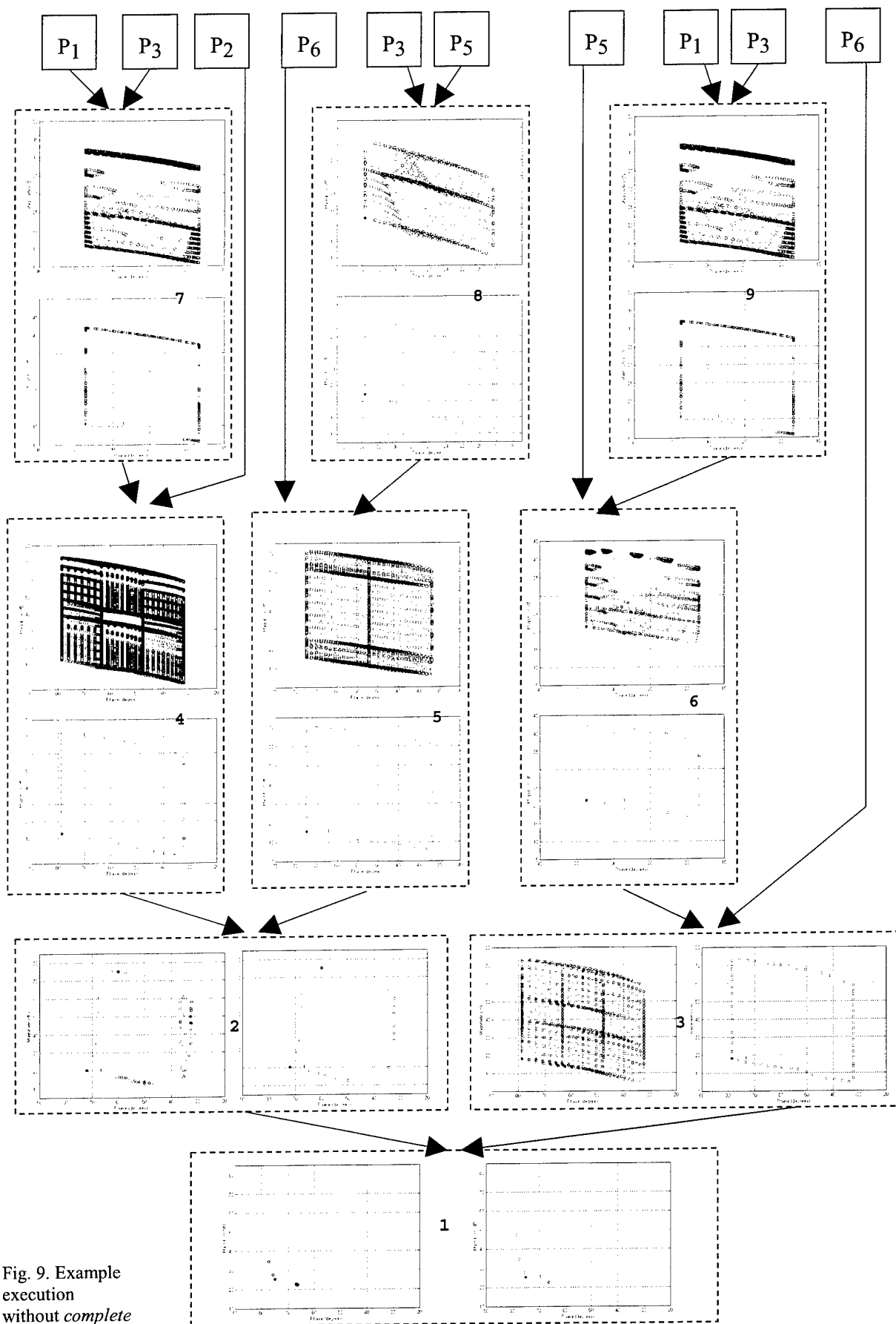


Fig. 9. Example execution without *complete* routine.

FREQUENCY DOMAIN FEEDFORWARD COMPENSATION

F.J. Pérez Castelo and R. Ferreiro Garcia

*Dept. Ingeniería Industrial. Universidad de La Coruña
javierpc@udc.es, Phone: 34 981 337400. Fax: 34-981-337401
ferreiro@udc.es, Phone: 34 981 167000. Fax: 34 981 167101*

Abstract: This work deals with some practical aspects of PID controllers regarding multivariable non-linear feedforward compensation. This contribution concerns the task of compensation for multivariable disturbances on the controlled variable. The strategy consists of establishing an adaptive function capable of compensating by means of a feedforward strategy all disturbance variables under any dynamic condition.

Keywords: QFT theory, frequency domain design, frequency domain identification, multivariable disturbances, multivariable feedforward compensation.

1. FEEDFORWARD CONTROL BACKGROUND.

Conventional feedforward control deals with the task of correcting the manipulated variable for disturbances on the controlled process. Most common industrial processes are disturbed by more than a variable. For instance, in heat exchangers, controlled temperature is disturbed from flow and temperature variations of heated fluid. Furthermore, they are disturbed also by variations of the operating point because dissipation heat may depend on the ambient and operating temperatures and by process parameters.

In conventional feedforward control (Shinsky 1980) an error must be detected in a controlled variable before the feedback controller can act to change the manipulated variable. Therefore, disturbances must upset the system before the feedback controller can do anything. It seems very reasonable that if a disturbance entering a process could be detected, a controller should begin to correct it before it upsets the process.

This is the basic idea of feedforward control. If disturbance can be measured, this result will be used

to send a signal through a feedforward control algorithm that makes appropriate changes in the manipulated variable so as to keep the controlled variable near its desired value.

Classical industrial controllers offer the possibility of compensation for only a disturbance variable entering the process, if such a disturbance can be measured.

The real problem concerning industrial control, in which a good performance is needed, requires the compensation task for more than a single disturbance variable included disturbance model parameters. In such a case, conventional controllers are not efficient and proposed adaptive controller takes advantage. Furthermore, disturbance variables are associated by non-linear functions. Non-linear feedforward compensator can be designed for non-linear systems.

An alternative to implement feedforward control systems in order to compensate multivariable disturbances, may be implemented by means of a frequency analysis procedure based in disturbance model identification by FFT algorithm.

2. SPECTRAL IDENTIFICATION

In order to get information related to system frequency response, it is necessary to implement a procedure by means of FFT algorithms. This information will be used later to design the corresponding PID controller. The application of FFT algorithms to the system dynamics by exciting it with sinusoidal signals of different frequencies permits the achievement of the magnitude and phase angle at concrete frequencies, but also subharmonic components originated by external disturbances are to be found.

The identification task starts searching for the ultimate frequency (w_{relay}) with system phase angle response $-\pi$ rad performing the Relay Feedback Analysis (Åström.K.J et al., 1989). This frequency will be the key for the control frequencies selection used in the regulator design (Ferreiro et al., 1995). The feedback PID controller and the perturbation lead/lag feedforward compensator (Figure 1,2 and 3) will be designed in function of the performance specification indicated by the designer. The control frequency (w_{cp}) for the feedback controller and the time constants (τ_a , τ_r) for the lead/lag feedforward compensator will be obtained as fraction of the w_{relay} and the control system performance specifications. With the FFT algorithm the following information will be found about the plant, working in open-loop configuration:

- The magnitude $M = |G(jw_{cp})|$ and phase $P = \angle G(jw_{cp})$ at the control frequency (w_{cp}) selected for the design of the feedback PID regulator.
- The central frequency of high frequency disturbances.

The performance specification includes datas like: phase margin (ϕ_M), settling time, overshoot and bandwidth. With such data proportional gain, integral and derivative parameters can be achieved deterministically (Phillips et al., 1995 and Åström.K.J et al., 1984).

The design expressions for three types of regulators are presented in Table1. The contribution angle θ_c corresponds with the regulator phase angle at the control frequency (w_{cp}). Proportional gain, integral and derivative parameters are achieved deterministically (Table 1) for PI and PD regulators. Design criteria can be achieved by selecting frequencies at which the contribution angle achieves acceptable regulators in terms of relative stability. Then the control frequency (w_{cp}) can vary in order to verify the design restrictions.

From frequency analysis by means of a digital signal processor algorithm which implements the FFT

(Decimation in Frequency) (Oppenheim et al., 1989), it is possible to introduce further computer-based calculations to identify salient characteristics, disturbance characteristics and system frequency response with some a priori knowledge.

Table 1:Design Equations for a concrete Phase Margin

$\theta_c = \angle G_c(jw_c) = 180 + \phi_M - \angle G_p(jw_c)$	
Design Equations	Restrictions
$Kp = \frac{\cos(\theta_c)}{ G_p(jw_c) }$ $T_d w_c = \tan(\theta_c)$	$0 < \theta_c < \frac{\pi}{2}$
$Kp = \frac{\cos(\theta_c)}{ G_p(jw_c) }$ $\frac{-1}{T_i w_c} = \tan(\theta_c)$	$0 > \theta_c > \frac{3\pi}{2}$
$Kp = \frac{\cos(\theta_c)}{ G_p(jw_c) }$ $T_d = \frac{\tan(\theta_c) + \sqrt{\tan(\theta_c)^2 + \frac{4}{K_t}}}{2w_c}$ $T_i = K_t T_d \quad 2 \leq K_t \leq 8$	$\frac{\pi}{2} > \theta_c > \frac{3\pi}{2}$

3. DESIGN ALGORITHM.

As we can see in Figure 1 ,2 and 3 the controller will be composed by a PID controller and a Lead/Lag Feedforward compensator.

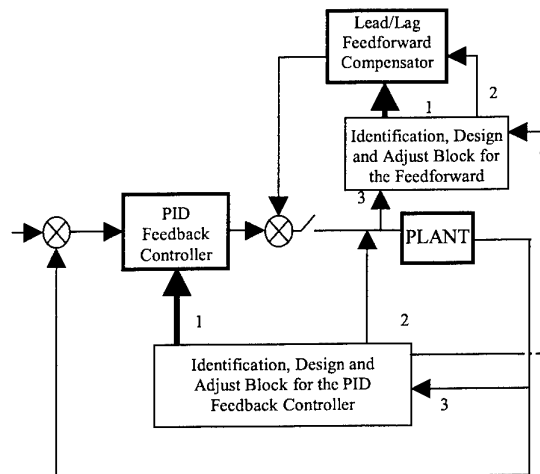


Figure 1. General configuration

The feedback one will be working all the time and will be adapted to give response to changes in operating conditions. Its input will be the error obtained as the difference between the set point and the controlled variable.

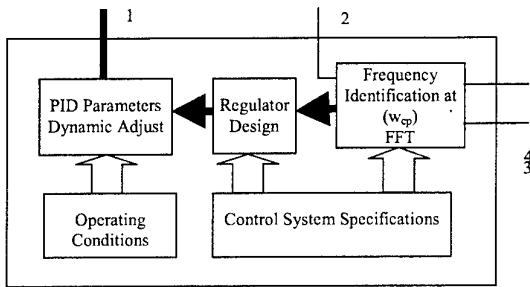


Figure 2. Identificación, Design and Adjust Block for the PID Controller

The lead/lag feedforward compensator will give response to any disturbance. In the identification process the manipulated variable measured under different operating conditions will be stored in order to estimate the manipulated variable during the control system performance.

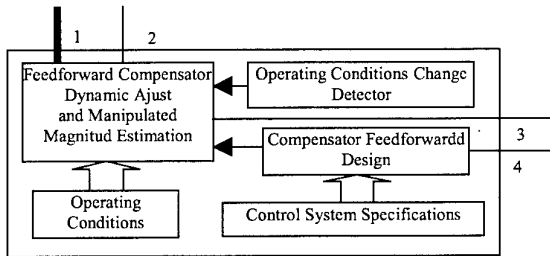


Figure 3. Identificación, Design and Adjust Block for the Feedforward Compensator

Its input (output 2 Figure 3) will be the error between the manipulated variable estimation when a variation in the disturbance variable is detected and the real system manipulated variable before the perturbation. Then the design algorithm will be related to the development of both elements. The design objective is to obtain two crisp sets look-up tables where we will map a complete set of PID parameters and the lead/lag time constants for any combination of operating conditions. This set of parameters will be obtained trying to give optimum responses depending on the design criteria specified for every concrete controller. As explained in section 2 the fuzzy adaptive design procedure is based in the plant identification by frequency techniques obtaining w_{relay} and subsequently w_{cp} , τ_a and τ_r .

It is important to mention that it is necessary to obtain these frequencies for any combination of operating conditions if we want to map the system nonlinearities.

The Figure 4 shows a PID design block diagram

(Åström.K.J et al., 1984) as important part of the fuzzy adaptive procedure. Input data is divided into two types:

- Data concerning the definition of the performance specification.
- Data concerning the dynamic system behaviour.

The design procedure has to follow the next sequence of actions:

1. Take the system to a steady state under a concrete operating conditions
2. Store the value of the manipulated variable (MV).
3. Apply the Relay Feedback Analysis.
4. Select the control frequency
5. Identify frequency system response (magnitude and phase) applying FFT at the control frequency
6. Verification of the design restrictions. If not come back to the step 3.
7. Application of the design expressions, obtaining the controllers parameters.
8. Choice of lead/lag time constants for the lead/lag feedforward compensator.

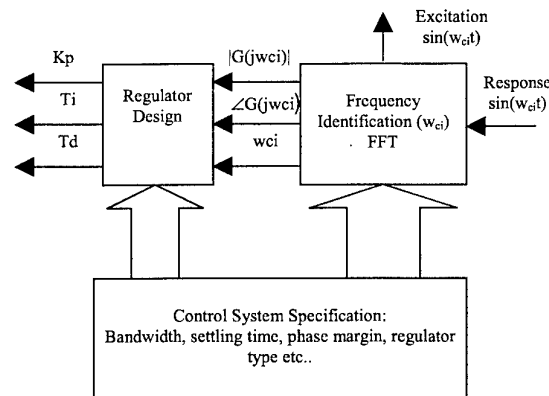


Figure 4. PID design block diagram

During the design process we can find that for some control frequencies to obtain acceptable regulators it is not possible. In these cases it is necessary to restart the design, searching control frequencies that will generate stable controllers.

Applying the above method for different system operating conditions we will built a crisp set look-up table with a complete set of controller parameters and time constants. The defuzzyfication method will be performed by least square regression procedure (Johansson et al., 1993, Brown et al., 1994) obtaining polynomials expressions for every PID parameter, lead/lag time constants and manipulated variable estimation as function of the operating conditions. These expressions permit to adapt in real time during the system performance the regulator parameters as

soon as the plant mathematical models change due to its implicit nonlinearities.

3. CASE STUDY.

A tank system is used to check the performance of the algorithm due to its nonlinear characteristics. The Tank system model is given by the expression (1)

$$\frac{d}{dt} [A(h)h] = q_i - q_o = q_i - a\sqrt{2gh} \quad (1)$$

- A(h) tank section (m2)
h tank level (m)
q_i, q_o input, output liquid flow (m3/sec.)
a outlet pipe section (m2)
g gravity (9.8 m/sec.2)

A tank with the following characteristics was used to verify experimentally the controller.

- Height = 10m
Base cross section diameter = 1m
Top cross section diameter = 4m
q_{imax}=3.514 m³//sec.
a_{max}=0.251 m²

The tank section is a function of the h variable. Taking it into account the equation (1) is converted in equation (2) which represents the mathematical model of our tank system

$$\pi \left[\frac{dh}{dt} + \frac{d}{dt} \left(\frac{h^3}{100} \right) + \frac{d}{dt} \left(\frac{h^2}{5} \right) \right] = q_i - a\sqrt{2gh} \quad (2)$$

The design procedure starts identifying the system by frequency techniques. First of all, it will be applied the relay Feedback Analysis (Figure 5) and secondly working with the open loop configuration we introduce sinusoidal stimulus to our plant, processing its responses by the FFT algorithm (Figure 6)

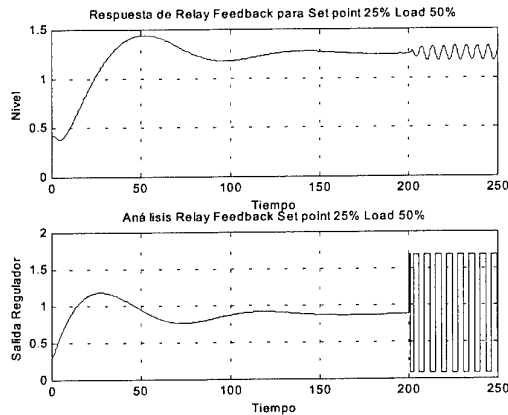


Figure 5. Relay Feedback Analysis

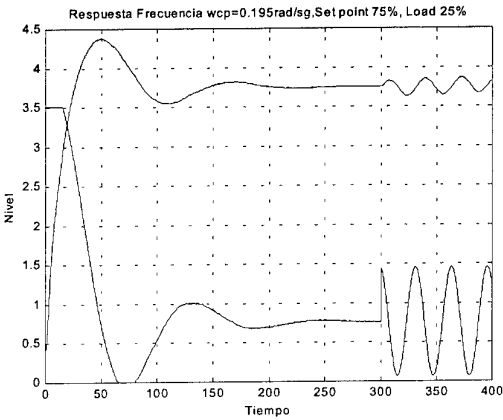


Figure 6. Frequency Response Analysis

The objective is to find, for every combination of operating conditions (set point and load) the frequency (w_{relay}) with system response phase -180 deg. It has been specified a set of performance specifications (time response, bandwidth and phase margin) initially. A slow time response trying to avoid great overshoots and a phase margin of 65 deg are some of these specifications.

The control frequency (w_{cp}) has been selected as fraction of w_{relay} (0.2 w_{relay} in this case) and the lead/lag unit pole and zero just the same (w_{ccf}=0.5w_{relay}=1/τ_a w_{cpf}=w_{relay}=1/τ_r). The results of the application of the algorithm is presented in Table 2. The Feedback controller is a PI and Feedforward compensator a lead/lag unit.

Table 2. Design Algorithm Results

Frequency Identification		LOAD					
		25%		50%		75%	
SET POINT	25%	W _{relay11} =1.005 M.V.=0.4395		W _{relay12} =1.04 M.V.=0.8781		W _{relay13} =1.08 M.V.=1.318	
		W _{cp11} =0.201	W _{cpf11} =1	W _{cp12} =0.208	W _{cpf12} =1	W _{cp13} =0.216	W _{cpf13} =1
		0.37	W _{ccf11} =0.5	0.32	W _{ccf12} =0.5	0.36	W _{ccf13} =0.5
		-94.7°		-90°		-106°	
	50%	W _{relay21} =0.94 M.V.=0.6226		W _{relay22} =0.63 M.V.=1.237		W _{relay23} =0.65 M.V.=1.863	
		W _{cp21} =0.188	W _{cpf21} =0.94	W _{cp22} =0.126	W _{cpf22} =0.63	W _{cp23} =0.13	W _{cpf23} =0.65
		0.244	W _{ccf21} =0.47	0.32	W _{ccf22} =0.31	0.62	W _{ccf23} =0.32
		-108°		-90°		-78.3°	
	75%	W _{relay31} =0.973 M.V.=0.7594		W _{relay32} =0.973 M.V.=1.525		W _{relay33} =0.973 M.V.=2.284	
W _{cp31} =0.1946		W _{cpf31} =0.97	W _{cp32} =0.1946	W _{cpf32} =0.97	W _{cp33} =0.1946	W _{cpf33} =0.97	
0.155		W _{ccf31} =0.48	0.155	W _{ccf32} =0.48	0.157	W _{ccf33} =0.48	
	-110°		-94.7°		-94.74°		
Parameters PID		LOAD					
		25%		50%		75%	
SET POINT	25%	K _{PP11} =2.5 35 T _{IP11} =13.45		K _{PP12} =2.83 T _{IP12} =10.31		K _{PP13} =2.74 T _{IP13} =29.23	
	50%	K _{PP21} =4.07 T _{IP21} =43.32		K _{PP22} =2.83 T _{IP22} =17.02		K _{PP23} =1.29 T _{IP23} =10.32	
	75%	K _{PP31} =6.42 T _{IP31} =58.74		K _{PP32} =6.05 T _{IP32} =13.9		K _{PP33} =5.97 T _{IP33} =13.92	

With the information of Table2 it is possible, applying numerical analysis perform a defuzzification procedure by means of polynomial expressions. These expressions has as independent variables the set point and the load and as dependent variables the controller parameters. Then the defuzzification process will be performed by least square regression procedure, obtaining the polynomial expressions. The expressions (3) represents the functions that relates the operating conditions to the manipulated variable estimation (MV), the PID parameters and the limit cycle frequency.

$$\begin{aligned}
 K_{pp} &= -2.385 + 19.13x + -8.68x^2 + 16.73y + -66.14xy + 52.72x^2y + 0.28y^2 + \\
 &-21.52xy^2 + 32.32x^2y^2 \\
 1/Tip &= -0.1637 + 0.7329x + -0.8513x^2 + 1.9757y + -7.2847xy + 7.1781x^2y + \\
 &-2.5498y^2 + 9.3053xy^2 + 32.32x^2y^2 \\
 w_{relay} &= -0.842 + 9.692x + -9.696x^2 + 9.99y + -7.80xy + -52.62x^2y + 52.4y^2 + \\
 &41.84xy^2 + -41.92x^2y^2 \\
 MV &= -0.0656 + 0.3716x + -0.4016x^2 + 1.1778y + 2.13xy + 0.5808x^2y + -0.3y^2 + \\
 &1.6976xy^2 + -1.824x^2y^2
 \end{aligned}
 \tag{3}$$

The variables x and y represent the operating conditions set point and load. The universe of discourse for both variables is [0,1].

Now the identification and controller design procedures are finished. The control system behaviour under different operating conditions and disturbances will be tested.

4. RESULTS AND CONCLUSIONS.

Initially the system time response is tested modifying by steps the set point and the load at the same time during the experiment. Three combinations of set point and load have been tested (0.25,0.25), (0.5,0.5) and (0.75,0.75).

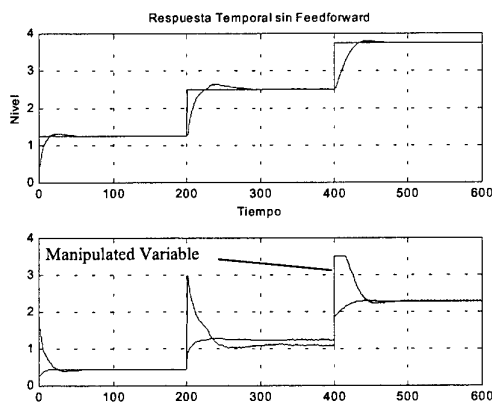


Figure7. System Time Response

In this first experiment we just try to evaluate the feedback controller element without using the perturbation feedforward compensator. Trying to observe how we can obtain quick time responses a control frequency $w_{cp}=0.2w_{relay}$ is selected and designed the corresponding set of controllers. The results are represented in Figure 7.

The second experiment was designed to analyze at the same time the controller performance under different operating conditions and disturbances. These conditions are set point (25%), load (25%) and a load perturbation.

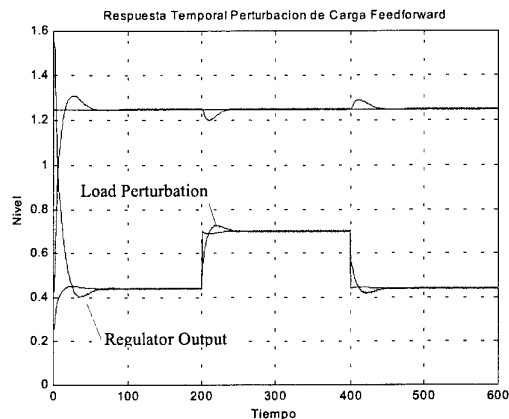


Figure 8. Feedback Controller Time Response under Disturbances

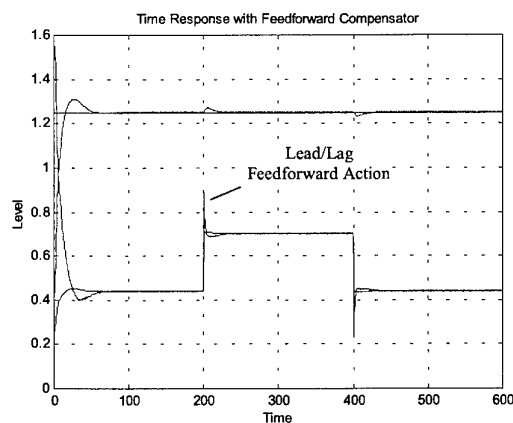


Figure 9. Feedforward Compensator Time Response

In Figure 8 and 9 the effect of the load perturbation with and without lead/lag feedforward compensator is represented. Its clear the correction effect of the lead/lag unit avoiding system long transient periods out of the operating point under load disturbance conditions.

The results show how valve modulation activity is correct in the three conditions where energy demanded for rapid following is achieved under good valve modulation, depending on the required tracking

speed. It is possible to achieve performance while keeping robustness of a controlled system under load changes in acceptable limits as per time response of results, where feedforward compensation of loads and set points with inherent modelling errors do not distort too much the response and avoids the limitation of the integral action.

The adaptive frequency method has been revealed as effective in feedforward dynamic compensation where uncertainties from environmental conditions are met, and some points are to be raised as follows:

- Low man machine interaction is needed for the adjustment task
- Acceptable time response to disturbances
- Robustness in both cases, that is under parameter variations and relative stability

REFERENCES

- Åström.K.J, Wittenmark B, *Adaptive Control*, Addison-Wesley Publishing. Chap 10, pp. 343-371,372-395, 1989
- Åström.K.J and T. Hagglund, "Automatic Tuning of Simple Regulators with Specifications on Phase and Amplitude Margins", *IFAC 1984 Automatica* Vol. 20 No. 5 pp 645-651, 1984
- Brown Martin and HarrisChris 1994 Neurofuzzy Adaptive Modelling and Control Prentice Hall Ltd pp364-406 pp 411-430
- Ferreiro García R. And Pérez Castelo F.J., *Adaptive PID Controller Applied on Marine DP Control Using Frequency Techniques*, Proceedings of the 3rd IFAC-CAMS'95 , 1995
- Johansson Rolf, *System Modeling Identification* Prentice-Hall. pp 78-93, 1993
- Oppenheim Alan V. and Ronald W. Scahafer *Discrete-Time Signal Processing*, Prentice-Hall Chap 10 582-605 Chap11, pp 696-713, 1989
- Phillips Charles L. and H. Troy Nagle, Jr.,. *Digital Control Systems. Analysis and Design*, Prentice-Hall, Inc. Englewood Cliffs,N.J., U.S.A. pp. 315-319 pp.404-413, 1995
- Shinskey F.G. *Process Control Systems* McGraw-Hill 1980

CPP, LQG or GPC?[†]

T O'Mahony & C. J. Downing

*Department of Electronic Engineering, Cork Institute of
Technology, Cork, IRELAND.*

Abstract: The robust control of a dc servo-motor is considered using three different control strategies; the cancellation pole-placement (CPP) controller, the linear quadratic gaussian (LQG) controller and the generalised predictive controller (GPC). The process is difficult to control being high-order, non-minimum phase, underdamped and non-linear. A proposed modification of the CPP controller which involves restructuring as a two degree-of-freedom controller, is shown to produce performance comparable to the LQG and GPC designs and, surprisingly, to have superior high-frequency robustness for this application

Keywords: Generalised Predictive Control, Linear Quadratic Control, Robust Control, Cancellation Pole-Placement Control, Real-time Control.

1. INTRODUCTION

This paper considers the design and implementation of three digital control strategies for a dc servo-motor system. The selected techniques are the cancellation pole-placement (CPP) controller, the linear quadratic gaussian (LQG) controller and the generalised predictive controller (GPC). All three control laws are designed to yield the same nominal tracking performance and a similar (nominal) degree of robustness. The controllers are then evaluated in terms of

- (a) robust performance
- (b) deterministic disturbance rejection
- (c) sensitivity to high-frequency noise

It could be argued that such a comparison is of little relevance in that, assuming the necessary degrees of freedom, each controller can be designed to yield identical performance. In theory this is certainly true, each controller can be designed to place the closed-loop poles at identical locations. In practice, however, performance is dictated not just by what is theoretically achievable but also by the availability and simplicity of the tuning parameters that equip the

controller. Thus for a successful practical implementation the control law should have parameters that directly affect

- 1) performance
- 2) robustness

Furthermore these parameters should be easily adjustable to achieve the requisite performance and/or degree of robustness.

A frequent criticism of the GPC and, particularly, of the CPP controller is that they lack the simple robustness-enhancing 'tuning knob'. In the GPC case an observer polynomial - the T -polynomial - may be incorporated to enhance robustness but its selection is not always intuitive and few systematic design techniques exist. The problem is exacerbated with the CPP controller in that the only tuning parameter available is the desired closed-loop transfer function. Hence while nominal performance is trivial to specify, the design of a robust control law is problematic. To overcome these deficits O'Mahony and Downing (2001, 2000) have recently proposed novel tuning strategies for each of these control laws that are based in the frequency domain and which directly enhance the robustness of the controllers.

[†] This research was funded by the CIT Scholarship Scheme. The authors wish to gratefully acknowledge this support.

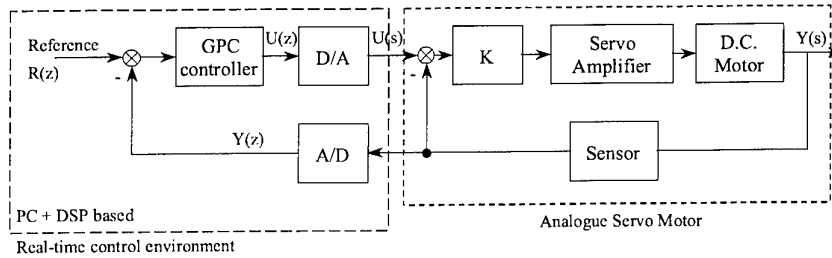


Figure 1: Experimental set-up of voltage controlled dc motor

Thus one of the contributions of this paper is to evaluate these proposals, in real-time, on a difficult system, and to compare the resultant performance with that of a well established technique e.g. the LQG.

A somewhat surprising outcome of this study is the level of performance achieved with the CPP controller. Frequently, in the literature, this controller is commended for its simplicity but dismissed due to the plethora of practical problems that besiege it. For example, Isermann (1981) notes that "the design of cancellation controllers has to be restricted to sufficiently damped, asymptotically stable processes with minimum phase behaviour". Yet in this application the CPP controller is successfully applied to a process that exhibits oscillatory poles, non-minimum phase behaviour and considerable non-linear characteristics. Furthermore if utilised in a two degree-of-freedom structure the CPP controller is shown to perform equivalently to the "more advanced" LQG and GPC designs in terms of robust performance and disturbance rejection, but displays superior immunity to the effects of high-frequency noise.

This paper proceeds with a brief outline of the real-time process in §2.0, for which a linear model is developed in §3.0. In §4.0 the process of tuning each of the controllers is elaborated while §5.0 and §6.0 are devoted to performance evaluation. Finally in §7.0 some conclusions are drawn.

2. DC MOTOR

The experimental rig used to evaluate the performance of these controllers is a voltage controlled dc motor as illustrated in figure 1. The control target can be position, speed or torque, among others. In this application, position will be utilised as the controlled variable.

An analogue proportional controller is supplied with the dc motor and employed to stabilise the motor. The combination of motor plus proportional controller is considered to be the system under control and the various controllers were designed on this premise. The control objective is to accurately

and rapidly track any changes in set-point. The control design is achieved using MATLAB and implemented in real-time using the dSPACE real-time control environment. In essence this real-time environment resolves the issues of coding and implementation thus enabling the control system designer to concentrate on the design aspects of the application.

3. IDENTIFICATION

A model of the dc motor may be directly estimated by recourse to parameter estimation techniques such as Least Squares, see, for example, Ljung (1987). With this technique it is necessary to select the model structure *a-priori*. Assuming a second-order model of the form -

$$G_m(z^{-1}) = \frac{b_1 z^{-1} + b_2 z^{-2}}{1 + a_1 z^{-1} + a_2 z^{-2}} \quad (1)$$

the coefficients a_1 , a_2 , b_1 and b_2 may be obtained by applying a standard test input signal such as a step and recording the result. Application of the LS algorithm to these signals resulted in the following model coefficients -

$$\begin{aligned} a_1 &= -1.554; & a_2 &= 0.802 \\ b_1 &= 0.113; & b_2 &= 0.1312 \end{aligned} \quad (2)$$

A sampling interval of $\tau_s = 0.05 \text{ sec}$ was utilised. Note that this discrete-time model is non-minimum phase (NMP) with a zero located at $z = -b_2/b_1 = -1.161$.

To test the accuracy of the model a step input was applied to both the model and the physical system, as illustrated in figure 2. For the estimated 2nd-order model it is evident that a perfect fit was not obtained. This is primarily due to the fact the motor, like most physical systems, has high-frequency dynamics which are not captured by the second-order model. However, it was felt that this model captured the dominant characteristics of the dc motor and therefore constitutes a valid simplification. Moreover, if a robust controller design philosophy is pursued, the resulting controllers will perform well despite the model uncertainty.

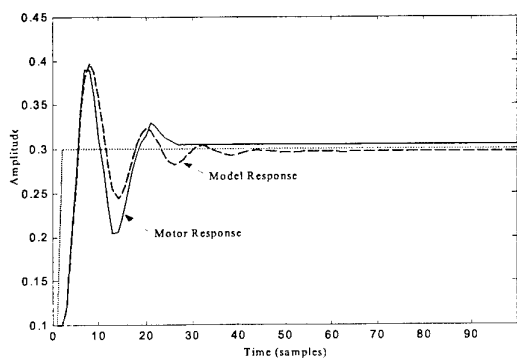


Figure 2: Model validation: 2nd-order model versus actual plant data

4. CONTROLLER DESIGN

A difficulty with any controller comparison is that the authors familiarity with their favoured technique (in this case GPC) over the contesting solutions may unintentionally introduce bias into the results. To minimise this possibility the controllers considered here were designed to yield similar performance, though this aspiration is understandably limited by the available design parameters that equip the individual controllers. Since the GPC is, in essence, a two degree-of-freedom (2-DOF) controller a fair comparison dictated that a similar flexibility be available in the other two techniques. Hence the general 2-DOF structure of Vilanova & Serra (1997) was proposed to extend the standard CPP controller to provide the requisite degrees of freedom. Likewise a polynomial version of the LQG controller, as advocated by Grimbale (1994), was implemented which enables the servo response to be specified independent of the feedback controller. All three controllers were therefore designed to yield the same nominal response to set-point changes. This ideal response model, $M_i(z)$, was specified as second-order overdamped, with a settling time of 1 second i.e.

$$M_i(z^{-1}) = \frac{0.0359z^{-1} + 0.0294z^{-2}}{1 - 1.483z^{-1} + 0.5488z^{-2}} \quad (3)$$

The feedback components of each controller were then designed to yield approximately the same robustness index - a delay margin of 0.75sec - as elucidated presently.

4.1 Cancellation pole-placement design

The design of the CPP controller centres around the selection of a single tuning parameter, the desired closed-loop transfer function or complementary sensitivity function, T . Given this transfer function the controller is calculated using

$$G_c(z^{-1}) = \frac{1}{G_m} \cdot \frac{T}{1 - T} \quad (4)$$

Thus while nominal tracking performance is easily specified via T , few strategies exist to aid the robust design of this controller. In O'Mahony and Downing (2001) it was noted that if

$$\frac{T}{G_m} \leq 1 \quad \forall \omega < \omega_o \quad (5)$$

where ω_o is the closed-loop bandwidth, then the *input sensitivity function*, $M(z^{-1}) = G_c/(1 + G_c G_m)$ would also be less than one at all relevant frequencies. This ensures that the controller possesses good high-frequency properties and hence that the closed-loop is relatively insensitive to high-frequency stimuli arising as a result of measurement noise or unmodelled dynamics. This simple guideline was used to choose the closed-loop transfer function T such that a robust CPP control law resulted. In general however, such a design may impinge upon the servo-performance and result in sluggish responses to set-point changes. To offset this disadvantage the two degree-of-freedom (2-DOF) control structure, presented by Vilanova and Serra (1997) and illustrated in figure 3, is utilised. In this realisation the servo response is characterised by the open-loop controller denoted as G_s , whereas the feedback and robustness properties depend completely on the feedback or regulator controller denoted G_R . Each controller can be arbitrarily designed according to the desired behaviour of the associated loops.

The design of the 2-DOF CPP controller began with the specification of the regulator transfer function, T_R . A fourth-order transfer function was utilised which satisfied equation 5 and is defined by:

$$T_R(z) = \frac{0.0004(z + 7.58)(z + 0.76)(z + 0.077)}{(z - 0.779)(z - 0.67)(z - 0.7)^2}$$

and the feedback or regulator controller, G_R , was calculated from equation 4 with T replaced by T_R . Note that to achieve a stable control law the model, G_m , has to be modified to eliminate the NMP zero.

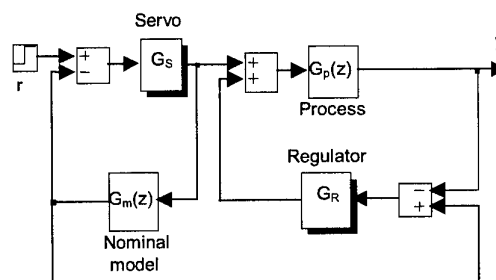


Figure 3: Realisation of 2-DOF CPP Controller

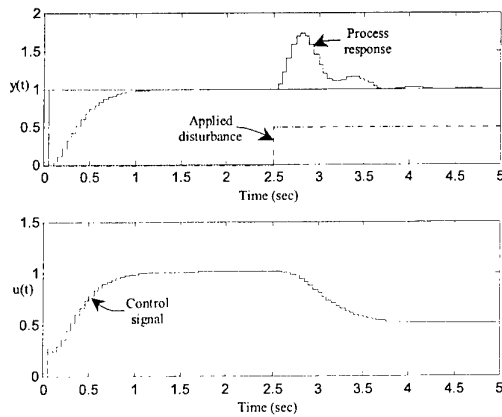


Figure 4: Performance of 2-DOF CPP controller

An optimal solution to this problem is to replace the unstable zeros by their reciprocal, Peterka (1972). Analysis of the resulting control law yielded a gain margin, G_m , of 13dB's, a phase margin, Φ_m , equal to 86° and a delay margin, Δ_m , of 0.76sec. The servo control law was subsequently designed to achieve the one second settling time by setting $T_s = M_i$ of equation 3 and solving equation 4 to obtain the controller G_s . The control performance was evaluated using Simulink with the results shown in figure 4.

4.2 Linear quadratic gaussian design

The design of the LQG controller entails choosing three transfer functions. Two of these, $Q(z^{-1})$ and $R(z^{-1})$ appear in the LQG cost function as

$$J = E\{Q e^2(t) + R u^2(t)\}$$

whereas the third W_i is used to dictate the ideal input/output response. The design of the LQG controller may be achieved by applying a two-stage synthesis procedure, where, in the first stage, the regulator dynamics are specified through the dynamic weights Q and R . Subsequently the user is completely free to choose an ideal servo response and the algorithm, outlined by Grimble (1994), enables a suitable reference controller to be systematically designed.

Consider the block diagram of figure 5, below. It is trivial to define the following sensitivity functions:

Sensitivity function:

$$S = \frac{y(t)}{d(t)} = \frac{1}{1 + G_c G_m}$$

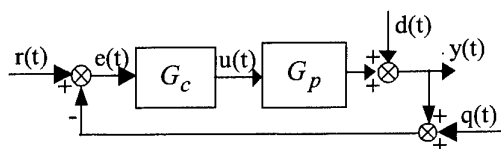


Figure 5: Simple Closed-loop Control System

Complementary sensitivity function:

$$T = \frac{y(t)}{q(t)} = \frac{G_c G_p}{1 + G_c G_m}$$

Input sensitivity function:

$$M = \frac{u(t)}{q(t)} = \frac{G_c}{1 + G_c G_m}$$

It is well known that the sensitivity function, S , is predominantly used to investigate the low-frequency performance of the controller, in particular the response to disturbances and set-point trajectories. To achieve good low-frequency performance S must have low gain at low frequencies and, ideally, unity gain at high frequencies. In contrast both of the other sensitivity functions may be used to analyse the high-frequency controller performance. To minimise actuator activity it is required that M have good high-frequency roll-off in addition to having low gain at high frequencies. Similarly if T has low gain and good roll-off at high frequencies then the effect of measurement noise on the process response will be minimal. In addition T also determines the controller sensitivity to mis-modelling since:

$$\left\| \frac{1}{\Delta_m} \right\| < T; \quad \forall \omega \quad (6)$$

if stability is to be guaranteed, Doyle (1979). In equation 6 Δ_m represents the upper bound of the multiplicative modelling uncertainty. The frequency weights Q and R may be designed by noting that Q predominantly affects the low-frequency properties of the controller and hence determines the response to disturbances, tracking ability and performance robustness. If Q is chosen such that this filter has high-gain at low frequencies it will effectively penalise S at these frequencies and ensure that S is suitably shaped. Introducing an integrator in Q introduces integral action in the feedback controller and guarantees that step disturbances will be rejected and that step-like trajectories will be accurately tracked. Conversely the control weighting R is usually defined to have high-gain at high frequencies such that both T and M are heavily penalised in this frequency region, which results in improved stability robustness and measurement noise rejection.

Using this philosophy suitable values for Q and R were determined, by trial-and-error, to be-

$$Q = \frac{0.12}{1 - z^{-1}} \quad R = \frac{0.48}{(1 - 0.2z^{-1})(1 - 0.4z^{-2})}$$

Analysing the resulting feedback controller yielded the following margins: $G_m = 23dB's$, $\Phi_m = 81^\circ$ and $\Delta_m = 0.77sec$. The design was completed by letting W_i equal to the ideal response model M_i and solving to determine the servo or reference controller. The resulting Simulink performance is illustrated in figure 6.

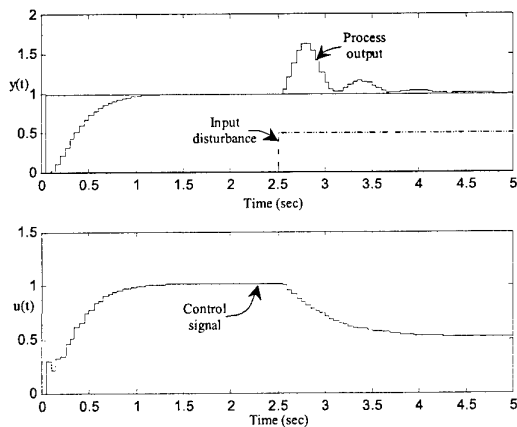


Figure 6: Performance of LQG controller

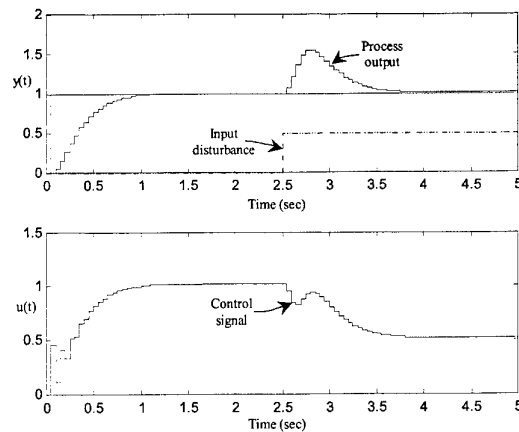


Figure 7: Performance of GPC

4.3 Generalised predictive controller design

The GPC can also be designed utilising a two-stage strategy. Initially the servo parameters may be selected to realise the desired nominal response to set-point changes and subsequently a single design polynomial, denoted the T -polynomial, may be utilised to enhance the regulator performance or increase the robustness of the controller. A difficulty with the GPC strategy is the large number of parameters (six in all) which must be initialised prior to commissioning. Preliminary work on these parameters was mainly concerned with their effect on the servo performance and resulted in the development of a number of tuning rules to yield a variety of servo performances, Lambert (1987) and Söeterboek (1992). However, these rules usually require the simultaneous specification of a number of parameters and, hence, are less than intuitive. This difficulty was assuaged with the work of McIntosh *et al* (1991) who presented a number of simple tuning strategies which allowed the user to vary the closed-loop speed of response over a full range by adjusting a single active tuning parameter whilst all other servo parameters remain fixed. One of these strategies, the so called *detuned model-following configuration* utilises a polynomial - the $P(z^{-1})$ polynomial - to place the closed-loop poles and hence GPC can be set up to follow the closed-loop model $M(z^{-1}) = 1/P(z^{-1})$. Letting

$$P(z^{-1}) = 1 - 1.483z^{-1} + 0.5488z^{-2}$$

with the remaining parameters initialised as outlined by McIntosh *et al* (1991), completed the design of the GPC servo response. The properties of the feedback controller, in particular the robustness of the control law - may now be improved by including the T -polynomial. Again a frequency-domain approach, see O'Mahony and Downing (2000), was utilised where $T(z^{-1})$ was designed to guarantee robust stability i.e. to ensure that equation 5 was satisfied at all frequencies for the estimated model uncertainty. This philosophy led to the following

parameterisation of the T -polynomial-

$$T(z^{-1}) = (1 - 0.17z^{-1})^2 (1 - 0.14z^{-1})^2 (1 - 0.33z^{-1})$$

The GPC controller yielded the following margins: $G_m = 13dB's$, $\Phi_m = 73^\circ$ and $\Delta_m = 0.75sec$ with the Simulink performance of figure 7.

5. MODEL UNCERTAINTY AND ROBUST PERFORMANCE

The requirement for good high-frequency closed-loop performance is consistently referred to in the robust control literature and is primarily due to the fact that model uncertainty tends to be predominantly high-frequency in nature. In the case of the dc motor model uncertainty arises from (a) neglected dynamics and (b) non-linearities over the operating range of the motor. The former is evident from figure 2 and was discussed in §3.0. The non-linearity displayed by the plant is primarily a function of the magnitude of the applied step as illustrated in figure 8(a) where a number of step inputs of different magnitudes are applied to the motor and the resulting responses

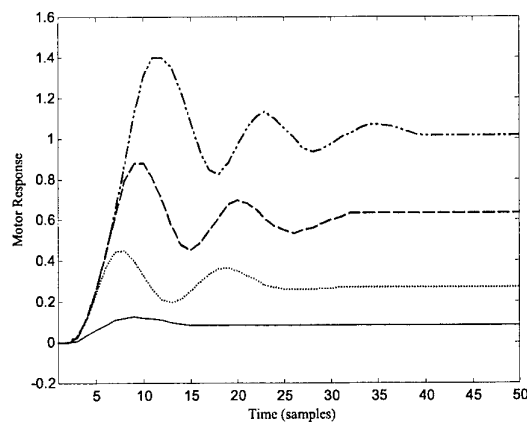


Figure 8(a): Open-loop response of dc motor at different operating regions.

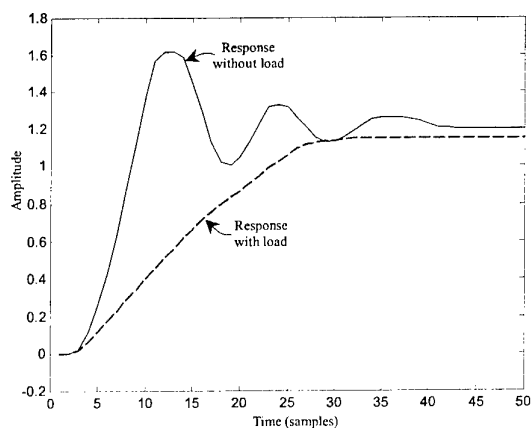


Figure 8(b): Open-loop response of dc motor with, and without applied load

recorded. The process dynamics also vary considerably with the applied load as illustrated by figure 8(b) where the unloaded response is compared with the response that results when 100% load is applied.

The real-time performance of all three controllers is illustrated in figures 9, 10 and 11. Figure 9 illustrates the closed-loop response for small set-point changes while figure 10 depicts the response for larger set-point variations - in both cases the motor is unloaded. In Figure 11 the performance of all three control laws is compared when 100% load is applied to the motor. Clearly all three controllers perform well (almost equivalently) despite the significant dynamic variations present. It could be argued that, of the contesting designs, the GPC performs better for relatively small uncertainties (figures 9 and 10) in that very tight tracking with minimal overshoot was achieved. However, in the presence of more severe mis-modelling (figure 11) the LQG and CPP design perform slightly better in that lower overshoot results.

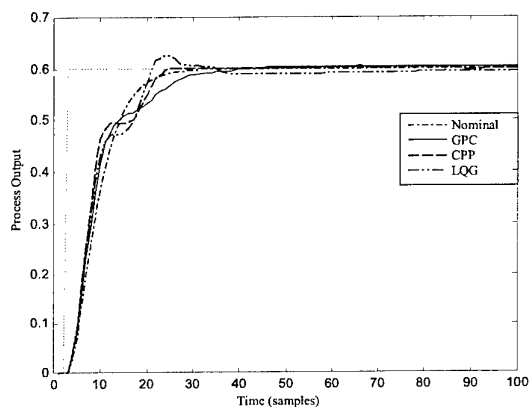


Figure 9: Performance of three controllers for small set-point change

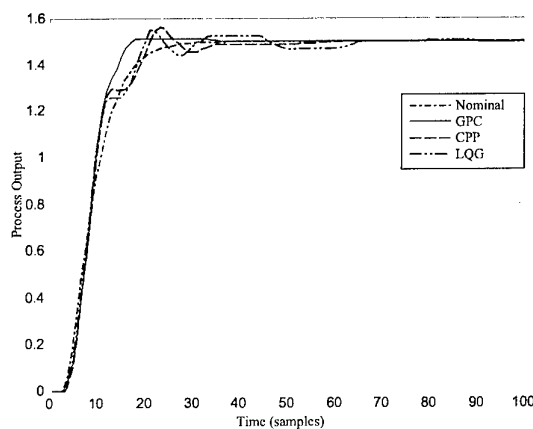


Figure 10: Performance of three controllers for large set-point change

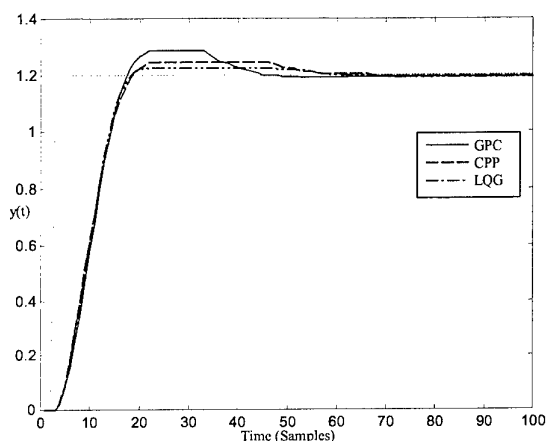


Figure 11: Real-time comparison of the three control laws for fully-loaded motor

6. DISTURBANCE COMPENSATION

The foregoing analysis has experimentally evaluated the servo performance of the three controllers in the presence of considerable model-mismatch and illustrated the robust performance of each of the designs. However, a contesting requirement is that of disturbance rejection, and the design of any servo-system requires that the controller effectively reject any disturbances that may result in the controlled variable deviating from the set-point. Thus the performance in the presence of two different types of disturbances is evaluated. Firstly a deterministic disturbance, in the form of a step load offset, was applied to the motor. As noted by Shinskey (1990) such load upsets are particularly demanding as they contain a wide spectrum of frequencies and demand a permanent shift in controller output. This disturbance was added to the process input and the combined signal then applied to the motor. The results are illustrated in figure 12.

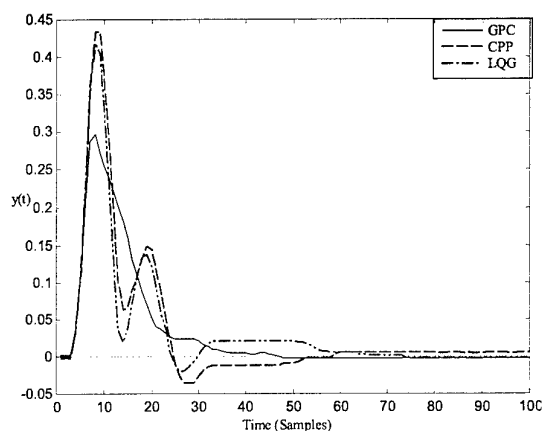


Figure 12: Deterministic disturbance rejection

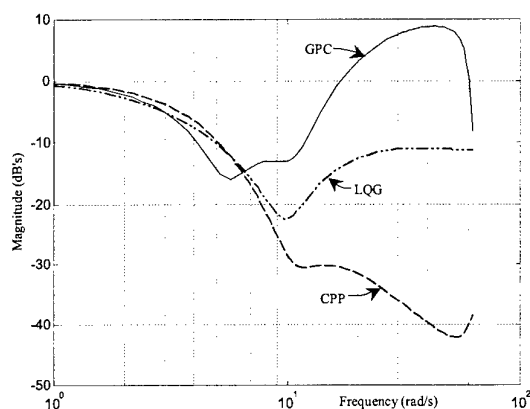


Figure 13: Input sensitivity function

In addition the effect of measurement noise was evaluated. Theoretically this may be accomplished by examining the *input sensitivity function* as illustrated in figure 13 for each of the designs. Most significantly the performance of the three controllers varies considerably in this regard. The chosen GPC design is clearly unsatisfactory with an input sensitivity function of almost +10dB's at high-frequencies. Thus while this controller is relatively robust to mis-modelling it is quite sensitive to the effects of high-frequency measurement noise. In contrast both the LQG and CPP controllers are suitably parameterised at high frequencies and should perform well in practice. This is verified by the results of figure 14 which illustrates the performance of each of the controllers in real-time. As indicated by figure 13 the CPP design is least sensitive and displays a smooth control signal while the performance of the LQG design is also acceptable.

7. CONCLUSION

In this paper three alternative 2-DOF control laws were designed and evaluated in real-time on a dc servo-motor system. It should be noted that though the GPC and LQG controllers have 2-DOF structures

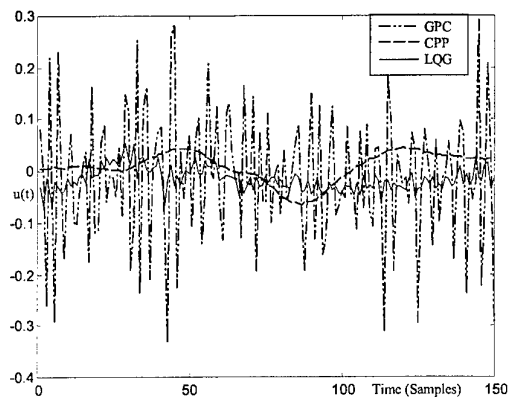


Figure 14: Control signal deviations in the presence of measurement noise

the servo and regulator dynamics cannot be independently designed. In the GPC case the servo parameters affect the regulator loop, though the regulator parameter, the T -polynomial, does not affect the nominal servo performance. Hence tuning begins by setting the servo parameters and subsequently the T -polynomial is designed to supply any additional robustness requirements. If the servo parameters are subsequently changed the regulator performance will be affected and might require the re-design of the T -polynomial. The situation is reversed for the LQG controller in that the regulator parameters affect the servo performance and consequently must be designed first. Subsequently the tracking controller is determined. As with the GPC if the regulator parameters are subsequently modified the tracking controller will need to be re-designed to maintain the desired closed-loop behaviour. Thus an advantage of the proposed CPP control law is that the tracking and regulatory controllers are completely independent and may be arbitrarily designed according to the requirement of each loop.

Furthermore since each loop is equipped with only a single tuning parameter the controller design is simple and may be easily adjusted for performance/robustness. This is not the case for the GPC where five parameters dictate the tracking performance and must be initialised *a-priori*. With the LQG controller the regulator loop requires that two transfer functions (four polynomials) be designed prior to implementation.

Considering the simplicity of the CPP structure, the performance achieved is rather unexpected. In terms of robust performance the controller performance equals that of the GPC or LQG controllers. The disturbance rejection capability is practically identical to that achieved by the LQG and in terms of the integral of absolute error (IAE) criterion, no worse than that achieved by the GPC. As indicated by figures 13 however, the GPC design utilised in

this application is very susceptible to the effects of high-frequency measurement noise and both the control signal and process output exhibit very large variance. The use of either the LQG or CPP controllers results in a significantly reduced process variance and both perform almost identically in this regard. However, the CPP controller results in a much smoother control signal and is consequently the controller of choice for this application.

8. REFERENCES

- Doyle, J.C., (1979), 'Robustness of multiloop linear feedback systems', *Proc. 17th IEEE Con. Decision & Control*, pp 12-18
- Grimble, M.J., (1994), *Robust Industrial Control: Optimal Design Approach for Polynomial Systems*, Prentice-Hall International, UK.
- Isermann, R., (1981), *Digital Control Systems*, Springer-Verlag Berlin, Heidelberg.
- Lambert, E.P., 1987, 'Process control applications of long-range prediction', *D. Phil. Thesis*, Oxford University
- Landau, I.D., R. Lozano & M. M'Saad, (1998), *Adaptive Control*, Springer-Verlag, London.
- Ljung, L., (1987), *System Identification*, Prentice-Hall, Inc., NJ
- McIntosh, A., S. Shah & D. Fisher, 1991, 'Analysis and tuning of adaptive generalised predictive control', *Canadian J. of Chem. Eng.*, Vol. 69, pp 97-110
- O'Mahony, T., & C.J. Downing, (2001), 'Robust design of the cancellation pole-placement controller', Submitted to *Irish Signals and Systems Conference 2001*, Maynooth, Ireland.
- O'Mahony, T., & C.J. Downing, (2000), 'Structurally Stable Synthesis of the Generalised Predictive Controller', *Proc. Irish Signals & Systems Conf*, NUI Galway, Galway, Ireland.
- Peterka, V., (1972), 'A steady-state minimum variance control strategy', *Kybernetika*.
- Shinskey, F.G., (1990), "How good are our controllers in absolute performance and robustness?", *Measurement & Control*, Vol. 23, pp 114 - 121
- Söeterboek, R., 1992, *Predictive Control: A unified approach*, Prentice-Hall
- Vilanova, R., & I. Serra, (1997), 'Realisation of two-degree-of-freedom compensators', *IEE Proc.-Control Theory Appl.*, Vol. 144, No. 6, pp. 589-595

On Horowitz's Contributions to Reset Control*

Yossi Chait and C.V. Hollot

College of Engineering
University of Massachusetts Amherst
Amherst, MA 01003

Abstract

History shows that Prof. Isaac Horowitz was often ahead of the curve in his feedback control research, especially in developing quantitatively-driven design procedures. In some topics, his work was so out of line with the main stream that it has received virtually no recognition from the control community until a few decades later. In this paper we present recent research that was directly motivated by Horowitz's pioneering work on reset controllers in the 1970's. Reset controllers are linear controllers that reset some of their states to zero when their inputs reach a threshold. Horowitz motivated their use by showing that with qualitative design, they can exhibit better performance tradeoffs than those in linear, time-invariant systems. This paper supports and advances his thinking by presenting recent theoretical and experimental results on reset control.

*This material is based upon work supported by the National Science Foundation under Grants No. CMS-9313764 and CMS-9800612 and by Philips Research Laboratories.

1 Introduction

It is well-appreciated that Bode's gain-phase relationship [1] places a hard limitation on performance tradeoffs in linear, time-invariant (LTI) feedback control systems. Specifically, the need to minimize the open-loop high-frequency gain often competes with required high levels of low-frequency loop gains and phase margin bounds. To illustrate this point, consider the standard linear feedback control system in Figure 1. The plant $P(s)$ represents the dynamics of a typical electro-mechanical system modeled as a double integrator for the rigid-body dynamics and a single resonance below 100 Hz to capture structural flexibility. The generic loop frequency response $|PC(j\omega)|$ is required to have sufficient bandwidth and large low-frequency gain for speedy response and positioning. Conversely, $|PC(j\omega)|$ needs to be small at high frequencies to suppress residual vibration. We plot $|PC(j\omega)|$ corresponding to a stable closed loop against these two specifications in Figure 1 to illustrate this tradeoff.

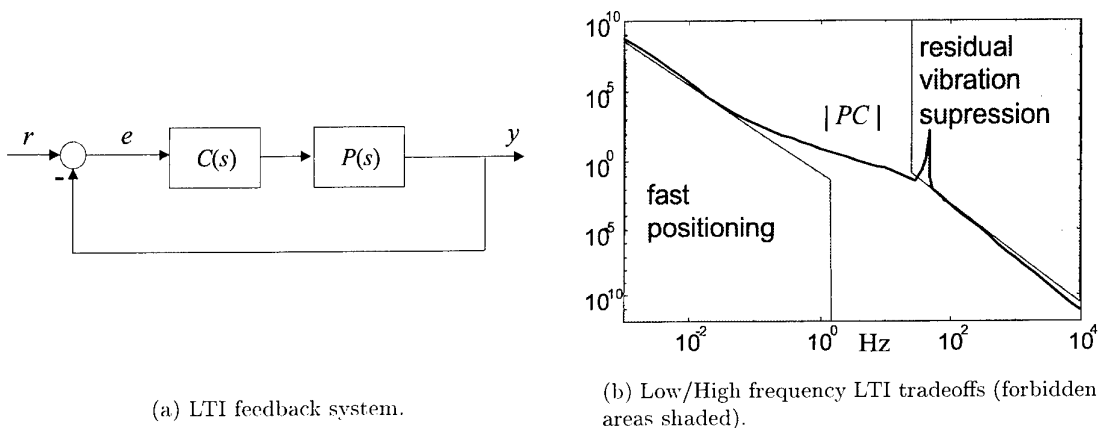


Figure 1: Tradeoffs in LTI systems.

This low/high frequency performance tradeoff is defined by Bode's gain-phase relation which limits how fast $|PC(j\omega)|$ can transition through unity-gain while maintaining closed-loop stability and adequate phase margins¹. In this context, to achieve additional residual vibration suppression, one needs to sacrifice bandwidth and positioning speed. Another factor which exacerbates this tradeoff is the non-collocation of actuators and sensors which, technically speaking, results in right-half plane zeroes in $P(s)$. The fact that one cannot reduce $|PC(j\omega)|$ infinitely fast beyond crossover implies that there exists a frequency range near this crossover where sensor noise is amplified. Horowitz termed this necessary evil as the "cost of feedback" [1].

The above inherent conflict in LTI control motivated researchers to consider, as early as the 1950's, classes of "hard" nonlinearities, including elements such as reset, limiter and saturation; e.g., see [2]-[10]. This paper focuses on the so-called class of reset controllers which are LTI systems with mechanism and law to reset some or all the controller states to zero. For example, the grand-daddy of reset controllers is the Clegg integrator which is a linear integrator whose output is reset to zero whenever its input crosses zero [3]. The describing function for this reset element has magnitude slope equivalent to that of a linear integrator, but with only 38.1° degrees of phase lag. This 51.9°

¹A typical loop gain slope at cross-over is at best -30 dB/dec in a minimum phase system.

degree improvement in phase lag over its linear counterpart suggests the possibility of a compensator supplying the required bandwidth with a much reduced gain at high frequencies. However, despite this favorable describing function, it was not until the work of [11] that a quantitative control design procedure was developed around Clegg integrator, and [12] further generalized the resetting concept to higher-order systems. In fact, the objective of this paper is to motivate Horowitz's contributions to reset control through recent theoretical, simulation and experimental work.

Reset control action resembles a number of popular nonlinear control strategies including relay control [13], sliding mode control [14] and switching control [15]. A common feature to these is the use of a switching surface to trigger change in control signal. Distinctively, reset control employs the same (linear) control law on both sides of the switching surface. Resetting occurs when the system trajectory impacts this surface. This reset action can be alternatively viewed as the injection of judiciously-timed, state-dependent impulses into an otherwise LTI feedback system. This analogy is evident in the paper where we use impulsive differential equations; e.g., see [16] and [17], to model dynamics. This connection to impulsive control helps to draw comparison to a body of control work [18] where impulses were introduced in an open-loop fashion to quash oscillations in vibratory systems. We also would like to point out other recent research and applications of reset control found in [19]-[21].

In terms of applications, the class of electro-mechanical systems is a natural fit for reset control. For example, a storage device's read/write head during seek mode slews to a specific track on the memory medium (magnetic or optical) to gather data. At high speeds, the head typically exhibits undesired mechanical vibrations at the end of a slewing movement. Even though the head may be nominally positioned over the desired track at this time, read/write cannot commence until this residual vibration sufficiently damps out. From a servo design viewpoint, settling time is the single most overriding factor limiting performance improvement in some storage devices. As it turns out, reduction of settling time involves a tradeoff; that is, the faster (larger control bandwidth) the read/write head slews towards its destination track, the more it vibrates when slewing stops. Unfortunately, LTI control is hamstrung by Bode's gain-phase relation to sufficiently improve this situation. This tradeoff phenomenon is not specific to the storage devices industry, but is endemic to a large class of electro-mechanical systems where high-performance is critical. It is our experimental experience with such systems that motivated us to explore control solutions outside the realm of LTI controllers.

The paper is organized as follows. The next section provides a conclusive example to demonstrate the advantage in using reset control. After that, Section 3 writes out the dynamical equations of reset control systems and in Section 4 we present recent theoretical results on this class of reset control systems. Finally, Section 5 describes Horowitz's design procedure for FORE reset systems followed by three applications.

2 Motivation: Overcoming Limitations of Linear Control [22]

In this section we give an example comparing reset to linear feedback control. In this example, control specifications are not achievable by any linear feedback control, but achievable using reset. Consider the standard linear feedback control system in Figure 1 where the plant $P(s)$ contains an integrator. Assume that $C(s)$ stabilizes. In [23] it was shown that the tracking error e due to a unit-step input satisfies

$$\int_0^\infty e(t)dt = \frac{1}{K_v}$$

where the velocity constant K_v is defined by $K_v \triangleq \lim_{s \rightarrow 0} sP(s)C(s)$. Alone, this constraint does not imply overshoot in the step response y ; i.e., $y(t) \geq 1$ for some $t > 0$. However, introduction of an additional, sufficiently stringent time-domain bandwidth constraint will. To see this, consider the notion of rise time t_r introduced in [23]:

$$t_r = \sup_T \left\{ T : y(t) \leq \frac{t}{T}, t \in [0, T] \right\}.$$

The following result (see [22]) is quite immediate.

Fact: If $t_r > \frac{2}{K_v}$; i.e., the rise time is sufficiently slow, then the unit-step response $y(t)$ overshoots.

To illustrate this result consider the plant $P(s)$ in Figure 1 as a simple integrator. In addition to closed-loop stability suppose the design objectives are the following:

- Steady-state error no greater than 1 when tracking a unit-ramp input.
- Rise time greater than 2 seconds when tracking a unit-step.
- No overshoot in the step response.

To meet the error specification on the ramp response, this linear feedback system must have velocity error constant $K_v \geq 1$. Since $t_r > 2 \geq \frac{2}{K_v}$, the above Fact indicates that no stabilizing $C(s)$ exists to meet all the above objectives. However, these specifications can be met using reset control with a first-order reset element (FORE) described by

$$\begin{aligned} \dot{u}_r(t) &= -bu_r(t) + e(t); & e(t) &\neq 0 \\ u_r(t^+) &= 0; & e(t) &= 0 \end{aligned}$$

where b , the FORE's pole, is chosen as $b = 1$. Indeed, it can be shown using results from Section 4 that that this reset system is asymptotically stable and has zero steady-state tracking error e to constant r . Figure 3 shows a simulation of this control system's tracking error e to a unit-ramp

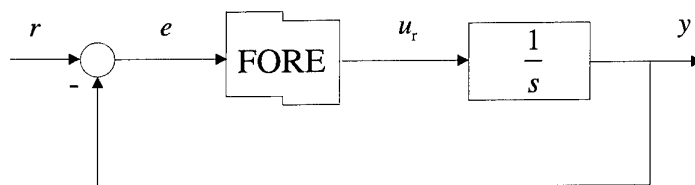
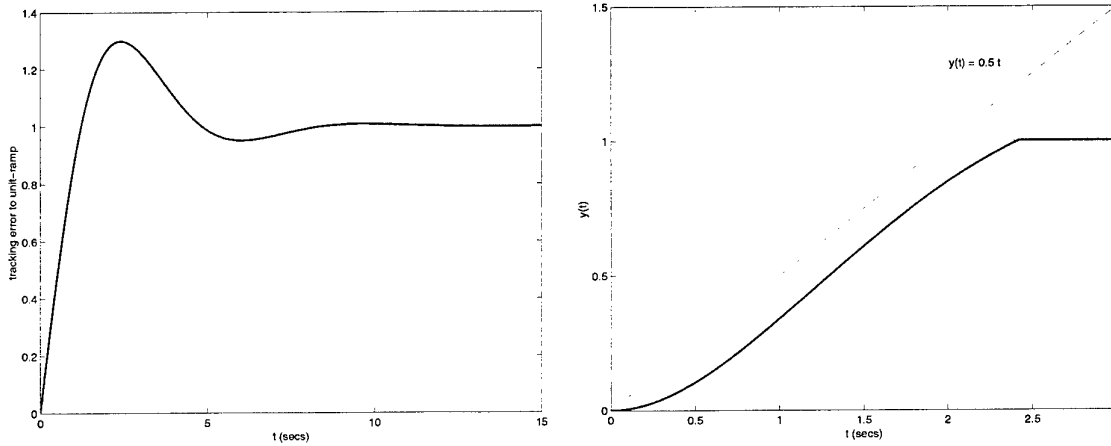


Figure 2: Reset control of an integrator using a first-order reset element.

input. The steady-state error is one. In Figure 3 we also show its response y to a unit-step input and see that its rise time t_r is greater than 2 seconds and has no overshoot². Thus, this reset control system meets the previously stated design objectives that were not attainable using linear feedback control.

²The step response in Figure 3 is deadbeat. This occurs since $(u, y) = (0, r)$ is an equilibrium point.



(a) Tracking-error e to a unit-ramp input r .

(b) Output response y to a unit-step input r .

Figure 3: Responses of the reset control system in Figure 2.

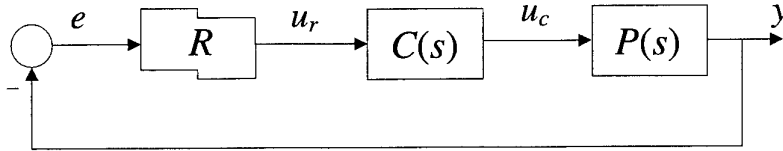


Figure 4: Block diagram of the reset control system.

3 The Dynamics of Reset Control Systems

The class of reset control systems considered in this paper is shown in Figure 4 where the reset controller R is described by the impulsive differential equation (IDE) (see [16])

$$\begin{aligned} \dot{x}_r(t) &= A_r x_r(t) + B_r e(t); & e(t) &\neq 0 \\ x_r(t^+) &= A_{Rr} x_r(t); & e(t) &= 0 \\ u_r(t) &= C_r x_r(t) \end{aligned} \quad (1)$$

where $x_r(t) \in \mathbf{R}^{n_r}$ is the reset controller state and $u_r(t) \in \mathbf{R}$ is its output. The matrix $A_{Rr} \in \mathbf{R}^{n_r \times n_r}$ identifies that subset of states x_r that are reset. For example, in this paper we will assume that the last n_{rr} states x_{rr} are reset and use the structure $A_{Rr} = \begin{bmatrix} I_{n_r - n_{rr}} & 0 \\ 0 & 0 \end{bmatrix}$.

Illustrations of (1) include the Clegg integrator [3] described by

$$A_r = 0; \quad B_r = 1; \quad C_r = 1; \quad A_{Rr} = 0$$

and the FORE [12] having

$$A_r = b; \quad B_r = 1; \quad C_r = 1; \quad A_{Rr} = 0. \quad (2)$$

The linear controller $C(s)$ and plant $P(s)$ have, respectively, state-space realizations:

$$\begin{aligned}\dot{x}_c(t) &= A_c x_c(t) + B_c u_r(t) \\ u_c(t) &= C_c x_c(t)\end{aligned}$$

and

$$\begin{aligned}\dot{x}_p(t) &= A_p x_p(t) + B_p u_c(t) \\ y(t) &= C_p x_p(t)\end{aligned}$$

where $x_c(t) \in \mathbf{R}^{n_c}$, $x_p(t) \in \mathbf{R}^{n_p}$ and $y(t) \in \mathbf{R}$. The closed-loop system can then be described by the IDE

$$\begin{aligned}\dot{x}(t) &= A_{cl}x(t); \quad x(t) \notin \mathcal{M}; \quad x(0) = x_0 \\ x(t^+) &= A_R x(t); \quad x(t) \in \mathcal{M} \\ y(t) &= C_{cl}x(t)\end{aligned}\tag{3}$$

where

$$x \triangleq \begin{bmatrix} x_p \\ x_c \\ x_r \end{bmatrix}; \quad A_{cl} \triangleq \begin{bmatrix} A_p & B_p C_c & 0 \\ 0 & A_c & B_c C_r \\ -B_r C_p & 0 & A_r \end{bmatrix}; \quad A_R \triangleq \begin{bmatrix} I_{n_p} & 0 & 0 \\ 0 & I_{n_c} & 0 \\ 0 & 0 & A_{Rr} \end{bmatrix}; \quad C_{cl} \triangleq \begin{bmatrix} C_p & 0 & 0 \end{bmatrix}$$

and where the *reset surface* \mathcal{M} is the set of states for which $e = 0$. More precisely,

$$\mathcal{M} \triangleq \{\xi : C_{cl}\xi = 0; \quad [0 \ 0 \ I_{n_{rr}}]\xi \neq 0\}.$$

As a consequence of this definition,

$$x(t) \in \mathcal{M} \Rightarrow x(t^+) \notin \mathcal{M}.$$

The times $t = t_i$ at which the system trajectory x intersects the reset surface \mathcal{M} are referred to as *reset times*. These instants depend on initial-conditions and are collected in the ordered set:

$$\mathcal{T}(x_o) \triangleq \{t_i : t_i < t_{i+1}; x(t_i) \in \mathcal{M}, i = 1, 2, \dots, \infty\}.$$

The solution to (3) is piecewise left-continuous on the intervals $(t_i, t_{i+1}]$. We define the *reset intervals* τ_i by

$$\begin{aligned}\tau_1 &\triangleq t_1; \\ \tau_{i+1} &\triangleq t_{i+1} - t_i, \quad i \in N.\end{aligned}$$

We make the following assumption on the set of reset times:

Resetting Assumption: *Given initial condition $x_0 \in \mathbf{R}^n$, the set of reset times $\mathcal{T}(x_o)$ is an unbounded, discrete subset of \mathbf{R}_+ .*

Unboundedness of the set of reset times implies continual resetting. If this condition is not satisfied, then, after the last reset instance, the reset control system behaves as its base-linear system. We avoid such trivial cases. Discreteness of $\mathcal{T}(x_o)$, together with this unboundedness, guarantees the existence and continuation of solutions to (3). Finally, in absence of resetting; i.e., $A_{Rr} = I$, the resulting linear system is called the *base-linear* system.

4 Theory [24]-[29]

An impediment to more widespread use and acceptance of reset control undoubtedly lies with the fact that such systems are nonlinear and nonsmooth and lack a specifically tailored theoretical framework to address stability and performance issues. The problem of analyzing closed-loop stability of feedback systems with reset controllers appears to be the main factor for their limited use in applications until recently. Moreover, even simple, low-order plants can be destabilized by a Clegg integrator, even though describing function analysis would predict otherwise. For example, the plant

$$CP(s) = \frac{(3+a)s+1}{s^2+3s-a}$$

is stabilizable by a linear integrator for all a , hence, describing function analysis would "predict" that the loop is stable when a Clegg integrator is introduced³. However, as our new stability results in [24] show, the Clegg system to be unstable if $|(5+2a)-2| > 1$ and stable otherwise. As a matter of fact, the system is unstable if $a = -6$ while describing function analysis inaccurately "predicts" stability.

Motivated by this situation, in this section we present a number of recent results that can be used to analyze stability, transient and asymptotic behaviour of reset control systems (proofs are omitted and can be found in the references).

4.1 Stability

First, we state some general Lyapunov-like stability conditions for our reset control systems which are similar to the analysis in [16] and [30].

Theorem 1: *Under the Resetting Assumption, the reset control system described in (3) is quadratically stable⁴ if and only if there exists a $\beta \in \mathbf{R}^{n_{rr}}$ such that*

$$H_\beta(s) \triangleq [\beta C_p \ 0 \ I_{n_{rr}}] (sI - A_{cl})^{-1} \begin{bmatrix} 0 \\ I_{n_{rr}} \end{bmatrix} \quad (4)$$

is strictly positive real (SPR)⁵.

Theorem 1 gives an easily-testable condition for the quadratic stability of the reset control systems described by (3). This condition is also key in showing that reset control systems enjoy other properties. Before we present these results, we formally introduce first-order reset elements. Consider the reset control system with a reference input as shown in Figure 5 and described by the following IDE

$$\begin{aligned} \dot{x}(t) &= A_{cl}x(t) + B_{cl}r(t); & x(t) \notin \mathcal{M}; & x(0) = 0, \\ x(t^+) &= A_R x(t); & x(t) \in \mathcal{M}, & \\ y(t) &= C_{cl}x(t) \end{aligned} \quad (5)$$

³The describing function of a Clegg integrator is $\frac{1.619}{j\omega} \exp^{-j38.15^\circ}$.

⁴See [29] for a definition of quadratic stability for this class of reset systems.

⁵A transfer function $X(s)$ is said to be *strictly positive real* if $X(s)$ is asymptotically stable, and $\text{Re}[X(j\omega)] > 0$, $\forall \omega \geq 0$.

where

$$B_{cl} = \begin{bmatrix} 0 \\ 1 \end{bmatrix}; \quad A_R = \begin{bmatrix} I & 0 \\ 0 & 0 \end{bmatrix}$$

and where

$$\mathcal{M} \triangleq \{\xi : r(t) - C_{cl}\xi = 0; \quad [0 \ 0 \ I_{n_{rr}}]\xi \neq 0\}.$$

Analyzing the BIBO stability of (5) requires every bounded input⁶ r to produce a bounded output

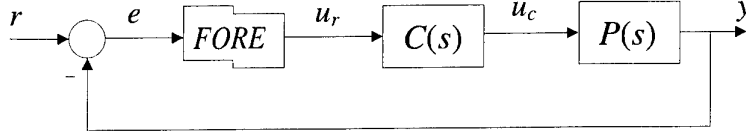


Figure 5: Block diagram of a FORE reset control system.

y . To begin this analysis we let x_ℓ be the state of the base-linear system; that is:

$$\dot{x}_\ell(t) = A_{cl}x_\ell(t) + B_{cl}r(t); \quad x(0) = 0$$

and take $z \triangleq x - x_\ell$. We partition

$$x = \begin{bmatrix} x_L \\ x_r \end{bmatrix}; \quad z = \begin{bmatrix} z_L \\ z_r \end{bmatrix}; \quad x_\ell = \begin{bmatrix} x_{\ell L} \\ x_{\ell r} \end{bmatrix}.$$

Applying the transformations:

$$\begin{aligned} z_L(t) &\triangleq x_L(t) - x_{\ell L}(t); \\ z_r(t) &\triangleq x_r(t) - x_{\ell r}(t) \end{aligned}$$

to (5) we obtain:

$$\begin{aligned} \dot{z}_p(t) &= Az_L(t) + Bz_r(t) \\ \dot{z}_f(t) &= -Cz_L(t) - bz_r(t); \quad t \notin \mathcal{T}(0) \\ z_r(t_i^+) &= -x_{\ell r}(t_i); \quad t \in \mathcal{T}(0). \end{aligned} \tag{6}$$

Before we present our next result we need to flesh out a hidden problem. Specifically, we need to rule out the possibility that the reset times τ_i converge to zero. This is still an open problem. However, in real time implementations, the sampling time establishes a lower limit on τ_i . With the standing assumption that there exists a lower bound σ such that $\tau_i \geq \sigma$, $\sigma > 0$, we can now state our BIBO stability result.

Theorem 2: *The reset control system (5) is BIBO stable if it is quadratically stable; i.e., there exists a β such that $H_\beta(s)$ in (4) is SPR.*

⁶A signal z is said to *bounded* if there exists a constant M such that $|z(t)| < M$ for all t .

4.2 Steady-State Performance

In this section we study the steady-state performance of the reset control system in (5) and show that it enjoys an internal model principle and steady-state superposition property. We introduce an *internal model principle* for the reset control systems by considering a model of the reference signal r inside the loop as part of $L(s) = P(s)C(s)$. We can state the following theorem.

Theorem 3: *Under the Resetting Assumption, if the loop $L(s)$ contains an internal model of r , and if there exists a β such that $H_\beta(s)$ in (4) is SPR, then the reset control system described in (5) achieves asymptotic tracking of the reference input r .*

We now introduce an additional input to the control system as shown in the Figure 6. This system can be described by

$$\begin{aligned} \dot{x}(t) &= A_{cl}x(t) + B_{cl}r_1(t) + B_{cl}r_2(t); & x(t) \notin \mathcal{M}; & x(0) = x_0 \\ x(t^+) &= A_R x(t); & x(t) \in \mathcal{M}, \\ y(t) &= C_{cl}x(t) \end{aligned} \quad (7)$$

where

$$\mathcal{M} \triangleq \{\xi : r_1(t) + r_2(t) - C_{cl}\xi = 0; [0 \ 0 \ I_{n_{rr}}]\xi \neq 0\}.$$

The next result gives a steady-state superposition result. If the loop $L(s)$ contains an internal model of one of the inputs signals, say r_2 , then this result claims that the steady-state response to $r_1 + r_2$ is simply the steady-state response to r_1 .

Corollary 4: *Consider the reset control system with two inputs r_1 and r_2 described in (7). Suppose the Resetting Assumption is in force, $L(s)$ contains an internal model of r_2 and there exists a β such that $H_\beta(s)$ is strictly positive real (SPR). Then, the steady-state error, $\lim_{t \rightarrow \infty} e(t)$ is independent of r_2 .*

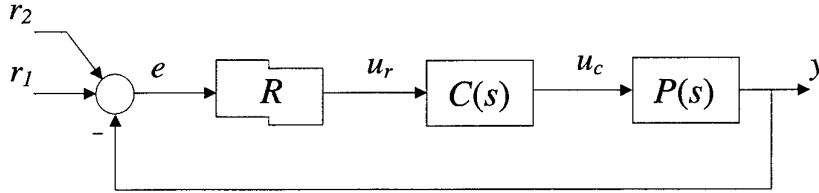


Figure 6: Block diagram of a reset control system with two inputs.

4.3 Transient Performance

In this section we analyze the reset control system (5) for a special class of second-order loops. We consider the case of $r(t) \equiv r_0$ and prove that the step-response maximum occurs during the time interval $(t_1, t_1 + \tau_0)$. The proof of the following can be found in [26].

Theorem 5: *Consider the reset control system described in (5) utilizing FORE with $PC(s) = \frac{(s+b)\omega_n^2}{s(s+2\zeta\omega_n)}$ and $r(t) \equiv r_0$. Let $M_r \triangleq \sup_{t>0} |y(t) - r_0|$ denote the step-response maximum. Then,*

$$M_r = \max_{t \in [t_1, t_1 + \tau_0]} |y(t) - r_0|.$$

From Theorem 5 the step response maximum M_r is equal to the peak response in the first reset interval $[t_1, t_1 + \tau_0)$. In [12], this overshoot value has been explicitly computed in terms of b, ζ , and ω_n as repeated below:

$$M_r = e^{-\frac{\pi\zeta}{\sqrt{1-\zeta^2}}} - \Delta$$

where

$$\Delta = \begin{cases} \frac{\alpha[4\beta^2\zeta^2e^{-\zeta\mu} - 2\zeta\beta(1-4\zeta^2\beta)e^{-\mu/\zeta\beta}]}{1-4\zeta^2\beta+4\zeta^2\beta^2}; & \zeta \geq 0.5 \\ \frac{\alpha[\beta^2e^{-\zeta\mu} - \beta(1-2\zeta\beta)e^{-\mu/\beta}]}{1-2\zeta\beta+\beta^2}; & \zeta \leq 0.5 \end{cases},$$

$$\alpha = e^{\frac{-\zeta}{\sqrt{1-\zeta^2}} \arccos \zeta}; \quad \beta = \frac{\omega_c}{b}; \quad \mu = \frac{\pi - \arccos \zeta}{\sqrt{1-\zeta^2}}$$

and where ω_c is the unity-gain crossover frequency of $|L(j\omega)|$.

Since the reset control system (5) behaves as a linear system before its first reset, then its rise time is that of its base-linear system ($\approx \frac{1.8}{\omega_n}$). The 2% settling time t_s can be computed using [26] adjacent intervals of y are shown to be scaled copies of each other. Indeed, using this, the settling time is computed as

$$t_s = \frac{k\pi}{\sqrt{1-\zeta^2}\omega_n}$$

where k is the smallest integer satisfying $|p_{11}(\tau_0)|^k M_r < 0.02$.

5 Experiments [27],[31],[32]

In this section we describe three applications of Horowitz's FORE controller, two experimental and one in simulation (complete details are shown only for the first). Before we proceed, let us review the unique design procedure developed in [11] and [12].

5.1 Horowitz's Design Procedure [11],[12]

Consider a reset system as shown in Figure 4. As mentioned in the introduction, the design of the reset controller proceeds in two steps and involves interplay between the design of the linear element C and the reset network FORE. The rationale introduced in [12] is to first design C so that the linear closed-loop response satisfies both the disturbance rejection and sensor-noise suppression specifications (at the expense of violating the gain/phase margin constraint). The next step involves choosing pole b in FORE to improve the overshoot response. [12] showed that resetting action reduces overshoot. Indeed, under a standard assumption of dominant second-order response, they related this overshoot to the crossover frequency ω_c ($|L(j\omega_c)| = 1$) and phase margin of the linear design and the pole of the reset element as shown in Figure 7. Finally, it is crucial to understand that performance does come with blind reset. In fact, doing so most likely will result in a worse performance than that of the underlying LTI system (see [32]).

It is important to note that the design procedures in [11] and [12] do not involve describing function analysis. They studied in detail the transient behavior of a feedback system with either Clegg or FORE reset element subjected to step inputs. By assuming second-order dominance, they computed the resulting overshoot (Figure 7) and discovered the possibility of increased undershoot

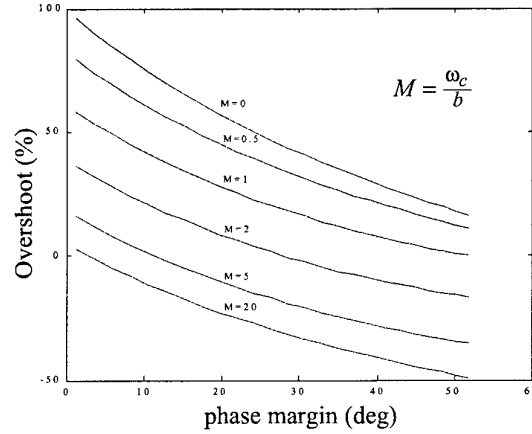


Figure 7: Reset control system for the flexible mechanism.

following the overshoot. The detailed and unique analysis in [12] of the nonlinear transient behavior which includes a departure from second-order dominance and noise response is a must read for its invaluable QFT-like design insight.

5.2 Flexible Mechanical System

The benefits of reset control have also been realized in experimental settings. Here we describe a laboratory setup in which we applied both linear and reset control to the speed control of the rotational flexible mechanical system shown in Figure 8. This system consists of three inertias connected via flexible shafts. A servo motor drives inertia J_3 and the speed of inertia J_1 is measured via a tachometer. The controller was implemented using dSPACE tools [33]. A more complete description of this experiment can be found in [27].

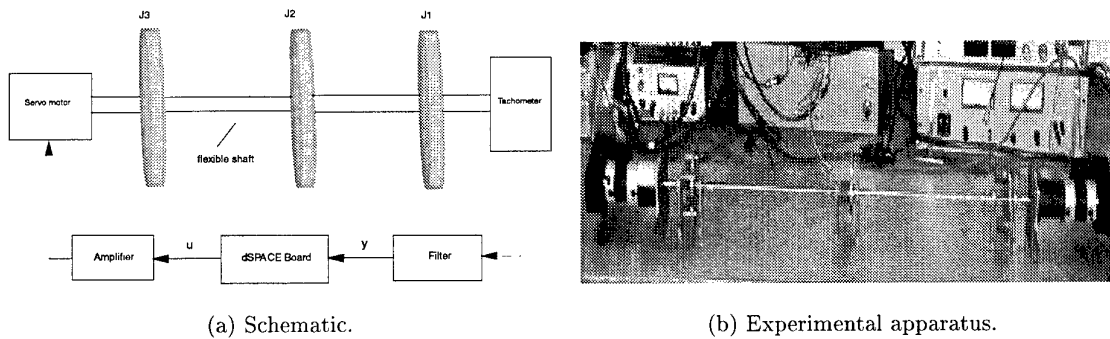


Figure 8: The experimental rotational flexible mechanical system.

A block diagram of a linear feedback control system is shown in Figure 9 where the plant $P(s)$ was identified from frequency-response data of the flexible mechanical system as:

$$P(s) = \frac{46083950}{(s + 1.524)(s^2 + 3.1s + 2820)(s^2 + 3.62s + 9846)}.$$

We posed the following specifications to illustrate the limitations and tradeoffs in LTI design and their subsequent relief using reset control:

1. *Bandwidth constraint:* The unity-gain cross-over frequency ω_c , defined by $|PC(j\omega_c)| = 1$, must satisfy $\omega_c > 3\pi$.
2. *Disturbance rejection:* Low-frequency disturbances are to be rejected; specifically,

$$\left| \frac{y(j\omega)}{d(j\omega)} \right| \leq 0.2, \quad \text{when } \omega \leq \pi;$$

3. *Sensor-noise suppression:* High-frequency sensor noise is to be suppressed; i.e.,

$$\left| \frac{y(j\omega)}{n(j\omega)} \right| \leq 0.3, \quad \text{when } \omega \geq 10\pi;$$

4. *Asymptotic performance:* Zero steady-state tracking error to constant reference r and disturbance d signals.
5. *Overshoot:* Overshoot in output y to a constant reference r should be less than 20%.

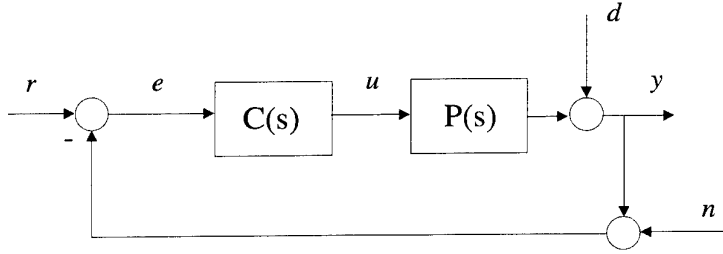


Figure 9: Block diagram of the linear control system.

The first two constraints translate into minimum-gain requirements on the open-loop gain $|PC(j\omega)|$ at low frequencies while the third specification places an upper bound on this gain at high frequencies. The fourth specification requires $C(s)$ to contain an integrator and the fifth specification requires a phase margin of approximately 45° assuming second-order dominance.

Using classical loop-shaping techniques we were unable to meet all of the above specifications. To illustrate this difficulty, consider two candidate, stabilizing LTI controllers:

$$C_1(s) = \frac{1281489(s + 4.483)(s^2 + 3.735s + 2851)(s^2 + 5.158s + 10060)}{s(s^2 + 295.1s + 22330)(s^2 + 126.2s + 8889)(s^2 + 239s + 27560)}$$

and

$$C_2(s) = \frac{1075460(s + 7)(s^2 + 3.662s + 2798)(s^2 + 5.419s + 9876)}{s(s + 209.6)(s + 35.8)(s^2 + 132.8s + 12050)(s^2 + 375.9s + 66930)}.$$

Figure 10 compares the Bode plots of the corresponding loops $L_1(j\omega) = C_1(j\omega)P(j\omega)$ and $L_2(j\omega) = C_2(j\omega)P(j\omega)$. Loop L_1 fails to satisfy the sensor-noise suppression specification at $\omega = 10\pi$. This specification can be met by reducing the gain of $L_1(j\omega)$ as done with $L_2(j\omega)$. This is verified by the

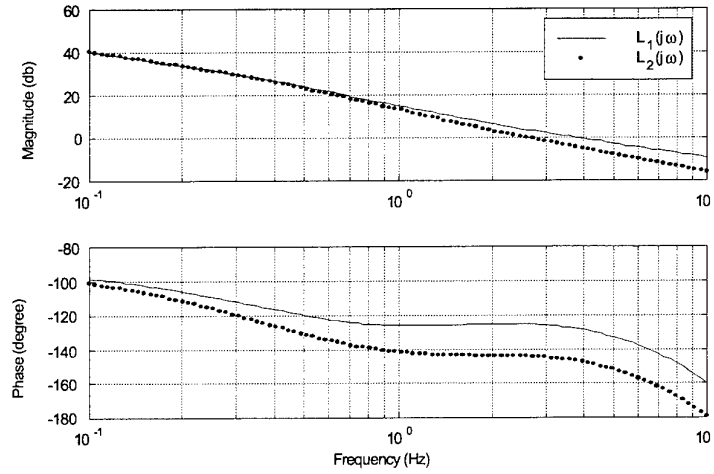
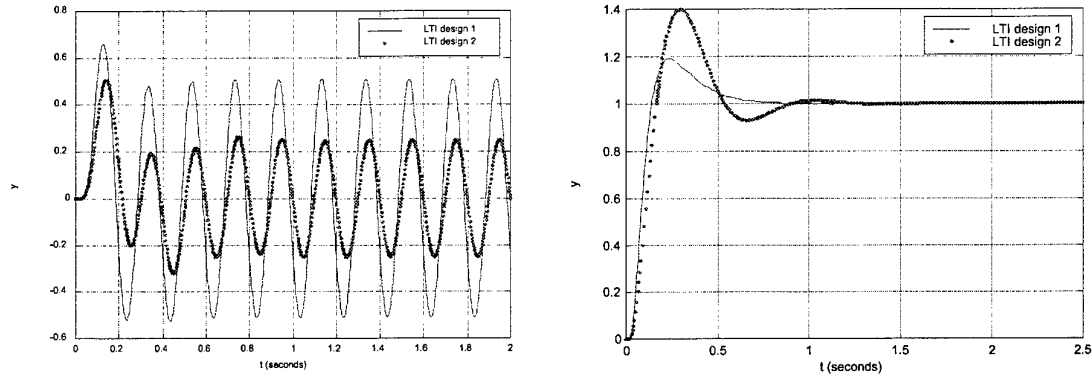


Figure 10: Bode plots of L_1 and L_2 .

time response y to 5 Hz sinusoidal noise n in Figure 11. Since both designs stabilize and since both low-frequency gains are constrained by the first two specifications, Bode's gain-phase relationship [1] dictates that $L_2(j\omega)$ must have correspondingly larger phase lag as verified in the phase plot of Figure 10. The reduced gain in $L_2(j\omega)$ comes at the expense of a smaller phase margin and hence larger overshoot as shown in the step responses in Figure 11. Extensive tuning of these controllers failed to yield a design meeting all specifications.



(a) Simulated output y to $n(t) = \sin(10\pi t)$.

(b) Simulated output y to $r(t) = 1$.

Figure 11: Comparison between LTI designs L_1 and L_2 .

Now we turn to reset control design where we exploit its potential to satisfy the above specifications. The design procedure consists of two steps as developed in [11] and [12]. First, we design a linear controller to meet all the specifications - except for the overshoot constraint; $C_2(s)$ is a suitable choice. The second step is to select the FORE's pole b to meet the overshoot specification. In this respect, Figure 7 provides a guideline for this choice and we selected $b = 14$. The resulting reset control system is shown in Figure 12. Note that the H_β theorem (Theorem 1), developed as

an analysis tool. can be use to modify the loop response at the frequency range where the SPR condition is violated. In this application, however, the results in Section 4 show that this reset control system is quadratically stable and asymptotically tracks constant reference inputs r .

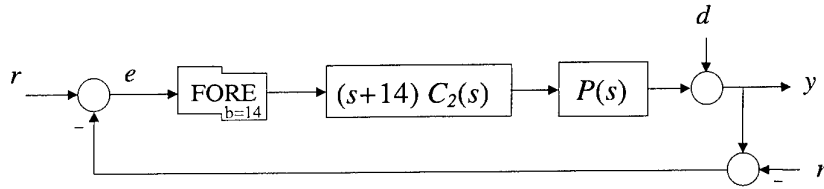


Figure 12: Reset control system for the flexible mechanism.

We also compare the performance of the LTI (using L_1) and reset control systems. Figure 13 shows that the reset control system has better sensor-noise suppression to a 5 Hz sinusoid which does not come at the expense of a worse transient response (as seen in the LTI tradeoff experienced by controller $C_2(s)$). The reset control system has comparable transient response as shown in Figure 13⁷.

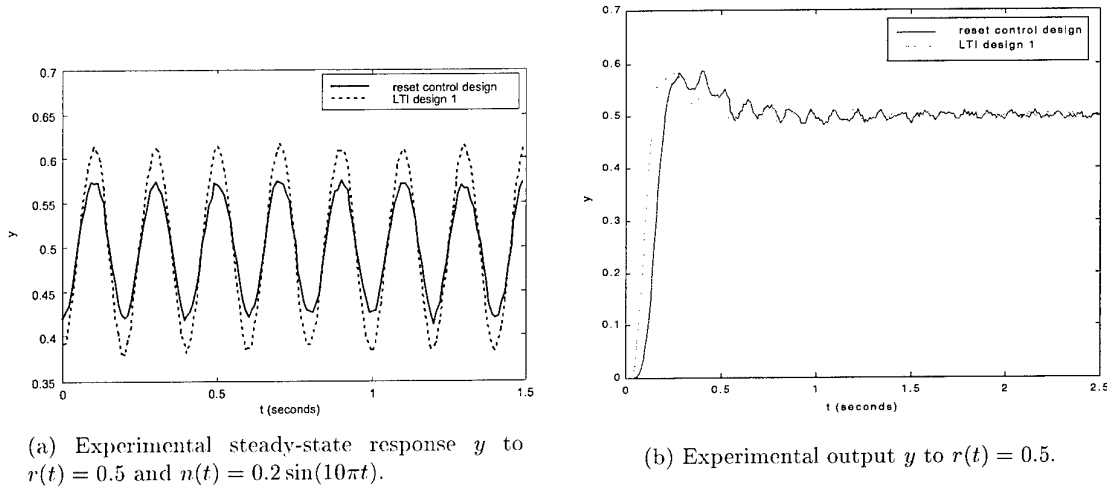


Figure 13: Comparison of reset and LTI performance.

Finally, we compare the performance of the LTI (using L_1) and reset control systems to white-noise (Figure 14).

5.3 Tape Backup

This feedback control design problem involves disturbance attenuation and sensor-noise suppression for a tape-speed control system. There are several subsystems in a tape-transport system such as the tape-speed and the tape-tension control subsystems. We focus on the tape-speed control subsystem consisting of a motor and belt-driven capstan wheel as shown in Figure 15. The capstan's friction force pulls the tape past the read/write head and a frequency-to-voltage converter measures the

⁷The small steady-state oscillation is due to ripple in the the tach-generator.

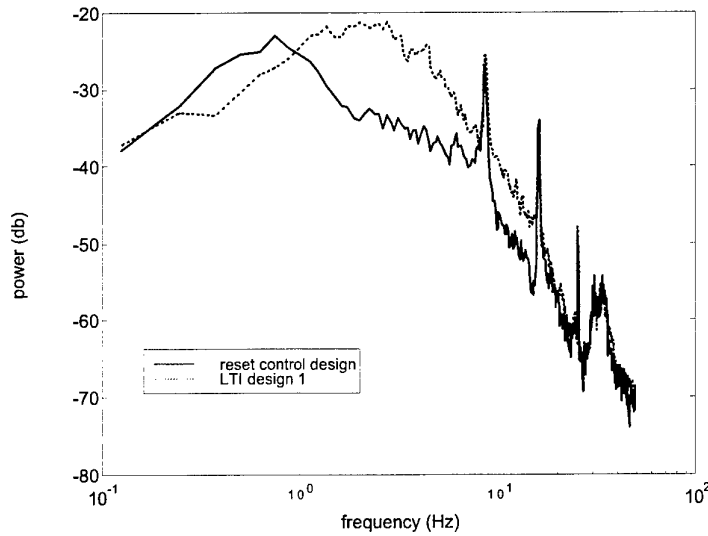
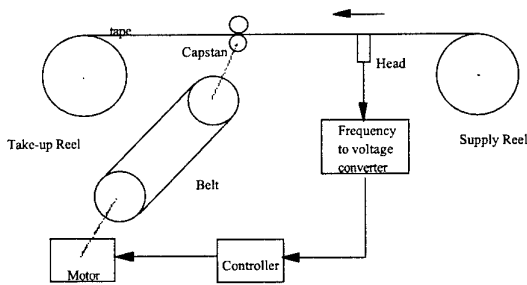
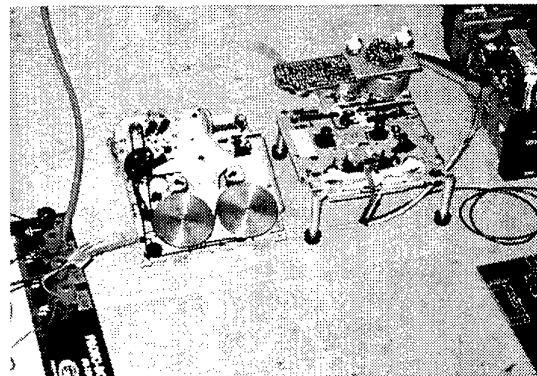


Figure 14: Comparison of output y power spectra when n is white sensor noise.

tape-speed error relative to a 3.15 kHz master-tape speed. This tape-speed error signal is then fed back to the controller. Unlike conventional tape devices that use motor current as a measure of tape speed, this scheme measures tape-speed errors directly, thus providing a more accurate measurement of the physical variable to be controlled. In this context, P represents the dynamics from the motor voltage u (volts) to the tape speed error y (volts) as measured by the frequency to voltage converter, d is the lumped disturbance accounting for eccentricities and mechanical load variations and n models sensor noise. Eccentricities produce periodic disturbances related to the rotational speed of various mechanical parts such as reels, capstan, etc', while mechanical load variations are modeled by a broadband disturbance signal.



(a) Schematic.



(b) Apparatus.

Figure 15: The tape backup system.

The controllers were digitally implemented on a TMS320C30 DSP system (32-bit floating point,

33 MHz 16-bit, volts dynamics range A/D and D/A channels) using a 1 kHz sampling rate. The controller integrator was implemented using an analog operational amplifier since it had a larger dynamic range than possible in this digital implementation.

To simulate the step disturbance d and sensor noise n , a square-wave (with four-second period) and 10 Hz sinusoid, respectively, is introduced at the output of the frequency-to-voltage converter (see Figure 15). The response to this excitation was measured for both the linear and reset controllers. The experimental results are shown in Figure 16. They show that both systems have similar disturbance rejection and transient behavior. Reset control improves sensor-noise suppression by 4 – 5 dB. Finally, the tape-speed servo was excited with filtered white noise n (50 Hz bandwidth) and measured the averaged voltage spectra of the frequency-to-voltage converter output for both the linear and reset control systems. The results, plotted in Figure 16, show that reset control provides an improvement in broadband sensor-noise suppression of 4 – 6 dB over the 3 – 10 Hz frequency range

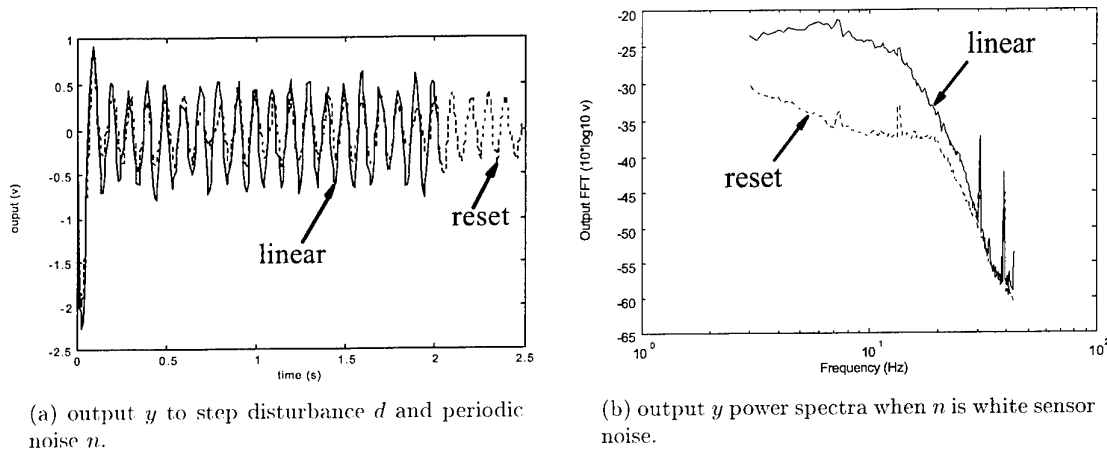


Figure 16: Comparison of reset and linear responses.

A more complete description of this experiment can be found in [31] and [32]. It is interesting to note the slight difference between the original FORE block diagram in [12] and the one used in these (e.g., Figure 12) experiments. [31] suggested that since between reset instances FORE behaves like the LTI $\frac{1}{s+b}$, then the controller $C(s)$ be augmented with the zero $s+b$. This innovation completely decouples the two design steps in [12]. Indeed, all the FORE implementations discussed in this Section use this idea.

5.4 Wafer Stage

From a control design view point, a semiconductor wafer stage exhibits similar difficulties seen in data-storage devices as described earlier. The schematic shown in Figure 17 is a prototype wafer stage experimental setup consisting of an airfoot (to minimize friction), a translator and a chuck (please refer to [35] and [36] for more details).

Three-dimensional position control is achieved by linear motors and a laser interferometer provides position information with a resolution of 13 nanometer (nm). The performance objective is to precisely and quickly position the semiconductor wafer stage. Once positioned, the masked wafer is exposed to light as part of the photo-lithography process in semiconductor manufacture.

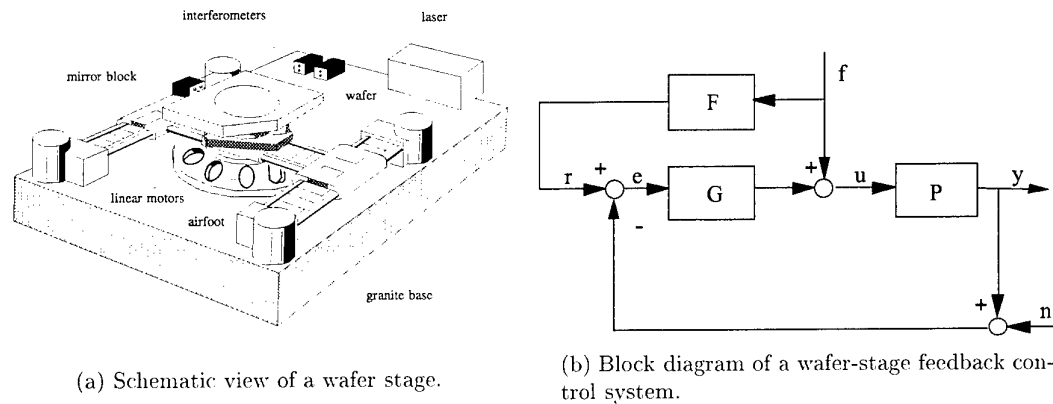


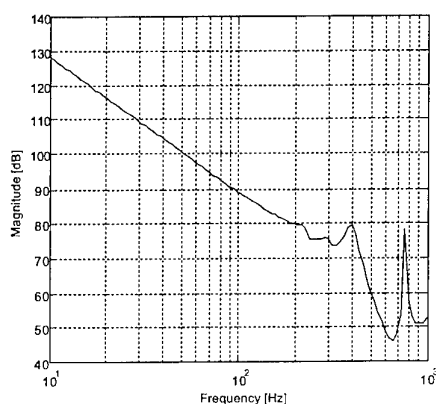
Figure 17: A wafer stage.

A typical process involves moving the stage through 20 positions each 10 mm apart. Due to the fine features of the laser-generated mask, position accuracies of 50 nm (50×10^{-9} m) are required. Since this mechanical positioning system is inherently flexible, there exists a tradeoff between the speed at which the wafer stage is translated and the resulting residual vibration. To illustrate, consider the block diagram of a wafer-stage feedback control system in Figure 17 where P denotes a single-axis of wafer-stage dynamics relating input force u to wafer stage position y . F and G respectively denote feedforward and feedback compensators and e the tracking error. The control objective is to minimize the time for a 10 mm point-to-point repositioning of y .

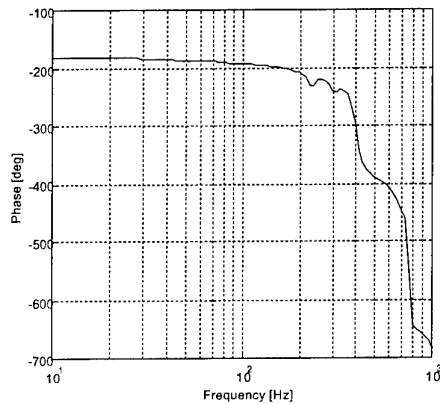
An experimental set-up of this wafer stage is described in [35]. They identified a 16th-order model of a non-minimum phase P which is described by the frequency response in Figure 18. The key specification is the tracking error e settling time of 50 nm. The control design consists of designing the command signal f as well as the compensators G and F . To briefly illustrate achievable performance, consider the design of [35] where f is the classic bang-bang command signal.

Alternative command signals f have been suggested (e.g., [37]-[40]) to minimize this residual vibration. Some techniques simply minimize the high-frequency content of the command signal while more sophisticated techniques minimize the frequency content of the command signal at the plant's resonances. Such techniques can significantly improve performance. For example, [35] designed a so-called "limited jerk" command signal which reduced the 50 nm settling time. However, while careful design of command signals can suppress residual vibration, its success depends on accurate knowledge of the plant's resonances. In addition, attenuation of the command signal's spectrum necessarily reduces the input energy thereby slowing setpoint response. This leads to the question of whether the feedback compensator G can be redesigned to improve settling time. From control design viewpoint, a high-bandwidth feedback loop is needed for small rise time and fast settling time. However, a high-bandwidth loop also amplifies those plant resonances near crossover, thus contributing to residual vibration. Hence, speed and suppression of residual vibration are conflicting objectives for feedback of such systems as concluded in [35]. Despite this seemingly negative scenario, one can dramatically reduce settling time through the novel use of so-called reset control.

A comparison of the residual tracking errors between the linear and reset controllers with bang-bang command is shown in Figure 19. The settling times are 0.158 sec and 0.140 sec, respectively,



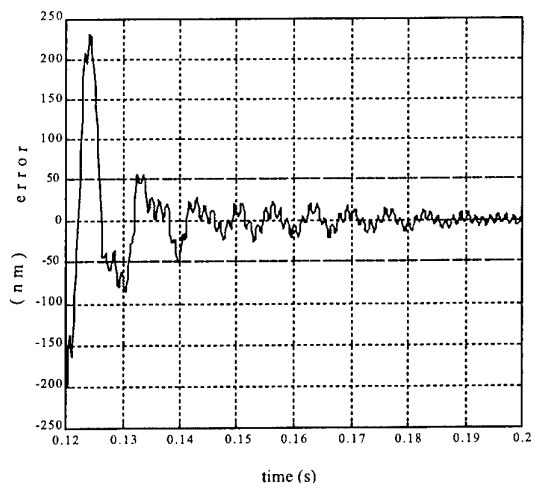
(a) Magnitude.



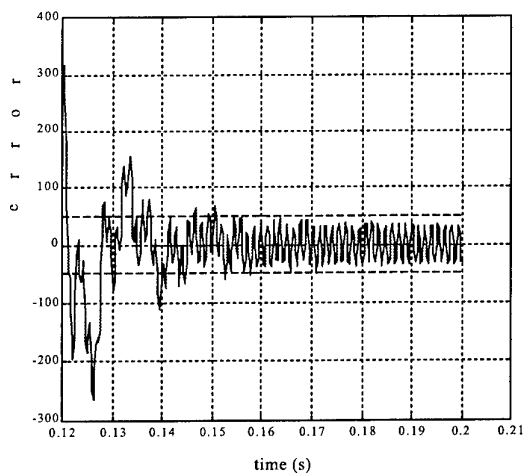
(b) Phase.

Figure 18: Frequency response of the wafer stage in the x-direction.

showing an improvement due to the reset action. Moreover, reset action reduced the steady-state amplitude of the residual vibration by factors of 3 and 1.5 for bang-bang. This property can be an important factor in future control of wafer stages since increased positional accuracy will be needed to keep pace with shrinking semiconductor circuit dimensions.



(a) reset control.



(b) LTI control.

Figure 19: Comparison of stage tracking errors for bang-bang command.

6 Conclusions

This paper described recent theoretical and experimental work in the area of reset control systems what was motivated by Prof. Horowitz's pioneering work. The experimental work directly borrowed from his quantitative design procedure, and the theory evolved around his unique FORE element. It appears to the authors that reset control is an important class of controllers that calls for further research and more experimentation by control engineers.

Acknowledgment

This work is a result of fruitful collaboration with our past and present graduate students Orhan Beker, Qian Chen, Hanzhong Hu and Yuan Zheng.

References

- [1] Horowitz, I.M., *Synthesis of Feedback Systems*, Academic Press, New York, 1963.
- [2] Lewis, J.B., "The Use of Nonlinear Feedback to Improve the Transient Response of a Servomechanism," *Trans. AIEE*, Vol. 71(II), pp. 449-453, 1953.
- [3] Clegg, J.C., "A Nonlinear Integrator for Servomechanism," *AIEE Transactions Part II, Application and Industry*, Vol. 77, pp. 41-42, 1958.
- [4] Bailey, A.R., "Stabilization of Control Systems by the Use of Driven Limiters," *Procs. IEE*, Vol. 113(1), pp. 169-174, 1966.
- [5] Foster, W.C., Giesecking, D.L., and Waymayer, W.K., "A Nonlinear Filter for Independent Gain and Phase (With Applications)," *Trans. ASME J. Basic Engineering*, Vol. 88, pp. 457-462, 1966.
- [6] Balasubramanian, R., Atherton, D.P., "Performance of Feedback Systems with Nonlinear Phase-Advance Compensators to Gaussian Inputs," *Electronic Letters*, Vol. 3(12), pp. 563-565, 1967.
- [7] Gelb, A., and Vander Velde, W.E., *Multiple-Input Describing Functions and Nonlinear System Design*, McGraw-Hill Book Co., New York, 1968.
- [8] Zoss, L.M., Witte, A.G., and Marsch, J.E., "A Nonlinear Three Response Controller With Two Response Adjustment," *Procs. Advances in Instrumentation*, Vol. 23, pp. 1-6, 1968.
- [9] Atherton, D.P., *Nonlinear Control Systems*, Van Nostrand Reinhold Co., London, 1975.
- [10] Karybakas, C.A., "Nonlinear Integrator with Zero Phase Shift," *IEEE Trans. Industrial Electronics Control Instrumentation*, Vol. IECI-24(2), pp. 150-152, 1977.
- [11] Krishnan, K.R., and Horowitz, I.M., "Synthesis of a Nonlinear Feedback System with Significant Plant-Ignorance for Prescribed System Tolerance," *International Journal of Control*, Vol. 19, pp. 689-706, 1974.

- [12] Horowitz, I.M., and Rosenbaum, P., "Nonlinear Design for Cost of Feedback Reduction in Systems with Large Parameter Uncertainty," *International Journal of Control*, Vol. 24, No. 6, pp. 977-1001, 1975.
- [13] Tsypkin, Y.Z., *Relay Control Systems*, Cambridge University Press, Cambridge, UK, 1984.
- [14] Decarlo, R.A., "Variable Structure Control of Nonlinear Multivariable Systems: A Tutorial," *IEEE Proceedings*, Vol. 76, No. 3, pp. 212-232, 1988.
- [15] Branicky, M.S., "Multiple Lyapunov Functions and Other Analysis Tools for Switched and Hybrid Systems," *IEEE Transactions on Automatic Control*, Vol. 43, pp. 475-482, 1998.
- [16] Bainov, D.D., and Simconov, P.S., *Systems with Impulse Effect: Stability, Theory and Application*, Halsted Press, New York, 1989.
- [17] Haddad, W.M., Chellaboina, V., and Kablar, N.A., "Nonlinear Impulsive Dynamical Systems Part I: Stability and Dissipativity," *Proceedings of Conference on Decision and Control*, Phoenix, AZ, pp. 4404-4422, 1999.
- [18] Singer, N.C., and Seering, W.P., "Preshaping Command Inputs to Reduce System Vibration," *Transactions of the ASME*, Vol. 76, No. 3, pp. 76-82, 1990.
- [19] Bobrow, J.E., Jabbari, F., and Thai, K., "An Active Truss Element and Control Law for Vibration Suppression," *Smart Materials and Structures*, Vol. 4, pp. 264-269, 1995.
- [20] Bupp, R.T., Bernstein, D.S., Chellaboina, V., and Haddad, W.M., "Resetting Virtual Absorbers for Vibration Control," *Proceedings of the American Control Conference*, Albuquerque, NM, pp. 2647-2651, 1997.
- [21] Haddad, W.M., Chellaboina, V., and Kablar, N.A., "Active Control of Combustion Instabilities via Hybrid Resetting Controllers," *Proceedings of the American Control Conference*, Chicago, IL, pp. 2378-2382, 2000.
- [22] Beker, O., Hollot, C.V., and Chait, Y., "Plant with Integrator: An Example of Reset Control Overcoming Limitations of Linear Feedback," ECE Department Technical Note ECE07.13.2000, University of Massachusetts Amherst; also *IEEE Transactions on Automatic Control*, 2000, to appear.
- [23] Middleton, R.H., "Trade-offs in Linear Control System Design," *Automatica*, Vol. 27, no. 2, pp. 281-292, 1991.
- [24] Hu, H., Zheng, Y., Chait, Y., and Hollot, C.V., "On the Zero-Input Stability of Control Systems Having Clegg Integrators," *Proceedings of the American Control Conference*, Albuquerque, NM, pp. 408-410, 1997.
- [25] Beker, O., Hollot, C.V., Chen, Q., and Chait, Y., "Stability of A Reset Control System Under Constant Inputs," *Proceedings of the American Control Conference*, San Diego, CA, pp. 3044-3045, 1999.
- [26] Chen, Q., Hollot, C.V., Chait, Y., and Beker, O., "On Reset Control Systems with Second-Order Plants," *Proceedings of the American Control Conference*, Chicago, IL, pp. 205-209, 2000.

- [27] Chen, Q., *Reset Control Systems: Stability, Performance and Application*, Ph.D. Dissertation, University of Massachusetts, Amherst, 2000.
- [28] Chen, Q., Hollot, C.V., and Chait, Y., "BIBO Stability of a Class of Reset Control Systems," *Proceedings of the 2000 Conference on Information Sciences and Systems*, Princeton, NJ, TP8-39, 2000.
- [29] Hollot, C.V., Beker, O., Chait, Y., and Chen, Q., "On Establishing Classic Performance Measures for Reset Control Systems, in *Proceedings of the Robust Control Workshop 2000*, Newcastle, December, 2000.
- [30] Ye, H., Michel, A.N., and Hou, L., "Stability Analysis of Systems with Impulse Effects," *IEEE Transactions on Automatic Control*, Vol. 43, No. 12, pp. 1719-1723, 1998.
- [31] Zheng, Y., *Theory and Practical Considerations in Reset Control Design*, Ph.D. Dissertation, University of Massachusetts, Amherst, 1998.
- [32] Zheng, Y., Chait, Y., Hollot, C.V., Steinbuch, M., and Norg, M., "Experimental Demonstration of Reset Control Design," *IFAC Journal of Control Engineering Practice*, Vol. 8, No. 2, pp. 113-120, 2000.
- [33] dSPACE Experiment Guide, dSPACE Inc., Paderborn, Germany, 1999.
- [34] Slotine, J.E., and Li, W., *Applied Nonlinear Control*, Prentice-Hall Inc., New Jersey, 1991.
- [35] de Roover, D., and Sperling, F.B., "Point-to-Point Control of High Accuracy Positioning Mechanism," *Procs. ACC*, pp. 1350-1354, 1997.
- [36] de Roover, D., *Motion Control of a Wafer Stage*, Ph.D. Dissertation, Delft University of Technology, The Netherlands, 1997.
- [37] Meckl, P.H., and Seering, "Controlling Velocity-Limited Systems to Reduce Residual Vibration," *Procs. IEEE Int. Conf. Robotics & Automation*, Philadelphia, pp. 1428-1433, 1988.
- [38] Bhat, S.P., and Miu, D.K., "Experiments on Point-to-Point Positioning Control of Flexible Beams Using Laplace Transform Technique- Part II: Closed-Loop," *ASME J. Dynamics Systems, Measurements, and Control*, Vol. 113, pp. 438-443, 1990.
- [39] Singer, N.C., and Seering, W.P., "Preshaping Command Inputs to Reduce System Vibration," *ASME J. Dynamics Systems, Measurements, and Control*, Vol. 112, pp. 76-82, 1990.
- [40] Meckl, P.H., and Kineeler, R., "Robust Motion Control of Flexible Systems using Feedforward Forcing Functions," *IEEE Trans. Control Systems Technology*, Vol. 2(3), pp. 245-254, 1994.

QFT CONTROLLER SYNTHESIS USING EVOLUTIVE STRATEGIES

C. Raimúndez, A. Baños, A. Barreiro

Universidad de Vigo and Universidad de Murcia, Spain

e-mail: [cesareo,abarreiro]@uvigo.es, abanos@dif.um.es

Abstract: Evolution Strategies (ES) are stochastic optimization techniques obeying an evolutionist paradigm, that can be used to find global optima over a response hypersurface. The current investigation focuses on robust controller synthesis under QFT methodology, using the unsupervised learning capabilities of ES's issued from their evolutionist paradigm. ES has proven efficiency over high dimensional search spaces. QFT synthesis can be considered as a low dimension problem but highly non linear due mainly to the boundaries and Hurwitz conditions for the closed loop transfer function. In [4] following also the evolutionist paradigm (Genetic Algorithms), a loop-shaping proposal can be found.

Keywords: Evolution Strategies, QFT synthesis, QFT loop-shaping

1 INTRODUCTION

One of the most important steps in QFT synthesis is loop shaping of the open loop transfer function, in order to satisfy specifications given as boundaries. This step has been usually done manually by trial and error, and obviously a good design is strongly based on the experience of the designer. Although loop shaping can be clearly alleviated by the use of efficient CAD programs, including the popular Matlab QFT Toolbox [2], there is a need for developing methods for automatic loop shaping, overall in those problems where a high order controller is necessary, being this an important open problem.

It is well known that optimal loop shaping is a hard nonlinear optimization problem, and although there is a number of theoretical results that may be found useful [6, 1] as well as nonlinear programming [12] and convex optimization techniques [3], an efficient (non-conservative) and complete solution to the problem has not yet been found. Recently, as an alternative to these optimization techniques, Chen and Ballance [4] have applied genetic algorithms (GA's) to this problem. Comparison with the Evolutionary Strategies (ES's) approach can be done observing that in GA's the search space is a chromosomal length consequence, and for a many scaled parameterization problem (polynomial coefficients), the *a priori* chromosomal codification can insert unnecessary non linearities and limitations in the search space. The ES's has a native multiscaled behaviour and has good hill-climb properties. Also the ES's *know* the search space dimension while the GA's does not (chromosomal codification destroys that nice information).

In this work, evolution strategies are used to find an optimal loop shaping, using algorithms developed previously by the first author [9]. This technique has also been used for approaching other difficult optimization problems, e. g. Hamiltonian controller synthesis [10]

The ES's developed application can be used for building con-

trollers with numerator and denominator given degrees. Can also be used to improve previous hand made controllers. The process can be started from scratch or from a previous seed found through an interpolation procedure. That interpolating facility can be used when we know by heart the closed loop possible shape. Points are given interactively at the boundary frequencies and the facility gives as result the best Hurwitz interpolating pair $\{G_c(\pi, s), G_p(s)\}$ where $G_c(\pi, s)$ is the controller configured by the π parameters, and $G_p(s)$ is the nominal plant. This result can be used as a seed in an ES's global searching procedure. The examples presented in this paper were all obtained directly from scratch.

2 PRELIMINARIES

Simulated Evolution is based on the collective learning processes within a population of individuals, in the quest for survival [7]. Each individual represents a search point in the space of potential solutions to a given problem.

There are currently three main lines of research strongly related but independently developed in simulated evolution : Genetic Algorithms (GA), Evolution Strategies (ES), and Evolutionary Programming (EP). In each of these methods, the population of individuals is arbitrarily initialized and evolves towards better regions of the search space by means of a stochastic process of selection, mutation, and recombination if appropriate.

These methods differ in the specific representation, mutation operators and selection procedures. While genetic algorithms emphasize chromosomal operators based on observed genetic mechanisms (e.g., cross-over and bit mutation), evolution strategies and evolutionary programming emphasize the adaptation and diversity of behavior from parent to offspring over successive generations.

Evolution is the result of interplay between the creation of new

genetic information and its evaluation and selection. A single individual of a population is affected by other individuals of the population as well as by the environment. The better an individual performs under these conditions the greater is the chance for the individual to survive for a longer while and generate offsprings, which inherit the parental genetic information.

The main contributions in the evolutionary computation approach are:

- Model regularity independence.
- Parallelization to cope with intensive cost fitness computation.
- Population search \times individual search (classical).
- General meta-heuristics.
- Good convergence properties.

Evolution strategies lead to algorithms that reproduce the process of neo-Darwinian organic evolution. The reader is directed to [7] for a general survey and [9] for applications in control. The main ingredients are:

t Time or epoch.

$\#(\pi, \sigma)$ Individual.

π Exogenous parameters. (Search Space).

σ Endogenous parameters. (Adaptation).

$P(t)$ Population. $P(t) = \cup_i^n \#(\pi_i, \sigma_i)$

$\Phi(f(\pi))$ Fitness. $\Phi(f(\pi)) : \mathbb{R}^{\|\pi\|} \rightarrow \mathbb{R}^+$

operators (Mutation, Selection, Variation, etc.)

Briefly, After the fitness definition, the evolution procedure follows according [11] the next algorithm:

```

 $t \leftarrow 0$ 
initialize  $P(t)$ 
evaluate  $\Phi(P(t))$ 
while not terminate
   $P'(t) \leftarrow \text{variation } P(t)$ 
  evaluate  $\Phi(P'(t))$ 
   $P(t+1) \leftarrow \text{select } P'(t) \cup Q$ 
   $t \leftarrow t+1$ 
end

```

Here Q is a special pot of individuals that might be considered for selection purposes, e.g. $Q = \{\emptyset, P(t), \dots\}$. An offspring population $P'(t)$ of size λ is generated by means of variation operators such as recombination and/or mutation from the population $P(t)$. The offspring individuals $\#(\pi_i, \sigma_i) \in P(t)$ are

evaluated by calculating their fitness represented by $\Phi(f)$. Selection of the fittest is performed to drive the process toward better individuals.

In evolution strategies the individual consist on two types of parameters: *exogenous* π which are points in the search space, and *endogenous* σ which are known too as *strategic parameters*, thus $\# = \#(\pi, \sigma)$. Variation is composed of *mutation* and *self-adaptation* performed independently on each individual. Thus

$$\#(\pi', \sigma') \leftarrow \text{mutate}(\#(\pi, \cdot)) \cup \text{adapt}(\#(\cdot, \sigma)) \quad (1)$$

where mutation is accomplished by

$$\pi'_i = \pi_i + \sigma_i \cdot N(0, 1) \quad (2)$$

and adaptation is accomplished by

$$\sigma'_i = \sigma_i \cdot \exp\{\tau' \cdot N(0, 1) + \tau \cdot N(0, 1)\} \quad (3)$$

where $\tau' \propto (\sqrt{2n})^{-1}$ and $\tau \propto (\sqrt{2\sqrt{n}})^{-1}$.

$N(0, 1)$ indicates a normal density function with expectation zero and standard deviation 1, and n the dimension of the search space ($n = \|\pi\|$).

Selection is based only on the response surface value of each individual. Among many others are specially suited:

- Proportional. Selection is done according to the individual relative fitness $p(\#_i) = \frac{\Phi(f(\pi_i))}{\sum_k \Phi(f(\pi_k))}$
- Rank-based. Selection is done according to indices which correspond to probability classes, associated with fitness classes.
- Tournament. Works by taking a random uniform sample of size $q > 1$ from the population, and then selecting the best as a survival, and repeating the process until the new population is filled.
- (λ, μ) . Uses a deterministic selection scheme. μ parents create $\lambda > \mu$ offsprings and the best μ are selected as the next population [$Q = \emptyset$].
- $(\lambda + \mu)$. Selects the μ survivors from the union of parents and offsprings, such that a monotonic course of evolution is guaranteed [$Q = P(t)$]

3 LOOP SHAPING BY EVOLUTION STRATEGIES

In the following it is assumed that a set of boundaries has been computed for the corresponding frequencies. The problem of fitting a rational transfer function to these boundaries is considered, by using evolution strategies. The main assumption is that the number of zeros and poles has to be previously specified.

Search Space A real polynomial $X_n(s)$ is represented by

$$X_n(s) = \sum_{i=0}^{i=n} c_i s^i = \begin{cases} c_n \prod_{i=1}^{n/2} (s^2 + a_i s + b_i) & n \text{ even} \\ c_n (s + b_0) \prod_{i=1}^{n/2} (s^2 + a_i s + b_i) & n \text{ odd} \end{cases} \quad (4)$$

where the binomial $(s^2 + a_i s + b_i)$ can have real or complex roots, depending on whether $a_i^2 - 4b_i \geq 0$ or not. The controller $G_c(s)$ is a transfer function represented by

$$G_c(s) = \frac{N_m^c(s)}{D_n^c(s)} = K \frac{(s + z_0) \prod_{i=1}^{m/2} (s^2 + a_i s + b_i)}{(s + p_0) \prod_{j=1}^{n/2} (s^2 + c_j s + d_j)} \quad (5)$$

where the terms $(s + z_0)$ and $(s + p_0)$ appeared only when the numerator and/or denominator degrees m, n are odd. This parameterization of the controller defines the search space π , given by

$$\pi = \left\{ K, z_0, \{a_i, b_i\}_{i=1}^{m/2}, p_0, \{c_i, d_i\}_{i=1}^{n/2} \right\} \quad (6)$$

An alternative search space could be

$$G_c(s) = \frac{N_m^c(s)}{D_n^c(s)} = \frac{\sum_i^m b_i s^i}{\sum_i^n a_i s^i} \quad (7)$$

where

$$\pi = \{ \{b_i\}_{i=0}^m, \{a_i\}_{i=0}^n \} \quad (8)$$

However, in the case of high order controllers is preferable to use 6 instead 8 because of the scale differences between the coefficients in the second formulation. The first formulation is also amenable for easily assuring, when demanded, controller inner stability as well as cancellation.

Feasible Search Space Among all posible controllers, we select those which make stable the closed loop system. The nominal plant is represented by

$$G_p(s) = \frac{N_p^p(s)}{D_q^p(s)} \quad (9)$$

so the closed loop transfer function

$$G(s) = \frac{N_m^c(s) N_p^p(s)}{D_n^c(s) D_q^p(s) + N_m^c(s) N_p^p(s)} \quad (10)$$

Hurwitz representatives are allowed and non Hurwitz are punished and so excluded from the search.

Boundary Associated Penalties

Boundaries are weighted following [5] according to barrier functions (Fig. 1). We prefer the smooth barrier instead drastic

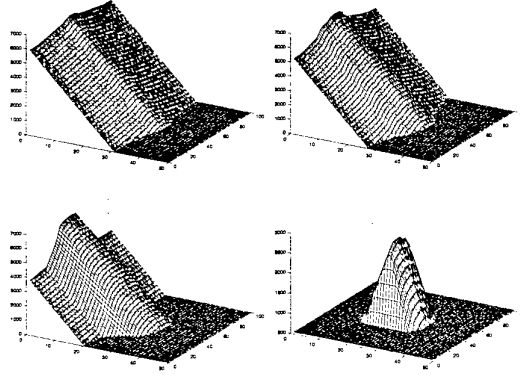


Figure 1: Typical boundary barriers. The horizontal plane corresponds to the Nichols plane. In the vertical axis is represented the barrier value

because the ES's intrinsic knowledge feedback is more graded and helpful.

Fitness Function.

For a given controller, that is a given individual or element of the search space π , the fitness function include the quantity that is to be optimized as well as the restriction of the problem. In our case, it contains the boundaries through the barrier function, and the cut-off frequency and the high-frequency gain as measures to be minimized.

function fitness(π)

given $G_c(\pi, j\omega)$

calculate $D(\pi, j\omega) = 1 + G_c(\pi, j\omega)G_p(j\omega)$

if $D(\pi, j\omega)$ is Hurwitz

$f = k_1 \omega_c + k_2 \mathcal{B}(G_c(\pi, j\omega)G_p(j\omega)) + k_3 \mathcal{C}(G_c(\pi, j\omega)G_p(j\omega))$

else

$f = \infty$

end

return f

Here k_1, k_2, k_3 are ranging constants, ω_c the cut-off frequency, $\mathcal{B}(\cdot)$ the boundaries barrier function and $\mathcal{C}(\cdot)$ the feedback cost.

4 CASE STUDY

The problem considered is the autopilot design problem proposed by [12]. The goal is find a feedback controller G_c , and a forward controller G_r for the family of plants

$$\mathcal{G}_p = \left\{ G_p(s) = \frac{k(1 + \frac{s}{z})}{s(1 + \frac{s}{p})(1 + 2\xi(\frac{s}{\omega_n}) + (\frac{s}{\omega_n})^2)} \right\} \quad (11)$$

k, z, p, ξ, ω_n according to:

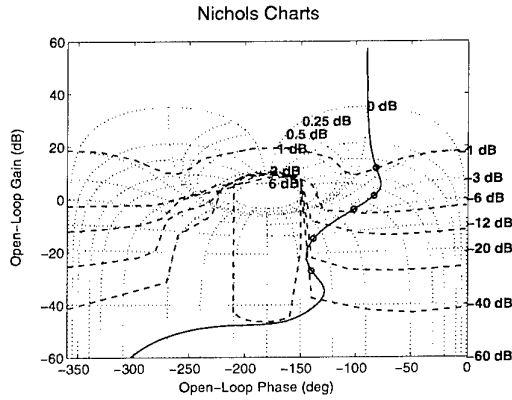


Figure 2: Evolutive Strategies Solution for 3th order controller

	nominal	
k	0.2	[0.2, 2.0]
z	0.5	[0.5, 0.75]
p	1.0	[1.0, 10.0]
ω_n	5.0	[5.0, 6.0]
ξ	0.8	[0.8, 0.9]

such that the closed loop system is stable and in addition

$$T_L(\omega) \leq \left| G_r(j\omega) \frac{G_p(j\omega)G_c(j\omega)}{1 + G_p(j\omega)G_c(j\omega)} \right| \leq T_U(\omega) \quad (12)$$

The technique described in the above Section is applied. As a result, a third order controller

$$G_c(s) = 3.66 \frac{s^2/96.6128 + s/7.571 + 1}{s^3/885474 + s^2/8132.8 + s/49.5633 + 1} \quad (13)$$

The Nichols plots of the boundaries and the fitting of the open loop function is given in fig. 2. The boundaries were built from the nominal plant at the frequencies 0.2, 1.0, 2.0, 5.0, 10.0 and 1000.0 [rad/s].

For comparison purposes a fitting with a proper third order controller has been made. The result is

$$G_c(s) = 3.44 \frac{(s/1.45 + 1)(s/5.55 + 1)(s/17.21 + 1)}{(s/0.49 + 1)(s/41.22 + 1)(s/146.58 + 1)} \quad (14)$$

while the solution proposed by Thomson [12] is:

$$G_c(s) = 5 \frac{(s/2 + 1)(s/4 + 1)(s/6 + 1)}{(s/0.5 + 1)(s/80 + 1)(s/100 + 1)} \quad (15)$$

Comparison of results for this case can be seen in figures 3, 4 and 5. The order 4th controller can be also easily obtained,

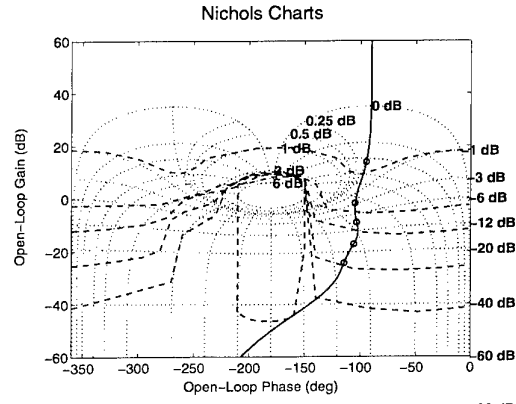


Figure 3: Thomson's 3th order solution

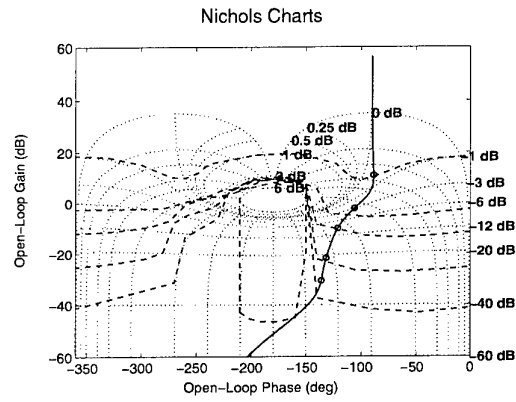


Figure 4: Evolutive Strategies solution

with the results shown in figure 6 and the indices evolution can be seen in fig. 7

$$G_c(s) = 77.38 \frac{(s + 0.428)(s + 2.62)(s + 7.235)(s + 37.885)}{(s + 0.42)(s + 0.9)(s + 89.023)(s + 212.25)} \quad (16)$$

As a result, it can be seen that evolution strategies gives 3th order controller that results in a loop gain transfer function with small static gain and small cut-off frequency. The solution found for the 4th order controller had almost the same shape, thus no much improvement was attained with the higher order controller in this case.

Closing the applications we show a couple of examples extracted from the MATLAB toolbox (demo1,demo2) that also where solved in [4]

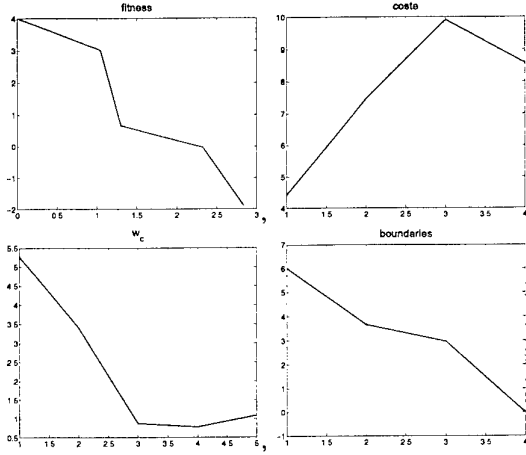


Figure 5: From left to right, top down: fitness, feedback cost, cutoff frequency, barriers penalty for the 3th controller. Those are bilogarithmic plots in which horizontal axis measures $\log_{10}(\text{fitness_evaluations})$

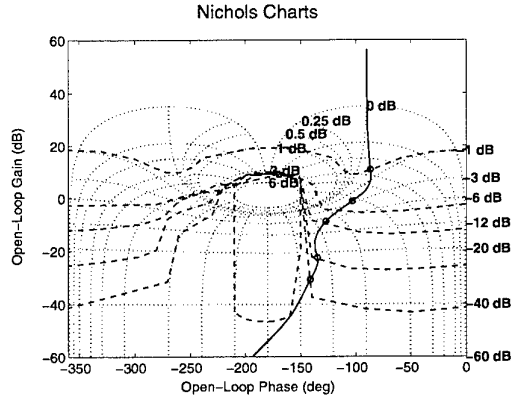


Figure 6: and Evolutive Strategies Solution 4th order

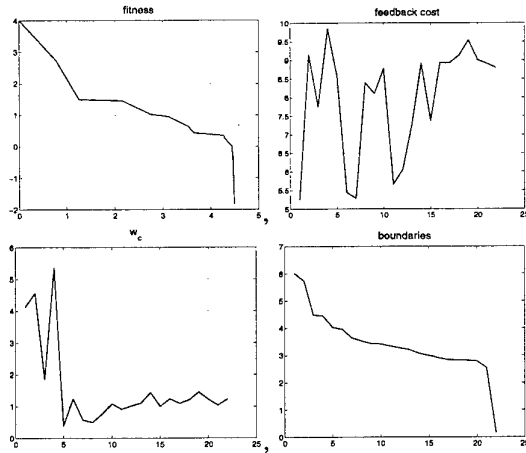


Figure 7: From left to right, top down: fitness, feedback cost, cutoff frequency, barriers penalty for the 4th controller. Those are bilogarithmic plots in which horizontal axis measures $\log_{10}(\text{fitness_evaluations})$

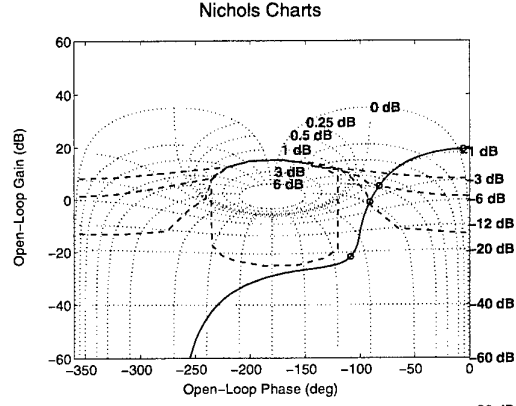


Figure 8: demo1. Nichols chart (controller 1×2)

4.1 demo1

$$\mathcal{G}_p = \left\{ G_p(s) = \frac{k}{(s+a)(s+b)} \mid k \in [1, 10], a \in [1, 10], b \in [20, 30] \right\} \quad (17)$$

closed loop specifications

- 1) Robust stability.
- 2) Robustness margin

$$\left| \frac{G_p(j\omega)G_c(j\omega)}{1 + G_p(j\omega)G_c(j\omega)} \right| \leq 1.2 \quad \forall G_p \in \mathcal{G}_p, \omega \geq 0 \quad (18)$$

- 3) Output perturbation rejection:

$$\left| \frac{Y(j\omega)}{D(j\omega)} \right| < \left| \frac{(j\omega)^3 + 64(j\omega)^2 + 748(j\omega) + 2400}{(j\omega)^2 + 14.4(j\omega) + 169} \right|, \omega < 10 \quad (19)$$

- 4) Input perturbation rejection

$$\left| \frac{Y(j\omega)}{V(j\omega)} \right| < 0.01, \omega < 50 \quad (20)$$

ES's solution:

$$G_c(s) = \frac{140.69(s/104.82 + 1)}{(s/104.82 + 1)^2 + 6.537} \quad (21)$$

[4] solution:

$$G_c(s) = 379 \frac{s/42 + 1}{(s/247)^2 + s/247 + 1} \quad (22)$$

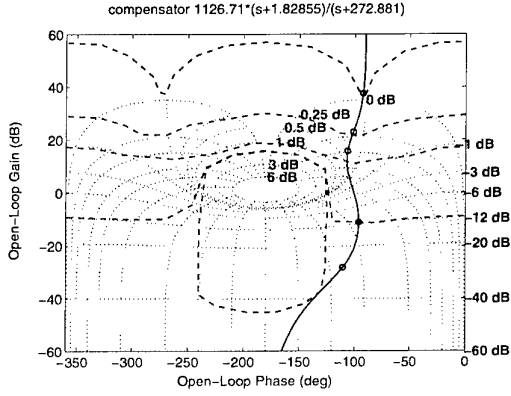


Figure 9: demo2. ES's Nichols chart (controller 1x1)

4.2 demo2

$$\mathcal{G}_p = \left\{ G_p(s) = \frac{ka}{s(s+a)} : k \in [1, 10], a \in [1, 10] \right\} \quad (23)$$

Closed loop specifications:

$$\left| \frac{G_p(j\omega)G_c(j\omega)}{1 + G_p(j\omega)G_c(j\omega)} \right| \leq 1.2 \quad \forall G_p \in \mathcal{G}_p, \omega \geq 0 \quad (24)$$

$$T_L(\omega) \leq \left| F(j\omega) \frac{G_p(j\omega)G_c(j\omega)}{1 + G_p(j\omega)G_c(j\omega)} \right| \leq T_U(\omega) \quad (25)$$

$$T_L(\omega) = \left| \frac{120}{(j\omega)^3 + 17(j\omega)^2 + 828(j\omega) + 120} \right| \quad (26)$$

$$T_U(\omega) = \left| \frac{0.6854(j\omega + 30)}{(j\omega)^2 + 4(j\omega) + 19.752} \right| \quad (27)$$

ES's solution:

$$G_c(s) = 1126.71 \frac{s + 1.82855}{s + 272.881} \quad (28)$$

[4] solution:

$$G_c(s) = \frac{6.753 \times 10^6 s + 1.3947 \times 10^7}{s^2 + 3.4834 \times 10^3 s + 1.6218 \times 10^6} \quad (29)$$

[2] solution:

$$G_c(s) = \frac{3.0787 \times 10^6 s^2 + 3.5365 \times 10^8 s + 3.8529 \times 10^8}{s^3 + 1.5288 \times 10^3 s^2 + 1.0636 \times 10^6 s + 4.2810 \times 10^7} \quad (30)$$

5 ACKNOWLEDGEMENTS

This work has been supported by CICYT under project DPI2000-1218-C04-02 and DPI2000-1218-C04-03

References

- [1] Ballance, D. J., and Gawthrop, P. J., "Control systems via a QFT approach", Proc. Control'91, 476-481, 1991.
- [2] Borghesani, C., Chait, Y., Yaniv, O., Quantitative Feedback Theory Toolbox User Manual, Control and Dynamical Systems 107-81 California Institute of Technology, Pasadena, CA 91125, The Math Work Inc., 1995
- [3] Chait, Y., "Optimal automatic loop-shaping of QFT controllers via convex optimization", Proc. Symposium on QFT and other frequency domain methods and applications, Univ. Of Strathclyde, U.K., pp. 13-27, 1997.
- [4] Chen, W., Ballance, D. J., Li, Y., Automatic Loop-Shaping in QFT Using Genetic Algorithms, Centre for Systems & Control, University of Glasgow, University of Glasgow - Internal Report, 1998
- [5] Fiacco, A. V., McCormick, G. P. Nonlinear Programming: Sequential Unconstrained Minimization Techniques. John Wiley and Sons, Inc. 1968.
- [6] Gera, A., and Horowitz, I., "Optimization of the loop function", International Journal of Control, 31, 389-398, 1980.
- [7] Hans-Paul Schwefel and Rudolph G. *Contemporary Evolution Strategies* In: Advances in Artificial Life. Third International Conference on Artificial Life, vol. 929 of Lecture Notes in Artificial Intelligence, pages 893-907. Springer, Berlin. 1996.
- [8] Horowitz, I., Quantitative Feedback Design Theory (QFT), QFT Publications, Boulder, Colorado, 1993.
- [9] Raimundez, J. C., Evolutive strategies and their application in controller synthesis, Ph. D. Thesis, University of Vigo, 1997.
- [10] Raimundez, J. C., "Hamiltonian controller synthesis using evolutive strategies", NCN Workshop on Dynamics, Bifurcations and Control, Germany, 2001.
- [11] Thomas Bäck, Ulrich Hammel, Hans-Paul Schwefel *Evolutionary Computation: Comments on the History and Current State* In: IEEE Trans. on Evolutionary Computation, vol. 1 n° 1, April 1997.
- [12] Thompson, D. F., "Optimal and suboptimal loop shaping in Quantitative Feedback Theory", Ph. D. Thesis, School of Mechanical Eng., Purdue University, West Lafayette, IN, 1990.

A METHOD FOR NONLINEAR QUANTITATIVE STABILITY

Alfonso Baños* and Isaac Horowitz**

**Dept. Informática y Sistemas, Universidad de Murcia,
Campus Espinardo, 30071, Murcia, Spain.*

***Prof. Emeritus, Dept. Applied Mathematics, Weizmann Institute of Science,
Rehovot, Israel, and Dept. of Electrical and Computer Engineering, University of
California, Davis, USA.*

Abstract: This work makes use of the Schauder fixed point theorem to develop a quantitative approach to the stability problem of nonlinear QFT designs. The method is applied to nonlinear systems having a linear high-frequency behavior, and is specially well suited for systems with hard memoryless nonlinearities.

Keywords: QFT, stability, nonlinear systems

1. INTRODUCTION

Quantitative Feedback Theory (QFT) has been developed for nonlinear and/or time varying systems ([1]). Several rigorous techniques are available in the literature for usual closed-loop specifications such as tracking or disturbance attenuation. However, the (BIBO) stability of these designs has not been explicitly considered. The reason is that the designs inherently achieve the desired specified performance over the specified sets of command and disturbance inputs. The latter sets must be compact, but can have arbitrary numbers of elements. If one is concerned about the effect of any other conceivable input class, he need only include it in the final total input sets. Also, It is easy to formulate the sets so that small deviations in any input, results in small deviations in the output. However, this paper shows that for a specific nonlinear problem class, one can readily formally include *quantitative* BIBO stability in the design process. Some previous ideas in this direction are given in [2].

Alternatives approaches to nonlinear stability in QFT have been developed recently [3-5], based on absolute

stability results such as that the Circle and Popov criteria, that has been adapted as synthesis tools, generating specific stability bounds. Absolute stability results may be conservative in many cases, thus it becomes apparent the strong interest in developing another approaches to nonlinear stability. One direction is the application of multiplier theory and harmonic balance [5]. In this work, an approach based on Schauder fixed point theorem is developed, using typical QFT reasonings, to develop *quantitative* stability results.

It is worthwhile to mention that a very important area of research in stability of nonlinear systems has its roots in the application of the contraction mapping fixed point theorem. One of the seminal works in this direction is [6], from where small-gain theorem, loop transformations, etc.. can be derived. This work emphasizes the use of a less restrictive fixed point result, that is Schauder theorem, for deriving practical rules in order to design stabilizing feedback compensator in the presence of potentially large uncertainty.

2. QUANTITATIVE STABILITY

Let $\varphi_\theta: U \rightarrow Y$ be a nonlinear system parameterized by the parameter vector $\theta \in \Theta$, with U and Y linear spaces of inputs and outputs signals, respectively. Let $U_S \subset U$ and $Y_S \subset Y$ be subsets of bounded signals in their respective spaces. Consider an uncertain nonlinear plant defined as the set $\varphi = \{\varphi_\theta | \theta \in \Theta\}$, and that each nonlinear system φ_θ may be decomposed in the following way (Fig. 1): for each output y in Y_S such that $y = \varphi_\theta(u)$ for some input u in U_S ,

$$y = \varphi_\theta u = P_{y,\theta}(u + d_{y,\theta}) \quad (1)$$

where $P_{y,\theta}$, a linear time-invariant system with transfer function $P_{y,\theta}(s)$, defines the set $\mathbf{P} = \{P_{y,\theta} | y \in Y, \theta \in \Theta\}$, and the disturbance signal $d_{y,\theta}$ defines the set $\mathbf{D} = \{d_{y,\theta}, y \in Y, \theta \in \Theta\}$. For bounded outputs, the corresponding disturbance set \mathbf{D}_S is also defined as $\mathbf{D}_S = \{d_{y,\theta} | y \in Y_S, \theta \in \Theta\}$. It is assumed that $\mathbf{D}_S \subset U_S$, that is that the disturbance is a bounded signal when corresponding to a bounded output.

Consider the systems φ and \mathbf{P} embedded in a two degrees of freedom feedback structure, following Fig. 2, where we have considered r and d as inputs to the feedback system, for stability purposes. A standard definition of BIBO closed-loop stability is the following: the nonlinear feedback system is stable if for every bounded signals $r \in R_S$ and $d \in U_S$, we have that $u \in U_S$ and $y \in Y_S$.

The second structure in Fig. 2 poses a linear feedback problem, where the disturbance signal is now $d_L = d + d_{y,\theta}$, where obviously $d_L \in U_S$ when $d \in U_S$ and $d_y \in \mathbf{D}_S$. We would like the linear system to be stable in the above sense: for every bounded signals $r \in R_S$ and $d_L \in U_S$, and for every $\theta \in \Theta$, we have that $u_L \in U_S$ and $y_L \in Y_S$. If G can be designed to stabilize the linear feedback system in that way, then for each reference input r , each disturbance input d , and each parameter vector θ , a mapping $\varphi: Y \rightarrow Y$ is defined for each bounded output y in Y_S . It is given by

$$y_L = \varphi(y) = P_{y,\theta} G(1 + P_{y,\theta} G)^{-1} Fr + P_{y,\theta} (1 + P_{y,\theta} G)^{-1} (d_{y,\theta} + d) \quad (2)$$

and $\varphi(Y_S) \subseteq Y_S$ if the feedback system is stable. If, in addition, every mapping φ is continuous over Y_S , a convex and compact subset of a Banach space, Schauder fixed point theorem is applicable. Thus, for every bounded signals $r \in R_S$, $d \in \mathbf{D}_S$ and every $\theta \in \Theta$ there exists a bounded signal $y^* \in Y_S$ that satisfy (note that the fixed point y^* depends on the signals r , d , and the parameter vector θ , however by notational simplicity it is not explicitly shown)

$$y^* = \varphi(y^*) = P_{y,\theta} G(1 + P_{y,\theta} G)^{-1} Fr + P_{y,\theta} (1 + P_{y,\theta} G)^{-1} (d_{y,\theta} + d) \quad (3)$$

from where

$$y^* + GP_{y,\theta} y^* = P_{y,\theta} Fr + P_{y,\theta} (d_{y,\theta} + d) \quad (4)$$

and finally using the decomposition (1)

$$\begin{cases} y^* = P_{y,\theta} (u^* + d_{y,\theta} + d) = \varphi_\theta(u^* + d) \\ u^* = GFr - Gy^* \end{cases} \quad (5)$$

that is, y^* is also the output of the nonlinear feedback system, that becomes stable in the sense that for every bounded signals r and d , we have that y^* is also bounded. A similar reasoning can be done to show that u^* is also bounded, then the nonlinear feedback system is stable.

The above method is rather general. Two simplifying assumptions are: i) choose $d_{y,\theta} = 0$ in (1) and then solve the equivalent linear problem using the first QFT nonlinear method, and ii) choose $P_{y,\theta}$ independent on the output y and then applying the second QFT nonlinear method. In practice, it is more convenient to choose $P_{y,\theta}$ independent of the output y . Thus the second QFT nonlinear method is applicable, that will be the approach followed here.

Moreover, the designer may be interested in a more restricted sense of stability, in which the set Y_S may be related with the size of the inputs r and d , e.g. finite gain stability: the output is bounded by a linear function of the inputs bounds. In this sense, not only the output is bounded for bounded inputs, in addition the size of the output is proportional to the input size (see Section 3). The class of nonlinear plants that will be first considered in this work is the given by the following differential equation

$$y^{(n)}(t) + f_y(y(t), y'(t), \dots, y^{(n-1)}(t), \theta) = u^{(m)}(t) + f_u(u(t), u'(t), \dots, u^{(m-1)}(t), \theta)$$

corresponding to nonlinear systems in which the leading derivatives enter linearly, thus the system have a linear high frequency behavior. The set of bounded outputs can be defined with respect to the set of references and disturbances inputs as

$$Y_S = \left\{ y \in Y \mid \|y\| \leq \alpha_0 \|r\| + \beta_0 \|y\| \leq \beta_1, \dots, \|y^{(n-1)}\| \leq \beta_{n-1}, r \in R_S, d \in D_S \right\}$$

where β_0 is an allowed bias over the output $y(t)$, and both the gain α_0 , the bias β_0 , and the rest of bounds are finite constants.

3. CASE STUDY: UNCERTAIN VAN DER POL SYSTEM

An uncertain Van der Pol system is given by [7]

$$\begin{aligned} \mathcal{P}_\theta : u &\rightarrow y, \ddot{y} + A\dot{y}(By^2 - 1) + Ey = ku \\ A &\in [1, 3], B \in [1, 4], E \in [-2, -1], k \in [30, 120] \\ \theta &= (A, B, E, k) \end{aligned} \quad (7)$$

By simplicity, in the following we consider two cases:

- i) stability with respect to disturbances, that is $r = 0$,
- and ii) stability with respect to references, $d = 0$.

A possible decomposition of the nonlinear plant is (note that as discussed above, the linear equivalent plant does not depend on y , thus second QFT method is applicable)

$$\begin{cases} P_\theta(s) = \frac{k}{s^2 - As + E} \\ d_{y,\theta} = -\frac{AB}{k} \dot{y}y^2 \end{cases} \quad (8)$$

Case #1: $r = 0$

a) Definition of bounded inputs and outputs

$$D_S = \{d \in L_\infty, \|d\| \leq \delta_0, \|\dot{d}\| \leq \delta_1\} \quad (9)$$

$$Y_S = \{y \in L_\infty, \|y\| \leq \beta_0, \|\dot{y}\| \leq \beta_1\} \quad (10)$$

$$D_{L,S} = \left\{ d_L = d + d_{y,\theta} \mid d \in D_S, d_{y,\theta} = -\frac{AB}{k} \dot{y}y^2, y \in Y_S, A \in [1, 3], B \in [1, 4] \right\} \quad (11)$$

b) Stabilization of the linear equivalent problem (the method based on specifications over the dc-gain of closed loop transfer functions is used [1]). First, the output must be bounded according to (10)

$$\begin{cases} T_d(0)\mu_d \|d_L\| \leq \beta_0 \\ T_d(s) = \frac{P(s)}{1 + P(s)G(s)} \\ d_L \in D_S \Rightarrow \|d_L\| \leq \|d\| + \|d_{y,\theta}\| \leq \delta_0 + 0.4 \cdot \beta_1 \beta_0^2 \end{cases} \quad (12)$$

and although an exact solution is possible, a reasonable approximate solution can be obtained, by doing $T_d(0) \equiv 1/G(0)$, resulting in

$$G(0) \geq \frac{(\delta_0 + 0.4\beta_1\beta_0^2)\mu_d}{\beta_0} \quad (13)$$

In addition, the first derivative of the output must be bounded to guarantee that the output is bounded to satisfy (10). Then

$$T_d(0)\mu_d \|\dot{d}_L\| \leq \beta_1 \quad (14)$$

or making simplifying assumptions as above

$$\frac{1}{G(0)}\mu_d \left\| \dot{d} + \frac{AB}{k}(\ddot{y}y^2 + 2\dot{y}^2) \right\| \leq \beta_1 \quad (15)$$

now assuming that the maximum value of the second derivative of the output is given by β_2 , we obtain

$$\frac{1}{G(0)}\mu_d(\delta_1 + 0.4(\beta_2\beta_0^2 + 2\beta_1^2)) \leq \beta_1 \quad (16)$$

and finally

$$G(0) \geq \frac{(\delta_1 + 0.4(\beta_2\beta_0^2 + 2\beta_1^2))\mu_d}{\beta_1} \quad (17)$$

Clearly, the solution will be the maximum of right hands of (13)-(17), that is

$$G(0) \geq \max \left(\frac{(\delta_0 + 0.4\beta_1\beta_0^2)\mu_d}{\beta_0}, \frac{(\delta_1 + 0.4(\beta_2\beta_0^2 + 2\beta_1^2))\mu_d}{\beta_1} \right) \quad (18)$$

c) Some numeric values for $\mu_d = 1.3$ and $\beta_2 = 100$ (this bound has to be chosen large enough)

δ_0 ($\ d\ \leq \delta_0$)	δ_1 ($\ \dot{d}\ \leq \delta_1$)	β_0 ($\ y\ \leq \beta_0$)	β_1 ($\ \dot{y}\ \leq \beta_1$)	$G(0)$
1	5	1	5	17
1	5	0.05	5	26
3	10	1	5	18.2
3	100	1	5	41.6
3	100	3	5	125
3	100	3	50	79.3

The table indicates that relatively low values of $G(0)$ guaranty quantitative stability with respect to disturbances.

Case #2: $d = 0$

a) Definition of bounded inputs and outputs

$$R_S = \{r \in L_\infty, \|r\| \leq \rho_0, \|\dot{r}\| \leq \rho_1\} \quad (19)$$

$$Y_S = \{y \in L_\infty, \|y\| \leq \alpha_0 \|r\| + \beta_0, \|\dot{y}\| \leq \beta_1, r \in R_S\} \quad (20)$$

$$D_{L,S} = \{d_L = d_{y,\theta} \mid d_{y,\theta} = -\frac{AB}{k} \dot{y}y^2, y \in Y_S, A \in [1, 3], B \in [1, 4]\} \quad (21)$$

b) Stabilization of the linear equivalent problem. First, the output must be bounded according to (20)

$$\begin{cases} T_r(0)\mu_r\|r\| + T_d(0)\mu_d\|d_L\| \leq \alpha_0\|r\| + \beta_0 \\ T_d(s) = \frac{G(s)P(s)}{1+P(s)G(s)} T_r(s) = \frac{P(s)}{1+P(s)G(s)} \\ r \in R_s \Rightarrow \|r\| \leq \rho_0 \\ d_i \in D_s \Rightarrow \|d_L\| \leq 0.4 \cdot \beta_1(\alpha_0\|r\| + \beta_0)^2 \end{cases} \quad (22)$$

Again by using $T_r(0) \equiv 1$ and $T_d(0) \equiv 1/G(0)$, a reasonable approximate solution is given by the quadratic inequality

$$0.4\beta_1\alpha_0^2\mu_d\|r\|^2 + (0.8\beta_0\beta_1\alpha_0\mu_d - (\alpha_0 - \mu_r)G(0))\|r\| + 0.4\beta_0^2\beta_1\mu_d - \beta_0G(0) \leq 0 \quad (23)$$

that should be satisfied for $\|r\| \leq \rho$. Of course, the treatment is easier for the case $\alpha_0 = 0$. Because of the solution of (23) is more involved, only the case $\alpha_0 = 0$ will be treated here for simplicity. Then, for $\alpha_0 = 0$ (23) is reduced to the linear inequality.

$$\mu_rG(0)\|r\| + 0.4\beta_0^2\beta_1\mu_d - \beta_0G(0) \leq 0 \quad (24)$$

which is easily solved by doing

$$(\mu_r\rho_0 - \beta_0)G(0) + 0.4\beta_0^2\beta_1\mu_d \leq 0 \quad (25)$$

and finally the solution is (being $\beta_0 > \mu_r\rho_0$)

$$G(0) \geq \frac{0.4\beta_0^2\beta_1\mu_d}{\beta_0 - \mu_r\rho_0} \quad (26)$$

Also the first derivative of the output must be bounded to guarantees that the output is satisfy (20). Then, a condition similar to (15) is obtained:

$$\mu_r\|\dot{r}\| + \frac{1}{G(0)}\mu_d\left\|\frac{AB}{k}(\ddot{y}y^2 + 2\dot{y}^2)\right\| \leq \beta_1 \quad (27)$$

from where (being $\beta_1 > \mu_r\rho_1$)

$$G(0) \geq \frac{0.4\mu_d(\beta_0^2\beta_2 + 2\beta_1^2)}{\beta_1 - \mu_r\rho_1} \quad (28)$$

The solution is the worst-case value, given by

$$G(0) \geq \max \left\{ \frac{0.4\beta_0^2\beta_1\mu_d}{\beta_0 - \mu_r\rho_0}, \frac{0.4\mu_d(\beta_0^2\beta_2 + 2\beta_1^2)}{\beta_1 - \mu_r\rho_1} \right\} \quad (29)$$

c) Some numeric values (for $\mu_d = 1.3$, $\beta_2=100$ —this bound has to be chosen large enough)

ρ_0 ($\ r\ \leq \rho_0$)	ρ_1 ($\ \dot{r}\ \leq \rho_1$)	β_0 ($\ y\ \leq \beta_0$)	β_1 ($\ \dot{y}\ \leq \beta_1$)	$G(0)$
1	5	2	20	69
1	5	5	20	127
1	5	5	50	175
3	5	5	50	590
3	5	10	50	425
3	20	10	50	426

As a result, assuming the linear equivalent problem is solved for (linear) stability, affordable dc-gain values of the feedback compensator are obtained for the stability of the nonlinear control system. Comparing Case #1 and Case #2, it is seen that the values of the required dc-gain $G(0)$ are bigger in the second case. This is quite reasonable, since in this case the compensator has to deal not only with the reference input, but also with the disturbances given by the nonlinear dynamics. In any case, typical values of $G(0)$ in the different design given in the literature [7,8] are big enough to conclude that those designs also guaranty quantitative stability in the sense define above.

4. HARD NONLINEARITIES

The quantitative stability method developed in Section 2 is specially well-suited for systems with hard nonlinearities $z = N(y)$ which can be decomposed as $z = Ky + \eta(y)$, where $|\eta(y)| \leq M$. This type of systems include common nonlinearities such as Coulomb friction, backlash, deadzone, etc. In the framework of QFT, these systems have been studied in [9]. In the following, the quantitative stability method is applied to these type of systems. In general, we assume that the nonlinearity η can be represented as a disturbance d_y , associated to the closed loop output y . For example, in the Example 1 of [9], where the control of a motor driving a load is considered, the plant can be transformed to the system of Fig. 3, where in this case $|\eta(y)| \leq 0.2$.

It will be briefly shown how the quantitative stability method can be easily applied obtaining very efficient results. Here we define bounded signals spaces as $R_s = D_s = L_\infty$, and

$$Y_s = \{y \in L_\infty \mid \|y\| \leq \beta_0, \|\dot{y}\| \leq \beta_1\}$$

Assuming that the linear equivalent feedback system (taking d_y as a disturbance) is stable (note that for linear time invariant systems L_∞ -stability and L_2 -stability are equivalent), the nonlinear original system will be automatically stable. Note that in this case no extra conditions are needed, providing that the

constants β_0 and β_1 are computed *a posteriori*. Thus the only conditions are that the closed-loop linear transfer functions, from the inputs of the feedback system (for example the reference r and a disturbance d) and d_y to the rest of signals be stable. Obviously, some extra restrictions can be incorporated to shape these transfer functions in order to obtain appropriate tracking and/or disturbance attenuation, and thus obtaining less conservative bounds β_0 and β_1 . This is a very convenient method for guarantying stability for this type of nonlinear systems. Note that underlying theory based on Schauder fixed point theorem gives a rigorous answer to the problem.

5. CONCLUSIONS

In QFT nonlinear designs it is guarantied that for a prescribed set of references and/or disturbances, the closed loop output belong to a set of acceptable outputs. In general, small deviations from those references and disturbances, that is inputs to the control systems, result in bounded outputs. The incorporation of BIBO stability for more general inputs is possible without leaving the QFT framework. In this work, quantitative stability has been introduced, in the sense that for given inputs bounds and specified output bounds, conditions have been derived over the open loop functions. The result is based on an appropriate application of Schauder fixed point theorem.

ACKNOWLEDGEMENTS

This work has been supported by CICYT under project DPI2000-1218-C04-03 ("FRENODEL: Frequency domain techniques in nonlinear control systems: effects of hard nonlinearities in electromechanical systems")

REFERENCES

- Horowitz, I., *Quantitative Feedback Theory-QFT* (Vol. 1), QFT Press, 4470 Grinnell Ave., Boulder, Colorado 80305, USA, 1993. This is available (in America) from I. Horowitz: 0132012@aol.com, and elsewhere from A. Baños: abanos@dif.um.es.
- Horowitz, I., and Baños, A., "Fundamentals of Nonlinear QFT", in A. Baños, F. Lamnabhi-Lagarigue and F. J. Montoya (eds.), *Advances in Nonlinear Control*, Lectures Notes in Control and Information Science 264, Springer-Verlag, pp. 61-134, 2001.
- Baños, A. and A. Barreiro, "Stability of nonlinear QFT using robust absolute stability criteria", *International Journal of Control*, vol. 73, no. 1, pp. 74-88, 2000.
- Barreiro, A. and A. Baños, "Nonlinear robust stabilization by conicity and QFT techniques", *Automatica*, vol.36, no. 9, 2000.
- Baños, A. Barreiro, F. Gordillo, and J. Aracil, "Nonlinear QFT Synthesis based on harmonic balance and multiplier theory", in A. Isidori, F. Lamnabhi-Lagarigue, and W. Respondek (eds.), *Nonlinear Control in the Year 2000*, Lectures Notes in Control and Information Science #259, Springer-Verlag, London, 2000.
- Zames, G., "Functional analysis applied to nonlinear feedback systems", *IEEE Transactions on Circuit Theory*, pp. 392-403, 1963.
- Horowitz, I. and Schur, D., "Control of uncertain Van der Pol plant", *International Journal of Control*, 32, 2, 199-219, 1980.
- Baños, O. Yaniv, and F. J. Montoya, "Nonlinear QFT based on local linearization", in S. G. Tzafestas and G. Schmidt (eds.), *Progress in System and Robot Analysis and Control Design*, Lecture Notes in Control and Information Science #243, Springer-Verlag, pp. 251-262, 1992.
- Oldak, S., Baril, C., and Gutman, P. O., "Quantitative design of a class of nonlinear systems with parametric uncertainty", QFT Symposium, Wright Laboratory, 1992.

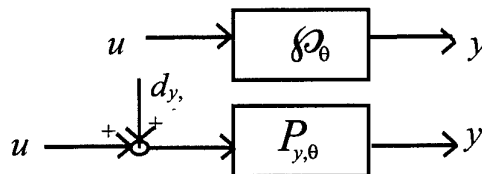


Fig. 1: Decomposition of the nonlinear plant in a LTI plant + disturbance

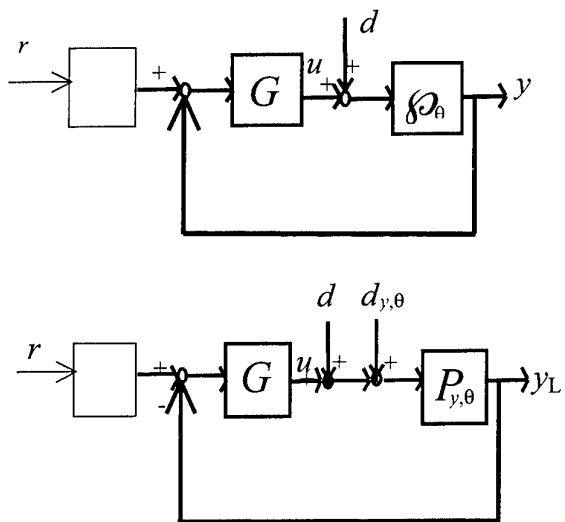


Fig. 2: Nonlinear control system and equivalent linear control system

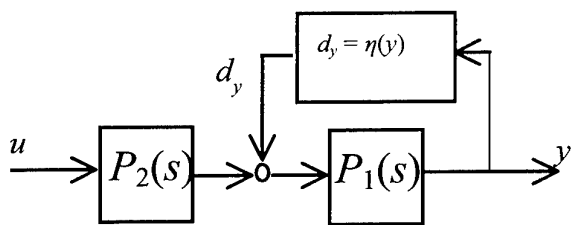


Fig. 2: Example of nonlinear plant with memoryless nonlinearities

List of Authors

Aranda, J.	73; 223	Raimúndez, C.	291
Baños, A.	123; 247; 291; 297	Rao, P. S.	107
Barreiro, A.	291	Rueda Rodríguez, T. M.	79
Barreras, M.	231	Ruipérez, P.	73
Bentley, A. E.	47	Salas, A.	151
Berenguel, M.	123	Schneider, E.	203
Bhattacharyya, S. P.	31	Sheela, S.	177
Boje, E.	63; 107	Tadeo, F.	113
Bondia, J.	133	Ukpai, U.	39
Borshchevsky, M.	9	Valle, F. Del	113
Cardoso, A.	215	Velasco González, F. J.	79
Castillejo, J.	231	Villanueva, J.	67
Cervera, J.	247	Vital, P.	231
Chait, Y.	269	Wikander, J.	95
Cruz, J. M. de la	73	Xiang, F.	95
Díaz, J. M.	73; 223	Yang, S. F.	239
Dormido, S.	223		
Dormido Canto, S.	223		
Dourado, A.	215		
Downing, C. J.	207; 261		
Egaña, I.	67		
Eitelberg, E.	1; 141		
Ferreiro García, R.	255		
Galvez, J. M.	85		
Ganzelmeier, L.	203		
García-Sanz, M.	ix; 67; 193; 231		
Gil-Martínez, M.	193		
Gomes da Silva, A.	85		
González, L.	151		
Gueta, R.	9		
Gutman, P. O.	9		
Helbig, J.	203		
Hollot, C. V.	269		
Horesh, E.	9		
Horowitz, I.	57; 247; 297		
Houpis, C. H.	171		
Hwang, C.	239		
Jayasuriya, S.	39		
Keel, L. H.	31		
Kotecha, K.	161		
López García, E.	79		
Machado, L.	85		
Moreno, J. C.	123		
Moyano Pérez, E.	79		
Nataraj, P. S. V.	161; 177		
O'Brien, M.	207		
O'Mahony, T.	261		
Pérez, O.	113		
Pérez Castelo, F. J.	255		
Picó, J.	133		
Prakash, A. K.	177		
Pratt, P.	207		